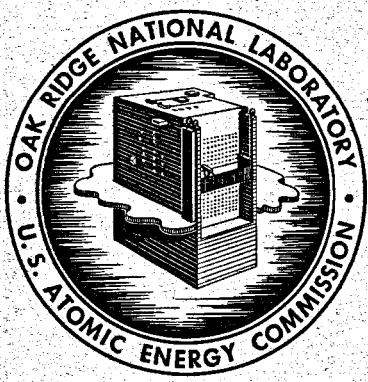


325  
12/7/64

ORNL-3708  
UC-80 - Reactor Technology  
TID-4500 (35th ed.)

MOLTEN-SALT REACTOR PROGRAM  
SEMIANNUAL PROGRESS REPORT  
FOR PERIOD ENDING JULY 31, 1964



OAK RIDGE NATIONAL LABORATORY  
operated by  
UNION CARBIDE CORPORATION  
for the  
U. S. ATOMIC ENERGY COMMISSION

Printed in USA. Price \$7.04. Available from the Clearinghouse for Federal Scientific and Technical Information, National Bureau of Standards, U.S. Department of Commerce, Springfield, Virginia

**LEGAL NOTICE**

This report was prepared as an account of Government sponsored work. Neither the United States, nor the Commission, nor any person acting on behalf of the Commission:

- A. Makes any warranty or representation, expressed or implied, with respect to the accuracy, completeness, or usefulness of the information contained in this report, or that the use of any information, apparatus, method, or process disclosed in this report may not infringe privately owned rights; or
- B. Assumes any liabilities with respect to the use of, or for damages resulting from the use of any information, apparatus, method, or process disclosed in this report.

As used in the above, "person acting on behalf of the Commission" includes any employee or contractor of the Commission, or employee of such contractor, to the extent that such employee or contractor of the Commission, or employee of such contractor prepares, disseminates, or provides access to, any information pursuant to his employment or contract with the Commission, or his employment with such contractor.

ORNL-3708

Contract No. W-7405-eng-26

MOLTEN-SALT REACTOR PROGRAM

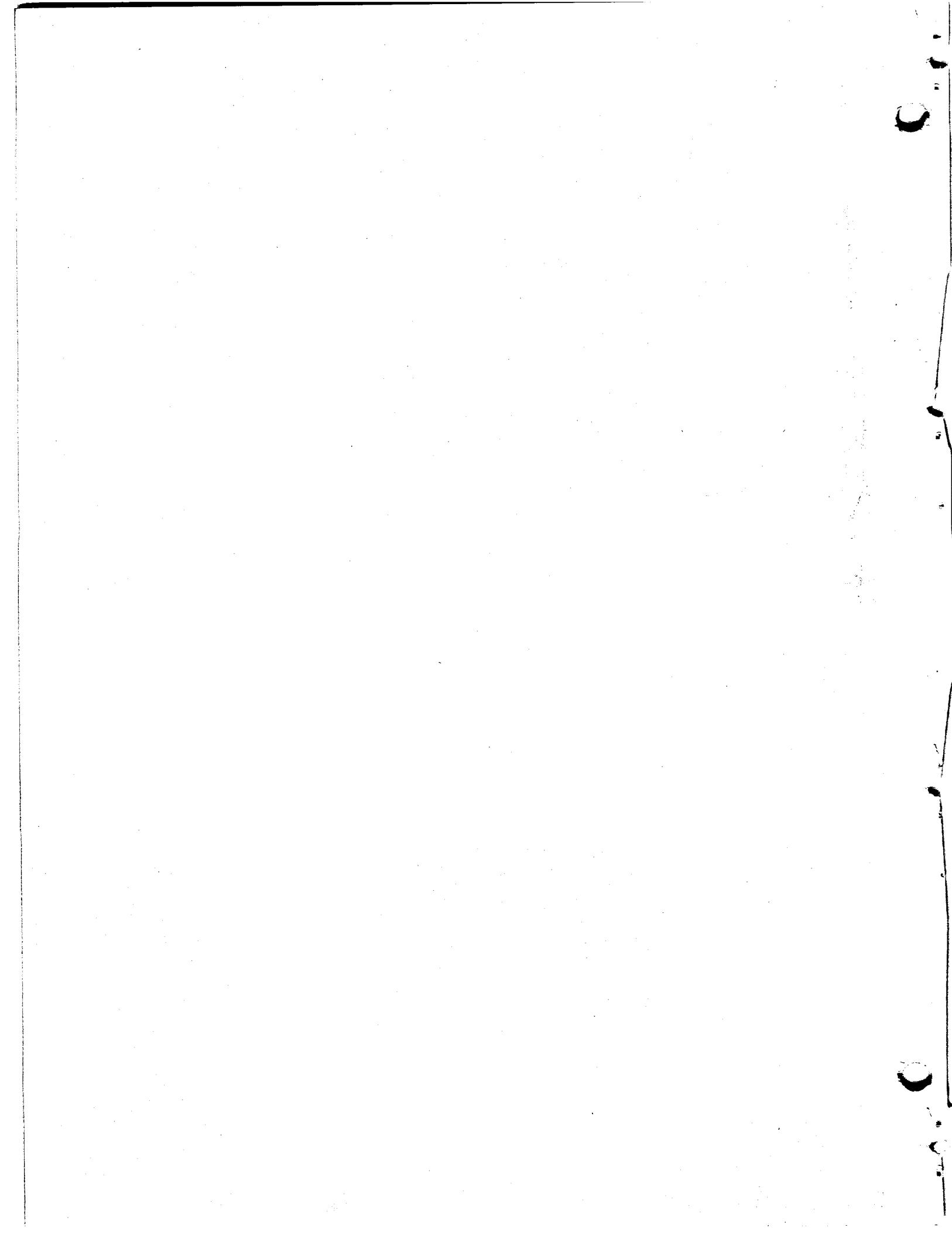
SEMIANNUAL PROGRESS REPORT

For Period Ending July 31, 1964

R. B. Briggs, Program Director

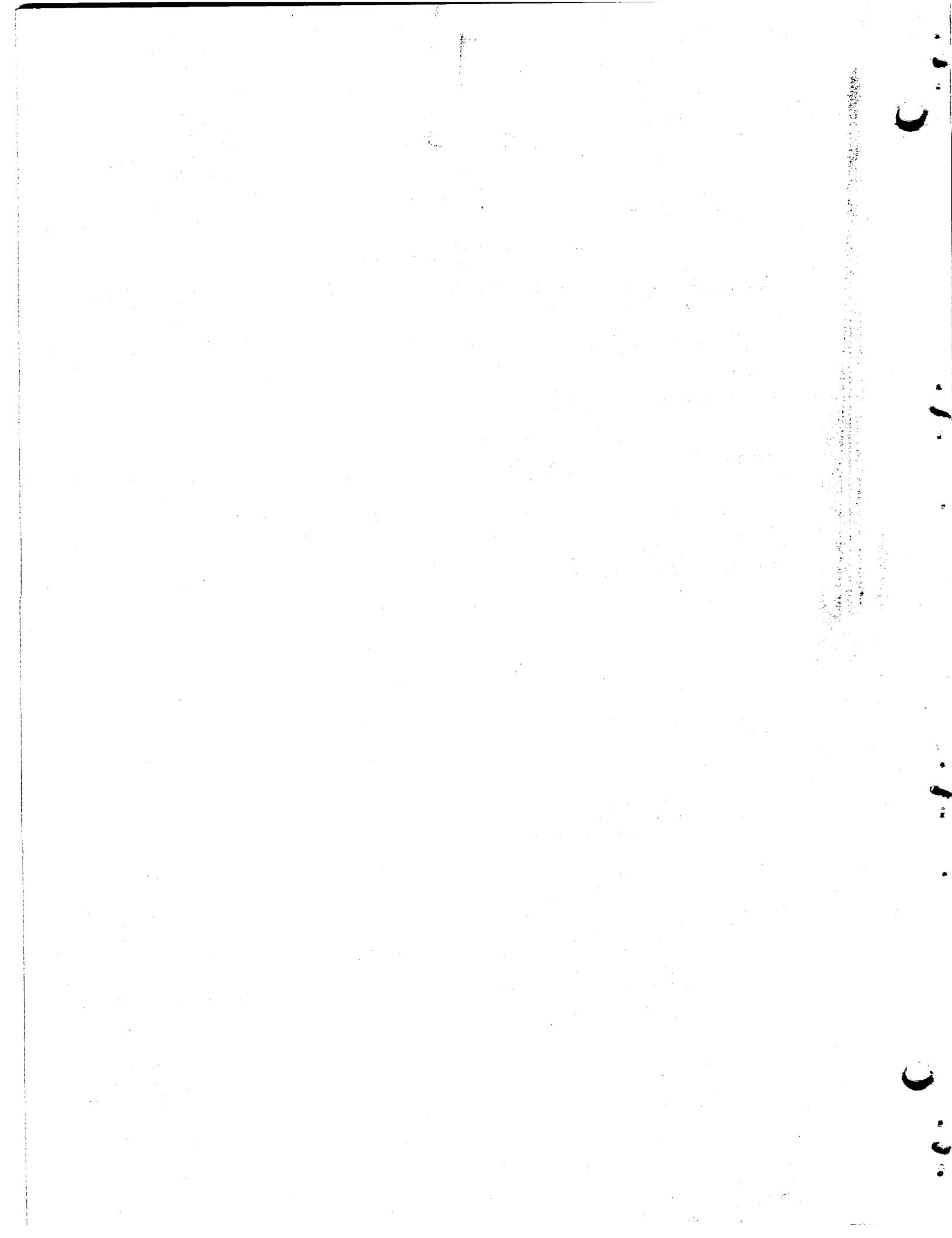
NOVEMBER 1964

OAK RIDGE NATIONAL LABORATORY  
Oak Ridge, Tennessee  
operated by  
UNION CARBIDE CORPORATION  
for the  
U.S. ATOMIC ENERGY COMMISSION



## CONTENTS

|   |     |
|---|-----|
| INTRODUCTION.....   | 1   |
| THE PLACE OF MOLTEN-SALT REACTORS IN THE AEC PROGRAM -<br>E. E. Sinclair.....                   | 1   |
| MOLTEN-SALT POWER REACTORS AND THE ROLE OF THE MSRE IN THEIR<br>DEVELOPMENT - R. B. Briggs..... | 3   |
| MSRE DESIGN AND CONSTRUCTION - W. B. McDonald.....  | 22  |
| NUCLEAR CHARACTERISTICS OF THE MSRE - R. J. Engel.....  | 83  |
| INSTRUMENTATION AND CONTROL OF THE MSRE - J. R. Tallackson.....                                 | 115 |
| PUMP DEVELOPMENT - A. G. Grindell and P. G. Smith.....  | 147 |
| COMPONENT DEVELOPMENT IN SUPPORT OF THE MSRE -<br>Dunlap Scott, Jr.....                         | 167 |
| REMOTE MAINTENANCE OF THE MSRE - Robert Blumberg.....   | 190 |
| FUEL PROCESSING FACILITY - R. B. Lindauer.....  | 201 |
| PLANS FOR OPERATION OF THE MSRE - P. N. Haubenreich.....  | 205 |
| CHEMICAL BASIS FOR MOLTEN-SALT REACTORS - W. R. Grimes.....                                     | 214 |
| EFFECTS OF RADIATION ON THE COMPATIBILITY OF MSRE MATERIALS -<br>F. F. Blankenship.....         | 252 |
| PREPARATION OF MSRE FUEL, COOLANT, AND FLUSH SALTS -<br>J. H. Shaffer.....                      | 288 |
| FUTURE CHEMICAL DEVELOPMENT - H. F. McDuffie.....   | 304 |
| ANALYTICAL CHEMISTRY FOR THE MOLTEN-SALT REACTOR - J. C. White....                              | 320 |
| METALLURGICAL DEVELOPMENTS - A. Taboada.....  | 330 |
| MSRE GRAPHITE - W. H. Cook.....   | 373 |



## INTRODUCTION

This semiannual report is a collection of papers that were presented at a general information meeting on the Molten-Salt Reactor Experiment at the Oak Ridge National Laboratory, August 18 and 19, 1964. It describes the design and construction of the Experiment, the related research and development, and is intended to bring the reader up to date on the status of the general technology of molten-salt thermal-breeder reactors.

Previous progress reports of the Molten-Salt Reactor Program are listed below:

|           |  |
|-----------|--|
| ORNL-2474 | Period Ending January 31, 1958               |
| ORNL-2626 | Period Ending October 31, 1958               |
| ORNL-2684 | Period Ending January 31, 1959               |
| ORNL-2723 | Period Ending April 30, 1959                 |
| ORNL-2799 | Period Ending July 31, 1959                  |
| ORNL-2890 | Period Ending October 31, 1959               |
| ORNL-2973 | Periods Ending January 31 and April 30, 1960 |
| ORNL-3014 | Period Ending July 31, 1960                  |
| ORNL-3122 | Period Ending February 28, 1961              |
| ORNL-3215 | Period Ending August 31, 1961                |
| ORNL-3282 | Period Ending February 28, 1962              |
| ORNL-3369 | Period Ending August 31, 1962                |
| ORNL-3419 | Period Ending January 31, 1963               |
| ORNL-3529 | Period Ending July 31, 1963                  |
| ORNL-3626 | Period Ending January 31, 1964               |

## THE PLACE OF MOLTEN-SALT REACTORS IN THE AEC PROGRAM

E. E. Sinclair

This meeting was organized so that interested parties may learn about the status of molten-salt reactor technology and inspect the Molten-Salt Reactor Experiment (MSRE) before it goes into operation. As you know, the MSRE is just about ready for prenuclear operation, and the timing for this meeting was selected with that fact in mind.

As a representative of the Atomic Energy Commission, which is supporting the development of molten-salt reactor technology, I have agreed to describe "the place of molten-salt reactors in the AEC program." As a matter of fact, this is very easily done by reference to the 1962 AEC Report to the President, which delineates the objectives of this Nation's reactor development programs. In discussing the program for the long-range future (i.e., the development of breeders which will fully utilize nuclear resources), the Report states in part: "Although breeding in the thorium-uranium 233 cycle can build upon experience gained with less advanced reactors ... vigorous and specific efforts will be required to attain breeding on a significant scale. Both fuel and blanket systems must be pushed. Attention should be directed at methods of continuous removal of fission products, including the use of fluid fuels (such as fused uranium salts) and blanket materials. Experimental reactors designed to breed must be built and operated. Hopefully, within the next several years, the program will achieve the stage where operating prototypes will be appropriate."

From this statement and the AEC support of the molten-salt program here at ORNL, it is evident that the AEC looks to molten-salt reactor technology for the near-term accomplishment of breeding on a significant scale in the Th-<sup>233</sup>U cycle. There is, of course, no obvious reason why molten-salt technology could not be developed for fast breeding in the uranium-plutonium cycle, and perhaps this will someday be done. The salt system that has been developed here, however, quite naturally lends itself to thermal breeding in the Th-<sup>233</sup>U cycle; and it is the objective of this program to develop and demonstrate a reactor system which will exploit this capability.

Although the forthcoming operation of the MSRE will not achieve this objective alone, it is an exceedingly important and necessary step toward the goal. The MSRE, being a small single-region machine, is not designed to breed, but it does tie all the pertinent technology developed thus far together into a relatively simple operating system. Its operation is expected to supply the information and confidence needed to proceed with the next and, perhaps final, step of the demonstration program: the design, construction, and operation of a two-region thermal breeder sufficiently large to permit scale-up to commercial sizes.

It would be wishful thinking to suppose that there will be no "bugs" in the MSRE as designed and built. The history of reactor development suggests that there will be bugs or minor difficulties unforeseen in design or caused by errors in construction. These are unwanted but are more or less expected. It is also possible that operation of the MSRE will uncover some truly unexpected major problems. I personally do not expect any, because the technology base that has been worked out for the MSRE is very broad and thorough. In my view the MSRE is much better off in this respect than has been the case for some past reactor experiments.

Today and tomorrow, this technological base which has been developed for the MSRE will be explained in detail. I hope you are as favorably impressed as I am, by the broad coverage, yet thoroughness, of the developments that have been conducted here at ORNL. I venture to predict that there will be another information meeting here in the not too distant future to introduce the operation of a molten-salt breeder prototype. I hope to see you all here at that time.

---

MOLTEN-SALT POWER REACTORS AND THE ROLE OF THE MSRE  
IN THEIR DEVELOPMENT

R. B. Briggs

Realization of a system that makes full use of the potential energy in thorium to produce cheap electricity is the primary mission of reactor development at the Oak Ridge National Laboratory. That system must be an efficient breeder system. An advanced converter may be a worthwhile step in the development, but an advanced converter does not reach the goal. No matter how good the conversion ratio, if it is significantly less than 1, the amount of uranium that must be mined to make up the deficit in fissionable material is greater than the amount of thorium that must be mined to compensate for the thorium converted to  $^{233}\text{U}$  and burned. For example, if the conversion ratio is 0.90, the  $^{235}\text{U}$  from 20 tons of natural uranium will be burned with each ton of thorium consumed. Even with a conversion ratio of 0.99, the  $^{235}\text{U}$  from 2 tons of uranium must be supplied with each ton of thorium.

One feature of the Th- $^{233}\text{U}$  fuel system is that breeding should be possible with thermal and intermediate reactors as well as with fast reactors. Many technical and economic factors combine to favor the thermal breeders; so we have chosen to emphasize them in our program. Our studies lead us to believe that molten-salt reactors are the most promising of the several possible thermal breeder reactors for achieving a satisfactory breeding gain and producing cheap electricity.

Our estimate<sup>1</sup> of the breeding performance of a two-fluid, graphite-moderated thermal breeder is shown in Table 1. The neutron yields and losses are known with less accuracy than the numbers imply, but the table was prepared to show some of the smaller losses and to balance.

We see that the uranium and thorium concentrations and the ratio of uranium to carbon atoms can be adjusted to obtain a good balance between the neutron yield and the parasitic absorptions in moderator and in carrier salts. This leaves a net of about 12 neutrons per 100 neutrons absorbed in fuel for production of excess  $^{233}\text{U}$ . The losses to  $^{233}\text{Pa}$  can

Table 1. Performance Estimate for Molten-Salt Breeder Reactor

|  |  |        |        |        |        |        |        |        |
|--|--|--------|--------|--------|--------|--------|--------|--------|
| Fuel salt composition, mole %  | 0.4UF <sub>4</sub> -63LiF-36.6BeF <sub>2</sub> |        |        |        |        |        |        |        |
| Blanket salt composition, mole %   | 15ThF <sub>4</sub> -67LiF-18BeF <sub>2</sub>   |        |        |        |        |        |        |        |
| Moderator-fuel ratio, N(C)/N(U)  | 5100   |        |        |        |        |        |        |        |
| Volume fraction of fuel salt in core   | 0.16   |        |        |        |        |        |        |        |
| Volume fraction of fertile salt in core  | 0.071  | 0.070  | 0.069  | 0.068  | 0.068  | 0.066  | 0.065  | 0.066  |
| Thorium inventory, metric tons for<br>1000 Mw (electrical)                       |  |        |        | 270    |        |        | 140    |        |
| Fertile stream cycle time, days  | 35   | 35     | 35     | 50     | 100    | 200    | 200    | 50     |
| Fuel stream cycle time, days   | 11   | 23     | 31     | 55     | 55     | 72     | 84     | 50     |
| Total <sup>233</sup> U, <sup>235</sup> U, and <sup>233</sup> Pa inventory,<br>kg | 880  | 860    | 860    | 900    | 1020   | 1220   | 1220   | 880    |
| Net neutron yield, $\bar{\eta}e$   | 2.2137   | 2.2131 | 2.2128 | 2.2120 | 2.2115 | 2.2103 | 2.2097 | 2.2095 |
| Neutron losses:  |  |        |        |        |        |        |        |        |
| <sup>233</sup> U absorptions   | 0.9172   | 0.9150 | 0.9139 | 0.9111 | 0.9095 | 0.9053 | 0.9034 | 0.9021 |
| <sup>235</sup> U absorptions   | 0.0828   | 0.0850 | 0.0861 | 0.0889 | 0.0905 | 0.0947 | 0.0966 | 0.0979 |
| <sup>232</sup> Th fission  | 0.0019   | 0.0019 | 0.0018 | 0.0018 | 0.0018 | 0.0018 | 0.0018 | 0.0018 |
| <sup>233</sup> Pa absorptions ( $\times 2$ )                                     | 0.0120   | 0.0117 | 0.0116 | 0.0113 | 0.0112 | 0.0108 | 0.0106 | 0.0214 |
| <sup>236</sup> U absorptions   | 0.0106   | 0.0115 | 0.0119 | 0.0132 | 0.0140 | 0.0164 | 0.0176 | 0.0165 |
| <sup>237</sup> Np absorptions  | 0.0004   | 0.0010 | 0.0010 | 0.0008 | 0.0008 | 0.0010 | 0.0011 | 0.0010 |
| <sup>135</sup> Xe absorptions  | 0.0050   | 0.0050 | 0.0050 | 0.0050 | 0.0050 | 0.0050 | 0.0050 | 0.0050 |
| Sm absorptions   | 0.0001   | 0.0001 | 0.0001 | 0.0002 | 0.0003 | 0.0005 | 0.0005 | 0.0003 |
| Other fission product absorptions  | 0.0218   | 0.0267 | 0.0317 | 0.0422 | 0.0442 | 0.0532 | 0.0631 | 0.0478 |
| Corrosion product absorptions  | 0.0008   | 0.0008 | 0.0008 | 0.0008 | 0.0008 | 0.0008 | 0.0008 | 0.0008 |
| Moderator absorptions  | 0.0291   | 0.0286 | 0.0286 | 0.0287 | 0.0287 | 0.0287 | 0.0287 | 0.0287 |
| Fuel carrier absorptions   | 0.0284   | 0.0302 | 0.0302 | 0.0302 | 0.0291 | 0.0301 | 0.0301 | 0.0301 |
| Thorium carrier absorptions  | 0.0177   | 0.0199 | 0.0198 | 0.0196 | 0.0195 | 0.0192 | 0.0190 | 0.0192 |
| Loss of delayed neutrons   | 0.0043   | 0.0043 | 0.0043 | 0.0043 | 0.0043 | 0.0043 | 0.0043 | 0.0043 |
| Leakage  | 0.0016   | 0.0016 | 0.0016 | 0.0016 | 0.0016 | 0.0016 | 0.0016 | 0.0016 |
| Chemical processing losses   | 0.0022   | 0.0022 | 0.0022 | 0.0022 | 0.0022 | 0.0022 | 0.0022 | 0.0022 |
| Net breeding gain  | 0.0778   | 0.0676 | 0.0622 | 0.0501 | 0.0480 | 0.0347 | 0.0232 | 0.0288 |
| Net fuel yield, % per full power year  | 8.6  | 8.0    | 7.3    | 5.6    | 5.0    | 2.8    | 1.9    | 3.4    |

be kept low by providing an ample inventory of thorium. Losses to fission products must be kept low, and this can be done by processing the fissile and fertile streams on short cycles - cycles that would be prohibitively expensive if they involved storage, shipment, dissolution, extraction, and refabrication of solid fuel elements, but that should be acceptably cheap if they involved only simple on-site physical and chemical separations from liquid fuels and blankets.

We can readily obtain a breeding gain and fuel yield of 5%, a specific power of 1 Mw (electrical) per kilogram of fissile material and 4 Mw (electrical) per metric ton of thorium. In the studies from which the data in Table 1 were taken, we assumed that  $^{233}\text{Pa}$  could not be separated easily from the fertile stream; thus we were limited to rapid removal of  $^{233}\text{U}$  by the fluoride volatility process. Our chemists have evidence that  $^{233}\text{Pa}$  in very low concentration can be separated from the fertile stream on solid adsorbents. With developments such as this and use of the shorter fuel cycles, we should be able to push the breeding gain to 8%, the yield to 10%, and the specific powers to about 2 Mw (electrical) per kilogram of fissile material and 10 Mw (electrical) per metric ton of thorium. Any type of breeder reactor with performance characteristics equal to the more conservative ones listed above would be an accomplishment of major importance. One with the more advanced characteristics would be an outstanding achievement.

Our belief that molten-salt reactors can produce cheap electricity is founded, in part, on favorable estimates of costs for conceptual designs - fuel costs<sup>2</sup> of 0.5 to 1.5 mills/kwhr and capital costs<sup>3,4</sup> of \$125 to \$145/kwhr. These estimates were made several years ago and were equal to, or less than, those for competitive systems. We have observed no later development, technical or economic, that should adversely affect the outlook for molten-salt reactors.

The costs for a large molten-salt reactor really cannot be estimated accurately enough to be the primary basis for developing a new reactor system. To develop a power reactor technology is a long and expensive business. A new type of reactor merits consideration for such development only if it has basic characteristics which give it considerable long-term promise. Early large-scale versions must produce competitive power, but there must be potential for bettering the competitive position through improvements which lead to larger unit power output, higher thermal efficiency, and better utilization of fuel. Molten-salt reactors have these important basic characteristics.

Low capital costs are promoted by the following characteristics. Fuel and blanket salts have vapor pressures below 1 atm up to 2600°F, and they have good heat-transfer and fluid-flow properties. Thus, molten-salt reactors are low-pressure, high-temperature heat sources, and units can be designed to supply steam to one or more of the largest modern turbine-generator sets. The salts do not undergo violent chemical reactions with air or with a variety of coolants. Volatile fission products can be purged continuously. These characteristics, when combined with the low pressure, can be used to simplify containment.

Uranium, thorium, and plutonium fluorides are sufficiently soluble in appropriate carrier salts for the fuel and blanket liquids to be true solutions. The solubility increases with temperature, so the solutions are thermally stable; they are also stable to radiation. There is no need to resort to slurries or to provide equipment for recombining decomposition products.

The fuel solutions generally have a high negative temperature coefficient of reactivity. Xenon-135 can be removed continuously. Fuel can be added while the reactor is at full power by means of relatively simple equipment. Only a small amount of excess reactivity must be controlled. These attributes should lead to simplified nuclear control and safety systems.

Several characteristics promote low fuel costs. The good radiation stability permits long burnup where desirable. On the other hand, there are no fuel elements to fabricate, the reactors can be designed for good neutron economy, and the fluids can be handled conveniently; so we have the opportunity to remove bred material and fission products on short cycles and to obtain good breeding ratios at low cost. For example, the fluoride volatility process can be used to remove  $^{233}\text{U}$  from the fluoride salt of a thorium breeder blanket without otherwise changing the liquid.

Low operating costs are obtained by building large units that operate continuously. Materials are available to contain the salts at high temperature with little corrosion. Well-designed equipment, carefully fabricated of these materials, should require little maintenance.

Some characteristics of the salt systems tend to make the cost high. Since the salts melt at 850 to 950°F, we must make provision for preheating the reactor equipment to a high temperature before the salts are admitted and we must prevent them from freezing. We must provide an intermediate heat-transfer system or a specially designed steam generator to keep water from coming in contact with the salt and to isolate the reactor from high pressure in the event of a leak. The chemical reaction on mixing is not violent; but hydrogen fluoride is generated and it is corrosive. Also, zirconium and uranium oxides precipitate from the salts in contact with moisture.

Lithium fluoride is a constituent of fuel and blanket salts, and the separated isotope  $^7\text{Li}$  must be used to obtain low parasitic absorption of neutrons. Stainless steel and Inconel will contain the salts satisfactorily at 1000 and possibly 1200°F, but more expensive materials must be used at higher temperature. INOR-8 is preferred at 1300 to 1500°F. Refractory metals - molybdenum and niobium - and graphite appear to be the best container materials for higher temperatures. The graphite must be coated or otherwise specially processed to have low permeability to salt and gaseous fission products.

Since the reactors involve the handling of large quantities of mobile fission products, some special precautions must be taken in the containment. Also, the equipment in the circulating systems becomes radioactive and must be serviced by remote maintenance methods.

We believe that the advantages of molten-salt reactors can greatly outweigh the disadvantages in well-designed and well-developed plants. When demonstrated, they should assure the molten-salt thermal breeders a prominent place in our nuclear power industry.

With the preceding as an introduction, I would like to discuss briefly some general features of a molten-salt thermal breeder reactor. Typical compositions of fuel and blanket salts for the breeder are shown in Table 2. They consist of uranium and thorium fluorides dissolved in a lithium fluoride-beryllium fluoride carrier salt. We use beryllium fluoride to obtain mixtures with low liquidus temperatures and lithium fluoride to obtain good fluid properties. Fluorine, beryllium, and  $^{7}\text{Li}$  all have low neutron absorption cross sections, and the fluorides offer advantages in processing the fuels.

Although these salts have moderating properties, additional moderator is required to make a thermal reactor. Graphite is the preferred moderator because it can be used in direct contact with the salts, thus eliminating the need for a low-cross-section cladding material. The salts do not wet graphite and will not enter the pores at pressures as high as 200 psi if the pore openings are less than about  $0.4\text{ }\mu$  in diameter. An experimental grade of graphite that satisfies this requirement was obtained for the MSRE; additional development and improvement of that material should produce one that would meet all the requirements of a large power reactor.

The costs of the salts should be compared with those of other reactor materials. Typical coolants costs are a few cents per cubic foot for  $\text{H}_2\text{O}$ ;  $\$1.20/\text{ft}^3$  for helium at 500 psi;  $\$12/\text{ft}^3$  for sodium;  $\$92/\text{ft}^3$  for lead;  $\$110/\text{ft}^3$  for a heat-transfer salt composed of lithium, sodium, and potassium fluorides; and  $\$1400/\text{ft}^3$  for  $\text{D}_2\text{O}$ . Fuels cost about  $\$3500/\text{ft}^3$  for natural uranium oxide,  $\$45,000/\text{ft}^3$  for a 2.2% enriched uranium oxide for a boiling or pressurized-water reactor, and  $\$320,000/\text{ft}^3$  for a  $\text{UO}_2\text{-PuO}_2$  mixture in a large fast breeder. The costs for fuels do not include fabrication. Thus we see that the fuel salts are relatively cheap fuel mixtures, but they are expensive heat-transfer fluids and must be used efficiently.

A concept of a two-fluid breeder reactor<sup>5</sup> is shown in Fig. 1. We generally favor this type, in which the fuel is pumped through the reactor core and then through external heat exchangers. The core can be made compact without the necessity for providing large amounts of heat-transfer surface in a small volume, and it can be made almost entirely of high-purity graphite. The heat exchanger can be made compact and efficient and of the most corrosion-resistant materials without regard for their neutron cross sections. Gaseous fission products can be stripped from the circulating fuel rapidly and continuously to hold the loss of neutrons to  $^{135}\text{Xe}$  to a very low level. The cost and the high radiation level of the circulating fuel dictate that the components be closely coupled.

Figure 1 represents a reactor that would produce 1200 Mw of heat for generating 500 Mw of electricity. The reactor has a core about 8 ft in diameter by 8 ft high, completely surrounded by a 3-ft-thick blanket of

Table 2. Compositions, Properties, and Costs of Typical Fuel and Blanket Salts

|  | Cost<br>(\$/lb) | Core of Two-Region<br>Breeder |      |                    | Blanket of Two-Region<br>Breeder |      |                    |
|--|-----------------|-------------------------------|------|--------------------|----------------------------------|------|--------------------|
|  |                 | Mole %                        | Wt % | \$/ft <sup>3</sup> | Mole %                           | Wt % | \$/ft <sup>3</sup> |
| <b>Salt constituent</b>  |                 |                               |      |                    |                                  |      |                    |
| UF <sub>4</sub> <sup>a</sup> (74% <sup>233</sup> U and <sup>235</sup> U)       | 4.200           | 0.3                           | 2.7  | 13,700             |                                  |      |                    |
| ThF <sub>4</sub>   | 5.50            |                               |      |                    | 15                               | 64   | 770                |
| LiF <sup>b</sup>   | 16              | 63                            | 48.0 | 920                | 67                               | 24   | 840                |
| BeF <sub>4</sub>   | 7               | 36.7                          | 49.3 | 410                | 18                               | 12   | 180                |
|  |                 |                               |      | 15,000             |                                  |      | 1790               |
| Density, lb/ft <sup>3</sup>  |                 |                               | 120  |                    |                                  | 220  |                    |
| Liquidus temperature, °F   |                 |                               | 850  |                    |                                  | 930  |                    |
| Heat capacity, Btu ft <sup>-3</sup> (°F) <sup>-1</sup>                         |                 |                               | 65   |                    |                                  | 65   |                    |
| Thermal conductivity, Btu ft <sup>-1</sup> hr <sup>-1</sup> (°F) <sup>-1</sup> |                 |                               | 3    |                    |                                  | 3    |                    |
| Viscosity at 1200°F, lb ft <sup>-1</sup> hr <sup>-1</sup>                      |                 |                               | 20   |                    |                                  | 15   |                    |

<sup>a</sup>Fissile material values at \$5450/lb.

<sup>b</sup>Lithium-7 (99.996%) values at \$55/lb as LiOH.

fertile salt. A 1-ft-thick graphite reflector is installed between the blanket and the reactor vessel.

The core is an assembly of graphite prisms 7-1/2 in. square and about 8 ft long. The corners of adjacent prisms are machined to form vertical passages of circular cross section about 5 in. in diameter. The fuel salt flows in bayonet tubes of impermeable graphite which are inserted into these vertical passages. The outer tubes are 3.75 in. ID with walls 0.5 in. thick and they are brazed to a metal plenum. The inner tubes are 2.4 in. ID with walls 0.25 in. thick. They are joined to the inner plenum by mechanical joints since some leakage of fuel can be tolerated at this point.

The graphite-moderator assembly is supported by graphite structural members in the blanket. The annulus between the fuel tubes and the moderator and the regions between the core and the reactor vessel are filled with blanket fluid, which is maintained at a slightly higher pressure than that of the fuel stream. If a leak develops, fertile material will enter the fuel stream, and the reactivity will decrease.

Fuel salt enters the core from the inlet plenum at 1125°F, passes down through the annulus in the bayonet tubes, rises through the inner

UNCLASSIFIED  
ORNL-LR-DWG 46040RA

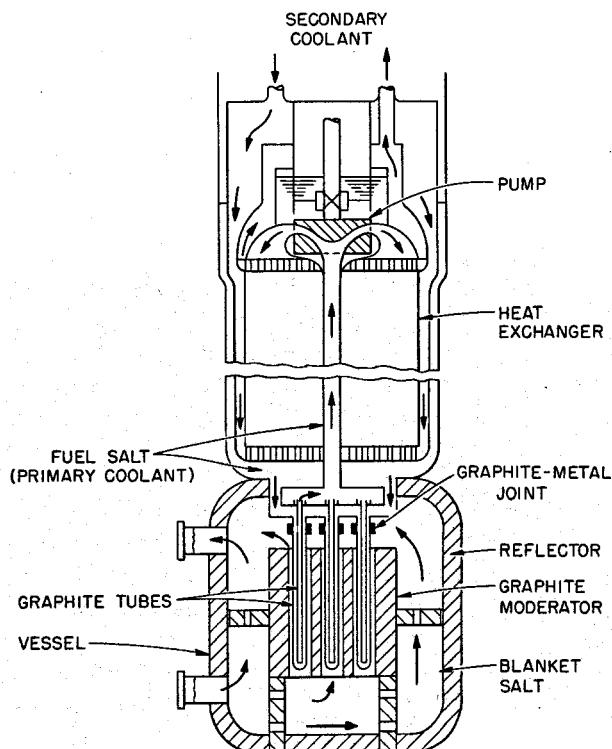


Fig. 1. Molten-Salt Breeder Reactor.

tubes, and is discharged at an average temperature of 1300°F. It is collected in the outlet plenum and passes up through a duct to the impeller chamber of the pump, then through the heat exchanger, and back to the reactor inlet. Changes in volume of the fuel are accommodated in the space in the pump tank above the impeller. The flow rate of the fuel is 40,000 gpm. This is one-third to one-half the flow rate specified for water-cooled and sodium-cooled reactors with the same electrical output. The maximum velocity in the graphite tubes is 25 fps, and the maximum temperature is 1400°F.

The blanket salt is pumped through an external heat exchanger at a rate of 5000 gpm. The temperatures are about the same as those for the fuel stream.

The coolant salt (a mixture of lithium, potassium, and sodium fluorides) in an intermediate circuit is pumped through the fuel and blanket heat exchangers at a rate of 50,000 gpm (entering at 950°F and leaving at 1100°F) and then through steam generators, superheaters, and reheaters. The steam cycle can be varied over a considerable range to suit local conditions and the preference of the user. In our studies, we have held the steam temperature to 1050°F, and the pressure has been varied between 1800 and 3500 psi. With one stage of reheat and several stages of feedwater heating, the net thermal efficiency is in the range of 42 to 45%.

Reactors of this general configuration can be conceived with multiple pumps and heat exchangers and heat outputs much greater than 1200 Mw. Our engineers estimate that as much as 5 Mw of heat (equivalent to 2 Mw of electricity) can be extracted from the reactor for each cubic foot of fuel salt in the reactor core and heat-removal systems.<sup>6</sup> Plants with high performance like this are the goal of the thermal-breeder development and can be built when we learn that the graphite structures and the heat exchangers will operate for many years without maintenance.

Early versions of the breeder may have to sacrifice some in performance in order to make use of lower flow velocities and more conventional equipment and to provide better access for maintenance. One such concept of a 2400-Mw reactor is shown in Figs. 2 and 3. The graphite region is about 12 ft square by 15 ft high. It consists of graphite bars that are 7-3/4 in. square over a 10-ft length in the center and are reduced to 5 in. in diameter over the end sections. The reduced sections are in the end blankets. Groups of nine bars are assembled into 2-ft-square modules. Fuel salt flows through 3-1/2-in.-diam holes in the centers of the bars, up through one bar and down through an adjacent bar in the same module. Pipes which are brazed to the bars are connected to concentric inlet and outlet headers at the bottom of each module. The inlet headers are welded or brazed into a plenum in the bottom of the reactor vessel, and the outlet header is connected by a mechanical joint. The modules are fixed and supported by the piping at the bottom and are guided by a grid at the top. We show access to the bottom of the reactor from a subpile room for making the connections. However, the center bar of each module has no fuel channel and can be withdrawn separately from above. Our experience with remote and semiremote maintenance gives us assurance that tools can be devised to make and break the joints from either end.

UNCLASSIFIED  
ORNL-DWG 64-6959R

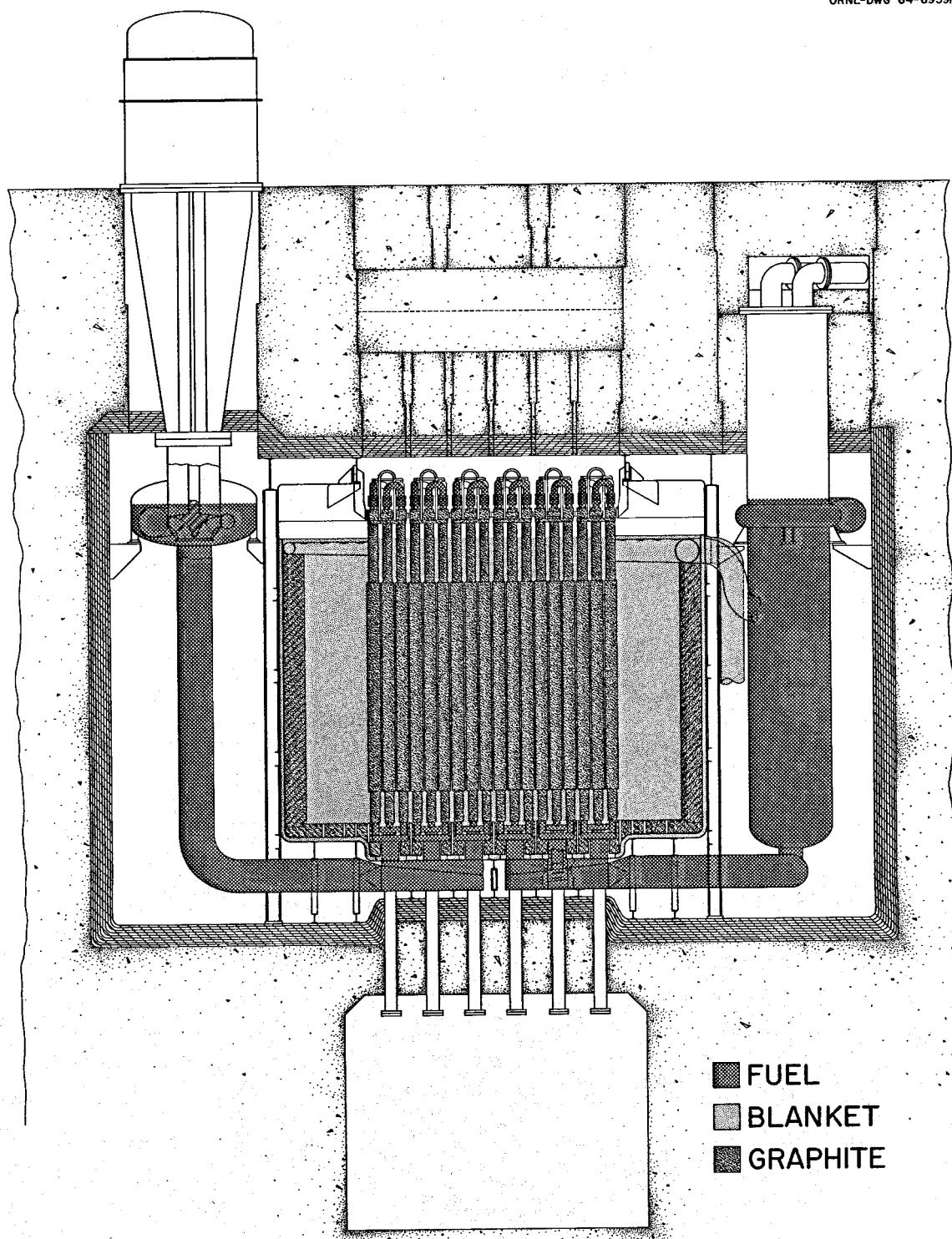


Fig. 2. Two-Region Molten-Salt Breeder.

The graphite structure is contained in a reactor vessel that is about 20 ft in diameter and 25 ft high. A graphite reflector is installed next to the vessel wall. The interstices of the core and the reflector and the space between the core and the reflector are filled with blanket salt. The atmosphere over the blanket is helium or argon.

UNCLASSIFIED  
ORNL-DWG 64-7465

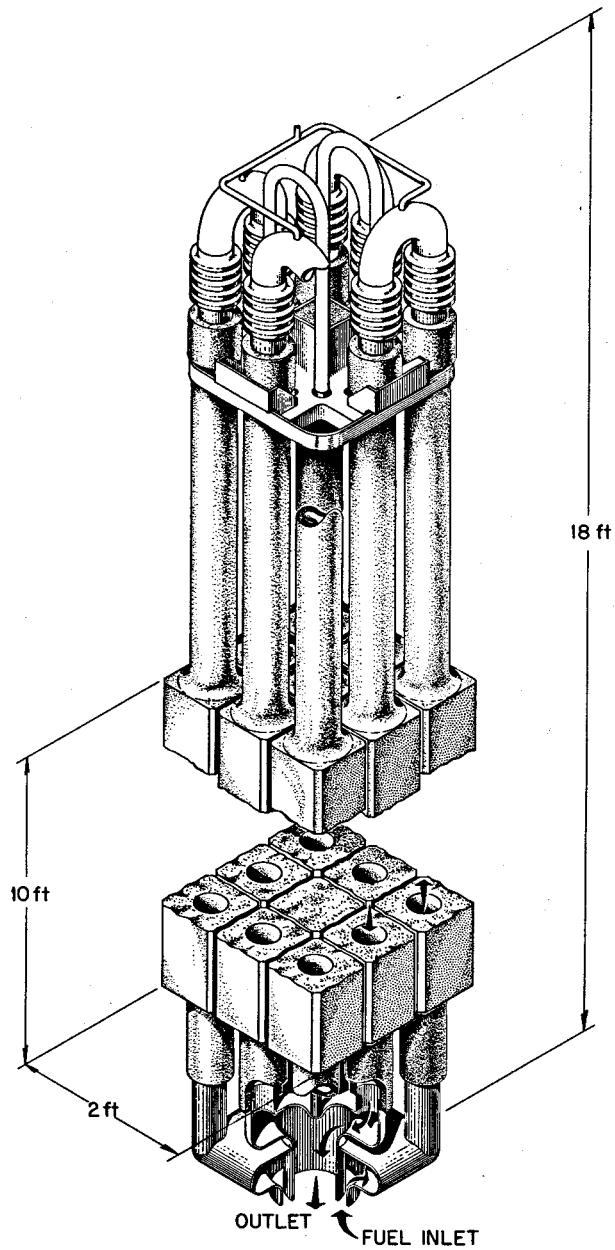


Fig. 3. Core Module for Molten-Salt Breeder Reactor.

The reactor vessel is centered in a 36-ft-diam containment vessel. Heat exchangers, pumps for fuel and blanket salts, and heaters are installed in the annulus, with access from above for maintenance. The containment vessel is insulated and surrounded by concrete shielding.

In an arrangement such as this we can attain a performance of 2.5 Mw of heat (1 Mw of electricity) or better per cubic foot of fuel salt.

The reactors become high-performance breeders when they are directly connected to processing plants that can remove low concentrations of bred materials from the blanket salt and fission products from the fuel salt at moderate cost. In fact, our early enthusiasm for the molten-salt reactor as a breeder was based largely on the development of the fluoride volatility process — a process that makes it economically feasible to hold the inventory of  $^{233}\text{U}$  to a very low level in a molten-salt blanket.

A flow diagram<sup>7</sup> of a processing scheme for a molten-salt breeder reactor is shown in Fig. 4. Krypton and xenon are removed in the reactor by sparging the fuel salt with helium in the pump bowl. The off-gas is passed through charcoal beds, where the fission products are absorbed and the helium is recycled to the reactor.

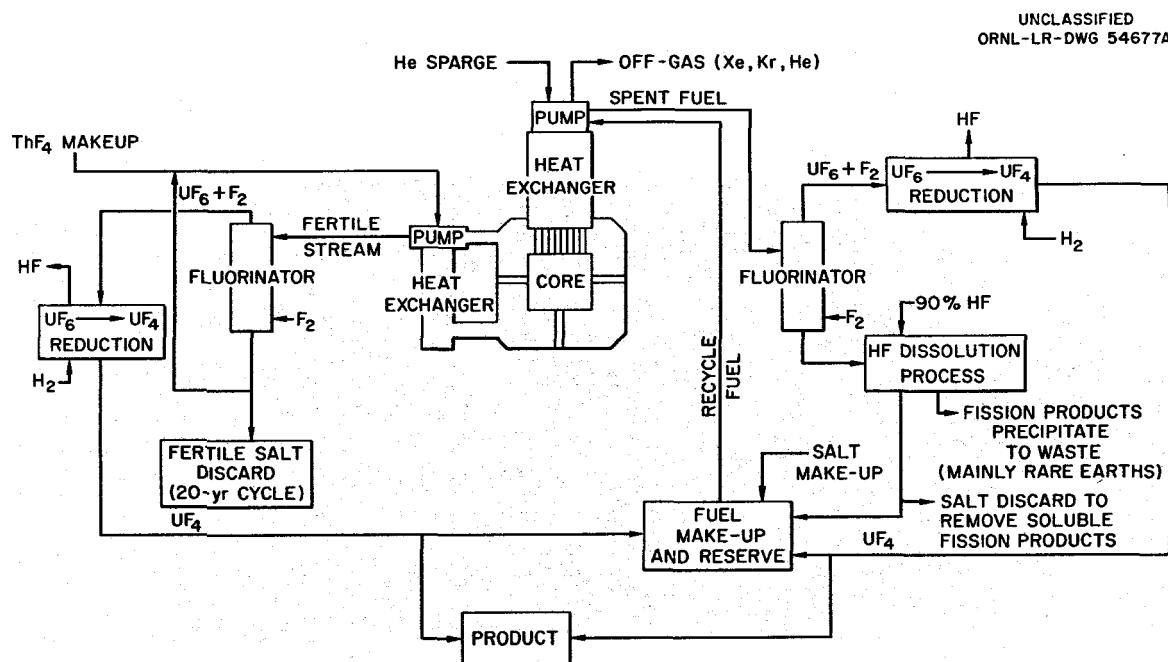


Fig. 4. Fuel Processing Cycles for Molten-Salt Breeder Reactor.

Side streams of fuel and blanket salt are removed from the reactor for processing in a facility at the reactor site. The complete fuel and blanket charges, respectively, are processed in 10 to 60 days (3 to 15% burnup of fissile material) and 35 to 200 days (equivalent to 300 to 1700 Mwd per metric ton of exposure) to obtain the corresponding breeding gain shown in Table 1. The fuel salt is first treated with fluorine. The  $\text{UF}_4$  is converted to volatile  $\text{UF}_6$  and swept out of the fluorinator. The  $\text{UF}_6$  is then reduced back to  $\text{UF}_4$  with hydrogen in a flame reducer and returned to the reactor.

The uranium-free salt, containing fission products, is dissolved in 90% hydrofluoric acid. Rare earths and zirconium salts are insoluble and are separated by filtration. The solution containing lithium and beryllium fluorides and some soluble fission products (principally Cs, Rb, Sr, Ba, Te, Se, Nb, Cd, Ag, and Te) is evaporated to dryness. Part of the salt is discarded to rid the system of the soluble fission products, and the rest is melted, combined with the recovered uranium, and returned to the reactor.

The blanket salt is fluorinated to remove the bred uranium as the hexafluoride, sparged with helium to remove traces of fluorine, and recycled directly to the blanket. Since such a small fraction of fissions occurs in the blanket, the fission-product-removal step is unnecessary. The fission product poison level is controlled by replacing the blanket salt on a 20-year cycle. Protactinium is not removed from the fertile stream in this process; its concentration rises until the decay rate equals its production rate. Loss of neutrons to protactinium is controlled by adjusting the volume of the fertile salt.

The  $\text{UF}_6$  from the fertile stream fluorinator is reduced to  $\text{UF}_4$  with hydrogen and blended with the fuel stream for recycle to the reactor. Excess production is sold.

Because the methods outlined above involve only minor chemical manipulations to the bulk of the salts, we believe that they will permit us to achieve high conversion ratios and low fuel costs in plants of 1000-Mw (electrical) capacity and possibly in smaller plants. However, these methods may well be superseded by even better ones. We mentioned earlier that the  $^{233}\text{Pa}$  precursor of  $^{233}\text{U}$  can be adsorbed from the blanket salt and the effect of this on the reactor performance. Within the past month, M. J. Kelly, one of our chemists, has shown that the carrier salts can be separated from rare-earth fission products by vacuum distillation. This promises to be a substantial improvement over the HF dissolution method and has other important implications regarding methods of operating and controlling the reactors.

Except for the fluoride volatility process, we have been discussing reactor and processing concepts. Concepts have real value when enough basic technology is developed for us to convert them into authentic engineering designs.

Molten-salt reactors are not entirely new. Much of their technology was developed here at ORNL in 1951 to 1958 in the Aircraft Nuclear Propulsion Program. A proof-of-principle experiment with molten-salt fuel - the Aircraft Reactor Experiment - was built and, in 1954, operated successfully for several hundred hours at 1200 to 1500°F, with periods of nuclear operation at power levels as high as 2.5 Mw. But a large power breeder reactor differs in many ways from an aircraft power plant. The fuels and some materials must be different to obtain good breeding ratios. The power levels must be considerably higher; methods must be available for processing fuel and blanket salts efficiently; and costs are important. On the other hand, the weight and size are not restricted. A reactor for producing power for a modern turbogenerator can operate at considerably lower temperature than a power plant for a supersonic aircraft. Extreme compactness is a virtue but not a necessity.

Research and development for civilian power reactors was undertaken in 1957. By 1960 enough favorable experimental results were obtained to indicate that a molten-salt thermal breeder should be feasible, but that experience with an operating reactor was essential to prove the feasibility. At about this same time the importance of breeding to the long-range utilization of nuclear fuels, and particularly to the utilization of thorium, was gaining increased attention. Interest in the breeding potential of the molten-salt reactors, their capacity to use the heat efficiently to produce electricity, and in the characteristics that should permit this to be achieved at low cost led the Atomic Energy Commission to authorize design and construction of the Molten-Salt Reactor Experiment (MSRE) in the summer of 1960.

The MSRE is needed to investigate some essentials of chemistry, materials, engineering, and operation of the molten-salt reactor concepts. The major physics questions are related to uncertainties in the breeding ratios. They can finally be resolved only by a material balance over a large plant.

The central problem of the thermal breeder reactor is to prove the suitability of graphite for the core structure. The graphite must have low permeability to salt and fission products; it must have long life under reactor conditions; and it must be obtainable in large size. In 1960 this kind of graphite was a laboratory curiosity. Procurement of material for the MSRE was a step in development of graphite for large reactors. Operation of the MSRE will provide us with essential data about the long-term compatibility of graphite with salts and structural material in the reactor environment.

We know a great deal about the chemistry of molten salts in the absence of radiation and have some knowledge of radiation effects. But the complex environment of a power reactor cannot be duplicated in a simple capsule or in-pile loop. Operation of fuel and blanket salts in a reactor is essential to the investigation and demonstration of their compatibility with graphite and structural materials under radiation. The predicted behavior of fission products must be confirmed, and their distribution in the reactor systems must be established.

INOR-8 (Hastelloy N or Inco 806), a new nickel alloy containing 17% molybdenum, 7% chromium, and 4% iron, was developed specifically to have good strength and to contain reactor fuel and blanket salts with little corrosion at high temperature. This is a preferred material for molten-salt power reactors. Experience is needed with the construction of reactor components and piping and with the behavior of commercial materials during long exposure in a reactor plant.

The practicality of molten-salt reactors depends on our ability to maintain the radioactive equipment by remote or semiremote methods. We have had considerable experience with maintenance of radioactive equipment in aqueous homogeneous reactors, but the problems encountered depend very much on the types of fuels and materials used in the reactors and on their interactions. We need some experience with radioactive molten-salt systems to establish criteria for the design of large reactors.

The salts in the reactor equipment and piping must be kept molten at all times. This should be easy in all but the steam generators after some fission products have accumulated in the salts. However, heaters will be needed for preheating the systems and for maintaining the high temperatures in the absence of fission product heat. We require experience with the design, operation, and maintenance of heating equipment for radioactive systems.

Finally, we need general operational experience with a molten-salt reactor in order to establish the criteria for the design of a practical power plant. We cannot predict the detailed behavior of the plant and equipment or the day-to-day problems that can arise with its operation and with the containment of radioactivity or the numerous small improvements that, in total, can greatly simplify the operation and increase the confidence in a new device.

We have designed, developed, and are now preparing to operate the MSRE to test much of the technology of the thermal breeder reactor. A flow diagram for the reactor systems is shown in Fig. 5. The reactor produces 10 Mw of heat while operating at 1200°F. The base pressure in the system is 5 psig at a free surface in the pump bowl. Fuel salt is pumped at a rate of 1250 gpm through the shell of the heat exchanger and through the reactor vessel. The average increase in temperature as the fuel passes through the core is 50°F at 10 Mw.

A coolant salt in an intermediate circuit circulates through the tubes of the heat exchanger to remove heat from the fuel. The heat is dissipated to the atmosphere in an air-cooled radiator. Power recovery is not an objective of this experiment, so we have included no power-generation equipment.

Drain tanks are provided for storing fuel and coolant salts when the reactor is not operating. Drainage of the fuel to the storage tank is the primary shutdown mechanism.

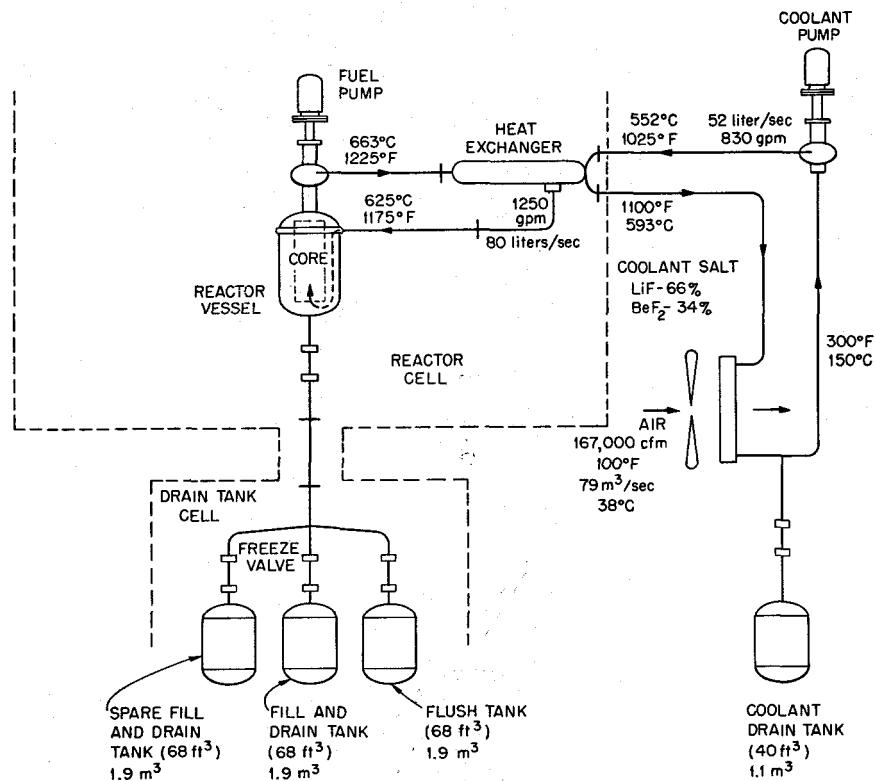
UNCLASSIFIED  
ORNL-LR-DWG 59158A

Fig. 5. MSRE Flow Diagram.

A drawing of the reactor vessel is shown in Fig. 6. The vessel is about 5 ft in diameter and 8 ft high, including the nozzle on the top. The core is an assembly of graphite bars 2 in. square by 5 ft long. Fuel salt circulates in direct contact with the graphite through channels machined in the sides of the bars. Three control rods operate in thimbles installed through the access nozzle. A channel is also provided for irradiating graphite and metal specimens in salt in the core. Five full-length core bars can be withdrawn by removing the thimble assembly.

All equipment that contains salt is made of INOR-8. The graphite is a new material that satisfies many of the requirements for graphite for the breeder. All vessels and pipes that contain salts are heated. Considerable design and development effort was spent in making essential equipment replaceable.

An elevation of part of the MSRE building is shown in Fig. 7. The reactor vessel, pump, and heat exchanger are installed in one cell. The drain tanks are in an adjoining cell. These cells constitute the secondary containment and will be sealed when fuel is in the reactor. The coolant system is in a shielded area. Ventilation and access to the area are controlled, but no other secondary containment is necessary.

The MSRE is primarily an experiment in reactor technology. We realize the importance of the fuel and blanket processing to achievement of the final goal but have chosen to prove the feasibility of the reactor systems before proceeding with development of some of the processing concepts. However, it proved to be advisable to install equipment at the reactor site for fluorinating and hydrofluorinating the fuel. This equipment is being installed in a cell adjacent to the drain tank. We believe

UNCLASSIFIED  
ORNL-LR-DWG 61097RIA

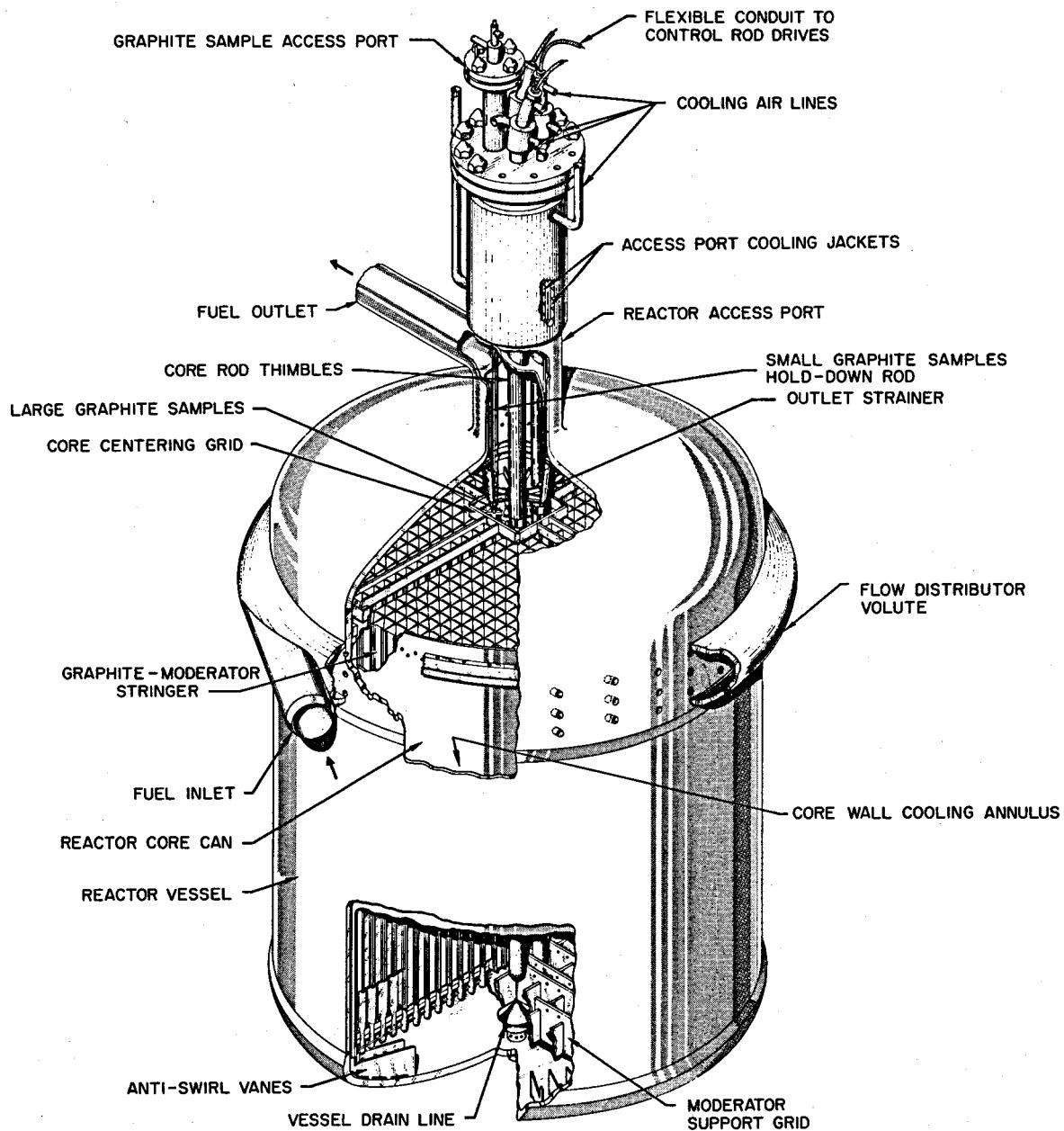


Fig. 6. MSRE Reactor Vessel.

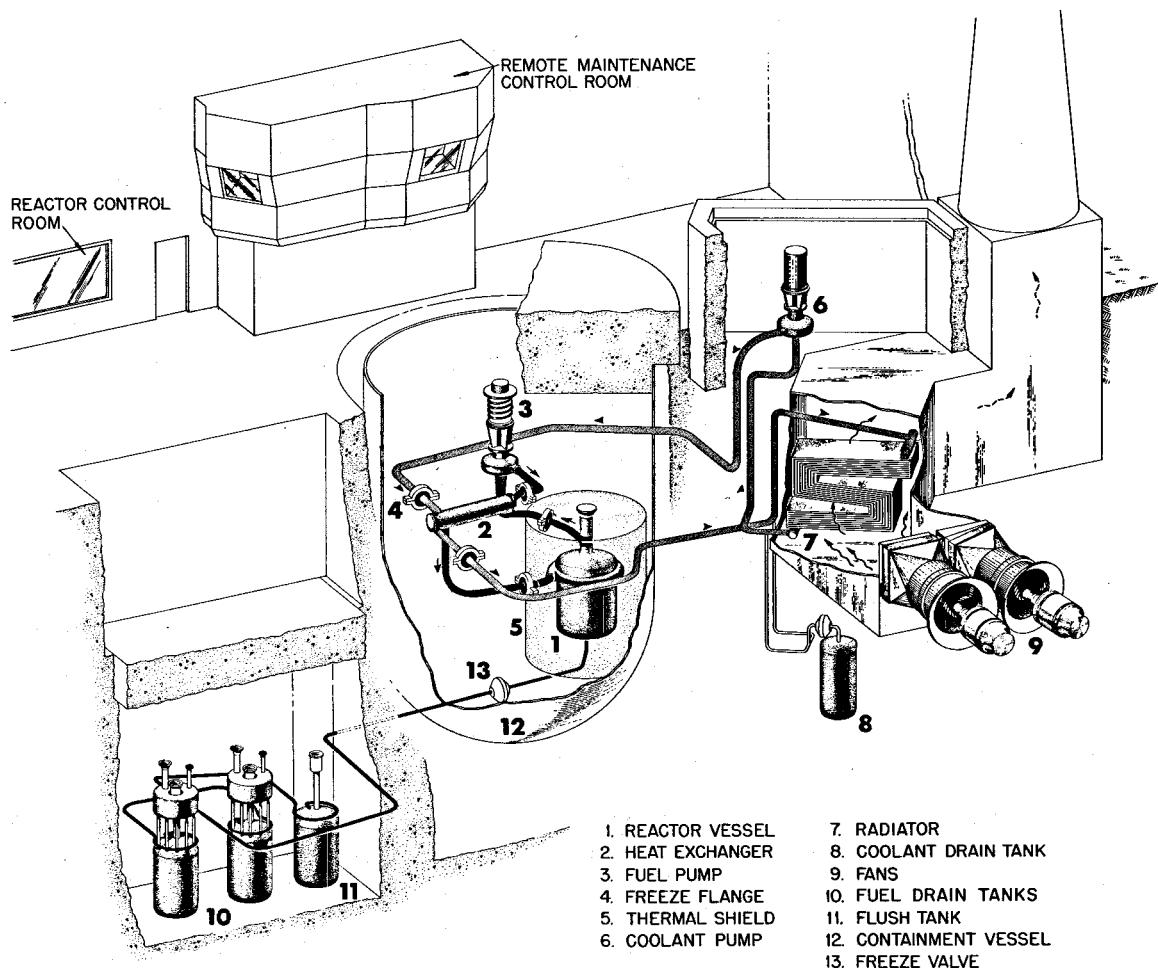
UNCLASSIFIED  
ORNL-DWG 63-1209R

Fig. 7. Elevation of Part of MSRE Building.

that its use will help considerably to demonstrate the advantages of on-site processing for liquid fuels.

The MSRE was fitted into an existing building; the reactor was installed in an existing containment vessel that was modified to provide a flat top. The drain tank cell and some other areas are new, but most of the facility was modified only slightly for the MSRE. This resulted in some compromises in the design and an installation so compact as to give some the impression of complexity. The power level was held to 10 Mw as a sensible maximum for an experiment; but criticality considerations dictated the size of the reactor vessel, and the size of the reactor vessel dictated the flow rate of the fuel. Except for the amount of heat-transfer surface in the heat exchanger and radiator, this small installation is more nearly representative of a 40- to 60-Mw reactor.

Suppose that good operation of the MSRE and detailed engineering studies of large plants give convincing evidence of the promise of molten-salt reactors for breeding and producing low-cost power. Where do we go from the MSRE? Three areas need special attention in progressing to large power breeder plants: (1) the graphite core structure needs additional work; (2) the fuel and blanket processing must be brought to a satisfactory stage of development; and (3) large-scale equipment must be developed and operated. Pilot-plant demonstration of elements of the core and of the fuel and blanket processes should be done in a modification of the MSRE or in a thermal breeder test facility. But, primarily, we want molten-salt reactors to be useful, and they will be useful when operated by a utility to produce power.

We believe that the MSRE can be followed by a power reactor prototype. Much of the large equipment can be modeled after equipment being developed for sodium reactors. The graphite development and the processing development do not have to be complete. A reactor similar in design to the concept shown in Fig. 2, but with graphite throughout the blanket, can be fueled with a mixture of the fuel and blanket salts, shown in Table 2, to make a one-fluid advanced converter reactor. This reactor would require very little in the way of processing to have very low fuel costs. It could be used to test graphite elements as well as other major equipment for the breeder. It could eventually be changed into a breeder by installing proved graphite assemblies in the core and additional facilities for processing fuel and blanket streams. Such a prototype is the keystone of any plan for making an early profit on the effort invested in the development of molten-salt reactors.

Up to this point we have mentioned only the thermal breeder and a possible precursor (the advanced converter) and the relationship of the MSRE to them. However, there are other interesting and important possibilities for molten-salt reactors. J. A. Lane has suggested that  $^{235}\text{U}$  and plutonium may become very cheap in the future and that a molten-salt reactor with its high thermal efficiency and simple fuel would be ideal for burning this material in small reactors to generate 50 to 250 Mw (electrical). P. R. Kasten has proposed the development of an intermediate breeder reactor with the molten-salt fuel cooled internally by the molten-salt blanket.

For many years fast reactors with molten-salt fuels have been judged to be impractical. The inventory in externally cooled versions was always prohibitive. Internally cooled designs had too low a specific power, or the salt temperature was too high, or too much structural material was required. E. S. Bettis has suggested molten lead as a direct-contact coolant for molten-salt reactors. He has proposed some designs to achieve very high specific power in large fast reactors. Preliminary experiments have shown molten lead to be immiscible and unreactive with fluoride and chloride salts.

None of the reactors that have received serious consideration in the past have made use of the full high-temperature potential of the molten-salt fuels. There is no need to go to temperatures above 1400°F in the

reactors to provide the highest temperature steam that can be used to advantage in today's steam cycles. However, A. Fraas<sup>8</sup> suggested that the potassium vapor cycle being developed for space applications should one day be a good topping cycle for the conventional steam cycle to raise the thermal efficiency to about 55%. He proposed a molten-salt reactor operating at about 1900°F as a good heat source for the combined cycle.

To propose that the MSRE will solve all the problems of all these reactors would be to exaggerate. But most of the experience with the reactor and with the handling of the fuels will apply to all. We have encountered problems in building the reactor and will encounter more in starting and operating it. However, our experience with the test loops and construction gives us full confidence that we have a good reactor. We expect the MSRE to provide an impressive beginning for the development of a variety of useful power reactors.

#### References

1. L. G. Alexander et al., Thorium Breeder Reactor Evaluation. Part I. Fuel Yield and Fuel Cycle Costs in Five Thermal Breeders, ORNL-CF-61-3-9, p. 150 (March 1961).
2. L. G. Alexander et al., Thorium Breeder Reactor Evaluation. Part I. Fuel Yield and Fuel Cycle Costs in Five Thermal Breeders, ORNL-CF-61-3-9, p. 147 (March 1961).
3. Oak Ridge National Laboratory, Capital Investment for 1000 MWe Molten Salt Converter Reference Design Power Reactor, Sargent & Lundy - 1994 (Dec. 27, 1962).
4. L. G. Alexander et al., Cost of Power from a 1000-MWe Molten-Salt Converter Reactor, ORNL report (in preparation).
5. L. G. Alexander et al., Thorium Breeder Reactor Evaluation. Part I. Fuel Yield and Fuel Cycle Costs in Five Thermal Breeders, ORNL-CF-61-3-9, p. 69 (March 1961).
6. L. G. Alexander et al., Thorium Breeder Reactor Evaluation. Part I. Fuel Yield and Fuel Cycle Costs in Five Thermal Breeders (appendices), ORNL-CF-61-3-9, p. 10.
7. L. G. Alexander et al., Thorium Breeder Reactor Evaluation. Part I. Fuel Yield and Fuel Cycle Costs in Five Thermal Breeders (appendices), ORNL-CF-61-3-9, p. 87.
8. A. P. Fraas et al., A Potassium-Steam Binary Vapor Cycle for Nuclear Power Plant, ORNL-3584 (May 1964).

MSRE DESIGN AND CONSTRUCTION

W. B. McDonald

Introduction

The Molten-Salt Reactor Experiment (MSRE) is a circulating fuel, graphite-moderated, single-region reactor designed for a heat generation rate of 10 Mw. The fuel employs a molten mixture of lithium, beryllium, and zirconium fluoride salts as a solvent for uranium or thorium and uranium fluorides. Heat generation occurs as the fuel flows through machined passages in the graphite core, and heat is transferred from the fuel salt to a similar coolant salt in a shell-tube heat exchanger. Finally, the heat is dissipated to air in an air blast radiator. Since power recovery is not an objective of this experiment, no electric power generation equipment is utilized.

It is intended in this section to give a general description of the design of the MSRE systems, pointing out the most salient features and presenting data of general interest, and to describe the major features of the reactor and facility construction. The reader having interest in a more detailed exposition of the MSRE design is referred to ORNL-TM-728, Molten-Salt Reactor Experiment, Part I, Reactor Design.

Description of MSRE Equipment and Process

The simplified drawing in Fig. 1 shows the general arrangement of major equipment items. The primary fuel system consists of the reactor vessel in which heat is generated, a heat exchanger for transfer of heat from fuel salt to coolant salt, a sump-type centrifugal pump for circulating the fuel salt, and connecting piping.

The secondary coolant system consists of a coolant-salt pump, a radiator in which heat is transferred from coolant salt to air, and piping which connects the pump, heat exchanger, and radiator.

Both the primary and secondary systems are connected to drain tank systems for storage of the fuel, coolant, and flushing salts.

Reactor Vessel and Graphite Core

The reactor vessel is a 5-ft-diam, 8-ft-high tank containing a 55-in.-diam by 64-in.-high graphite core structure. A cutaway drawing of the reactor is shown in Fig. 6, p. 18. Design data for the reactor vessel and the graphite core are presented in Table 1.

At the design point of 10 Mw (thermal) the fuel salt enters the flow distributor near the top of the vessel at 1175°F and 20 psig. The fuel then spirals downward in turbulent flow through a 1-in. annulus between the vessel wall and the core can, cooling the vessel wall to within 5°F of the bulk temperature of the entering fuel salt. Straightening vanes welded to the bottom head of the reactor vessel remove the rotational component and direct the fuel upward in laminar flow through the 0.4- by 1.2-in. channels machined in the 67-in.-long graphite bars of the core matrix. There are about 1140 of these flow passages in which heat is generated by the fissioning of the  $^{235}\text{U}$  constituent of the fuel salt.

When filled, the core, having a nominal volume of 90 ft<sup>3</sup>, contains 20 ft<sup>3</sup> of fuel salt and 70 ft<sup>3</sup> of graphite. At 10 Mw, with no fuel absorbed by the graphite, 1.4 Mw of heat is generated in the fuel outside

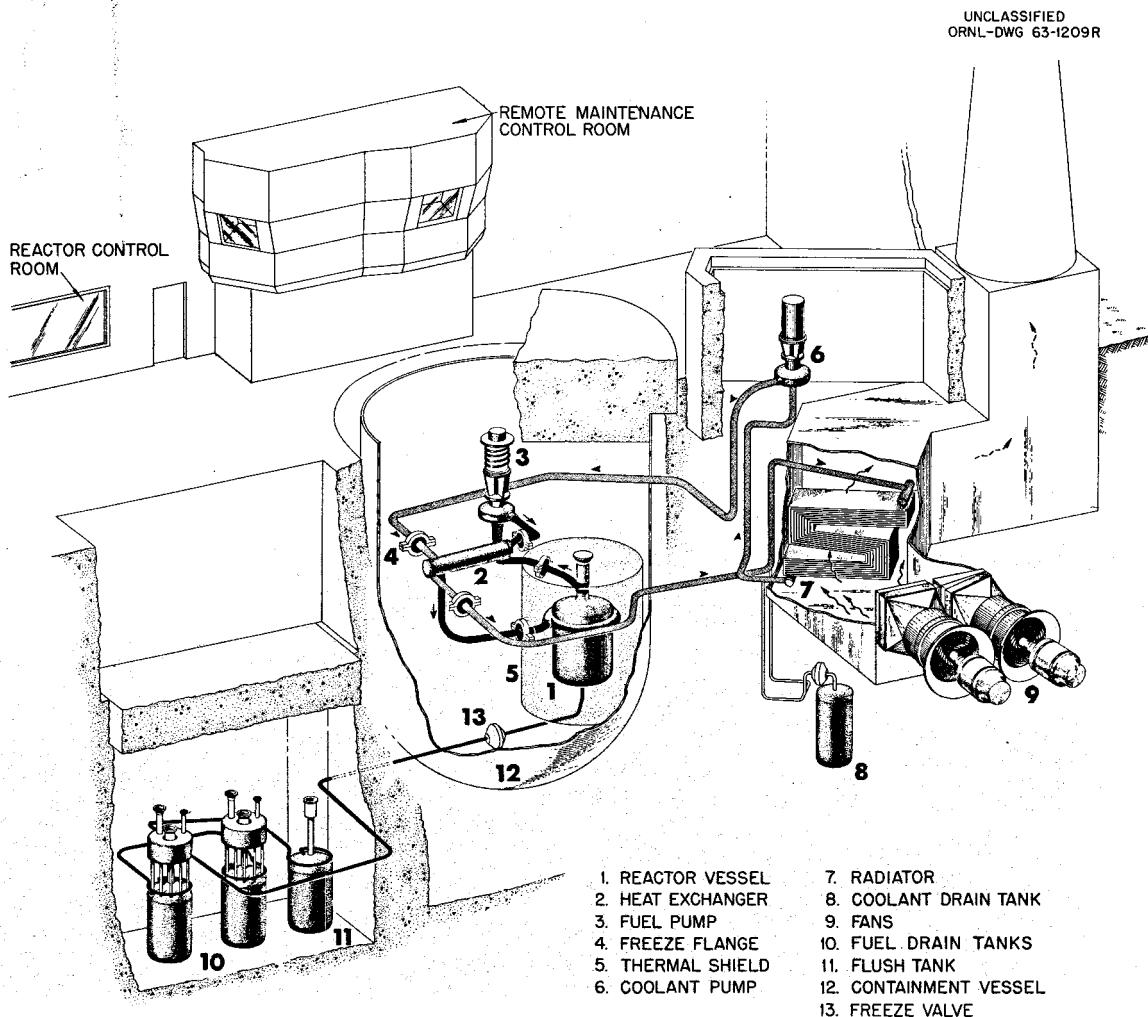


Fig. 1. MSRE Flow Diagram.

Table 1. Reactor Vessel and Core Design Data and Dimensions

|  |                             |
|--|-----------------------------|
| Construction material                                | INOR-8                      |
| Inlet nozzle, sched 40, in., iron pipe size          | 5                           |
| Outlet nozzle, sched 40, in., iron pipe size         | 5                           |
| Core vessel  |                             |
| OD, in.  | 59-1/8 (60 in. max)         |
| ID, in.  | 58                          |
| Wall thickness, in.                                  | 9/16                        |
| Overall height, in. (to center line of 5-in. nozzle) | 100-3/4                     |
| Head thickness, in.                                  | 1                           |
| Design pressure, psi                                 | 50                          |
| Design temperature, °F                               | 1300                        |
| Fuel inlet temperature, °F                           | 1175                        |
| Fuel outlet temperature, °F                          | 1225                        |
| Inlet  | Constant area distributor   |
| Cooling annulus ID, in.                              | 56                          |
| Cooling annulus OD, in.                              | 58                          |
| Graphite core  |                             |
| Diameter, in.  | 55-1/4                      |
| Number of fuel channels (equivalent)                 | 1140                        |
| Fuel channel size, in.                               | 1.2 x 0.4 (rounded corners) |
| Core container                                       |                             |
| ID, in.  | 55-1/2                      |
| OD, in.  | 56                          |
| Wall thickness, in.                                  | 1/4                         |
| Height, in.  | 68                          |

the nominal core volume, 0.6 Mw is generated in the graphite, and 8.0 Mw is generated in the fuel within the core, giving an average power density of 14 kw/liter in the nominal core. The maximum power density is calculated to be 31 kw/liter.

The thermal conductivities of both the fuel salt and the graphite are such that, even with laminar flow, the maximum graphite temperature is only about 60°F above the temperature of the adjacent fuel. The nuclear average and maximum temperatures of the graphite are estimated to be about 1255 and 1300°F respectively. The fuel exit temperature in the hottest channel is about 1260°F. The mixed fuel leaves the plenum at the top of the reactor at 1225°F and 7 psig.

A 10-in.-diam access port on top of the reactor vessel is designed to permit the insertion of graphite and metal samples and three 2-in.-diam thimbles for control rods into the core at the region of highest neutron flux. The control rod poison elements are composed of short 1-in.-diam cylinders of Inconel-clad gadolinium oxide, assembled on a flexible Inconel hose to permit passage around two bends that form an offset in each thimble. The control rods have an individual worth of 2.8%  $\Delta k/k$  and a combined worth of 6.7%  $\Delta k/k$ . At the maximum withdrawal rate of 0.5 in./sec, normally limited to one rod at a time, the change in reactivity is 0.04% ( $\Delta k/k$ )/sec. Simultaneous insertion of the three rods at a rate of 0.5 in./sec causes a change in reactivity of 0.09% ( $\Delta k/k$ )/sec. The control rods and rod drives are cooled by circulation of ambient cell atmosphere through the flexible hoses and the thimbles.

#### Fuel Pump

A sump-type centrifugal pump, shown in Fig. 2, having a vertical shaft with an overhung impeller, takes its suction directly from the reactor. The impeller rotates at 1160 rpm to discharge 1200 gpm at a head of 49 ft of fluid. The 75-hp drive motor is directly coupled to the shaft, and the complete assembly is about 8 ft high. The pump and motor are hermetically sealed to prevent the escape of volatile fission products to the reactor cell.

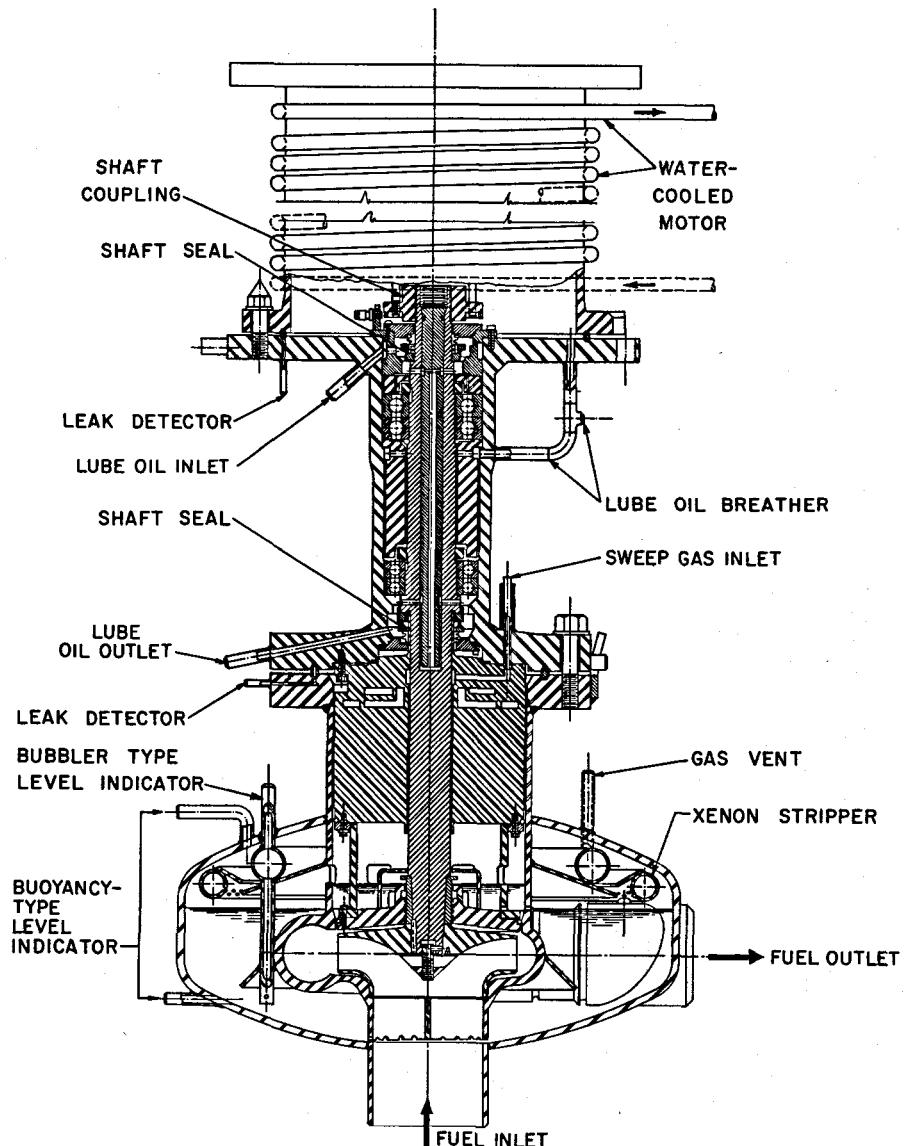
The 36-in.-diam pump bowl serves both as the pump sump and as the normal expansion volume for the fuel salt. Gas-bubbler-type level indicators are used to accurately determine the position of the free fluid surface in the pump bowl. An overflow tank having a volume of 5.5 ft<sup>3</sup> is located beneath the pump and is connected to the gas space above the free surface of the fuel in the pump bowl. Although this tank is not normally used, its volume is sufficient to provide for the free expansion of the fuel salt under all emergency conditions.

A sampling and enriching system, located in a hot cell in the high-bay area above the reactor, is connected directly to the pump bowl and provides means for extracting a 10-g sample of salt for analysis or adding 90 g of fuel to alter the fuel concentration or to compensate for fuel burnup.

About 65 gpm of the pump output is recirculated in the pump bowl to facilitate the release of entrained or dissolved gases from the salt. These gases, containing highly radioactive xenon and krypton, are carried to the off-gas disposal system by about 200 ft<sup>3</sup>/day (STP) of helium flowing through the gas space of the pump bowl. This helium also serves as a cover gas to exclude air and water vapor from the salt.

A sealed external pumping system supplies oil to lubricate the ball bearings and rotary seals on the pump shaft and to remove heat, generated

UNCLASSIFIED  
ORNL-LR-DWG-56043-AR



MSRE FUEL PUMP

Fig. 2. Cross Section of MSRE Fuel Pump.

by friction or nuclear radiation, from metal parts not cooled by the salt. The helium purge enters the pump below the lower shaft seal. A small part of it flows upward to sweep out oil vapor leaking through the seal, and the remainder flows downward along the shaft to the pump bowl, preventing the radioactive gases from reaching the oil. The latter flow eventually enters the off-gas system.

The drive motor and the pump rotary assembly are separately removable. This facilitates remote removal and replacement of the rotary assembly, if required.

#### Primary Heat Exchanger

The horizontal shell-and-tube heat exchanger shown in Fig. 3 is about 16 in. in diameter and more than 8 ft long. It contains 159 1/2-in.-OD by 0.040-in.-wall U-tubes approximately 15 ft long, with an effective heat transfer surface of  $\sim 254 \text{ ft}^2$ . At the 10-Mw performance level the salt discharged by the fuel pump flows through the shell side, where it is cooled from 1225 to 1175°F. The coolant salt circulates through the tubes

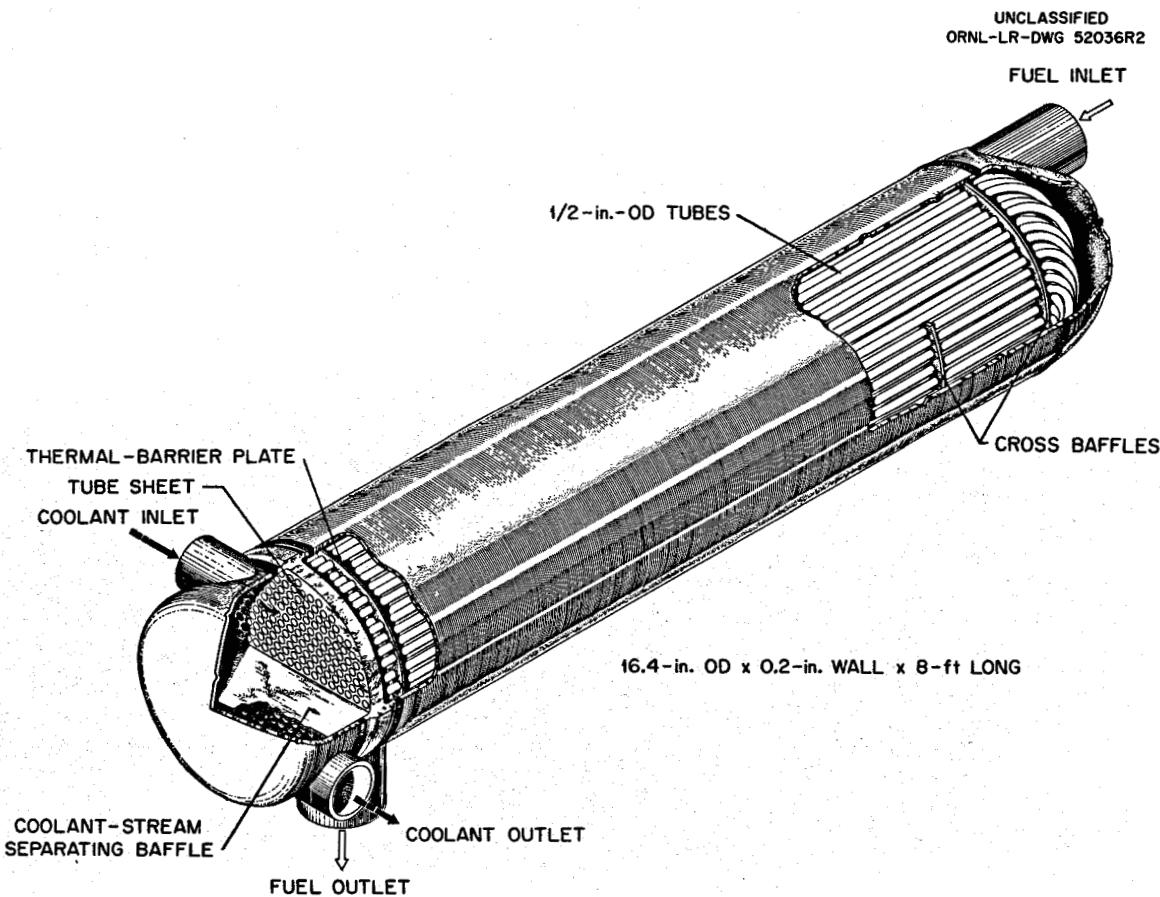


Fig. 3. Primary Heat Exchanger for MSRE.

at 850 gpm, entering at 1025°F and leaving at 1100°F. In the event of a heat exchanger tube failure, it is desired that leakage be from coolant to fuel. So the shell side of the primary heat exchanger is at lower pressure than the tube side.

The shell side contains 25%-cut cross-baffles on 12-in. spacing to achieve cross flow through the shell. INOR-8 spacing bars are tightly laced in two directions through spaces between the triangular-pitched tubes to eliminate tube flutter and vibration. A flow-impingement baffle is placed on the downstream side of the shell entrance nozzle to prevent direct impingement of the high-velocity salt stream upon the tubes.

The most significant design data for the primary heat exchanger are presented in Table 2.

#### Coolant Pump

The coolant salt is circulated by a sump-type centrifugal pump identical in most respects to the fuel pump. Major differences are the elimination of provisions for removal of radioactive gases and the overflow tank. The pump has both float-type and gas-bubbler-type level indicators in the pump bowl. The pump is driven by a 75-hp, 1750-rpm motor and delivers 850 gpm at a head of 78 ft of fluid.

#### Radiator

Heat transported by the coolant salt is discharged to air in the radiator shown in Fig. 4. Seven hundred square feet of cooling surface is provided by 120 tubes, 0.75 in. in diameter by 30 ft long, arrayed in 10 banks, each containing 12 tubes. The tubes in each bank are butt-welded at both ends to common headers which are in turn connected to larger flow distribution and collection headers at the entrance and exit ends.

Cooling air is supplied to the radiator by two 250-hp axial blowers, having a combined capacity of 200,000 cfm. At a power level of 10 Mw, the salt enters the radiator at 1100°F and leaves at 1025°F, resulting in a cooling-air temperature rise of 200°F. To guard against freezing of the salt in the radiator tubes, quick-closing doors, automatically actuated upon sudden reduction of reactor power, are provided to shut off the air flow, and the radiator is heated by banks of electric heaters inside the enclosure. The doors can be adjusted at any position between fully open and fully closed, and remotely actuated dampers can be adjusted to bypass air around the radiator to regulate the heat removal rate.

Pertinent design data for the MSRE radiator are given in Table 3.

#### Drain Tank Systems

Four tanks, with associated piping, heating and cooling equipment, and valving, are provided for safe storage of the salt mixtures when the fuel- and coolant-salt circulating systems are not in operation. A fill-

Table 2. Design Data for Primary Heat Exchanger

|  |  |
|--|--|
| Construction material                            | INOR-8                                   |
| Heat load, Mw                                    | 10                                       |
| Shell-side fluid                                 | Fuel salt                                |
| Tube-side fluid                                  | Coolant salt                             |
| Layout   | 25%-cut cross-baffled shell with U-tubes |
| Baffle pitch, in.                                | 12                                       |
| Tube pitch, in.                                  | 0.775 triangular                         |
| Active shell length, ft                          | ~6                                       |
| Overall shell length, ft                         | ~8                                       |
| Shell diameter, in.                              | 16                                       |
| Shell thickness, in.                             | 1/2                                      |
| Average tube length, ft                          | 14                                       |
| Number of U-tubes                                | 159                                      |
| Tube size, in.                                   | 1/2 OD, 0.042 wall                       |
| Effective heat transfer surface, ft <sup>2</sup> | ~254                                     |
| Tube-sheet thickness, in.                        | 1-1/2                                    |
| Fuel salt holdup, ft <sup>3</sup>                | 6.1                                      |
| Design temperature, °F                           |  |
| Shell side                                       | 1300                                     |
| Tube side  | 1300                                     |
| Design pressure, psig                            |  |
| Shell side                                       | 55                                       |
| Tube side  | 90                                       |
| Allowable working pressure, <sup>a</sup> psig    |  |
| Shell side                                       | 75                                       |
| Tube side  | 125                                      |
| Hydrostatic test pressure, psig                  |  |
| Shell side                                       | 800                                      |
| Tube side  | 1335                                     |
| Terminal temperature, °F                         |  |
| Fuel salt  | 1225 inlet; 1175 outlet                  |
| Coolant  | 1025 inlet; 1100 outlet                  |
| Effective log mean temperature difference, °F    | 133                                      |
| Pressure drop, psi                               |  |
| Shell side                                       | 24                                       |
| Tube side  | 29                                       |
| Nozzles  |  |
| Shell, in. (sched 40)                            | 5  |
| Tube, in. (sched 40)                             | 5  |
| Fuel-salt flow rate, gpm                         | 1200 (2.67 cfs)                          |
| Coolant-salt flow rate, gpm                      | 850 (1.85 cfs)                           |

<sup>a</sup>Based on actual thicknesses of materials and stresses allowed by ASME Code.

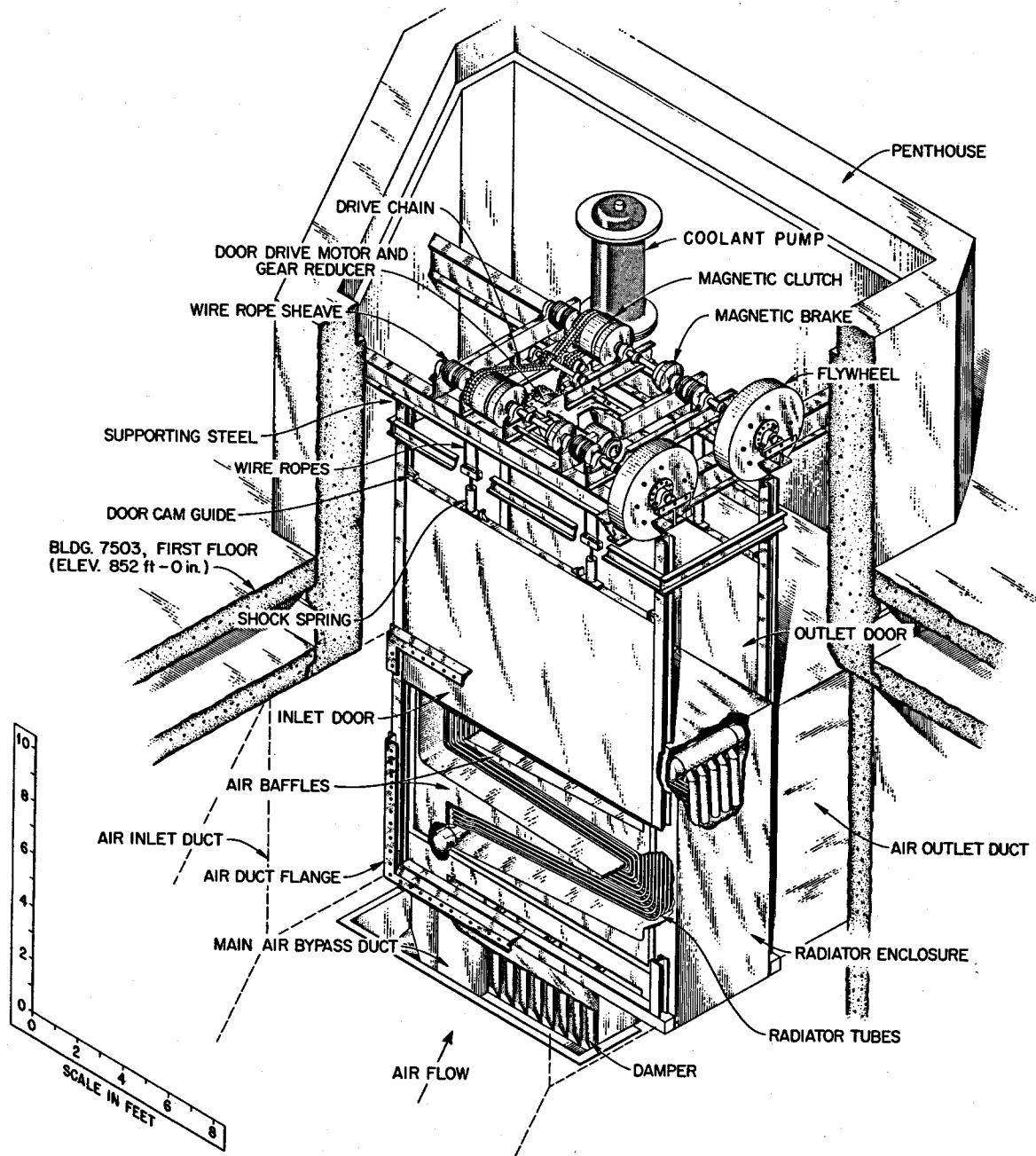
UNCLASSIFIED  
ORNL-LR-DWG 55841R2

Fig. 4. MSRE Radiator Coil and Enclosure.

and-drain line connects two fuel-salt drain tanks and one flush-salt tank to the reactor vessel. One drain tank is provided for the coolant salt.

During operation, salt is held in the fuel and coolant systems by means of freeze valves. In simplest form, a freeze valve consists of a flattened section of pipe, associated heating and cooling devices, and instrumentation which permit freezing and melting a salt plug as required for unmodulated flow.

Table 3. Radiator Design Data

|   |                                   |
|---|-----------------------------------|
| Construction material   | INOR-8                            |
| Duty, Mw  | 10                                |
| Temperature differentials, °F   |                                   |
| Salt  | Inlet 1100; outlet 1025           |
| Air   | Inlet 100; outlet 300             |
| Air flow, cfm at 9.9 in. H <sub>2</sub> O   | 200,000                           |
| Salt flow (at average temperature), gpm   | 830                               |
| Effective mean ΔT, °F   | 862                               |
| Overall coefficient of heat transfer,<br>Btu ft <sup>-2</sup> hr <sup>-1</sup> (°F) <sup>-1</sup> | 58.5                              |
| Heat transfer surface area, ft <sup>2</sup>   | 706                               |
| Design temperature, °F  | 1250                              |
| Maximum allowable internal pressure<br>at 1250°F, psi   | 350                               |
| Operating pressure at design point, psi   | 75                                |
| Tube diameter, in.  | 0.750                             |
| Wall thickness, in.   | 0.072                             |
| Tube length, ft   | 30                                |
| Tube matrix   | 12 tubes per row, 10<br>rows deep |
| Tube spacing, in.   | 1-1/2                             |
| Row spacing, in.  | 1-1/2                             |
| Subheaders, in., iron pipe size, sched 40   | 2-1/2                             |
| Main headers, in., ID (1/2 in. wall)  | 8                                 |
| Air side ΔP, in. of H <sub>2</sub> O  | 9.9                               |
| Salt side ΔP, psi   | 19.8                              |

Provisions have been made for remotely cutting the drain tank piping at preselected points for the removal of components, and for making brazed joints at those points.

A fuel-salt drain tank is shown in Fig. 5. The tank is 50 in. in diameter and 86 in. high. Its 80-ft<sup>3</sup> volume is sufficient to hold in a noncritical geometry all the salt that can be contained by the fuel-salt circulating system. The tank is provided with a low-pressure, gravity-circulated cooling system, capable of removing 100 kw of fission product decay heat by boiling water in 32 bayonet tubes that are inserted in thimbles in the tank.

The flush-salt tank is similar to the fuel-salt tank, except that it has no thimbles or cooling system. New flush salt is similar in composition to fuel salt, but without fissile or fertile materials. It is used to wash the fuel-salt circulating system before fuel is added and after fuel is drained, and the only decay heat is from the small quantity of fission products that it removes from the equipment.

The coolant-salt tank resembles the flush-salt tank, but it is 40 in. in diameter by 78 in. high and has a volume of 50 ft<sup>3</sup>.

The tanks are provided with devices to indicate high and low levels and with weigh cells to indicate the weight of the tanks and their contents with sufficient accuracy to determine the quantity of salt in the circulating system at any time.

#### Piping and Flanges

The major components of the fuel-salt and coolant-salt circulating systems are interconnected by 5-in. sched 40 piping. The fill-and-drain lines are 1-1/2-in. sched 40 pipe in which the freeze valves are located.

Since equipment and techniques have not been developed for remote welding of piping, special flanges are used in the fuel-salt circulation system to permit removal and replacement of radioactive components. These flanges, designated freeze flanges, utilize a ring of frozen fuel salt between the flange faces to prevent liquid leakage and a conventional O-ring-type, helium-buffered, leak-monitored joint to prevent the escape of fission-product-contaminated gases.

#### Heating Equipment

All the components and connecting piping in the salt circulating systems are heated electrically to maintain all portions of the system above the salt liquidus temperature of 840 to 850°F. The equipment is preheated before salt is added, and the heaters are continuously energized during reactor operation to ensure that there is no uncontrolled freezing of the salt in the piping and that the salt can be drained when necessary. The total capacity of the heaters is about 1930 kw; however, the actual power load is less than half of this. Normally, the power is

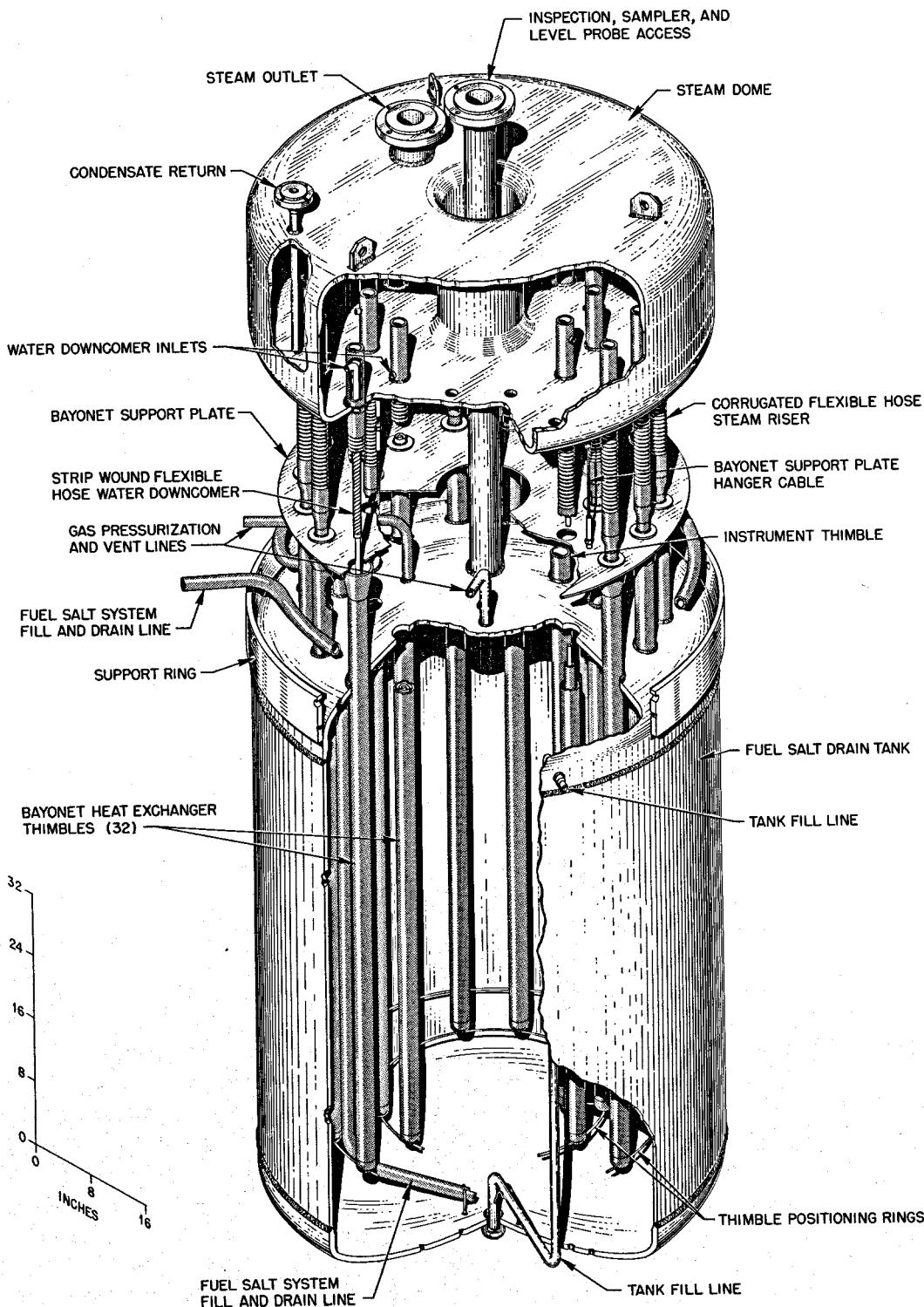
UNCLASSIFIED  
ORNL-LR-DWG 61719

Fig. 5. Fuel-Salt Drain Tank.

supplied by TVA lines; however, about 300 kw can be provided by the diesel electric emergency power supply.

The heaters used are generally of three types: (1) molded ceramic units with embedded Nichrome elements, (2) Inconel-sheathed tubular heaters with Nichrome elements and magnesium oxide electrical insulation, and (3) resistance heating of the pipe wall by connecting the pipe across the secondary taps of low-voltage, high-current transformers. Most heating units in the reactor and drain tank cells can be replaced, if required, by remote manipulation. Heating units in areas having negligible radioactivity during shutdown are replaceable by direct contact maintenance only.

To minimize dusting, multiple-layer reflective-type thermal insulation is generally used with remotely replaceable heating units. The permanent heaters are insulated with low-thermal-conductivity ceramic fiber or expanded silica materials.

At least one thermocouple is provided on the piping for each heater unit. Anticipated "cold spots" in the piping have additional thermocouples.

#### Materials of Construction

The salt-containing piping and components are fabricated from INOR-8 - a special nickel-molybdenum alloy of the Hastelloy family, having good resistance to corrosion attack by the fuel and coolant salts at temperatures at least as high as 1500°F. The mechanical properties are superior to those of the austenitic stainless steels, and the alloy is weldable by established procedures. Most of the INOR-8 equipment was designed for 1300°F and 50 psig service, assuming an allowable stress of 2750 psi.

Stainless steel piping and valves are used in the helium supply and off-gas systems. INOR-8, Inconel, and Monel are used in the fuel reprocessing system.

#### Major Auxiliary Systems

In addition to the fuel-salt and coolant-salt circulating systems, three major auxiliary systems are required for operating the MSRE. These are the cover- and off-gas systems, instrumentation and control systems, and the fuel reprocessing system. These systems are discussed in detail elsewhere and are only briefly described here.

#### Cover- and Off-Gas Systems

A helium cover-gas system protects the oxygen-sensitive fuel from contact with air or moisture. Commercial helium is supplied from a tank trailer, located outside the building, and is passed through a purification system to reduce its oxygen and water content below 1 ppm before it

is admitted to the reactor systems. A flow of 200 ft<sup>3</sup>/day (STP) is passed continuously through the fuel pump bowl to transport the fission product gases to activated charcoal adsorber beds. The radioactive xenon is retained on the charcoal for a minimum of 90 days, and the krypton is retained for 7-1/2 days, which is sufficient for all but the <sup>85</sup>Kr to decay to insignificant levels. The <sup>85</sup>Kr is maintained well within tolerance, the effluent gas being diluted with 21,000 cfm of air, filtered, monitored, and dispersed from a 3-ft-diam, 100-ft-high steel containment ventilation stack.

The cover-gas system is also used to pressurize the drain tanks to move molten salts into the fuel and coolant circulating systems. The gas effluent from these operations is passed through charcoal beds and filters before it is discharged through the off-gas stack.

#### Instrumentation and Control Systems

Nuclear and process control are important to the operation of the MSRE. The reactor has a negative temperature coefficient of  $6.4 \text{ to } 9.9 \times 10^{-5}$  ( $\Delta k/k$ )/°F, depending on the type of fuel that is being used. The excess reactivity requirements are not expected to exceed  $2 \times 10^{-2} \Delta k/k$  at the normal operating temperature. The three control rods have a combined worth of  $5.6 \text{ to } 7.6 \times 10^{-2} \Delta k/k$ , depending upon the fuel composition. Their major functions are to eliminate the wide temperature variations that would otherwise accompany changes in power and xenon poison level and to make it possible to hold the reactor subcritical at a temperature 200 to 300°F below the normal operating temperature. They have some safety functions, most of which are concerned with the startup of the reactor. Rapid action is not required of the control rods; however, a magnetic clutch is provided in the drive train to permit the rods to drop into the thimbles with an acceleration of 0.5 g as a convenient way of providing insertion rates that are more rapid than the removal rates. Burnup and growth of long-lived fission product poisons are compensated by adding fuel through the sampler-enricher. Complete shutdown of the reactor is accomplished by draining the fuel salt into the storage tanks in the drain tank cell.

When the reactor is operated at power levels above a few hundred kilowatts, the power is controlled by regulating the air flow, and thereby the rate of heat removal, at the radiator. The power level is determined by measuring the flow rate and temperature difference in the coolant-salt system. The control rods operate to hold the fuel outlet temperature from the reactor constant, and the inlet temperature is permitted to vary with power level. At low power the control rods operate to hold the neutron flux constant, and the heat withdrawal at the radiator or the input to the heaters on piping and equipment is adjusted to keep the temperature within a specified range.

Preventing the salts from freezing, except at freeze flanges and valves, and protecting the equipment from overheating are among the most important control functions. Temperatures are monitored in about 400

places in fuel and coolant systems, and the heating and cooling equipment is controlled to maintain temperatures within specified ranges throughout the systems.

Digital computer and data handling equipment are included in the instrumentation to provide rapid compilation and analysis of the process data. This equipment has no control function, but gives current information about all important variables and warns of abnormal conditions.

#### Fuel Processing System

Batches of fuel salt or flush salt which have been removed from the reactor circulating system can be processed in separate equipment to permit their reuse or to recover the uranium.

Salts that have been contaminated with oxygen to the saturation point (about 80 ppm of O<sub>2</sub>), and thus tend to precipitate the fuel constituents as oxides, can be treated with a hydrogen-hydrogen fluoride gas mixture to remove the oxygen as water vapor. These salts can then be reused.

A salt batch unacceptably contaminated with fission products, or one in which it is desirable to drastically change the uranium content, can be treated with fluorine gas to separate the uranium from the carrier salt by volatilization of UF<sub>6</sub>. In some instances the carrier salt will be discarded; in others uranium of a different enrichment, thorium, or other constituents will be added to give the desired composition.

The processing system consists of a salt storage and processing tank, supply tanks for the H<sub>2</sub>, HF, and F<sub>2</sub> treating gases, a high-temperature (750°F) sodium fluoride adsorber for decontaminating the UF<sub>6</sub>, several low-temperature portable adsorbers for UF<sub>6</sub>, a caustic scrubber, and associated piping and instrumentation. All except the UF<sub>6</sub> adsorbers are located in the fuel processing cell below the operating floor.

After the uranium has been transferred to the UF<sub>6</sub> adsorbers, they are transported to the ORNL Volatility Pilot Plant at X-10, where the UF<sub>6</sub> is transferred to product cylinders for return to the diffusion plants.

#### General Plant Arrangement

The general arrangement of Building 7503 is shown in Fig. 6. The main entrance is at the north end. Reactor equipment and major auxiliary facilities occupy the west half of the building in the high-bay area. The east half of the building contains the control room, offices, change rooms, instrument and general maintenance shops, and storage areas. Additional offices are provided in a separate building to the east of the main building.

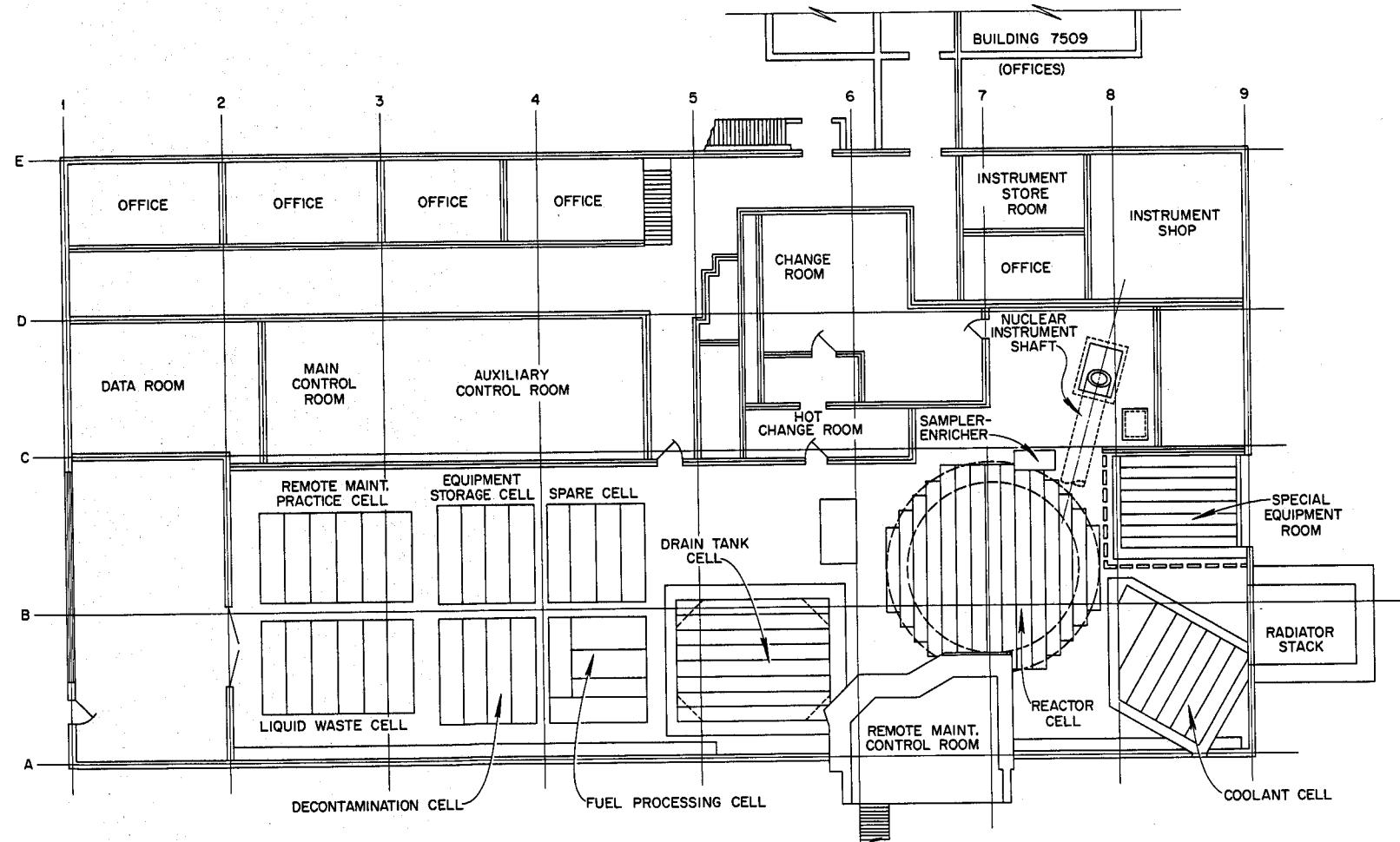


Fig. 6. MSRE Plant Layout, Plan (Above 852-ft Level).

Equipment for ventilation of the operating and experimental areas is located south of the main building. A small cooling tower and small buildings to house stores and the diesel-electric emergency power equipment are located west of the main building.

The reactor primary system and the drain tank system are installed in shielded, pressure-tight reactor and drain tank cells, which occupy most of the south half of the high-bay area. These cells are connected by an open 3-ft-diam duct and are thus both constructed to withstand the same design pressure of 40 psig, with a leakage rate of less than 1 vol % per day. A vapor-condensing system, buried in the ground south of the building, is provided to keep the pressure below 40 psi during the maximum credible accident by condensing the steam in vapors that are discharged from the reactor cell. When the reactor is operating, the reactor and drain tank cells are sealed, purged with nitrogen to obtain an atmosphere that is less than 5% oxygen, and maintained at about 2 psi below atmospheric pressure.

The reactor cell is a carbon steel containment vessel 24 ft in diameter and 33 ft in overall height. The top is flat and consists of two layers of removable concrete plugs and beams for a total thickness of 7 ft. A thin stainless steel membrane is installed between the two layers of plugs and welded to the wall of the steel vessel to provide a tight seal during operation.

The reactor cell vessel is located within a 30-ft-diam steel tank. The annular space is filled with a magnetite sand and water mixture, and there is a minimum of 2 ft of concrete shielding around the outer tank. In addition to this shielding, the reactor vessel is surrounded by a 14-in.-thick steel and water thermal shield.

The drain tank cell adjoins the reactor cell on the north. It is a 17-1/2-ft by 21-1/2-ft by 28-ft-high rectangular tank, made of reinforced concrete and lined with stainless steel. The roof structure, including the membrane, is similar to that of the reactor cell.

The coolant cell abuts the reactor cell on the south. It is a shielded area with controlled ventilation but is not sealed.

The blowers that supply cooling air to the radiator are installed in an existing blower house along the west wall of the coolant cell.

Rooms containing auxiliary and service equipment, instrument transmitters, and electrical equipment are located along the east wall of the reactor, drain tank, and coolant cells. Ventilation of these rooms is controlled, and some are provided with shielding.

The north half of the building contains several small shielded cells in which the ventilation is controlled, but which are not gastight. These cells are used for storing and processing the fuel, handling and storing liquid wastes, and storing and decontaminating reactor equipment.

The high-bay area of the building over the cells mentioned above is lined with metal, has all but the smaller openings sealed, and is provided with air locks. Ventilation is controlled, and the area is normally operated at slightly below atmospheric pressure. The effluent air from this area and from all other controlled-ventilation areas is filtered and monitored before it is discharged to the atmosphere. The containment ventilation equipment consists of a filter pit, two fans, and a 100-ft-high stack. They are located south of the main building and are connected to it by a ventilation duct to the bottom of the reactor cell and another along the east side of the high bay.

The vent house and charcoal beds for handling the gaseous fission products from the reactor systems are near the southwest corner of the main building. The carbon beds are installed in an existing pit that is filled with water and covered with concrete slabs. The vent house and pit are also controlled-ventilation areas. Gases from the carbon beds are discharged into the ventilation system upstream from the filter.

Maintenance of equipment in the fuel circulating and drain tank systems will be by removal of one or more of the concrete roof plugs and use of remote handling and viewing equipment. A heavily shielded maintenance control room with viewing windows is located above the operating floor for operation of the cranes and other remotely controlled equipment. This room will be used, primarily, when a large number of the roof plugs are removed and a piece of highly radioactive equipment is to be transferred to a storage cell.

Equipment in the coolant cell cannot be approached when the reactor is operating, but since the induced activity in the coolant salts is short-lived, the coolant cell can be entered for direct maintenance shortly after reactor shutdown.

#### Description of Major Areas; Status of Construction and MSRE Installation

##### General

A general view of Building 7503 is shown in Fig. 7. This area was originally constructed for the Aircraft Reactor Experiment and later modified for the Aircraft Reactor Test, which was canceled in 1957. Some accommodations in the MSRE design were necessary to fit the experiment into the existing structures, and extensive modifications were required in the sections of the building that house the reactor and fuel-salt circulation system, the coolant-salt circulation system, and the fuel-salt drain tanks. A shielded remote-maintenance control room was added. The existing reactor containment vessel height was increased by about 8-1/2 ft, and the shielding walls, roof plugs, cell wall penetrations, supports, and other structural features were extensively modified. Considerable excavation was needed within the high bay to make room for the drain tank cell. The penthouse for the coolant system and the radiator duct were extensively modified.

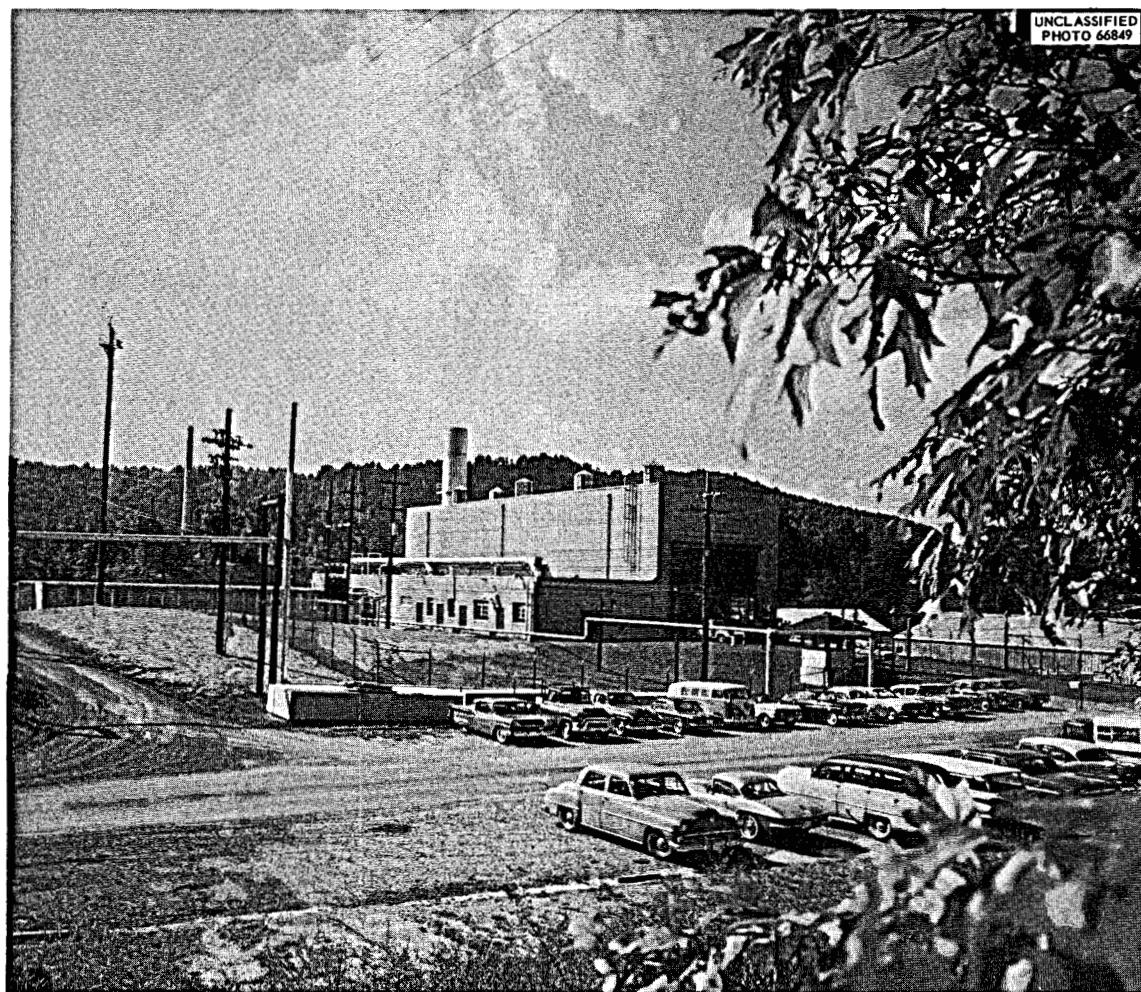


Fig. 7. North View of Building 7503.

In modifying the existing buildings for the MSRE, the areas were divided into five classifications:

Class I. These areas have high radiation levels at all times once the reactor has operated at power and highly radioactive fuel or wastes have been handled in the equipment. They include the reactor cell, drain tank cell, fuel-processing cell, liquid waste cell, charcoal bed pit, etc. The equipment in these areas must withstand relatively high radiation levels and, in most cases, must be maintained by remote-maintenance methods. Direct maintenance will be possible in the fuel-processing and liquid-waste cells, but the equipment must first be decontaminated.

Class II. Areas in this classification are not accessible when fuel salt is in the primary circulating system but can be entered within a

short time after the salt has been drained. The coolant-salt area, which includes the radiator, coolant pump, and coolant-salt drain tank, is in this category. The west tunnel and the unshielded areas of the blower house are other examples. Equipment in these areas can be repaired by direct approach.

Class III. These are areas that are accessible during periods of low-power operation of the reactor, such as the special equipment room and south electric service area, but cannot be entered if the power is above 1 Mw. The equipment in these areas can be inspected and repaired without draining the reactor.

Class IV. These are areas that are accessible or habitable at all times, except under the conditions described below in Class V. These areas include office spaces, control rooms, etc.

Class V. The maintenance control room will be the only habitable area during maintenance operations when large, radioactive components are being removed from the reactor cell. The rest of the MSRE site must be evacuated. This shielded room contains remote control units for the cranes and TV cameras.

#### Building

Above grade, Building 7503 is constructed of steel framing and asbestos cement corrugated siding with a sheet metal interior finish. Reinforced concrete is used in almost all cases below the 850-ft elevation.

Floor plans at the 852- and 840-ft levels are shown in Figs. 6 and 8. The general location of equipment is also shown in Fig. 6, and an elevation view is shown in Fig. 9.

The west half of the building above the 852-ft level is about 42 ft wide, 157 ft long, and 33 ft high. This high, or crane, bay area houses the reactor cell, drain tank cell, coolant-salt penthouse, and most of the auxiliary cells.

The eastern half of the building above the 852-ft elevation is 38 ft wide, 157 ft long, and about 12 ft high. Offices for operational personnel are located along the east wall of the north end. The main control room (Fig. 10), auxiliary control room, and a room used for the data logger, computer, and by the shift supervisor on duty are located across the hall on the western side. The large hall provides ample space for an observation gallery. Windows behind the control panels enable the operating personnel to view the top of the reactor cell and other operating areas of the high bay. The change rooms are located near the center of the building. The southeastern corner is used for an instrument shop, instrument stores, and offices for instrument department supervisory personnel.

Most of the western half of the building at the 840-ft level is occupied by the reactor cell, drain tank cell, and auxiliary cells. The

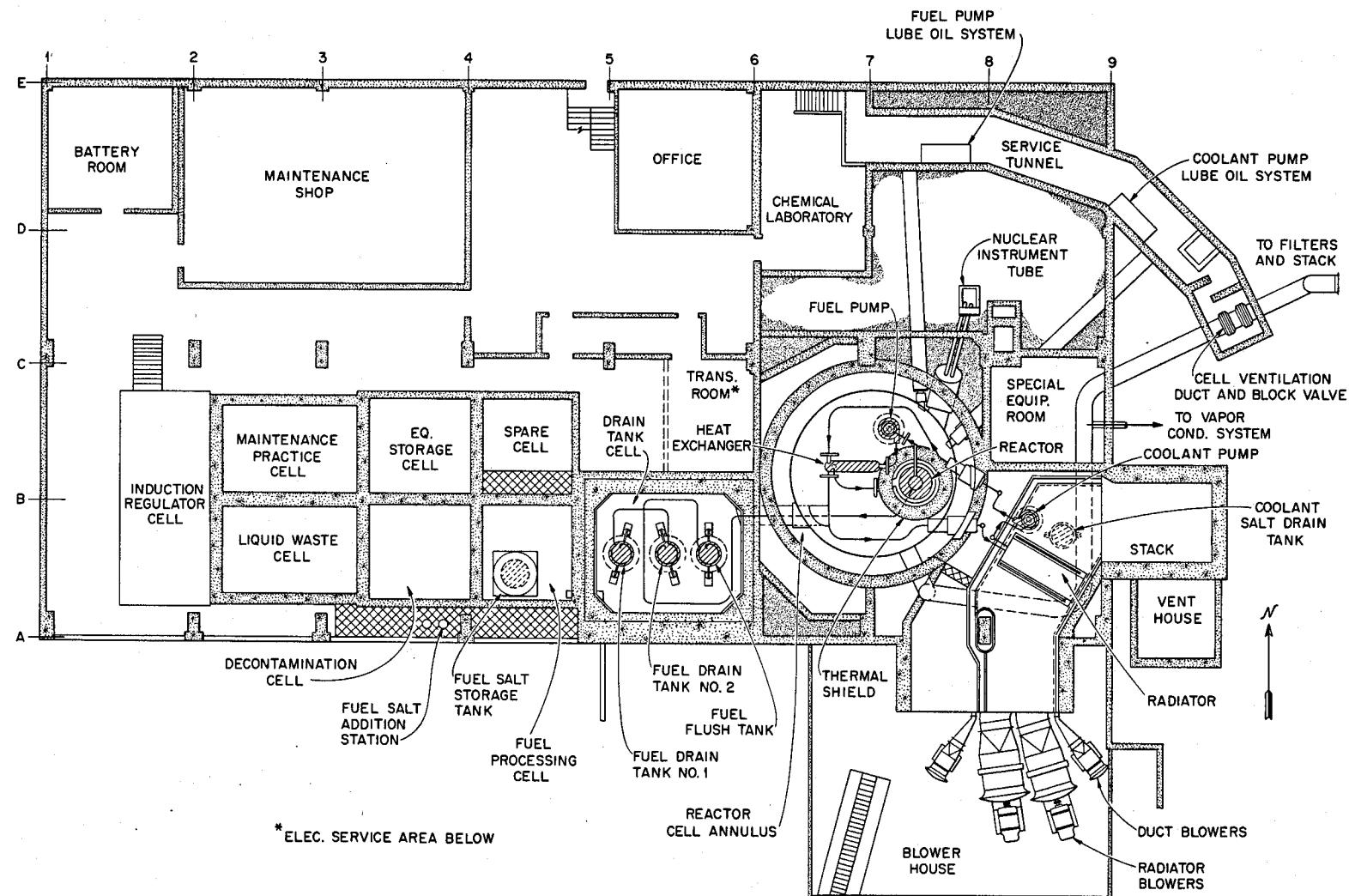


Fig. 8. MSRE Plant Layout at 840-ft Level.

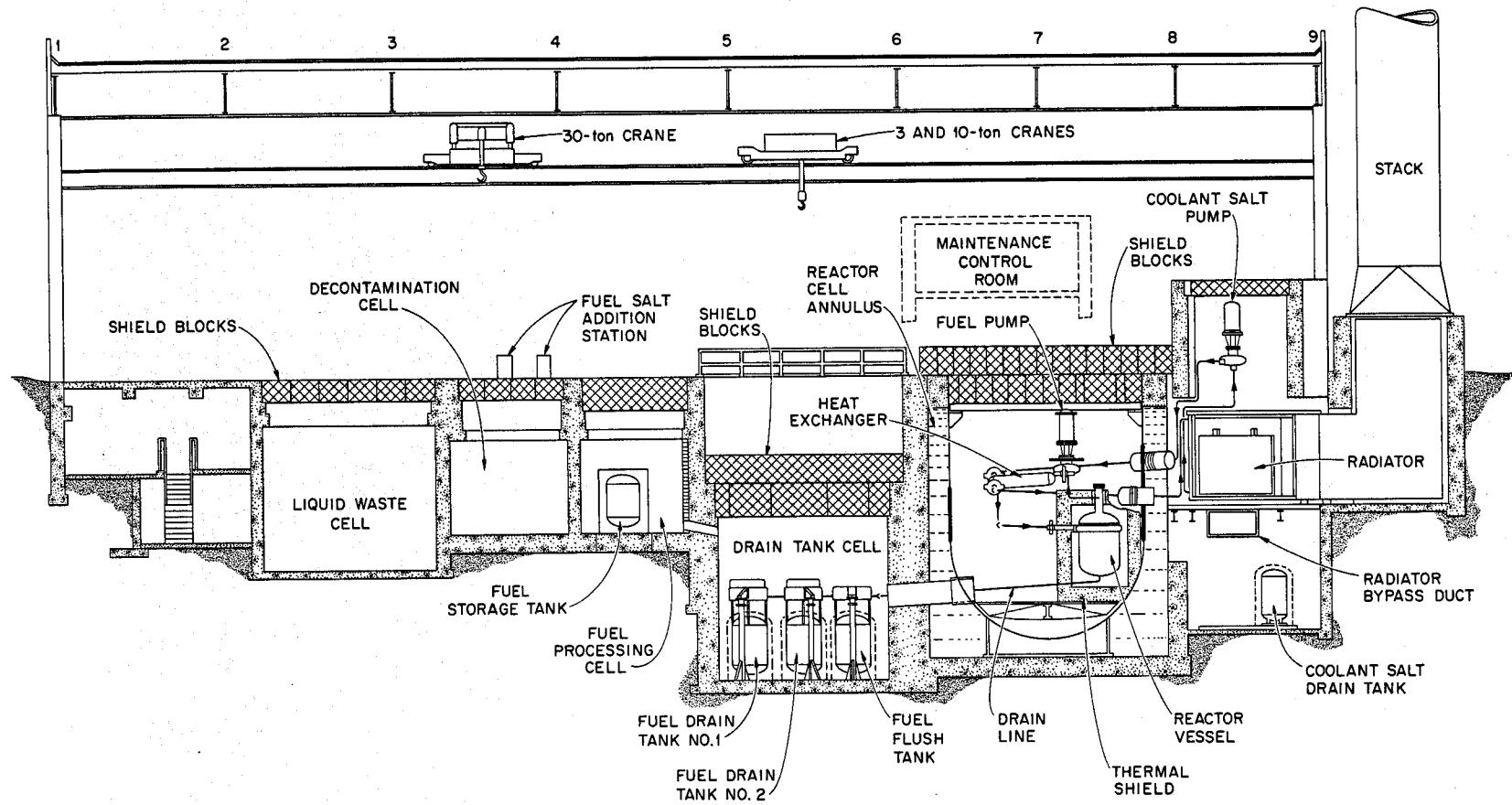


Fig. 9. MSRE Plant Layout, Elevation.

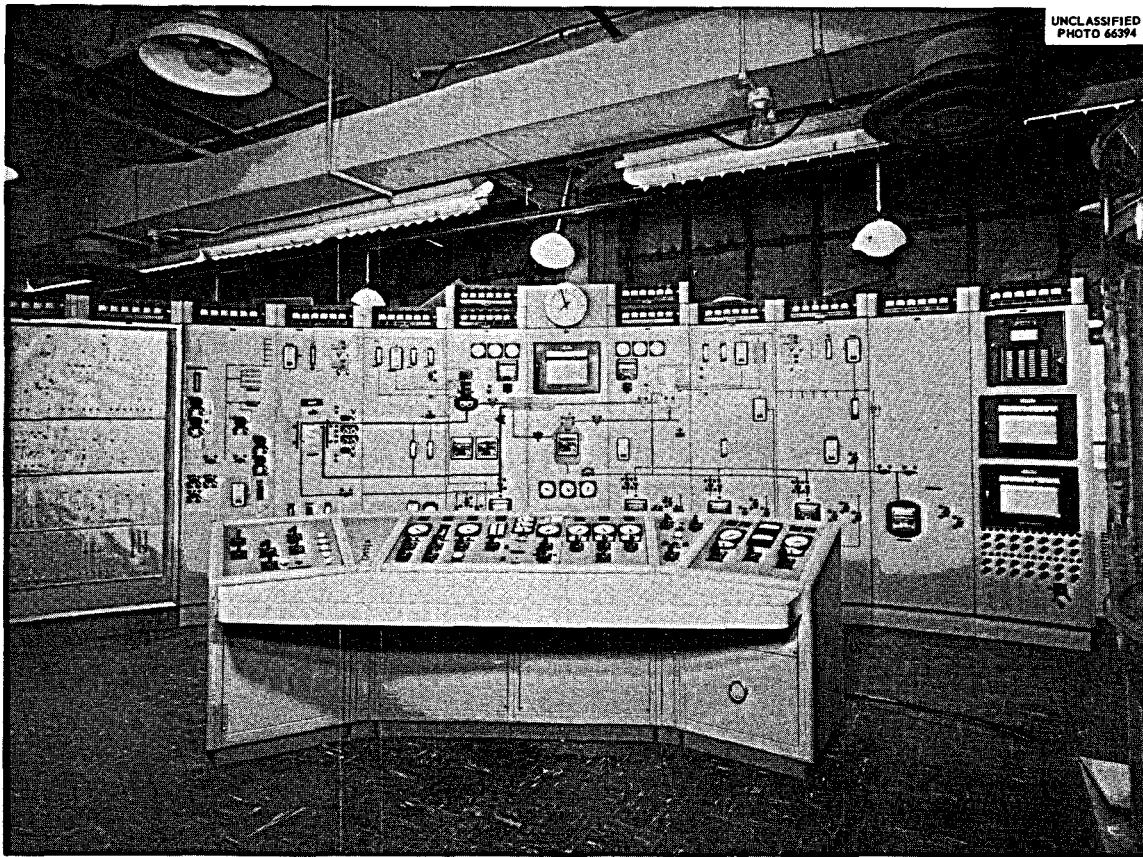


Fig. 10. MSRE Main Control Room.

emergency nitrogen cylinder station is located against the west wall in the northwest corner of this level. Switch boxes used in the heater circuits are located across the aisle between columns A and C (see Fig. 6). Behind these switch boxes is an 8- by 40-1/2-ft pit with a floor elevation of 831-1/2 ft. This pit contains heater circuit induction regulators with some heater transformers mounted above. It is accessible from the 840-ft level by stairs located at the east end. Additional induction regulators and rheostats are located at column line C between columns 2 and 3. The heater control panels and thermocouple scanner panels are installed along column line C between columns 3 and 4.

The batteries for the 48- and 250-v dc emergency power supply are in an 18- by 18-ft battery room in the northeast corner. The motor generators and control panels for the 48-v system are in an area west of the battery room. The main valves and controls for the fire protection sprinkler system are installed along the north wall.

A maintenance shop area is provided between columns 2 and 4. The process-water backflow preventer is installed on the east wall between columns 2 and 3.

The area between column lines 4 and 6 houses the main lighting breakers, switch boxes and transformers, the intercom control panel, water heater, and air conditioners for the main control room and transmitter room, as well as a lunchroom and meeting room for maintenance personnel. The transmitter room is located between column lines 5 and 6.

The service room, 16 by 27 ft, located at the northeast corner of the 840-ft level, serves as a small chemistry laboratory and as an access to the service tunnel. The instrument panels for the fuel and coolant lube oil systems are located in this area.

Reactor Cell. The reactor cell, shown in Fig. 9, is a cylindrical carbon steel vessel 24 ft in diameter and 33 ft in overall height (extending from the 819- to 852-ft elevation), with a hemispherical bottom and a flat top. The lower 24-1/2 ft (819- to 843-1/2-ft elevation) was built for the ART in 1956. It was designed for 195 psig at 565°F and was tested hydrostatically at 300 psig. The hemispherical bottom is 1 to 1-1/4 in. thick. The cylindrical portion is 2 in. thick except for the section that contains the large penetrations, where it is 4 in. thick.

This vessel was modified for the MSRE in 1962 by lengthening the cylindrical section 8-1/2 ft (843-1/2- to 852-ft elevation). Several new penetrations were installed, and a 12-in. section of 8-in. sched 80 pipe, closed by a pipe cap, was welded into the bottom of the vessel to form a sump. The extension to the vessel was 2 in. thick, except for the top section, which was made as a 7-1/4- by 14-in. flange for bolting the top shield beams in place. The flange and top shield structure were designed for 40 psig and the completed vessel was tested hydrostatically to 48 psig, measured at the top of the cell. Both the original vessel and the extension were made of ASTM A201 grade B fire-box-quality steel. Material for the extension was purchased to specification ASTM A300 to obtain steel with good impact properties at low temperature. Steel for the original vessel was purchased to specification ASTM A201.

All the welds on the reactor cell vessel were inspected by magnetic particle methods if they were in carbon steel, or by liquid penetrant methods if they were in stainless steel. All butt welds and penetration welds were radiographed. After all the welding was completed, the vessel was stress relieved by heating to 1150 to 1200°F for 7-1/2 hr.

Calculated stresses in the vessel were well below those permitted by ASME Boiler and Pressure Vessel Code Case 1272N-3. Allowable stresses for ASTM A201 grade B steel were taken as 16,500 psi for general membrane stresses, 24,750 for general membrane plus general bending plus local membrane stresses, and 45,000 psi for combined primary and secondary stresses.

Two layers of 3-1/2-ft-thick shield blocks for the reactor cell are supported by a channel formed into a ring and welded to the inside of the cell wall. The cavity in the channel is filled with steel shot to provide shielding for the cracks between edges of the blocks and the cell wall. One-half-inch steel plate stiffeners are installed at 9° intervals. The top of the channel is at the 848-1/2-ft elevation.

Two beams provide the rest of the support for the bottom layer of blocks. These beams were built of 36-in. WF 150-lb I-beams with angle iron and steel plate stiffeners. The cavities were filled with concrete for shielding. The beams rest on a built-up support plate assembly, which is welded to the side of the cell at the 847-ft 7-in. elevation.

Offsets, 6-1/4 by 26 in., are provided in the ends of the bottom blocks to fit over the support beams. Guides formed by angle iron assure proper alignment. Several of the bottom blocks have stepped plugs for access to selected parts of the cell for remote maintenance.

The sides of the blocks are recessed 1/2 in. for 14 in. down from the top. With blocks set side by side and with a 1/2-in. gap between, a 1-1/2-in. slot is formed at the top. One-inch-thick steel plate 12 in. high is placed in the slots for shielding. The 11-gage ASTM-A240 type 304 stainless steel membrane is placed on top of the bottom layer of blocks and is seal-welded to the sides of the cell. Cover plates are provided over each access plug. These are bolted to the membrane and are sealed by neoprene O-rings. A 1/8-in. layer of Masonite is placed on top of the membrane to protect it from damage by the top layer of blocks.

The top blocks are beams that reach from one side of the cell to the other. The ends of these blocks are bolted to the top ring of the cell with fifty 2-1/2-in. No. 4 NC-2 studs, 57-1/4 in. long, made from ASTM-A320 grade L7 bolting steel. These studs pass through holes that were formed by casting 3-in. sched 40 pipes in the ends of the blocks. Cold-rolled steel washers, 9 in. long by 9 in. wide by 1 in. thick, and standard 2-1/2-in. No. 4 NC-2 nuts are used on each stud.

A removable structural steel platform (elevation 823-1/2 ft at top) forms a floor in the reactor cell vessel and a base for supporting major pieces of equipment.

The reactor cell vessel is installed in another cylindrical steel tank that is referred to here as the shield tank. This tank is 30 ft in diameter and 35-1/2 ft high (elevation 816-1/2 to 852 ft). The flat bottom is 3/4 in. thick, and the cylindrical section is 3/8 in. thick. The shield tank sits on a reinforced concrete foundation that is 34-1/2 ft in diameter by 2-1/2 ft thick. The reactor vessel cell is centered in the shield tank and supported by a 15-ft-diam, 5-ft-high cylindrical skirt made of 1-in.-thick steel plate, reinforced by appropriate rings and stiffeners. The skirt is joined to the hemispherical bottom of the reactor cell in a manner that provides for some flexibility and differential expansion and is anchored to the concrete foundation with eighteen 2-in.-diam bolts.

From elevation 816-1/2 to 846 ft, the annulus between the shield tank and the reactor cell vessel and skirt is filled with magnetite sand and water for shielding. The water contains about 200 ppm of a chromate rust inhibitor, Nalco-360. A 4-in.-diam overflow line to the coolant cell controls the water level in the annulus.

The region beneath the reactor cell vessel inside the skirt contains only water, and steam will be produced there if a large quantity of salt is spilled into the bottom of the reactor cell. An 8-in.-diam vent pipe is provided to permit the steam to escape at low pressure. This pipe connects into the skirt at the junction with the reactor cell and extends to elevation 846 ft, where it passes through the wall of the shield tank and terminates as an open pipe in the coolant cell.

From elevation 846 to 852 ft, the annulus between the reactor cell and shield tank is filled with a ring of magnetite concrete. The concrete ring improves the shielding at the operating floor level and provides some stiffening for the top of the reactor cell vessel. The concrete ring is supported from the wall of the shield tank, and the reactor cell wall is free to move through the ring and to expand and contract relative to the shield tank.

Numerous penetrations were installed through the walls of the reactor cell and shield tank to provide for process and service piping, for electrical and instrument leads, and for other accesses. The penetrations are 4- to 36-in.-diam pipe sleeves welded into the walls of the reactor cell and the shield tank. Since the reactor cell will be near 150°F when the reactor is operating and the temperature of the shield tank may at times be as low as 60°F, bellows were incorporated in most of the sleeves to permit radial and axial movement of one tank relative to the other without producing excessive stress. The bellows are covered with partial sleeves to prevent the sand from packing tightly around them.

Several other lines are installed directly in the penetrations with welded seals at one or both ends, or they are grouped in plugs which are filled with concrete and inserted in the penetrations. The major openings are the 36-in.-diam neutron instrument tube and drain tank interconnection and the 30-in.-diam duct for ventilating the cell when maintenance is in progress. The original tank contained several other 8- and 24-in.-diam penetrations, and they were either removed or closed and filled with shielding.

All the components and connecting piping, which were first fitted together on a precision assembly jig outside the cell, have been installed in the cell, as shown in Fig. 11. All thermocouple and heater leads have been installed and connected to the thermocouple and heater remote disconnects. All leak detector tubing, helium, air, and water piping, together with associated valving, have been installed. No additional installation work is required for prenuclear testing with flush salt. Before the addition of fuel salt and making the MSRE critical, the sampling and enriching system and the control rods and rod drives must be installed.

Drain Tank Cell. The drain tank cell shown in Fig. 6 is 17 ft 7 in. by 21 ft 2-1/2 in., with the corners beveled at 45° angles for 2-1/2 ft. The flat floor is at the 814-ft elevation, and the stainless steel membrane between the two layers of top blocks is at the 838-ft 6-in. elevation. The open pit extends to the 852-ft elevation.

The cell was designed for 40 psig, and when completed in 1962 it was hydrostatically tested at 48 psig (measured at the elevation of the membrane, 838-1/2 ft).

The bottom and sides have a 3/16-in.-thick stainless steel liner, backed up by heavily reinforced concrete, magnetite concrete being used where required for biological shielding. The liner is welded to an angle-iron grid work at approximately 8-in. spacing, with 1/2-in. plug welds. The angle irons are welded to reinforcement rods embedded in the concrete.

Vertical columns in the north and south walls are welded to horizontal beams embedded in the concrete of the cell floor. The tops of the columns are welded to horizontal 36-in. WF 160 I-beams running east and west. These have stiffeners welded to them on approximately 6-in. centers. A slot is provided at the top of these I-beams at elevation 842 ft 1 in. to 842 ft 4-3/8 in. by welding a 1-1/4-in. plate to the web of the beam. Eighty-two 3-1/4- by 4-1/2- by 10-in. steel keys are wedged into this slot to hold down the top blocks.

The top of the cell is composed of two layers of reinforced concrete blocks with an 11-gage (A-204 type 304 stainless steel) membrane between

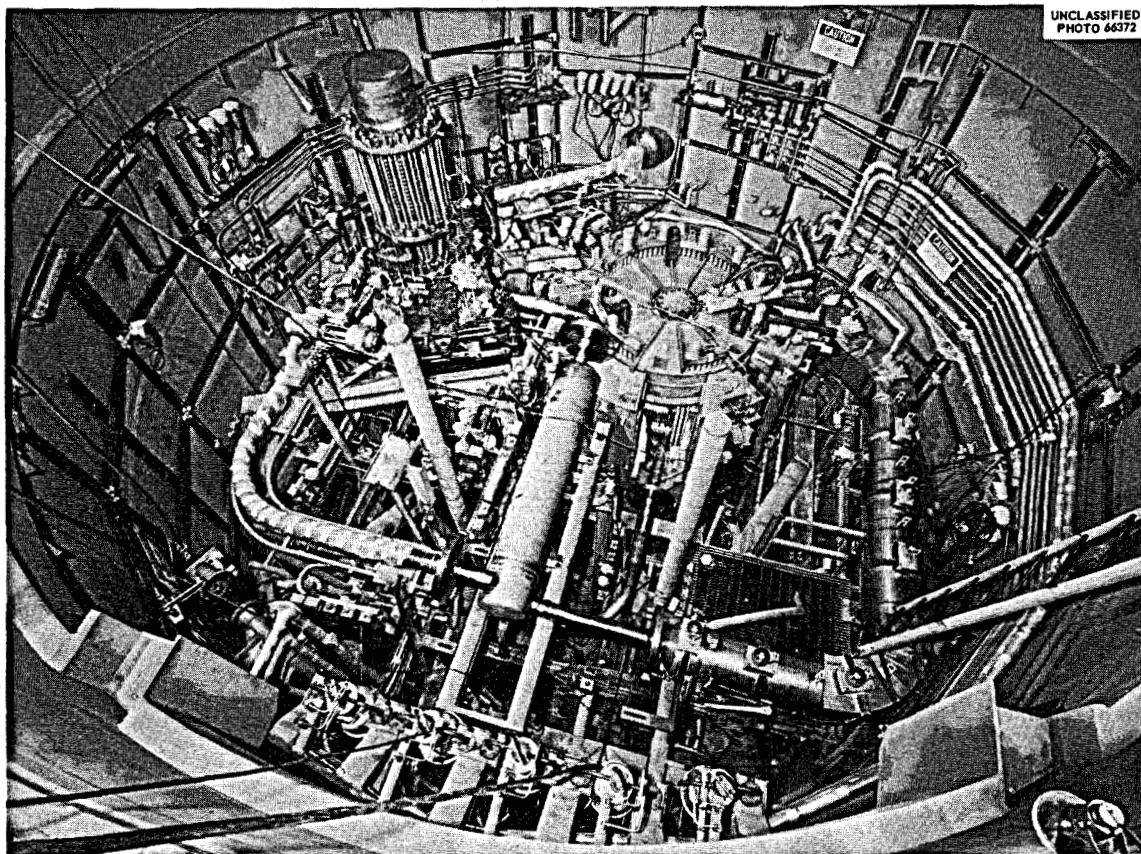


Fig. 11. Fuel-Salt Circulation System in Reactor Cell.

them. Both layers of blocks are ordinary concrete (density 150 lb/ft<sup>3</sup>). The bottom layer is 4 ft thick and the top layer is 3-1/2 ft thick.

The blocks are arranged to facilitate remote maintenance. One side of the lower blocks, which run east and west, is supported by a ledge at an elevation of 834-1/2 ft. The other side of these and the ends of the north-south blocks are supported by beams that extend from the east to the west side of the cell. These beams are built up of 24-in. 104.9-lb I-beams with angle-iron and steel-plate stiffeners. The cavities are poured full of concrete for shielding. These rest on a built-up support plate assembly, which is welded to the side of the stainless steel liner and is anchored into the concrete walls. Offsets, 4-1/4 by 25-1/2 in., are provided in the ends of the bottom blocks to fit over the support beams. V grooves formed by angle irons assure proper alignment. The sides of the bottom blocks are recessed 1/2 in. for 14 in. down from the top. With two blocks side by side and with a 1/2-in. gap between the sides at the bottom, a 1-1/2-in. slot is formed at the top. One-inch steel plates, 12 in. high, are put into the slots to provide biological shielding.

The 11-gage (ASTM A-240 type 304 stainless steel) sealing membrane is placed on top of the bottom blocks (elevation 838 ft 6 in.) and is seal-welded to the sides of the cell. A 1/8-in. layer of Masonite is placed on top of the seal pan to protect it from damage during installation of the top blocks. The top blocks are beams that reach from the north side to the south side of the cell. They are held down by the eighty-two 3-1/4- by 4-1/2- by 10-in. steel keys discussed previously. These are inserted into slots in the top beams of the north and south sides of the cell and are driven in approximately 4 in., leaving approximately 5 in. bearing on the ends of the blocks. There are approximately four keys for each end of each block. A 1-1/2-in. 6 NC square nut is welded to the top of each key to aid in removing and handling the keys.

The floor elevation is 814 ft at the highest point along the west wall and slopes 1/8 in./ft to a trench along the east wall. The trench slopes 1/8 in./ft toward the south and terminates in a sump in the south-east corner. The sump consists of a 10-in.-long section of 4-in. sched 40 pipe and a 4-in. butt-welded cap (347 stainless steel).

Numerous lines are installed through the walls of the drain tank cell to provide for process and service piping, electrical and instrument leads, and for other accesses. These enter through 3/4- to 6-in. pipe or pipe sleeve penetrations that are welded to the stainless steel liner and cast into the concrete walls. Lines are installed in these individually or grouped in plugs that are filled with concrete and inserted.

Figure 12 shows the salt storage vessels and associated equipment, installed in the drain tank cell. All tanks, tank furnaces, steam cooling equipment, and associated piping have been installed in the drain tank cell. Leak testing and other required check-out tests have been conducted on installed equipment. Except for the installation and check-out of some remotely removable pipe heater insulation units, this cell is ready to accept the flush salt.

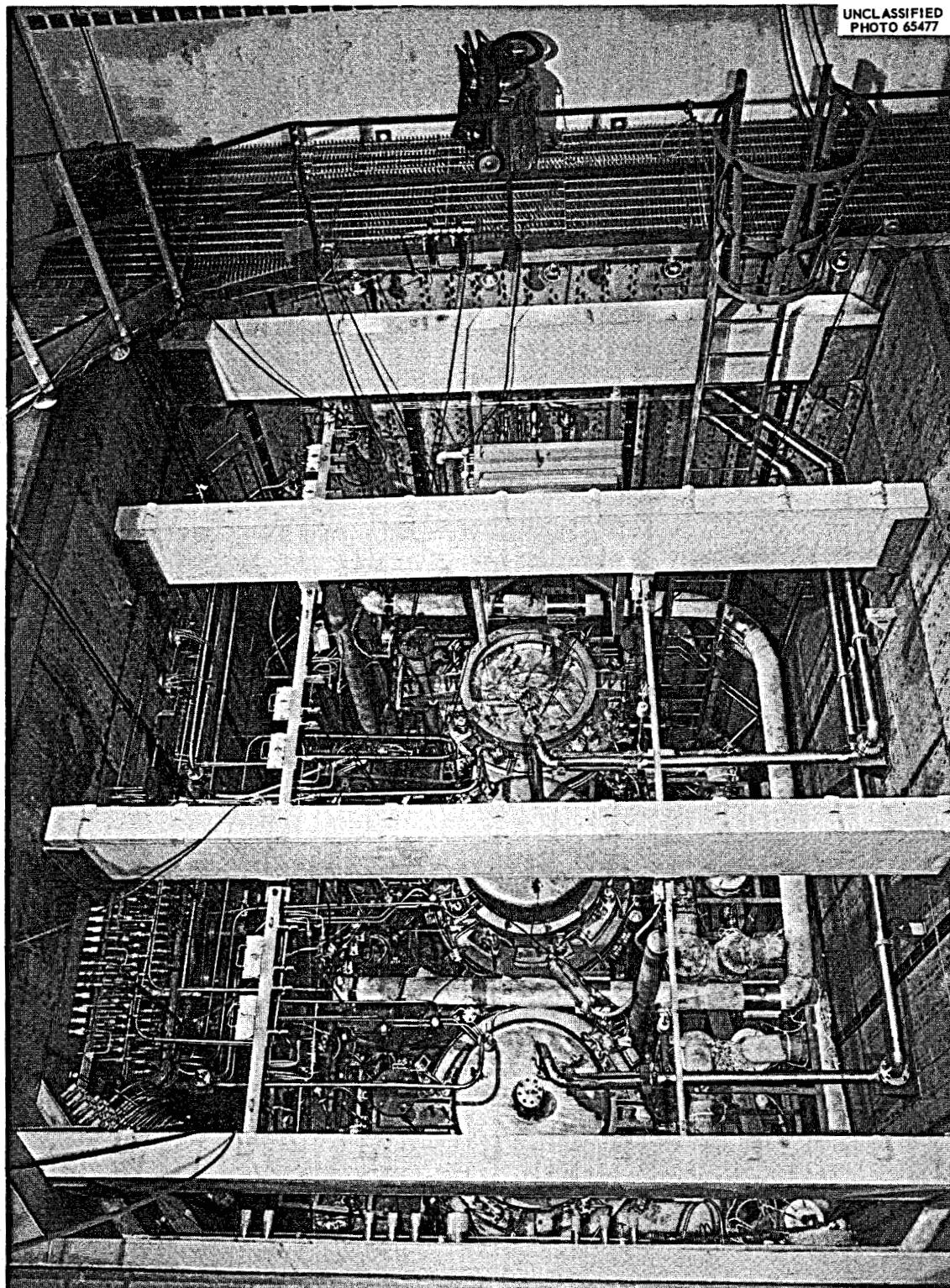


Fig. 12. Drain Tank Cell Equipment Installed.

Coolant Cell and Coolant Drain Tank Cell. Except for two lines in the reactor cell which connect the coolant-salt circulating system to the heat exchanger, all coolant-salt piping is located in the coolant and coolant drain tank cell, shown in Fig. 6. The top section of the coolant cell is a concrete enclosure (penthouse) which rises from the southwest corner of the high bay to an elevation of 863 ft 3 in. The walls are ordinary reinforced concrete 24 in. thick except for the south corner, which is 15-1/2 in. thick. Additional shielding for this corner is provided by the 2-ft-thick base for the stack, which goes to the 859-ft elevation. A 4-in. ledge at elevation 861 ft 9 in. on the southeast and northeast sides of the penthouse supports the bottom layer of the top shield blocks. These are constructed of 12-in.-thick reinforced ordinary concrete. The 12-in.-thick top shielding blocks rest on the bottom blocks. The 1/2-in. gaps between plugs in each layer are staggered for better shielding. Ledges at the 862-ft 9-in. elevation on the northeast side and at the 861-ft 9 in. elevation on the other sides are provided for shielding.

The bottom of the coolant radiator is at elevation 836 ft 1-3/4 in. The floor of the coolant stack enclosure, located south of the radiator, is at elevation 835 ft 5 in., and the 2-ft-thick reinforced regular concrete walls extend to the 859-ft elevation.

A 1-1/4-in. steel grating and/or 11-gage sheet metal pan at elevation 834 ft 11 in. separates the coolant cell from the coolant drain tank cell. Thus, the coolant drain tank cell is below ground level on all sides. The elevation of the concrete floor is 820 ft. It is bounded by the reactor cell annulus on the northeast and by the special equipment room on the east.

Two penetrations from the reactor cell terminate in the coolant cell or coolant drain tank cell. The wall between the coolant and coolant drain tank cells and the special equipment room is 16 in. thick to the 835-ft 5-in. elevation and 12 in. thick above this. Existing openings between the cells are closed by stacked magnetite concrete blocks to enable proper ventilation of both areas and to provide adequate shielding. A 6-ft-wide concrete ramp with 2-ft stairs in the center (slope 7 in 12) extends from the northwest corner of the coolant drain tank cell to the blower house at the 840-ft elevation. This is closed off by stacked magnetite blocks.

Shielding from the coolant pump and from piping is provided by 8 ft of barytes blocks stacked above the 835-ft elevation between the radiator housing and reactor shield.

All equipment for the coolant-salt system has been installed. Figure 13 shows the coolant pump and the radiator door-lift mechanism. The installed radiator is shown in Fig. 14, and the main blowers are shown in Fig. 15. The installed coolant drain tank equipment, located at the level below the radiator, is shown in Fig. 16. This system has been checked out and is ready to receive the coolant salt.

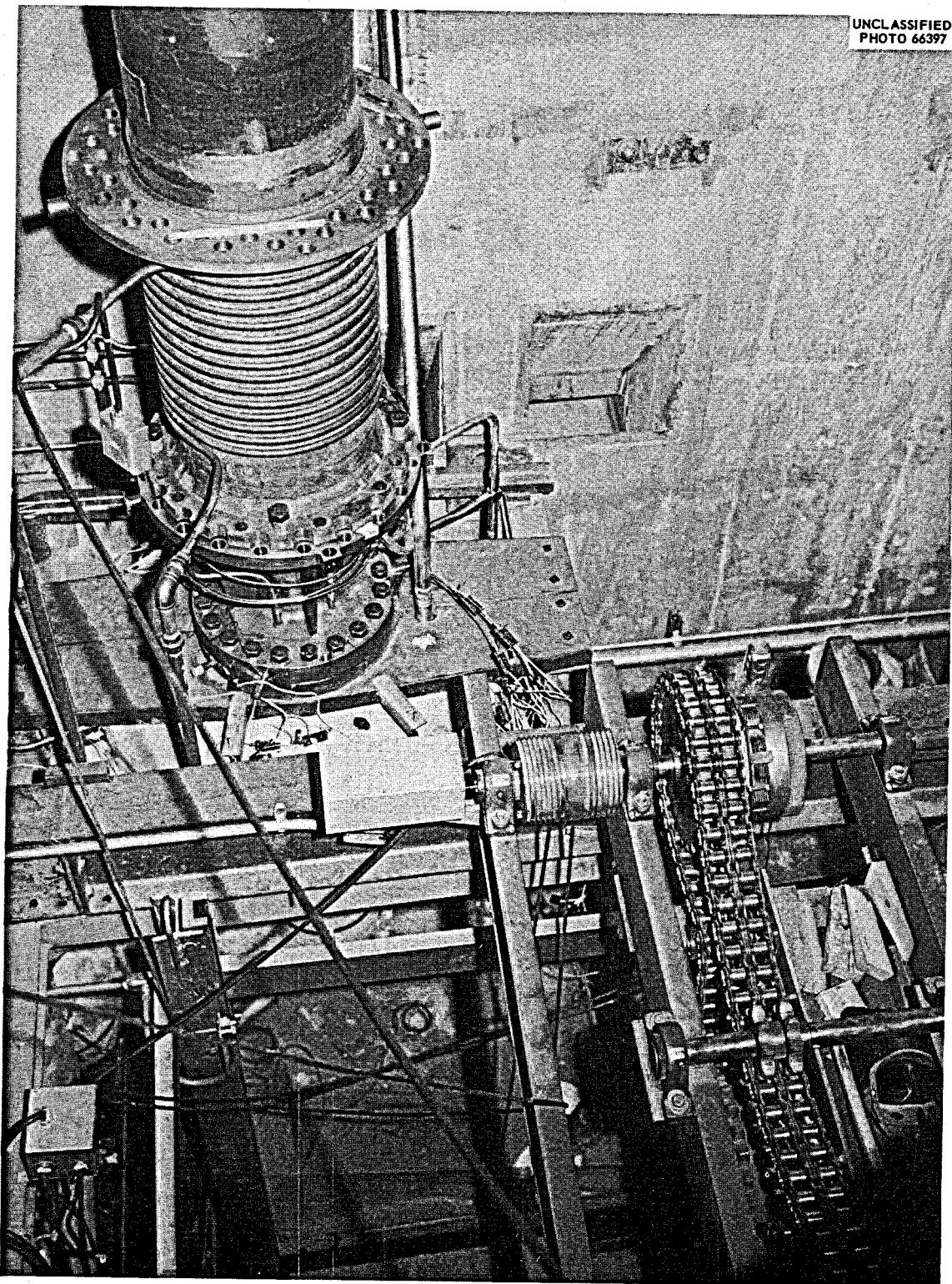


Fig. 13. Coolant Pump and Radiator Door-Lift Mechanism.

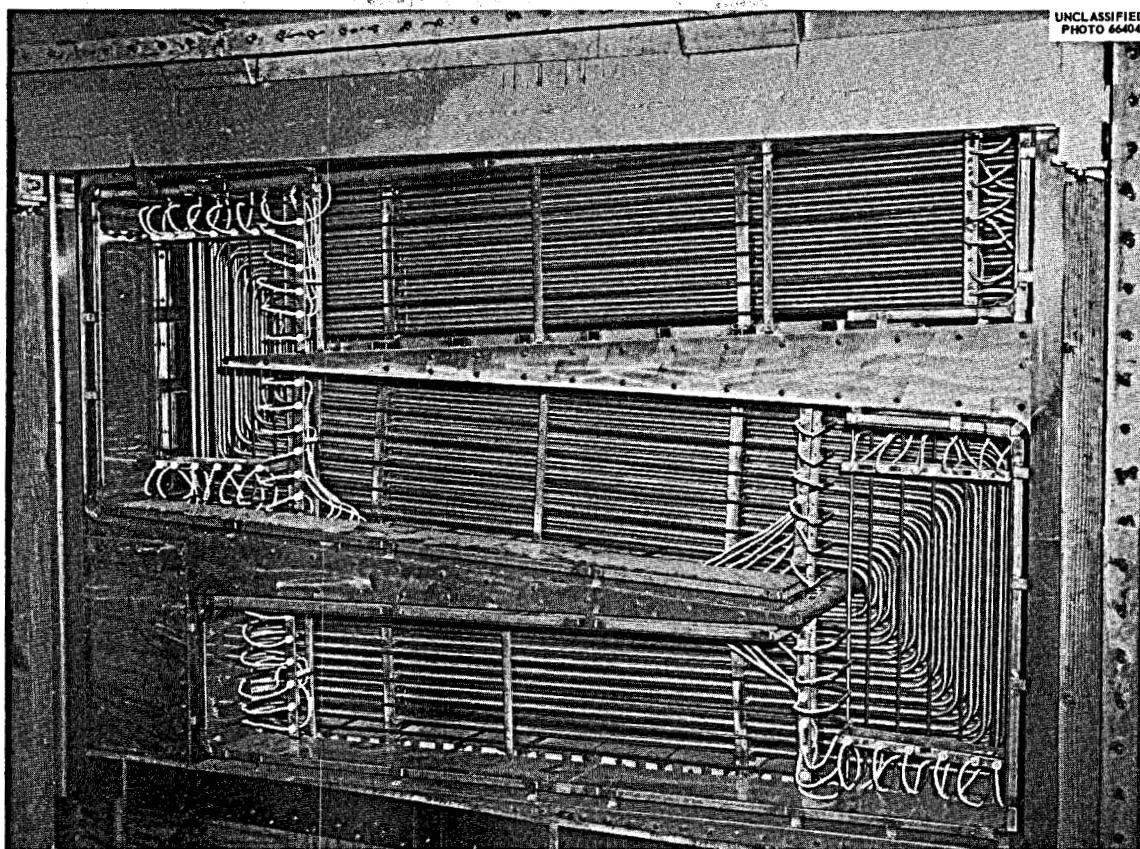


Fig. 14. MSRE Radiator, as Installed.

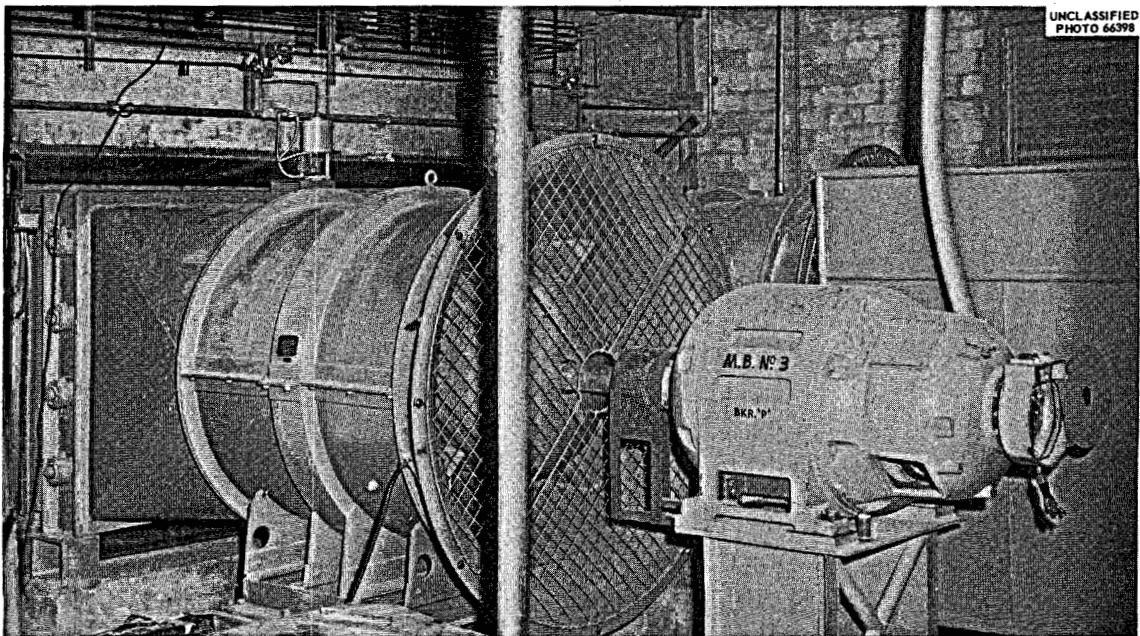


Fig. 15. Main Blowers for MSRE Coolant System.

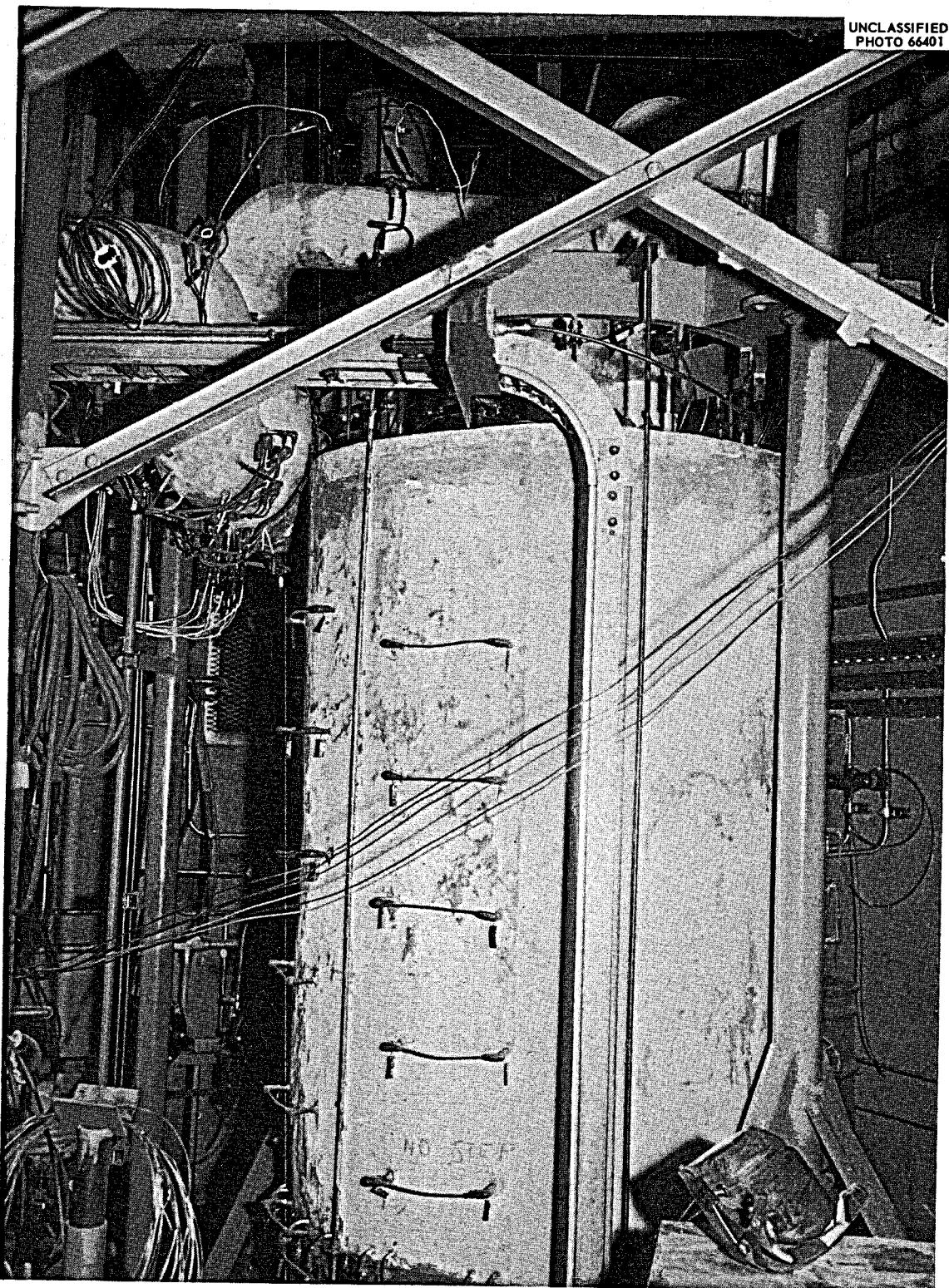


Fig. 16. Coolant Drain Tank.

Special Equipment Room. The major items of equipment located in the special equipment room are the component coolant blowers, the containment boxes for the fuel pump cover gas and bubbler lines, the 30-in.-diam cell ventilation duct, and the rupture disks and lines to the vapor-condensing system. This cell is located southeast of the reactor cell and, as discussed previously, has a common wall with the coolant cell and coolant drain tank cell. The other walls are 12-in.-thick reinforced concrete below ground level. The cell is 15 ft 11 in. by 17 ft. The floor elevation is 828 ft 7 in., except for a 5-ft by 15-ft 11-in. by 3-ft-deep pit which runs east and west, 2 ft 3 in. from the south wall.

The top consists of two rows of removable concrete shield plugs with staggered joints. Each row of blocks is 1 ft thick. The bottom row is supported by a 4-in. ledge at the 850-ft elevation. Containment is provided by ventilation from the stack fans.

Figure 17 shows the equipment in the special equipment room as installed, checked out, and ready for operation. Only the lines to the vapor-condensing system are yet to be installed.

Pump Room. The pit pump and sump pumps are located in the pump room. This room is under the north end of the special equipment room. It is 7-1/2 ft wide by 15 ft 3 in. long by 6 ft 7 in. high with a floor elevation of 820 ft. A 3- by 3-ft sump, near center of the north wall, extends to the 811-ft elevation. Access to the pump room is through a 3- by 4-ft hatch near column C-8. This equipment is installed.

Service Tunnel. The fuel and coolant lube-oil systems shown in Fig. 18 and the reactor cell ventilation block valves are installed in the

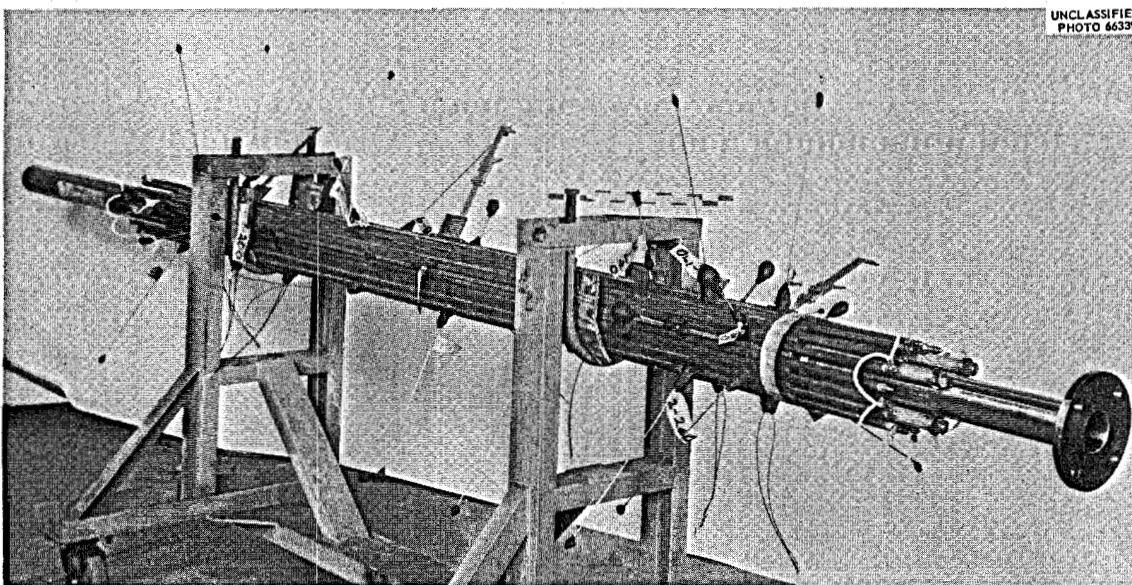


Fig. 17. Equipment Installed in Special Equipment Room.

service tunnel. This tunnel is 7 ft wide by 11 ft high by approximately 67 ft long. It passes under the southeast corner of the 7503 building and extends south and west outside the building. The floor elevation is 833 ft 3 in. Normal access is from the service room on the 840-ft level; however, a 3- by 3-ft hatch near the west end provides access from outside the building. This hatch is normally closed by a sheet-metal-covered wooden lid. Containment is controlled by ventilation.

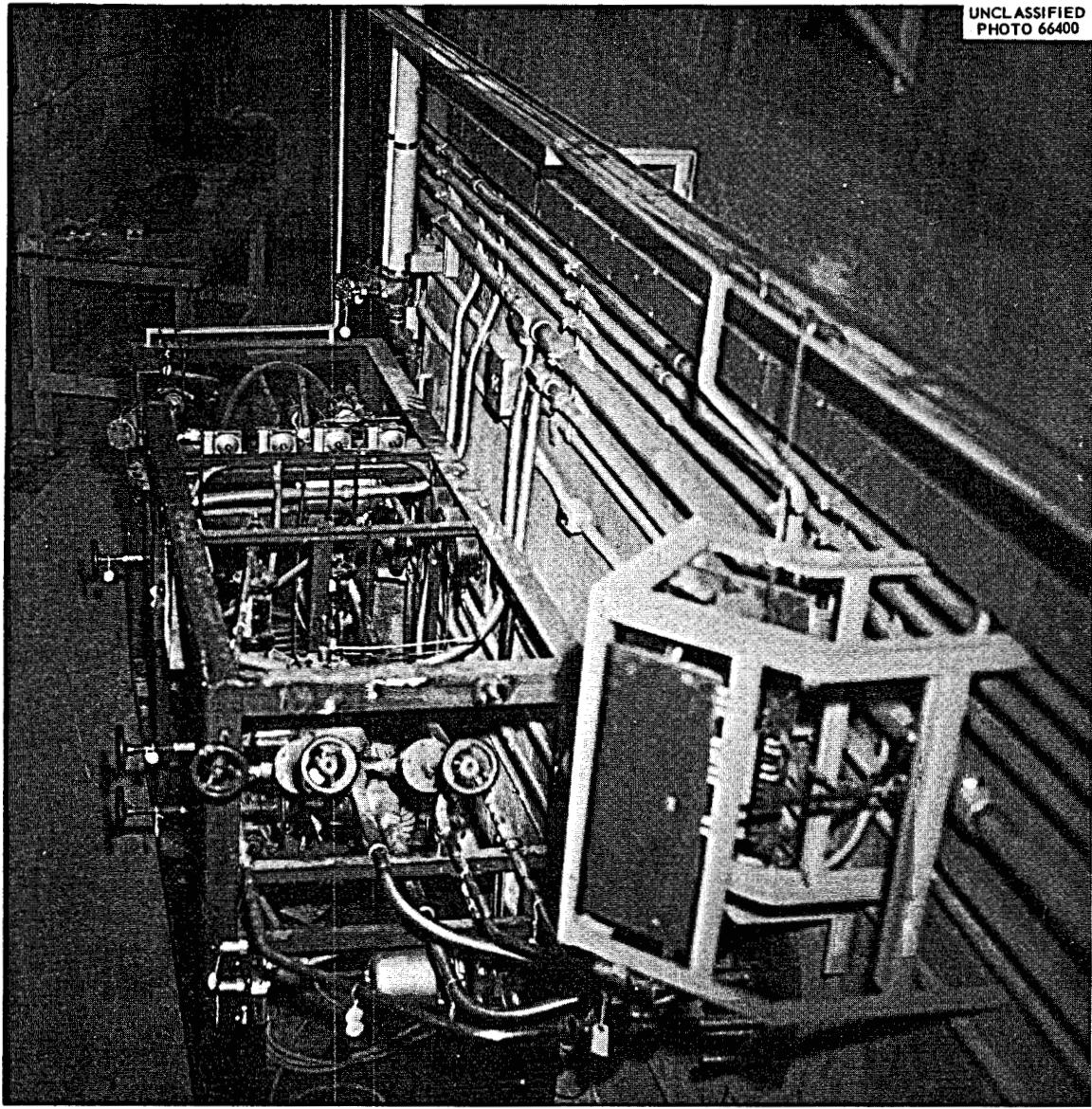


Fig. 18. Typical Lube-Oil System for Fuel and Coolant Pumps.

Transmitter Room and Electric Service Areas. The area north and west of the reactor cell annulus at elevation 831 ft (west tunnel) connects by a narrow passage to a similar area north and east of the reactor cell annulus (east tunnel). These extend eastward under the 840-ft floor to a 24-in.-thick concrete wall 12 ft north of column line 6. This entire area is called the south electric service area. Six penetrations from the reactor cell and eighteen from the drain tank cell terminate in this area. The walls, except for those joining the reactor or drain tank cells, are located below ground level. The ceiling, which connects with the transmitter room, is 24-in.-thick reinforced concrete with a 3-ft 7-1/2-in. by 6-ft 7-1/2-in. by 24-in.-thick concrete plug for access to the area. This plug has a 4- by 12-in. offset on all sides for shielding.

The north electric service area is located north of the 24-in.-thick concrete wall mentioned above. The floor of this room is at the 824-ft elevation. Many of the drain tank cell penetrations terminate in this area as well as some from the spare cell. The ceiling of this area and the floor of the transmitter room above is 2- to 4-in.-thick reinforced concrete poured on "Q" decking No. 3-16. Containment is by controlled ventilation. A 2- by 3-ft manhole with a hinged steel door provides access from the transmitter room.

The floor of the transmitter room is at the 840-ft elevation. The 5-in. floor of the high bay (elevation, 852 ft) is the ceiling of the transmitter room. A 5-ft by 9-ft 3-1/2-in. plug can be removed from the high-bay floor so that the high-bay crane can be used to remove the shielding plug on the 840-ft level between the transmitter room and the south electric service area. This room is approximately 16 by 20 ft and contains the leak detector system and instrumentation for the drain tank weigh cells, pump level and speed, sump level, component cooling air, etc.

Auxiliary Cells. Six smaller cells are located between columns 2-5 and A-C. Removable concrete blocks provide access from the high-bay area at the 852-ft elevation. Containment of each is by control of ventilation and discharge of the air through the filters to the stack. Descriptions of their projected uses are given below.

Fuel Processing Cell - The fuel storage tank and other in-cell equipment for hydrofluorinating or fluorinating the fuel or flush salt are located in this cell. The absorber cubicle is located east of this cell at the 852-ft level.

Decontamination Cell - This cell contains a decontamination tank. Both tank and cell are used for underwater maintenance and storage of contaminated equipment.

Liquid Waste Cell - The liquid waste tank, sand filter, and cell sump jet block valves are located in this cell.

Remote Maintenance Cell - The liquid waste pump and waste tank exhaust blower are located in this cell. It will also be used as a remote maintenance practice cell.

Hot Storage Cell - This cell will be used to store contaminated equipment removed from the reactor or drain tank cell.

Spare Cell - The absolute filter in the chemical processing cell air exhaust line and the flame arrester in the chemical processing off-gas line are located in this cell.

High-Bay Containment Enclosure. The high-bay containment enclosure between columns 2-8 and A-C is 42 by 136 ft with a ceiling elevation of 885 ft 4 in. The containment extends east near column 8 to include the neutron instrument tube and to provide room for the fuel-salt sampler.

A false ceiling and containment seal is installed 15 ft above the floor between columns 8-9 and B-C. The containment walls extend from this elevation to 885 ft 4 in. along column line C from columns 8 to 9, west along column line 9 to column A, then north along column A to column 8. Thus the coolant cell penthouse is included in the high-bay area and the high-bay crane can be used for handling equipment and shielding blocks in this cell. A 10- by 12-ft loading hatch and Bilco door in the false ceiling of the area between columns 8-9 and B-C is used for moving small equipment into or out of the containment enclosure and for removal of fuel- and coolant-salt samples. A 12- by 12-ft door located at column line 2 is used for removal of larger equipment. The framework of the high bay is Stran Steel construction with a 16-gage iron sheet metal skin skip-welded to it. The cracks were sealed with fiberglass tape and Carbofine paint.

Emergency exits are provided at the southeast corner and near the center of the east wall. Since this area is considered as a contaminated zone, normal entrance and exit is through the hot change house, located east of the high bay, and through the regular change room.

Maintenance Control Room. A 19-ft 8-in. by 14-ft 9-in. maintenance control room is located along the west side of the high-bay containment between the reactor and drain tank cells. The floor elevation is 862 ft and the ceiling 870-1/2 ft. The west side is corrugated asbestos to match the building. The roof is 12-in.-thick concrete, the south side 2-ft-thick concrete, and the north and south sides 3- to 3-1/2-ft-thick concrete for shielding. A zinc bromide-filled viewing window is located on the west side near the south end and another on the northwest corner of the room for use during remote maintenance. Access to the maintenance control room is via stairs which terminate at ground level west of the building.

A 6-ft by 19-ft 8-in. electric equipment room located below the maintenance room has a floor elevation of 852 ft. This is accessible through a hatch in the southeast corner of the maintenance control room.

#### Off-Gas Area

The off-gas area, consisting of a vent house and absorber pit, is shown in Fig. 8.

The vent house is 12 by 15 ft with an operating floor level of 848 ft. The sloping roof attaches to the south end of the 7503 building at the 857-1/2-ft elevation.

A 5- by 9- by 3-ft-deep containment enclosure is located along the east side of the vent house. This contains the reactor and drain tank off-gas lines, instruments, valves, etc. The bottom of this enclosure is at the 839-1/2-ft elevation. The east and west sides are reinforced concrete; the north and south ends and top at the 842-1/2-ft elevation are constructed of mild steel angle irons and 1/8-in. plate (ASTM A-7). The joints are caulked to prevent leakage. Hand valves have shielded extension handles which permit them to be operated from the vent-house floor. Pipe caps are installed for containment when the valves are not being operated. Five feet of barytes blocks are stacked on top of the containment enclosure. A 17-in.-diam removable plug is installed above the control valves and check valves to facilitate remote maintenance.

The west side of the vent house has a floor elevation of 844-1/2 ft and is used for off-gas lines not requiring shielding and for stacked block shielding for the reactor and drain tank off-gas lines.

A 5- by 15-ft valve pit with the bottom at an elevation of 841 ft is located south of the vent house. The off-gas lines pass through this pit before entering the absorber beds, shown after fabrication in Fig. 19. The outlet lines are also located in this pit. The inlet valves are contained in a 2-1/2- by 4- by 2-ft-high containment box which has a top elevation of 845-3/4 ft. Seventeen inches of steel plate is used above this box for shielding. Shielded extension handles permit operation of the valves from the operating floor at an elevation of 848 ft. Pipe caps are installed for containment when the valves are not being operated. The liners between the charcoal beds and the pit go through a 9- by 18-in. penetration, where they are grouted in place using Embeco expansion grout.

The charcoal bed pit has a 10-ft inside diameter with 14-in.-thick concrete walls. The bottom of the pit is at an elevation of 823 ft 9 in. The pit is filled with water to an elevation of 846 ft for shielding. Two 10-1/2-ft-diam by 18-in.-thick barytes concrete blocks are supported by a ledge at the 846-1/2-ft elevation. The top block is caulked to obtain an airtight seal. Additional barytes concrete blocks are stacked on top of these to give a minimum of 5-1/2 ft of shielding. A 4-ft annulus around the outside of the charcoal bed pit is filled with stabilized aggregate from the 848-ft to the 849-ft 5-in. elevation.

The off-gas from the charcoal bed goes through the valve pit mentioned previously, where unshielded extension handles permit operation from the 848-ft elevation.

Installation of the charcoal adsorbers and associated valving and piping is nearing completion.

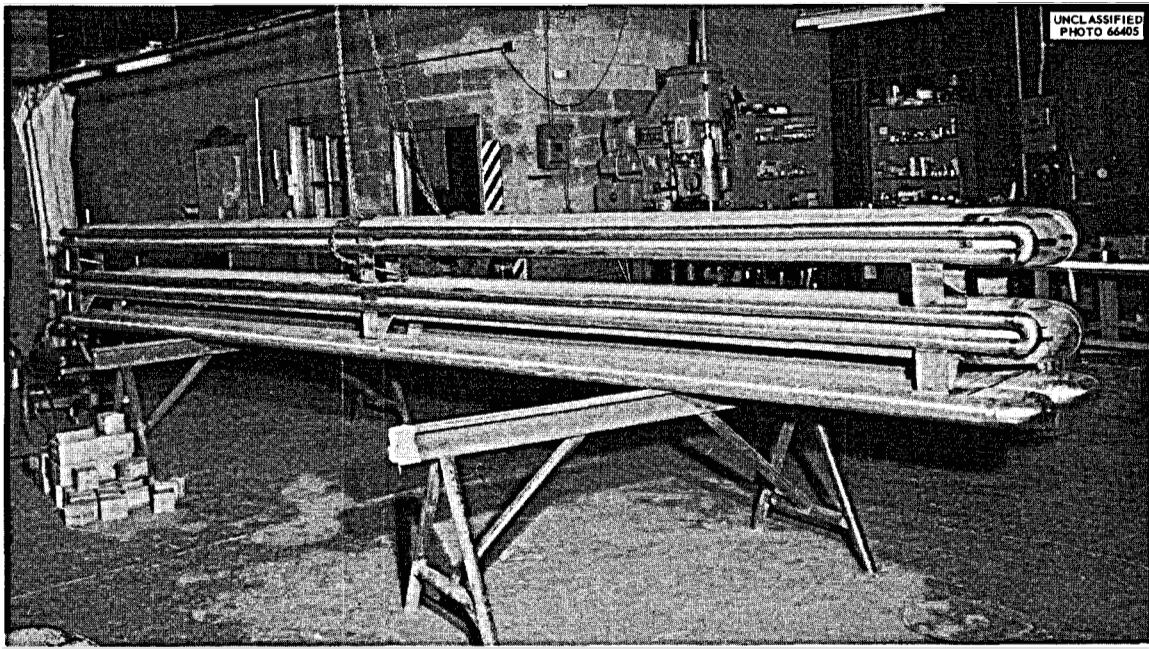


Fig. 19. Charcoal Adsorber Beds for MSRE Off-Gas System.

#### Stack Area

The stack area is located south of Building 7503. All off-gas and containment ventilation air passes through roughing and absolute filters before being discharged up the stack.

These filters are located in a pit 60 ft south of Building 7503. The pit is 26-1/2 by 18-3/4 ft with a sloping floor. The floor elevation at the north end is 850 ft and the south end is 848 ft. The walls are 1-ft-thick concrete. The roof plugs are 18-in.-thick concrete with a 3-in. offset at the center. This offset rests on a ledge 9 in. down from the top of the pit. The elevation of the top of the pit is 857 ft. The roof blocks are caulked to prevent leakage.

A 3-ft 3-in. by 5-ft 6-in. valve pit is attached to the filter pit on the southeast corner. This houses the filter pit drain valves and water level indicators. The walls and removable roof plug are 8-in.-thick concrete. The floor and roof are at 845- and 857-ft elevations.

The two 21,000-cfm stack fans and the associated 3-ft-diam by 100-ft-high steel stack are located south of the filter pit.

All construction and equipment installations associated with the stack, filter house, and ventilation ducts are completed.

Vapor-Condensing Tanks

The vapor-condensing system water tank, expansion tank, and associated piping are located west of the stack area. As mentioned previously, the rupture disks and connections to the reactor cell exhaust duct are located in the special equipment room. The tanks and piping for this system are nearing completion, but are yet to be installed.

Blower House

The blower house is 36 by 43 ft with floor and ceiling elevations of 838 and 856 ft respectively. The north, south, and west walls are louvered to provide air inlet to the two coolant blowers and two annulus blowers located in the south half of the room. The air from the blowers passes through the radiator area of the coolant cell and out the 10-ft-diam by 70-ft-high steel stack located just north of the vent house. Top elevation of this stack is 930 ft.

Gas coolant pump No. 3, which supplies air to freeze valves in the coolant drain tank cell and fuel processing cell, is located between column lines 7 and 8.

A ramp leading to the coolant drain tank cell begins at the northwest corner of the blower house.

The cooling water equipment room, housing the cooling-water control panel, storage tanks, flowmeters, and treated-water circulation pumps, is located in the southwest corner of the blower house.

The stairs leading to the maintenance control room are located just west of the blower house. The area under the stairs is used for the fluorine gas trailer, hydrogen and hydrogen fluoride gas cylinders, etc., which are used in processing the fuel salt.

All equipment in this area has been installed.

Diesel House

The 30- by 72-ft diesel house is located 36 ft west of Building 7503 between column lines 3 and 5 and adjoins the switch house on the east. It has corrugated asbestos siding and a pitched roof with an elevation of 858 ft at the center and 852 ft at the sides.

The three diesel generator units, Fig. 20, and their auxiliaries are located at the east end of the north half of the building. The 5000-gal diesel fuel storage tank is located approximately 100 ft north of the diesel house.

The helium cover-gas treatment equipment, Fig. 21, and emergency helium supply cylinders are located just west of the diesels. The helium supply trailer is located outside the west end of the building.

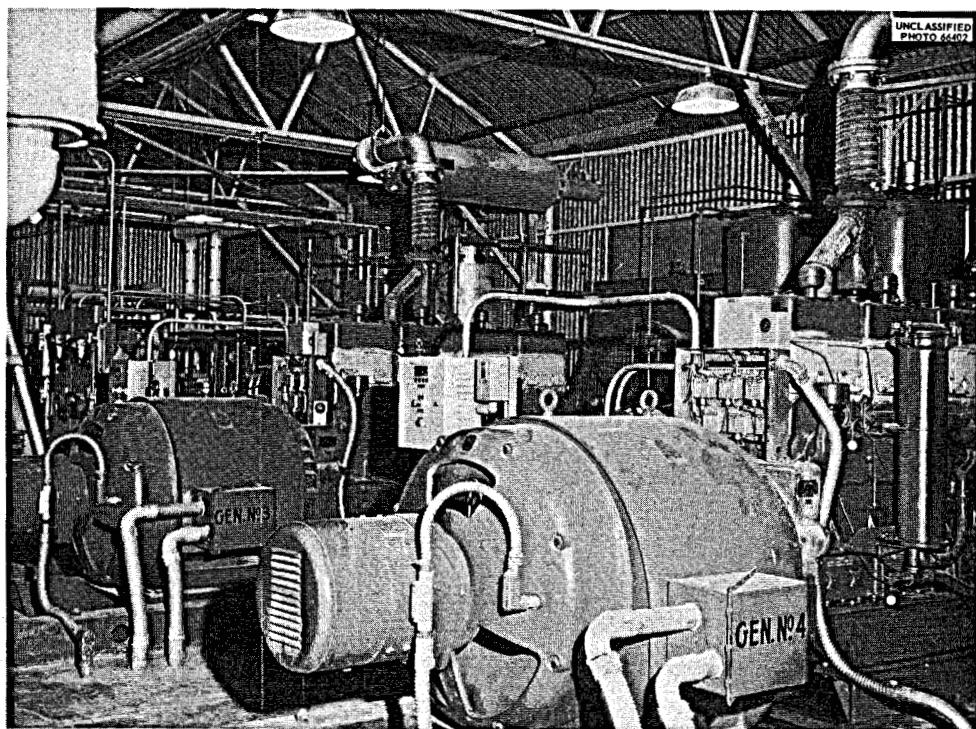


Fig. 20. Diesel Generator Installation.

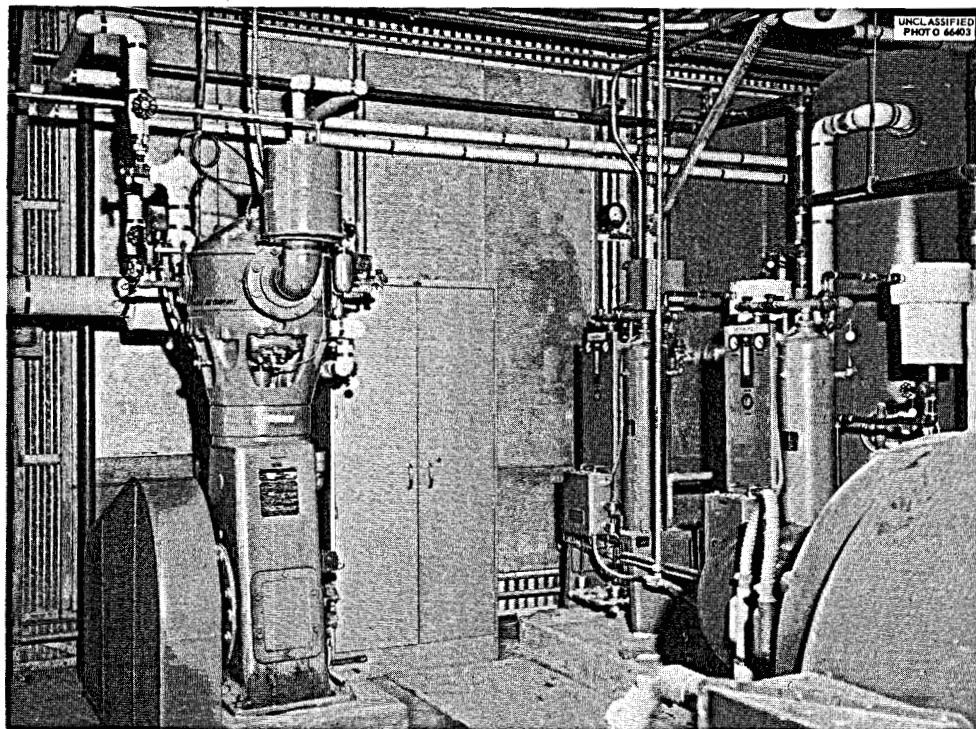


Fig. 21. Helium Cover-Gas Treatment Equipment and Instrument Air Compressor.

The tower-water-to-treated-water heat exchanger is located along the west end inside the building.

The instrument air compressors and auxiliary air compressor are along the south side (see Fig. 21).

Installation of equipment in this area is completed.

#### Switch House and Motor Generator House

The switch house, which is 30 by 36 ft, adjoins the diesel house on the west and Building 7503 on the east. It has corrugated asbestos siding with a flat roof at the 852-ft elevation. The floor elevation is 840 ft.

The main switchgear for the 480-v feeder lines and the diesel generator controls are located in this area.

A 15- by 16-ft motor generator room, located north of the east end of the switch house and accessible from the switch house, contains two motor generators and their control panels. The process power substation is located west of the motor generator room.

Electrical installation in this area is completed.

#### Inlet Air Filter House

The high-bay inlet air filter and steam heating units are located in the inlet air filter house. This 12- by 20-ft concrete block building is located just west of the 7503 building. The floor elevation is 840 ft 6 in., and the flat roof is at an elevation of 850 ft 11 in.

#### Procurement and Fabrication of Major Components

When project status was attained for the MSRE, it was thought desirable to have the major components for the salt circulating systems made by industrial fabricators who were experienced in producing reactor components such as nuclear code vessels, heat exchangers, reactor containment vessels, etc. Engineering drawings and specifications, welding qualification procedures, and inspection procedures were prepared which were consistent with this approach.

Requests for bids on the reactor vessel, radiator, heat exchanger, and the several salt storage tanks were sent out to several companies considered to have the greatest amount of experience in nuclear component fabrication. After these companies had reviewed the drawings and specifications, a prebid conference was held at which representatives of these companies were briefed on the properties and fabricability of INOR-8 and interpretations of the specifications were made, if unclear to any prospective bidder.

Since INOR-8 was a new alloy, and since considerable precision machining and flaw-free welding were required, all companies invited declined to submit lump-sum bids for producing the components. Further negotiations disclosed that most felt too many uncertainties existed to justify lump-sum bids, although most had considerable experience with other alloys of the Hastelloy family. Some of the companies expressed an interest in producing the components under a cost-plus-fixed-fee contract. It was decided, however, to fabricate the components in Union Carbide Corporation shops, since craftsmen in these shops had several years' experience in INOR-8 fabrication and the shops were well equipped for fabrication of units of this size. The major portion of the INOR-8 component fabrication was done in the Y-12 shops.

#### Special Materials Procurement

All contracts for special materials were fixed price and ordered on the basis of competitive bids.

INOR-8. Most of the INOR-8 plate, bar stock, and tube rounds were produced by the Stellite Division of Union Carbide Corporation. Some of the ingots were produced by the International Nickel Company and Alvac Metals. The extrusion of seamless pipe and tubing was done by Michigan Seamless Tube Company, Wall Tube Company, and the International Nickel Company. Forged pipe fittings were produced by Taylor Forge. Approximately two years were required to complete all INOR-8 procurement.

Typical INOR-8 prices were:

|                            |                  |
|----------------------------|------------------|
| Rolled plate               | \$3.00 per pound |
| Forged bar                 | 4.50 per pound   |
| Tubing (1/2-in. diam)      | 6.00 per foot    |
| Pipe (5-in.-diam sched 40) | 225.00 per foot  |

Graphite. The 6000 lb of special graphite bars for the MSRE core were extruded, processed, and machined by the Carbon Products Division of Union Carbide Corporation for a fixed price of about \$194,000.

This graphite, which has low salt absorption and low permeability to gases, has been produced only in the laboratory and in small sizes prior to this order. Approximately 2-3/4 years were required to produce the final machined bars to the quality and tolerances required for the MSRE core assembly.

Fabrication. Although some development of fabrication methods and procedures was required, in general it was found that INOR-8 presented no more problems than Inconel or various stainless steels if procedures were closely followed.

The Y-12 shops, during peak periods, used ten welders qualified in INOR-8 welding procedures. These welders made 1300 x-ray-quality welds requiring only 55 repairs. Out of 3300 welds which required liquid penetrant inspection of each pass, only 1015 minor repairs to removed dye indications were required.

To meet the peak demands, during the 2-1/2-year fabrication period, approximately 40 craftsmen were utilized at Y-12 and 10 craftsmen at the X-10 and Paducah shops.

Representative costs for making reactor-grade welds to MSRE specifications are: (1) precision fitting and welding of top head to reactor vessel (60 in. diam by 1 in. thick), about \$2900, or \$187 per foot of weld; and (2) fitting to reasonable tolerances and welding of bottom head to fuel storage tank (50 in. diam by 1/2 in. thick), about \$620, or \$47 per foot of weld.

Data concerning cost of major components are shown in Table 4.

Fabrication Process. A photographic presentation of the completed major components is made in the following pages, together with pictures of the more significant stages of fabrication.

Drain Tanks. Figure 22 shows the rolled shell for a typical drain tank. These shells were rolled, machined, and welded to a tolerance of approximately 1/16 in. in order to give good weld fit-up with the beads. Figure 23 shows the bayonet tubes assembled to the top head of a fuel drain tank, and Fig. 24 shows the completed tank. The steam dome cooling assembly is shown in Fig. 25.

Table 4. Cost of Major MSRE Components

| Component                                     | Weight<br>(lb) | WO Cost<br>(dollars) | INOR-8 Cost<br>(dollars) | Graphite<br>Cost<br>(dollars) |
|---|----------------|----------------------|--------------------------|-------------------------------|
| Reactor                                       | 9,500          | 200,000              | 50,000                   | 200,000                       |
| Heat exchanger                                | 2,100          | 80,000               | 28,000                   |                               |
| Radiator (less enclosure)                     | 3,500          | 62,000               | 61,000                   |                               |
| Fuel flush tank                               | 3,200          | 22,000               | 20,000                   |                               |
| Fuel drain tanks and steam domes <sup>a</sup> | 11,600         | 108,000              | 90,000                   |                               |
| Coolant drain tank                            | 1,800          | 19,000               | 9,000                    |                               |

<sup>a</sup>Two duplicate units.

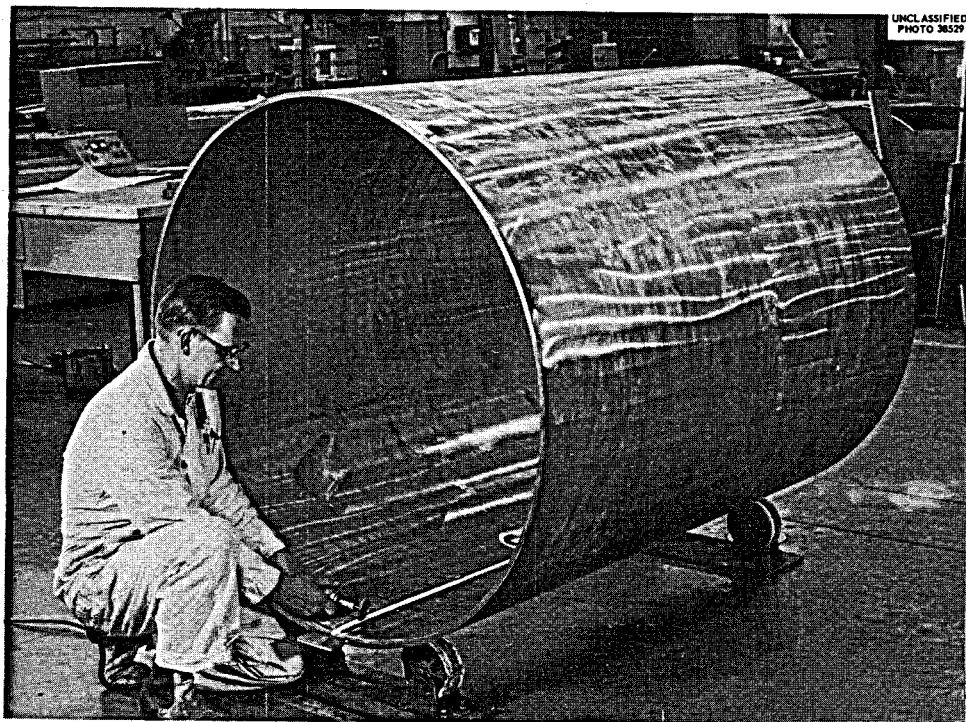


Fig. 22. Typical Rolled Shell for Fuel Drain Tank.

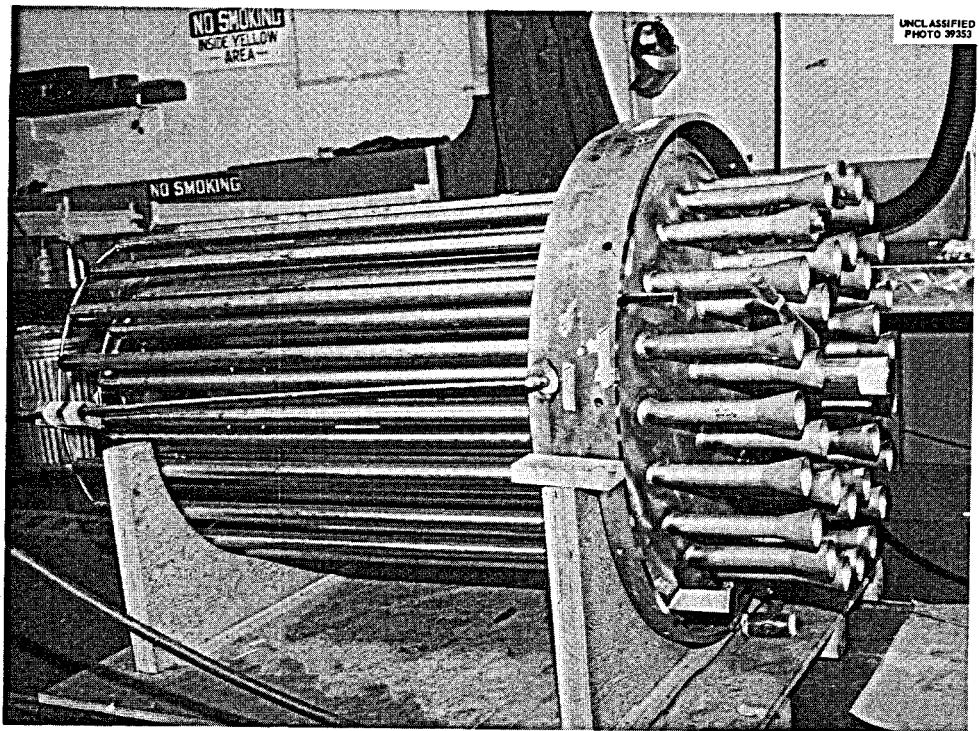


Fig. 23. Fuel Drain Tank Bayonet Tubes Assembled to Top Head.

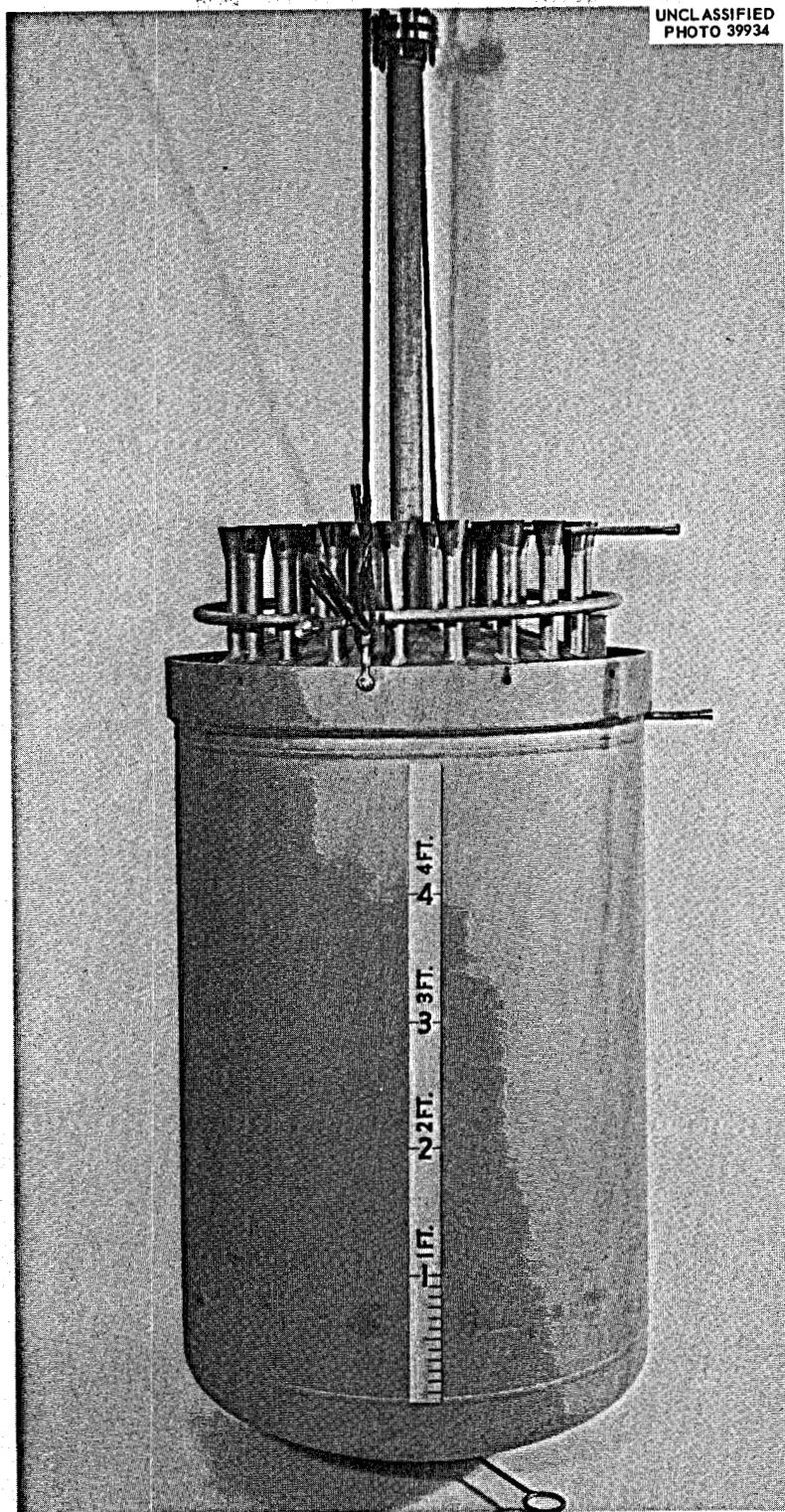


Fig. 24. Completed Fuel Drain Tank.

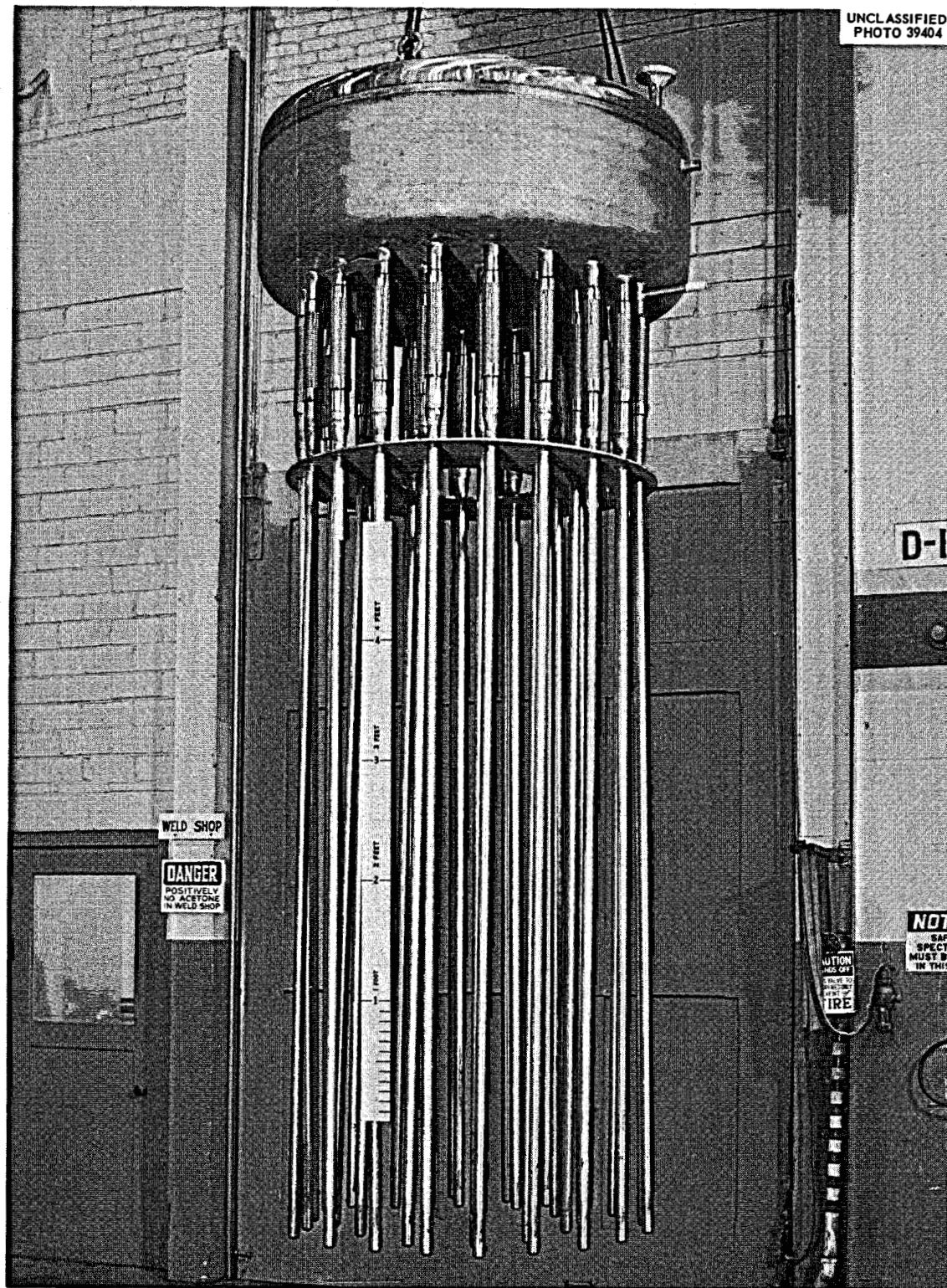


Fig. 25. Completed Steam Dome Cooler for MSRE Drain Tanks.

Heat Exchanger. The shell, entrance-exit plenum, and tube bundle are shown in Fig. 26, and Fig. 27 shows the completed unit. The semi-automatic tube-to-tube-sheet welding process is shown in Fig. 28.

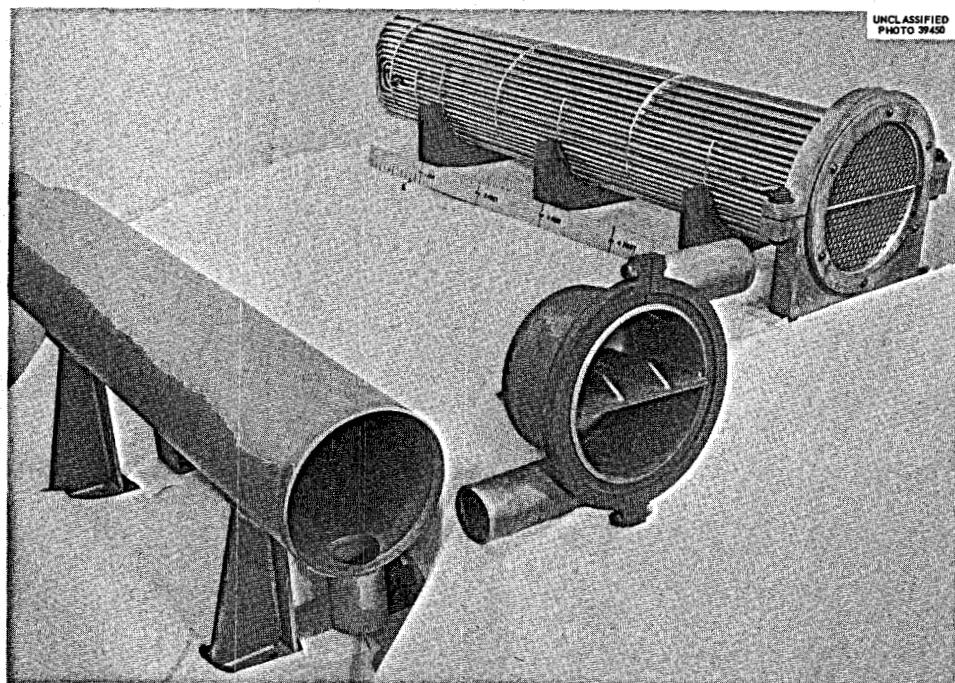


Fig. 26. Components for MSRE Primary Heat Exchanger.

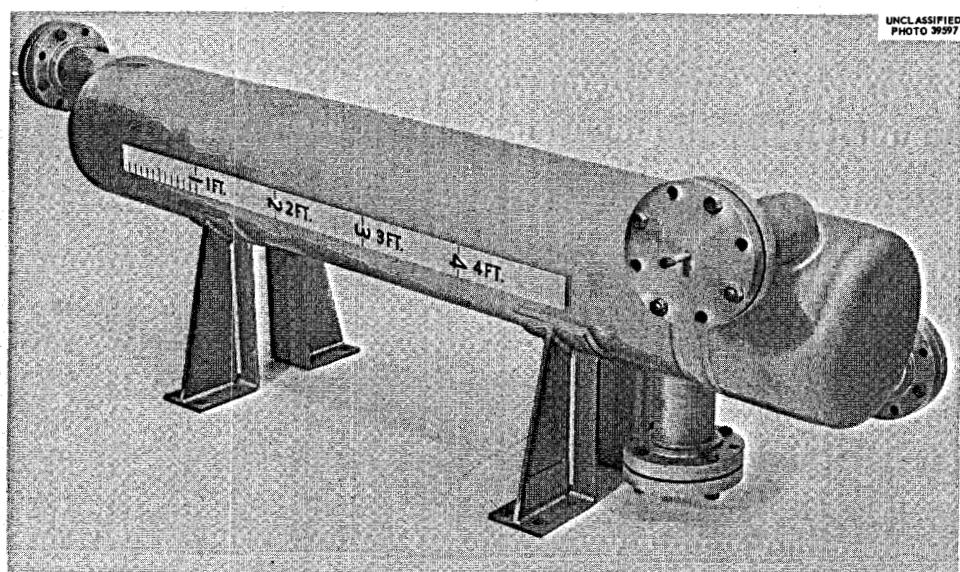


Fig. 27. Completed Heat Exchanger.



Fig. 28. Welding Heat Exchanger Tubes to Tube Sheet.

Pumps. The MSRE fuel and coolant circulating pumps are very similar. Figure 29 shows the fuel pump bowl and volute in process. The rotary element assembly is shown in Fig. 30. The completed pump and drive motor assembly is shown during hot performance tests in Fig. 31.

Radiator. The radiator with its furnace enclosure, shown in Fig. 32, is one of the more complex MSRE components from the standpoint of fabrication. The main header in its early fabrication stage is shown in Fig. 33. A closeup of the tube-header assembly in process, with sheathed thermocouples attached, is shown in Fig. 34. The completed coil assembly, prior to its placement in the enclosure, is shown in Fig. 35.

Reactor and Core. As with all other MSRE components, extreme care and critical inspection went into the fabrication of the reactor vessel and core assembly. Figure 36 shows the machining of the bottom head for the vessel, and Fig. 37 shows the attachment of vanes to remove the swirl from the fuel and to direct its flow through the graphite core. Figure 38 shows the flow distribution and Fig. 39 the vessel ready for installation of the graphite core. The core assembly at the halfway point is shown in Fig. 40 and the completed assembly in its can in Fig. 41. The reactor access nozzle and the control rod thimbles are shown during fabrication in Fig. 42. The completed control rod thimble assembly is shown in Fig. 43, prior to final attachment to the completed vessel, which is shown in Fig. 44 ready for shipment to the reactor installation site.

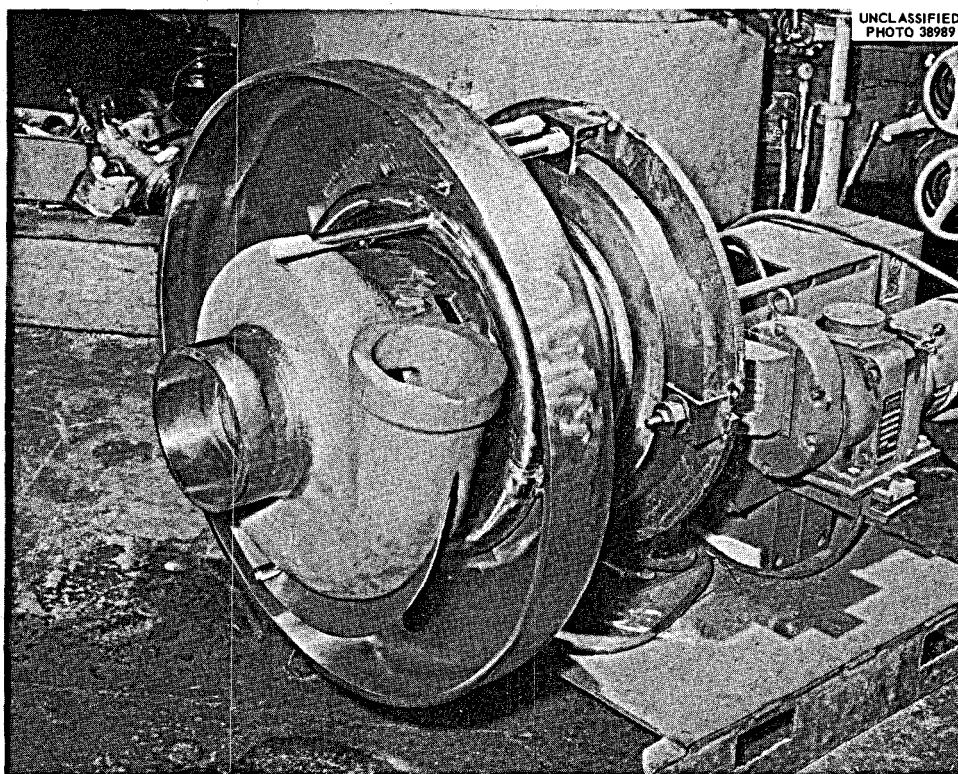


Fig. 29. Fabrication of Fuel Pump Bowl and Volute.

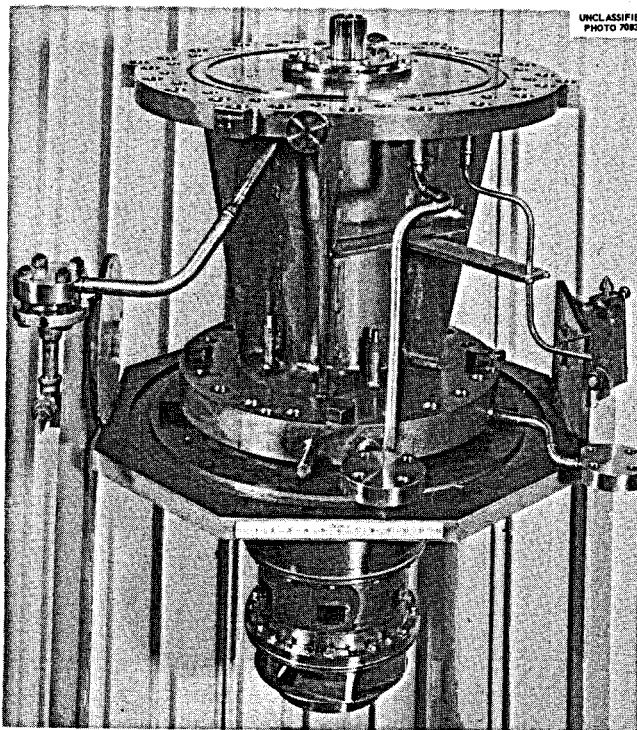


Fig. 30. Fuel Pump Rotary Assembly.

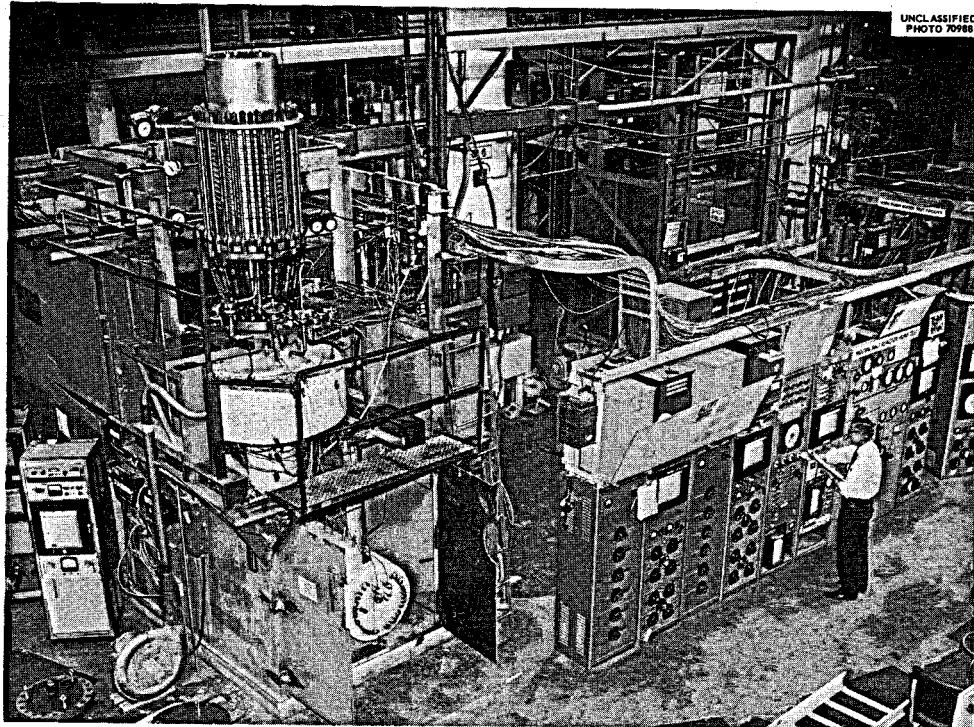


Fig. 31. Completed Fuel Pump on Hot Test Stand.

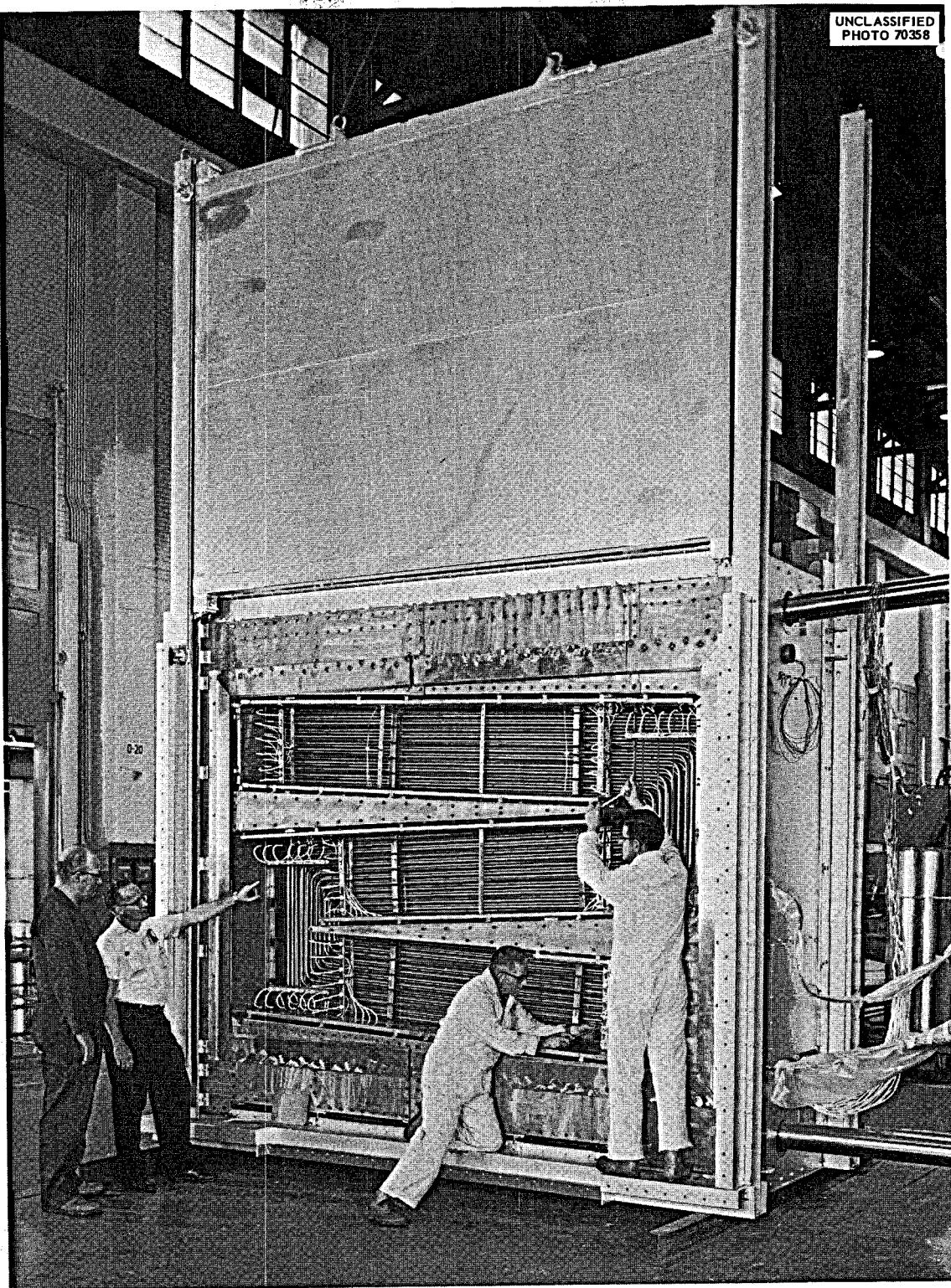


Fig. 32. MSRE Radiator and Furnace Enclosure.

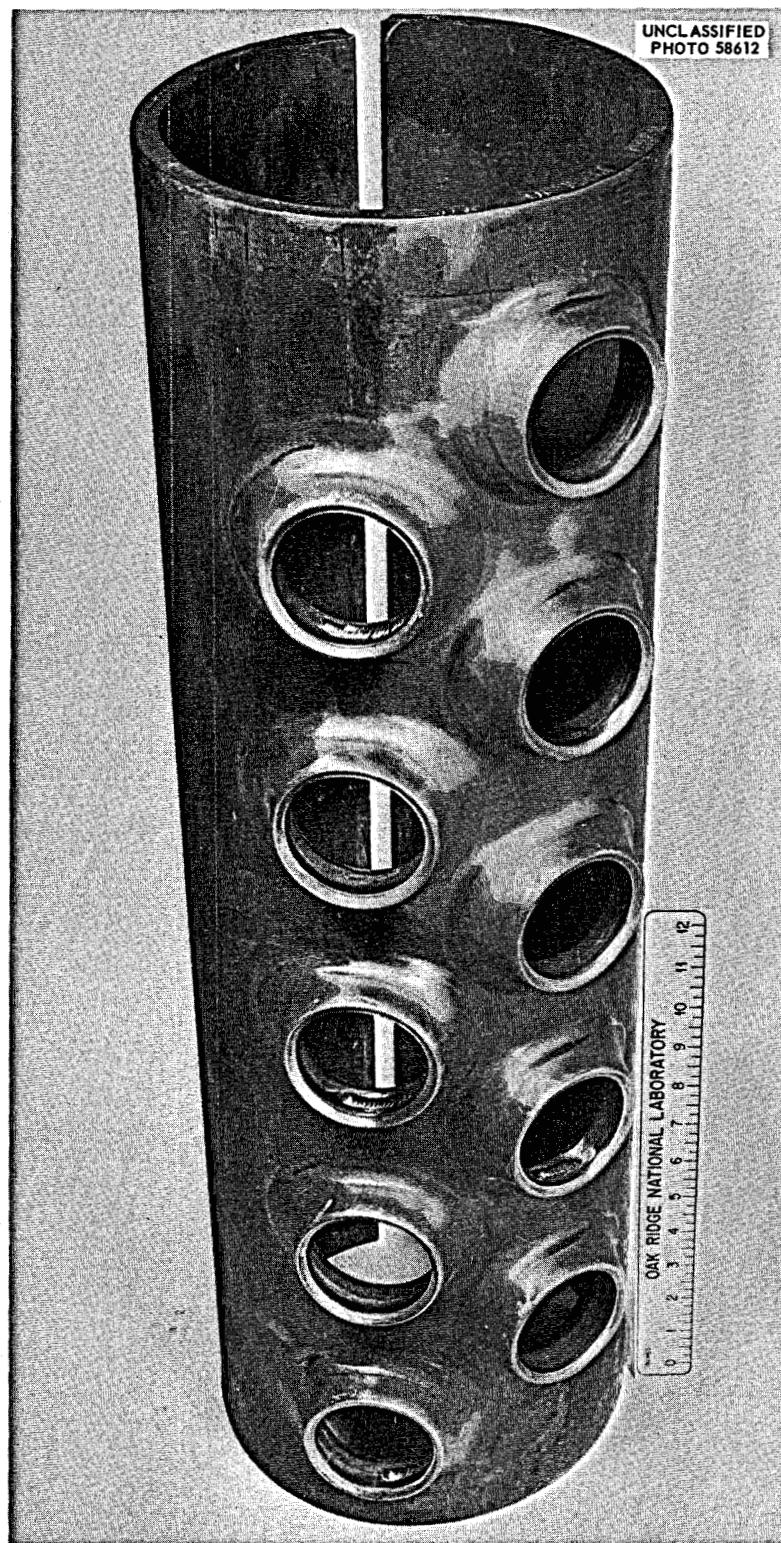


Fig. 33. Main Header for the MSRE Radiator In Process.

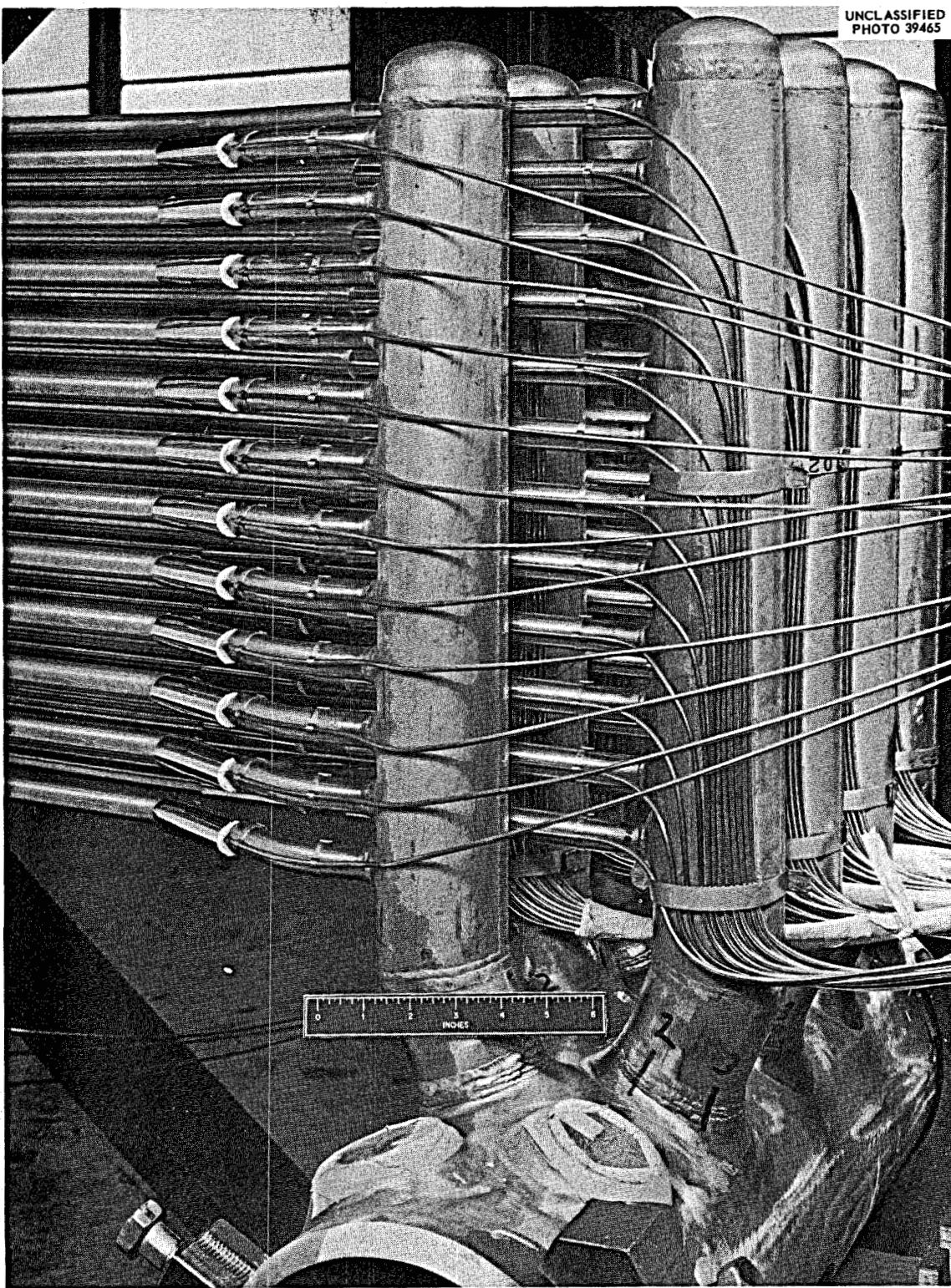


Fig. 34. Radiator Tube-to-Header Assembly with Thermocouples Attached to Each Tube.

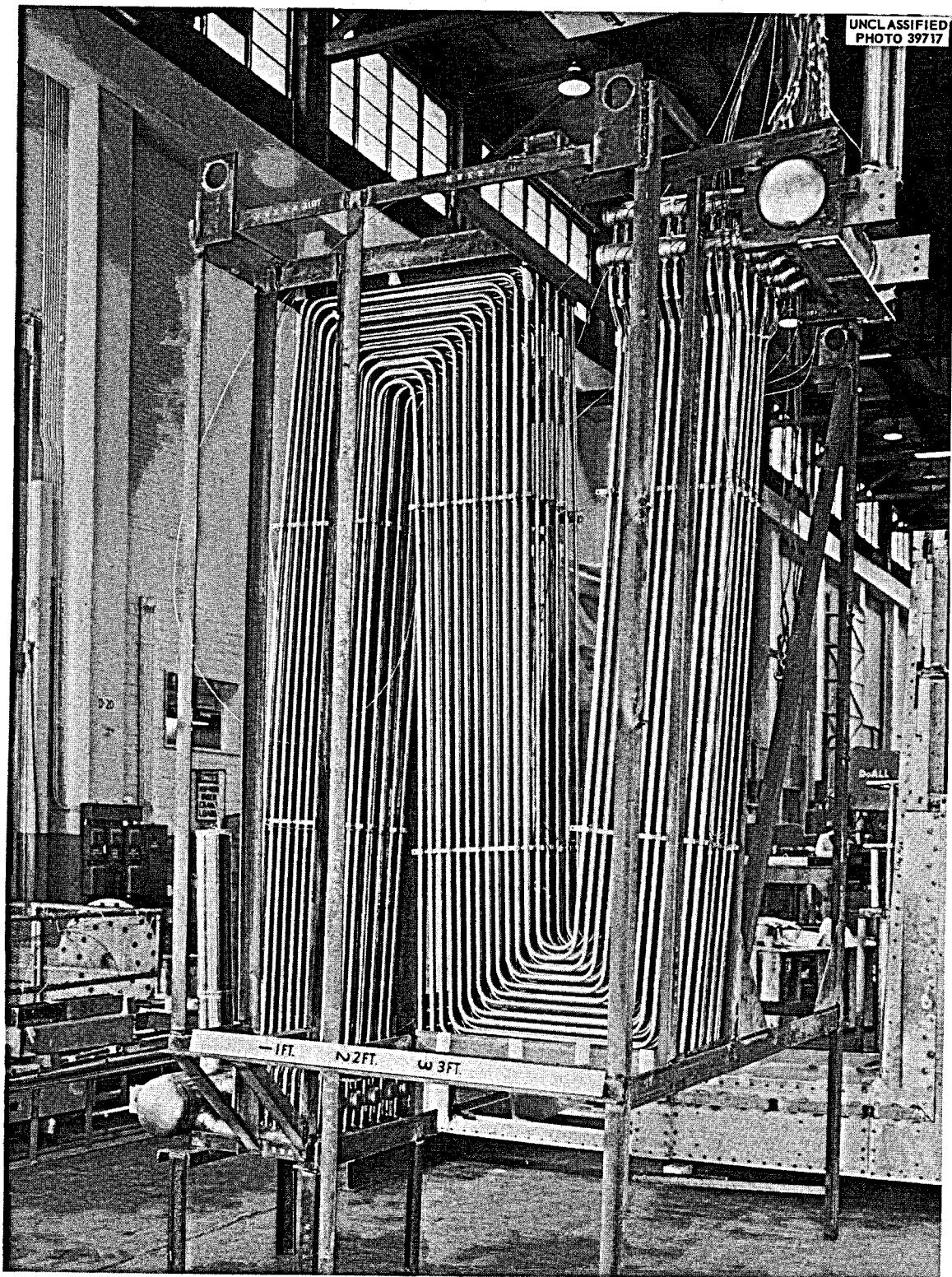


Fig. 35. Completed Radiator Coil.

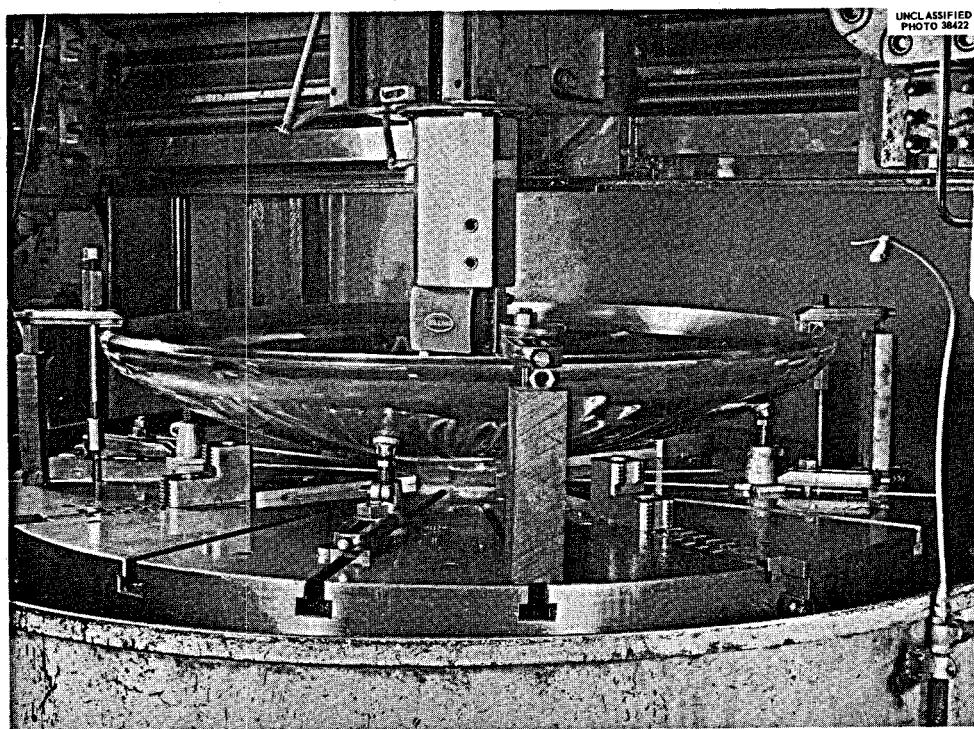


Fig. 36. Machining Bottom Head for Reactor Vessel.



Fig. 37. Attachment of Flow-Straightening Vanes to Reactor Vessel.

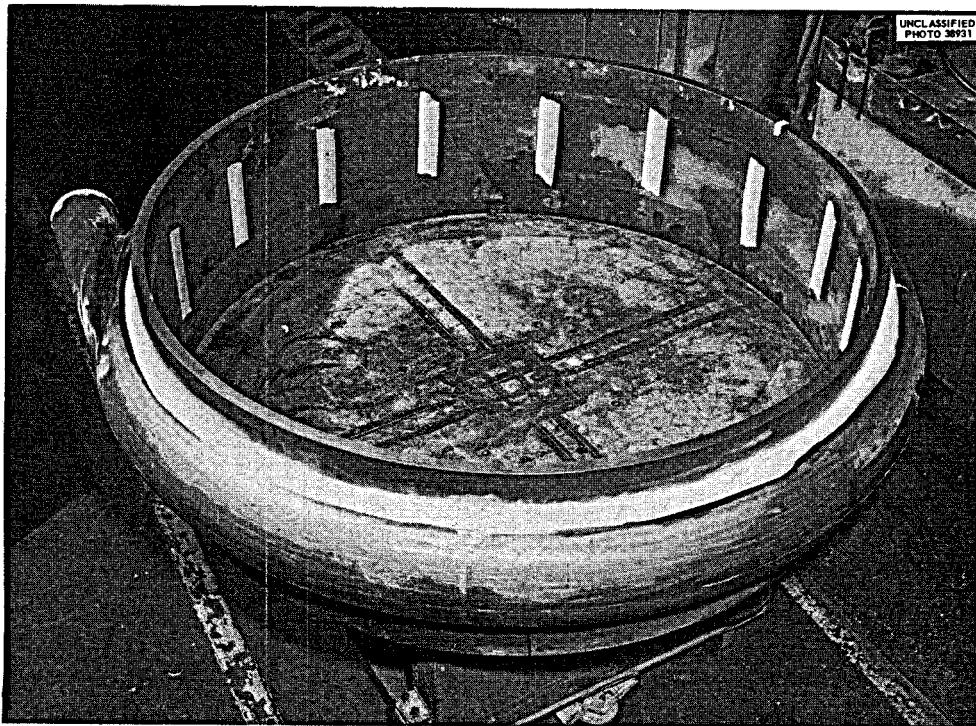


Fig. 38. Reactor Vessel Inlet Nozzle and Flow Distribution.

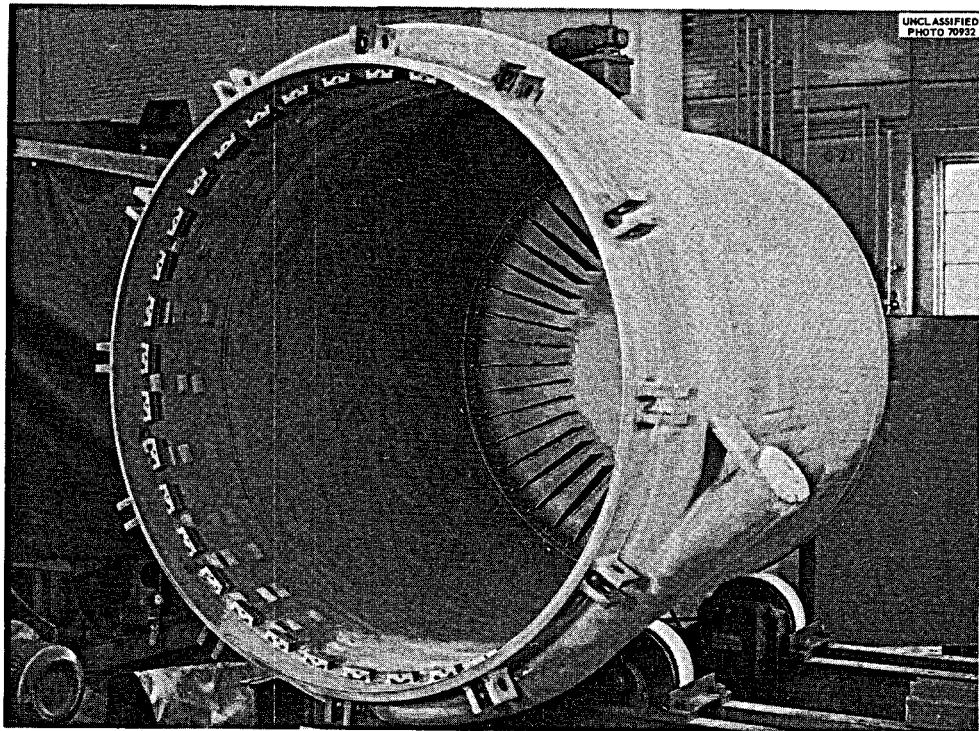


Fig. 39. Reactor Vessel Ready to Accept Graphite Core Assembly.

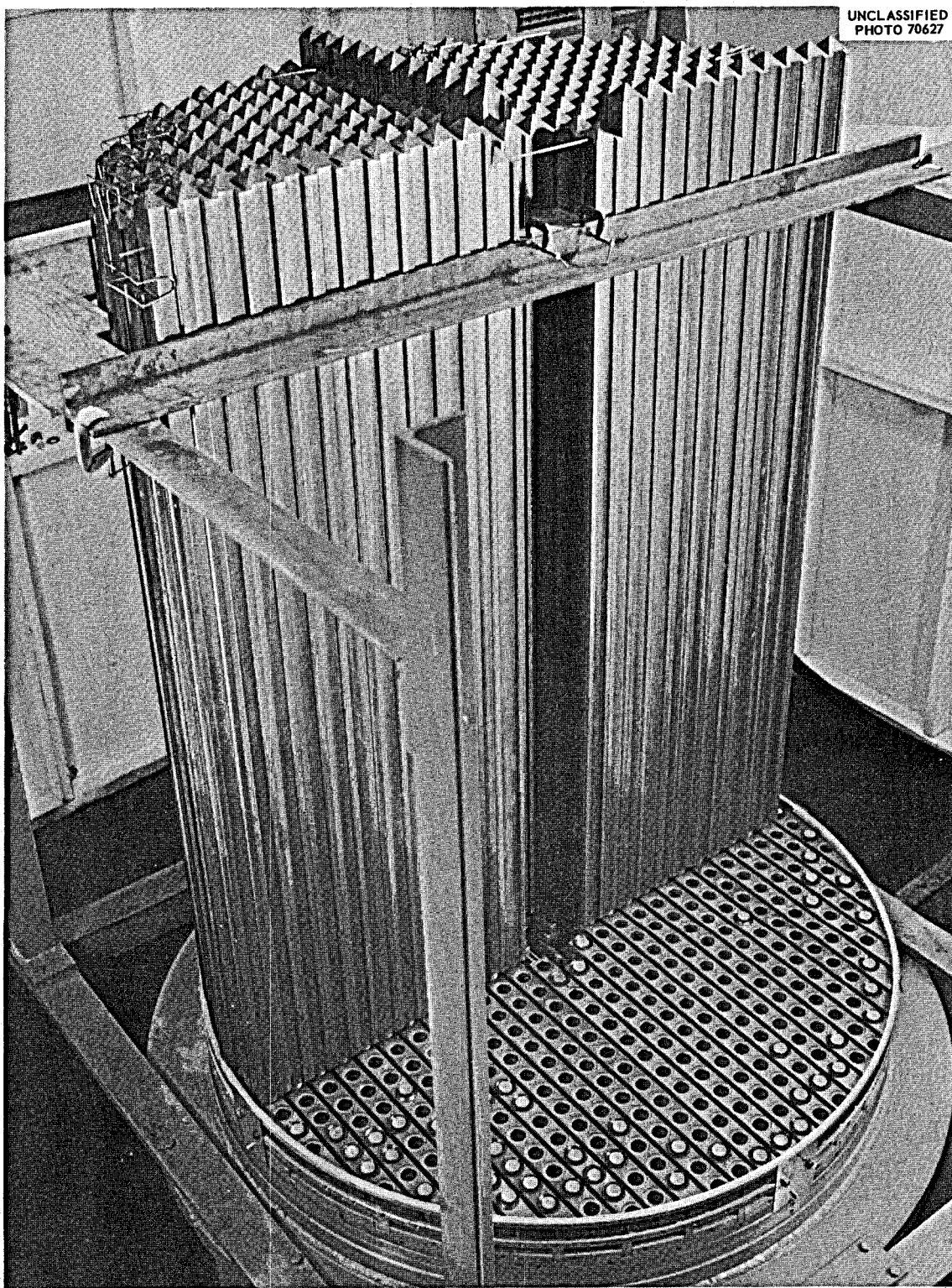


Fig. 40. Assembly of Graphite Bars into MSRE Core.

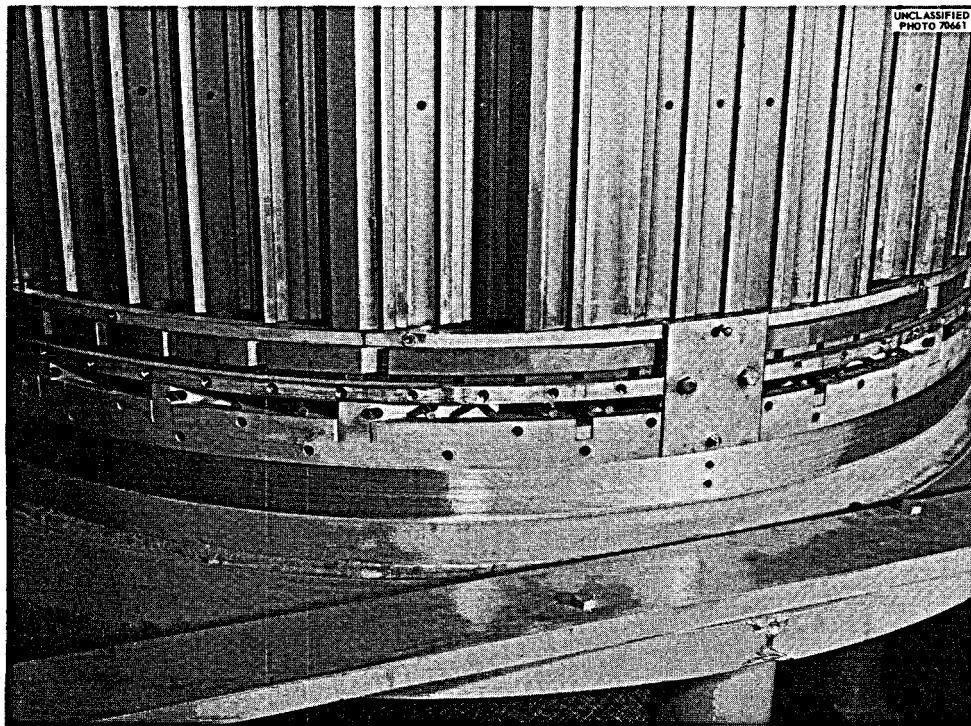


Fig. 41. Completed Graphite Core Assembly.

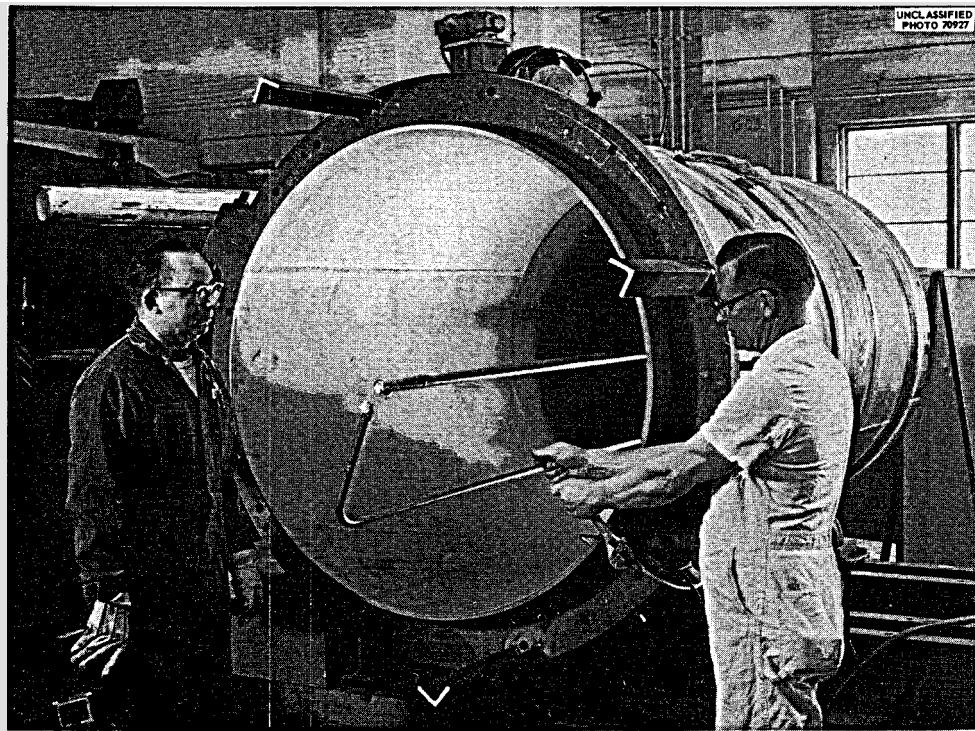


Fig. 42. Reactor Access Nozzle and Control Rod Thimbles In Process.

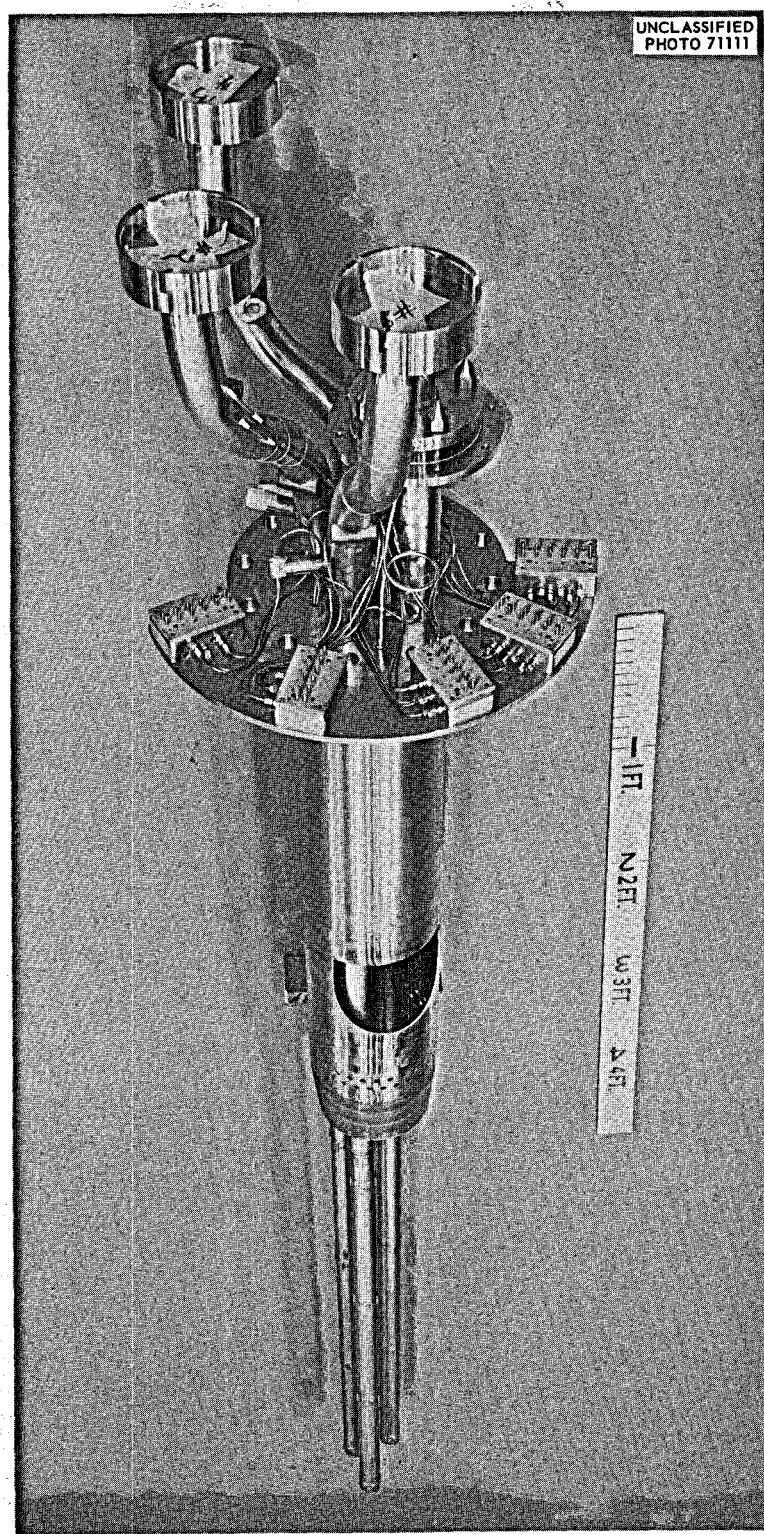


Fig. 43. Completed Control Rod Thimble Assembly.

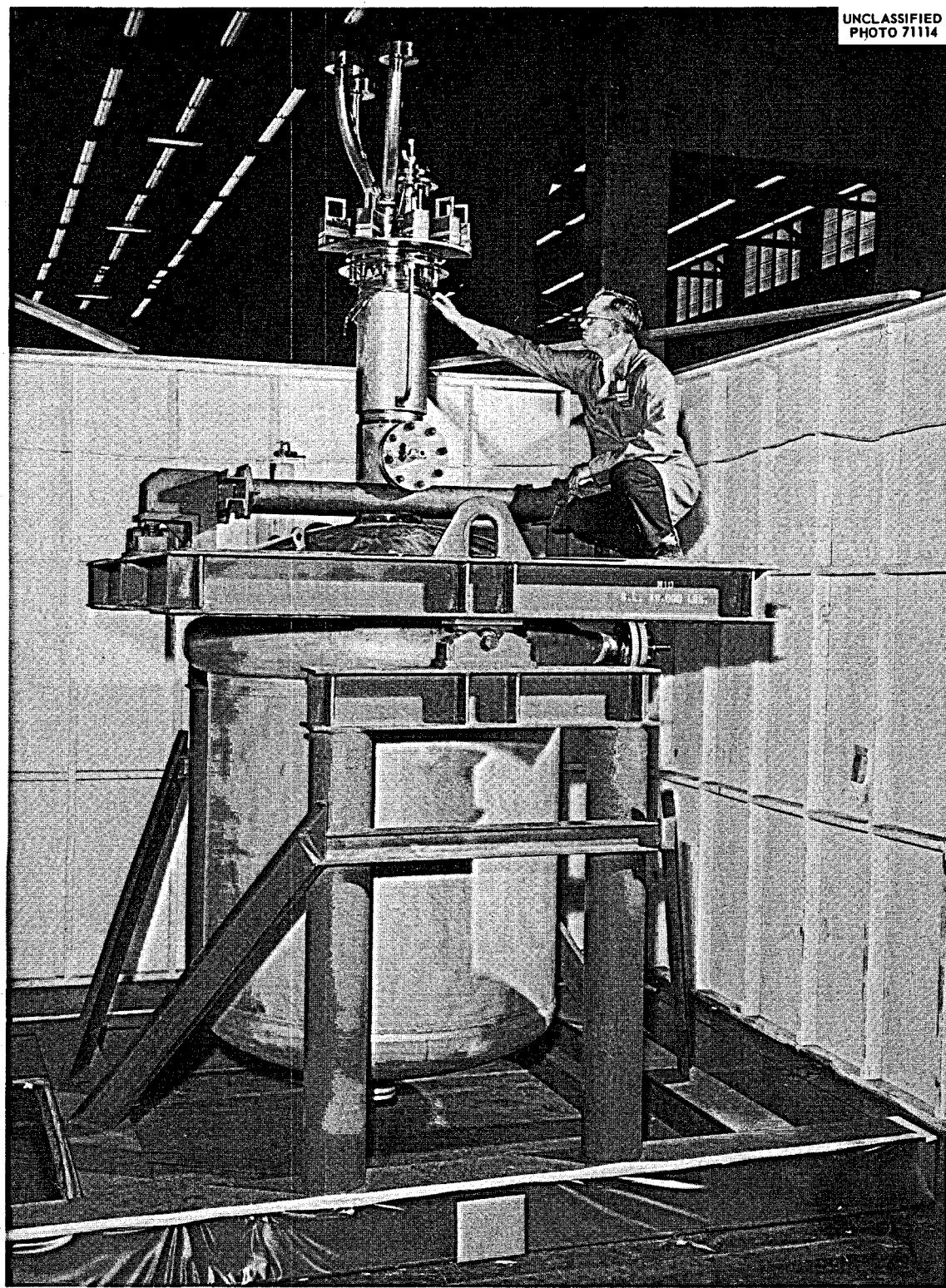


Fig. 44. Reactor Completed and Ready for Shipment to MSRE Site.

NUCLEAR CHARACTERISTICS OF THE MSRE<sup>1</sup>

R. J. Engel

Basis of Core Design

The basic concept of the MSRE is a cylindrical vessel containing a graphite matrix for neutron moderation through which a molten-salt fuel is circulated. To provide a logical basis for the core design, several preliminary studies were made to establish the dependence of a limited number of nuclear properties on important core parameters. Three combinations of the components of the fuel mixture were considered in these calculations; the nominal compositions and densities are listed in Table 1.

Effect of Core Size

The effect of core size on the critical concentration and mass of uranium was examined for a series of cores containing 8 vol % of type I fuel (Table 1). Calculations were made for two core heights (5.5 and 10 ft) and four diameters (3.5, 4.0, 4.5, and 5.0 ft). The resultant critical concentrations (in mole % total uranium) and critical masses (in kilograms of  $^{235}\text{U}$ ) are shown in Fig. 1. No allowance was made for uranium inventory in the circulating loop outside the core.

Effect of Fuel Volume Fraction

Two preliminary studies of the effect of fuel volume fraction were made in the range from 8 to 16 vol % using fuel mixtures I and II. These were superseded by a more detailed study using fuel III after mechanical design and chemical studies had established firmer values for the core size and fuel composition. The core used had a 27.7-in. radius and was 63 in. high. Uniform fuel volume fractions from 0.08 to 0.28 were considered, and system inventories were based on a fuel holdup of 38.4 ft<sup>3</sup> outside the core. In addition to the calculations of critical mass and inventory, preliminary calculations were made of the fuel temperature coefficient of reactivity and the reactivity effect associated with permeation of 7% of the graphite volume by fuel salt.\* The results of this study are summarized in Table 2 for the fuel volume fraction range from 12 to 28%.

Miscellaneous Studies

A number of calculations were made to evaluate at least the critical concentrations and masses for several other core configurations. In some cases neutron flux distributions were also obtained. The configurations considered included:

\*This fraction was at that time the estimated fraction of the graphite volume accessible to kerosene.

Table 1. Nominal Fuel Compositions and Densities Used in MSRE Survey Calculations

| Fuel type                    | I   | II  | III  |
|------------------------------|-----|-----|------|
| Composition, mole %          |     |     |      |
| LiF <sup>a</sup>             | 64  | 64  | 70   |
| BeF <sub>2</sub>             | 31  | 31  | 23   |
| ThF <sub>4</sub>             | 4   | 0   | 1    |
| ZrF <sub>4</sub>             | 0   | 4   | 5    |
| UF <sub>4</sub> <sup>b</sup> | 1   | 1   | 1    |
| Density, g/cm <sup>3</sup>   |     |     |      |
|                              | 2.2 | 2.2 | 2.47 |

<sup>a</sup>0.003% <sup>6</sup>Li, 99.997% <sup>7</sup>Li.

<sup>b</sup>93.5% <sup>235</sup>U, 6.5% <sup>238</sup>U.

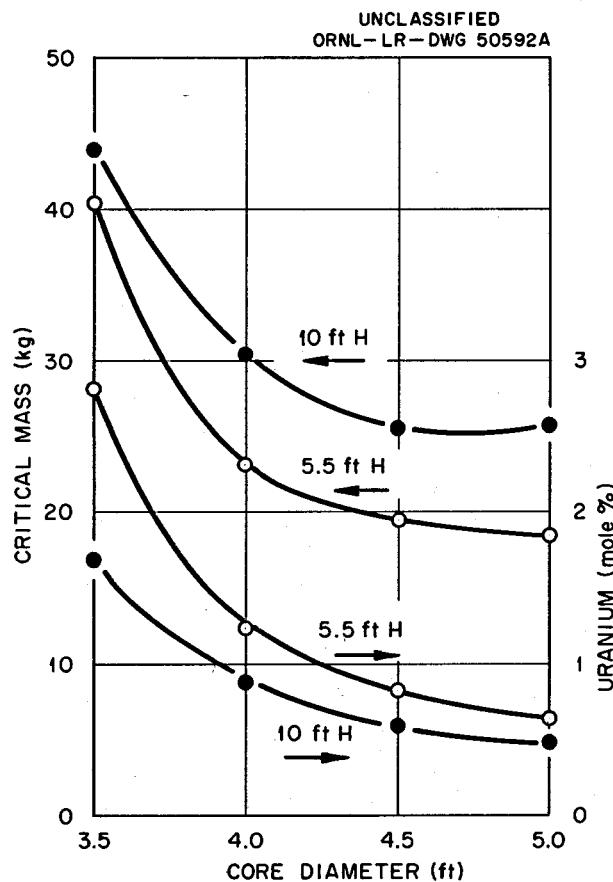


Fig. 1. Critical Concentration and Mass as a Function of Core Size.

Table 2. Effect of Fuel Volume Fraction on Nuclear Characteristics of MSRE

Core dimensions: radius, 27.7 in.; height, 63 in.

Nominal composition of fuel: LiF-BeF<sub>2</sub>-ZrF<sub>2</sub>-ThF<sub>4</sub>-UF<sub>4</sub>  
(70-23-5-1-1 mole %)

Temperature: 1200°F

Fuel density: 2.47 g/cm<sup>3</sup>

Graphite density: 1.90 g/cm<sup>3</sup>

| Fuel fraction, vol %   | 12    | 14    | 16    | 20    | 24    | 28    |
|--|-------|-------|-------|-------|-------|-------|
| Critical fuel concentration, mole % U                          | 0.296 | 0.273 | 0.257 | 0.238 | 0.233 | 0.236 |
| Critical mass, kg of <sup>235</sup> U                          | 11.0  | 11.8  | 12.7  | 14.8  | 17.4  | 20.5  |
| System <sup>235</sup> U inventory, <sup>a</sup> kg             | 51.0  | 48.6  | 47.4  | 47.1  | 48.7  | 52.4  |
| Fuel temperature coeff., ( $\delta k/k$ )/°F ( $\times 10^5$ ) | -3.93 | -3.83 | -3.70 | -3.44 | -3.16 | -2.86 |
| Permeation effect, <sup>b</sup> % $\delta k/k$                 | 11.4  | 9.7   | 8.3   | 6.1   | 4.6   | 3.5   |

<sup>a</sup>Core plus 38.4 ft<sup>3</sup> of fuel.

<sup>b</sup>Permeation by fuel salt of 7% of graphite volume.

1. Cores containing two concentric regions with different fuel volume fractions. Three combinations were evaluated.
2. Cores containing three concentric regions with different fuel volume fractions. Thirteen combinations were evaluated.
3. Cores in which the solid moderator was all in a reflector or partly in a reflector and partly in an island at the center of the core. Graphite, beryllium, and beryllium oxide were evaluated as solid moderators for both configurations.
4. Cores in which the fuel was confined within INOR-8 tubes. Three fuel volume fractions were evaluated for each of three tube thicknesses.

None of these configurations showed any significant advantage over the uniform, one-region core.

### Choice of Final Configuration

At an early stage of the design it was decided that the core would be approximately 4.5 ft in diameter and 5.5 ft high, after calculations showed that the critical mass was relatively insensitive to core size in this region (Fig. 1). A fuel volume fraction of 0.225 was chosen because it was near the minimum critical concentration of uranium and had a favorably low reactivity effect due to fuel permeation of the graphite. (The nominal fuel fraction was 0.24, but this was reduced to 0.225 because of mechanical considerations regarding the graphite moderator bars.)

### Basic Nuclear Properties

#### Description of Core

The final design of the core and reactor vessel is shown in Fig. 6 in the preceding paper. Fuel salt enters through a flow distributor near the top of the vessel and flows downward through an annular region outside the graphite to the lower head. Antiswirl vanes in the lower head direct the flow radially inward before it turns up to enter the fuel channels. After passing through the moderated portion of the core, the fuel leaves the reactor vessel from the upper head. The graphite moderator is supported by an INOR-8 grid which is suspended from the core can. The channeled region of the core consists of 2-in.-square, vertical graphite stringers, with half-channels machined into each face to provide fuel passages. The regular pattern is broken near the axis of the core, where three control rod thimbles and a sample assembly are located. Figure 2 shows a typical fuel channel and the arrangement around the core axis.

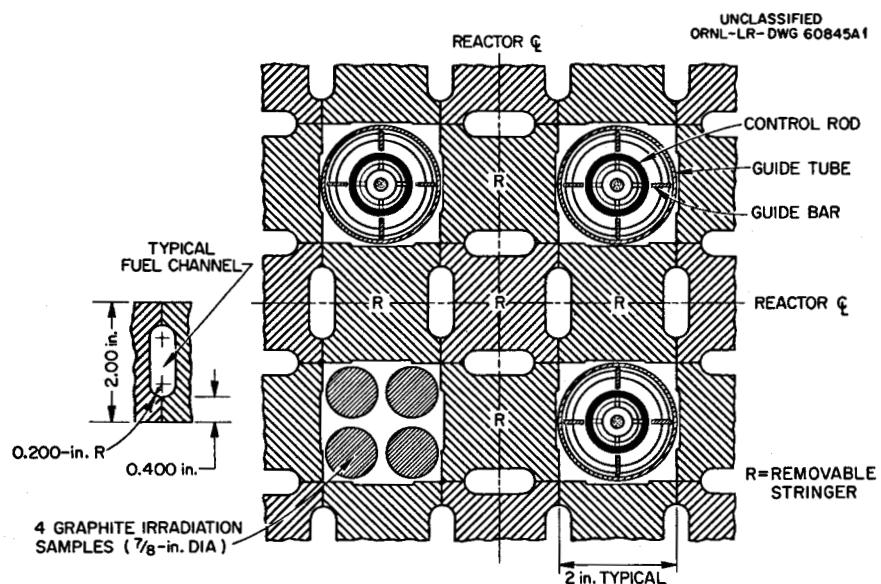


Fig. 2. MSRE Control Rod Arrangement and Typical Fuel Channel.

### Methods of Calculation

Most of the nuclear characteristics of the core were calculated for a somewhat simplified representation of the actual design which included as much detail as was practical. The actual configuration was approximated by a two-dimensional model in R-Z geometry (cylinder with angular symmetry) containing 20 regions with different compositions based on the fractions of salt, graphite, and structural material in each. Limitation of the model to two dimensions resulted in a large savings in computing time, and the representation was considered adequate for most purposes. The principal shortcoming of the model was the representation of the three control rod thimbles. These were approximated by a single, cylindrical shell of metal around a cylinder of low-density fuel to account for the extra fuel around the thimbles and the air inside them. Special mathematical models were used where accurate representation of the region around the control rods was required.

The nuclear characteristics of the reactor were calculated for three different fuel-salt mixtures with nominal compositions as shown in Table 3. In initial operation of the reactor a mixture very similar to fuel C will be used.

Table 3. MSRE Fuel Salts for Which Detailed Nuclear Calculations Were Made

| Fuel type                             | A     | B     | C     |
|---------------------------------------|-------|-------|-------|
| Salt composition, mole %              |       |       |       |
| LiF <sup>a</sup>                      | 70    | 66.8  | 65    |
| BeF <sub>2</sub>                      | 23.7  | 29    | 29.2  |
| ZrF <sub>4</sub>                      | 5     | 4     | 5     |
| ThF <sub>4</sub>                      | 1     | 0     | 0     |
| UF <sub>4</sub> (approx)              | 0.3   | 0.2   | 0.8   |
| Uranium composition, at. %            |       |       |       |
| <sup>234</sup> U                      | 1     | 1     | 0.3   |
| <sup>235</sup> U                      | 93    | 93    | 35    |
| <sup>236</sup> U                      | 1     | 1     | 0.3   |
| <sup>238</sup> U                      | 5     | 5     | 64.4  |
| Density at 1200°F, lb/ft <sup>3</sup> | 144.5 | 134.5 | 142.7 |

<sup>a</sup>99.9926% <sup>7</sup>Li, 0.0074% <sup>6</sup>Li.

Multigroup Calculations. The critical uranium concentration for each fuel was calculated by the use of MODRIC, a one-dimensional, multi-group neutron diffusion code. This program was used with 32 fast-neutron energy groups and a thermal energy cutoff at 0.4 ev. Fast group cross sections for most elements were generated by the use of GAM-I. However, the cross-section library that was available for this program did not include data for  $^{6}\text{Li}$ ,  $^{7}\text{Li}$ , and  $^{19}\text{F}$ . The slowing-down effects of these isotopes were simulated with an equivalent amount of oxygen, and absorption cross sections were compiled separately from basic data. Average cross sections for the thermal energy group were computed by the use of another program, THERMOS.

In addition to the critical concentrations, the MODRIC calculations produced sets of two-group constants for each region of the 20-region model. Three one-dimensional calculations were required to provide the necessary constants for all the regions with each fuel mixture. The MODRIC calculations also produced a neutron energy spectrum for each region (normalized to 1 neutron produced in the reactor).

Two-Group Calculations. Absolute spatial flux distributions at 10 Mw were calculated for the complete 20-region model using the two-dimensional, two-group neutron diffusion code EQUIPOISE-3. This program also served as a check on the critical concentrations produced by the one-dimensional calculations.

Other Calculations. The reactivity changes associated with changes in fuel and graphite temperature, fuel and graphite density, uranium concentration, and  $^{135}\text{Xe}$  concentration and poison fraction were calculated for a one-region, two-group model of the core. This model was also used to investigate the effect of the thermal-neutron cutoff energy on the temperature coefficients. The latter study revealed that, for this system, the temperature coefficients of reactivity would be underestimated if the thermal energy cutoff were less than 1 ev.

#### Summary of Results

The basic nuclear characteristics of the MSRE with each of the three fuel mixtures are summarized in Table 4. The critical concentrations shown are the results of the MODRIC calculations. These concentrations gave values for  $k_{\text{eff}}$  of 0.993, 0.997, and 0.993 for fuels A, B, and C, respectively, when used in the EQUIPOISE program. The thermal-neutron fluxes are direct results of the EQUIPOISE calculations, as are the prompt-neutron lifetimes. The reactivity coefficients were obtained from the single-region calculations. The temperature coefficients in this table reflect the 1-ev thermal energy cutoff. Fuel and graphite temperature coefficients of reactivity were also computed for fuel C using the EQUIPOISE results. The values for fuel and graphite were, respectively, 3 and 15% lower than those obtained with the single-region model. However, the multiregion results are not necessarily more accurate because of assumptions that were made regarding the spatial dependence of the thermal-neutron spectrum.

Table 4. Nuclear Characteristics of MSRE with Various Fuels

|  | Fuel A                 | Fuel B                 | Fuel C                                     |
|--|------------------------|------------------------|--|
| Uranium concentration, mole %  |                        |                        |  |
| Clean, noncirculating  |                        |                        |  |
| $^{235}\text{U}$   | 0.291                  | 0.176                  | 0.291                                      |
| Total U  | 0.313                  | 0.189                  | 0.831                                      |
| Operating <sup>a</sup>   |                        |                        |  |
| $^{235}\text{U}$   | 0.337                  | 0.199                  | 0.346                                      |
| Total U  | 0.362                  | 0.214                  | 0.890                                      |
| Uranium inventory, <sup>b</sup> kg   |                        |                        |  |
| Initial criticality  |                        |                        |  |
| $^{235}\text{U}$   | 79                     | 48                     | 77   |
| Total U  | 85                     | 52                     | 218  |
| Operating <sup>a</sup>   |                        |                        |  |
| $^{235}\text{U}$   | 91                     | 55                     | 92   |
| Total U  | 98                     | 59                     | 233  |
| Thermal-neutron flux, <sup>c</sup> neutrons<br>$\text{cm}^{-2} \text{ sec}^{-1}$ |                        |                        |  |
| Maximum  | $3.31 \times 10^{13}$  | $5.56 \times 10^{13}$  | $3.29 \times 10^{13}$                      |
| Average in graphite-moderated regions  | $1.42 \times 10^{13}$  | $2.43 \times 10^{13}$  | $1.42 \times 10^{13}$                      |
| Average in circulating fuel  | $3.98 \times 10^{12}$  | $6.81 \times 10^{12}$  | $3.98 \times 10^{12}$                      |
| Reactivity coefficient <sup>d</sup>  |                        |                        |  |
| Fuel temperature, ( $^{\circ}\text{F}$ ) <sup>-1</sup>                           | $-3.03 \times 10^{-5}$ | $-4.97 \times 10^{-5}$ | $-3.28 \times 10^{-5}$                     |
| Graphite temperature, ( $^{\circ}\text{F}$ ) <sup>-1</sup>                       | $-3.36 \times 10^{-5}$ | $-4.91 \times 10^{-5}$ | $-3.68 \times 10^{-5}$                     |
| Uranium concentration  | 0.2526                 | 0.3028                 | 0.1754 <sup>e</sup><br>0.2110 <sup>f</sup> |
| $^{135}\text{Xe}$ concentration in core, (atom/barn-cm) <sup>-1</sup>            | $-1.28 \times 10^8$    | $-2.04 \times 10^8$    | $-1.33 \times 10^8$                        |
| $^{135}\text{Xe}$ poison fraction  | -0.746                 | -0.691                 | -0.752                                     |
| Fuel salt density  | 0.190                  | 0.345                  | 0.182                                      |
| Graphite density   | 0.755                  | 0.735                  | 0.767                                      |
| Prompt-neutron lifetime, sec   | $2.29 \times 10^{-4}$  | $3.47 \times 10^{-4}$  | $2.40 \times 10^{-4}$                      |

<sup>a</sup>Fuel loaded to compensate for 4% 8k/k in poisons.<sup>b</sup>Based on 73.2 ft<sup>3</sup> of fuel salt at 1200°F.<sup>c</sup>At operating fuel concentration, 10 Mw.<sup>d</sup>At initial critical concentration. Where units are shown, coefficients for variable x are of the form  $(1/k)/(dk/dx)$ ; other coefficients are of the form  $(x/k)/(dk/dx)$ .<sup>e</sup>Based on uranium isotopic composition of clean, critical reactor.<sup>f</sup>Based on highly (~93%) enriched uranium.

Table 5 summarizes the neutron balance for the reactor with fuel C at the clean, critical condition. The large leakage values illustrate the relatively small "nuclear size" of the MSRE. This factor has an important effect on the size of the temperature coefficients of reactivity because changes in neutron leakage with temperature contribute heavily to the coefficients in this reactor.

Figures 3 and 4 show, respectively, the axial and radial distributions (at the position of maximum thermal flux) of the two-group neutron fluxes at 10 Mw with fuel C. The zero position for the axial distributions is the bottom of the graphite matrix in the core. The thermal flux distribution in the main portion of the core (0 to 65 in.) is very closely approximated by a sine distribution with an effective core height of 78 in. The depression in the radial distribution of the thermal flux near the axis is caused by the control rod thimbles and the extra fuel that surrounds them.

Table 5. Neutron Balance for Fuel C at the Clean, Critical Condition  
(per  $10^5$  neutrons produced)

| Region         | Absorptions      |                  |                   |          |      |        |
|----------------|------------------|------------------|-------------------|----------|------|--------|
|                | $^{235}\text{U}$ | $^{238}\text{U}$ | Salt <sup>a</sup> | Graphite | INOR | Total  |
| Main core      | 45,459           | 7252             | 4364              | 795      | 1380 | 59,250 |
| Upper head     | 3,031            | 928              | 675               | 1        | 131  | 4,766  |
| Lower head     | 1,337            | 449              | 294               | 0        | 1480 | 3,560  |
| Downcomer      | 1,496            | 338              | 203               | 0        | 0    | 2,037  |
| Core can       | 0                | 0                | 0                 | 0        | 3635 | 3,635  |
| Reactor vessel | 0                | 0                | 0                 | 0        | 3056 | 3,056  |
| Total          | 51,323           | 8967             | 5536              | 796      | 9682 | 76,304 |

| Surface | Leakage |      |        |
|---------|---------|------|--------|
|         | Fast    | Slow | Total  |
| Top     | 1,991   | 10   | 2,001  |
| Sides   | 19,619  | 1004 | 20,623 |
| Bottom  | 1,068   | 4    | 1,072  |
| Total   | 22,678  | 1018 | 23,696 |

<sup>a</sup>Constituents other than  $^{235}\text{U}$  and  $^{238}\text{U}$ .

### Later Refinements<sup>2</sup>

Some additional calculations have been made in an effort to define the basic nuclear properties of the reactor more precisely. An improved version of the cross-section program, GAM-II, which includes lithium and fluorine is now available. Calculations using this program indicate that the critical concentrations are overestimated by about 14%. This difference is due primarily to the slowing-down effect of inelastic neutron scattering by  $^{19}\text{F}$  which was not considered in the earlier calculations.

Some calculations were performed to evaluate the advantages of using 32 fast-neutron groups. Sets of multigroup cross sections with 32, 16, 8, and 4 fast groups were generated using the GAM-II program. These cross sections were used in one-dimensional diffusion calculations (MODRIC) of the critical concentration. All the calculations agreed to within 1% on

UNCLASSIFIED  
ORNL-DWG 63-8149A

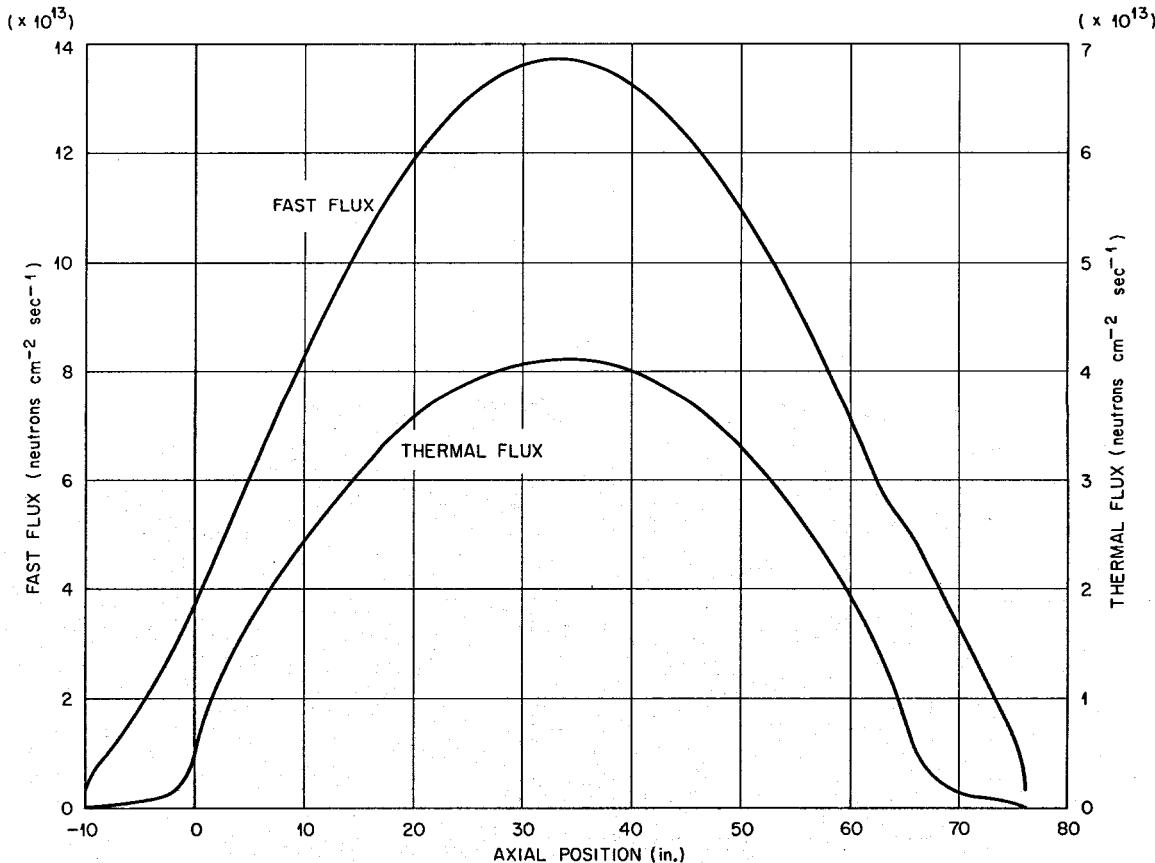


Fig. 3. Axial Distribution of Two-Group Fluxes 8.4 in. from Core Center Line, Fuel C.

UNCLASSIFIED  
ORNL-DWG 63-8151A

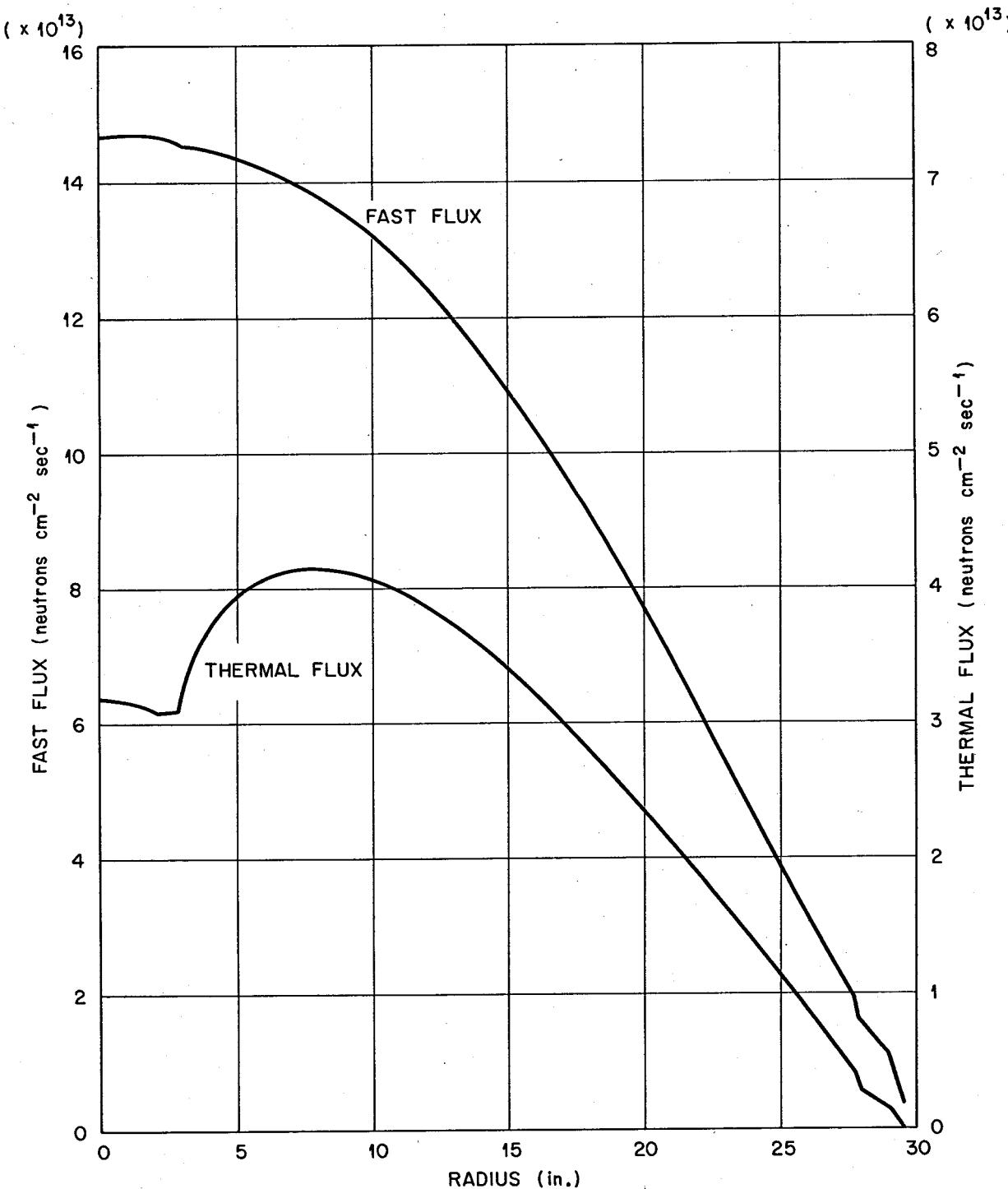


Fig. 4. Radial Distribution of Two-Group Fluxes near Core Midplane,  
Fuel C.

critical concentration, indicating the adequacy of the four-group treatment for future work.

#### Effects of Fuel Circulation

The fact that the fuel circulates through the MSRE core has a definite effect on some of the nuclear properties. Subjects that have been given separate consideration are the loss of some of the delayed neutrons and the effects of gas bubbles in the circulating stream.

Delayed Neutrons. Since the transit time through the active region of the core (where the fission density is substantial) is only about one-third the loop transit time, significant portions of the delayed neutrons from the longer-lived precursors are emitted outside the core, where they are lost to the chain reaction. Calculations have been made to evaluate this loss under steady-state operating conditions. For this purpose, the core was approximated as a single-region cylinder with uniform fuel flow velocity. The effect of the precursor movement on the axial distribution of the delayed-neutron emission densities is shown in Fig. 5. The source

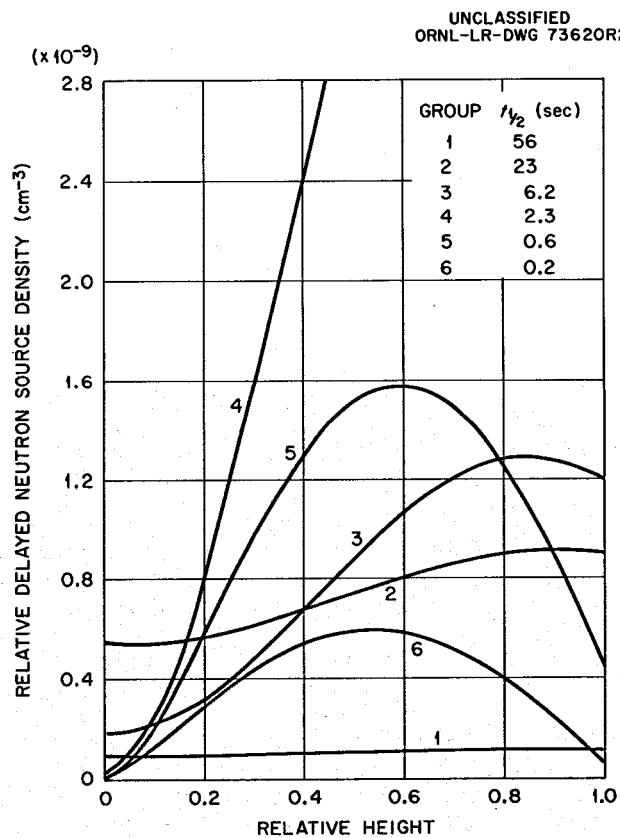


Fig. 5. Axial Distribution of Delayed-Neutron Source Densities in an MSRE Fuel Channel. Fuel circulating at 1200 gpm.

of delayed neutrons from the shortest-lived group of precursors has essentially the same distribution as the prompt-neutron flux. At the other extreme the distribution from the longest-lived group is nearly flat. The effects of the distorted source distributions and the lower average energies of the delayed neutrons on their nonleakage probabilities were included in the evaluation of the effective delayed-neutron fraction. The total effective fraction of delayed neutrons is 0.00362 at a 1200-gpm circulation rate and is 0.00666 in the static core. The total yield of precursors is 0.00641. The effective delayed-neutron fraction was used in subsequent kinetics calculations instead of trying to account for precursor transport during transient conditions.

Gas Bubbles. The use of the xenon-stripping device in the fuel-pump bowl results in the introduction of helium gas bubbles into the circulating fuel stream. At operating conditions the fuel in the core may contain about 1 vol % of helium bubbles. The presence of these bubbles makes the fuel compressible, causing a pressure coefficient of reactivity. In addition, the presence of the gas modifies the fuel temperature coefficient of reactivity because the density of the salt-gas mixture changes with temperature at a rate different from the density of the salt alone.

For rapid changes in pressure the mass of helium in the core remains essentially constant, and the reactor exhibits a positive pressure coefficient of reactivity. However, for very slow changes, the gas volume in the core is inversely proportional to the compression ratio between the pump bowl (where the gas is introduced) and the core. This leads to a negative pressure coefficient. The presence of gas increases the temperature coefficient of the mixture density; this leads to an increase in the size of the negative temperature coefficient of reactivity.

The magnitudes of the pressure and temperature coefficients of reactivity with entrained gas in the core are listed in Table 6 for a core temperature of 1200°F and a pump-bowl pressure of 5 psig.

During normal operation, the presence of entrained gas introduces additional power "noise" as fluctuations in core outlet pressure are converted to reactivity perturbations. In power excursions the gas enhances the negative temperature coefficient of reactivity of the fuel. At the same time, the pressure coefficient makes a positive contribution to reactivity during at least part of the power excursion. However, the relation between pressure rise and temperature rise in any credible excursion is such that the net reactivity feedback from the combined pressure and temperature effects is negative.

#### Control Rods

The MSRE contains three flexible control rods whose centers are located at three corners of a 4-in. square around the axis of the core. The rods operate in re-entrant INOR-8 thimbles, 2 in. in diameter with 0.065-in. walls. The poison elements are hollow cylinders, 1.08 in. OD by 0.84 in. ID and 1.3 in. long, containing 30 wt %  $\text{Al}_2\text{O}_3$  and 70 wt %

Table 6. Reactivity Coefficients with Entrained Gas in Core<sup>a</sup>

|  | Fuel A | Fuel B | Fuel C |
|--|--------|--------|--------|
| Fuel density coefficient of reactivity   | 0.190  | 0.345  | 0.182  |
| Fuel temperature coefficient of reactivity, $(^{\circ}\text{F})^{-1} (\times 10^{-5})$ |        |        |        |
| No gas or slow changes with gas  | -3.03  | -4.97  | -3.28  |
| Rapid changes with gas   | -3.14  | -5.17  | -3.39  |
| Pressure coefficient of reactivity, $\text{psi}^{-1} (\times 10^{-5})$                 |        |        |        |
| Slow changes with gas  | -3.8   | -7.0   | -3.7   |
| Rapid changes with gas   | +6.3   | +11.4  | +6.0   |

<sup>a</sup>Evaluated at  $T = 1200^{\circ}\text{F}$ ,  $P = 36.5 \text{ psia}$  (pump-bowl pressure, 5 psig).

$\text{Gd}_2\text{O}_3$ . Thirty-six such elements, each clad in Inconel, are used for each control rod.

#### Rod-Worth Calculations

The initial rod-worth calculations were done in two dimensions with two neutron energy groups (fast and thermal) with EQUIPOISE-3. For this purpose a horizontal cross section of the core was represented in X-Y geometry, and an equivalent axial buckling was applied. The poison elements were regarded as "black" to thermal neutrons and transparent to fast neutrons. The control rod "cells" were sized such that the perimeter of the square representation of each rod thimble was equal to that of the actual item. These calculations gave the reactivity effect associated with the insertion of three control rods completely through the core for each of the three fuels. The calculations were extended for fuel A to obtain the effects of various combinations of fully inserted rods. Other EQUIPOISE-3 calculations, in R-Z geometry with a single control cylinder, were used to estimate the variation in worth with insertion distance.

Table 7 lists the total control rod worths obtained from the EQUIPOISE-3 calculations. The worths of the various combinations listed for fuel A indicate the existence of appreciable interaction or "shadowing" between the rods. All values are for a clean reactor with uranium concentrations corresponding to the "just critical" condition without rods. Figure 6 shows the fractional worth of a rod or bank of rods as a function of fractional distance inserted. This curve is displaced somewhat to the left of the idealized  $\int \sin^2$  curve.

Subsequent calculations which considered epithermal absorptions in the poison elements have been made using the EXTERMINATOR program in two dimensions with the cross section of the core represented in R- $\theta$  geometry. Four neutron energy groups were used: a fast group, a thermal group, and two groups covering the important gadolinium resonances. Two calculations were made: one using the latest clean, critical uranium concentration computed for fuel C with GAM-II cross sections and one with fuel containing 1.9%  $\delta k/k$  of fission product poisons compensated by additional  $^{235}\text{U}$ . The results were, respectively, 5.51 and 5.22%  $\delta k/k$  for three rods. In the clean case, epithermal absorptions accounted for 12% of the rod worth.

Table 7. Control Rod Worths in the MSRE

| Fuel | Rod Configuration          | Worth<br>(% $\delta k/k$ ) |
|------|----------------------------|----------------------------|
| A    | Three rods in              | 5.6                        |
|      | Rod 1 in, rods 2 and 3 out | 2.4                        |
|      | Rod 2 in, rods 1 and 3 out | 2.3                        |
|      | Rods 1 and 3 in, rod 2 out | 4.4                        |
|      | Rods 1 and 2 in, rod 3 out | 4.1                        |
| B    | Three rods in              | 7.6                        |
| C    | Three rods in              | 5.7                        |

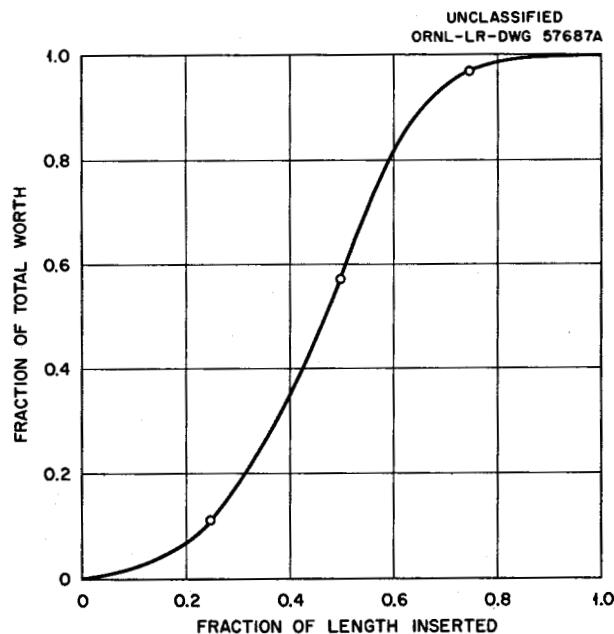


Fig. 6. Fractional Worth of a Rod or Bank of Rods as a Function of Distance Inserted.

### Control Requirements

Since the fuel in this reactor is fluid, it is not necessary for the control rods to perform flux-flattening functions for optimization of burnup and fuel-to-coolant heat transfer. In addition, the temperature distributions in the core are mild enough that temperature gradients are no problem. As a result the control rods can be operated in the simplest manner possible, consistent with good reactivity control.

In general, the two shim rods will be kept at equal distances of insertion, and the servo-operated regulating rod will be inserted deeper to keep the tip out of the "shadow" of the shim rods. The capability of adding uranium at any time to compensate for burnup and stable poison buildup permits steady operation at full power with the rods almost completely withdrawn. The only requirement is that the rods be deep enough so the insertion of negative reactivity is not delayed by travel time in regions of low effectiveness.

The driven speed of all three rods is 0.5 in./sec in both directions. This allows the regulating rod to change reactivity at 0.02 to 0.04%  $\delta k/k$  per second, depending on its position within the allowed operating range. Extensive analog computer studies indicated that this capability provides adequate control for all normal operations. The maximum capability for reactivity addition with all three rods moving in the region of maximum sensitivity is 0.08%  $\delta k/k$  per second for fuels A and C and 0.1% per second for fuel B.

The shim requirements to compensate for transient reactivity effects during operation are given in Table 8. These requirements, coupled with the control rod worths, allow for a shutdown margin of at least 3%  $\delta k/k$  at 1200°F for all operating conditions. The major uncertainty in the shim

Table 8. Rod Shim Requirements

| Cause                                    | Effect (% $\delta k/k$ ) |        |        |
|--|--------------------------|--------|--------|
|  | Fuel A                   | Fuel B | Fuel C |
| Loss of delayed neutrons                 | 0.3                      | 0.3    | 0.3    |
| Entrained gas                            | 0.2                      | 0.4    | 0.2    |
| Power (0-10 Mw)                          | 0.06                     | 0.08   | 0.06   |
| $^{135}\text{Xe}$ (equilibrium at 10 Mw) | 0.7                      | 0.9    | 0.7    |
| Samarium transient                       | 0.1                      | 0.1    | 0.1    |
| Burnup (120 g of $^{235}\text{U}$ )      | 0.03                     | 0.07   | 0.03   |
| Total                                    | 1.4                      | 1.9    | 1.4    |

requirements is that associated with  $^{135}\text{Xe}$ . Because of difficulties in calculating this quantity, its evaluation will be the subject of extensive experimental analysis. However, present indications are that the values given are conservative.

#### Core Temperatures

The distributions of the fuel and graphite temperatures in the core are of interest because of their effects on reactivity, particularly in connection with power changes. Overall temperature distributions were calculated for the nominal full-power conditions (i.e., a fuel flow rate of 1200 gpm and a temperature rise of 50°F) in the reactor. Results are presented for fuel C, but those for fuels A and B were practically the same.

#### Fuel Temperatures

For purposes of these calculations, the contents of the reactor vessel can be divided into a main core region, where most of the power

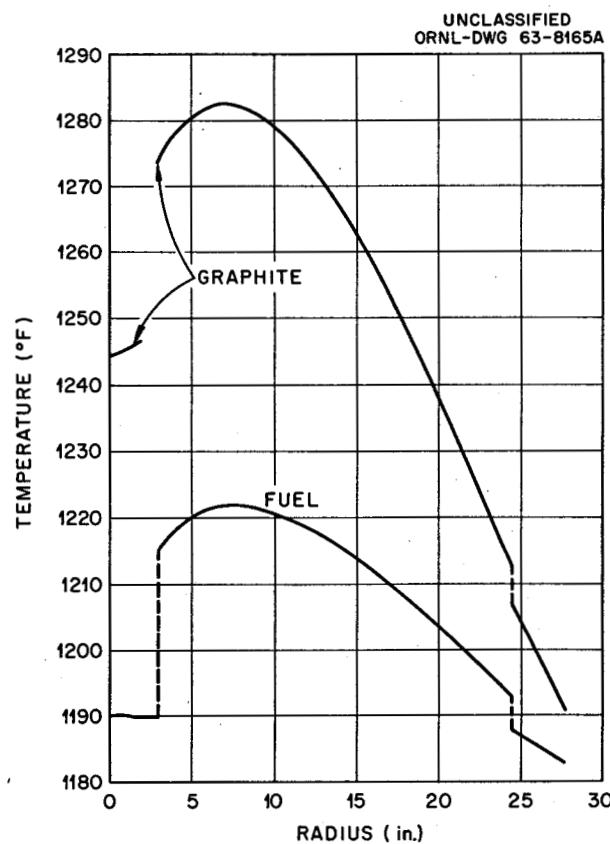


Fig. 7. Radial Temperature Profiles near the Core Midplane.

is generated, and a number of peripheral regions associated with the inlet and outlet. The main core region in this context is that portion that contains the graphite moderator.

Approximately 14% of the reactor power is produced in, or transferred to, the fuel as it flows through the peripheral regions. At 10 Mw this results in a  $3.6^{\circ}\text{F}$  temperature rise in the fuel before it enters the main core region and another  $3.4^{\circ}\text{F}$  rise as it flows through the upper head to leave the vessel.

The spatial distribution of the fuel temperature in the main core region was calculated by combining the fission-density distribution produced by EQUIPOISE-3 and the fuel-flow distribution predicted by hydraulic studies on a full-scale model of the reactor vessel. Axial conduction in the graphite was neglected, so heat produced in the graphite was transferred to the fuel with approximately the same axial distribution as that of the fuel heat source. The results of this calculation describe only the distribution of the average temperatures in the fuel channels. Variations in fuel temperature within individual channels are superimposed on this distribution.

Figures 7 and 8 show the overall radial temperature distribution near the core midplane and the axial distribution in the hottest fuel channel. These results are based on average fuel inlet and outlet temperatures of  $1175$  and  $1225^{\circ}\text{F}$  respectively. The low temperatures near the axis in the radial distribution result from the fact that the flow velocity in this region is about three times the average for the core.

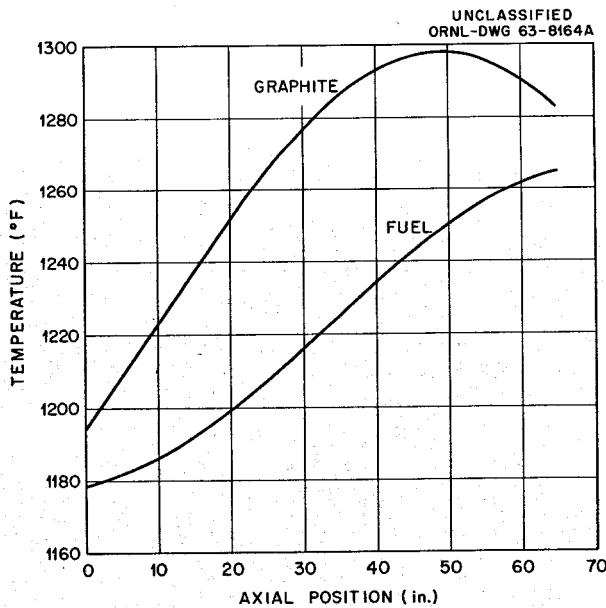


Fig. 8. Axial Temperature Profiles in Hottest Channel and Adjacent Graphite Stringer.

### Graphite Temperatures

Heat produced in the graphite by absorption of beta and gamma radiation and the elastic scattering of fast neutrons amounts to about 7% of the total heat produced in the reactor. Figures 9 and 10 show the radial and axial distributions of heat generation in the graphite. Since this heat must be transferred to the fuel for removal, the temperature of the graphite is, in general, higher than that of the fuel in the adjacent channels. The temperature difference is enhanced by the fact that the fuel near the channel walls is hotter than the average for the channel (Poppendiek effect). Permeation of the graphite by fuel, if it occurs, will also enhance the graphite-fuel temperature difference. Table 9 indicates the effect of fuel permeation on the maximum difference between the average temperature of a graphite stringer and the average for an adjacent fuel channel. The overall radial and axial temperature profiles in the graphite are shown in Figs. 7 and 8.

Table 9. Maximum Values of Graphite-Fuel Temperature Difference as a Function of Fuel Permeation

| Fuel permeation, vol % of graphite       | 0    | 0.5  | 2.0  |
|--|------|------|------|
| Graphite-fuel temperature difference, °F |      |      |      |
| Poppendiek effect in fuel                | 55.7 | 58.3 | 65.4 |
| Graphite temperature drop                | 5.5  | 6.7  | 9.8  |
| Total                                    | 61.2 | 65.0 | 75.2 |

### Average Temperatures

The concept of average temperatures has a number of useful applications in operating and in describing and analyzing the operation of the system. The bulk average temperature, particularly of the fuel, is essential for all material balance and inventory calculations. The nuclear average temperatures of the fuel and graphite, along with their respective temperature coefficients of reactivity, provide a convenient means of assessing the reactivity effects associated with temperature changes.

The fuel and graphite bulk average temperatures computed for the reference condition (1175°F inlet, 1225°F outlet) were 1199.5 and 1229°F respectively. Fuel permeation of 2% of the graphite volume increases the graphite average temperature by 4.4°F.

Nuclear average temperatures were obtained by weighting the temperature distributions with their nuclear importance functions. For the same reference conditions, the nuclear average temperatures of the fuel and

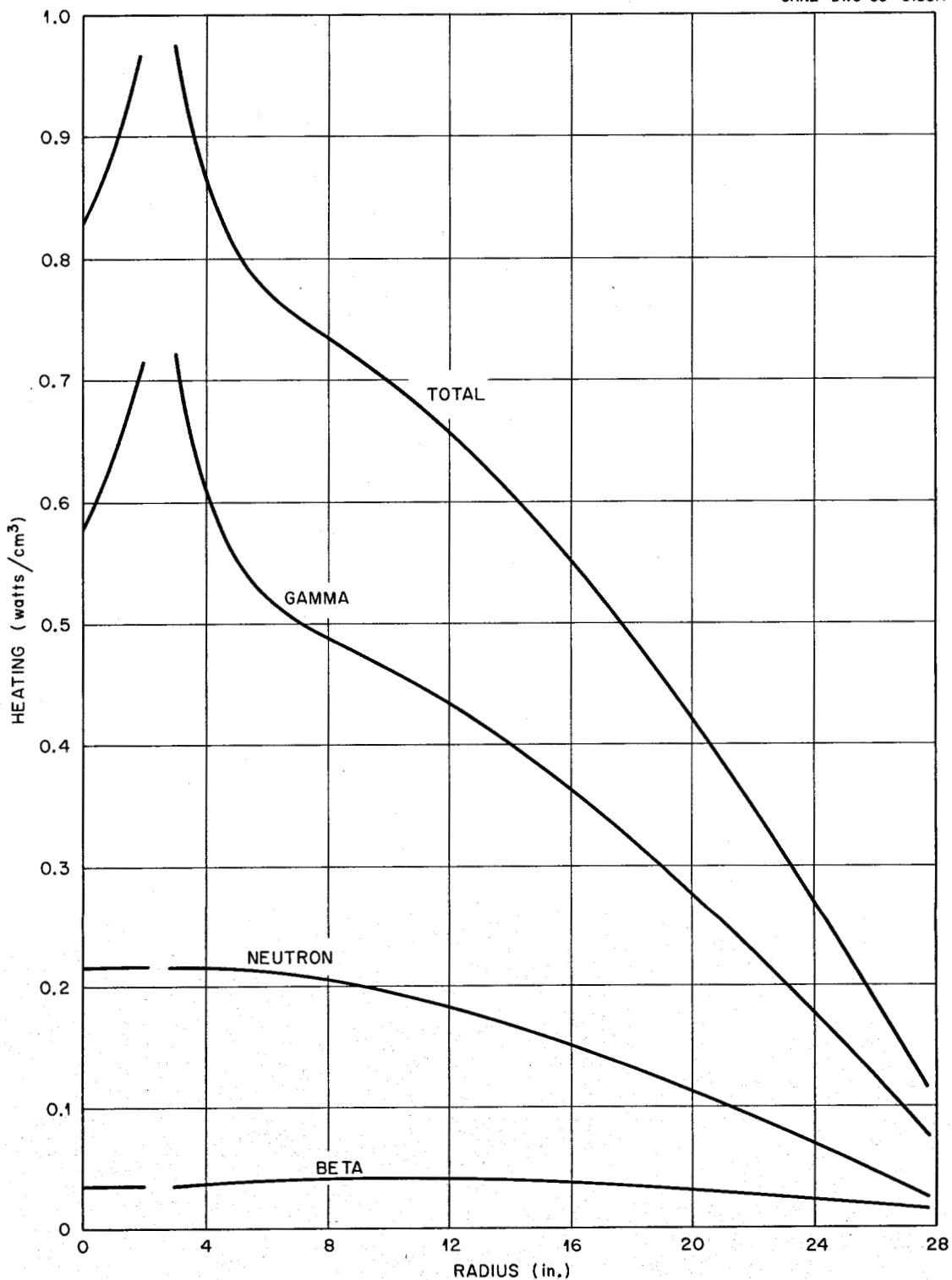
UNCLASSIFIED  
ORNL-DWG 63-8185A

Fig. 9. Heating in Graphite; Radial Distribution near Midplane at 10 Mw.

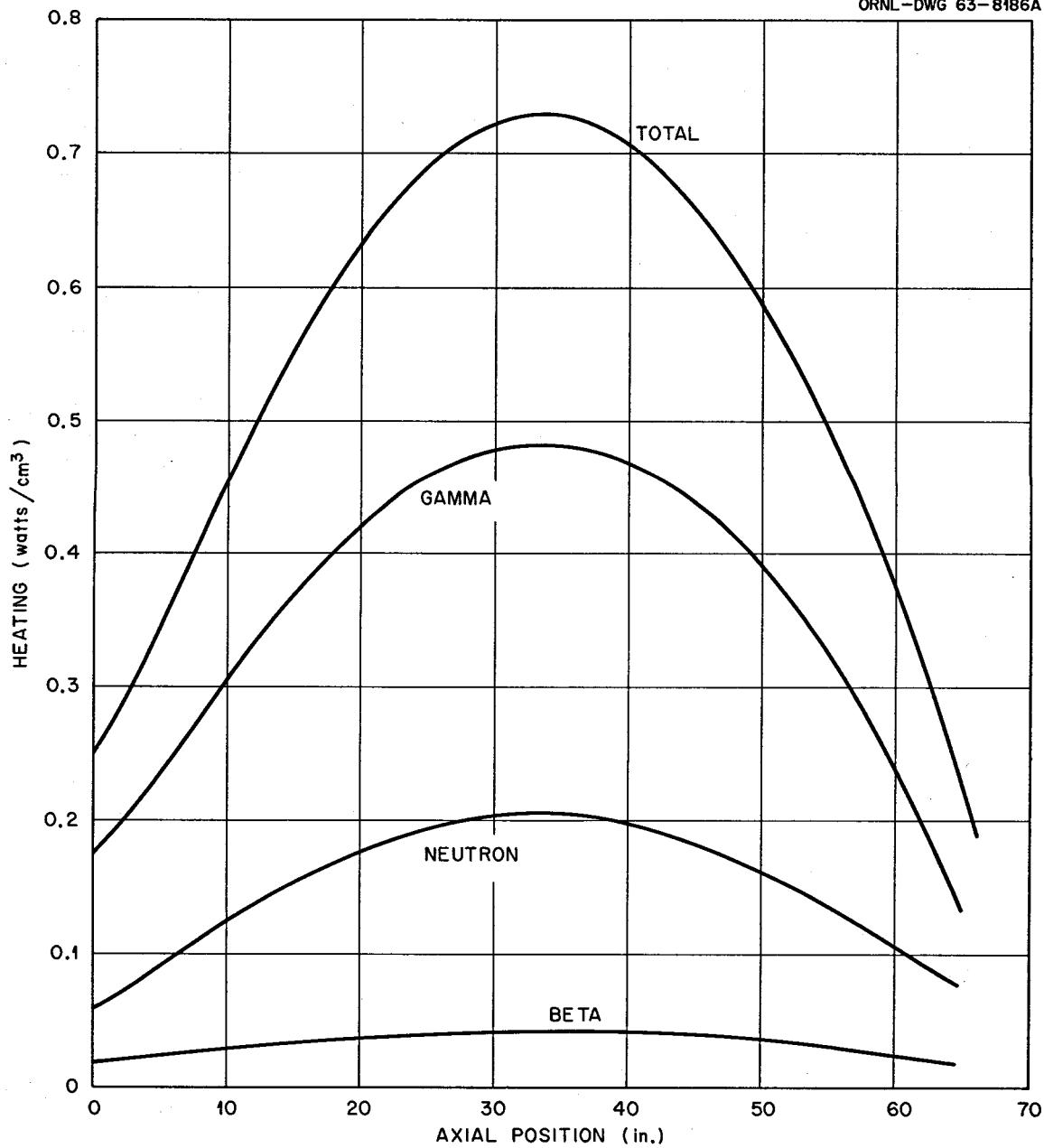
UNCLASSIFIED  
ORNL-DWG 63-8186A

Fig. 10. Heating in Graphite; Axial Distribution 8.4 in. from Core Center Line at 10 Mw.

graphite were 1211 and 1255°F respectively. The effect of 2 vol % fuel permeation in this case was an increase of 7°F in the graphite nuclear average temperature.

#### Power Coefficient of Reactivity

Whenever the reactor power is raised, temperatures of the fuel and graphite throughout the core must diverge. However, the shape of the temperature distributions at power and the relations between inlet, outlet, and average temperatures are inherent characteristics of the system which are not subject to external control. On the other hand, the position of the temperature distribution at power, relative to the temperature of the zero-power isothermal reactor, can be controlled by manipulation of the control rods. The amount of control rod manipulation, or reactivity change, required to maintain a particular temperature relation may be regarded as a power coefficient. Once the temperature behavior has been prescribed, it is possible to evaluate the power coefficient. However, this coefficient is not a constant since it depends on the arbitrary prescription of the temperature behavior. Values of the power coefficient of the MSRE and some pertinent temperatures for three fuels and three different modes of temperature control are given in Table 10.

#### Fission Product Poisoning

Operation of the reactor at power and changes in power level will produce changes in reactivity as fission products are built up and/or

Table 10. Power Coefficients of Reactivity and Temperatures at 10 Mw

| Mode of Control                           | Power Coefficient<br>[(% $\delta k/k$ )/Mw] |        |        | Temperature <sup>a</sup><br>(°F) |                   |                             |                             |
|---|---|--------|--------|----------------------------------|-------------------|-----------------------------|-----------------------------|
|   | Fuel A                                      | Fuel B | Fuel C | T <sub>(out)</sub>               | T <sub>(in)</sub> | T <sub>f</sub> <sup>*</sup> | T <sub>g</sub> <sup>*</sup> |
| Constant T <sub>(out)</sub>               | -0.006                                      | -0.008 | -0.006 | 1200                             | 1150              | 1186                        | 1230                        |
| Constant $\frac{T_{(out)} + T_{(in)}}{2}$ | -0.022                                      | -0.033 | -0.024 | 1225                             | 1175              | 1211                        | 1255                        |
| "Hands off"                               |   |        |        |                                  |                   |                             |                             |
| Fuel A                                    | 0   |        |        |                                  | 1191              | 1141                        | 1177                        |
| Fuel B                                    |   | 0      |        |                                  | 1192              | 1142                        | 1178                        |
| Fuel C                                    |   |        | 0      |                                  | 1191              | 1141                        | 1177                        |

<sup>a</sup>System isothermal at 1200°F at zero power.

destroyed. The negative reactivity effect due to the buildup of stable fission products, which depends primarily on integrated power, will be compensated by periodic additions of  $^{235}\text{U}$ . However, the transient effects, such as those due to  $^{135}\text{Xe}$  and  $^{149}\text{Sm}$ , will be compensated by control rod manipulation.

### Xenon-135

The reactivity effects associated with the buildup and decay (or removal) of  $^{135}\text{Xe}$  are expected to form a significant part of the shim requirements in this reactor. Because of this and the uncertainties in predicting the xenon behavior, this problem will be studied extensively during the operation of the reactor. Some preliminary calculations have been made, using rather gross assumptions, to estimate the xenon poisoning at full power.

Production Mechanisms. Xenon-135 is produced directly from fission of uranium as well as from the radioactive decay of  $^{135}\text{I}$  circulating with the fuel. In addition, there is a possibility that iodine, which presumably will not be stripped out in the pump bowl, may be trapped either in the graphite or on metal surfaces. Xenon produced from the decay of fixed iodine may have significantly different residence times, inside or outside of the core, than that produced in the circulating stream. The possibility of xenon production from fuel salt that is soaked into the graphite further increases the complexity of the problem.

Destruction Mechanisms. There are two major competing mechanisms for the removal of  $^{135}\text{Xe}$  from the circulating fuel. These are stripping in the pump bowl and migration to the unclad graphite moderator. Approximately 85% of the  $^{135}\text{Xe}$  that gets to the graphite is destroyed by neutron absorption, thus adding to the poisoning effect; the remainder decays to  $^{135}\text{Cs}$ . Both the xenon migration to the graphite and the stripping efficiency are highly uncertain, but it appears that 50% or more of the total  $^{135}\text{Xe}$  produced may be removed at the pump bowl. In addition to the major mechanisms, it is also necessary to consider the decay and burnup of xenon in the fuel itself. Different destruction rates for xenon produced from trapped iodine and from fuel soaked into the graphite should also be considered in a complete analysis.

Poisoning Effect. Preliminary calculations of the xenon poisoning were made for a range of pump-bowl stripping efficiencies and three assumed values of the xenon diffusion coefficient in graphite. In these calculations it was assumed that all the iodine circulated freely with the fuel and that all the xenon is produced in circulating fuel (no fuel soakup in graphite). The results are shown in Table 11. The expected values reflect a xenon diffusion coefficient in graphite of  $1.5 \times 10^{-5}$  ft $^2/\text{hr}$  ( $4 \times 10^{-6}$  cm $^2/\text{sec}$ ), and the maximum and minimum values show the effect of increasing and decreasing the parameter by a factor of 100.

An important assumption in these calculations was that all the circulating xenon was in solution in the salt. It has recently been

Table 11. Reactivity Effects of  $^{135}\text{Xe}$ 

|                                   |      | Fuel A or C | Fuel B |      |
|-----------------------------------|------|-------------|--------|------|
| Pump bowl stripping efficiency, % | 25   | 50          | 100    | 50   |
| Reactivity effect, % $\delta k/k$ |      |             |        |      |
| Expected                          | -1.2 | -0.7        | -0.5   | -0.9 |
| Minimum                           | -1.0 | -0.5        | -0.3   | -0.5 |
| Maximum                           | -1.7 | -1.2        | -0.9   | -1.5 |

shown that the presence of circulating helium bubbles, introduced by the stripper flow in the pump bowl, has a pronounced effect on the xenon behavior. Because of the extreme insolubility of xenon in molten salt, the addition of 1 vol % of circulating helium bubbles reduces the equilibrium xenon partial pressure (in the salt and bubbles) by a factor of about 40, for a given total amount of xenon in circulation. That is, about 98% of the circulating xenon will be in the bubbles. Since the xenon partial pressure provides the driving force for migration to the graphite, the preliminary calculations may overestimate the contribution to the poisoning by xenon in the graphite.

#### Samarium

Assuming that all the samarium circulates with the fuel, the buildup of this fission product will ultimately poison about 0.9%  $\delta k/k$  at 10 Mw. This level will be approached after about 100 days' operation at full power. This effect can be compensated by uranium addition to the fuel. However, each time the power is reduced to zero, the samarium poisoning will increase an additional 0.1% over a period of 7 days. This increase is burned out in about 7 days by operation at full power. Thus only the 0.1%  $\delta k/k$  samarium transient need be compensated by the control rods.

#### Low-Cross-Section Poisons

The large majority of the fission products may be regarded as an aggregate of low-cross-section nuclides. The poisoning effect of this group increases initially at a rate of about 0.003%  $\delta k/k$  per day at full power.

#### Neutron Sources

The presence of a neutron source that is independent of the fission chain reaction is essential to the safe and orderly operation of the reactor. Three classes of source neutrons will be available during the

operation of the MSRE. These include neutrons from the source that is inherent in the fuel itself, photoneutrons produced by decay of fission products, and the external source.

#### Inherent Source

The fact that the uranium is intimately mixed with the other constituents of the fuel salt provides a substantial source of neutrons from the interaction of alpha particles from the uranium with beryllium and fluorine. Some neutrons are also produced by the action of alpha particles on lithium, but this yield is negligible compared to that from fluorine and beryllium. Diffusion-plant enrichment of uranium in  $^{235}\text{U}$  also increases the  $^{234}\text{U}$  content, and about 97% of the alpha activity that leads to neutron production is due to  $^{234}\text{U}$ . Over half of the  $\alpha\text{-n}$  reactions take place in fluorine because of its high concentration in the fuel. The total yield of  $\alpha\text{-n}$  neutrons from the fuel in the core varies between 3 and  $4 \times 10^5$  neutrons/sec, depending on the choice of fuel. There is also an inherent source due to spontaneous fission, primarily of  $^{238}\text{U}$ , but this amounts to less than 1% of the  $\alpha\text{-n}$  source, even in fuel C, which contains about 0.6 mole %  $^{238}\text{U}$ . Since the inherent source is always present in the reactor when the fuel is there, it provides an absolutely reliable source whose presence need not be externally verified. The size of the inherent source has been shown to be adequate from the standpoint of reactor safety.

#### Photoneutron Source

Once the reactor has been operated at power, the action of gamma rays from the decay of fission products on the beryllium in the fuel provides an additional source of neutrons. This source provides a minimum of  $10^7$  neutrons/sec in the core for 50 days after operation at full power for 1 week.

#### External Source

From the standpoint of orderly operation, it is desirable to monitor the filling of the reactor (during routine startups) with the nuclear instruments from the start of this operation. Since detection of the inherent source requires that some fuel be in the reactor, an external source is required for this purpose. The external source will also serve a number of useful purposes during the initial startup program.

A thimble is provided for the insertion of a neutron source in the thermal shield which surrounds the reactor vessel. Because of the distance from the source thimble to the detectors on the opposite side of the reactor and the low sensitivity of the chambers (0.026 count/nv), a relatively large source will be required to produce a significant count rate ( $>2$  counts/sec) on the startup fission chambers when there is no fuel in the core. Calculations using the two-group, two-dimensional program EQUIPOISE BURNOUT indicate the need for a source of  $4 \times 10^7$  neutrons/sec for this purpose.

The source requirement could be met with an antimony-beryllium source, but the 60-day half-life of  $^{124}\text{Sb}$  dictates a substantially greater source to avoid frequent replacement. (The neutron flux in the thermal shield at the source tube is too low to maintain the  $^{124}\text{Sb}$  activity, even at full power.)

Because of uncertainties in the calculations of the source requirement, the final specification of the external source will be based on measurements to be made with the reactor vessel installed. The construction and startup schedule is such that there is time for procurement of a source after these measurements and before the source is needed for nuclear operation.

### Kinetics

A number of studies, using both digital and analog computer techniques, have been made to explore the kinetic behavior of the reactor. These calculations can be divided into two categories: those dealing with small disturbances such as random "noise" and changes in load demand that would be encountered in normal operation, and those dealing with major disturbances that arise from abnormal situations.

### Normal Operation

The reactor will be self-regulating during normal operation because of the negative temperature coefficients of both the fuel and graphite. The degree of self-regulation depends on the power level and is rather sluggish even at full power. A number of factors contribute to the slow response of the system. These include:

1. low power density in the core,
2. high heat capacities of the fuel and graphite,
3. low heat-transfer rate between fuel and graphite,
4. low heat production in the graphite,
5. long loop delay times between the heat sink at the radiator and the heat source in the core.

Figures 11 and 12 show the results of analog calculations of the system response to changes in load demand at the radiator, in the absence of external reactivity control. In both cases, slow changes in demand were started at zero time, and the temperature and power response of the reactor were recorded. The slow decrease in fuel temperatures after the increase in power and the increase after the power reduction reflect the attainment of the steady-state temperature distribution in the graphite. The slow power oscillation at low power was observed in all simulations and appears to be an inherent characteristic of the system.

During routine operation, some external reactivity control will be imposed through the use of a servo-operated regulating rod. This is ex-

pected to improve the response of the system and to minimize the "wallowing" at low power. At powers above 1 Mw the servo system will be used to regulate the reactor outlet temperature, with reset action based on the nuclear power level. At lower powers the neutron flux will be controlled directly, and the heat removal will be manually balanced against the production.

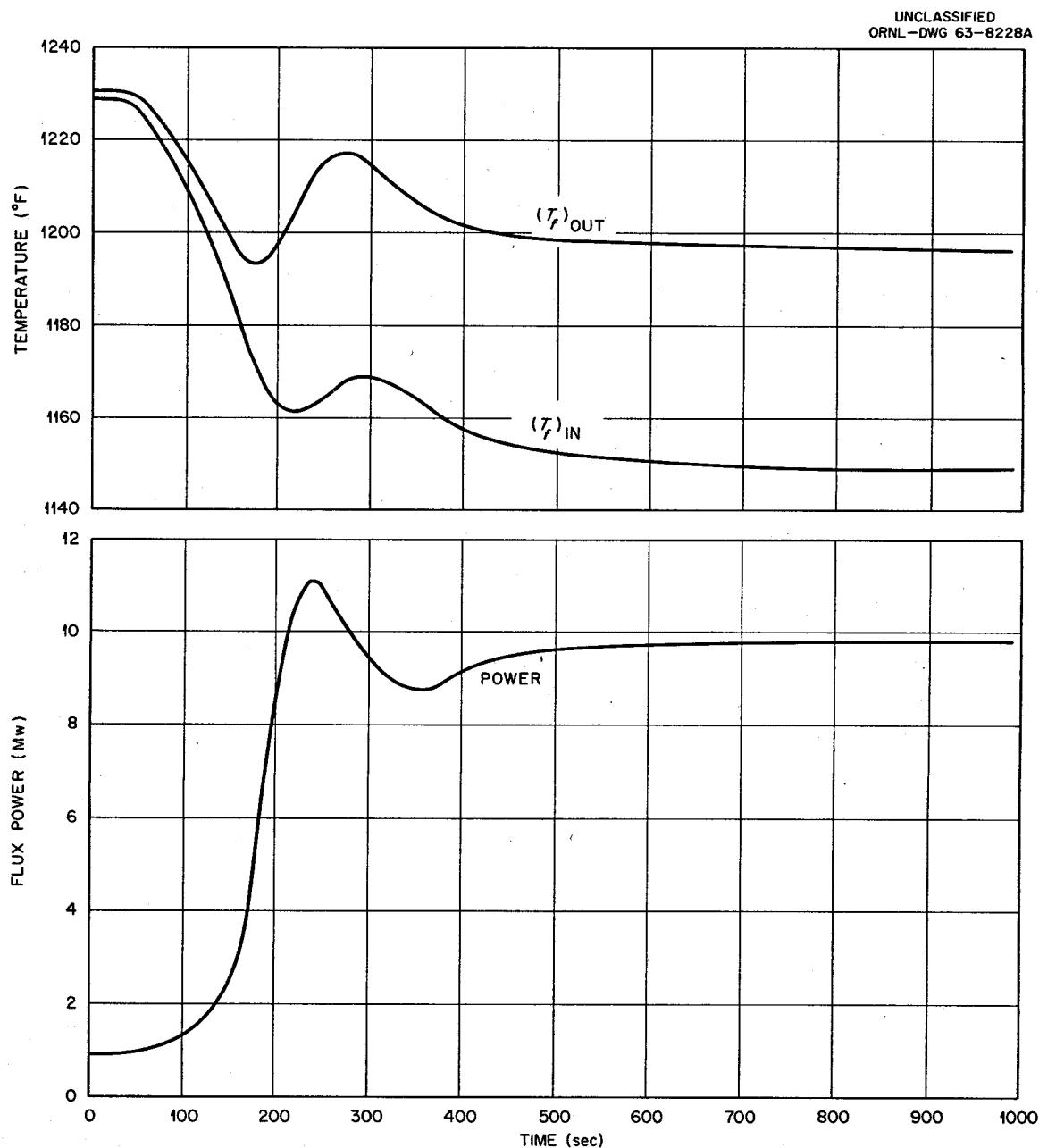


Fig. 11. Response of Nine-Region Model of MSRE to an Increase in Power Demand.

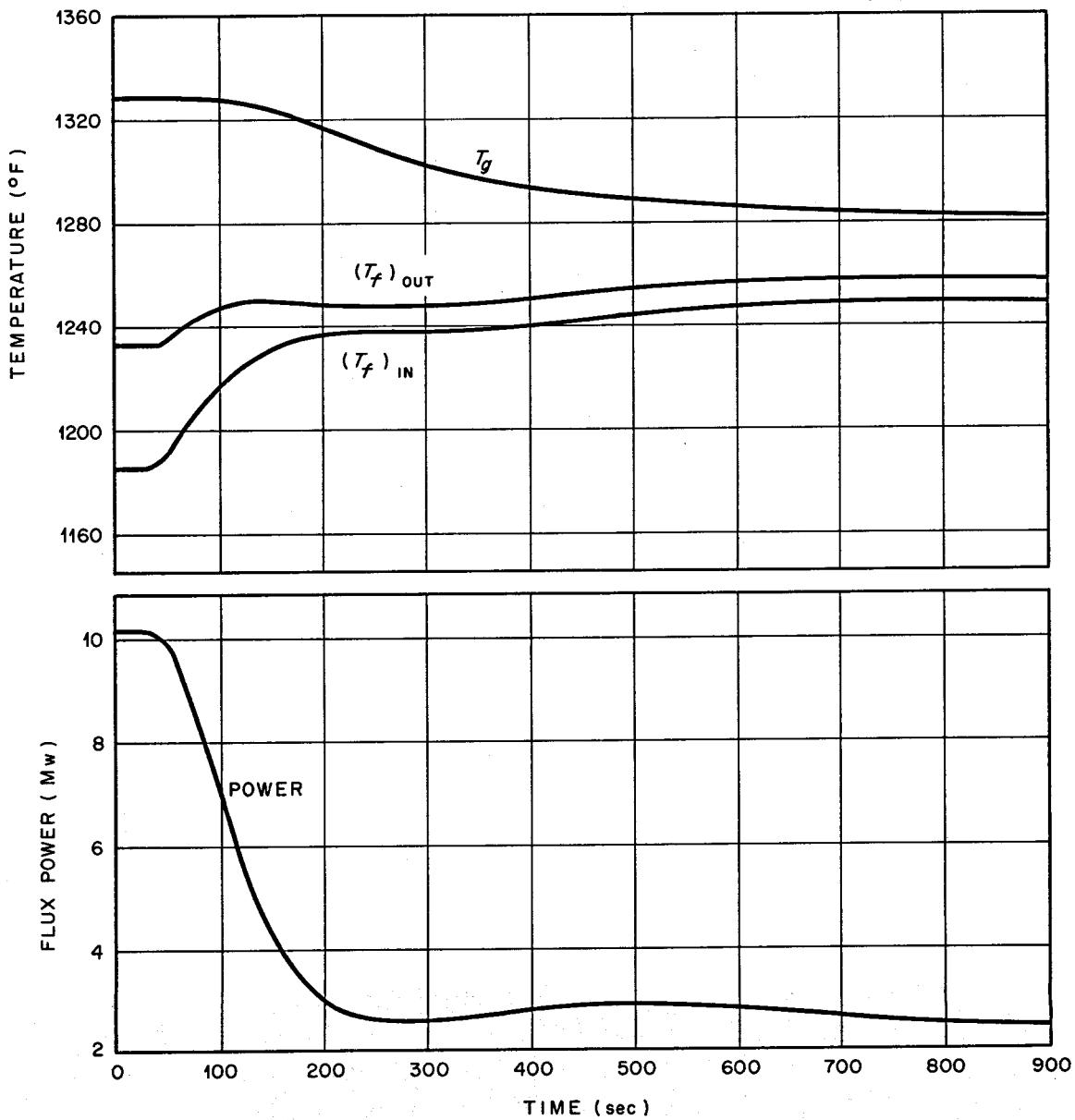
UNCLASSIFIED  
ORNL-DWG 63-8173A

Fig. 12. Response of Nine-Region Model of MSRE to a Decrease in Power Demand.

#### Abnormal Situations

The consequences of several, highly abnormal reactivity incidents have been examined in detail to characterize the inherent safety of the reactor and to evaluate the instrumented safety system. The excursions associated with reactivity accidents are inherently self-limiting by virtue of the negative temperature coefficient of reactivity of the fuel.

(The negative temperature coefficient of the graphite is of little value during a rapid excursion because of its long reaction time.) However, the action of the safety system is required to prevent equipment damage in the most severe cases considered.

One of the greatest possibilities for equipment damage in this system is collapse of the control rod thimbles. However, the pressure excursions calculated for the core were very small, and they always occurred before the temperature excursions reached the point where they might reduce the allowable stress on the thimbles.

The reactivity incidents considered, along with a brief description of how each might occur, are listed below. No attempt was made to evaluate the credibility of the occurrences.

1. Uncontrolled rod withdrawal - Simultaneous withdrawal of all three control rods, with criticality being attained while the rods are moving in the region of maximum differential worth, is postulated.
2. Cold slug accident - The fuel circulating pump is started with the core just critical at 1200°F while the fuel in the external loop is at 900°F.
3. Abnormal concentration of uranium during fuel addition - A slug of 120 g of  $^{235}\text{U}$ , added in the pump bowl, is assumed to go around the loop without dilution and enter the core as a "front" uniformly distributed to all fuel channels.
4. Displacement of graphite by fuel salt - Loss of an entire graphite stringer (62 in. long) from the center of the core and replacement by fuel salt is postulated.
5. Premature criticality during filling - The core is filled at the maximum possible rate with fuel salt in which the uranium concentration has been increased 60% by selective freezing in the drain tank. Criticality is achieved with the core 60% full.
6. Loss of fuel circulation - Failure of the power supply to the fuel circulating pump and the onset of natural-convection circulation are considered.
7. Loss of load - Instantaneous loss of all heat-removal capability at the radiator is assumed.

In all the events considered, except the filling accident, the reduction in reactivity obtained by dropping any two of the three control rods (with a 0.1-sec time delay and an acceleration of 5 ft/sec<sup>2</sup>) limited the power, temperature, and pressure excursions to easily tolerable values. In this context, tolerable values are those at which no damage to equipment in the reactor cell occurs. In the case of the fuel-pump power failure, an additional action, closure of the radiator doors, is required to avoid freezing the coolant salt in the radiator.

Aside from the filling accident, the incident with the greatest damage potential is the uncontrolled withdrawal of the control rods.

Figure 13 shows the results of a digital calculation of the transients produced by the rod withdrawal with fuel C in the reactor. The power at  $k = 1$  was 2 mw, the minimum attainable with only the inherent  $\alpha$ -neutron source present. If nothing were done to stop the rods, it is clear that intolerable temperatures would be reached. A rod scram at 15 Mw can limit the temperature excursion to a tolerable value, even if it is assumed that one of the three clutches fails to disengage. The effect of dropping two control rods, while the third continues to withdraw, is shown in Fig. 14. The actual response time of a prototype control rod was much shorter than that assumed for this analysis.

The filling accident represents a special case because the amount of reactivity available is not limited to that associated with a normal fuel loading. Prior to filling the reactor, the control rods will be withdrawn so that the core is just slightly subcritical when completely full. This provides a capability for rapid insertion of negative reactivity in the event of a power excursion during filling. However, the reactivity that could be added in the postulated accident is greater

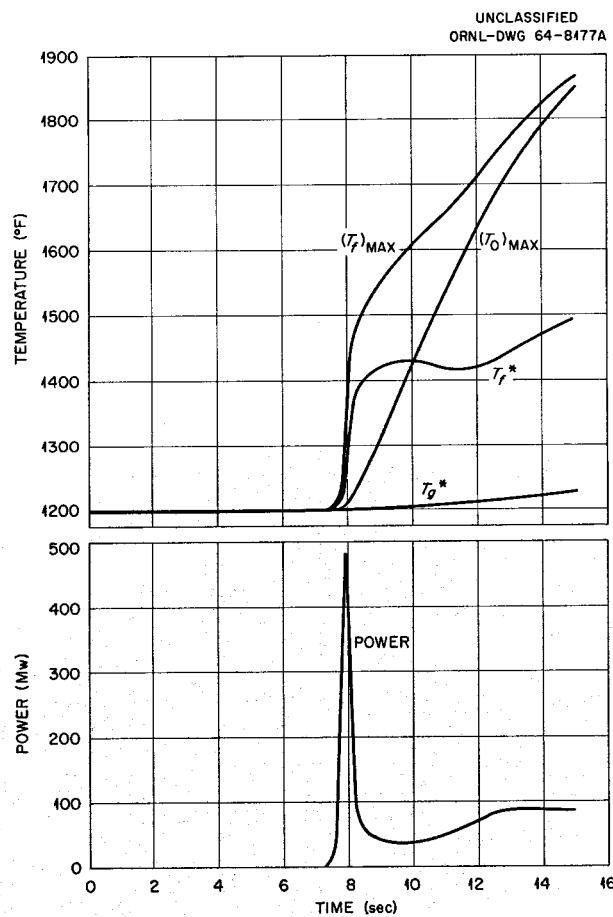


Fig. 13. Power and Temperature Transients Produced by Uncontrolled Rod Withdrawal, Fuel C.

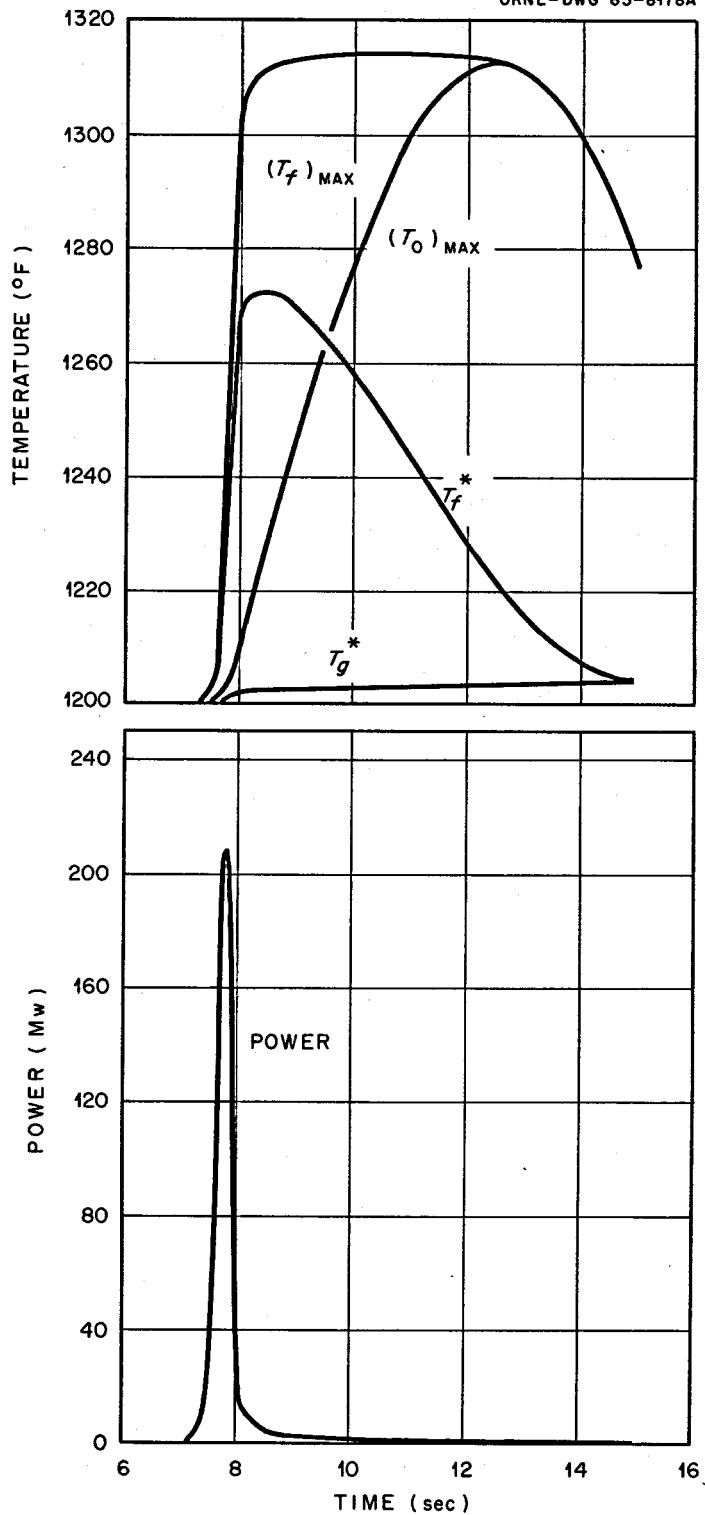
UNCLASSIFIED  
ORNL-DWG 63-8178A

Fig. 14. Effect of Dropping Two Control Rods at 15 Mw During Uncontrolled Rod Withdrawal, Fuel C.

than that which can be compensated by dropping two control rods. As a result it is necessary to stop fuel addition to limit this incident.

The occurrence of a high-flux signal causes, either directly or indirectly, three automatic actions, any one of which will stop the fill if it is in progress. (In the present design, this will occur at 20 kw during filling, but the analysis is based on its occurrence at 15 Mw.) These actions are closure of the helium supply valves to the drain tanks, opening of the drain-tank vent valves, and opening of equalizing valves between the drain tanks and the fuel loop. The least effective of these actions is that of stopping helium addition because this allows a "coastup" of the fuel level in the core and does not result in draining the fuel from the core. In analyzing the accident, it was assumed that only this one action actually occurred.

The calculated results of the postulated filling accident are shown in Fig. 15. The initial power excursion was checked by dropping two control rods at 15 Mw. However, the fuel coastup, due to failure of the vent and equalizing valves to open, resulted in a second critical event. The second excursion was slow enough so that only minor temperature rises were required, even with the reduced temperature coefficients applicable to the partly full core, to check it. If no further action were taken to insert the third control rod or to drain the fuel, the core would remain critical at some low power level.

#### Biological Shielding

The biological shielding above the reactor and drain-tank cells consists of 7 ft of concrete in two 42-in. layers with iron inserts to fill the cracks between blocks. The bottom layer above the reactor cell is barytes concrete, and the top layer is ordinary concrete. Both layers above the drain-tank cell are ordinary concrete. The shielding around the sides of the reactor cell is, for the most part, 3 ft of magnetite sand and water. Some additional shielding is provided by the thermal shield around the reactor vessel. This shield is 16 in. thick and is composed of about one-half iron and one-half water.

Extensive calculations have been made to evaluate the adequacy of the biological shielding. In general, it appears that, within the limits of the techniques available for evaluation, the biological shielding should be adequate. A few potential weak spots were recognized during the design. Provision has been made to stack additional concrete blocks in these areas if surveys during the initial approach to power indicate a need for them.

#### References

1. Most of this material has been reported in detail previously. See: P. N. Haubenreich et al., MSRE Design and Operations Report. Part III. Nuclear Analysis, ORNL-TM-730 (Feb. 3, 1964).
2. MSRP Semiann. Progr. Rept. Jan. 31, 1964, ORNL-3626, pp. 53-54.

UNCLASSIFIED  
ORNL-DWG 63-8182A

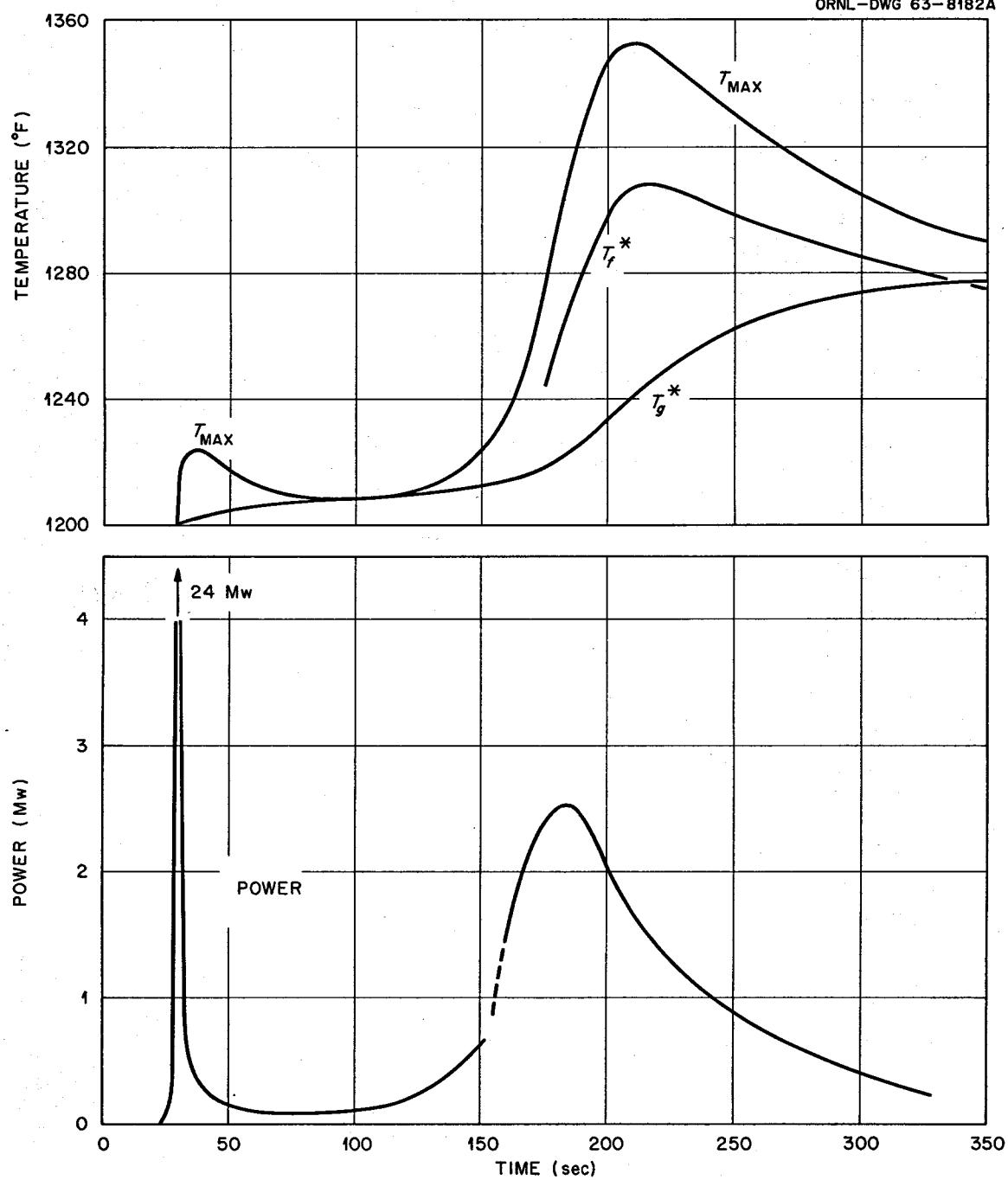


Fig. 15. Power and Temperature Transients Following Maximum Filling Accident.

INSTRUMENTATION AND CONTROL OF THE MSRE

J. R. Tallackson

Introduction

The purpose of the instrumentation and control system is to:

1. provide data to verify the designed performance,
2. provide information for reactor experiments,
3. provide safe, orderly operation of the reactor system.

I think you will conclude, as I proceed, that the MSRE is well equipped with instruments to meet both operational and experimental requirements. It is appropriate to point out that this is primarily an experimental system, one of the first of its kind. Therefore, it would be wrong to assume that the instrumentation and control equipment and its application is completely representative of any typical, future, molten-salt power reactor system.

Temperature

Temperature readings are the most important measurements in a system like this. High salt temperatures, which are thermodynamically desirable, must be limited and controlled lest they exceed limits imposed by materials and components; low salt temperature (freezing) can damage the system; and finally, steep gradients must also be avoided. These, then, are the reasons that the largest single concentration of instrumentation and control equipment is concerned with temperature.

Virtually all temperature measurements of consequence are made with Chromel-Alumel thermocouples. These are magnesium oxide insulated, Inconel sheathed, units and are welded or clamped to pipes or vessels. Most of the thermocouples are dual; that is, both the Chromel and Alumel wires are contained in a single sheath. A few selected couples in critical applications are made from two separately sheathed, single wires. A thermocouple failure, as by loss of a weld or clamp attachment, will then produce an open circuit and thereby signal that a failure has occurred.

We have been liberal in our use of thermocouples. Sufficient couples, with redundancy, have been installed, so that we can get temperature profiles of the tanks, the fuel and coolant salt piping, freeze valves, the pumps, and the radiator. More than 50% of these thermocouples are installed as a substitute for experience with the system and in order to obtain special data for a short time during early phases of the operation. Most of the temperature information now being gathered should not be required to run the machine.

Conventional methods for readout and data collecting from this number of points, such as multipoint recorders, would be an exercise in futility. We employ relatively new techniques to read temperatures and to use the temperature data effectively. Figure 1 is a block diagram of this temperature-measurement system.

Almost all the thermocouples are routed to the patch panel, so that any of the available readout methods can be applied to any given couple which comes into the patch panel.

The Operations Monitor is used for control system interlocking and to provide high or low limit alarms with a high degree of accuracy and with good reliability. It is in use at all times during reactor operation and not only indicates, with lamps, whether each temperature is within limits, but alarms both visually and audibly if any temperature goes beyond its particular, preset high or low value. It employs modular construction and is so designed that its capacity can be easily expanded or contracted. Circuitry consists entirely of transistors and magnetic amplifiers and is expected to be considerably more reliable and maintenance-free than comparable vacuum tube circuitry. The principal use of the Operations Monitor will be to monitor important temperatures at freeze valves in the fill and drain system and to provide control-system inter-

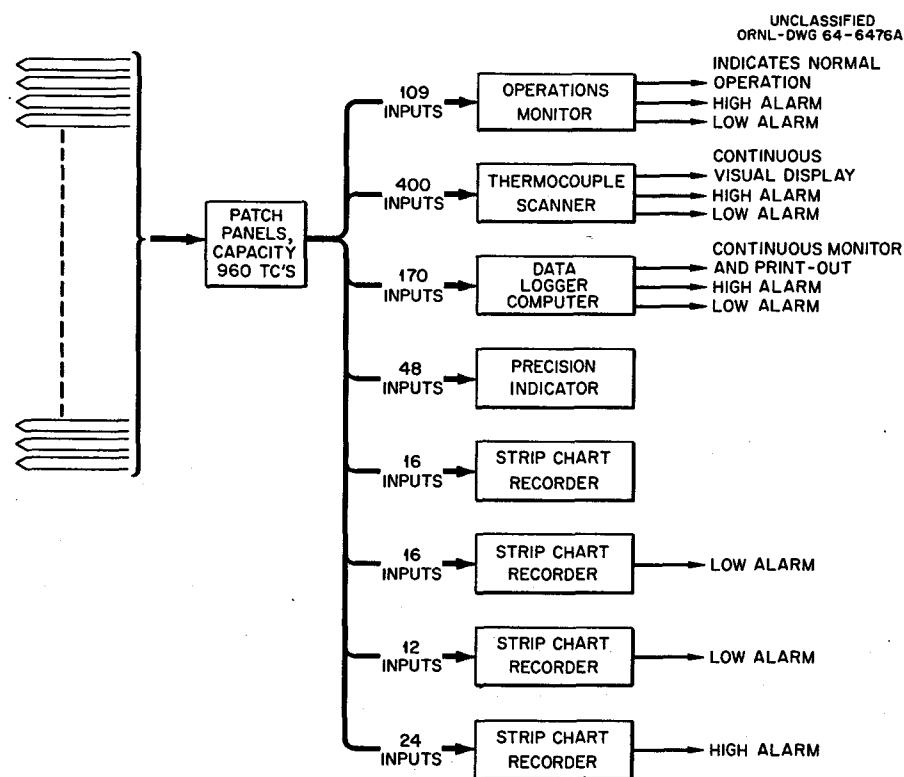


Fig. 1. Block Diagram of MSRE Temperature Measurement System.

lock signals based on these temperatures. The freeze flanges in the main salt loops and at the steam domes in the after-heat removal system are also monitored by this equipment.

The Thermocouple Scanner gives the operator an immediate and continuous picture of temperature profiles in the system. Figure 2 is a diagram of the system. You will note that this device operates in a straight-forward way; that is, a high speed selector switch is used to scan a group of 100 thermocouples, each couple being monitored every 50 msec and compared with a reference thermocouple. The difference is displayed on a 17-in. oscilloscope after suitable amplification. Temperature differences of 5°F are immediately apparent, and, if any couple differs by 50°F from the reference couple, it is annunciated. You will note that the scanner does not read absolute temperatures, only differences. A second thermocouple, adjacent to the reference couple, is therefore used with a precision temperature indicator to obtain the reading of the reference temperature.

The scanner will be most useful when the salt system, or a part of the system, is undergoing an operator-produced change in temperature, or when it becomes necessary to make certain that a particular piping loop

UNCLASSIFIED  
ORNL-LR-DWG 5891OR3A

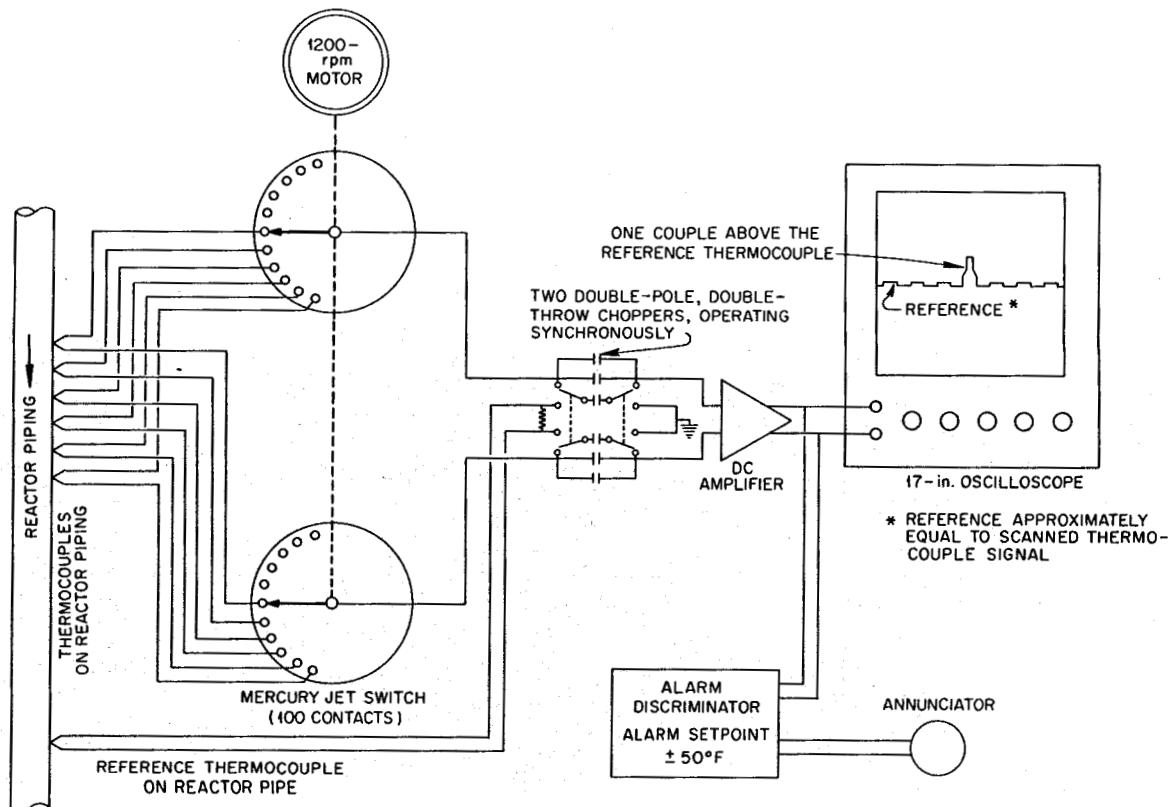


Fig. 2. Block Diagram of Temperature Scanning System.

or tank is at a uniform temperature, so that thermal gradients are minimized to unquestionably safe values. A typical situation occurs just before and during the filling of either the fuel- or the coolant-salt loop. The operator will be able to check temperatures around the loop and to make adjustments on the electrical heaters, as indicated by deviations on the oscilloscope.

Both the Operations Monitor and the Scanner have been thoroughly tested on experimental salt systems and test setups.

The Logger-Computer, which I will describe in more detail a little later, is capable of combining the operational features of both the Operations Monitor and the Scanner, but omitting the oscilloscope display, and, as we have it programmed, it is not used for control circuit interlocking.

#### More Important Process Measurements

Salt levels and flow rates are the most challenging measurement problems in the MSRE. Salt level in the drain tanks is measured in two ways. Pneumatic weigh cells are used to give a continuous indication of each tank's contents, and a two-point level detector tells us when salt level is at either 10 or 90% of tank capacity and gives us reference points for the weigh cell instrumentation. The level detector measures the voltage drop through the salt from electrodes suspended inside the tank. The weigh cell instrumentation is also used to provide control system interlocks when the reactor is being filled.

Weld-sealed pressure transmitters are used to measure helium pressures in lines to the drain tanks, and in the fuel pump bowl and the overflow tank. Salt levels in the fuel pump bowl and overflow tank are measured with submerged bubbler tubes and weld-sealed differential pressure transmitters. The output signal from all of these transmitters is electrical, and problems of transmission through the containment are thereby minimized.

We have also developed a float-type level transmitter, which gives a direct measurement of salt level without producing any major containment problems (see Fig. 3). No new concepts are involved. The float simply actuates the armature of a differential transformer which produces the signal. The magnetic coupling of the armature to the transformer coils is through the containment walls. The developmental problems involved pertain to environment, and results using this device are so encouraging that we have installed one on the coolant-salt pump bowl and will put a similar unit on the spare fuel-salt pump. We have operated one of these transmitters for more than two years on a test loop. Ninety percent (18,000 hr) of this time was at a temperature of 1250°F and 5% (1000 hr) at 1300°F. During this test period, the calibration shifted 0.2 in. (4%). A temperature change from 1000 to 1300°F causes a shift in indication of 0.3 in. (6%).

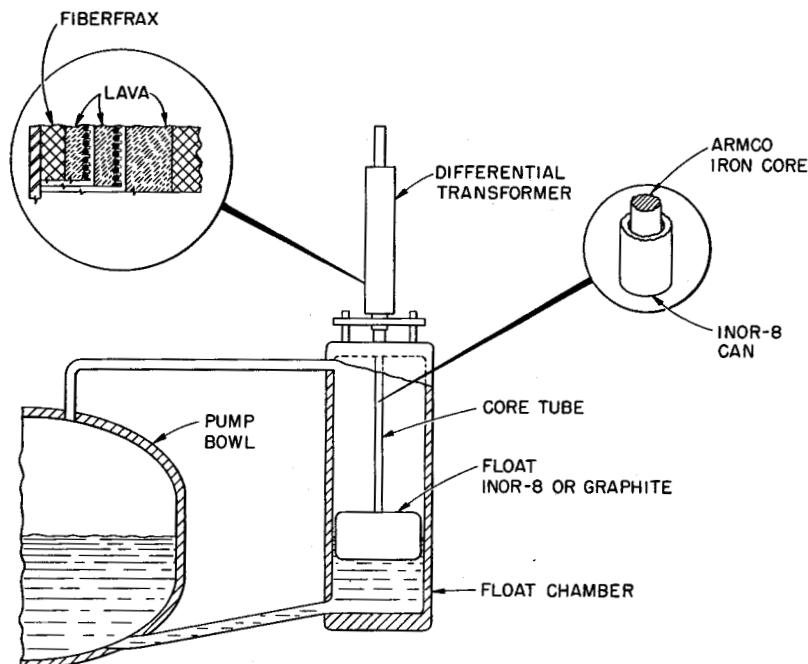
UNCLASSIFIED  
ORNL-DWG 64-7151A

Fig. 3. MSRE Float-Type Level Instrument.

A number of very small helium flows in the system are monitored with a flow element consisting of a packed bed of glass beads. Flow rate through this element is directly proportional to pressure drop, and this device is less subject to plugging and temperature effects than a capillary type element is.

Coolant-salt flow rate is measured by a Venturi and a specially designed differential pressure transmitter (Fig. 4). This transmitter is unusual in that intermediate NaK-filled capillary tubes, isolated by slack diaphragms, are used to transmit pressures from the molten salt to a silicone-oil-filled pneumatic transmitter of conventional design. A strain gage transducer has been added, so the output signal is electrical rather than pneumatic.

#### Nuclear Instruments

During normal operation from startup to full power, the MSRE will require three types of neutron sensors, namely: (1) fission chambers, (2) compensated ion chambers, and (3) safety chambers.

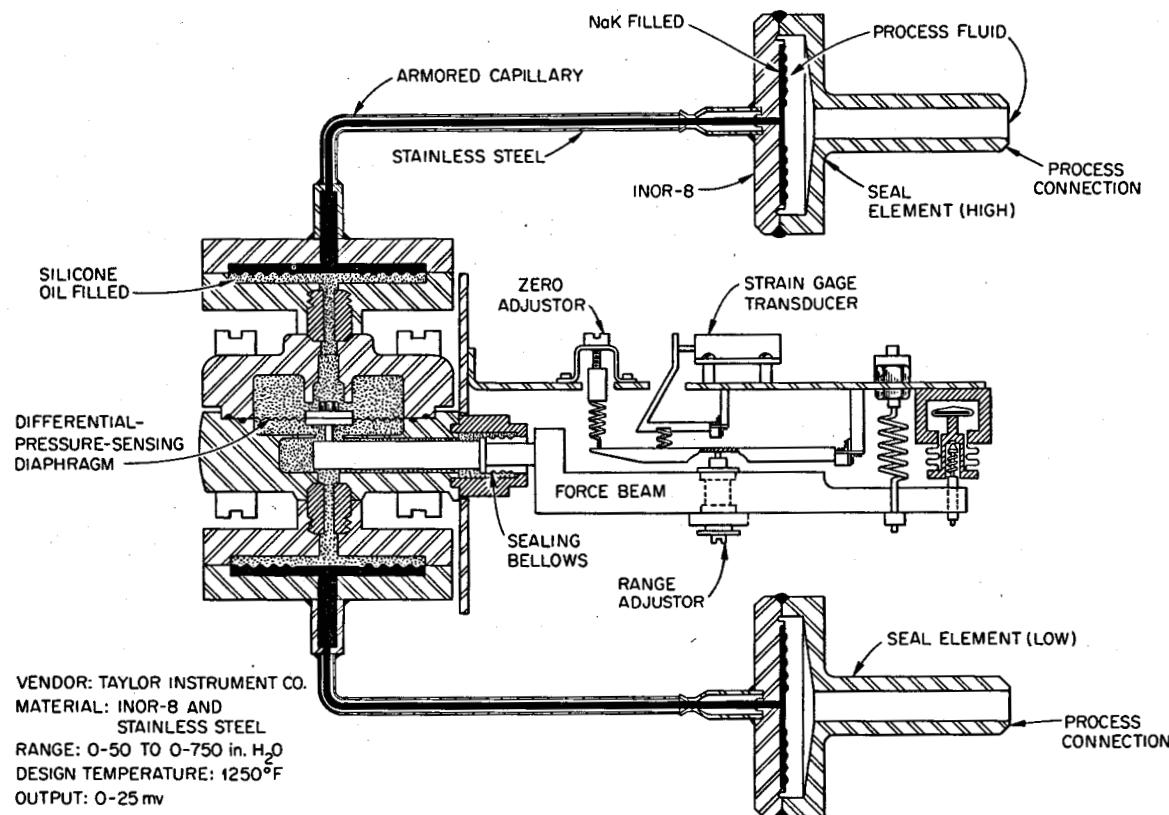
UNCLASSIFIED  
ORNL-LR-DWG 78815

Fig. 4. All-Welded, High-Temperature, NaK-Filled Differential-Pressure Transmitter.

For the initial critical experiments, four temporary channels of BF<sub>3</sub> counters will also be used. With the exception of two of the temporary BF<sub>3</sub> channels, all of the chambers are installed in a single penetration (Fig. 5). This penetration is 3 ft in diameter, is water filled, and contains a total of 10 internal guide tubes, which loosely retain and locate the chambers.

Figure 6 is a plan view of the reactor and the penetration.

During the early stages of design we provided two vertical holes in the shield for BF<sub>3</sub> counters and a third hole for the neutron source. Subsequently, analysis by Haubenreich and Engel showed that the majority of the neutrons at these locations will be source neutrons (as opposed to fission neutrons) which will have gotten to the counters by traveling around in the annular space between the shield and the core vessel. For that reason, we are putting the other BF<sub>3</sub> chambers directly opposite the source tube in the penetration.

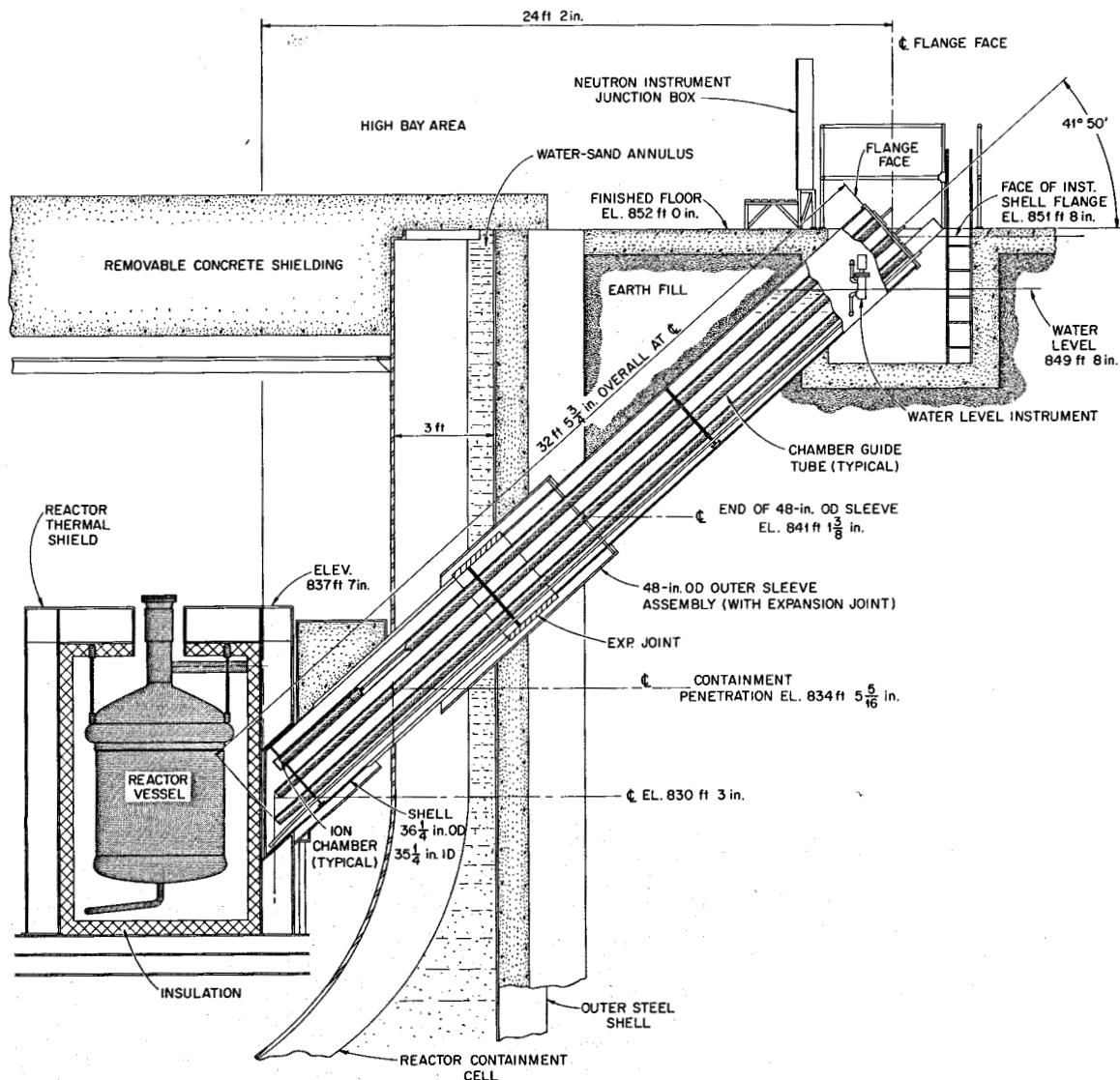
UNCLASSIFIED  
ORNL-DWG 64-625

Fig. 5. Elevation View of Nuclear Instrument Penetration.

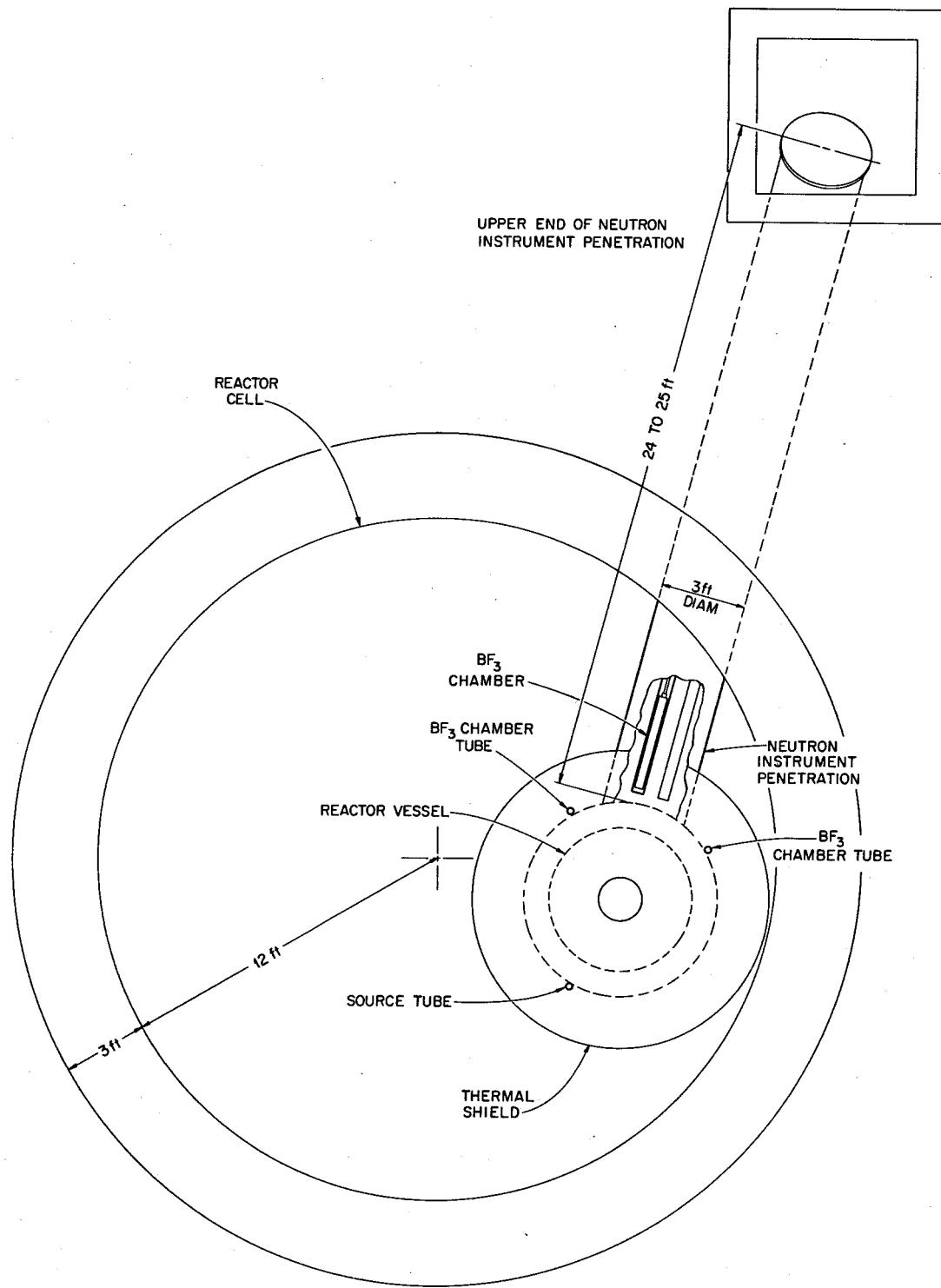
UNCLASSIFIED  
ORNL-DWG 64-984

Fig. 6. Plan View of Core Vessel, Showing BF<sub>3</sub> Counters in Shield and Source Location.

The fission chambers are the input sensors for the wide range counting system. This was described in an information meeting about two years ago. (see Fig. 7.). The fission chamber is moved by a servomotor, so that it maintains a constant, preset count rate for all values of reactor power sufficient to produce this count rate. If the attenuating medium surrounding the chamber produced ideal exponential attenuation, the log of reactor power would be proportional to the distance the chamber is withdrawn from its innermost position and the reactor period would be proportional to the velocity. Since this ideal situation is never attained, an adjustable trimming device, the function generator, is included in the servo to compensate for the deviation from true exponential neutron attenuation.

UNCLASSIFIED  
ORNL-DWG 64-1218R

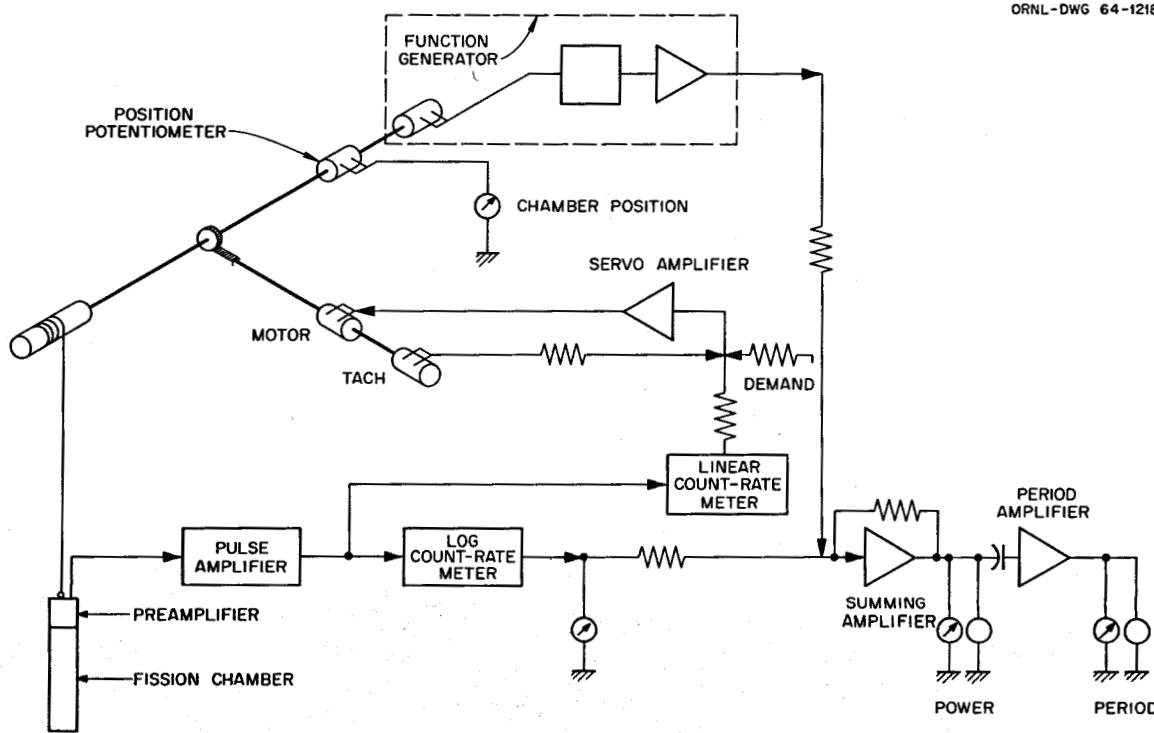


Fig. 7. Block Diagram of a Wide-Range Counting Channel.

The actual physical arrangement as used in the MSRE is shown in Fig. 8. Two compensated ion chamber channels are used to provide the most accurate flux information and for the input signal to the servo controller. Figure 9 is a highly simplified block diagram of these two channels.

By means of range switching on the picoammeters, an overall range of seven decades can be covered without changing chamber position or am-

plifier gain. In contrast to the wide range channels previously discussed, output is linear, and each range setting covers only half a decade, thereby giving good resolution. Output from either chamber and its range setting are continuously indicated and recorded on the main control board.

A third group of three chambers provides flux information, used as inputs to the safety system. These are uncompensated, neutron-sensitive ion chambers and have no function other than safety. They are effective in the power range from 1 kw to above 15 Mw.

UNCLASSIFIED  
ORNL-DWG 64-1219

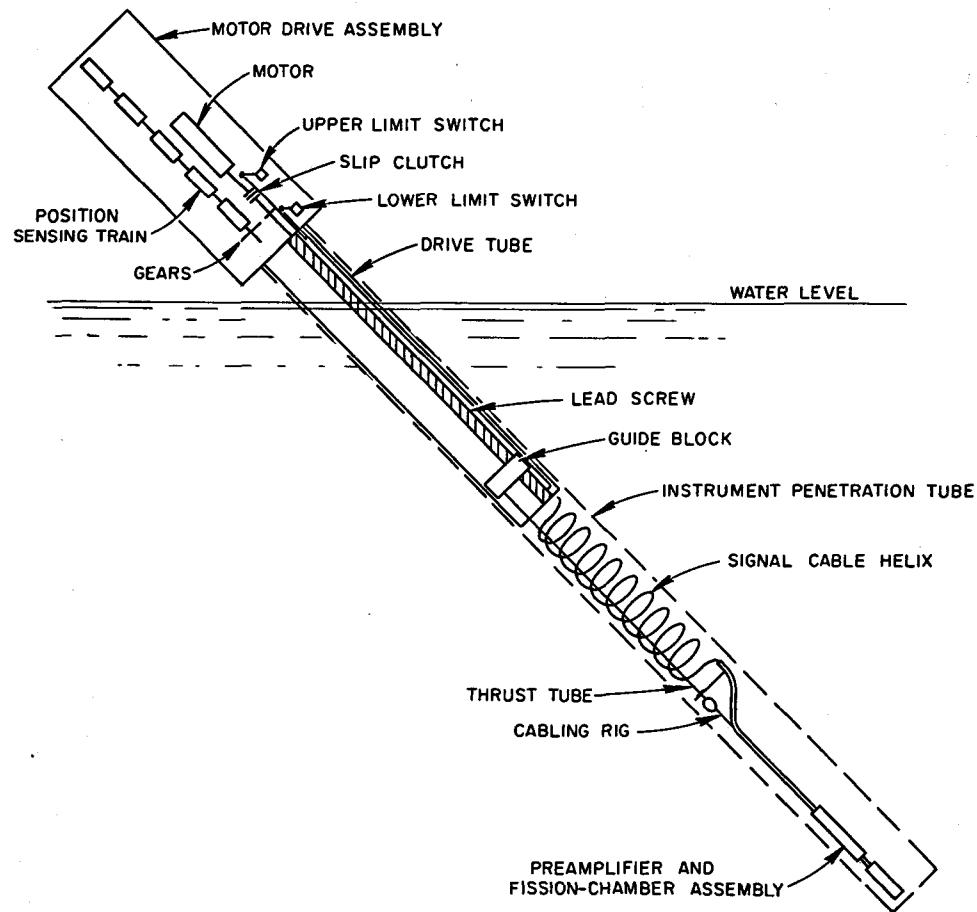


Fig. 8. Positioning Mechanism for Wide-Range Counting Channel.

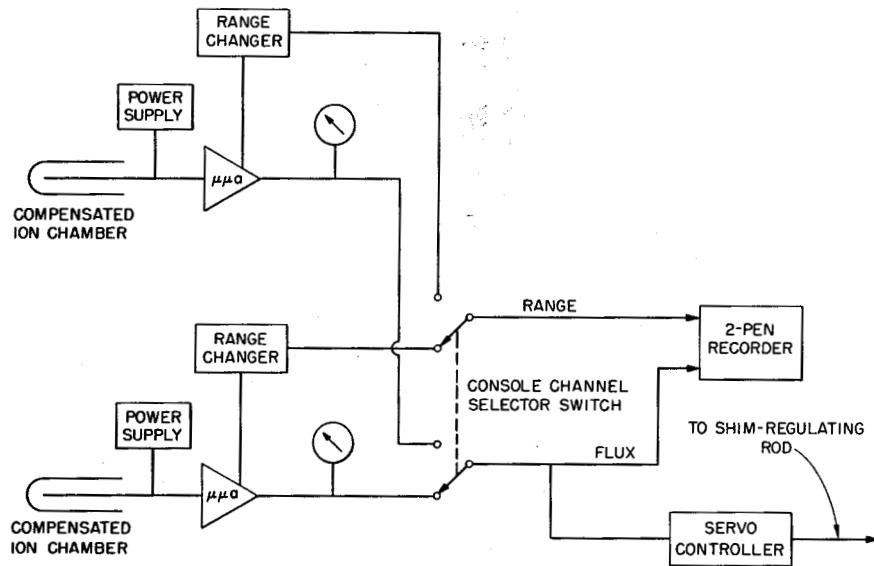
UNCLASSIFIED  
ORNL DWG 64-6480A

Fig. 9. MSRE Nuclear Instrumentation - Linear Flux Level Channels.

Rod Drives

Figure 10 is a diagram of a control rod drive. The articulated control rod is suspended from a sprocket chain driven by a gear-reduced ac servomotor. The three drives are identical; they include coarse and fine synchros to transmit rod position, an irreversible worm and gear set, and a potentiometer for the position input signal to the safety system. You will note that two parallel power transmission paths have been provided to the sprocket chain. One is via the electromagnetic clutch; the alternate drive path is through an overrunning clutch. The latter always provides a positive drive in the "insert" direction, and also maintains a positive connection to the drive, so that reverse torque at the output sprocket cannot produce accidental rod withdrawal. Any one of the three rods is capable of being used as the servo-controlled shim-regulating rod, by merely changing the electrical interconnections.

The shock absorber (shown in Fig. 11) used with this drive unit is somewhat unusual. It consists of a cylinder and a piston or plunger with the unique feature that the working "fluid" is composed of 3/32-in.-diam steel balls. The shock absorber assembly moves up and down with the rod. When the rod is scrammed, the cylinder halts at the stop blocks at the bottom of the housing. The rod and the plunger continue to move downwards, and the kinetic energy of the rod is absorbed as the steel balls are forced through the narrow annulus around the plunger into the upper part of the cylinder. This device is a development of the Vard Corporation, who are building the rod drives.

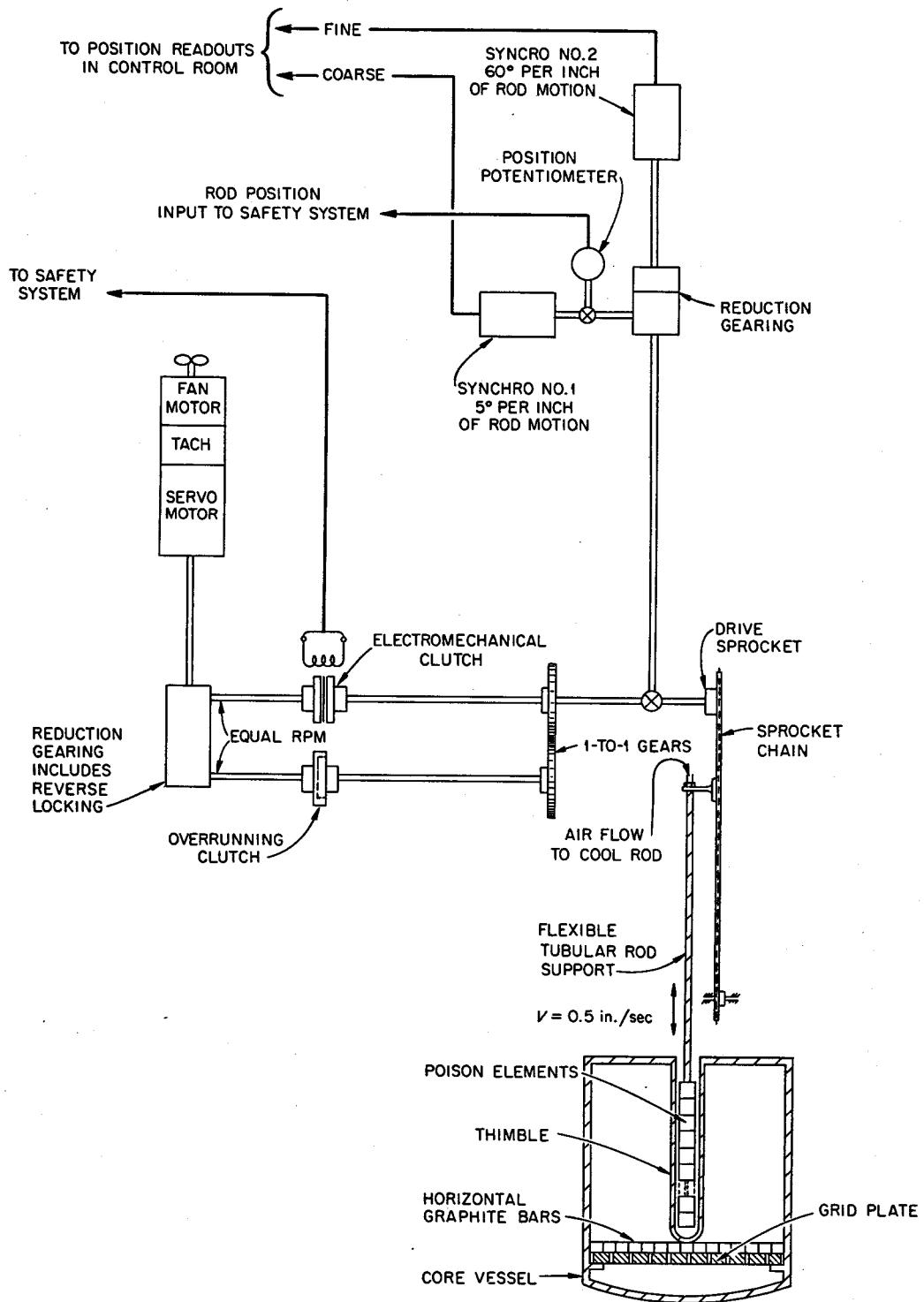
UNCLASSIFIED  
ORNL-DWG 63-8391

Fig. 10. Electromechanical Diagram of Control Rod Drive.

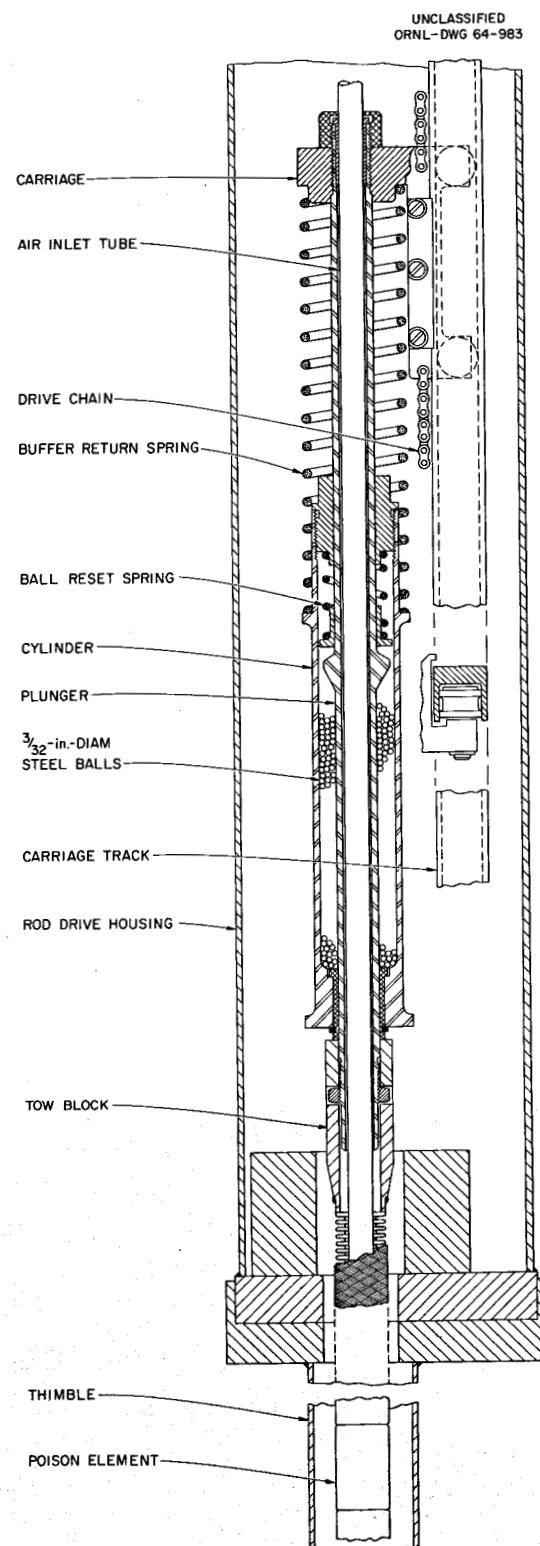


Fig. 11. MSRE Control Rod Drive - Shock Absorber Assembly.

Scram is effected by opening the clutch coil circuit, which disengages the clutch.

The curves in Fig. 12 give a comparison of actual scram performance with an arbitrary performance specification based on an acceleration of  $5 \text{ ft/sec}^2$  and a maximum release time or delay of 100 msec between the existence of scram conditions and actual disengagement of the clutch. Analysis has shown this to be adequate for any contrived situation. You will note that there is a wide margin of actual acceleration over that required. The actual acceleration obtained from tests of a prototype unit was  $13 \text{ ft/sec}^2$ .

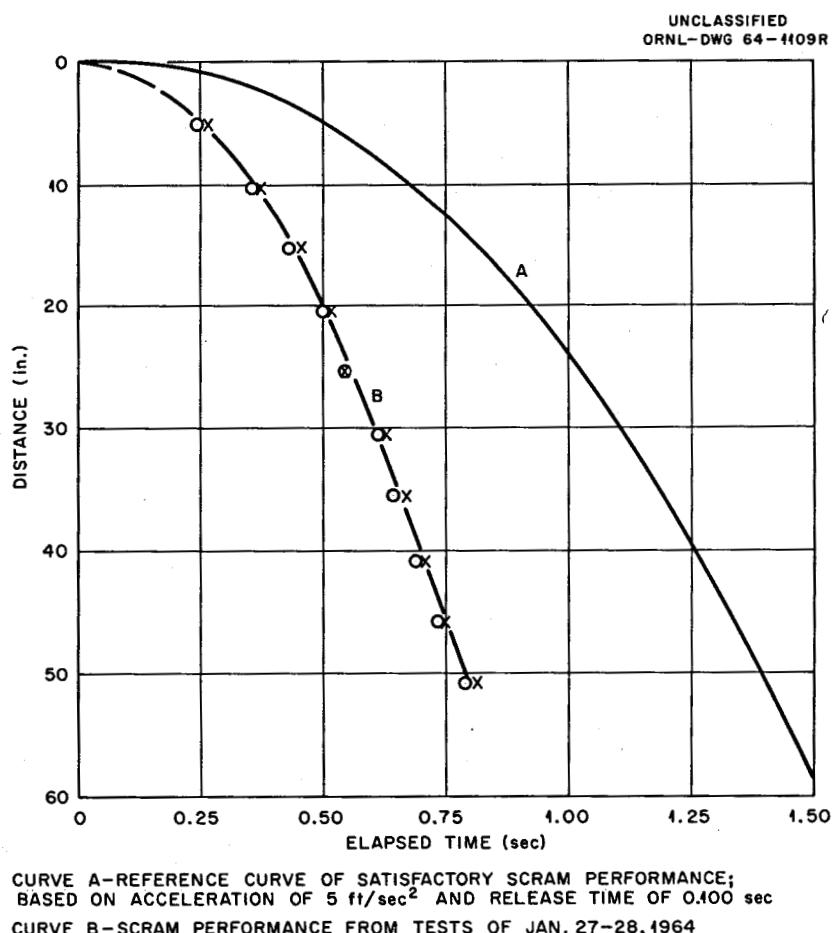


Fig. 12. MSRE Control Rod Height vs Time During Scram. Curve A — reference curve of satisfactory performance, based on acceleration of  $5 \text{ ft/sec}^2$  and release time of 0.100 sec. Curve B — scram performance from tests of January 27-28, 1964.

The curves in Fig. 13 have been calculated from the insertion distance vs time curves seen in Fig. 12 and the reactivity worth of two rods, starting from an initial withdrawal height of 51 in. Again we have a substantial margin of performance over that deemed adequate.

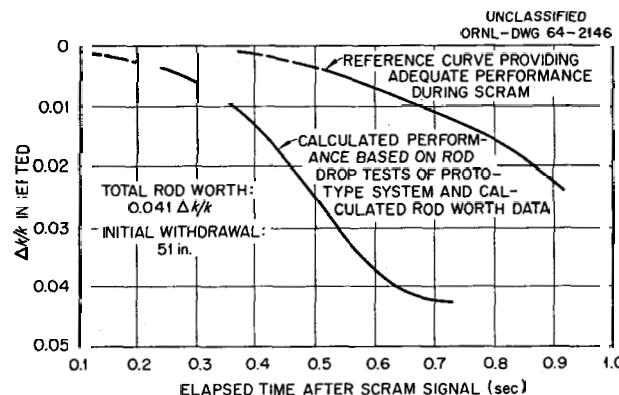


Fig. 13. MSRE Control Rods - Reactivity Insertion vs Time After Scram.

#### Safety System

The MSRE safety system is composed of reliable and redundant instrumentation, designed to protect the system and to ensure containment. Figure 14 is a block diagram of the system. We have extended the scope of the MSRE safety system beyond direct considerations of conditions in the core. The string of blocks on the left side of the diagram are conditions which initiate safety system action. Two of these, temperature and flux, call for a rod scram. Most of the remaining inputs and safety actions are concerned with various process instruments. The individual instruments and related equipment, which provide the input-output functions shown in the diagram, have been selected or designed with reliable operation as the first consideration. Redundancy, in the form of either two or three independent input channels, is used to produce the output action required. Periodic, in-service testing of all or a major portion of each channel is provided. For example, Fig. 15 shows three independent channels of temperature input information as we use it to scram the control rods or to drop the radiator doors. The instrumentation used to convert thermocouple emf to a usable signal is conventional, but for in-service testing we have added an additional pair of thermocouple junctions in series with the measuring junction on the pipe. During normal operation, both the added junctions are at the same temperature and hence produce no net signal. We can test the rod scram input circuitry by applying electrical heat to one of the added junctions, thus simulating a temperature rise at the reactor outlet. A temperature drop can be simulated by reversing the polarity of the artificially heated junction.

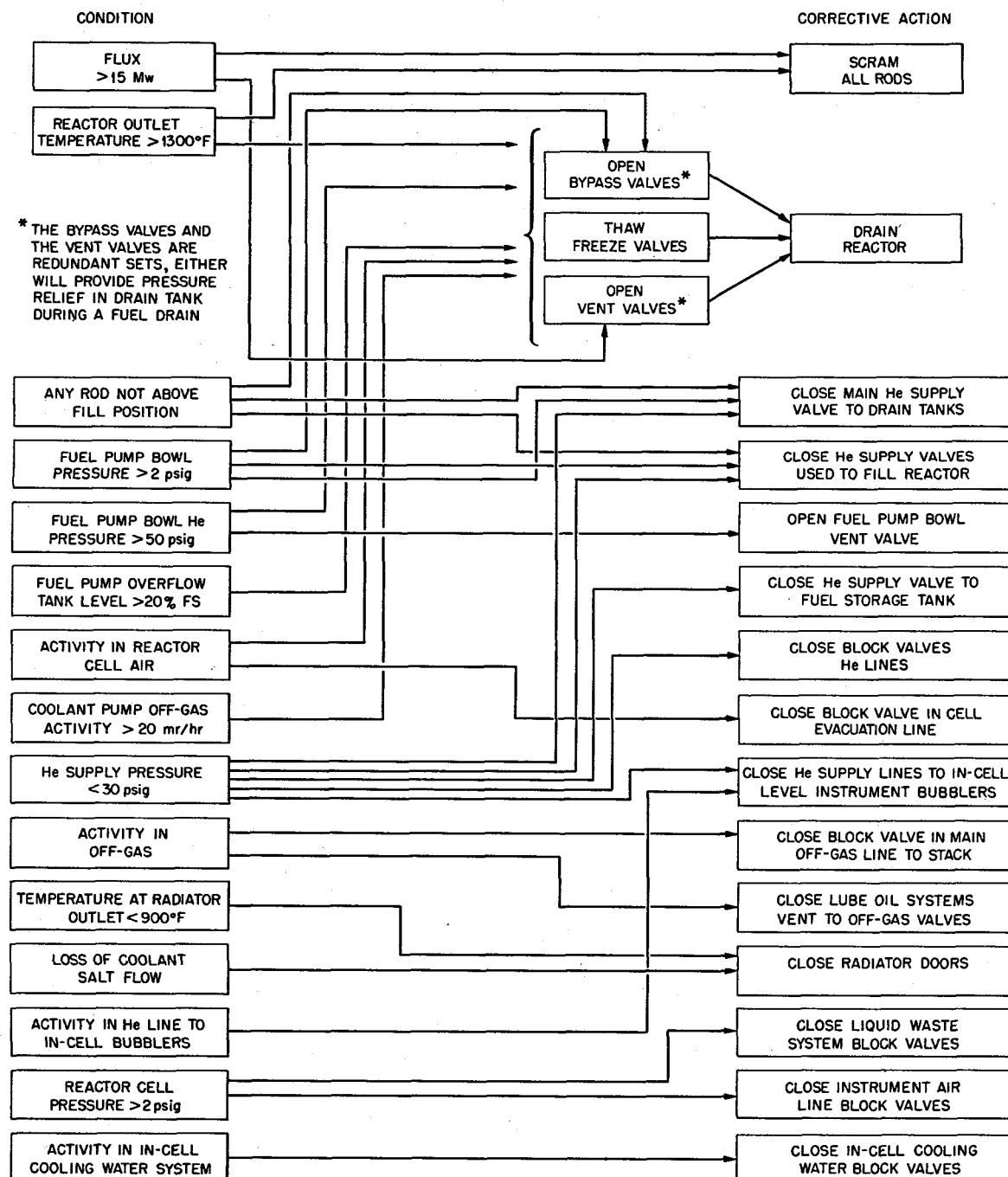
UNCLASSIFIED  
ORNL-DWG 64-637

Fig. 14. Block Diagram of MSRE Safety System.

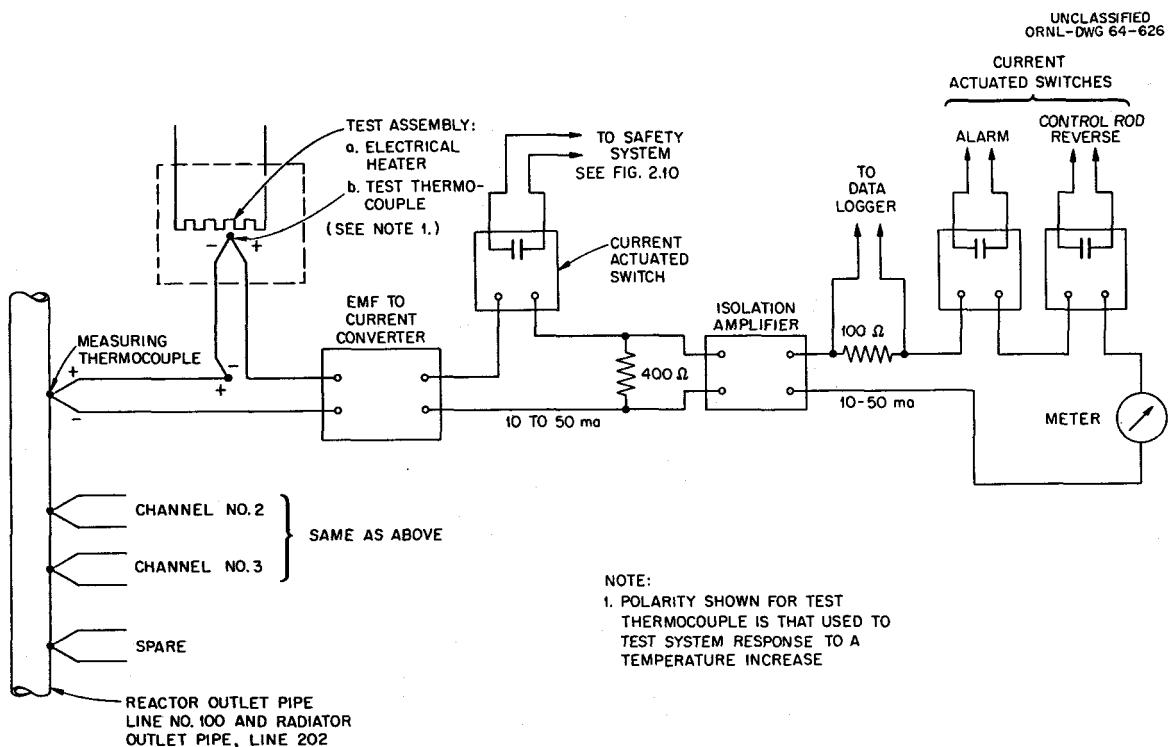


Fig. 15. Typical Temperature Measuring Channels Used in MSRE Safety System.

The three channel systems used to ensure containment are worth noting. Figure 16 shows the instrument setup used to close the block valves in the instrument air lines to in-cell pneumatic instruments when cell pressure exceeds 2 psig.

This 2 out of 3 system uses three independent pressure switches with diverse power sources to signal high pressure in the cell. Agreement of any two will initiate valve closure. This allows one nonoperating channel for either maintenance or testing. In service, routine testing is accomplished by manually opening, one at a time, the hand valves which lead to the nitrogen bottle and observing the pressure gages in the solenoid matrix. A similar technique is used with the three instrument channels used to measure the pressure of the inlet helium which enters the containment.

Rod scram is produced either by excess reactor outlet temperature or by excess flux. Figure 17 is a diagram, somewhat simplified, of the rod scram system. Each channel is independent. The neutron flux channels are continuously monitored to verify that the chambers are supplied with the correct voltage. The monitor unit provides means for testing channel response by simulating an excess flux signal. This is a 2 out of 3 coincidence system, and a rod scram will also be produced if any two input channels malfunction. This would occur if there were a loss of voltage to any two ion chambers.

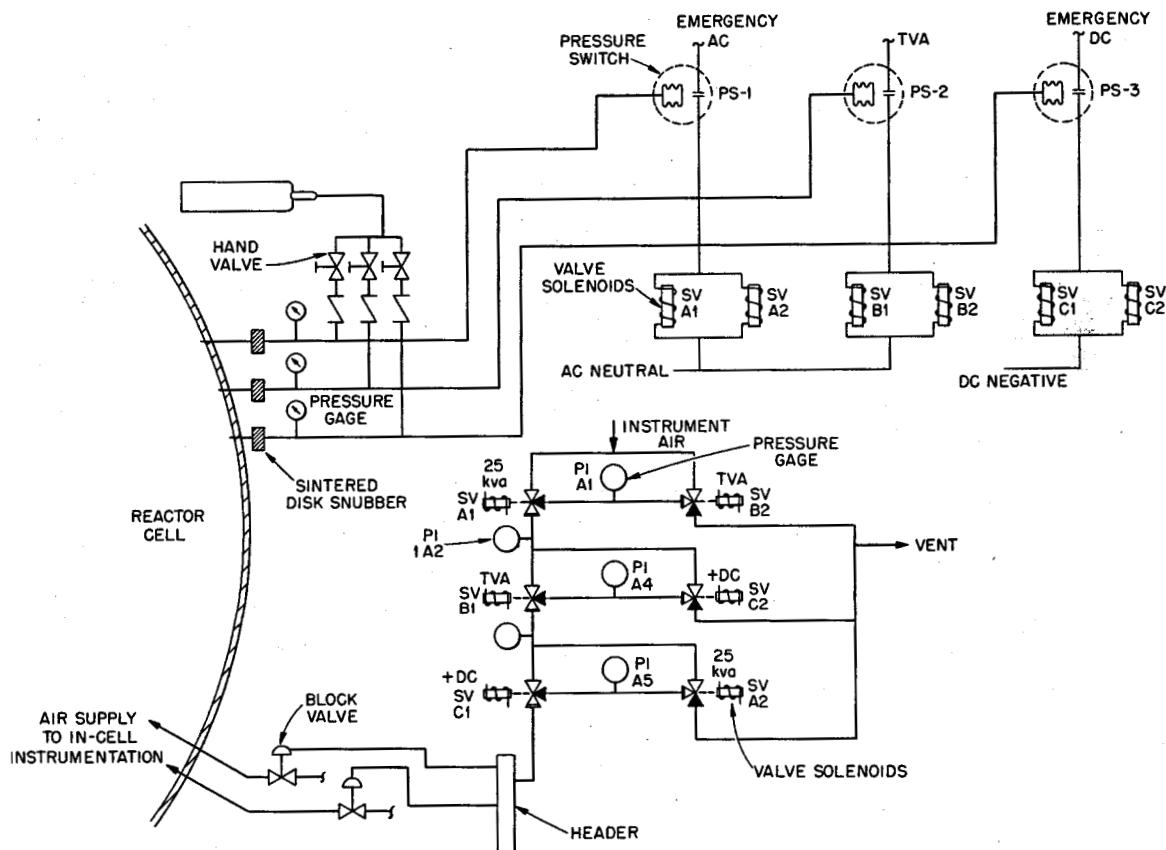
UNCLASSIFIED  
ORNL-DWG 64-6477A

Fig. 16. MSRE Redundant Instrumentation for Block Valves.

The electronic instrumentation making up this system is newly designed. It uses solid state modular construction and was not designed specifically for the MSRE or any other particular reactor. Rather, it is highly versatile in its capability of being adapted to a wide variety of design situations and is suitable for use in a wide variety of system configurations. For example, both the MSRE safety system and that of the High Flux Isotope Reactor use the same nuclear instrument components.

Figure 18 diagrams the system used for emergency closure of the radiator doors. A conservative analysis has shown that the coolant salt in the radiator can freeze in less than a minute in the worst situation. Since freezing and subsequent thawing may damage the radiator, a reliable system is employed to close the doors if the radiator outlet temperature becomes too low or if the coolant salt ceases to flow. The decision to scram the doors does not involve safety or containment; it was based solely on economic considerations.

UNCLASSIFIED  
ORNL-DWG 64-6479A

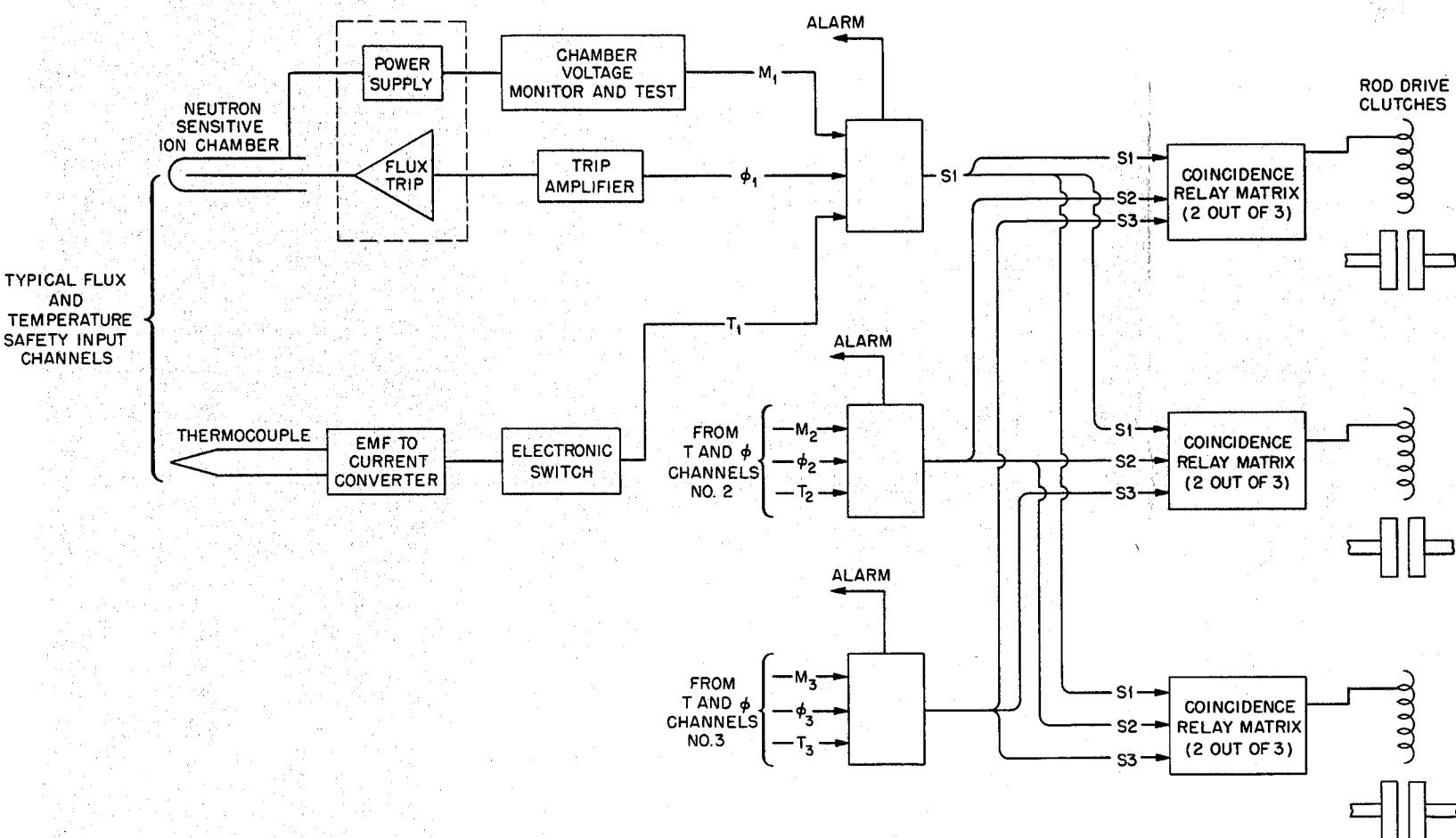


Fig. 17. Diagram of Rod Scram System.

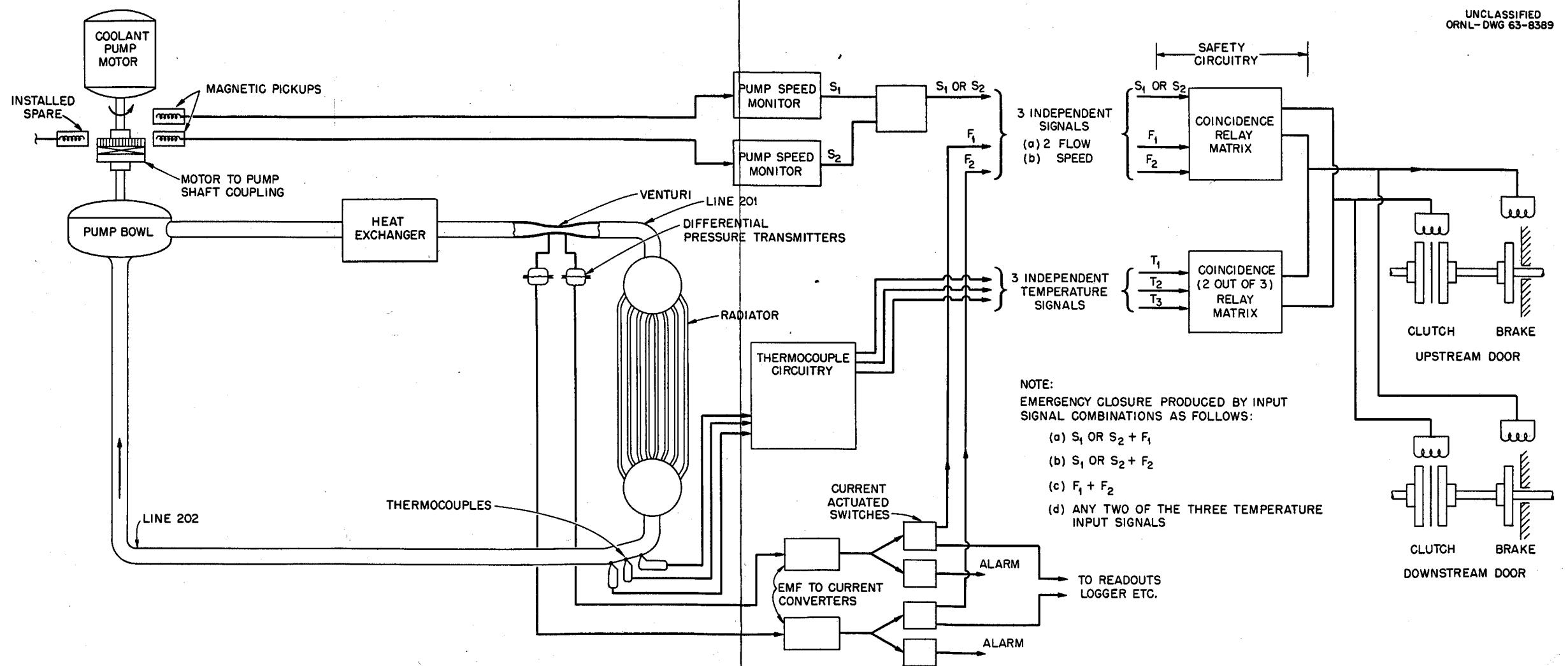


Fig. 18. Diagram of System Used for Emergency Closure of the Radiator Doors.

In addition to the safety instrumentation, there are several important control system interlocks which are not designed to as high a degree of reliability as the safety-grade protection. For example, there is a derivative signal from the drain tank weigh cells which is used to limit the reactor fill rate. We automatically insert or reverse the control rods if the reactor outlet temperature exceeds 1275°. This temperature is halfway between the design-point full-power temperature and the scram temperature. We also get an automatic reverse if power exceeds 12 Mw, if fuel level is too high in the overflow tank, or if, during startup, we are on a period of less than 10 sec or power exceeds 1.5 Mw.

#### Reactor System Control

Operation of the MSRE can be logically divided into two principal modes, and we use the control system to make the division. The first, or "prefill," mode includes those operations which are preparatory to nuclear operation, such as transfers of salt from the storage tank to the drain tanks, transfers among the drain tanks, circulation of helium in the fuel and coolant salt loops, and testing of all the various elements of the system. The last includes testing of pumps, cooling air and water systems, radiator doors and blowers, etc. The second mode, which we call "operate," includes nuclear operation of the system and aspects of operation, such as filling the system, which can lead directly to nuclear operation.

Figure 19 is a block diagram which shows, in a very broad sense, the more important restrictive and permissive interlocks in the control system.

The reactor may be operated either manually or with automatic control of the shim regulating rod. During the early phases of the design, we held the hope that the negative temperature coefficient would supply all the control required when the reactor was in the power range above 1 Mw. Analog simulation showed us that this would not be the case and that supplementary, external control would be required. This is the price we must pay to produce low-power-density design and to use an existing facility which imposes unfavorable piping geometry from the standpoint of control.

This reactor system is characterized by high heat capacity, long transport lags, low power density, and, consequently, a very sluggish temperature response to load and power changes. About half of the temperature coefficient is in the graphite moderator, which occupies nearly 80% of the core volume. It takes the graphite between 12 and 20 min to reach temperature equilibrium following a step change in reactor fuel-salt temperature. The transport lag from the radiator to the core is nearly 1/2 min in each direction; that is, it takes 25 sec for a change in radiator load to show up as a temperature change in the core, and the same length of time for a temperature change in the core to affect the loading at the radiator.

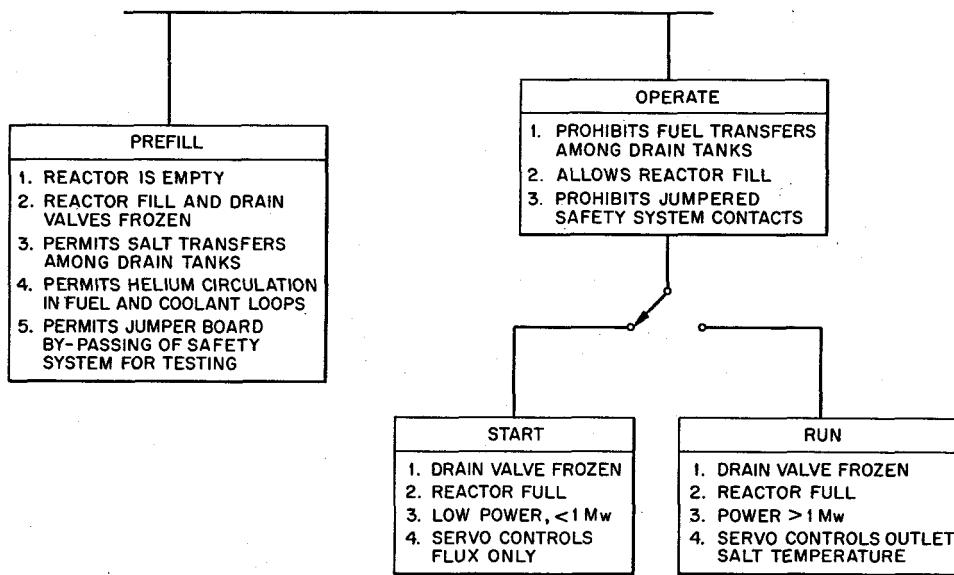
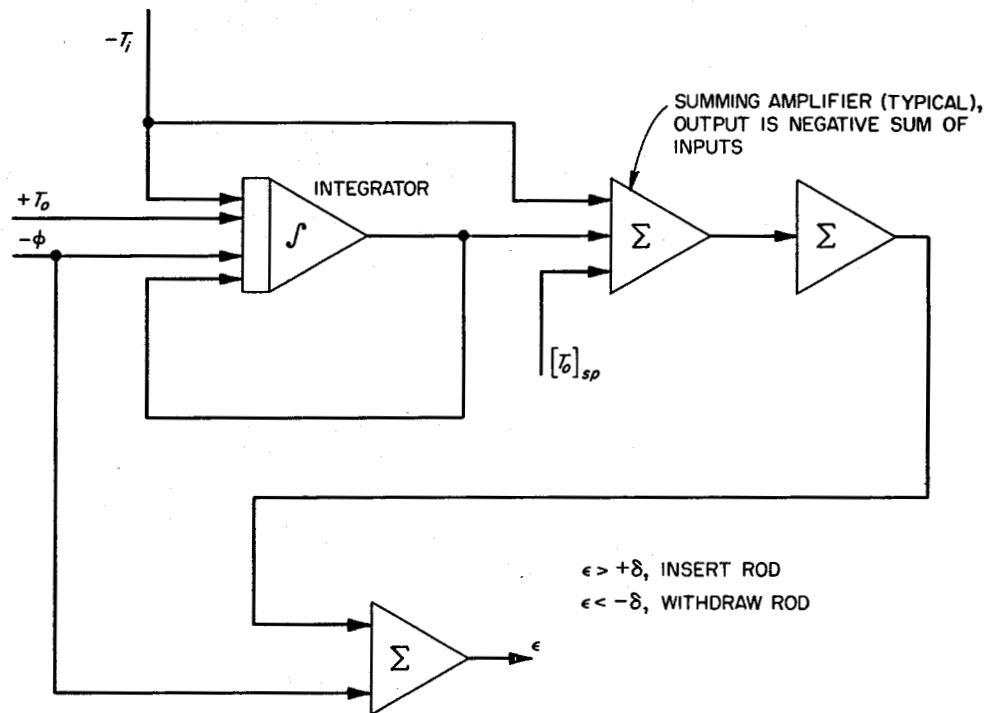
UNCLASSIFIED  
ORNL-DWG 64-6478A

Fig. 19. MSRE Control System Modes.

If there were no external control system, the analog simulation showed that in some situations the reactor would oscillate with very long periods around the average power demand level. These oscillations, while not dangerous, would be intolerable from an operating standpoint.

The controller which was developed as a result of these analog studies is diagrammed in Fig. 20. When the reactor is operating as a load-following power generator, the servo controller is used to hold the core outlet temperature constant. This mode of control is optimum thermodynamically and is what we would do if we were using the reactor to generate steam.

The controller is composed of four operational amplifiers; three are used for summing and for sign inversion, and the fourth is used as an integrator. Four inputs are used to attain control: flux, inlet temperature, outlet temperature, and outlet temperature set point. These inputs are combined. The controller can thus compare the reactor power, represented by flux, with the load, represented by the temperature drop across the core, and compute an error signal, calling for regulating rod action, should the two be different. The curves at the bottom of Fig. 20 show the open loop responses of the controller to step changes in flux, inlet temperature, and outlet temperature set point. This response curve for set point temperature is academic, since we use a low speed, motor driven potentiometer to make certain that we can't make step changes in temperature demand. The integrator produces, on a long time scale, a subtractive correction to the initial step inputs and gradually causes a reduction in the error signal. This scheme, using a long time constant integrator to reduce the error signal, also makes the controller insensitive to slow drifts in the inlet temperature and flux sensors.

UNCLASSIFIED  
ORNL-DWG 64-6206

$T_i$  = FUEL SALT TEMPERATURE, CORE INLET  
 $T_o$  = FUEL SALT TEMPERATURE, CORE OUTLET  
 $\phi$  = NEUTRON FLUX  
 $[T_o]_{sp}$  = SET POINT, FUEL SALT OUTLET TEMPERATURE

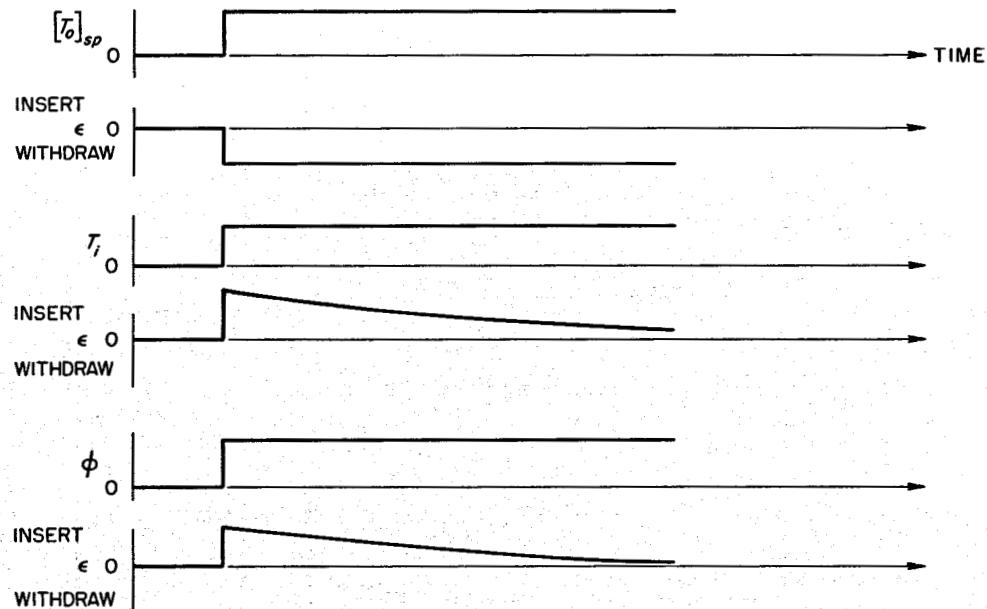


Fig. 20. Block Diagram of Servo Controller, Open Loop Responses to Step Inputs.

Below approximately 1 Mw, the controller is used as a simple flux comparator, and temperature control is by manual adjustment of system heaters. The results of an analog simulation of the reactor system using this controller are presented in Fig. 21.

Each regulating rod is capable of producing a total change of 2 to 3% in reactivity - considerably more than we care to put at the disposal of this or any other rod control servo. We have added a limit switching mechanism which reduces the effective stroke of the servo-controlled rod to an acceptable value.

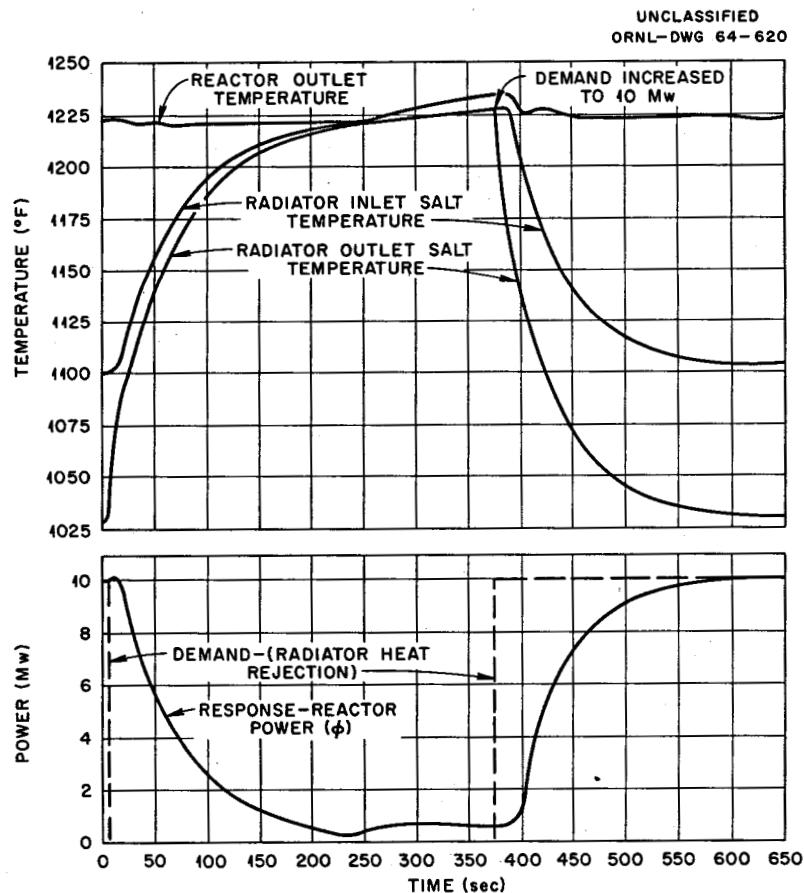


Fig. 21. Results of Analog Simulation of the Reactor System Using the Servo Controller.

The diagram on the left of Fig. 22 is strictly conceptual and shows what the limit switches accomplish. The motion of the control rod actually is remotely reproduced in the control room by a servomotor-driven cam which actuates the limit switches. A second motor is also coupled to the cam by means of a differential gear and locates the span of the limit switches with respect to the rod position, when shimming with the regulating rod.

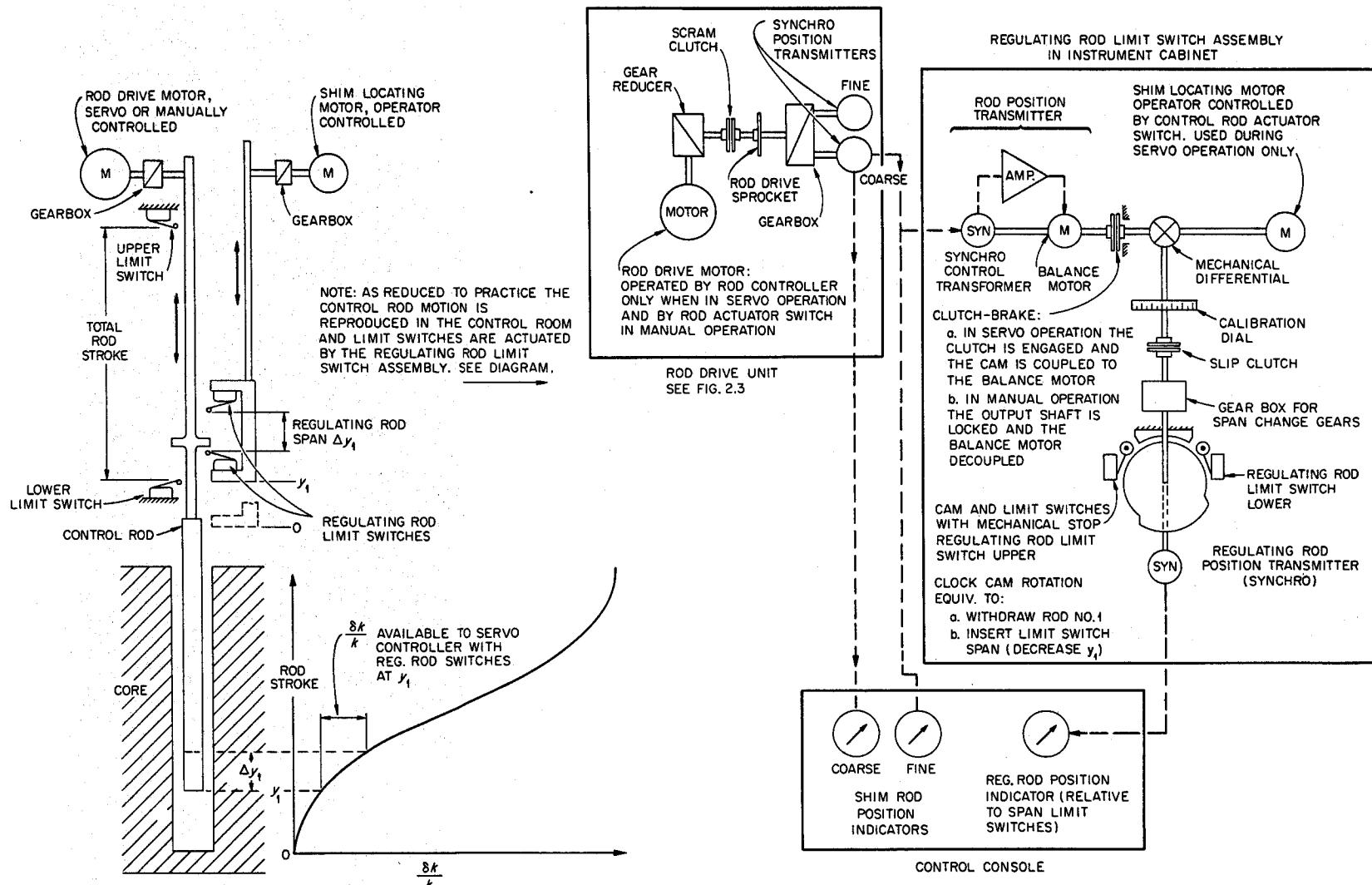


Fig. 22. Diagram of Regulating Rod Limit Switching Assembly.

A similar device has been operating very satisfactorily in the control system of the ORR for several years, and we have no reservations as to its use in the MSRE.

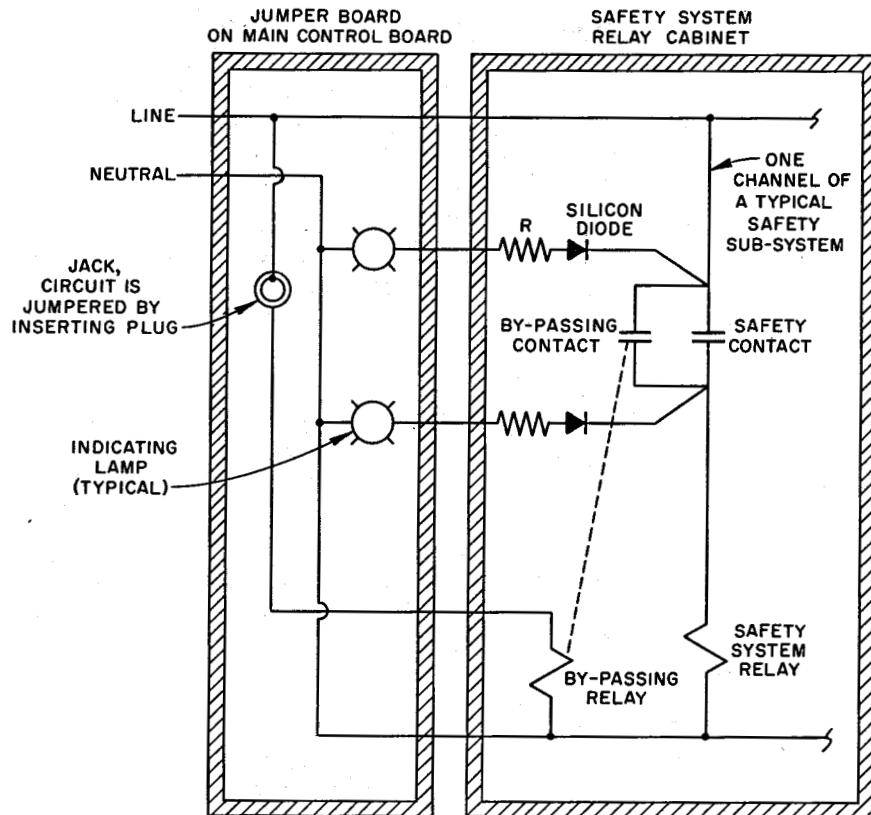
#### Load Control

Load, or reactor demand, is determined by the radiator door opening, by the by-pass damper position, and by the blowers. These components are all independently capable of affecting the load, and the manipulation of all of the pushbuttons, switches, etc., required to make load changes in a consistent and orderly fashion would be a burdensome task for a busy operator. These switching operations are programmed so that load changes may be accomplished by a single control switch at the console. Manual control of the various components responsible for the load is optional.

#### Circuit Jumpering

System checkout and tests of various parts of the reactor system, and the nonroutine operations required to conduct experiments, inevitably create conflicts and inconsistencies between operational requirements and prohibitions imposed by the control and safety system. An obvious example in the MSRE is the checking of the operation of the radiator doors when the system is empty and shut down. The safety system keeps the doors closed if salt (or pipe) temperature is below 900°F or if there is no coolant-salt circulation. Obviously, it is good practice to periodically check the operation of these doors. It isn't good practice to do this inspection by using clip leads to bypass interlocks or by temporarily rearranging the electrical interconnections on an informal basis.

A jumper board has therefore been mounted on the main control board to allow formal, administratively controlled bypassing of interlock and safety circuit contacts. Figure 23 is a diagram showing typical circuitry required to jumper a safety system contact. Actual contact bypassing is accomplished by relays which are energized when plugs are inserted in the board. Consider the situation in which there is a string of contacts ahead of a safety relay with several of these jumpers for bypassing. An open neutral could, conceivably, produce a sneak circuit via the lamps which might carry enough current to keep the safety relay energized, regardless of whether the safety contacts were open or closed. This is prevented by the silicon diodes which, in this situation, are back-to-back and prevent alternating current flow. The use of a bypassing jumper requires permission of the Operations Supervisor. Any jumper in the safety system circuitry prohibits switching into the "operate" mode. The jumper itself is visible from the control console, and each jumper or closed contact is indicated by a light on the jumper board. If any safety system contact is jumpered, an annunciator is actuated. The jumper board is designed as a graphic panel display of the control system circuitry and, in conjunction with the indicating lamps, gives the operator an immediate graphic display of the circuit condition of all vital control circuits.

UNCLASSIFIED  
ORNL-DWG 64-6080

NOTE: THE JUMPERS AND THE INDICATING LAMPS ARE ON THE MAIN CONTROL PANEL AND VISIBLE FROM THE OPERATOR'S CONSOLE.

Fig. 23. Diagram of Safety System Bypassing with Jumper Board.

#### Process Radiation Monitoring

The principal function of our process radiation monitors is to ensure containment; none of these monitors is used for routine operational control purposes.

We do monitor, with redundant input systems, the process lines from the containment which can provide a credible avenue of escape for contaminating radiation. These lines are, of course, equipped with block valves, which are closed automatically by the radiation monitoring equipment.

Line monitors are installed on the inlet helium supply lines to the fuel-salt loop and on lines from the containment in the off-gas system. These off-gas system monitors look at the cooling air flow in the secondary containment cell and at helium flows from the fuel- and coolant-salt loops, from the drain tanks, from the pump lube oil systems, and from the sampler-enricher. The off-gas is monitored again by the stack

gas monitor, just before being discharged to the atmosphere. The coolant pump off-gas should not contain any activity whatsoever. The origin of any activity in this line would be a leak in the heat exchanger, causing contamination of the coolant salt. Similarly, leakage of salt or fission product gases from the fuel-salt loop into the secondary containment would be detected by the monitors on the cell evacuation air line. Activity in either cell air or coolant pump off-gas initiates a drain and closes block valves in the lines involved.

The in-cell cooling water is also monitored for activity at the pump inlet pipe. This cooling water system circulates water to the fuel- and coolant-salt pumps, the in-cell air coolers, and the thermal shield. These monitors also produce automatic block valve closure.

Where radiation monitoring instruments are used to close block valves or to initiate an automatic drain, the input channels are redundant and the installation includes provisions for periodic testing with a source. In some cases, the redundancy is of the 2 out of 3 coincidence type for in-service testing.

We have also installed gamma chambers in the secondary containment cell around the reactor vessel, in the drain tank cell, and in the radiator pit. The fuel sampler-enricher and the lube oil systems are also equipped with individual radiation monitors.

#### Health Physics Monitoring

With respect to the individual instruments used, the MSRE health physics monitoring instruments are typical. That is, at strategic points in the building are located seven Constant Air Monitors to detect airborne contamination, and seven Beta-Gamma Monitors and seven Monitrons to detect sources of radiation. Readout from this scattered array of instruments is obtained locally at the instruments and centrally in the control room.

The control room alarm and annunciator instrumentation has been designed to meet ORNL requirements for health physics monitoring installations. Figure 24 is a block diagram of the health physics monitoring and alarm system. The system

1. indicates some types of instrument malfunction (i.e., an instrument failure evidenced by zero output produces an audible alarm and turns up a lamp showing which instrument is not functioning),
2. indicates by lamps and the audible alarm any instrument that exceeds the permissible health physics radiation level and provides a second indication at the high alarm level (3 times that of the health physics level for the Monitrons),
3. provides a control signal at any reasonable degree of coincidence. In the MSRE we have selected two groups of monitors so that if any two Monitrons out of six or any two Constant Air Monitors out of four are at the "high" alarm level, an automatic evacuation signal results.

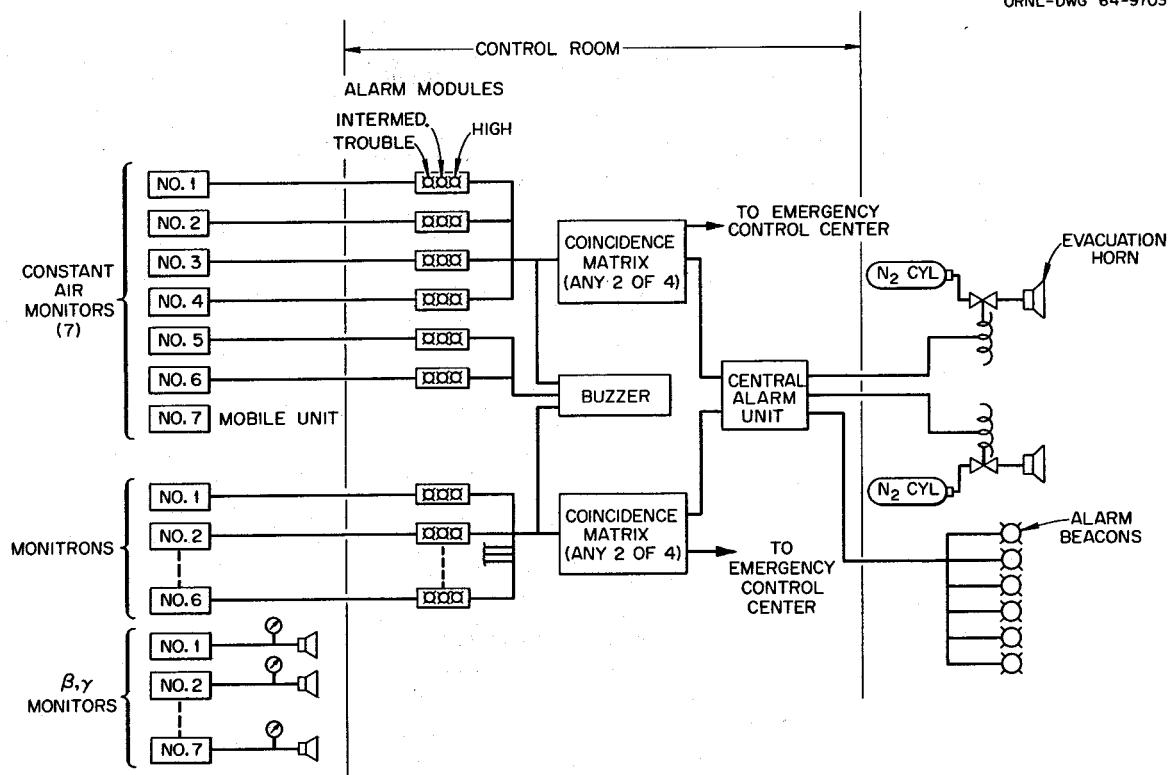


Fig. 24. Block Diagram of MSRE Health Physics Monitoring System.

This annunciation and alarm instrumentation, which ties the individual monitors together as a system, is of modular construction. The design of a health physics monitoring and alarm system is accomplished by the interconnection of a sufficient number of modules to meet design criteria for a particular facility.

All evacuation signals, whether produced automatically or administratively by the reactor operator or other responsible person on the site, are transmitted to the ORNL Emergency Control Center, where appropriate emergency procedures are set in motion. The automatic alarm can be blocked out by a key switch administratively controlled by the Chief of Operations when system testing or special maintenance is required.

The health physics instrumentation is not intended to be used for automatic control or system shutdown. Its main purpose is to provide reliable information to supervision on the site and to the Emergency Control Center.

### Beryllium Monitoring

We also monitor for beryllium contamination. The air passing out the radiator stack is sampled continuously with filter paper which is spectrographically analyzed once a minute. This operation is automatic, and the results are recorded. The reactor building contains 15 air sampling stations which draw building air through filter papers which are analyzed on a routine basis.

This beryllium monitoring operation is carried out by the Industrial Hygiene Department of the ORNL Medical Division.

### Data Logger-Computer

The MSRE instrumentation system is capable of generating a forbidding quantity of data. Our previous experience with large experimental systems equipped with typical strip chart recorders, indicators, etc., has shown that the recording, reduction, and evaluation of system data necessary for both routine operation and experimental purposes is a task of major proportions. In addition, conventional multi-point recorders, having long scanning periods, are inherently incapable of recording the frequency structure of all but very slow changes. Storage space for chart rolls must be provided, and truly accurate time referencing of all these rolls of data is always questionable. The problems of data reduction become particularly onerous and expensive when the design of a particular test is guided or determined by the results of the preceding test. There is, in these circumstances, a really large incentive to reduce the data reduction time which determines the nonproductive time between tests. An operation like the MSRE may cost \$4,000/day to run, and it is obvious that reductions in down time or nonproductive time will produce substantial savings.

For these reasons, we have added a logger-computer to the MSRE instrument system. Since our experience with systems of this type has been limited, we are proceeding with the logger-computer installation on a test and evaluation basis. Therefore, the design and operation of the MSRE is such that no vital functions involving data gathering, safety, or control are vested solely in the logger-computer. This enables us to rent the device on a month-to-month basis with credit toward ultimate purchase at our option. Figure 25 is a block diagram of the system.

The machine is capable of accepting a total of 350 analog plus 112 on-off contact inputs. These may have ranges from millivolts to volts of either ac or dc. During routine operation, the continuous scan rate is 90 points/sec, giving a maximum complete cycle time of 5 sec; this includes time for other computer functions during the scan. Data storage, either programmed or by operator command, is accomplished on either the magnetic or the paper tape units, or both, and in a format acceptable to our other large general purpose computers. The X-Y plotter can be programmed to automatically produce curves based on logged or computed data.

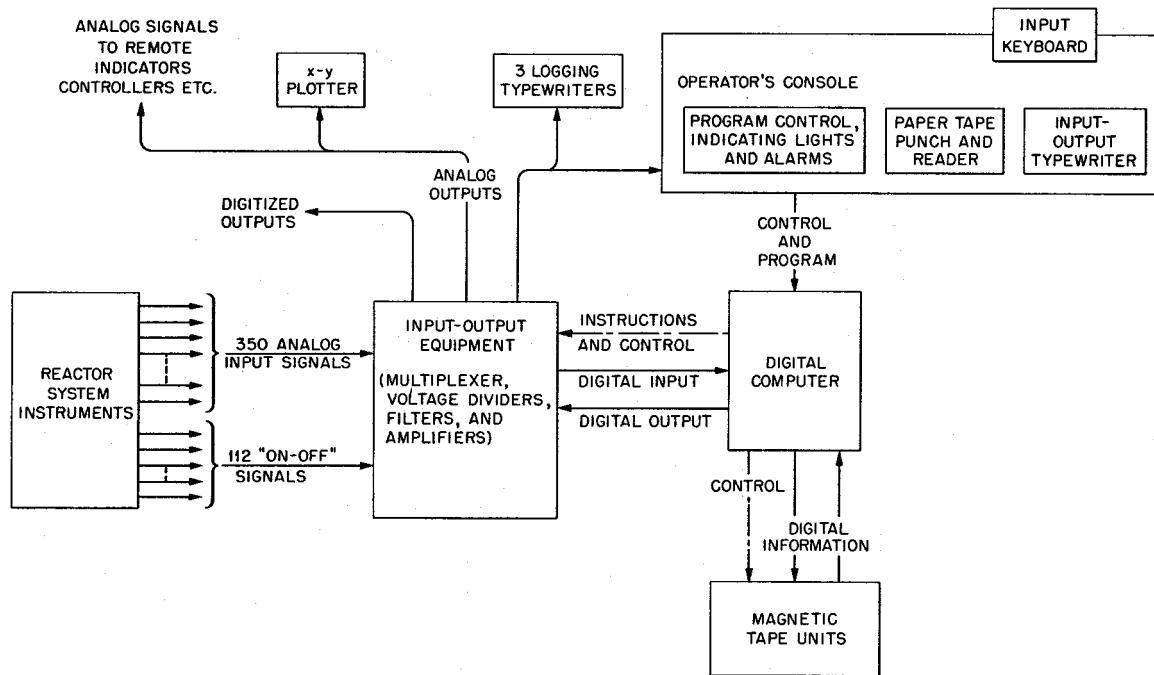
UNCLASSIFIED  
ORNL-DWG 64-6481A

Fig. 25. Block Diagram of MSRE Data Logger-Computer.

The scanned data are printed out routinely on the automatic typewriters in engineering units once an hour. They can be printed out at any time by operator request. In addition, there are printouts every 8 and 24 hr for summary and daily reports. The frequency of these routine printouts is at our option. The time of the log is printed and the instruments or sensors which produce the data are positively identified on the log sheet.

The machine continuously monitors the system operation. As the program now stands, approximately 150 input signals are compared with preset high and low limits. In the event that any of these input signals exceeds its limits, the equipment produces an alarm signal and prints out the off-limit signal. If a certain number of these 150 input signals reach the alarm limits, the system will pass into its fast scan mode. In the fast scan mode the system scans 64 preselected inputs continuously, taking about 1/4 sec for the complete scan cycle. The initiating signal is logged by the alarm typewriter, and the data are stored on magnetic tape which can subsequently be processed by the data system computer or, if desired, by one of our large, general purpose computer facilities.

The unit is also capable of producing 32 digitized output signals, readout, etc., should we so desire.

Typical calculations for which the machine is now being programmed are:

1. heat balance,
2. reactivity balance,
3. integrated power,
4. nuclear average temperature,
5. average temperatures and thermal cycling records of the salt pumps, which will be used to program laboratory tests by the metallurgy group,
6. a statistical survey of heat-exchanger temperatures, which will provide an evaluation of heat-exchanger performance.

The question of computer control of the reactor system inevitably arises when we discuss the application of this equipment. Existing programming plans do not include reactor or process control as part of its functions. The first reason, of course, is that we did not commit ourselves to making the unit an indispensable part of the design. Secondly, we want to gain experience with both the computer-logger and with the reactor before embarking on such a venture. I can, however, assure you that there is a substantial number of people who are eager and anxious to extend the use of the computer into the area of system control.

The initial programming is a joint effort by ORNL and the seller. We are developing a cadre of qualified personnel, drawn from the Instrumentation and Controls, the Reactor, and the Mathematics Divisions, to alter the machine operation and computational functions to suit the changing needs of the experimental program.

We are not installing this equipment on the assumption that it will effect immediate and obvious reductions in the cost of operating the MSRE. We do expect that, once we have learned to use it, we will extract more and better information in less time from the reactor system. This is a somewhat intangible cost saving, but it can be a very substantial one. Once experience and confidence in applying and using such equipment has been gained, I am confident that this or similar equipment will assume a greatly expanded role in large systems such as the MSRE.

PUMP DEVELOPMENT

A. G. Grindell

P. G. Smith

Introduction

The purpose of this report is to review the work done on producing the high-temperature salt pumps used in the Molten-Salt Reactor Experiment (MSRE) and the present status of that pump technology. It provides a brief description of the pumps, discusses in more detail certain distinguishing features of the pumps which have not been previously fully reported, describes noteworthy problems which were resolved during their design and testing, and gives a summary of the status of their technology.

Two of these pumps are required to circulate the salts in the MSRE, one in the fuel-salt and one in the coolant-salt circuits. Each pump must provide for the thermal expansion of the salt in its circuit and for the sampling of that salt. In addition, the fuel-salt pump must provide for the removal of  $^{135}\text{Xe}$  from the fuel salt and for the addition of fuel concentrate to the fuel salt as burnup progresses.

The detailed design of these pumps is based on precepts taken from many disciplines, including metallurgy, heat transfer, thermal stress analysis, hydraulic design of centrifugal pumps, mechanics, electrical machinery, and instrumentation and controls, and the Boiler and Pressure Vessel Code of the American Society of Mechanical Engineers. While we gratefully acknowledge the contributions from each of these disciplines to the production of satisfactory and reliable molten-salt pumps, we perforce limit ourselves to the discussion of noteworthy pump features and problems in this paper.

Salt Pump DesignGeneral Description

The fuel-salt pump will be used for purposes of demonstration in this presentation, and the few differences between it and the coolant-salt pump will be pointed out during the exposition. The fuel-salt pump, a hermetic sump-type centrifugal pump, consists of three main components: the pump tank, the rotary assembly, and the drive motor (see Fig. 1). These are supplemented with associated lubrication and purge-gas systems and instrumentation and controls. All the salt-wetted parts are constructed of Hastelloy N.

The pump tank is a semipermanent component in the fuel-salt circuit and is provided with two freeze flanges for convenient replacement. The motor and rotary assembly may be removed from the pump tank together or singly. The three main components are made hermetic by ring-joint flanges which are monitored by the leak-detection system.

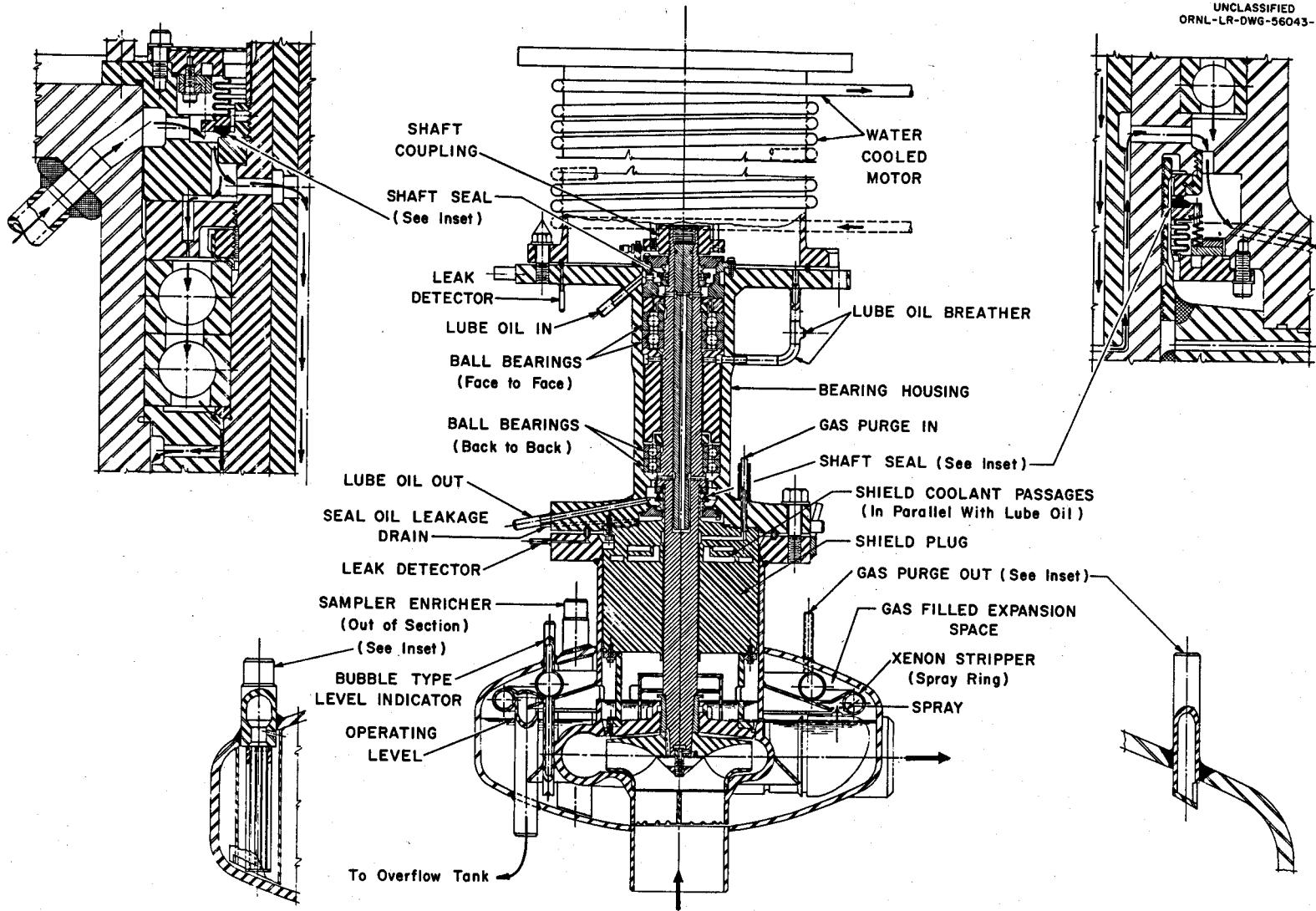


Fig. 1. MSRE Fuel Pump.

The pump tank contains the pump volute. During operation it houses the impeller and the shield plug, which are supported from the rotary assembly. It also contains the system liquid-gas interface, the spray device and gas purge for the removal of  $^{135}\text{Xe}$ , and the liquid-level instrumentation. The rotary assembly consists of the bearing housing, a pump shaft mounted on commercially available bearings, and upper and lower shaft seals. The shaft seals confine the circulated oil, which lubricates and cools the assembly, to the bearing housing.

The drive motor is of the squirrel-cage induction type, housed in a hermetic vessel. The electrical insulation system and the grease lubricant for the motor bearings are radiation resistant. A more complete and detailed description of this type of pump may be found in papers by Savage and Cobb<sup>1</sup> and Grindell, Boudreau, and Savage.<sup>2</sup>

#### Distinguishing Design Features Not Previously Reported

The MSRE salt pumps require certain features not found in conventional sump-type pumps. The pump tank contains a salt spray device to remove  $^{135}\text{Xe}$  from the circulating fuel salt and two elevated-temperature liquid-level indicators for molten-salt operation. A split purge-gas flow in the shaft annulus keeps oil vapors from the salt system and fission gases from the region of the lower shaft seal; the down-shaft purge also strips, dilutes, and removes  $^{135}\text{Xe}$  from the salt spray. Since the reactor vessel is used as the system anchor, the fuel pump is mounted on flexible supports to accommodate thermal expansions. A flow of nitrogen (cell air) removes nuclear-deposited heat from the upper section of the pump tank. The drive motor is specially enclosed. These features and the differences between the fuel- and coolant-salt pump designs are discussed in this section.

Nuclear-Poison-Removal Device. Some of the  $^{135}\text{Xe}$  poison is removed from the fuel salt by contacting a spray of the salt with helium in the fuel-pump tank. Approximately 50 gpm of salt is introduced through 291 small jets at a spray velocity of approximately 15 fps into the gas-filled portion of the fuel-pump tank. Here, the helium which enters the pump tank from the shaft annulus purge and that which is associated with the operation of the bubble-type liquid-level indicators remove the nuclear poison from the salt spray, dilute it, and carry it to charcoal traps.

It should be noted that this device is not included in the design of the coolant-salt pump.

Molten-Salt Liquid-Level Indicators. Two bubble-type liquid-level indicators are used to show the liquid level of fuel salt. They are identical except that one reaches to a 2-in. greater depth than the other. In this type of indicator a flow of helium passes through a tube inserted vertically into the salt from above the salt level. The difference in pressure between the gas supply to the level indicator and the gas space in the pump tank is a function of the depth of the tube in the salt. The gas flow from the indicators exits through the gas purge nozzle, helping to dilute and carry off fission gases, as mentioned above.

The coolant-salt pump also contains a buoyancy level indicator, which uses the output from a calibrated differential transformer to indicate level.

Gas Purge System. Helium enters the pump shaft annulus below the shaft lower seal. A portion of the helium (0.1 liter/min) flows upward in the annulus to reduce the migration of oil vapors from the lower seal leakage catch basin to the pump tank. A drain passage for the oil which leaks past the lower shaft seal conducts the flow of helium from the pump to the charcoal traps.

The remainder of the helium purge (2.3 liters/min) flows down the shaft annulus, reducing the migration of fission gases from the pump tank to the region of the lower shaft seal. This flow enters the pump tank gas space and dilutes and transports fission gases to charcoal traps.

Flexible Supports for the Fuel-Salt Pump. The fuel-salt pump is mounted on a horizontal plate which is supported at each end by the arrangement shown in Fig. 2. The end supports are identical and provide for three degrees of translational displacement. These supports are shown in Fig. 3. Roller bearings on the top surface of item 1 permit sideways translation of the pump support plate. Bearings on the upper side of item 1 mate with raceways in item 2 to permit forward and backward displacements of the pump. Item 2 is in turn supported by inclined linkages, attached to the base, which provide for vertical displacements. The weight of the pump system is counterbalanced with springs as shown and, as the salt piping system expands or contracts, the pump moves accordingly.

The coolant-salt pump is mounted in a rigid support.

Provisions for Cooling the Gas-Bounded Portion of the Pump Tank. The outside surface of the upper section of the fuel pump tank is gas cooled to remove nuclear-deposited heat. This is shown in Fig. 4. A distributor is fitted around the neck of the pump tank to distribute the flow of cooling gas (approximately 200 cfm of nitrogen) across the outer surface of the tank.

This cooling is not required on the coolant-salt pump tank.

Drive Motor. The pump drive motor is in a hermetic containment vessel, fabricated to meet the requirements of a Primary Nuclear Vessel as specified in the ASME Boiler and Pressure Vessel Code and appropriate Code Case Interpretations 1270N-2 and 1272N-4. Two grease-lubricated angular contact bearings, designed to operate continuously for  $10^4$  hr without maintenance or relubrication, support the shaft. The grease, Nuclear Radiation Resistant Grease-159, is reported<sup>3</sup> to be capable of withstanding  $3.4 \times 10^9$  rads total radiation dosage. The basic insulation system used in the motor windings consists of silicone-glass-mica laminates, silicone rubber over glass and type "ML" enamel, and multi-dip-impregnations of silicone varnish. These materials should be capable of withstanding an integrated radiation dose in excess of  $10^9$  rads.

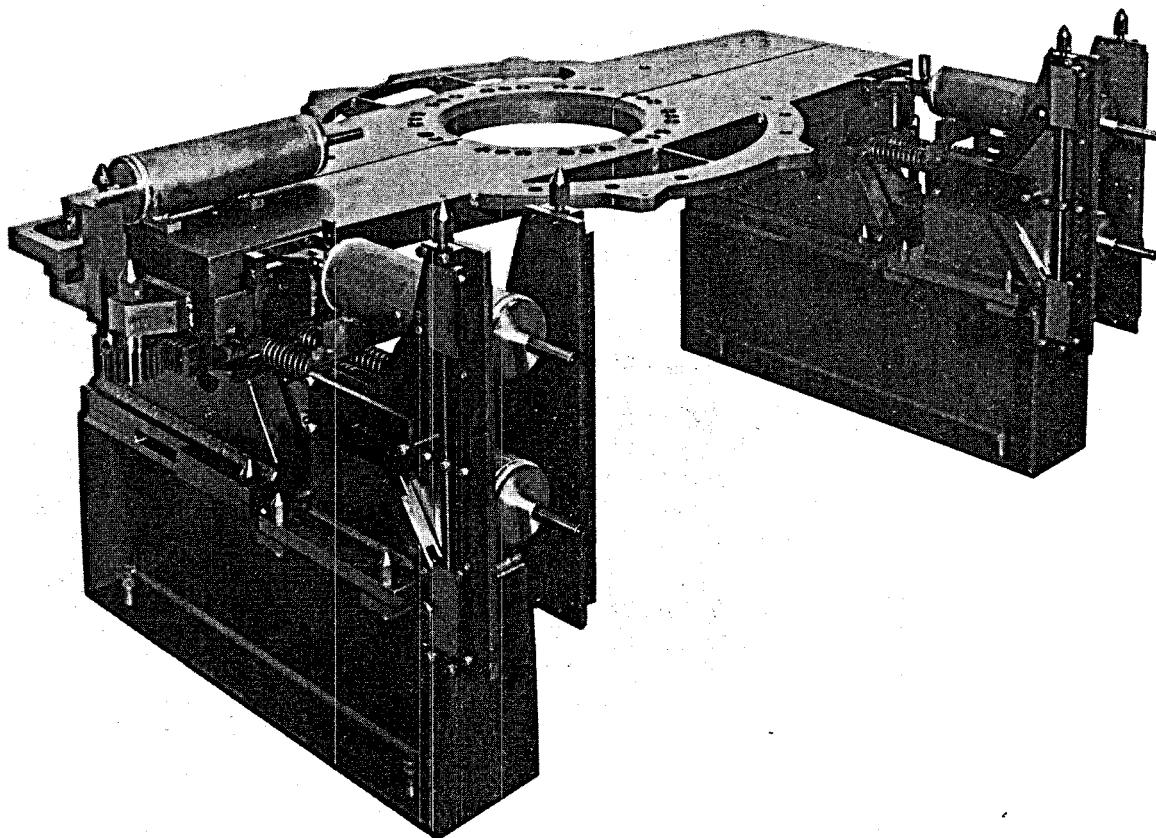
UNCLASSIFIED  
PHOTO 63422

Fig. 2. MSRE Fuel Pump Support.

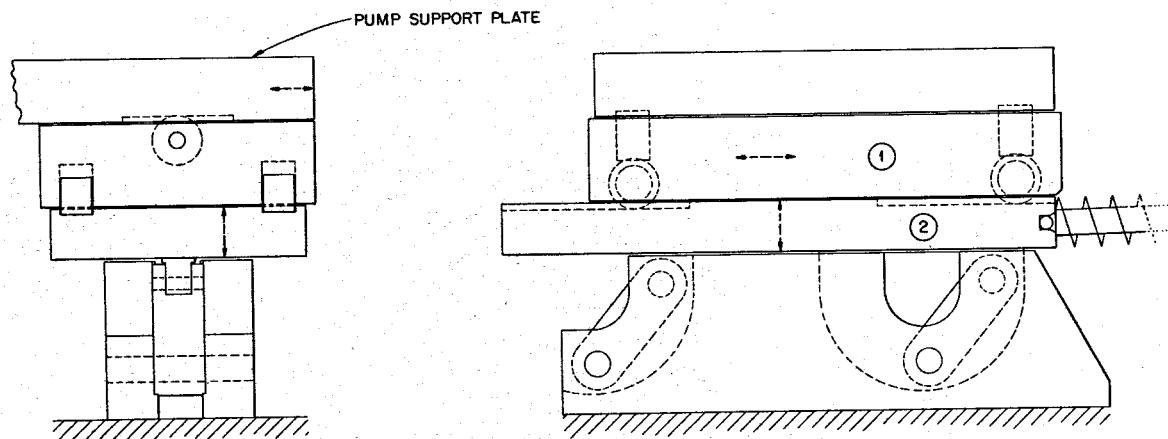
UNCLASSIFIED  
ORNL-DWG 64-6625

Fig. 3. Fuel Pump Support.

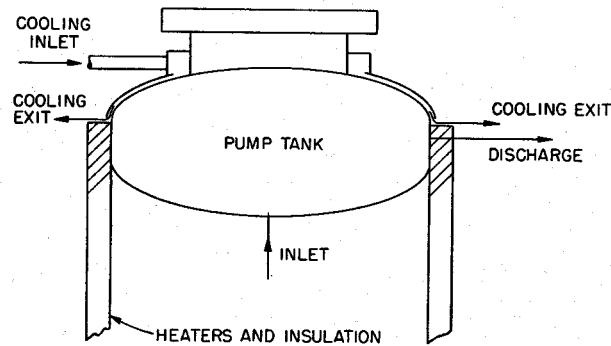
UNCLASSIFIED  
ORNL-DWG 64-6624

Fig. 4. Pump Tank Upper Shell Cooling.

Each of the salt pump motors is 75 hp, but the fuel-salt pump motor is 1200 rpm synchronous speed and the coolant pump motor is 1800 rpm.

#### Noteworthy Problems Resolved During Design and Development of Salt Pumps

During the design and development of these pumps, a number of noteworthy problems were resolved. The ability of the pump tanks to withstand the strain fatigue associated with thermal cycling from room to operating temperatures and from zero to full reactor power was investigated. The effectiveness of the purge-gas flow in the shaft annulus in limiting the back diffusion of fission gases was studied with the prototype pump using  $^{85}\text{Kr}$ . The need for maintaining this purge-gas flow to prevent plugging of the lower end of the pump shaft annulus with solidified salt was demonstrated. Attempts were made to determine the effectiveness of the device in the fuel-pump tank for removing fission gases. Adequate shaft running clearances to provide for off-design pump operation were deduced.

#### Pump Tank Thermal Stresses

The ability of the fuel- and coolant-salt pump tanks to sustain 100 reactor startup cycles from room temperature to 1200°F and 500 cycles from zero to full reactor power was studied. Values of the maximum thermal stress and the resultant strain fatigue associated with these cycles were computed and were compared with values of the thermal fatigue strength of Hastelloy N, deduced from metallurgical experiments. It was found that the upper section of the fuel pump tank required cooling, but the coolant pump tank did not require this cooling.

In analyzing the thermal stresses,<sup>4</sup> the configuration (Fig. 5) was considered to be composed of: (1) an internal cylinder, cylinder "A," extending from the volute to the junction with the spherical shell; (2) an external cylinder, cylinder "B," extending from the junction with the spherical shell to the top flange; and (3) the upper spherical shell of the pump tank.

Internal heat generation, conductive heat flow, convective and radiative heat transfer with the salt, and cooling of the shield plug and upper pump tank surfaces were the bases for calculating temperature distributions in the pump tank for various operating conditions with the generalized heat conduction code (GHT Code).<sup>5</sup> The axial temperature distributions of the volute support cylinder at various operating conditions and the effect of the gas cooling on the temperature distribution are shown in Fig. 6. The temperature distributions along the pump tank spherical shell (i.e., the upper section) for various operating conditions including cooling are shown in Fig. 7.

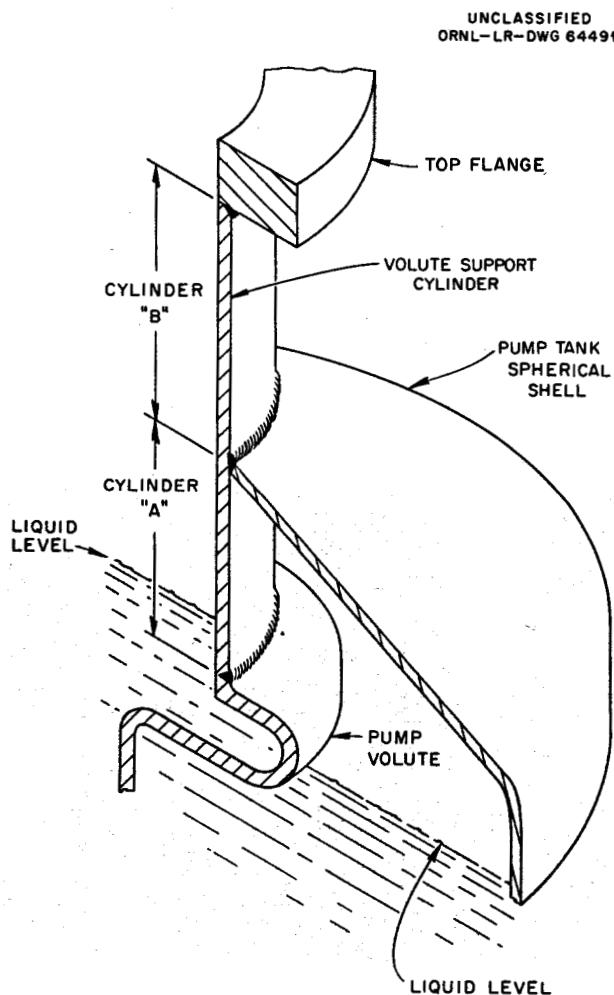


Fig. 5. Pump Tank and Volute Support Cylinder Geometry.

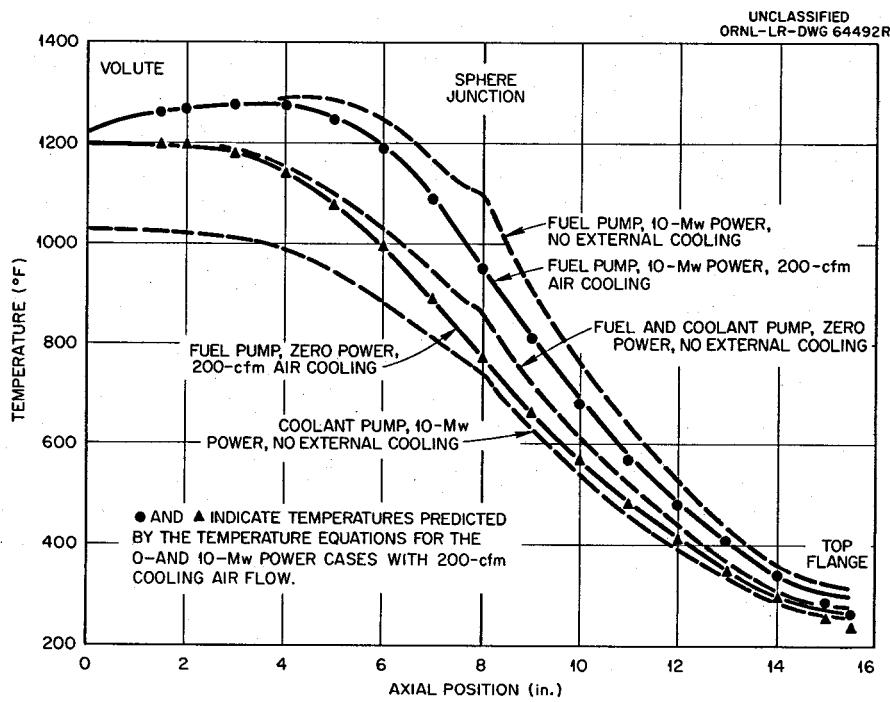


Fig. 6. Axial Temperature Distribution of Volute Support Cylinder at Various Operating Conditions.

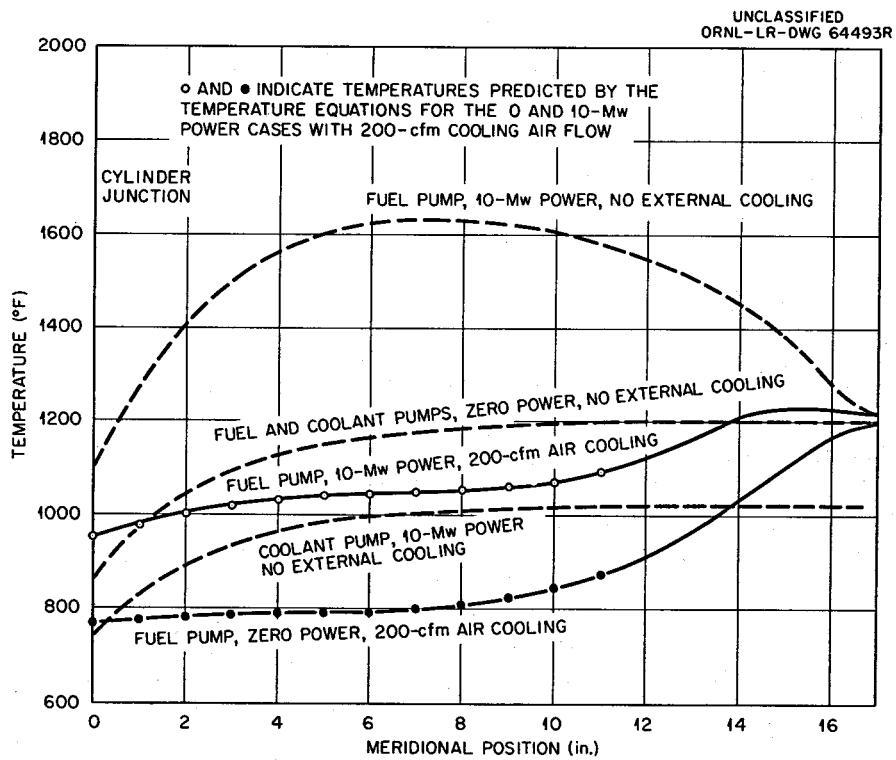


Fig. 7. Meridional Temperature Distribution of the Torispherical Shell at Various Operating Conditions.

An Oracle program was used to obtain the pressure stresses on the cylinder, and an IBM 7090 program was used to obtain the thermal stresses in the two cylinders and the sphere. The principal thermal stresses in the fuel pump at cylinders "A" and "B" for zero power operation with and without cooling are shown in Fig. 8. The stresses at cylinders "A" and "B" for 10-Mw power operation with and without cooling are shown in Fig. 9. The thermal stresses in the spherical shell for zero power operation with and without cooling are shown in Fig. 10. The stresses in the spherical shell for 10-Mw power operation with and without cooling are shown in Fig. 11.

The results of the strain-fatigue analysis are presented in Tables 1 and 2. The last column in each table, often referred to as a usage factor, is the decimal fraction of the strain-fatigue limit of Hastelloy N used up. By combining the usage factors in Tables 1 and 2 the data in Table 3 are obtained.

A usage factor of 0.8 or less indicates a safe operating condition.<sup>6</sup> At cooling air flow rates from 100-300 cfm the usage factor is less than 0.8, and a cooling air flow rate of 200 cfm has accordingly been selected for the MSRE.

A detailed report of the thermal-stress and strain-fatigue analyses for both the fuel- and coolant-salt pumps has been published.<sup>4</sup>

#### Back Diffusion of Fission Gases in the Pump Shaft Annulus

It has long been recognized that the migration of fission gases from the pump tank to the region of the shaft lower seal via the shaft annulus can polymerize leakage seal-oil and lead to plugging of the drain line for that leakage. A flow of purge gas down the shaft annulus was introduced to minimize this migration.

Back-diffusion tests,<sup>7</sup> using  $^{85}\text{Kr}$ , on the prototype pump measured the effectiveness of the shaft annulus purge. Figure 12 shows a schematic of the test setup. The upper end of the annulus through which the "down the shaft" purge flows contained a labyrinth seal with a 0.005-in. diametral clearance with the shaft. Krypton-85 was injected into the pump tank as shown. Count rate meters determined the concentrations of  $^{85}\text{Kr}$  in the pump tank off-gas and in the leakage oil catch basin at various flow rates of purge gas. Table 4 shows the data obtained during the tests. A count rate meter, capable of detecting a concentration as small as  $0.95 \times 10^{-10}$  curie/cm<sup>3</sup>, detected no  $^{85}\text{Kr}$  in the leakage oil purge gas. These data indicate the effectiveness of the purge gas to reduce the concentration of  $^{85}\text{Kr}$  in the catch basin by a factor of at least 20,000, compared with the concentration in the pump tank.

The radiation tolerance of the oil used with the MSRE pumps is  $10^7$  rads/g. With this amount of irradiation, the oil will flow and drain from the catch basin. The permissible source in the catch basin for the MSRE fuel pump for a dose of  $10^7$  rads per g of oil with 1-Mev beta radiation

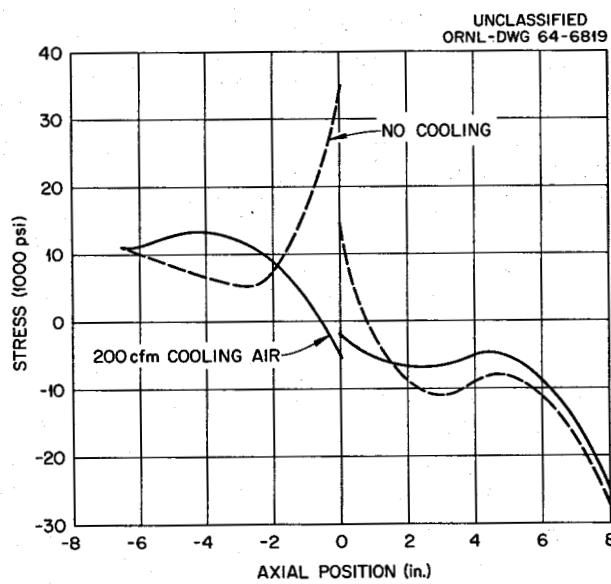


Fig. 8. Fuel Pump Principal Thermal Stresses at Cylinders "A" and "B" for Operation at Zero Power.

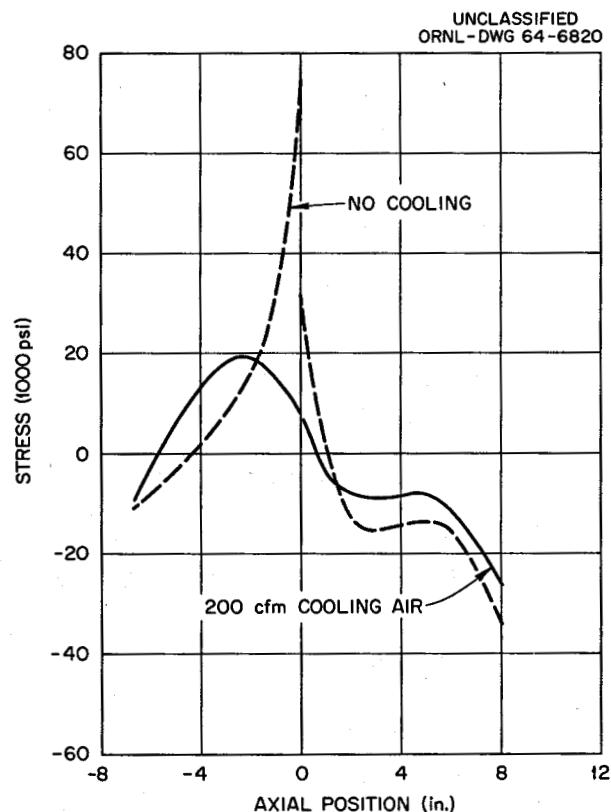


Fig. 9. Fuel Pump Principal Thermal Stresses at Cylinders "A" and "B" for Operation at 10 Mw.

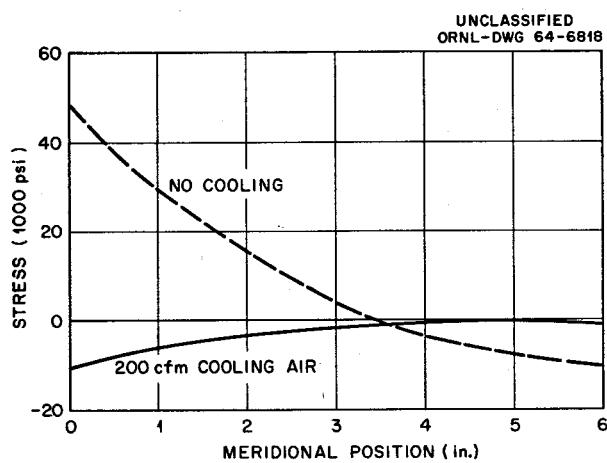


Fig. 10. Fuel Pump Principal Thermal Stresses at Spherical Shell for Operation at Zero Power.

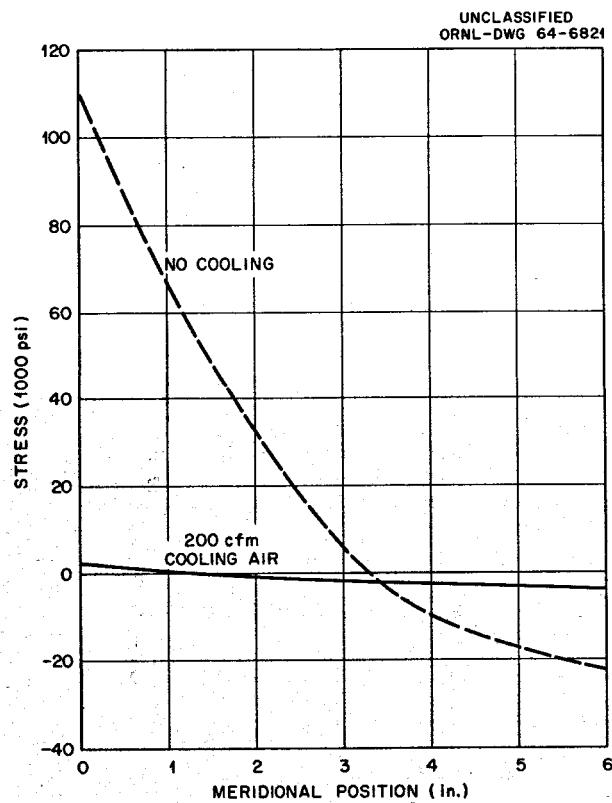


Fig. 11. Fuel Pump Principal Thermal Stresses at Spherical Shell for Operation at 10 Mw.

Table 1. Fuel Pump Strain Data for Heating Cycle (to 1200°F)

| Air Flow (cfm) | Maximum Stress Intensity (psi) | Stress Amplitude (psi) | Allowable Cycles | Cycle Fraction Per Cycle | Cycle Fraction in 100 Cycles, $P_1/N_1$ |
|----------------|--------------------------------|------------------------|------------------|--------------------------|---|
| 50             | 31,124                         | 15,562                 | 700              | 0.00143                  | 0.143                                   |
| 100            | 14,400                         | 7,200                  | 2,500            | 0.00040                  | 0.040                                   |
| 150            | 14,143                         | 7,072                  | 2,500            | 0.00040                  | 0.040                                   |
| 200            | 16,095                         | 8,048                  | 2,100            | 0.00047                  | 0.047                                   |
| 250            | 21,760                         | 10,880                 | 1,300            | 0.00077                  | 0.077                                   |
| 300            | 26,955                         | 13,477                 | 880              | 0.00114                  | 0.114                                   |

Table 2. Fuel Pump Strain Data for Power-Change Cycle from 0 to 10 Mw

| Air Flow (cfm) | Maximum Stress Intensity (psi) | Stress Amplitude (psi) | Allowable Cycles | Cycle Fraction Per Cycle | Cycle Fraction in 500 Cycles, $P_2/N_2$ |
|----------------|--------------------------------|------------------------|------------------|--------------------------|---|
| 50             | 37,971                         | 18,985                 | 520              | 0.00192                  | 0.961                                   |
| 100            | 24,763                         | 12,382                 | 1,000            | 0.001                    | 0.500                                   |
| 150            | 18,930                         | 9,465                  | 1,600            | 0.000625                 | 0.312                                   |
| 200            | 18,814                         | 9,407                  | 1,600            | 0.000625                 | 0.312                                   |
| 250            | 18,775                         | 9,388                  | 1,600            | 0.000625                 | 0.312                                   |
| 300            | 18,639                         | 9,320                  | 1,600            | 0.000625                 | 0.312                                   |

Table 3. Usage Factor as a Function of Air Flow Rate

| Air Flow (cfm) | Cycle Fraction in 100 Cycles, $P_1/N_1$ | Cycle Fraction in 500 Cycles, $P_2/N_2$ | Total Usage Factor, $\Sigma P_i/N_i$ |
|----------------|---|---|--------------------------------------|
| 50             | 0.143                                   | 0.961                                   | 1.10                                 |
| 100            | 0.040                                   | 0.500                                   | 0.54                                 |
| 150            | 0.040                                   | 0.312                                   | 0.352                                |
| 200            | 0.047                                   | 0.312                                   | 0.359                                |
| 250            | 0.077                                   | 0.312                                   | 0.389                                |
| 300            | 0.114                                   | 0.312                                   | 0.426                                |

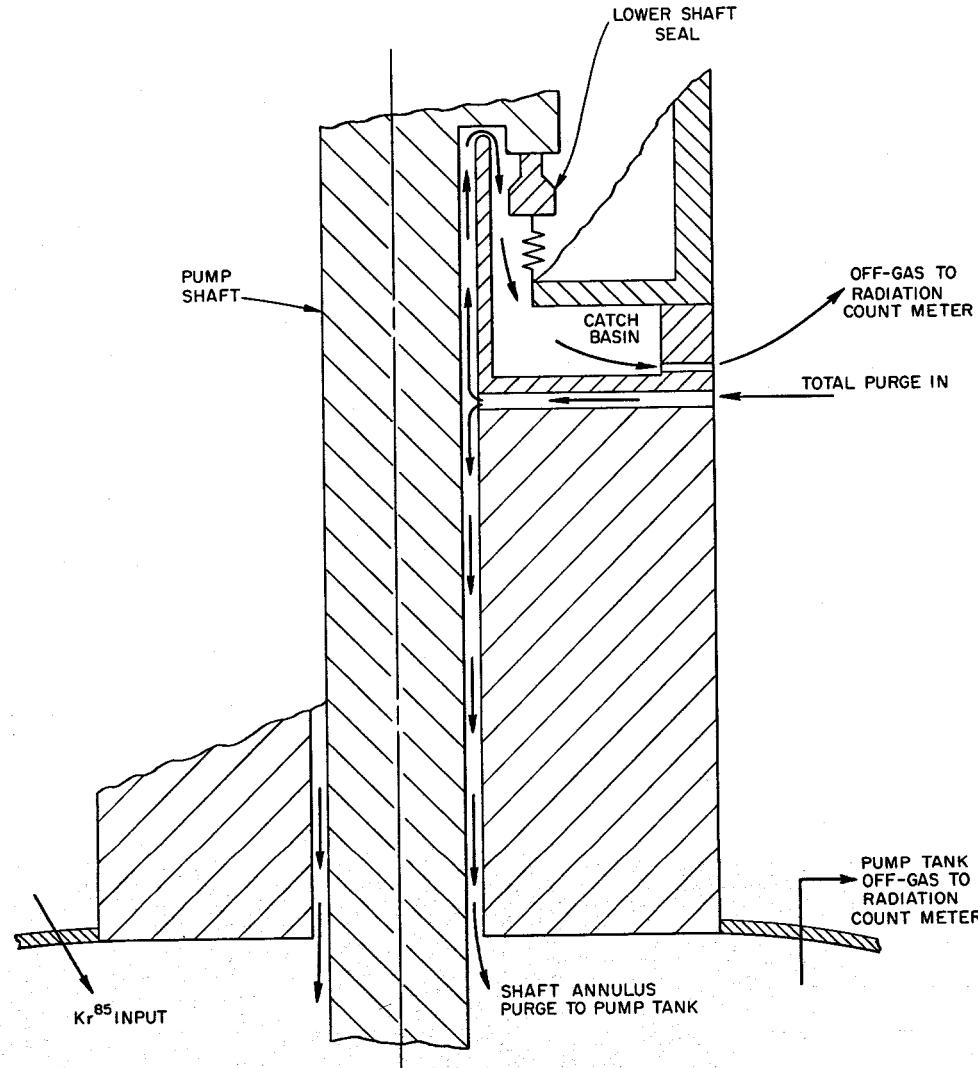
UNCLASSIFIED  
ORNL-DWG 63-6482

Fig. 12. Diagram for Purge Gas Flow in Shaft Annulus of MSRE Prototype Pump.

Table 4. Back-Diffusion Tests

| Shaft Purge<br>(liters/day) | Catch Basin Purge<br>(liters/day) | $^{85}\text{Kr}$ Concentration <sup>a</sup><br>in Pump Tank<br>(curies/cm <sup>3</sup> ) |
|-----------------------------|-----------------------------------|--|
| $\times 10^{-6}$            |                                   |  |
| 406                         | 487                               | 0.89   |
| 406                         | 487                               | 0.89   |
| 430                         | 497                               | 2.06   |
| 382                         | 481                               | 2.77   |
| 366                         | 354                               | 3.28   |
| 215                         | 360                               | 1.85   |
| 108                         | 360                               | 1.21   |
| 173                         | 673                               | 1.65   |
| 109                         | 360                               | 0.75   |
| 109                         | 681                               | 0.90   |
| 104                         | 681                               | 3.54   |

<sup>a</sup>Concentration values for catch basin were below the limit of detection.

is 0.13 curie. This is based on the conservative assumption that the leakage through the catch basin is 1 g/day and that all the energy of the beta emitters is absorbed by the oil. Since the volume of the catch basin is 423 cm<sup>3</sup>, the maximum permissible concentration in it is  $3.1 \times 10^{-4}$  curie/cm<sup>3</sup>. This concentration should not be exceeded, according to the data in Table 4, if the concentration in the MSRE fuel pump tank is maintained at less than 11 curies/cm<sup>3</sup>. The concentration of fission gas in the MSRE fuel pump is related to purge-gas flow as shown in Fig. 13. The data indicate that a flow of approximately 1400 liters/day will ensure that the concentration in the pump tank will be less than 11 curies/cm<sup>3</sup>. Purge-gas flows of 3300 liters/day down the shaft annulus and 1300 liters/day from the level indicators are available in the MSRE fuel pump.

#### Shaft Annulus Plugging

One 700-hr test<sup>8</sup> with molten salt at 1200°F was terminated when fluctuations in the power required by the motor led us to conclude that the shaft was rubbing, possibly in the shield plug. Inspection revealed the presence of solidified salt in the pump shaft annulus. Subsequent analysis of the prevailing operating conditions revealed that the pump tank pressure had exceeded the supply pressure of the gas to the shaft annulus by 5 psi and had caused the gas flow in the shaft purge annulus to flow upward instead of downward. The chemical composition of a sample of the material taken from the shaft annulus was very close to that of the salt being circulated. The results of x-ray and petrographic examinations of the sample indicated that the material was carried to the annulus as an entrained mist.

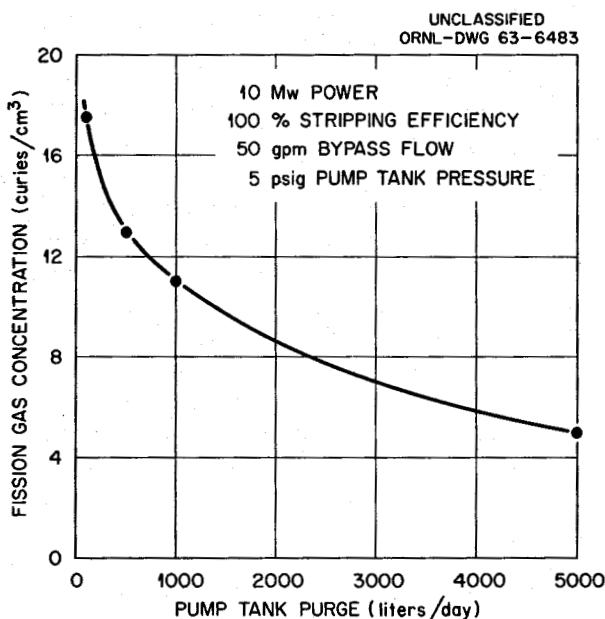


Fig. 13. Fission Gas Concentration in Pump Bowl vs Purge Flow Rate.

To prevent reoccurrence of this incident and to provide protection against the back diffusion discussed in the previous section, the gas flows to and from the pump tank are monitored to assure that gas flows down the shaft annulus. The flow rate of gas from the pump tank must equal the flow rate of the purge down the shaft annulus plus the flow rate of gas to the bubble-type level indicators.

#### Nuclear Poison Removal from the Fuel Salt

Simulating the removal of the  $^{135}\text{Xe}$  poison by helium contact with salt spray in the fuel pump tank, tests were made in the water test facility<sup>9</sup> with water (salt), dissolved carbon dioxide (xenon), and air (helium purge). However, since the applicability of these tests to the molten salt, xenon, and helium system in the reactor is doubtful, the results are not included here.

During the back-diffusion tests on the prototype pump, several attempts to determine the effectiveness of the spray device<sup>10</sup> using  $^{85}\text{Kr}$  failed. When the pump tank gas space was charged with  $^{85}\text{Kr}$  at a concentration of  $3.5 \times 10^{-6}$  curie/cm<sup>3</sup> and while the salt was circulating, attempts were made to detect the activity in the salt through the system piping and to determine the activity decrease with time. However, the instrumentation was unable to detect or measure any activity through the salt piping.

### Running Clearances to Accommodate Hydraulic Unbalance

Centrifugal pumps have a best-efficiency operating condition at which the various losses in the impeller and volute are minimum and the pressure distribution in the volute is uniform. During operation at this condition (see the balance line shown in Fig. 14), the net radial force on the impeller is nearly zero. During operation at higher and lower flows, the volute pressure distribution becomes non-uniform and a net radial force appears on the impeller. This force increases as the operating condition departs farther from the balance line, and operation at conditions which are off-design thus produces shaft deflections.

During the prototype pump tests with the 13-in.-diam impeller, a shaft seizure occurred.<sup>11</sup> Operation at off-design conditions produced a deflection of the shaft sufficiently large to cause rubbing of the hot, dry shaft against the bore of the shield plug at its lower end. The shaft was friction-welded to the bore of the shield plug over a length of about 4 in. (Fig. 15). The running clearances between the shaft and the shield plug were increased to 0.045 in. to avoid shaft seizure at anticipated off-design operating conditions.

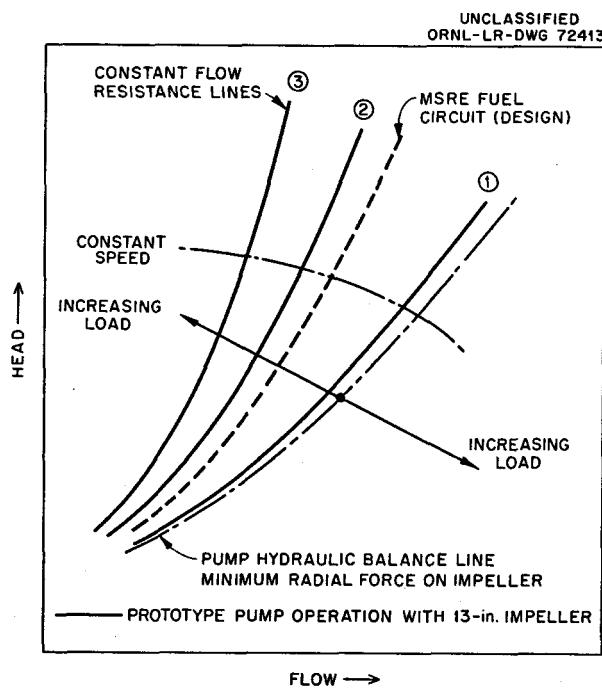


Fig. 14. Hydraulic Radial Unbalance of Centrifugal Pump Impeller.

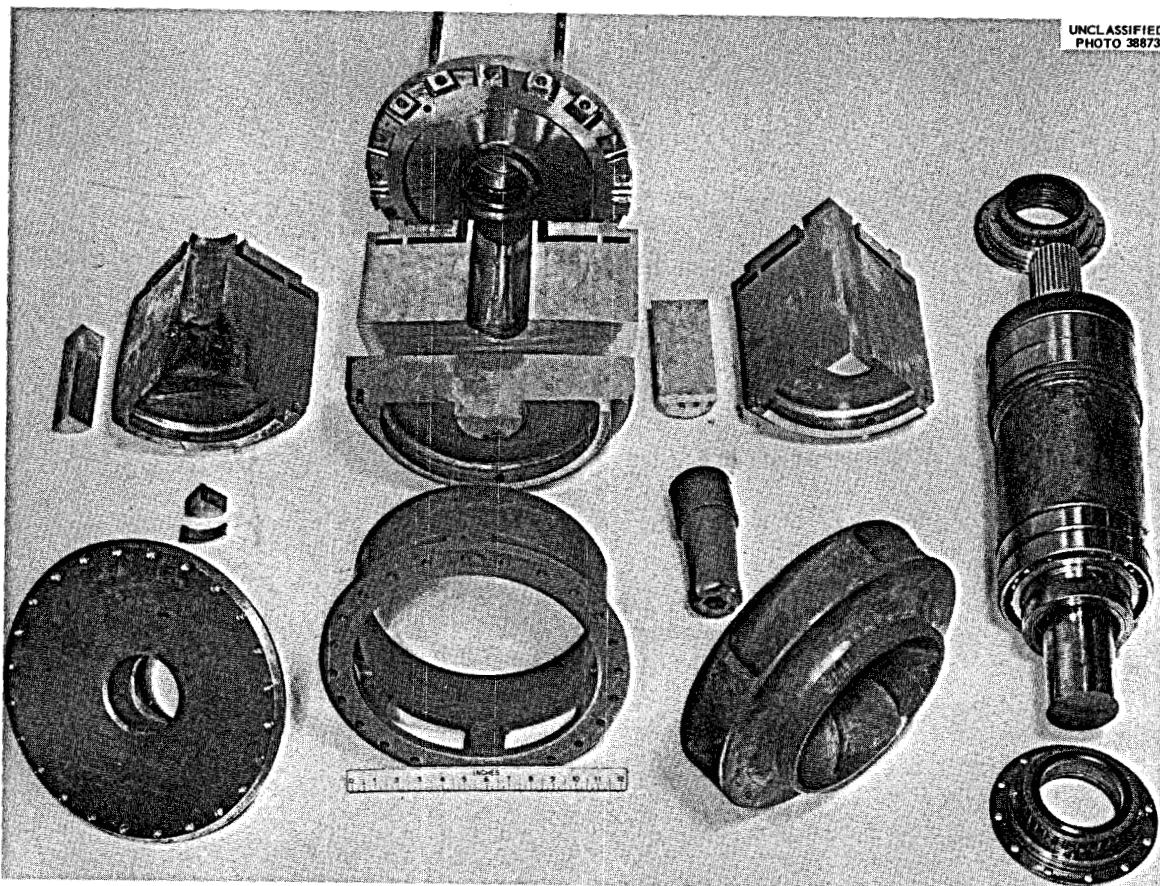


Fig. 15. Results of MSRE Prototype Pump Shaft Seizure.

#### Results of Tests with Prototype Pumps

Initial testing of the salt pumps was performed in a water test facility to verify the hydraulic performance characteristics and to develop the necessary baffles and guides to obtain satisfactory behavior of the liquid in the pump tank. Hot testing on the prototype pump followed. The hot tests were conducted to further verify the hydraulic performance during molten-salt operation and to ascertain the adequacy of the design to withstand the temperature and functional requirements.

#### Water Tests

Water tests<sup>9</sup> were performed with each of the salt pumps to obtain their hydraulic performance data for comparison with the manufacturers' reported performance. The pump characteristics were selected from the manufacturers' reported performances to fit the estimated system requirements in the MSRE. There was little difference between the performance obtained at ORNL and the manufacturers' performance.

### Prototype Pump Hot Tests

A large portion of the MSRE pump development consisted of work with the prototype pump. Table 5 enumerates the principal tests and gives the operating conditions, the impeller diameter, the test duration, the primary purposes of tests, and the reason for their termination. The problem of undissolved gas in the circulating salt was investigated in the prototype pump test facility. Measurements were made with a radiation densitometer to determine the content of undissolved gas in the circulating salt. The results are not reported, because the accuracy of the measurements is not yet certain.

### Status of Molten-Salt Pumps

#### Prototype Pump

Remaining Development Tests. Further measurements will be made of the concentration of undissolved gas in the circulating salt. Measurements will be continued with the radiation densitometer, and the effects of questionable variables on the results will be evaluated.

Because of shaft-rubbing incidents, the clearance between the shaft and the purge-gas labyrinth was increased from 0.005 in. to 0.010 in. An additional back-diffusion test with  $^{85}\text{Kr}$ , at various purge flow rates, will therefore be made, using the 0.010-in. clearance.

The pump and test facility will be used when required to investigate problems which may arise throughout the operation of the reactor.

Endurance Operation. As time permits, the prototype pump will be operated at 1200°F to investigate the endurance and reliability of the unit.

#### MK-1 Pumps

Each of the two salt pump rotary assemblies for the MSRE was operated satisfactorily at 1200°F, circulating salt, for approximately 100 hr in the prototype pump test facility prior to delivery to the MSRE. The MSRE pump drive motors were used to rotate the pumps for these tests. General behavior, performance of the bearings and seals, and hydraulic performance were observed. Adequacy of the running clearances was verified. The hydraulic performance data obtained with the coolant-salt pump has only minor value, however, since the impeller was matched with the fuel pump volute in the test facility.

The MK-1 fuel and coolant pumps, including their drive motors and lubrication systems, have been delivered to the MSRE.

Table 5. Prototype Pump Tests

| Test No.              | Molten-Salt Temp (°F) | Pump Shaft Speed (rpm) | Molten-Salt Flow (gpm) | Impeller Diameter (in.) | Test Duration (hr) | Primary Purposes of Test  | Reason for Termination                     |
|-----------------------|-----------------------|------------------------|------------------------|-------------------------|--------------------|---|--|
| 1                     | 80-1200               | 1150                   |                        | 13                      | 118                | Shakedown   |  |
| 1                     | 1200                  | 700-1030               | 750-1600               | 13                      | 217                | Hydraulic performance   | Shaft seizure                              |
| 2                     | 1200                  | 700-1030               | 750-1200               | 13                      | 96                 | Hydraulic performance   | Scheduled                                  |
| 3                     | 1200                  | 600-1150               | 400-1500               | 11-1/2                  | 1968               | Hydraulic performance   | Variable frequency motor-generator failure |
| 4                     | 1200                  | 1185                   | 1100                   | 11-1/2                  | 1848               | Back-diffusion tests  | Variable frequency motor-generator failure |
| 5                     | 1200-1320             | 1185                   | 1100                   | 11-1/2                  | 792                | Gas concentration tests in circulating salt, back-diffusion tests         | Scheduled                                  |
| 6                     | 1200                  | 1150                   | 1070                   | 11-1/2                  | 335                | Gas concentration tests in circulating salt                               |  |
| 6                     | 1000-1400             | 600-1150               | 500-1070               | 11-1/2                  | 368                | Hydraulic performance   | Shaft annulus plugging                     |
| 7                     | 1200                  | 1150                   | 1070                   | 11-1/2                  | 120                | Proof test of MSRE fuel pump lubrication stand and the fuel-pump supports |  |
| 7                     | 1100-1300             | 700-1150               | 600-1070               | 11-1/2                  | 409                |   | Scheduled                                  |
| 8                     | 1100-1300             | 1150                   | 1070                   | 11-1/2                  | 168                | Proof test of coolant pump lubrication stand and the fuel pump supports   | Scheduled                                  |
| Total operating time: |                       |                        |                        | 6439                    |                    |   |  |

MK-2 Fuel-Salt Pump

A modification of the MK-1 fuel-salt pump is under development. It contains the same impeller and volute in a pump tank which will provide an additional 6 ft<sup>3</sup> for thermal expansion of the system salt. The 36-in. diam of the tank was retained, but its height was increased approximately 9-3/4 in. Increasing the shaft length and thus the overhang of the impeller below the lower shaft bearing was necessitated. It was possible, however, to retain the MK-1 pump shaft diameter.

A mockup of the pump tank alone is being used in water tests to develop the hardware necessary to control the concentration of undissolved gas in the circulating liquid and to measure the rates of removal of carbon dioxide dissolved in the circulating liquid. The resulting tank configuration will be incorporated into the water test pump for further water testing. A hot salt test will be made with the final tank configuration.

MK-3 Fuel-Salt Pump

In the planning of the MK-3, an advanced salt pump design of larger capacity, advantage will be taken of the performance of MK-1 and MK-2 designs, the experience in the AEC program for the development of large sodium pumps, and the in-salt bearing experience at ORNL.<sup>12,13</sup> At the present time, a vertical sump-type pump, the upper end of the shaft supported by oil- or grease-lubricated radial and thrust bearings and the lower end supported by a salt-lubricated journal bearing, is the preferred design for the MK-3.

References

1. H. W. Savage and W. G. Cobb, Chem. Eng. Progr. 50, 445 (1954).
2. A. G. Grindell, W. F. Boudreau, and H. W. Savage, Nucl. Sci. Eng. 7, 83-91 (1960).
3. J. G. Carroll et al., Lubrication Eng. 18, 64 (1962).
4. C. H. Gabbard, Thermal-Stress and Strain-Fatigue Analysis of the MSRE Fuel and Coolant Pump Tanks, ORNL-TM-78 (Oct. 3, 1962).
5. T. B. Fowler, Generalized Heat Conduction Code for the IBM 704 Computer, ORNL-2734 (Oct. 14, 1959), and Supplement ORNL-CF-61-2-33 (Feb. 9, 1961).
6. Tentative Structural Design Basis for Reactor Pressure Vessels and Directly Associated Components (Pressurized, Water Cooled Systems) (esp. p. 31), PR 151987 (Dec. 1, 1958), U.S. Dept. of Commerce, Office of Technical Services.
7. MSRP Semiann. Progr. Rept. July 31, 1963, ORNL-3529, pp. 47-49.
8. Letter from P. G. Smith to R. B. Briggs, Shaft Plugging Incident; MSRE Prototype Fuel Pump, MSR-63-29 (Nov. 12, 1963) (internal use only).

9. P. G. Smith, Water Test Development of the Fuel Pump for the MSRE, ORNL-TM-79 (Mar. 27, 1962).
  10. MSRP Semiann. Progr. Rept. July 31, 1963, ORNL-3529, p. 44.
  11. Letter from A. G. Grindell to R. B. Briggs, MSRE Prototype Pump Shaft Seizure, MSR-62-67 (Aug. 27, 1962) (internal use only).
  12. P. G. Smith, ASLE (Am. Soc. Lubrication Engrs.) Trans. 4(2), 263-74 (1961).
  13. MSRP Semiann. Progr. Rept. Feb. 28, 1962, ORNL-3282, p. 56.
- 

#### COMPONENT DEVELOPMENT IN SUPPORT OF THE MSRE

Dunlap Scott, Jr.

The reliable performance of components and auxiliaries used in the circulation of molten salts was established by over 200,000 hr of accumulated loop operations and formed the basis for the specifications of components for the MSRE.

As an added ensurance of reliability and safety, prototypes of critical MSRE components were operated out-of-pile under conditions resembling those of the reactor.

In general, there are two phases of development work done on MSRE components. The first, in areas not well defined, consists in evolving component and system design specifications through experimentation. The second consists in operating prototypes of well-defined components for use in the MSRE to evaluate the adequacy of performance and safety. It is the purpose of this paper to discuss the effect of the development work in establishing the reliability of the MSRE components, and, mostly, it will cover only the second phase.

#### Core Hydraulics and Heat Transfer

First, I would like to discuss the core hydraulics and heat transfer. The first phase of development consisted in building and operating with water a 1/5 linearly scaled model as a rough, preliminary design check in establishing the acceptability of design concepts. The scale factor of 1/5 was chosen because, when the model was operated with water at 95°F with fluid velocities equal to the salt velocities in the reactor, the

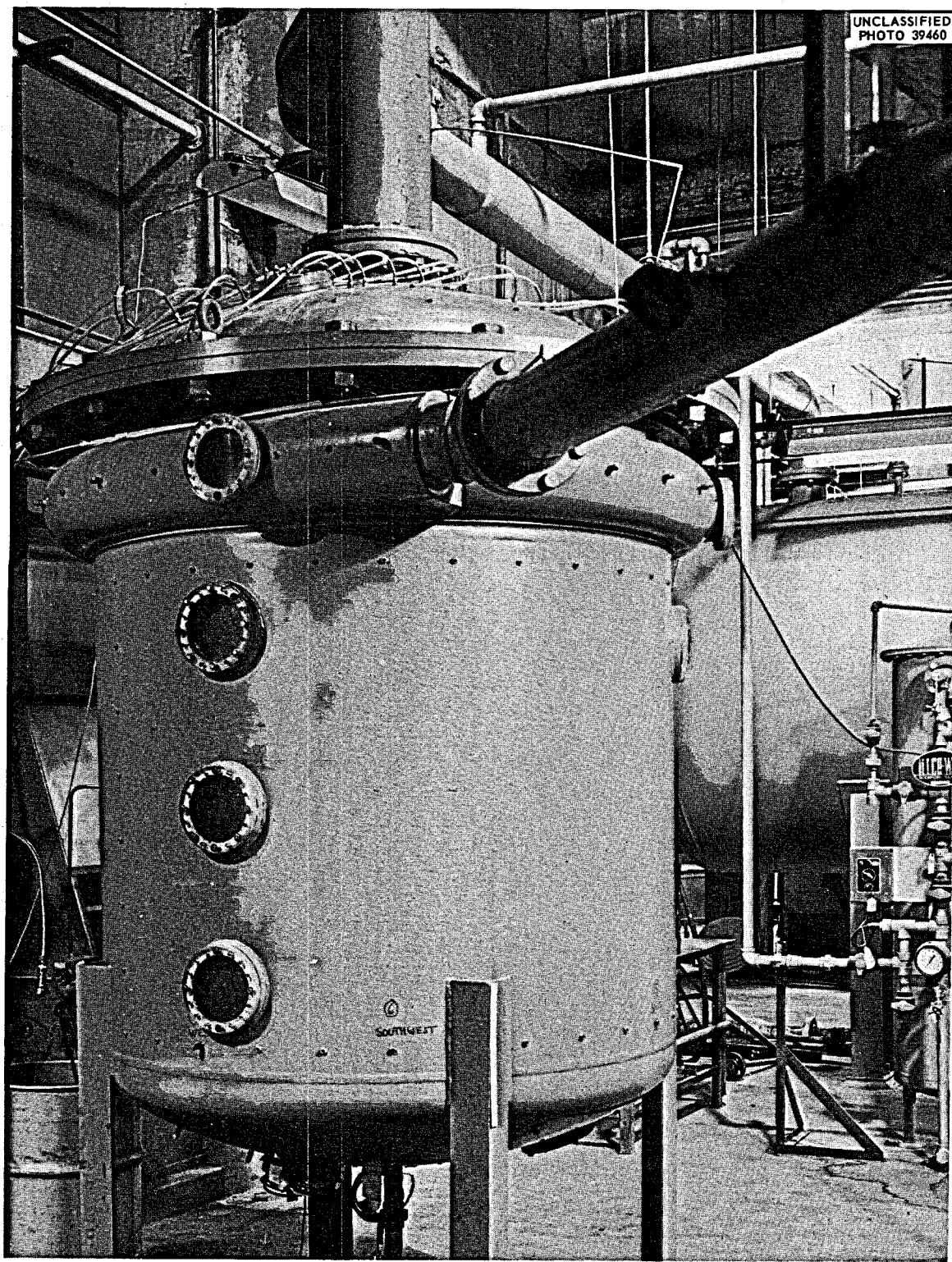


Fig. 1. Full-Scale Core Model.

model was fluid-dynamically similar to the reactor, and certain measurable parameters were related by a simple proportionality constant. This constant was 5 for the linear dimensions and fluid age, 1.38 for the turbulent heat transfer coefficient, and 1 for fluid velocity, Reynolds number, and relative fluid pressure gradients. The model was used principally to design the entrance volute, the flow distribution orifice assembly, and the antiswirl vane configuration in the bottom head.

The second phase of development used a full-scale core model, which is almost an exact duplicate of the reactor. Figure 1 shows this model. It is constructed of carbon steel, except for the core blocks and part of the moderator support grid, which are aluminum. Other differences, such as increased tolerances, were made for convenience and economics. Note the plastic windows, probe access holes, and the girth flange. All the initial data were taken with water as the fluid. This results in a Reynolds number for the model that is about four times that of the reactor. Later in the program, a thickening agent (JAGUAR-508, by Stein Hall and Co.) was added in order to more closely simulate the Reynolds numbers, and measurements which were suspected of having a strong dependence on the Reynolds number were repeated.

The areas in which measurements were made may be seen in Fig. 6, p.18. I shall quickly run through the measurement in the same order as the flow of fluid through the vessel: first, into the entrance volute, then through the flow distribution orifices, down the shell cooling wall annulus, into the lower head, through the core support lattice and core, into the upper head, and out the exit nozzle. Figure 2 gives the center-line velocity of the volute at three flow rates. The linear decrease in velocity indicates that the angular distribution of flow into the core wall cooling annulus is uniform. Since it is desirable to maintain high velocities and high heat transfer coefficients through the cooling annulus, the orifice holes were drilled at an angle to retain in the annulus the rotational flow established in the volute. Figure 3 is a plot of the resultant center-line velocity vs elevation in the annulus. The decrease in velocity results from the alteration of the tangential component. Measurements of the center-line velocity distribution around the core at the bottom of the annulus indicated that the flow to the lower head is uniform.

If the tangential component of the flow velocity were not removed by the antiswirl vanes in the lower head, it would produce an unfavorable vortex-type pressure distribution at the entrance into the moderator blocks. The antiswirl vanes performed well, as can be seen in Fig. 4. Due to the radial pressure distribution at the wall of the lower head, the pressure is a little higher in the center. This is in the right direction to promote higher flow rates through the center of the core. An additional attractive feature of this entrance condition in the lower head is the production of a jet at the wall, as shown in Fig. 5. This velocity profile was measured at a radius of 17 in. and a flow rate of 1200 gpm. A heat transfer coefficient of  $1200 \text{ Btu hr}^{-1} \text{ ft}^{-2} (\text{°F})^{-1}$  was calculated from these data. This jet did not persist much past this point, and, in fact, the flow over the vessel center line is gusty and

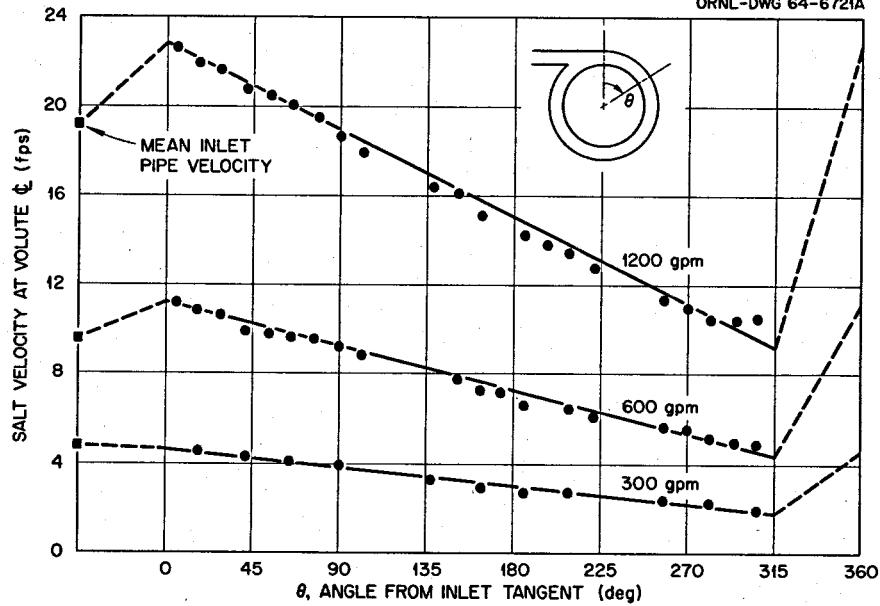
UNCLASSIFIED  
ORNL-DWG 64-6721A

Fig. 2. Center-Line Velocity Distribution in Volute.

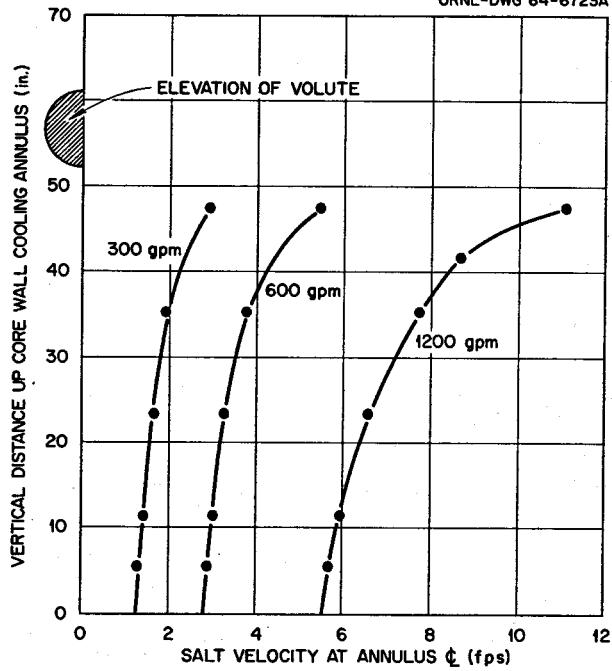
UNCLASSIFIED  
ORNL-DWG 64-6723A

Fig. 3. Center-Line Velocity Distribution vs Elevation in Cooling Annulus.

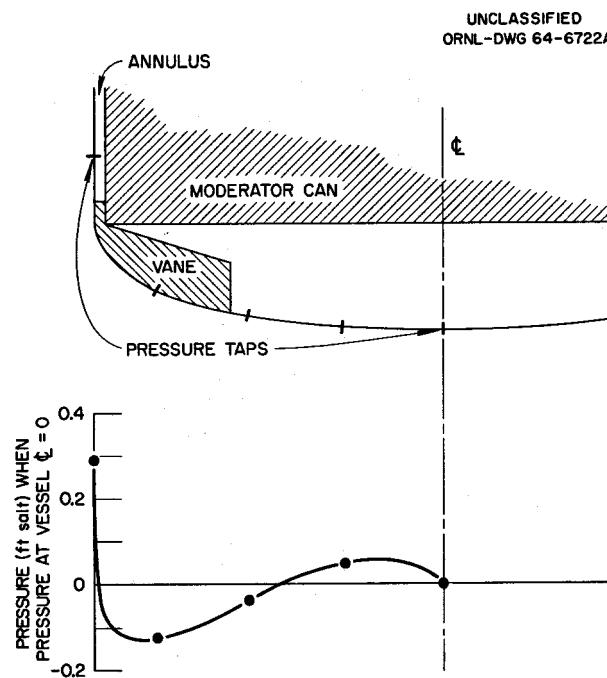


Fig. 4. Radial Pressure Gradient at Wall of Lower Head.

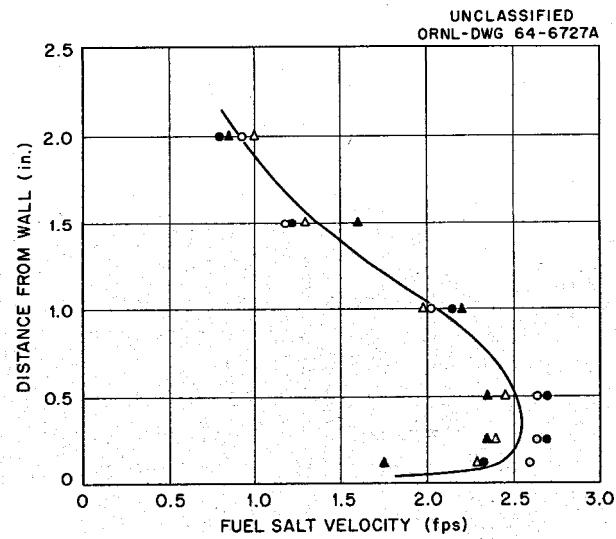


Fig. 5. Velocity Profile of Wall Jet in Lower Vessel Head at a Radius of 17 in. and a Flow Rate of 1200 gpm. Measurements were made at  $90^\circ$  to each other.

not predominant in any one direction. The results of measurements made with a heat meter in this region are shown in Fig. 6. There are some uncertainties in correlating the data at 4 in.; however, the results are believed to be within 50% and may be somewhat conservative, when thermal convention is included. Both curves indicate turbulence in this area.

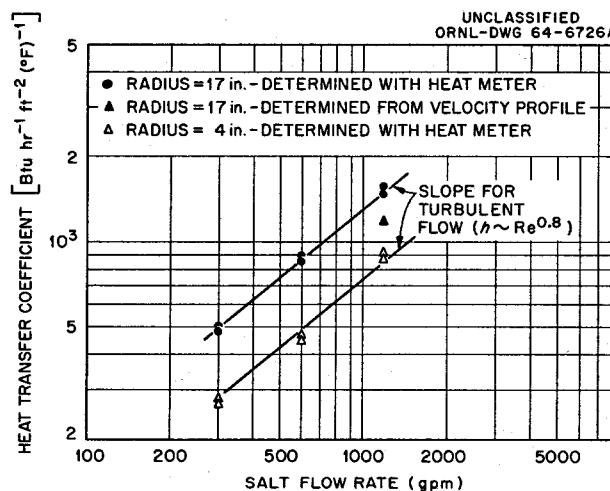


Fig. 6. Heat Transfer Coefficients in Lower Head of Reactor Vessel.

We now come to the moderator assembly, where the graphite support lattice and the moderator core blocks are. The support lattice consists of two layers of rectangular bars, one layer on top of, and perpendicular to, the other. The resultant square fuel passage holes are small, and the high fuel velocity through them produces an orificing effect. The velocity through the core blocks is much lower; consequently, the bulk of moderator assembly frictional head loss is taken in the lattice bars. The data in Fig. 7 were taken with water and later verified with a thickening agent, added for Reynolds number similarity. The total assembly pressure drop is shown along with the pressure drop across the lattice support measured in a separate mockup. These curves indicate turbulent flow in the moderator fuel channels, although it should be laminar since the Reynolds number in the channels is about 1000, based on the equivalent diameter. This disagreement only indicates that the entrance conditions persist well up into the channel. The flow distributions among the graphite channels are shown in Fig. 8. The two curves represent data taken in mutually perpendicular channels having different inlet conditions due to this support lattice, as shown in the sketch. To correct this deficiency, 1/10-in.-diam holes were drilled in the upper graphite support bars directly under the starved channels. This was the only change indicated necessary by the measurements. Note also that the flow decreases slightly with increasing radius, which reflects the radial pressure distribution measured in the lower head. Measurements made in the upper head indicated that no vortexing existed there. The overall pressure drop through the core, from the 5-in. inlet pipe to this 5-in. exit

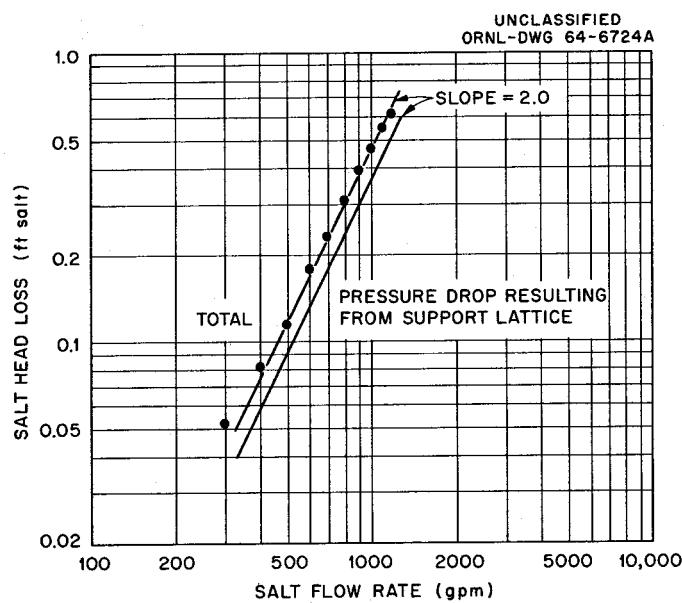


Fig. 7. Fuel Frictional Pressure Drop Across Moderator Assembly.

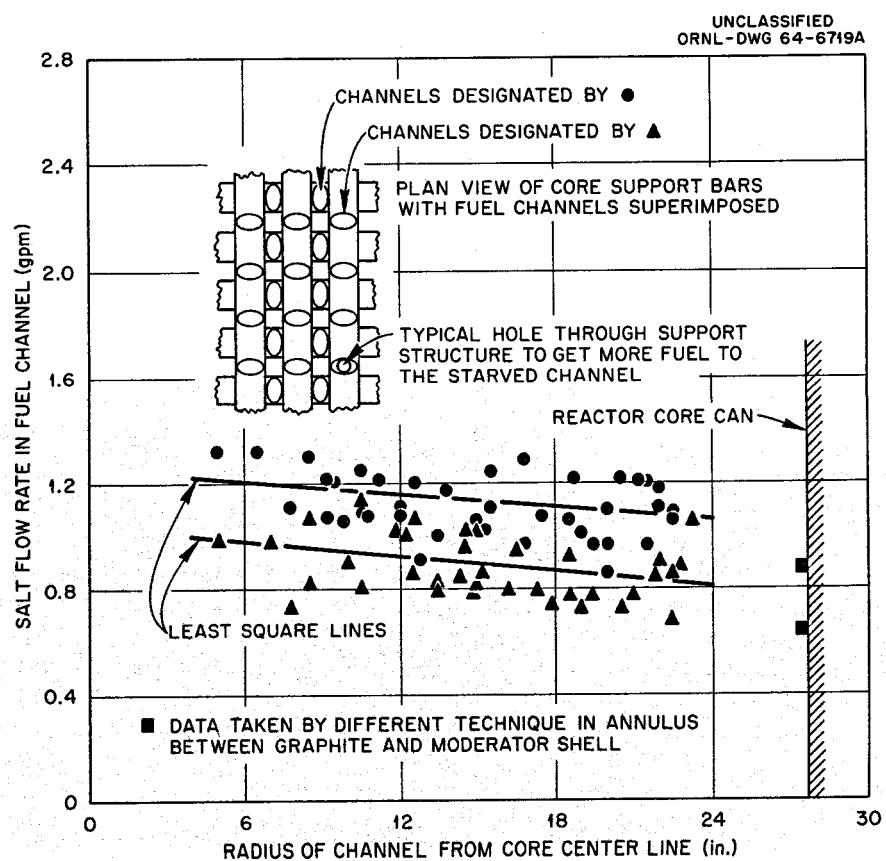


Fig. 8. Flow Distribution of Fuel Among Core Channels.

pipe, is given in Fig. 9. Note that the line has a slope of 2, which indicates that the pressure drop is independent of Reynolds number.

Experiments were run to study the tendency of solids to settle out in the lower head. It was found that solids with a specific gravity of 10 and less than  $300 \mu$  in size would continue through the lower head and up through the moderator, causing no problem.

In summary, the results of these tests indicate that the flow distribution within the reactor vessel assembly will provide adequate cooling to all parts of the assembly.

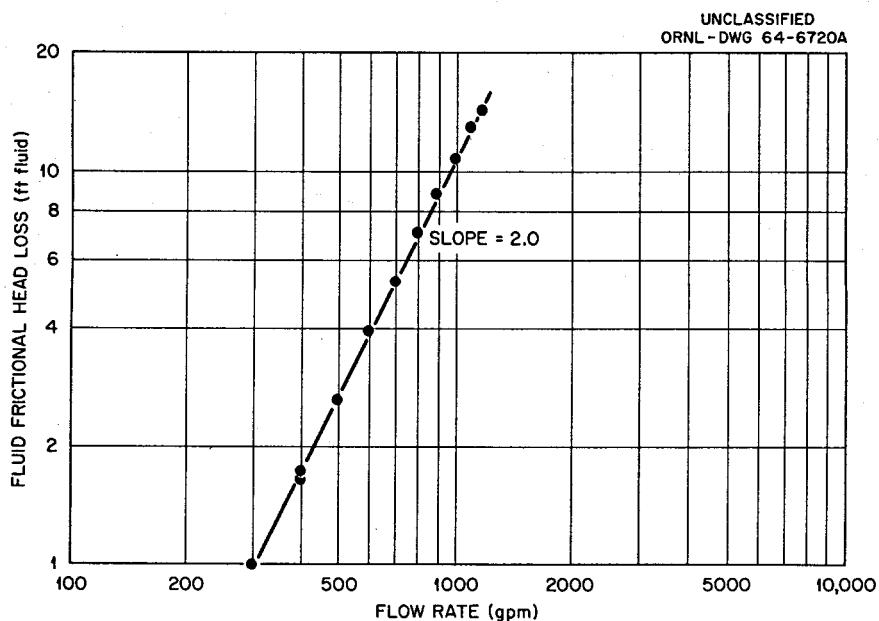


Fig. 9. Overall Fluid Frictional Head Loss Across MSRE Core.

#### Heat Exchanger

Hydraulic tests, similar to those just described for the reactor, were run on the primary heat exchanger. Figure 10 shows this test being performed last December. The initial tests indicated that the pressure drop through the tube side agreed with the calculations, but that the pressure drop on the shell side was excessive and that the tubes vibrated excessively at flow rates above 800 gpm in that side. The INOR-8 shell was removed, and a special stainless steel test shell was installed. As a result of subsequent tests, the tube vibrations were eliminated by attaching tight-fitting spacer bars to the baffle plates between the rows of tubes, and the pressure drop through the shell side was reduced by removing four tubes and increasing the size of the outlet nozzle. Figure 11 shows the fluid frictional head loss, as measured in the heat exchanger

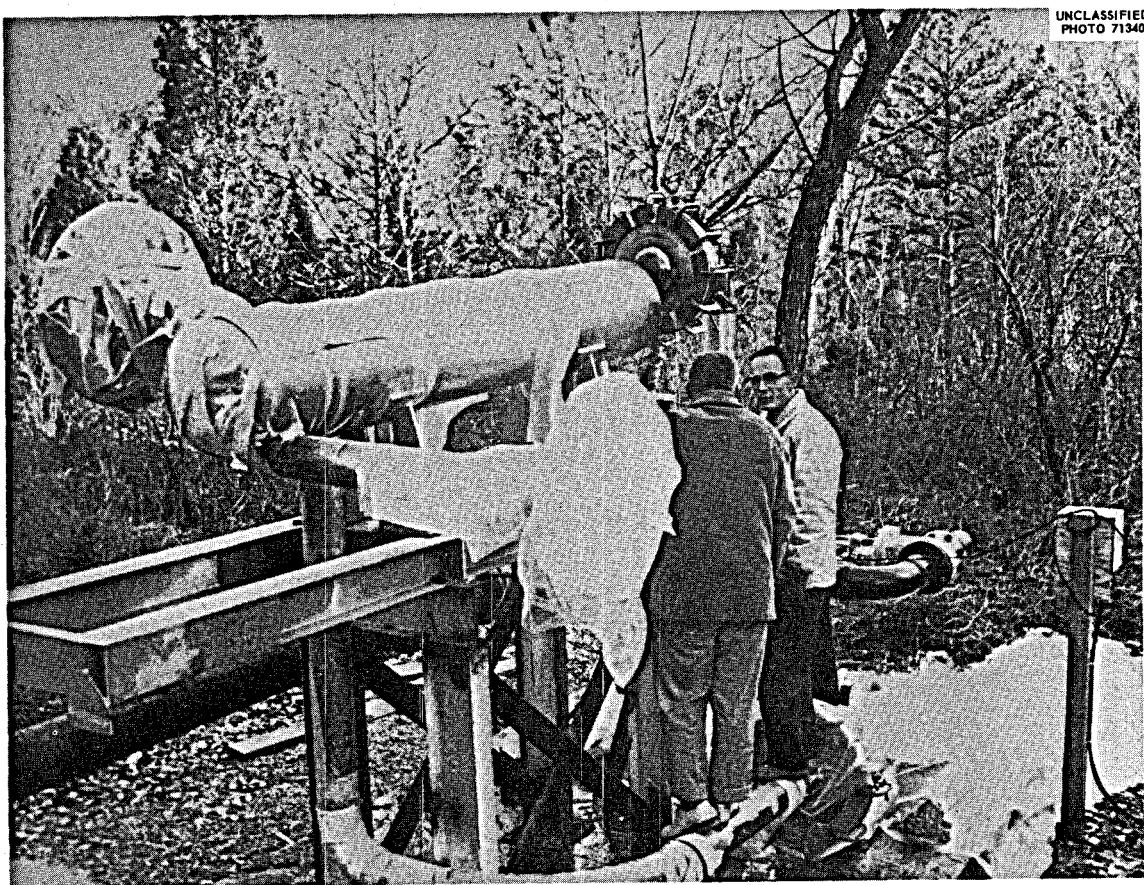


Fig. 10. Heat Exchanger Test.

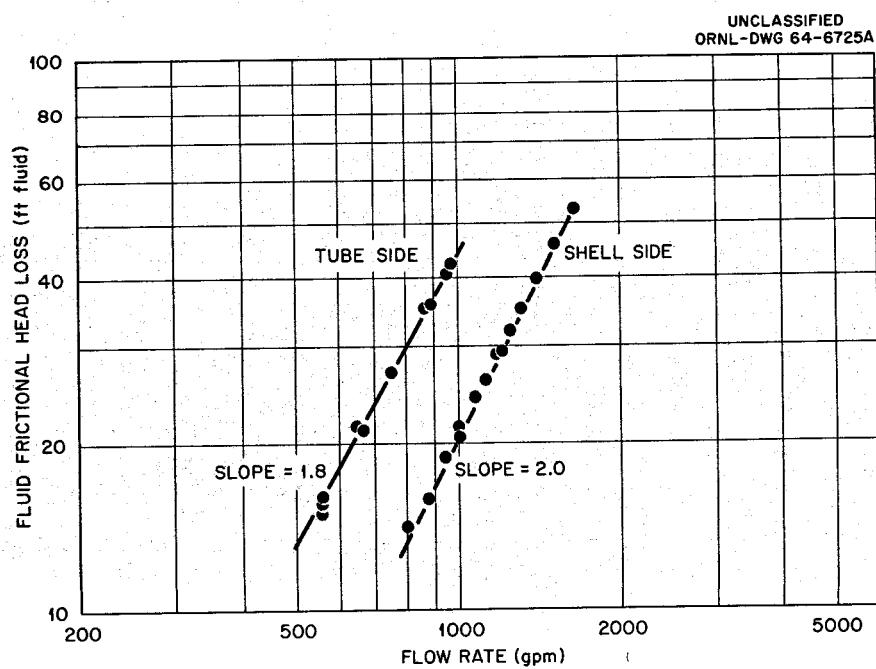


Fig. 11. Fluid Friction Head Loss in Primary Heat Exchanger.

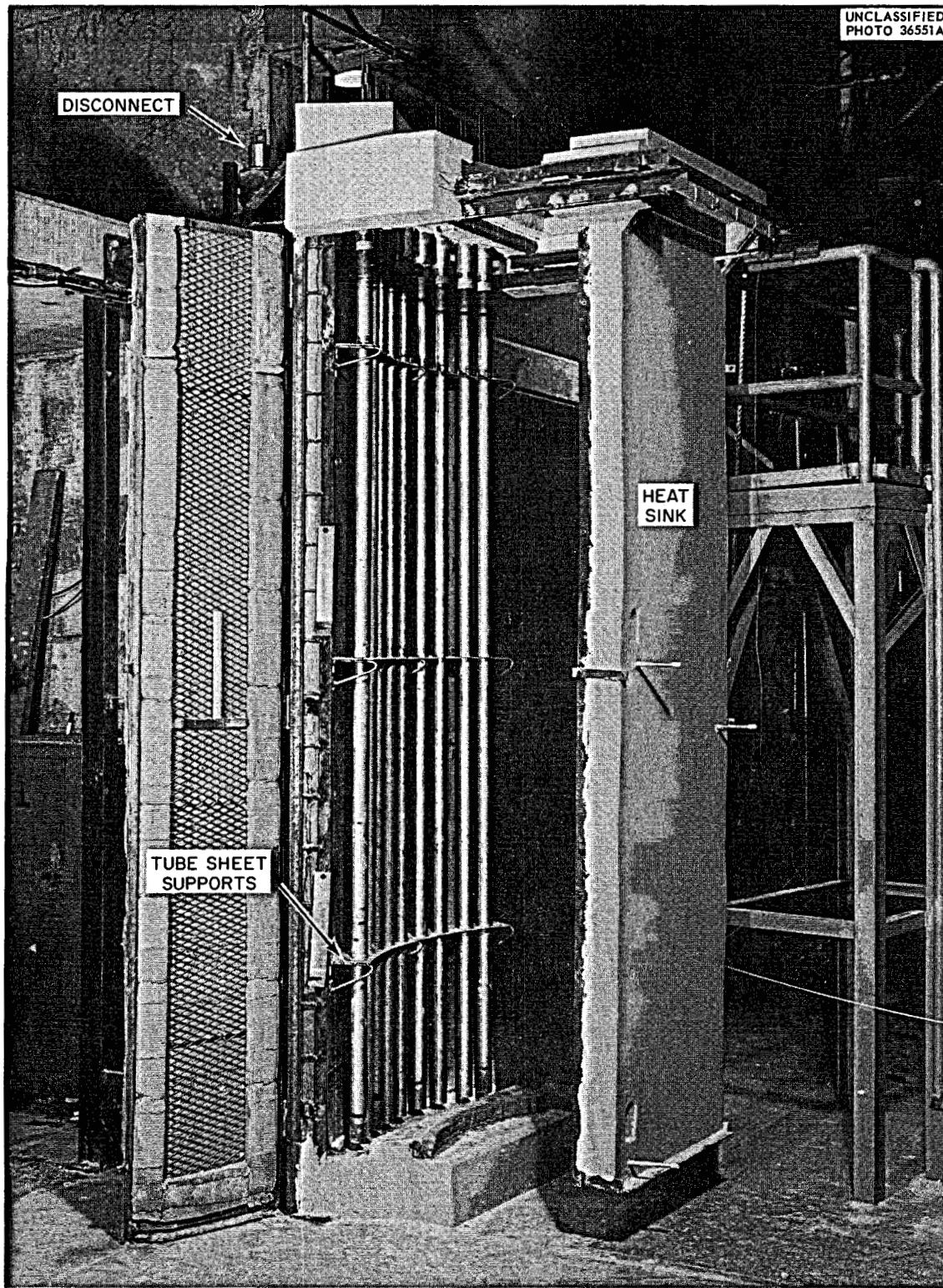


Fig. 12. Core Heater.

after the alterations were completed. The slopes of the two curves indicate that the pressure drop on the shell side is mostly due to entrance and exit losses and that the pressure drop on the tube side results mainly from frictional losses. We believe that the heat exchanger will now perform as originally planned.

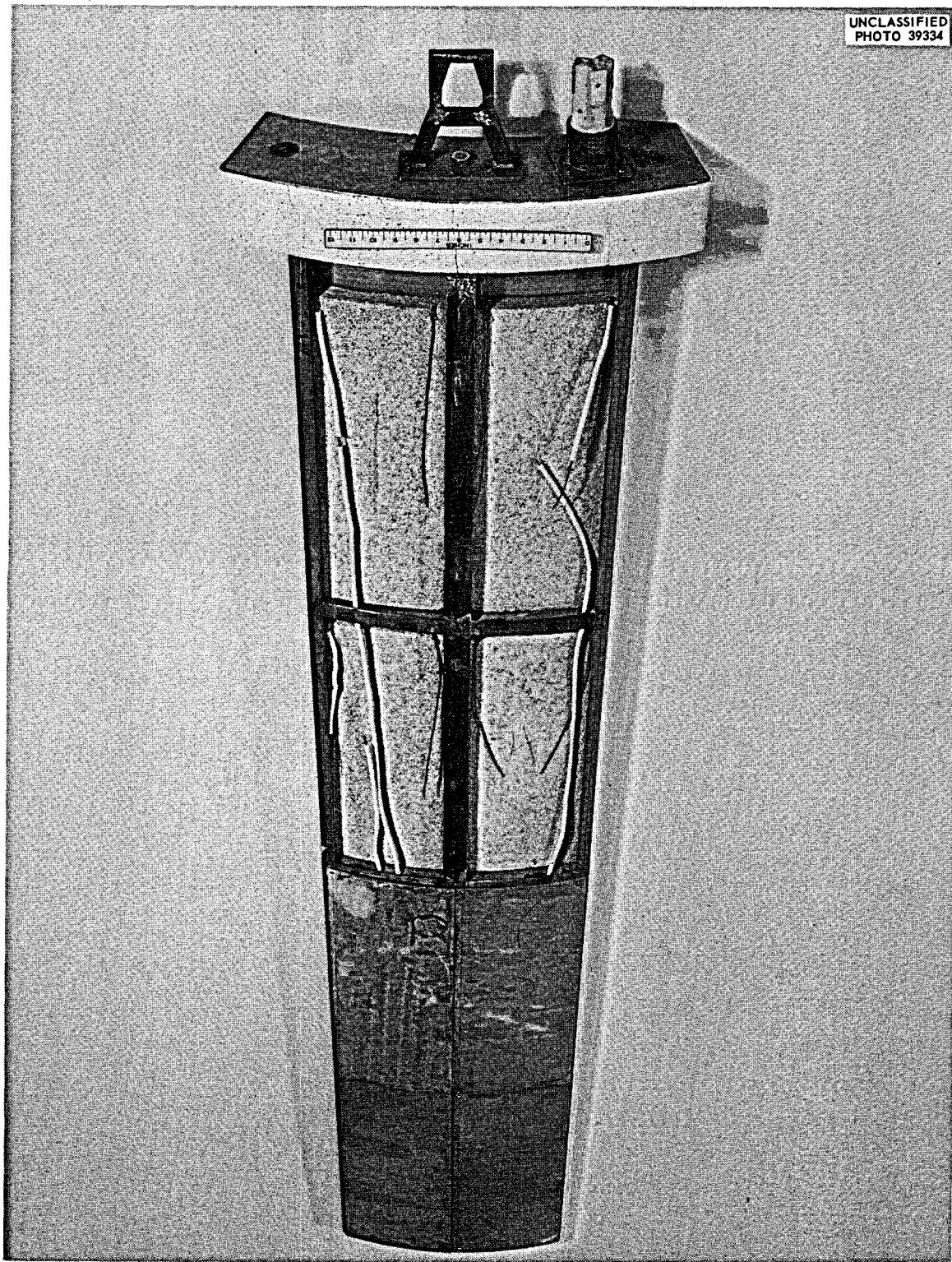
### Heaters

The next development area that I would like to discuss is concerned with the vessel and line heater and insulation packages. These units provide a controlled temperature distribution during heatup and cooldown as well as reduce the heat loss to the reactor and drain tank cell during high-temperature operation. Figure 12 shows a full-scale mockup of a section comprising 15% of the heater for the reactor furnace which was operated for 20,000 hr at 1250°F without incident.

A prototype of a single heater for the drain tank was operated at 1200°F over 10,000 hr without difficulty. Figure 13 shows the heater during assembly. The leads to the ceramic elements are interconnected by welding, and one of these welds failed early in the test operation. The design and inspection of the weld was improved, and no further trouble was encountered.

The heaters for the 5-in. pipes are enclosed in all-metal reflective insulation which was chosen because of the dusting problem normally encountered with refractory materials when much handling is required. Heater-insulation units of the type shown in Fig. 14 have operated with the interior above 1200°F for more than 5000 hr without difficulty or apparent deterioration, as would be indicated by a change in heat loss.

Another unit associated with the control of temperature of the vessels is the drain tank cooler, which is used to remove the afterheat following extended operation at full power. Figure 15 shows the parts for the test of a three-tube mockup of the original design of this cooler. The reentrant thimbles shown were immersed in a salt which was maintained between 1300 and 1400°F. The Inconel cooling bayonets, which include smaller concentric tubes for cooling water flow, were inserted into the thimble and cycled by allowing water to flow into the bayonets. Since the temperature of bayonets had been above 1300°F, the thermal shock from the water quench was terrific. Figure 16 shows a portion of the inner tube which had experienced more than 2600 such thermal cycles. The design of these tubes was changed in the area of the welds at the spacer fins, and new test units were constructed from INOR-8. These units have operated through more than 1000 thermal cycles with no evidence of cracking, even at the surface. On the basis of these tests, the drain tank cooler should operate without trouble through at least 100 reactor shutdowns from full power.



UNCLASSIFIED  
PHOTO 39334

Fig. 13. Drain Tank Heater During Assembly.

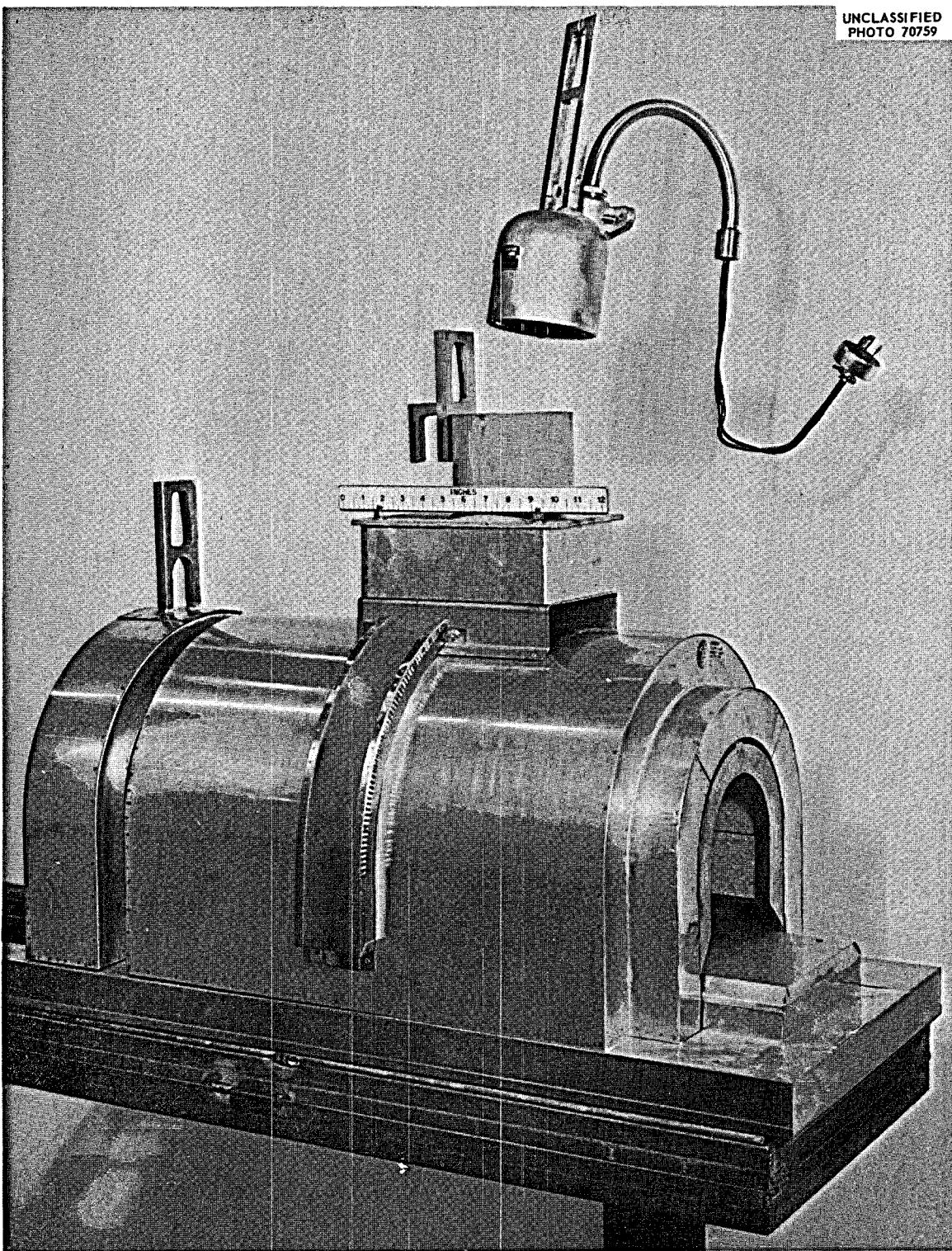
UNCLASSIFIED  
PHOTO 70759

Fig. 14. Pipe Heater.

### Freeze Flanges

Mechanical-type joints are provided in the 5-in. piping in the fuel- and coolant-salt system inside the reactor cell to permit the major equipment to be disconnected for removal and replacement. The so-called "freeze flange" type of joint was chosen because of its proven reliability in providing tight connections with zero salt leakage and insignificant gas leakage under all anticipated thermal-cycling conditions. Freeze flanges have been a part of molten-salt engineering development for several years. Flanges with integral cooling were incorporated in the Remote Maintenance Demonstrations Facility, where it was shown that they could withstand repeated thermal cycles and could be broken and reassembled. As a result of these preliminary tests, the design of the flange was improved to provide greater strength toward axial loads, to reduce the thermal stress, to improve the tightness of the buffer seal, and to remove the requirement of integral cooling. Flanges of the improved design (shown in Fig. 17) were thermal cycled between room temperature and 1300°F more than 100 times without significant changes which would indicate excessive thermal

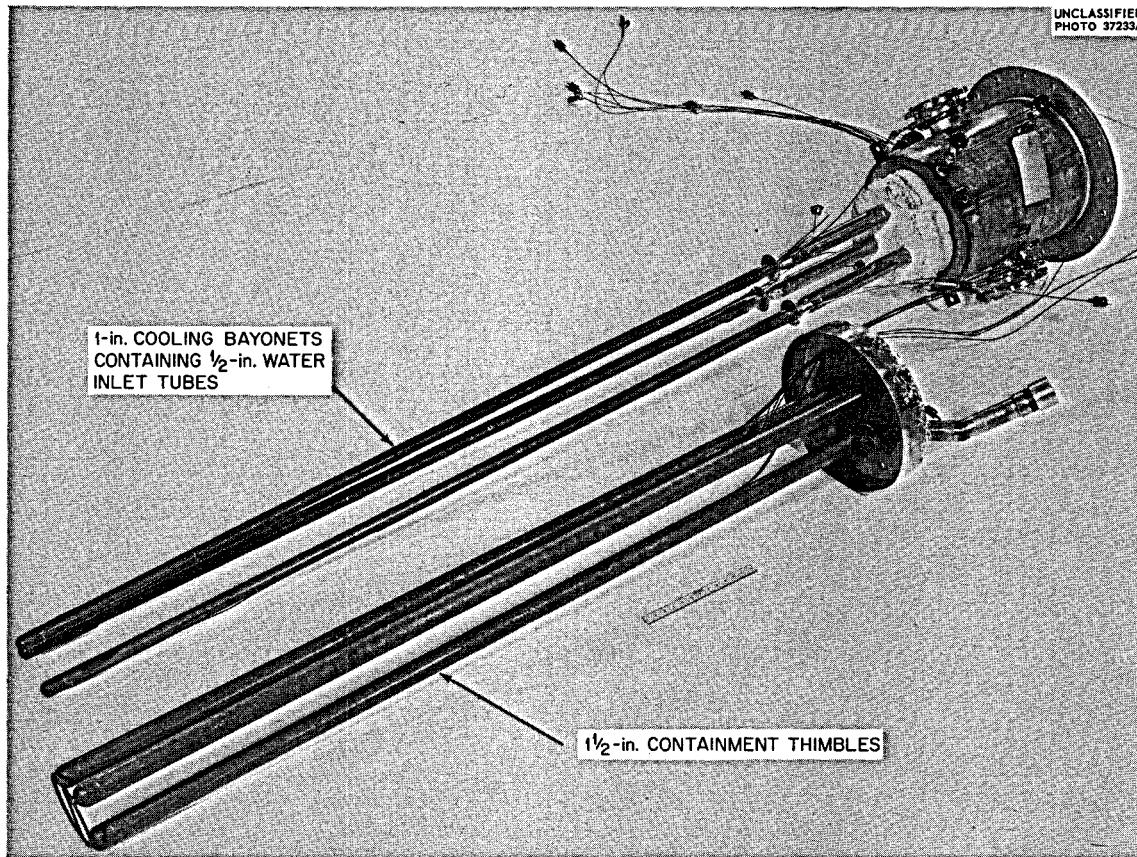


Fig. 15. Drain Tank Cooler Test Components.

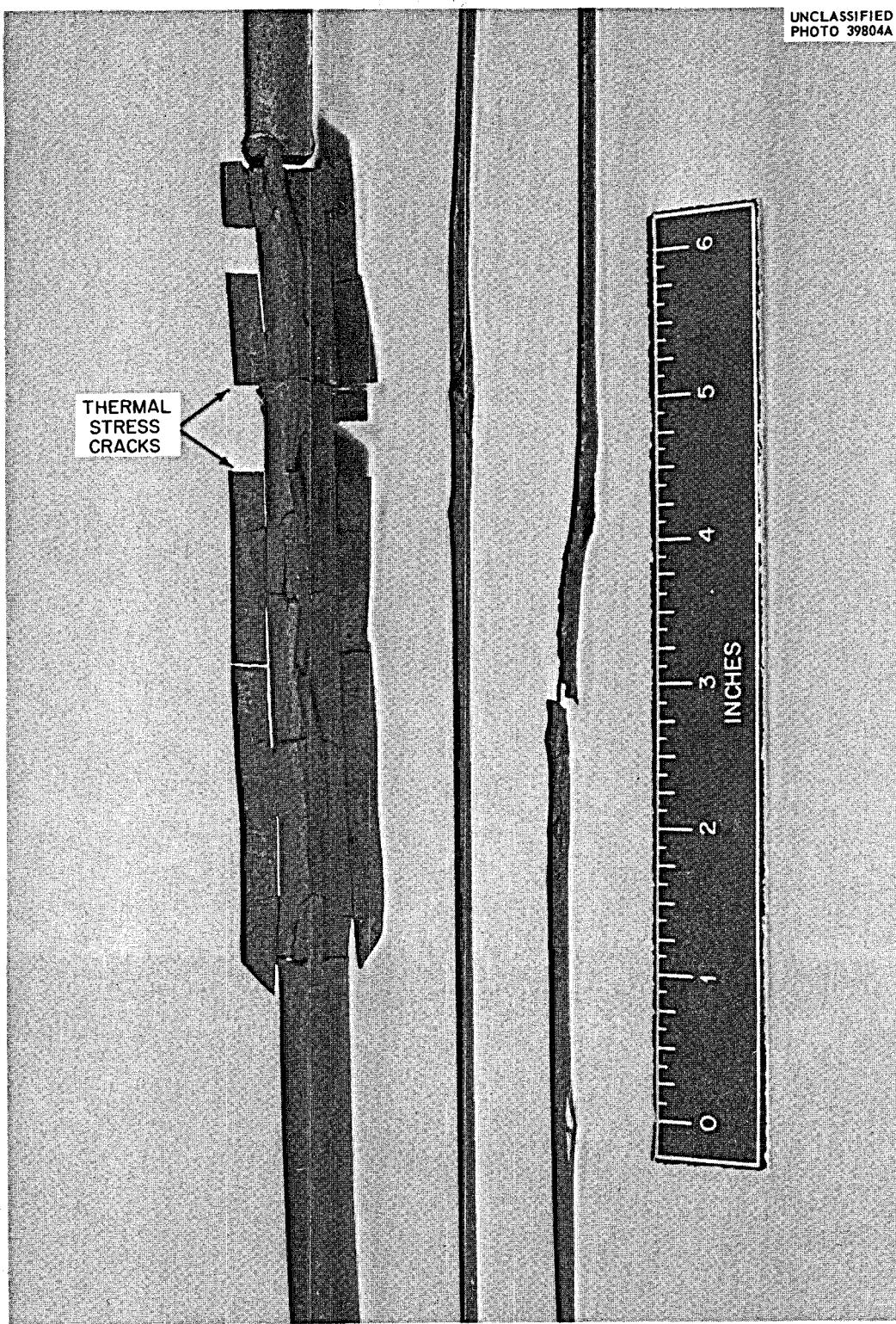


Fig. 16. Drain Tank Cooler 1/2-in. Tube.

stress. During all these tests the gas leakage from the buffer zone remained less than  $5 \times 10^{-4}$  std cm<sup>3</sup> of helium per second. It was found that a new flange would make up and seal satisfactorily with a flange which had experienced several thermal cycles from room temperature to 1300°F. In addition, there was a flange pair of this type incorporated in the prototype pump test loop, described in the section on pump development, and it has operated satisfactorily throughout that test. We have found nothing, from these or other tests, which would indicate problems with the use of these freeze flanges in the MSRE.

In addition to the work on freeze-flange disconnects, small, remotely maintainable buffered seal disconnects were developed for use in the sampler-enricher and the various gas lines of the MSRE. These disconnects satisfactorily demonstrated their reliability under extreme temperature conditions of operation.

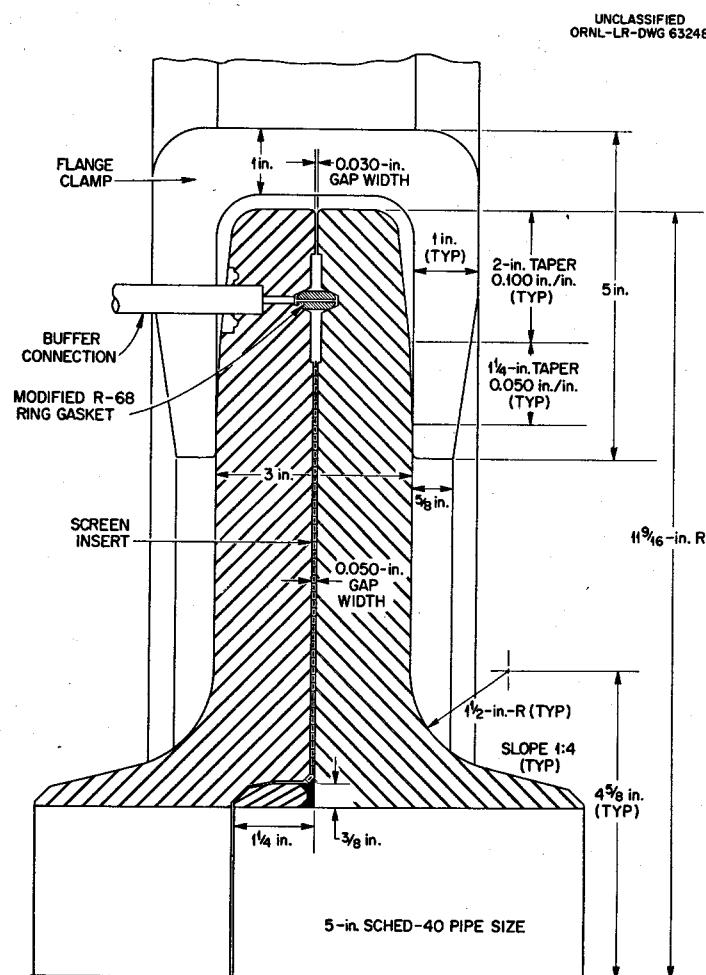


Fig. 17. Freeze Flange.

### Freeze Valves

A reliable high-temperature mechanical valve was not available at the start of this project. However, there was much experience with frozen plugs of salt in controlling the transfer of salt. It was necessary to develop and demonstrate a valve system which would operate reliably and give consistent indications of its condition. Many variations of freeze valves were built and tested; Fig. 18 shows the arrangement chosen for use in the reactor drain line at the drain tank.

This valve consists of a flattened section of pipe surrounded by an insulated air shroud, all of which is enclosed in a special removable pipe heater. It is characteristic of this valve that the frozen plug is formed within the insulated air shroud and that thawing must proceed from the ends of the plug toward the center. Since the energy for the thawing operation comes primarily from that stored in the removable pipe heater, the time required to open the valve is changed only slightly by a power failure. When it is required that a valve always remain frozen, the special pipe heater is allowed to cool to below the melting point of the salt. Valves of this type have operated through more than 100 freeze-thaw cycles without dimensional change, and require approximately 20 min to freeze and 15 min to thaw. They can be frozen even with salt flowing through them at rates of 300 in.<sup>3</sup>/hr. Results of these and other tests indicate to us that these freeze valves are satisfactory for the MSRE.

### Control Rod System

The control rod drive is shown in Fig. 19 along with the drive housing. The development problems with this control rod system for the MSRE resulted from the facts that the control rod must be flexible enough to go around an offset in the rod's path and that oil bath lubrication of the rotary parts of the drive mechanism is undesirable. The flexibility requirement created problems related to the effect of the stretch of the rod on position indication and wear at the contact surfaces in the path offset. A structural mockup of the control rod is shown in Fig. 20. Note the bellows inside the metal braid in the upper section and the wire cable inside the spiral hose in the lower section. This construction method was necessary to reduce the stretch of the rod, while permitting cooling air flow through the center. A method was developed which remotely calibrates the position of the bottom of the control rod with the remotely indicated position of the top of the rod by using this air flow. The wear problem was solved by incorporating graphite-bushed rollers into the guide thimble at the critical locations in the offset. These and other small changes were incorporated into the final design, and a prototype rod and guide thimble was then successfully operated at 1200°F through 38,000 full cycles of 102 in. of travel per cycle.

A radiation-resistant grease was used to lubricate the rotary elements of the control rod drive and proved satisfactory except at the worm drive section. The wiping action at the contact surface removed the grease there, causing overheating and destruction of the aluminum

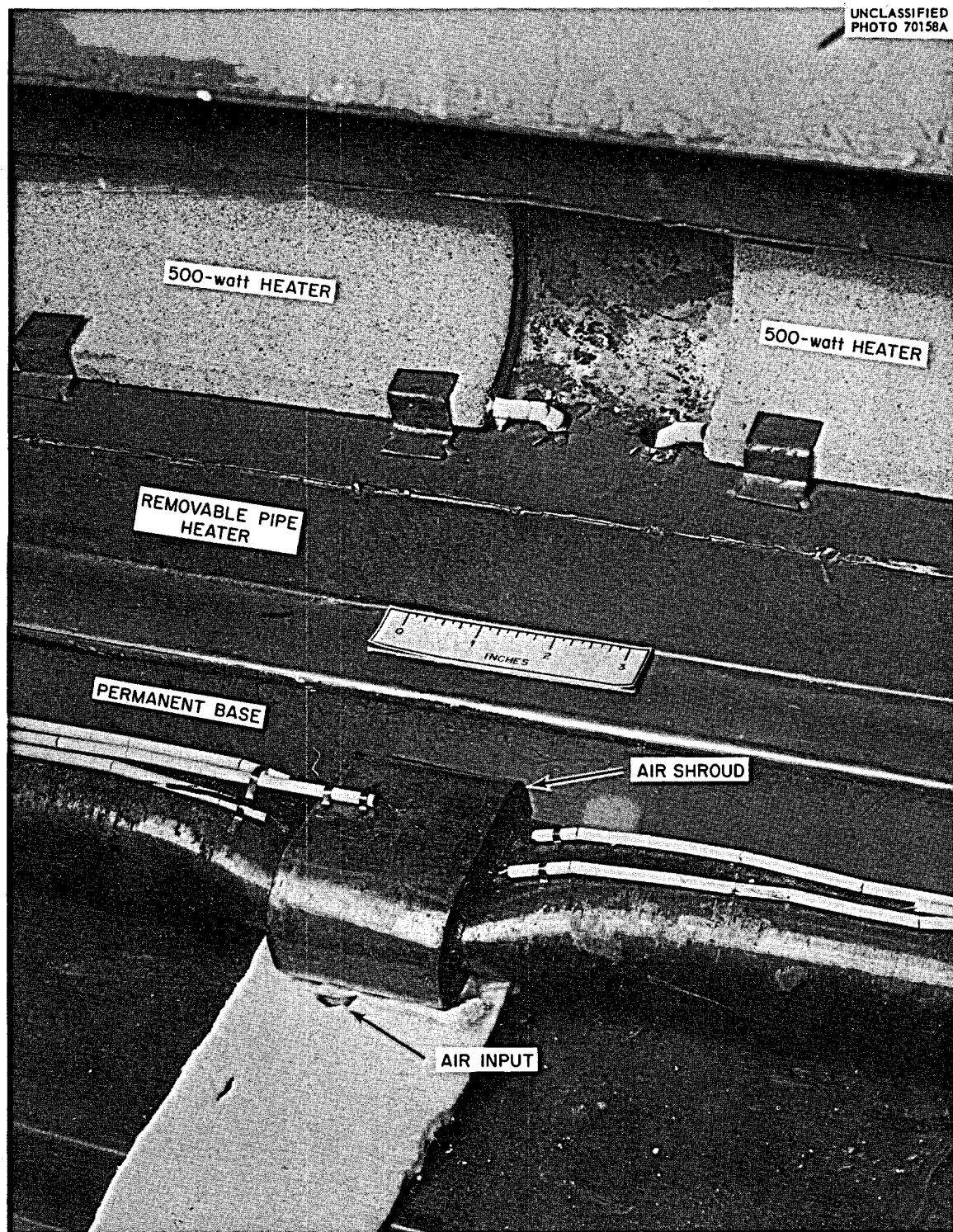


Fig. 18. Freeze Valve.

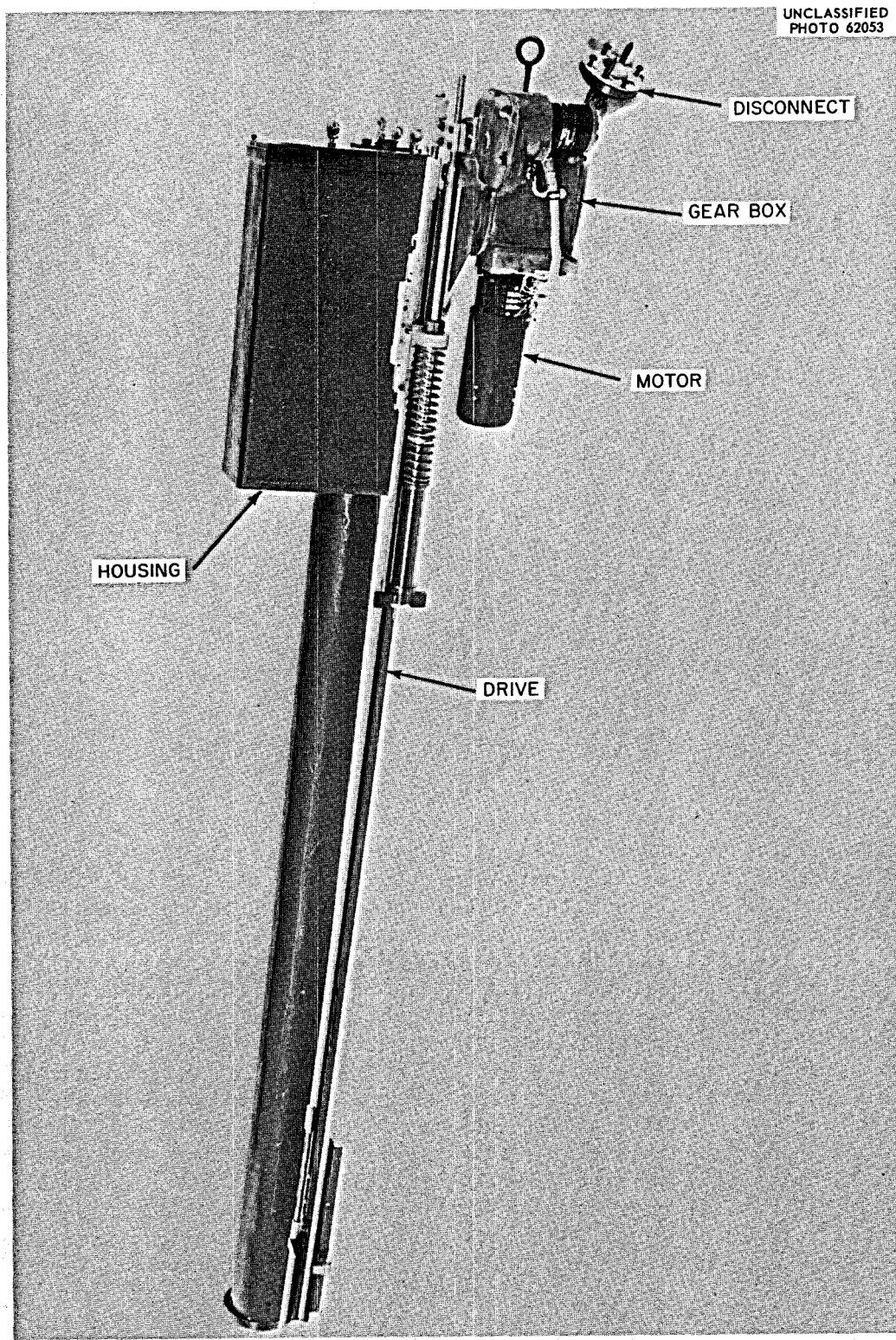
UNCLASSIFIED  
PHOTO 62053

Fig. 19. Control Rod Drive.

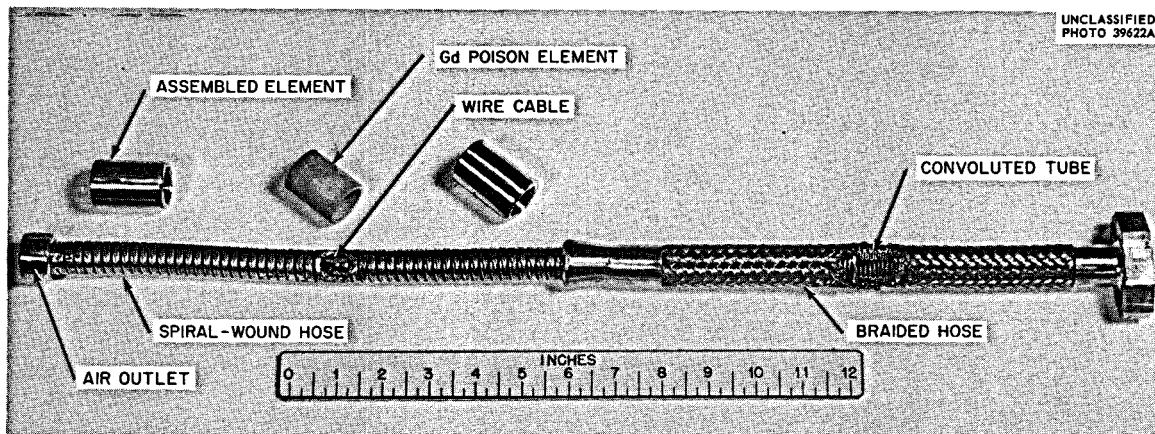


Fig. 20. Structural Mockup of MSRE Control Rod.

bronze worm wheel after 16,000 full stroke cycles. While this performance was considered adequate for the MSRE, testing of other materials has continued. A preliminary test using a hardened-steel pair of gears operated in excess of 29,000 full stroke cycles without significant wear. Gears of this type have been specified for use in the reactor. There have been some other changes as a result of the development testing, but they are in the category of optimization and do not affect the reliability.

#### Cover-Gas System

Another area examined for problems was the cover-gas system. This system consists of the inert-gas supply section, the distribution and control section, and the off-gas disposal sections. Of these, only the purification portion of the inert-gas supply section required experimental study, since the other sections are based on what has become a well-established technology. The inert-gas supply section consists of the supply and storage reservoirs, the oxygen- and water-removal units, and the on-line gas analysis section. On the basis of preliminary experiments, full-scale oxygen- and water-removal units were constructed and tested; the oxygen-removal unit is shown in Fig. 21. The test results indicated that, with a titanium bed temperature of 1200°F and an inlet oxygen concentration of 100 ppm, an outlet concentration of less than 1 ppm was maintained until 58% of the titanium sponge had been consumed. Since the average oxygen concentration at the inlet to the purifier for the MSRE is not expected to exceed 50 ppm, the life of a titanium charge should be six months or longer with a helium flow of 6000 liters/day. The performance of a commercial oxygen analyzer was checked during the helium purifier experiment and was deemed satisfactory after modification by the manufacturer.

The helium dryers were designed using the manufacturer's design parameter, and performance checks were limited to an occasional check of the water concentration at the dryer outlet. We determined that the dryer bed would require regeneration after 30 days of operation with an inlet moisture concentration of 50 ppm of H<sub>2</sub>O. Two dryers, installed in parallel for alternate operation in the MSRE, provide for the regeneration.

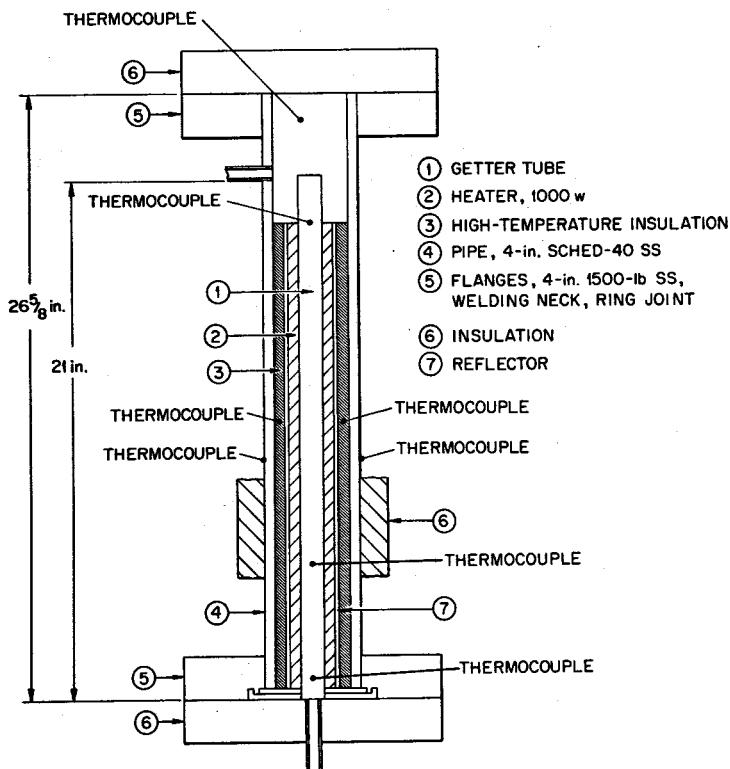
UNCLASSIFIED  
ORNL-LR-DWG 68585

Fig. 21. Oxygen-Removal Unit.

While no reliable method for the continuous detection of water in helium is available at this time, some work is continuing toward that goal, and in the meantime occasional checks will be made of the output of the purification section. The results of our tests indicate that the capacity and performance of the purification sections are more than adequate for use in the MSRE.

#### Sampler-Enricher

The major problem in the sampling and enriching of liquid-fuel reactors is the required penetration of the double containment. In general, the system developed for the MSRE uses a series of containment areas through which the sample moves after it is isolated from the circulating stream. Figure 22 shows the component arrangement for the sampler-enricher. Basically, it is a power-driven cable which lowers a small bucket into the liquid of the pump bowl. The cable then raises the bucket into a manipulator area for transfer into a shielded container for transport to the analytical chemistry hot cell. Figure 23 shows a sample and an enriching capsule of the type tested. Prototypes of critical components were assembled into a mockup of the sampler-enricher system, which was used to remove some 56 salt samples and to add 11 capsules of enriching salt to

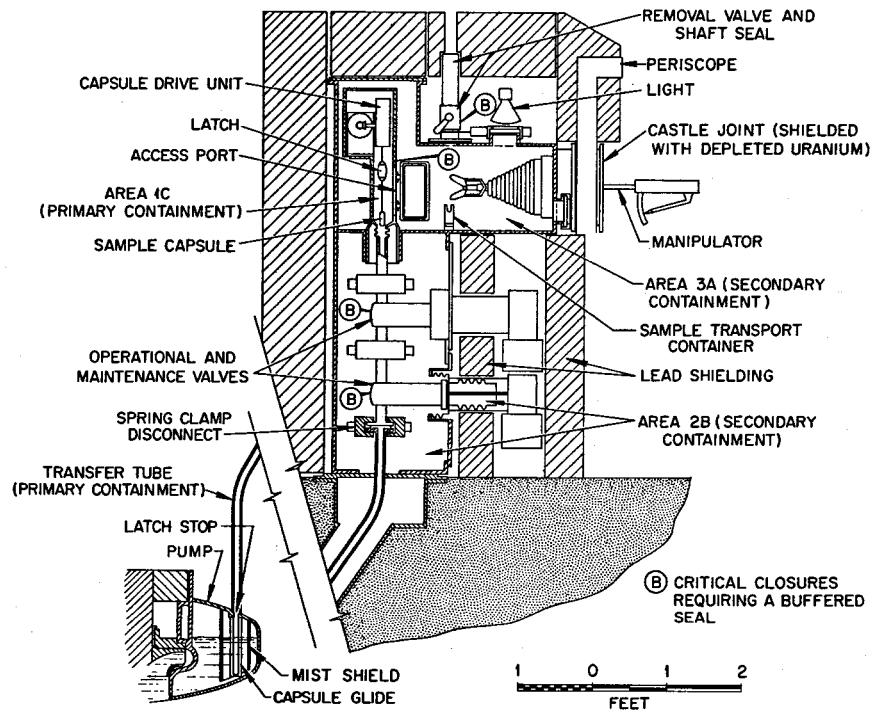
UNCLASSIFIED  
ORNL-DWG 63-5848R

Fig. 22. Component Arrangement for Sampler-Enricher.

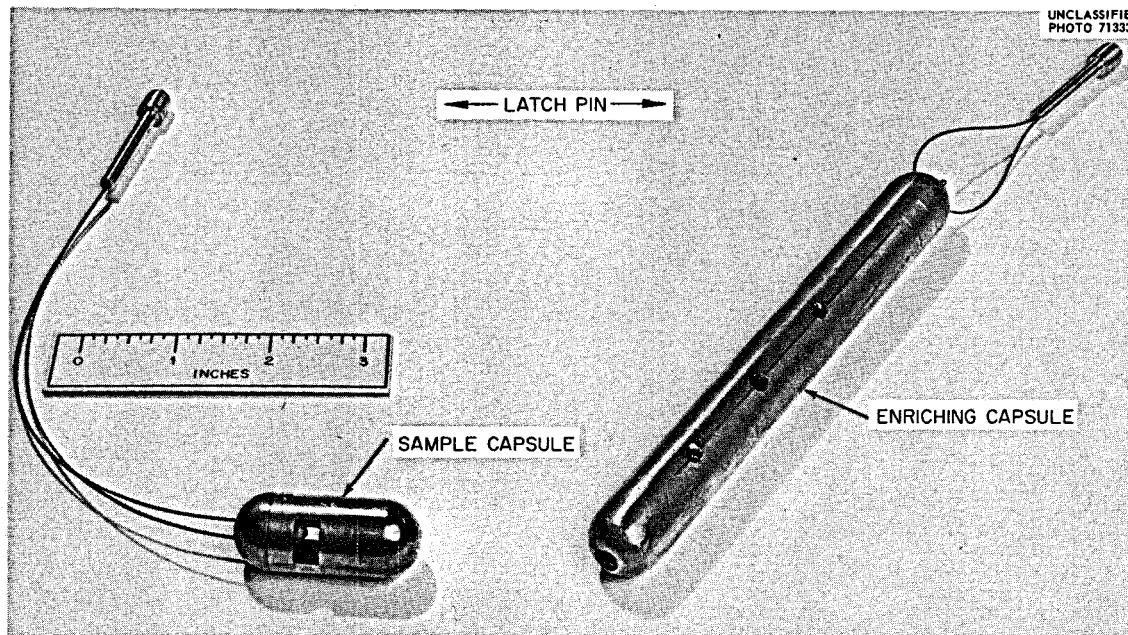


Fig. 23. Sample Capsule and Enriching Capsule.

a circulating loop. After some adjustments and minor alterations, the system operated reliably and safely. The results of the chemical analyses of the samples agreed within 1-1/2% with the results from samples taken with another proven method. These and other tests indicate that there should be no major difficulty with the use of these sampler systems in the MSRE.

#### Engineering Test Loop

The final area I would like to discuss concerns a collection of simulated MSRE components, the Engineering Test Loop, shown in Fig. 24. In this loop satisfactory performance of the freeze valves, level indicators, sampler-enricher, frozen salt-graphite access joint, and gas-handling system was demonstrated under simulated reactor operating conditions. A method of gas purging and salt flushing the system to remove oxide before operations with fuel was demonstrated. A method was demonstrated for the removal of oxide from the salt by treating with HF and hydrogen in the drain tank. The Engineering Test Loop was operated in excess of 15,400

UNCLASSIFIED  
ORNL-LR-DWG 54492A

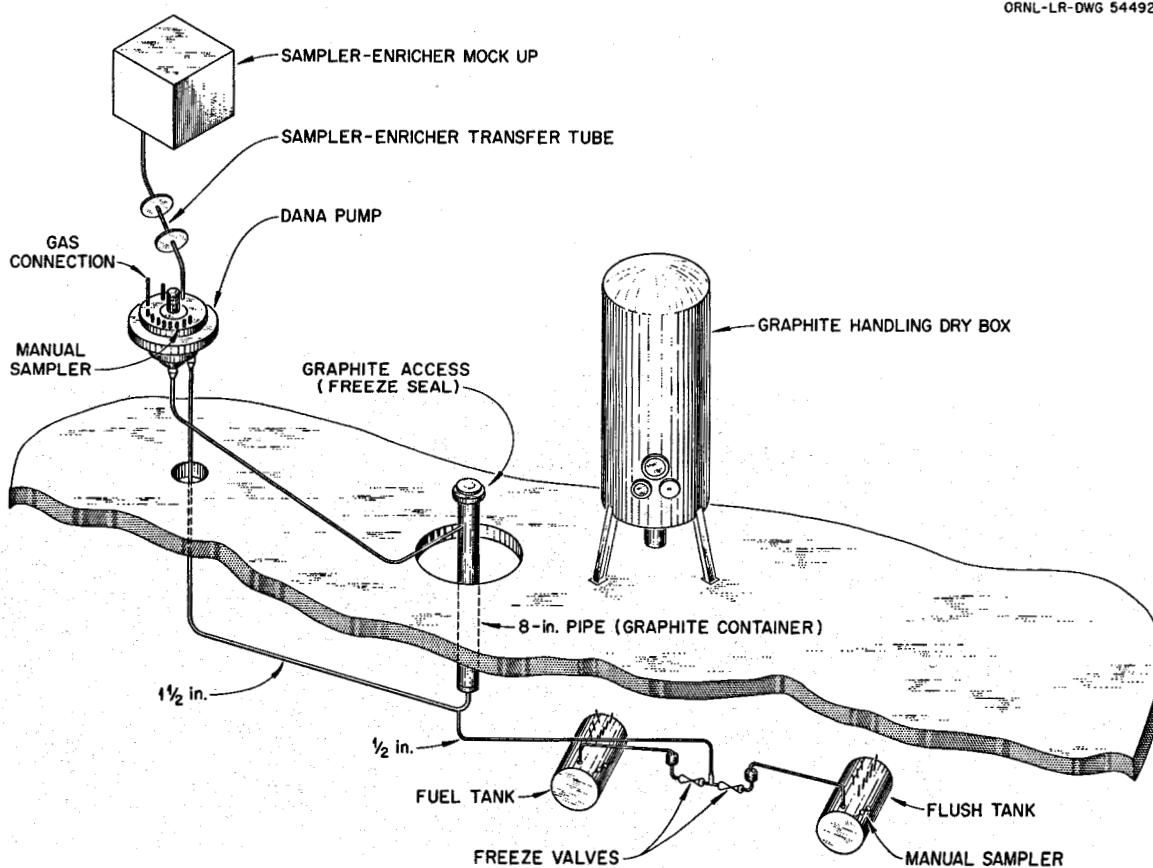


Fig. 24. Engineering Test Loop.

hr at 1200°F. The last 7000 hr of the test was conducted with LiF-BeF<sub>2</sub>-ZrF<sub>4</sub>-UF<sub>4</sub> salt to test the sampler-enricher and to follow the inventory of uranium added to the loop. The uranium concentration was varied from 0.1 mole % at the beginning of the period to about 0.7 mole % at the end. The results of the chemical analyses agreed with the book inventory of the additions within the experimental uncertainties of 3%. Metal and graphite samples were removed periodically for examinations, and no unusual changes were noticed.

#### Summary

In summary, the performance of the components tested has exceeded the requirements for the MSRE. In addition, the components needing maintenance have been made easily replaceable. Finally, the components and systems have been shown to be compatible when operated as a loop. This experience leads us to believe that the MSRE should have a long and uneventful life.

---

#### REMOTE MAINTENANCE OF THE MSRE

Robert Blumberg

To be attractive as a power producer, this reactor must possess a measure of serviceability. To this end the maintenance criteria influenced not only the system design but also the entire facility. The major requirement, stated simply, is that all the fuel-salt-carrying equipment and all other equipment that may fail in the reactor and the drain cell must be remotely replaceable.

Two structural types were considered. In the first, a large vessel with complex internals housed all the important elements of the system, such as the core, pump, heat exchanger, etc. Maintenance involved opening a large vessel closure and then working down, layer by layer, until the failed element was reached. This was discarded in favor of its counterpart, a system composed of a number of separate pieces of equipment joined by piping. This arrangement led to this set of guides or rules to make the MSRE capable of being easily maintained:

1. The system should be composed of several separate units joined by suitable disconnects.
2. Each unit should be accessible in the plan view of the reactor.
3. Removal and replacement should be considered in the design of each unit.
4. Maintenance equipment should be provided to handle the equipment from above.

It was originally planned to maintain the MSRE with a bridge-mounted manipulator, remotely controlled, using television for auxiliary viewing. However, because the MSRE was fitted into an existing building, there was not enough head room for this. The system that was adopted is a combination of the totally remote and the semidirect (long-handled) approaches. This combination of techniques stems from experience gained in operating the molten-salt remote maintenance demonstration facility<sup>1</sup> and in maintaining the Homogeneous Reactor Test (HRT).

Schematically, the method of maintenance is as follows. For small pieces of equipment such as heaters and valves, a portable maintenance shield, similar to the one developed for the HRT,<sup>2</sup> is set up over the opening left by the removal of two adjacent shield blocks. Long-handled tools are inserted through the portable shield (Fig. 1) to disconnect attachments and lift the unit out of the cell. Direct viewing is provided by built-in windows and lighting and by periscopes inserted through the shield. For large pieces of equipment, the portable shield and long-handled tools are used to prepare the item for a direct lift. This may involve disconnecting attachments, displacing the unit to provide clearance, and installing a lift fixture. The rest of the procedure is carried on by personnel from inside a shielded control room which overlooks both cells. From there, using remotely controlled cranes and a variety of accessories, sufficient shielding is removed from the cell roof to gain access to the item to be handled. The crane is then used to remove the item from the cell, put it into the storage pit, and replace the shielding blocks. Viewing is provided by windows in the wall of the control room and a pair of portable television cameras.

In summary, the MSRE, from a maintenance viewpoint, is a collection of replaceable parts joined by disconnects. Small parts will be maintained by long-handled tools inserted through a portable shield, and large parts will be prepared for removal with the long-handled tools and then removed by remote equipment. There are three general divisions that comprise the equipment to be used; the shielding, the long-handled tools, and the remote equipment.

#### Shielding

The reactor and drain cells are shielded by two layers of concrete blocks. For maintenance, the top layer is taken out of the way, and the upper surface of the lower layer then becomes the working floor for the maintenance crew. The lower layer has been designed to meet various needs of remote maintenance. First, the width of the blocks provides, as far as possible, a 2-ft modular grid to coincide with the 4-ft opening of the portable shield. Second, the blocks are laid out to allow convenient access to the major components in the cell. Third, penetrations through the block are provided where necessary, allowing access for tools without removing the shield block. Finally, the blocks are equipped with pickup sockets, which allow them to be handled remotely.

The portable maintenance shield is a device which is set up over any 4-ft opening in the shielding. It provides 12 in. of steel shielding for the personnel who will insert long-handled tools through bushed holes.

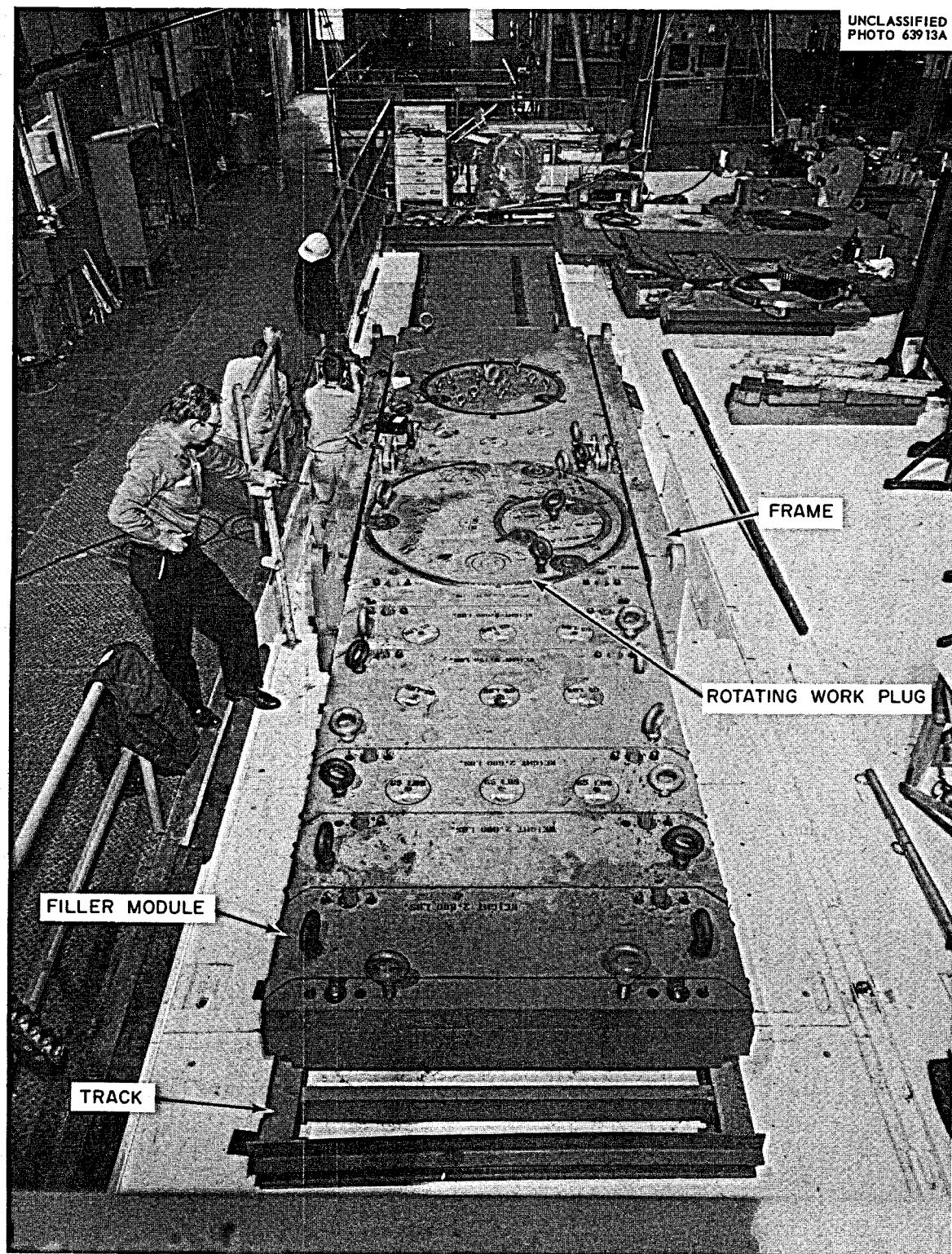


Fig. 1. MSRE Maintenance Shield.

For convenience, a total of 17 holes are provided at strategic locations. A combination of linear and rotary motions provides coverage over the entire 4-ft opening. Larger pieces of equipment, such as heaters and valves, are passed through the shield by opening the joint between two adjacent slabs of the portable shielding. A hole on the edge of one side of the joint is provided so the handling tool can support the equipment while it is made ready for removal. A motor provides the linear motion of the slide and can be operated from the control room. This permits evacuation of personnel when large openings are made in the shielding. Floodlights and windows are provided as plug-in inserts in the shield slabs and can be moved as required. Special cutouts and track sections have been provided for areas where interferences of the building facilities exist.

#### Long-Handled Tools

Most of the in-cell operations will be done with long-handled tools. Some typical examples are shown in Fig. 2. These tools have been made simple and sturdy, to the extent that whenever a choice exists between two designs, the factors of strength, reliability, and simplicity are

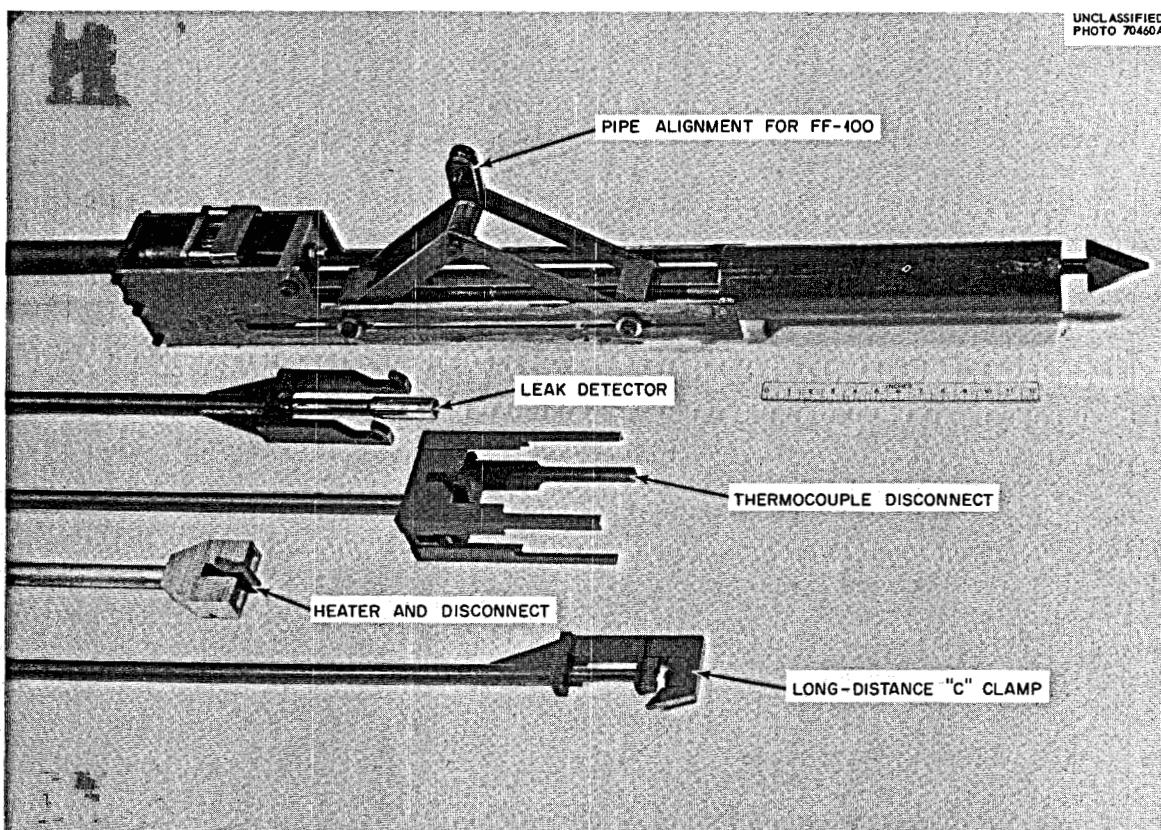


Fig. 2. Lower Ends of Five Miscellaneous Long-Handled Tools.

considered more important than appearance, ease of operation, and versatility. Experience has indicated that simple tools are more reliable than complex ones. Also, when they become contaminated, they are easier to clean, store, and maintain and are less expensive to replace. In general, the tools consist of a pipe mast with rods or cables inside to actuate movable parts at the working end. In some cases, they are merely extensions of simple tools such as socket wrenches, hooks, clamps, or pliers. In some cases, however, the basic character of the tool is masked in order to fulfill special requirements. An example of this is the thermocouple-disconnect tool. This is basically a hook that can be drawn up tight against a stop to give a solid grip on the disconnect handling bail. However, the alignment guides make the tool look somewhat more complex than a simple hook. An example of a more complex tool is the pipe alignment tool. It provides both vertical and horizontal motion for proper positioning of mating flanges. The heart of this device is a scissors jack and a lead screw. There are approximately 40 different long-handled tools.

The in-cell operations can be viewed through the lead glass windows in the portable shield (with or without binoculars) and also through a periscope which is inserted in the same manner as a long-handled tool. The periscope is a commercially available, 1.625-in.-diam instrument with radiation-resistant optics and both right-angle and straight-down objective lenses. It is sheathed in a 2-in.-OD stainless steel tube which protects it from contamination. Lighting is provided by special drop lights and built-in floodlights. In doing the maintenance, one individual observes the working end of the tool down in the cell with the scope and relays instructions to the tool operator. A third man will, perhaps, observe through the windows. Thus, the operation is a team effort and a high degree of skill is not as important as a good knowledge of the tools and the in-cell equipment.

#### Remote Equipment

When large openings are made in the cell (two lower shield blocks or more), high radiation levels make the high bay area uninhabitable for personnel. This situation will occur when handling blocks in preparation for semidirect maintenance, when the portable shield is spread apart to pass a large piece of equipment, or when handling large components such as the fuel pump bowl, heat exchanger, drain line, etc. During these times the reactor building is evacuated and the maintenance crew go into the shielded control room. The key piece of equipment that will be operated from there is the 30-ton crane. The equipment in the control room consists of the following:

1. two shield windows filled with zinc bromide, located to permit direct viewing of the high bay, the reactor, and the drain cells,
2. controls and monitors for three closed-circuit television cameras,
3. control boxes for operating both the 10- and 30-ton bridge cranes, including a switch to rotate the 30-ton crane hook,

4. a weigh cell readout indicating (in pounds) the load on the 30-ton crane,
5. switches to operate the slide of the portable shield.

Located outside the control room (in the high bay area) are a number of accessories to be used with the crane. They are all set up or supported so as to be available for pickup by the crane hook. These include:

1. a shield-block support beam pickup device,
2. two shield-block pickup tongs (one of which is shown in Fig. 3) equipped with cam devices which alternately open and close the tongs,
3. two portable camera stands with large handling bails, camera platforms, height adjustments, and heavy base plates for stability,
4. an assortment of lift fixtures to engage the crane hooks with the component to be handled.

UNCLASSIFIED  
ORNL-LR-DWG 61193

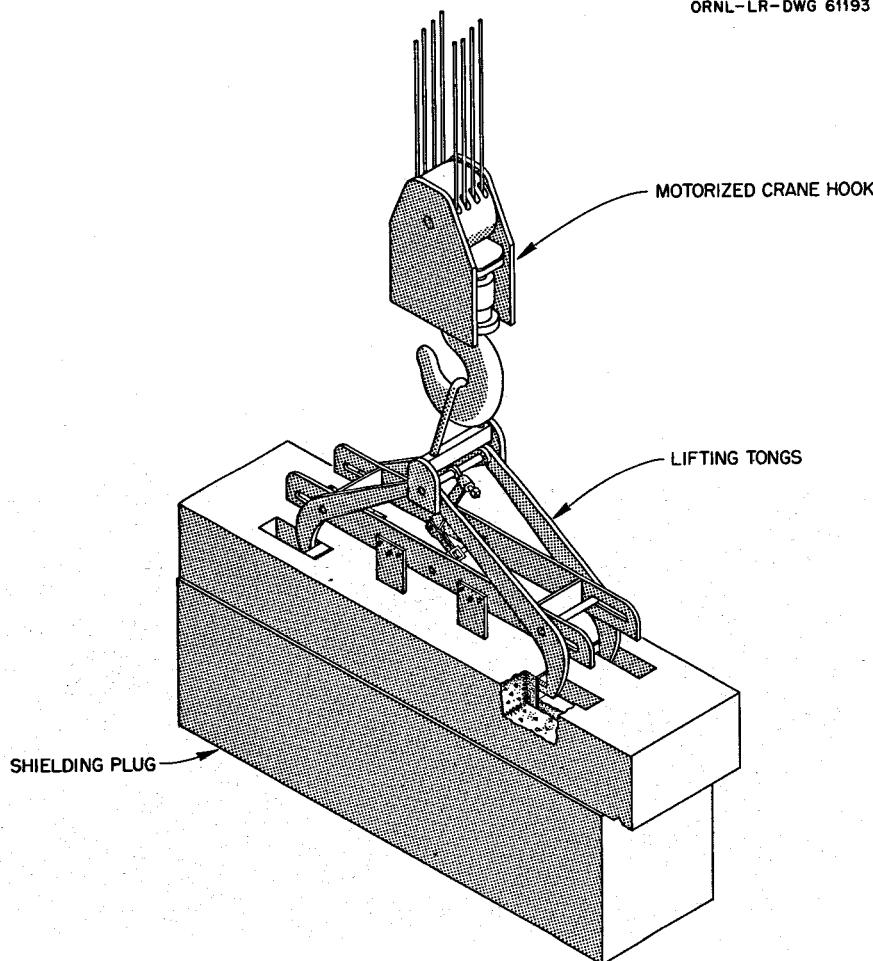


Fig. 3. Remotely Operated Lifting Tongs for Shielding Plugs.

At the present time, control room operations are limited to what can be done with the crane and its accessories. The complexity of the task arises in the differences between operating a crane remotely from the control room and operating it directly with a rigger crew. These differences are basically those of viewing, feel, and method of engaging the hook. Whereas a rigger crew will casually use slings, bars, shackles, etc., we have had to preplan all operations in order to have a suitable handling bail or socket available for the crane. The restricted viewing and feel of the operator inside the control room are augmented by binoculars, television, and the weigh cell. The crane controls feature extremely slow speeds. Further, specialized practice, familiarity with the equipment, and the elimination of speed and haste combine to make our capability approach that of ordinary crane usage.

#### The Development Effort

Starting from the idea of unit replacement and ending with a system capable of maintaining the MSRE required going through a series of activities which included design, development, testing, and the recording of information. Development programs were started as soon as problem areas were identified. The end products of these programs were actual working tools, operating procedures, and proven equipment.

#### Remote Operation of the 5-in. Freeze Flange

One major objective was to establish the technique of making and breaking the five special flanges which connect the primary loop components. By use of a full-scale mockup, where the sight, space, and distance restrictions were similar to those of the reactor, tools and techniques were worked out and refined. The overall procedure was separated as follows:

1. driving the flange clamps onto and off of the flanges with a design load of 40 tons (Fig. 4 shows the tools in place in the mockup),
2. storing the heavy clamp assembly on an in-cell bracket,
3. replacing a ring gasket without damaging its sealing surface,
4. covering the open piping to reduce the spread of contamination,
5. making up the flanges with sufficient force and precision to assure a good seal.

Six different tools are used to accomplish this manipulation, which can be considered to be a small extrapolation of existing long-handled tool experience.

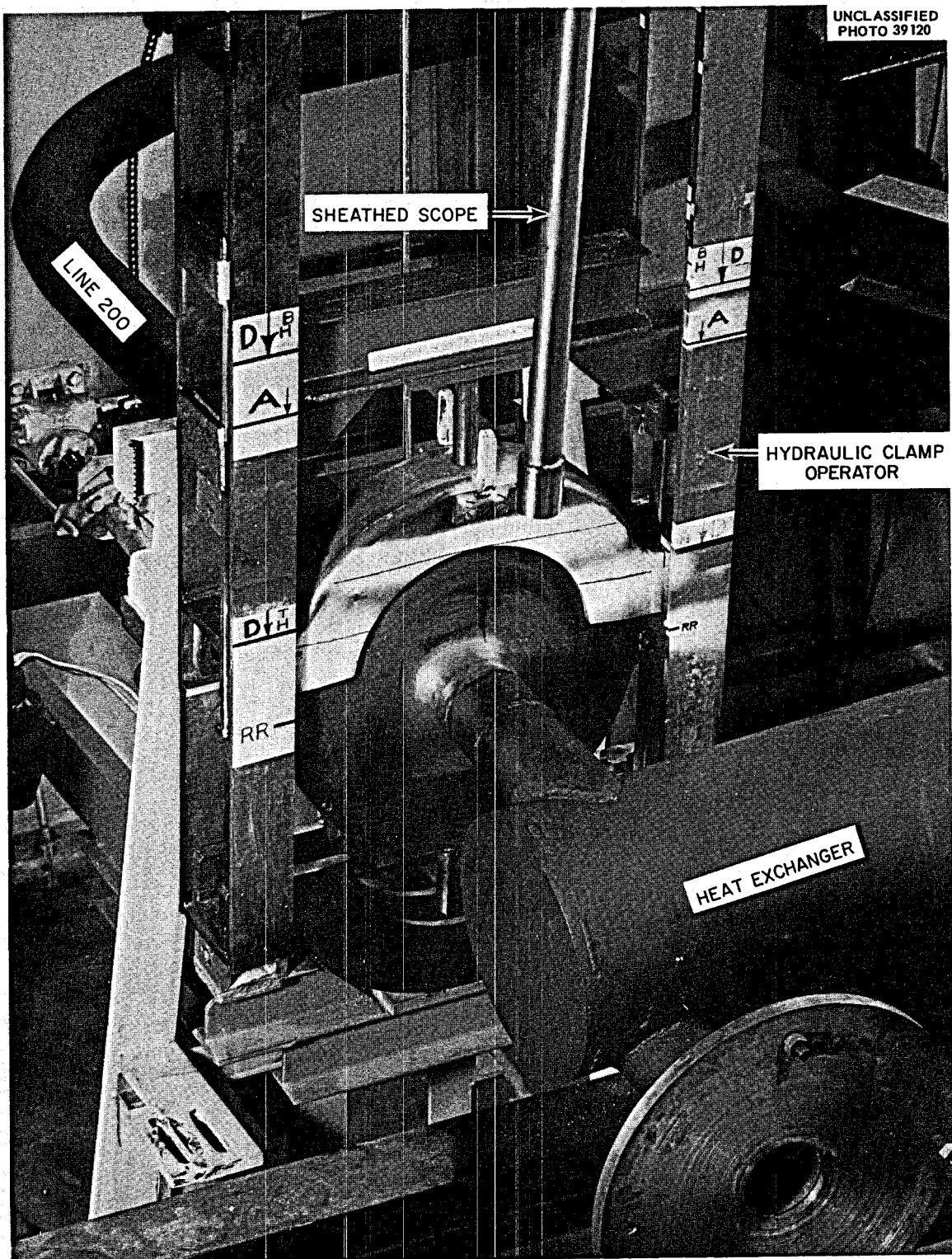


Fig. 4. Remote Assembly of Freeze-Flange Clamps.

Remote Cutting and Brazing

Besides the 5-in. piping of the primary system, the only other fuel-carrying lines that we must be able to be disconnect are the 1-1/2-in. pipes which interconnect the drain tanks, flush tank, and reactor vessel. A method of remotely cutting these lines and brazing them back together again has been developed for replacement of these components. The procedure is to lower a positioning vise into the cell onto a built-in platform. A pipe cutter, mounted on the vise, severs the pipe so that the failed component may be removed. Next, a pipe-tapering device, bolted to the platform and facing the pipe in the vise, machines the outside of the pipe, producing the male member of the joint. The furnace assembly, complete with induction heating coils, inert-gas purge, water cooling, thermocouples, and insulation, is slipped over the male joint. The replacement component, with the female portion of the joint and the end closure of the furnace, is lowered into place. A stationary vise then clamps onto the new piece. Figure 5 shows this part of the procedure. The furnace is closed, operated, and, when the melting temperature of the braze metal is reached, the positioning vise forces the joint together for optimum configuration while the metallurgical bonding takes place. After pressure testing, the furnace and the machinery are taken out of the cell, and the heaters and insulation are reinstalled. Long-handled

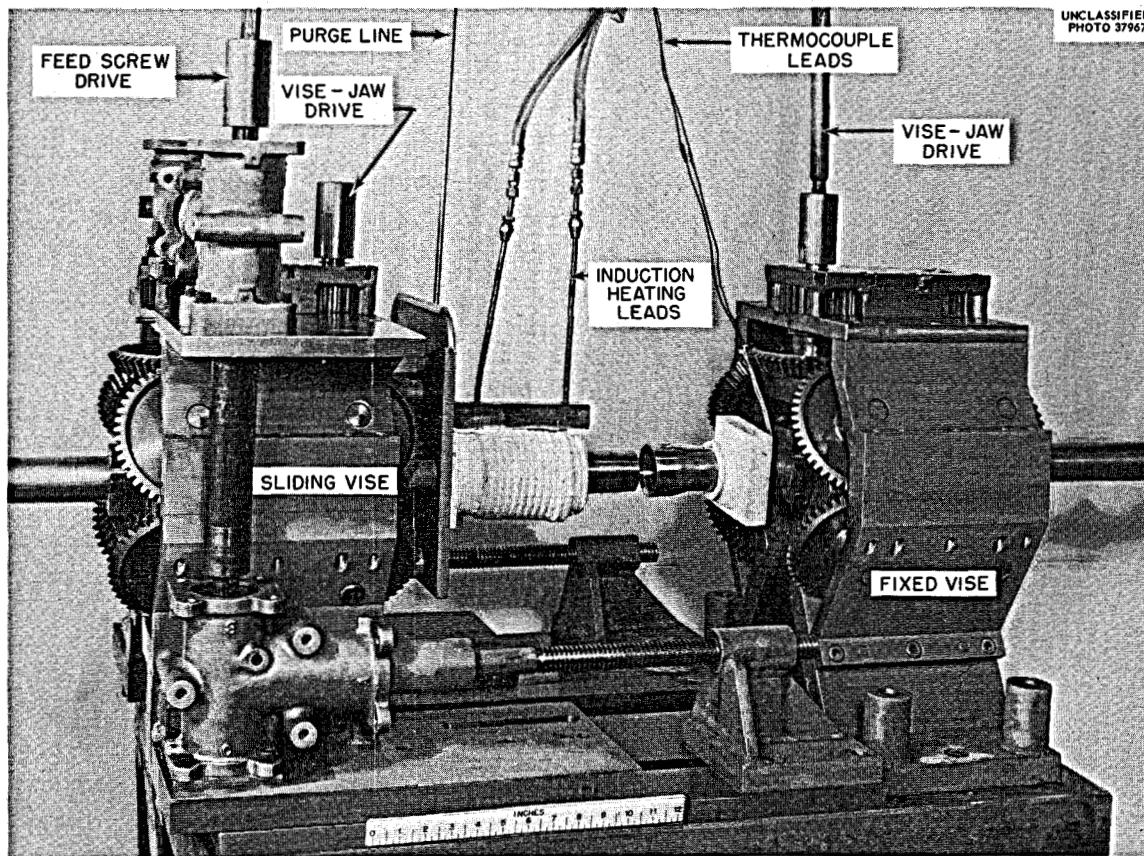


Fig. 5. Joint and Furnace Ready for Assembly.

tools, operated through the portable shield, are used to handle the machinery described. The process and equipment are described more completely in applicable sections of the MSRE design report and in the open literature.<sup>3</sup> Many joints have been produced this way under simulated reactor conditions, and all have successfully passed both destructive and nondestructive tests of their integrity. This process is a step toward the ultimate goal of highly reliable, easily maintained nuclear systems. Furthermore, it gives the MSRE the bonus of starting with an all-welded drain system.

#### Miscellaneous Development

Besides the above-mentioned problem areas, an effort was made to unify the design of all the equipment in the reactor that had to be maintained and to standardize it wherever possible.

The basic procedures for maintenance were evolved as information became available on radiation levels, head room requirements, component layout, and costs. The reactor design itself was continuously monitored to see that it reflected the needs of maintenance. Items whose function was principally maintenance were designed under the management of maintenance engineers. These items included the reactor access stand pipe, the in-cell jacking and aligning equipment, the portable maintenance shield, the long-handled tools, and the lift fixtures. A program of testing and demonstration was included in the construction schedule, and is now partially complete. The results of work in the drain cell are very encouraging.<sup>4</sup> Finally, procedures are being prepared<sup>5</sup> that will describe the maintenance equipment and how it is to be used at the MSRE.

#### Present Status

The status of the maintenance effort is summarized below. The work remaining is noted in parentheses, and the percentages are approximate. We estimate that four months of effort remain for one engineer and one technician.

| Activity   | Percent Complete |
|--|------------------|
| Developmental testing (set up mockup of graphite sample handling)  | 98               |
| Writing procedures   | 50               |
| Monitoring reactor design and construction (reactor cell assembly)                                       | 85               |
| Design of long-handled tools   | 92               |
| Fabrication and testing of long-handled tools  | 85               |
| Testing and demonstration at the reactor (reactor cell components, freeze flanges, and graphite sampler) | 30               |

Conclusions

From the beginning, the management of the MSRE considered the attainment of the maintenance objective important enough and difficult enough to warrant the investment of considerable time and effort. As a result of this preparation, we look forward to power operation with confidence in our capability. This is based on the following points.

1. every effort was made during the design and detailing stages to reflect the needs of maintenance;
2. we are using simple, straightforward methods that have been demonstrated before;
3. by the time the reactor goes to power, we will have tested working tools on actual reactor components;
4. tests at the site have shown that the tools work well and that we can improvise solutions in unanticipated situations.

We believe, therefore, that the MSRE can be maintained efficiently and safely with the equipment described.

References

1. W. B. McDonald and C. K. McGlothlan, Trans. Am. Nucl. Soc. 3(1), 191 (June 1960).
2. P. P. Holz, Dry Maintenance Facility for the HRT, ORNL-CF-60-10-85 (October 1960).
3. E. C. Hise, F. W. Cooke, and R. G. Donnelly, Remote Fabrication of Brazed Structural Joints in Radioactive Piping, ASME-63-WA-53.
4. R. Blumberg, internal memorandum, July 27, 1964.
5. R. Blumberg, Remote Maintenance Procedure, MSR-64-13 (Mar. 23, 1964) (internal use only).

FUEL PROCESSING FACILITY

R. B. Lindauer

A fuel processing facility for the MSRE is under construction, with completion scheduled for February 1965. The facility will be located in Building 7503 in a cell adjacent to the drain tank cell and will be operated from a separate panelboard in the high-bay area above the cell.

The facility has two functions. The first is to remove any oxide accumulation in the molten salt by sparging the salt with a mixture of hydrogen and hydrogen fluoride. The second is to recover uranium from the molten salt by sparging with fluorine and volatilizing the uranium as uranium hexafluoride. This second function should not be required until the program using the 30%-enriched fuel ends. At that time, both the flush and fuel salts will be fluorinated to remove the uranium of low enrichment. For the next phase of the program, 93%-enriched uranium will be added to the fuel salt.

The facility will handle 75-ft<sup>3</sup> batches of salt, which is about the volume of blanket salt which would be processed daily in a 1000-Mw (electrical) thermal breeder station on an 80-day cycle. The cost of the facility will be about \$350,000. This appears to be considerably less than comparable costs for large-scale, on-site processing plants which do not take advantage of the sharing of facilities with the reactor.

Flowsheet Description: H<sub>2</sub>-HF Treatment

Salt will be treated with H<sub>2</sub>-HF whenever it is suspected that oxide contamination has occurred. The flush salt will be treated after the initial flushing and shakedown operations and after flushing if the system has been opened for maintenance. Fuel salt could become contaminated through a leak in the system or by difficulties with the helium blanket system. Since operation of the reactor at power with a precipitate of zirconium oxide is not planned, processing will be required before the oxide solubility limit is exceeded. For fuel salt, this limit is about 80 ppm of oxide. During shakedown operations, however, the solubility limit of 210 ppm of BeO in flush salt may be exceeded.

A simplified flowsheet of the facility is shown in Fig. 1. The fuel processing facility is separated from the drain tanks by freeze valves. The fuel or flush salt is pressured by dry helium gas from the drain or the flush-salt tank to the fuel storage tank, where processing takes place. If the salt is fully irradiated fuel salt, a decay time of four days is required before transfer to allow for xenon decay, since the fuel processing facility is not vented through the large charcoal beds. If transfer of a fully irradiated fuel batch is desirable before 26 days' decay, it will be necessary to cool the batch in the fuel storage tank. This can be done by circulating the cell ventilation air through a space around the tank.

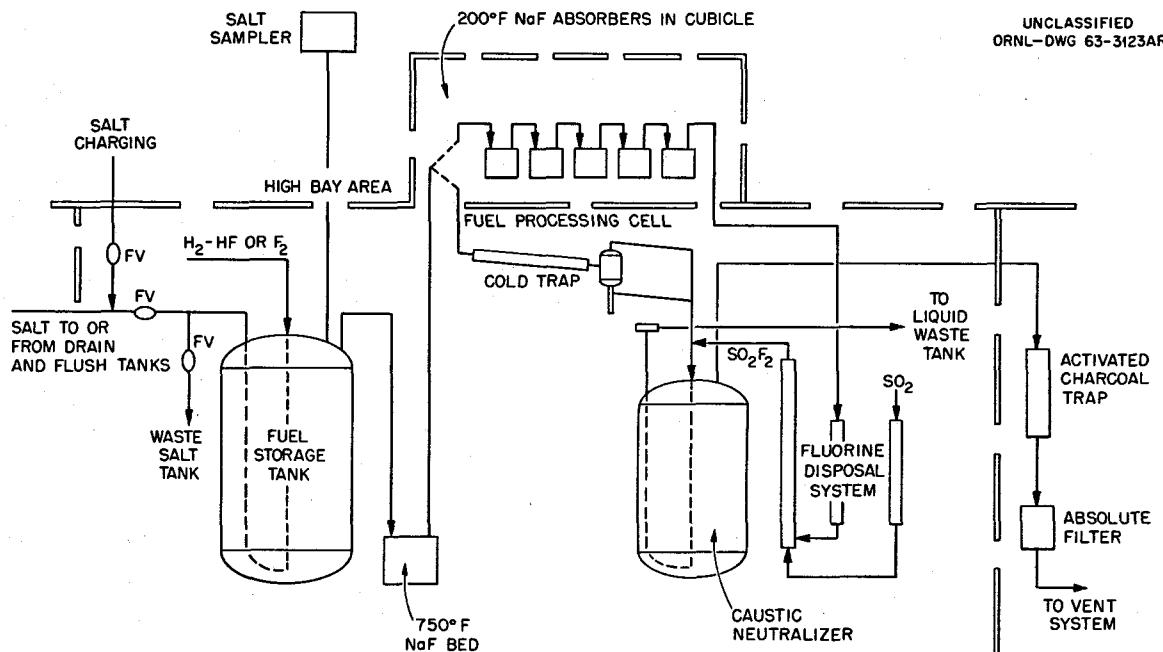


Fig. 1. MSRE Fuel Processing System.

The salt will be sparged with a gas mixture of probably 10 volumes of hydrogen to 1 volume of hydrogen fluoride at a total gas flow rate of 100 liters/min. The hydrogen is required in order to maintain a reducing condition in the melt and thereby minimize corrosion. The off-gas stream, consisting of hydrogen, helium, water, and excess hydrogen fluoride, passes through heated lines to a heated bed of sodium fluoride pellets. This bed will decontaminate the off-gas stream of volatilized corrosion and fission products. The gas stream then passes through the absorber cubicle, which is in the high-bay area above the cell. In this cubicle, the gas stream can either be sent through the absorber train for uranium recovery (as will be discussed later), or it can be sent directly back to the cell. For the hydrogen-hydrogen fluoride treatment, the gas stream next passes through a cold trap where water and part of the hydrogen fluoride are condensed. The oxide-removal rate is followed by observing the automatic siphoning of the small pot below the baffled vapor separator. The siphoned liquid, as well as the off-gas stream, is then bubbled through a 10% KOH solution to neutralize the unreacted HF. Off-gas from the caustic scrubber is passed through two successive activated-charcoal canisters, where any volatilized iodine will be removed, and then through a flame arrester before entering the cell ventilation duct. Air flow in this duct will be kept well above the 100 cfm required to keep the hydrogen content below the explosive limit of 4%. The caustic solution must be replaced after about two days of processing. The caustic solution is jetted to the liquid waste tank, from which it is pumped to the Melton Valley intermediate-level waste tanks.

Flowsheet Description: Fluorination

Since some fission product volatilization is expected during fluorination, the fuel salt should be allowed to decay for as long as the reactor operating schedule will allow. Fission product volatilization is minimized also by operating at as low a temperature as possible, about 50 to 100°F above the melting point or around 900°F. The most important fission products that form volatile fluorides are iodine, tellurium, niobium, ruthenium, and antimony. Experience has shown that most of the volatilized fission products are reduced to the metallic state and plate out on the equipment surfaces.

The molten salt is sparged with fluorine at a flow rate of 100 liters/min. About 2 hr is required for the conversion to UF<sub>5</sub> of all the UF<sub>4</sub> in a salt "C" (0.9 mole % UF<sub>4</sub>) fuel batch. At this time, evolution of UF<sub>6</sub> will begin, and the fluorine disposal system will be put in operation, although experience has shown that fluorine breakthrough will probably not occur until 1 mole of fluorine per mole of uranium has been added (about 4 hr at 100 liters/min). The fluorine disposal system reacts SO<sub>2</sub>, preheated to 400°F, with preheated fluorine in a preheated reactor to form inert SO<sub>2</sub>F<sub>2</sub>. When fluorine breakthrough occurs, as evidenced by an increase in the load on the preheater, the fluorine stream can be diluted with 50% helium, since utilization will be quite low by this time. Corrosion is expected to be high. In the Volatility Pilot Plant fluorinator, corrosion averaged about 1/2 mil/hr in a nickel vessel. Corrosion tests at Battelle Memorial Institute indicate the corrosion of INOR-8 to be somewhat less.

The off-gas from the fuel storage tank passes through the heated NaF bed, where considerable decontamination occurs both of volatilized fission and corrosion products. The UF<sub>6</sub> is then absorbed by low-temperature sodium fluoride in a series of absorbers in the cubicle in the high-bay area. With salt "C" it will be necessary to stop the fluorination twice to replace the absorbers. The loading of the absorbers is followed by observing the temperature of the bed. The bed is cooled by air flow around the absorbers, and the temperature should be kept below 300°F. At this temperature the UF<sub>6</sub> has a vapor pressure of 0.1 mm over the UF<sub>6</sub>·2NaF complex, and the uranium loss would be 190 g, or slightly less than 0.1%. The loaded absorbers will be sent to the Volatility Pilot Plant for desorption and cold trapping of the UF<sub>6</sub>. The radiation level at the surface of the unshielded absorbers should be less than 100 mr/hr and should pose no handling problem.

The SO<sub>2</sub>F<sub>2</sub> from the fluorine disposal system passes through the caustic scrubber. The excess SO<sub>2</sub> and the SO<sub>2</sub>F<sub>2</sub> will be partially neutralized by the caustic, and some fission product removal will be achieved. As mentioned before, the off-gas then passes through the charcoal trap before passing through the absolute filter, the containment filters, and the stack.

The heated line with a freeze valve is provided from the processing tank to outside the cell for removal of waste salt. This may not be

needed until operation of the MSRE has been terminated. At the present time the exact method of removal has not been determined; the waste salt will either be transported in cans and buried, or will be stored in an underground tank at the reactor site.

#### Equipment Description

In general, the fuel processing system is designed for direct maintenance. If maintenance is required after irradiated fuel salt has been processed, aqueous decontamination will be required. Exceptions to this are: (1) the sodium fluoride trap has been designed for remote replacement since plugging of this unit during fluorination is possible; (2) the two air-operated valves in the cell can be remotely replaced; and (3) all heaters on lines and equipment in the cell have duplicate spares installed. The roof plugs have been designed to permit use of the remote maintenance shield designed for the reactor, and the trap and valves are located under these removable roof plugs.

The fuel storage tank is an INOR-8 vessel 50 in. in diameter and 116 in. high. The height of the tank has been increased 30 in. over the height of the drain and flush tanks to minimize salt carry-over due to sparging. The tank is heated by four sets of tubular heaters which can be controlled independently. A 1-in. air space is provided around the tank through which the cell ventilation air can be diverted if necessary for cooling of an irradiated fuel salt batch. Salt inventory in the tank is determined by weigh cells similar to those in the drain tanks.

The sodium fluoride trap is a 20-in.-diam Inconel vessel, 14 in. high, designed to operate at 750°F. Tubular heaters are provided both on the outside and in a 4-in.-diam center pipe. The gas enters at the outside of a cylindrical baffle and flows down through the bed and up the inside of the baffle. The bed is loaded with 70 kg of 1/8-in. right-circular cylinders of NaF. This vessel is installed with ring-joint flanges which can be disconnected remotely, and it has remote disconnects for the electrical leads and thermocouples.

The sodium fluoride absorbers are constructed of carbon steel which is sufficiently resistant to fluorine at the temperatures involved and for the short duration of operation. These absorbers will be discarded after one use. The absorbers have a 14-in. OD with an internal cylindrical baffle similar to the NaF trap. They can be loaded to a bed depth of 6 to 10 in. Each absorber is mounted in an open-top container with an air distributor pipe at the bottom. The cooling air can flow up the outside of the absorbers and through a 2-in. center pipe. A thermowell is provided near the gas inlet for detecting UF<sub>6</sub> breakthrough from the preceding absorber and for regulating cooling air.

The caustic scrubber is a 42-in.-diam, 7-ft-high Inconel tank with a gas distributor. The tank has cooling-water coils on the outside to dissipate the heat from HF neutralization. A steam jet transfers the solution to the liquid waste tank.

The fluorine disposal system uses similar electrical preheaters for the SO<sub>2</sub> and the fluorine streams. The SO<sub>2</sub> heater is stainless steel; the fluorine heater is Monel. The heated streams are combined in the fluorine reactor, which is a 5-in. by 8-ft Monel pipe with a steam coil around the inlet half. Some heat is required to initiate the reaction, but once started, the reaction is exothermic, and the steam then functions as a coolant to keep the temperature around 400°F.

The salt sampler will be used mainly to determine if salt is satisfactory for return to the reactor after processing. After H<sub>2</sub>-HF treatment, the iron and HF content must be low. After fluorination, the sample should verify that all the uranium has been removed. The sampler is similar to the sampler-enricher for the reactor and is described in the chapter on "Component Development." It is actually the original mockup of the sampler-enricher with slight modifications and can be used for the chemical plant because the containment and pressure requirements are considerably less severe.

---

#### PLANS FOR OPERATION OF THE MSRE

P. N. Haubenreich

#### Introduction

#### Objectives

The purpose of the Molten-Salt Reactor Experiment, stated broadly, is to demonstrate that many of the desirable features of molten-salt reactors can presently be embodied in a practical reactor which can be operated safely and reliably and can be serviced without undue difficulty. The program which has been laid out for the MSRE is intended to provide that demonstration in a safe, efficient, and conclusive manner.

Although the complete success of the MSRE depends in part on the reactor being able to operate for long periods at full power, the test program recognizes that the success of a reactor experiment is not measured solely in megawatt-days. The tests and the experiments are designed to be penetrating and thorough, so that, when the experiment is concluded, not only will reliable operation and reasonable maintenance have been demonstrated, but there will be as many conclusive answers as possible to the important questions pertaining to the practicability of molten-salt reactors of this general type.

Areas to be Investigated

Chemistry and Materials. Some of the most important questions to be answered by the MSRE have to do with the behavior and interactions of the fuel salt, the graphite, and the container material in the reactor environment. The major points to be investigated in this area are:

1. fuel stability,
2. penetration of the graphite by the fuel salt,
3. graphite damage,
4. xenon retention and removal,
5. corrosion, and
6. behavior of corrosion products and nonvolatile fission products.

During operation, the principal means of investigation will be regular sampling and chemical analysis of the fuel salt, analysis of the long-term reactivity behavior, and determination of the isotopic composition of the xenon in the off-gas. Periodically, during shutdowns, specimens of graphite and of INOR will be removed from the core for examination.

Engineering. The MSRE incorporates some novel features and components which have been developed and designed specifically for molten-salt reactors. The test program will obtain performance data on these items, permitting evaluation of ideas and principles which could be employed in future reactors.

The broad heading of engineering also covers the extensive startup program which must be devoted to the checkout, calibration, and preliminary testing of the many more or less conventional devices and systems in the MSRE.

Reactor Physics. From the standpoint of reactor physics, the MSRE core is unique, but its nuclear design posed no serious problems. One reason for this apparent paradox is the simplicity of the core, which makes simple spatial approximations valid. Another reason is that the demands for accuracy in the predictions of the design are not severe. This situation arises because the fuel is fluid, permitting easy adjustment of the uranium loading, and eliminating hot spot problems associated with heat transfer from fuel to core coolant. For these reasons, the design did not employ extremely sophisticated calculational procedures, and there were no preliminary critical experiments. Instead, the physics part of the reactor test program is relied on to provide such accurate information on nuclear characteristics as may be required.

The program of reactor physics measurements begins with the experimental loading of uranium to attain criticality. Following this, experiments will be conducted to determine whether the system is stable and

safe. Accurate measurements of rod worth and of reactivity coefficients will be made to facilitate later analysis of the reactivity behavior during power operation. This analysis will be concerned with, among other things, the transient behavior of  $^{135}\text{Xe}$ . The reactivity behavior will also be scrutinized for anomalies which might indicate changes in conditions within the core.

#### Phases of Program

The testing and experimental operation of the MSRE are subdivided into phases which must follow in a natural sequence. They are:

1. precritical testing,
2. initial critical measurements,
3. low-power measurements, and
4. reactor capability investigations.

The precritical testing phase begins with part of the training of new operators; this consists of their checking the location of equipment and comparing the installed piping against the flowsheets. As systems are completed, leak testing, purging, filling, calibrating, and test operation are started. The precritical testing culminates in shakedown operation of the entire reactor system, with flush salt in the fuel system.

In the initial critical experiments, fuel salt will be loaded and enriched uranium will be added in increments to bring the concentration up to that required for operation. During this phase, the control rods will be calibrated and fuel concentration, temperature, and pressure coefficients of reactivity will be measured. Baseline data on the fuel chemistry and corrosion will also be obtained during this period.

After the critical experiments have been conducted at a few watts of nuclear power, the power will be raised to permit certain tests. These will include tests of the nuclear power servo-control system, tests of the automatic load control system, calibration of power indicators, and surveys of the biological shielding. The nuclear power will be less than 2 Mw during this period.

Capability investigations consist of two parts: the first, a step-wise approach to full power; second, extended operation. During the approach to full power, temperatures, radiation levels, and the nuclear power noise will be observed to determine whether any unforeseen condition exists which would restrict the attainable power level. Extended operation will test the reliability of equipment and long-term corrosion and fission product behavior. Maintenance will be carried out as required, and the reactor will be shut down periodically for removal of samples from the core. Long-range plans include chemical processing of the fuel salt and operation with different fuel salt compositions.

StaffOrganization

When the MSRE begins operation, about 43 persons will be employed at the reactor site. This staff is organized, as shown in Fig. 1, to perform the three primary functions: operations, analysis, and maintenance.

UNCLASSIFIED  
ORNL-DWG 64-9884

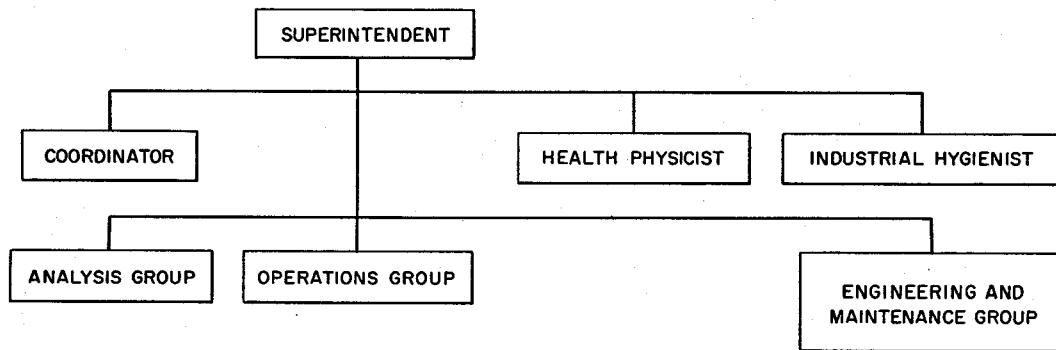


Fig. 1. Organization of MSRE Staff.

Operations. A senior engineer, called the Operations Chief, is in charge of the Operations Group and is responsible for the training, qualification, and performance of the men who actually handle the controls of the reactor. Another engineer assists him in these duties and also serves as relief Shift Supervisor.

There are four crews that operate the reactor on a rotating shift basis. Each crew consists of two engineers and three technicians. One engineer is the Shift Supervisor, who is responsible for all operations in the reactor area while he is on duty. The other Shift Engineer may operate any part of the reactor system or may direct the technicians in operations. A senior technician on each crew is designated Control Room Supervisor. He is the person who ordinarily operates the reactivity and load controls and maintains the control room log. The other two technicians attend to the operation of the auxiliary systems and to the manual collection of data.

Two additional technicians are assigned to the day shift, to take samples and to assist in special operations. They may also serve as relief for shift technicians who are sick or on vacation.

The organization of the Operations Group is shown in Fig. 2. All the personnel shown are members of the MSRE Operations Department of the ORNL Reactor Division.

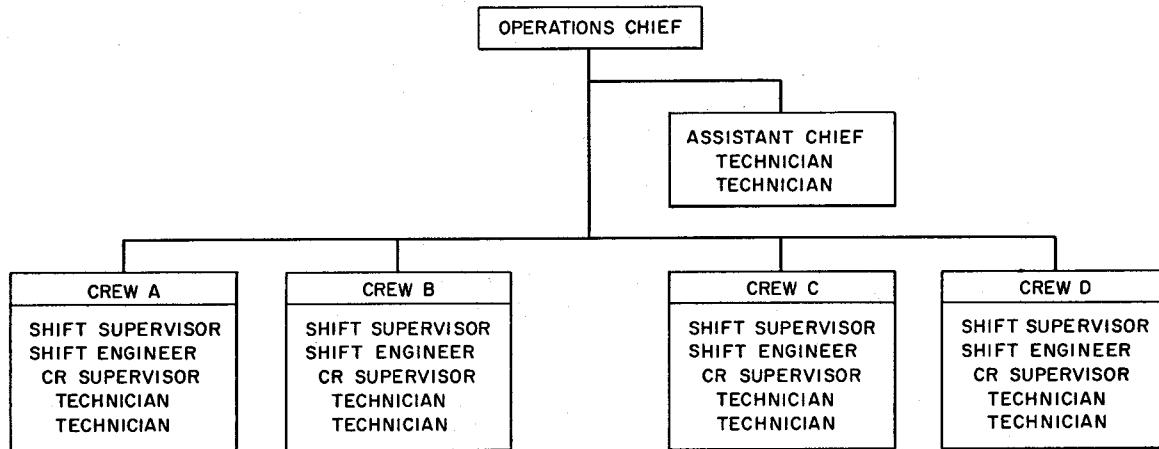


Fig. 2. Organization of Operations Group.

During the first several months of operation, while the reactor equipment and systems are being started and checked, each crew will have craftsmen attached to it to make any adjustments or minor repairs which may be required. A pipefitter, an electrician, and an instrument mechanic may be required on each shift at first.

Analysis. The group which is assigned to the analysis of the MSRE operation is represented in Fig. 3. The personnel assigned to nuclear and mechanical analysis are from the MSRE Operations Department of the Reactor Division. This group will also include loanees from Euratom (not shown). The other personnel are from the Reactor Chemistry, Metals and Ceramics, Chemical Technology, and Instrumentation and Controls Divisions.

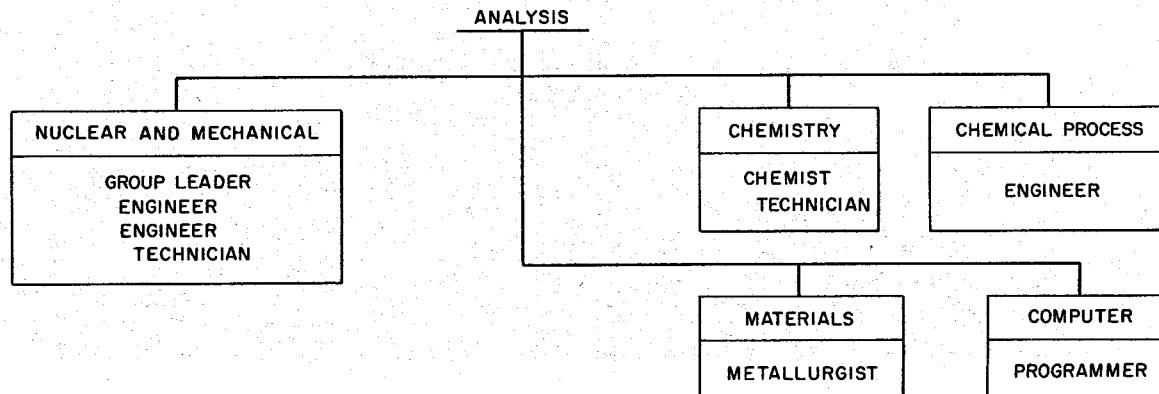


Fig. 3. Organization of Analysis Group.

Analysis personnel plan the experiments required in each field, prepare detailed procedures, and monitor and participate in the execution of the experiments. They then digest and evaluate the information and report the findings. An experienced computer programmer who participated in the initial programming of the on-line computer works with the other analysis personnel in collecting and reducing data.

Maintenance. The maintenance function includes semiremote maintenance of equipment in high radiation fields, normal maintenance of other equipment, design work associated with modifications, and procurement of parts and supplies. The personnel permanently assigned to this function are indicated in Fig. 4. The Instrumentation and Controls engineer and the Plant and Equipment engineer are from those respective ORNL divisions; the others are from the Reactor Division. Pipefitters, electricians, millwrights, riggers, and instrument mechanics will be assigned from the ORNL service organizations as required. The number of such craftsmen at the reactor site will fluctuate, depending on the status of the reactor.

When remote maintenance work is undertaken, specialists in this field will be called in from the Development Department of the Reactor Division.

UNCLASSIFIED  
ORNL-DWG 64-9887

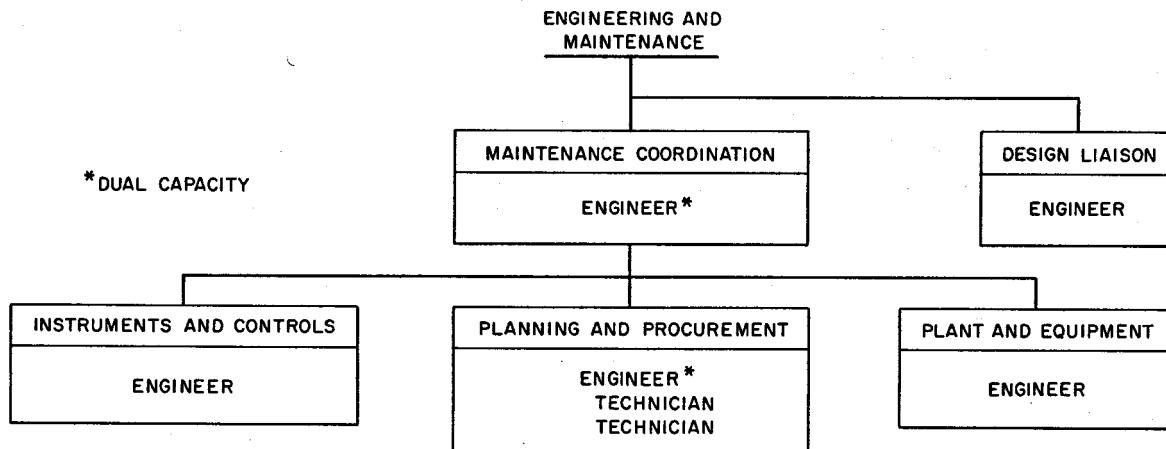


Fig. 4. Organization of Engineering and Maintenance Group.

Other Staff Members. Because the MSRE is an experiment, the operating conditions may be changed - within limits - and new phases may be added to the program, when analysis shows such changes and additions to be desirable. This flexibility requires that the various experiments be combined in an efficient manner and that the operations group be supplied with up-to-date instructions. This is the function of the coordinator (who also spends part of his time as a member of the nuclear and mechanical analysis group).

The operation and maintenance of the MSRE will be carefully monitored to avoid overexposure of personnel to direct radiation, radioactive contamination, or ingestion of beryllium. This will involve area monitoring, area surveys, and personnel monitoring. The Health Physics Division will monitor the radiation exposure and contamination; the Industrial Hygiene Department will monitor for beryllium. Representatives of these groups will work closely with the MSRE staff as indicated on the organization chart, Fig. 1.

#### Qualification and Training

The collective background of the MSRE staff includes many years of experience in reactor development, design, and operation. Six of the senior personnel participated in the operation of the Homogeneous Reactor Experiment No. 2, with duties similar to their present assignments, and six are graduates of ORSORT.

All the senior technical personnel were involved in the design and development of the MSRE for two to four years before joining the Operations Department. Their experience and special knowledge of the MSRE systems were put to use in the preparation of the operating procedures and other parts of the Design and Operations Report, in the writing of test procedures, and in the operator training program.

All the operating group, both engineers and technicians, were given an intensive two-week training program covering the theory, design, and layout of the entire reactor system. On-the-job training then began with detailed checking of the installation against flowsheets and drawings. This job thoroughly familiarized the operators with the physical layout of the MSRE. Visits to the ORR and to the molten-salt Engineering Test Loop were arranged in order to enable the operators to observe and participate in reactor operation and molten-salt sampling and transferring. One important purpose of the flush-salt operation is to give the operators experience in every phase of the operation except the nuclear and heat-removal aspects, which will be simulated insofar as possible.

At the conclusion of the precritical testing, there will be another period of intensive instruction, with special emphasis on nuclear experiments and operation. The operators will then be examined to ensure that they are thoroughly prepared and qualified to operate the MSRE safely and efficiently.

#### Use of Computer

An unusual feature of the MSRE operation will be the use of a high-speed digital computer, installed in the reactor building and directly connected to the reactor by sensing elements.

The Bunker-Ramo model 340 computer which will be installed uses 28-bit words, with 12,288 words in a magnetic core memory and 28,672 words

in a magnetic drum memory. It is designed for computer control applications and completes typical programs at a rate of over 70,000 operations/sec.

In the MSRE application, the computer will not exercise any direct control, and the reactor can be operated with the computer out of service. The functions of the computer include collecting and displaying data and performing on-line calculations for immediate and long-range purposes.

#### Computer Functions

A total of 273 signals from the reactor system are connected to the computer. Of these, 177 are temperatures; the remainder include pressures, flow rates, liquid levels, weights, fluxes, radiation levels, and control rod and radiator door positions. All of these are normally scanned once every 5 sec. Flux signals are repeated in the scan sequence so that the nuclear power is read once every 0.2 sec. A total of about 200 alarm points are entered in the computer, and any signal going beyond these limits produces an audible alarm and a printout on an alarm typewriter in the reactor control room. If any of 24 important variables go out of limits, the scanning is switched to a list of 64 selected variables, which is recorded on a magnetic tape once every 0.25 sec. Every 10 min the entire list of readings is stored on magnetic tape. The purpose of this storage is the retention of data for future analysis. All data on the tape are identified by point and time, so that they can be retrieved for use in tabulations, plots, or calculations.

The status of the reactor system and an up-to-date record of its operating history are typed out routinely by the computer on a preprinted sheet which is changed once a day. Fifty-four signals are typed once an hour, 186 signals are entered at 8-hr intervals, and 21 items, including calculated quantities, are entered on a daily report section of the sheet. Also on the preprinted sheet are the results of routine heat balances, taken at 4-hr intervals, and salt inventories, taken once each 8-hr shift. A reactivity balance, which will be described later, is typed out once an hour.

Most of the scheduled calculations can be initiated at any time by entering a simple demand signal through the computer console. Results of these calculations are typed out on another typewriter.

#### The Reactivity Balance

The reactivity balance is an important part of the analysis of the core behavior. Briefly, it consists of calculating the cumulative changes in reactivity produced by changes in fuel-uranium concentration, concentrations of  $^{135}\text{Xe}$  and other fission products in the core, core temperatures, and control rod positions. At the beginning of operation, when power levels are moderate, it will be assumed that there are no unforeseen mechanisms at work in the core, and the balance will be used to measure the reactivity which must be ascribed to xenon to make the net equal zero.

Analysis of the transient behavior of this apparent xenon effect will be used to help determine values for parameters affecting the xenon retention and removal. These quantities will then be put into a program which predicts xenon poisoning from the power history. After an adequate description of the  $^{135}\text{Xe}$  behavior becomes available, the reactivity balance will be used to detect anomalous developments. The reactivity balance is performed routinely every 5 min and is typed out once an hour. It may also be computed and printed out on demand.

### Schedule

#### Completion Dates

The assembly of the MSRE staff at the reactor site was completed at the first of July. (Most of the engineers had already been there for one to two months, working on the operating procedures and preparing training lectures.) The first two weeks in July were devoted to the initial training program. Following this, the operating crews began detailed checking of the installed piping and equipment, while continuing to receive classroom instruction. Visits to the ORR and the Engineering Test Loop were also made at this time.

The program of testing and calibration will be completed in the fall of 1964, and operation of the entire system (with flush salt) will begin. After the system has been shown to operate satisfactorily, it will be shut down, and final preparations will be made for nuclear operation. Fuel carrier salt will be charged into the reactor, and uranium will be added in the critical experiments. These experiments should begin in early spring, 1965, and full power be attained during the summer of 1965.

#### Uranium Content

The uranium used in the initial operation will contain only about 40%  $^{235}\text{U}$ . This is to be used instead of highly enriched material so that the total uranium concentration will be high enough to provide a large tolerance for  $\text{UF}_3$ . (If fluorine were lost from the fuel,  $\text{UF}_3$  would be formed, and if the  $\text{UF}_3/\text{UF}_4$  ratio got high enough, uranium might precipitate.) Experimental operation with the original fuel composition may last for about a year. If fluorine loss proves to be low, as expected, it is proposed to then strip the uranium from the salt (by fluorination in the storage tank) and add highly enriched uranium. Operation with the lower total uranium concentration would last perhaps another year. A year's operation with fuel of a third composition - one containing thorium - is contemplated. This would provide more experience with salt similar to that which might be used in a breeder reactor. We have not made plans for operation of the reactor beyond this point. Favorable experience and acceptance of molten-salt reactors as promising power breeders would probably lead to modification of parts of the plant and continuance of experiments important to the development of breeder reactors.

CHEMICAL BASIS FOR MOLTEN-SALT REACTORS

W. R. Grimes

Introduction

Nuclear reactors with liquid fuel and blanket systems have, in principle, advantages and disadvantages in comparison with more conventional reactor types. Ease in reactor control, ease of preparation of fuel and blanket, and the possibility of continuous side-stream processing of fuel and blanket are probably the most important advantages. Of the disadvantages, the increase in inventory imposed by the external circuitry and the necessity to achieve and to maintain the integrity of the complex and radioactive plumbing are the most obvious.

Molten-salt mixtures are versatile; they can serve as fuels, blankets, and coolants. With them a family of reactors, operating at low pressure and at usefully high temperature, can be provided. Whether such reactors can compete in the power market with other types depends upon the extent to which designers can optimize the advantages and minimize the disadvantages of each type. The intrinsic merit of the materials that must be used will, finally, control the extent to which such optimization can be accomplished. For liquid-fueled reactors such control will almost certainly lie in the nuclear properties and the chemical behavior of the materials. The thermodynamic behavior of molten-salt systems for use in nuclear reactors, with special emphasis on those for use in MSRE, is surveyed briefly in the following.

General Requirements for the Fluids<sup>1</sup>

Molten-salt reactors cannot be operated at all unless the minimum - though stringent - demands that the reactor makes upon its fluid fuel can be met. These minimum demands include the following. The fuel must dissolve more than the critical concentration of fissionable material at temperatures safely below the temperature of exit from the heat exchanger. The fuel must consist of elements of low (and preferably very low) capture cross section for neutrons of the energy spectrum typical of the chosen design. The mixture must be thermally stable, and its vapor pressure must be low over the temperature range proposed for operation. The fuel mixture must possess heat transfer and hydrodynamic properties adequate for its service as a heat-exchange fluid. It must be relatively non-aggressive toward some (otherwise suitable) material of construction, presumably a metal, and toward some suitable moderator material. The fuel must be stable toward reactor radiation, must be able to survive fission of the uranium (or other fissionable material), and must tolerate fission product accumulation without serious deterioration of its useful properties.

If molten-salt reactors are to be competitive, we must add to this impressive list the requirement of genuinely low fuel cycle cost; this clearly presupposes a cheap fuel and an effective turnaround and reuse of the unburned fissionable material, or an effective and economical decontamination and reprocessing scheme.

Blankets and coolants face requirements which differ in obvious ways. The radiation intensity in the blanket will be considerably less - in the coolant markedly less - than that in the fuel. Efficiency of the blanket as a heat transfer fluid may be relatively unimportant; but a high concentration of fertile isotope is essential, and an effective recovery of bred material is likely to be vital.

### Choice of Salt Composition

#### General Considerations

The compounds which are desirable constituents of fuels for thermal breeders are those that can be prepared from beryllium, bismuth, boron-11, carbon, deuterium, fluorine, lithium-7, nitrogen-15, oxygen, and the fissionable and fertile isotopes. For an epithermal reactor this list can probably be augmented somewhat, and a thermal reactor intended to burn  $^{235}\text{U}$  and to obtain a modest conversion of  $^{232}\text{Th}$  to  $^{233}\text{U}$  might use (as diluents) the compounds prepared from the elements listed in Table 1.

Of the known compounds containing useful concentrations of hydrogen (or deuterium), only the hydroxides of the alkali metals, the saline hydrides of lithium and calcium, and certain interstitial hydrides (e.g., zirconium hydride) show adequate thermal stability in the 1000 to 1300°F temperature range. [Acid fluorides (e.g.,  $\text{KHF}_2$ ) might be permissible in low concentrations at lower temperatures.] The hydrides are very strong reducing agents and are most unlikely to be useful components of any uraniferous liquid fuel system. Alkali hydroxides dissolve extremely small quantities of uranium compounds at useful reactor temperatures and are very corrosive at such temperatures to virtually all useful metals. Hydrogen-rich compounds, which might provide self-moderation to molten fuels, do not seem capable of use as fuels or coolants.

The nonmetals carbon, nitrogen, silicon, sulfur, phosphorus, and oxygen each form only high melting and generally unsuitable binary compounds with the metals of Table 1. From these nonmetals, however, a wide variety of oxygenated anions are available. Nitrates, nitrites, sulfates, and sulfites can generally be dismissed as lacking adequate thermal stability, and silicates as having undesirably high viscosities. Phosphates, borates, and carbonates are not so easy to dismiss without study, and phosphates have, in fact, received some attention. The several problems of thermal stability, corrosion, solubility of uranium and thorium compounds, and, especially, radiation stability would seem to make their use doubtful.

Table 1. Elements or Isotopes Which May Be  
Tolerable in High-Temperature  
Reactor Fuels

| Material    | Absorption Cross Section<br>(barns) |
|-------------|-------------------------------------|
| Nitrogen-15 | 0.000024                            |
| Oxygen      | 0.0002                              |
| Deuterium   | 0.00057                             |
| Carbon      | 0.0033                              |
| Fluorine    | 0.009                               |
| Beryllium   | 0.010                               |
| Bismuth     | 0.032                               |
| Lithium-7   | 0.033                               |
| Boron-11    | 0.05                                |
| Magnesium   | 0.063                               |
| Silicon     | 0.13                                |
| Lead        | 0.17                                |
| Zirconium   | 0.18                                |
| Phosphorus  | 0.21                                |
| Aluminum    | 0.23                                |
| Hydrogen    | 0.33                                |
| Calcium     | 0.43                                |
| Sulfur      | 0.49                                |
| Sodium      | 0.53                                |
| Chlorine-37 | 0.56                                |
| Tin         | 0.6                                 |
| Cerium      | 0.7                                 |
| Rubidium    | 0.7                                 |
| Zinc        | 1.06                                |
| Niobium     | 1.1                                 |
| Strontium   | 1.16                                |
| Barium      | 1.17                                |
| Yttrium     | 1.27                                |
| Nitrogen    | 1.88                                |
| Potassium   | 1.97                                |

If the oxygenated anions are eliminated, only fluorides and chlorides remain. Chlorides offer mixtures that are, in general, lower melting than fluorides; in addition,  $\text{UCl}_3$  is probably more stable than  $\text{UF}_3$ , with respect to the analogous tetravalent compounds. For thermal reactors, fluorides appear much more suitable for reasons which include (1) usefulness of the element without isotope separation, (2) better neutron economy, (3) higher chemical stability, (4) lower vapor pressure, and (5) higher specific heat per unit weight or volume.

Fluoride mixtures are, accordingly, preferred as fuel, blanket, and coolant mixtures for thermal reactors. The fluoride ion is insufficient to moderate the neutrons in cores of reasonable size; additional moderator is, accordingly, required. The fluoride ion, however, moderates too well to permit its use in genuinely fast reactors. In such reactors chloride mixtures, using  $^{35}\text{Cl}$ , will certainly be preferred.

#### Choice of Active Material

Uranium Fluoride. Uranium hexafluoride is a highly volatile compound clearly unsuited as a component of high-temperature liquids. The compound  $\text{UO}_2\text{F}_2$ , though relatively nonvolatile, is a strong oxidant which should prove very difficult to contain. Fluorides of pentavalent uranium ( $\text{UF}_5$ ,  $\text{U}_2\text{F}_9$ , etc.) are not thermally stable and should prove prohibitively corrosive if they could be stabilized in solution.

Uranium tetrafluoride is a relatively stable, nonvolatile, and non-hygroscopic material, which is readily prepared in high purity. It melts at  $1036^\circ\text{C}$ , but this very high freezing point is markedly depressed by several useful diluent fluorides. Pure, crystalline uranium trifluoride is stable, under inert atmospheres, to temperatures above  $1000^\circ\text{C}$ , but it disproportionates at higher temperatures by the reaction



Uranium trifluoride is appreciably less stable in molten fluoride solutions than in the crystalline state. It is tolerable in reactor fuels only insofar as the equilibrium activity of  $\text{U}^0$  which results is sufficiently low to avoid reaction with the moderator graphite or alloying with the container metal.<sup>2</sup> Appreciable concentrations of  $\text{UF}_3$  (see below) are tolerable in  $\text{LiF-BeF}_2$  mixtures such as those proposed for MSRE. In general, however, uranium tetrafluoride must be the major uraniferous compound in the fuel.

Thorium Fluoride. All the normal compounds of thorium are quadrivalent;  $\text{ThF}_4$  (melting at  $1115^\circ\text{C}$ ) must be used in any thorium-bearing fluoride melt.

#### Choice of Fluoride Diluents

The fuel system for thermal reactors of the types given most attention to date will require low concentrations (0.2 to 2 mole %) of uranium.

The properties (especially the melting temperature) of such fuels will be controlled by the composition of the diluent mixture. Blanket mixtures (and perhaps fuel systems for one-region converters or breeders) will require considerable concentrations of high-melting  $\text{ThF}_4$ . These fluids must, if they are to be compatible with the temperature requirements of large steam turbines and are to retain a reasonable margin of safety between the minimum reactor operating temperature and the freezing point of the fuel, be completely molten at  $975^\circ\text{F}$  ( $525^\circ\text{C}$ ). It is clear that the diluent fluoride system must be low melting and must be capable of large depressions of the freezing points of the active fluorides.

Simple consideration of the nuclear properties leads one to prefer as diluents the fluorides of Be, Bi,  $^7\text{Li}$ , Mg, Pb, Zr, Ca, Na, Sn, and Zn (in that order). Equally simple considerations (Table 2) of the stability of diluent fluorides toward reduction by common structural metals, however, serve to eliminate  $\text{BiF}_3$ ,  $\text{PbF}_2$ ,  $\text{SnF}_2$ , and  $\text{ZnF}_2$  from consideration.

No single fluoride can serve as a useful diluent for the active fluoride. The compound  $\text{BeF}_2$  is the only stable one listed whose melting point is close to the required level; this compound is too viscous for use in the pure state.

The very stable and high melting fluorides of the alkaline earths and of yttrium and cerium do not seem to be useful major constituents of low-melting mixtures. Mixtures containing about 10 mole % of alkaline earth fluoride with  $\text{BeF}_2$  melt below  $500^\circ\text{C}$ , but the viscosity of such melts is almost certainly too high for serious consideration.

Some of the possible combinations of alkali fluorides have suitable freezing points. Equimolar mixtures of  $\text{LiF}$  and  $\text{KF}$  melt at  $490^\circ\text{C}$ , and mixtures with 40 mole %  $\text{LiF}$  and 60 mole %  $\text{RbF}$  melt at  $470^\circ\text{C}$ . The ternary systems  $\text{LiF-NaF-KF}$  (see Fig. 1) and  $\text{LiF-NaF-RbF}$  have lower melting regions than do these binaries. All these systems will dissolve  $\text{UF}_4$  at concentrations up to several mole % at temperatures below  $525^\circ\text{C}$ . They might well prove useful as reactor fuels if no mixtures with more attractive properties were available.

Mixtures with useful melting points over relatively wide ranges of composition are available if  $\text{ZrF}_4$  is a component of the system. Phase relationships in the  $\text{NaF-ZrF}_4$  system (Fig. 2) show low melting points over the interval 40 to 55 mole %  $\text{ZrF}_4$ . A mixture of  $\text{UF}_4$  with  $\text{NaF}$  and  $\text{ZrF}_4$  served as fuel for the Aircraft Reactor Experiment. The phase diagram<sup>3</sup> of this ternary system is shown as Fig. 3.

The compounds  $\text{ZrF}_4$  and  $\text{UF}_4$  have very similar unit cell parameters and are isomorphous. They form a continuous series of solid solutions with a minimum melting point of  $765^\circ\text{C}$  for the solution containing 23 mole %  $\text{UF}_4$ . This minimum is responsible for a broad, shallow trough which penetrates the ternary diagram to about the 45 mole %  $\text{NaF}$  composition. A continuous series of solid solutions without a maximum or a minimum exists between  $\alpha\text{-}3\text{NaF}\cdot\text{UF}_4$  and  $3\text{NaF}\cdot\text{ZrF}_4$ ; in this solution series the temperature drops sharply with decreasing  $\text{ZrF}_4$  concentration. A continuous

Table 2. Properties of Fluorides for Use in  
High-Temperature Reactors

| Compound                              | Free Energy<br>of Formation<br>at 1000°K<br>(kcal/F atom) | Melting<br>Point<br>(°C) | Absorption Cross<br>Section <sup>a</sup> for<br>Thermal Neutrons<br>(barns) |
|---------------------------------------|---|--------------------------|---|
| <b>Structural metal<br/>fluorides</b> |   |                          |   |
| CrF <sub>2</sub>                      | -74   | 1100                     | 3.1   |
| FeF <sub>2</sub>                      | -66.5   | 930                      | 2.5   |
| NiF <sub>2</sub>                      | -58   | 1330                     | 4.6   |
| <b>Diluent fluorides</b>              |   |                          |   |
| CaF <sub>2</sub>                      | -125  | 1330                     | 0.43  |
| LiF                                   | -125  | 870                      | 0.033 <sup>b</sup>  |
| BaF <sub>2</sub>                      | -124  | 1280                     | 1.17  |
| SrF <sub>2</sub>                      | -123  | 1400                     | 1.16  |
| CeF <sub>3</sub>                      | -118  | 1324                     | 0.7   |
| YF <sub>3</sub>                       | -113  | 1144                     | 1.27  |
| MgF <sub>2</sub>                      | -113  | 1270                     | 0.063   |
| RbF                                   | -112  | 790                      | 0.70  |
| NaF                                   | -112  | 1000                     | 0.53  |
| KF                                    | -109  | 880                      | 1.97  |
| BeF <sub>2</sub>                      | -104  | 545                      | 0.010   |
| ZrF <sub>4</sub>                      | -94   | 912                      | 0.180   |
| AlF <sub>3</sub>                      | -90   | 1040                     | 0.23  |
| ZnF <sub>2</sub>                      | -71   | 872                      | 1.06  |
| SnF <sub>2</sub>                      | -62   | 213                      | 0.6   |
| PbF <sub>2</sub>                      | -62   | 850                      | 0.17  |
| BiF <sub>3</sub>                      | -50   | 727                      | 0.032   |
| <b>Active fluorides</b>               |   |                          |   |
| ThF <sub>4</sub>                      | -101  | 1115                     |   |
| UF <sub>4</sub>                       | -95.3   | 1035                     |   |
| UF <sub>3</sub>                       | -100.4  | 1495                     |   |

<sup>a</sup>Of metallic ion.

<sup>b</sup>Cross section for <sup>7</sup>Li.

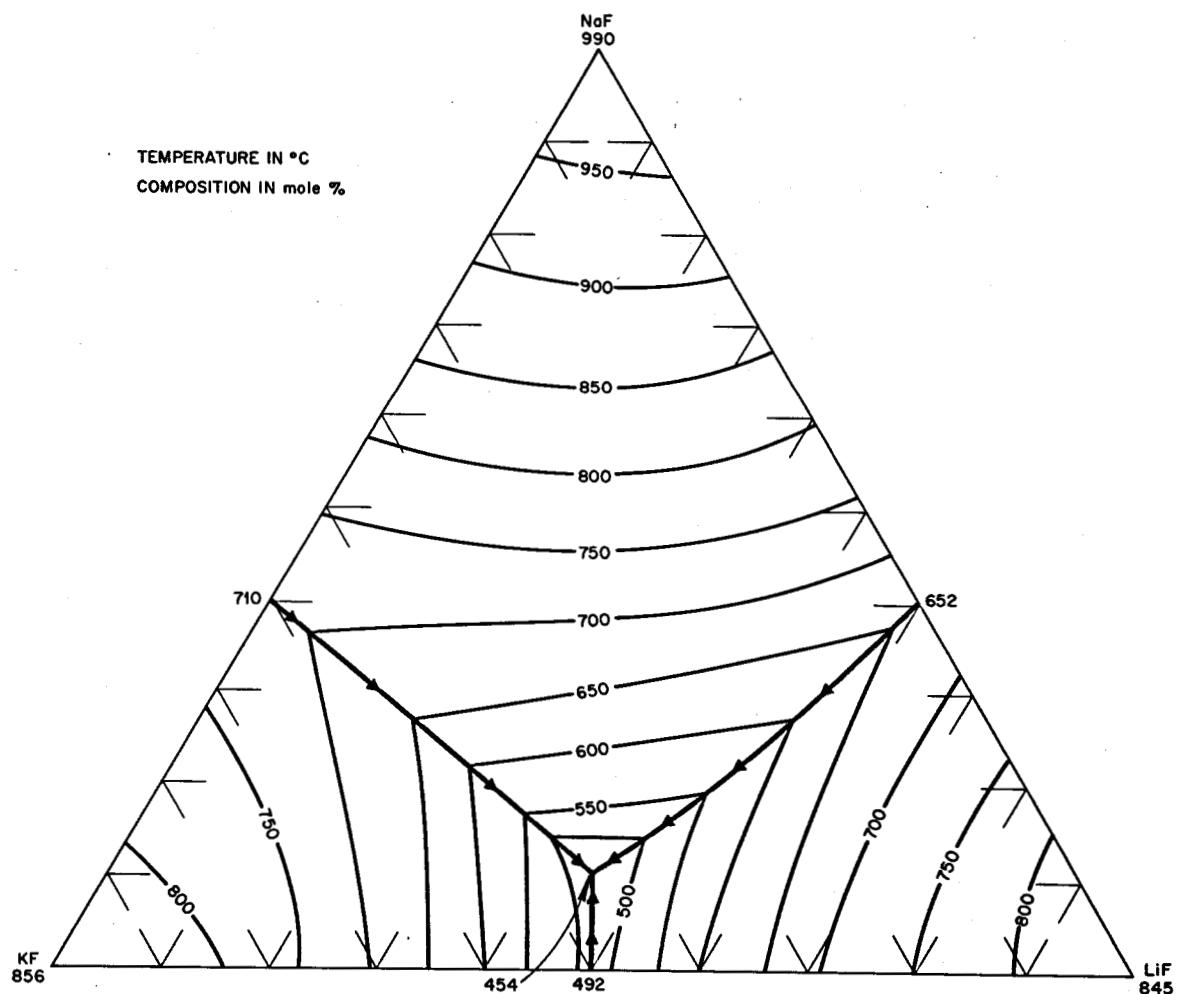
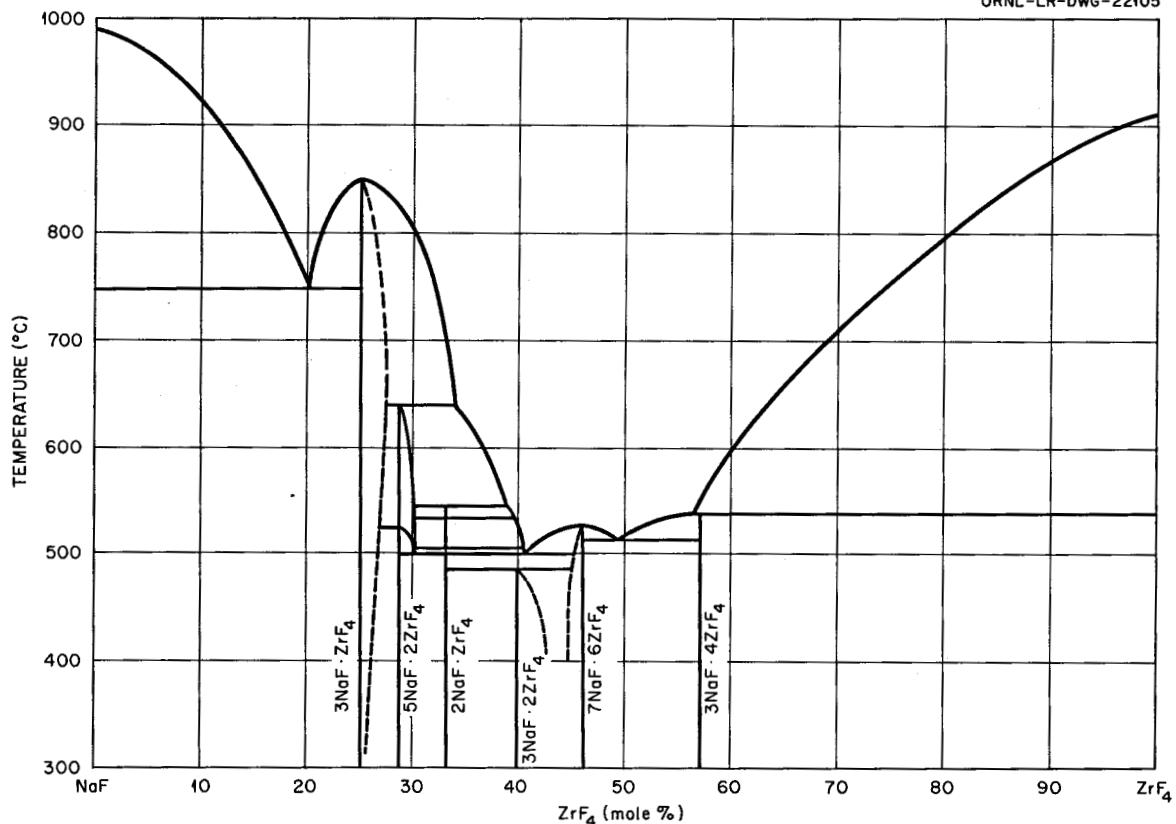
UNCLASSIFIED  
ORNL-LR-DWG 1199A

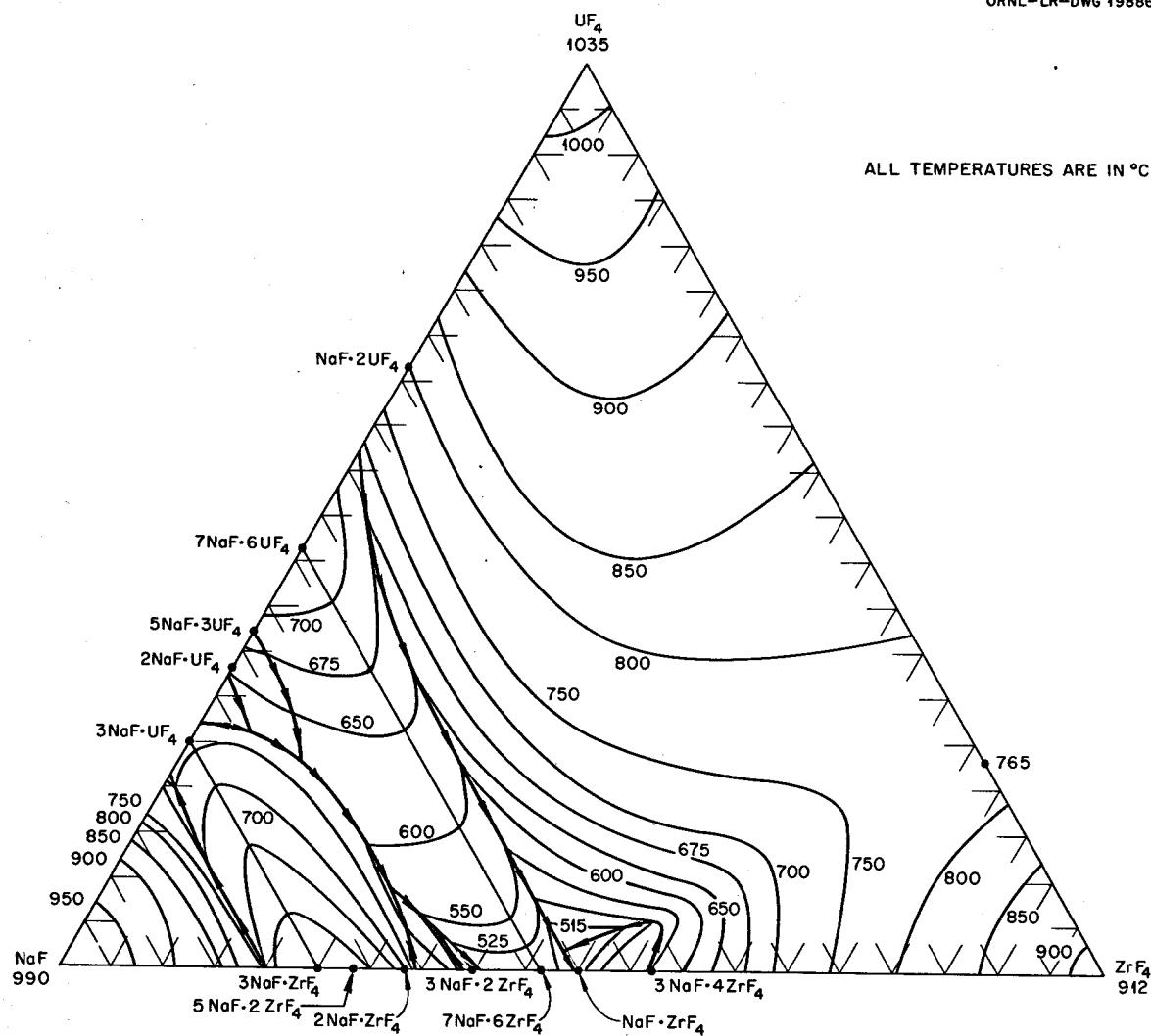
Fig. 1. The System LiF-NaF-KF.

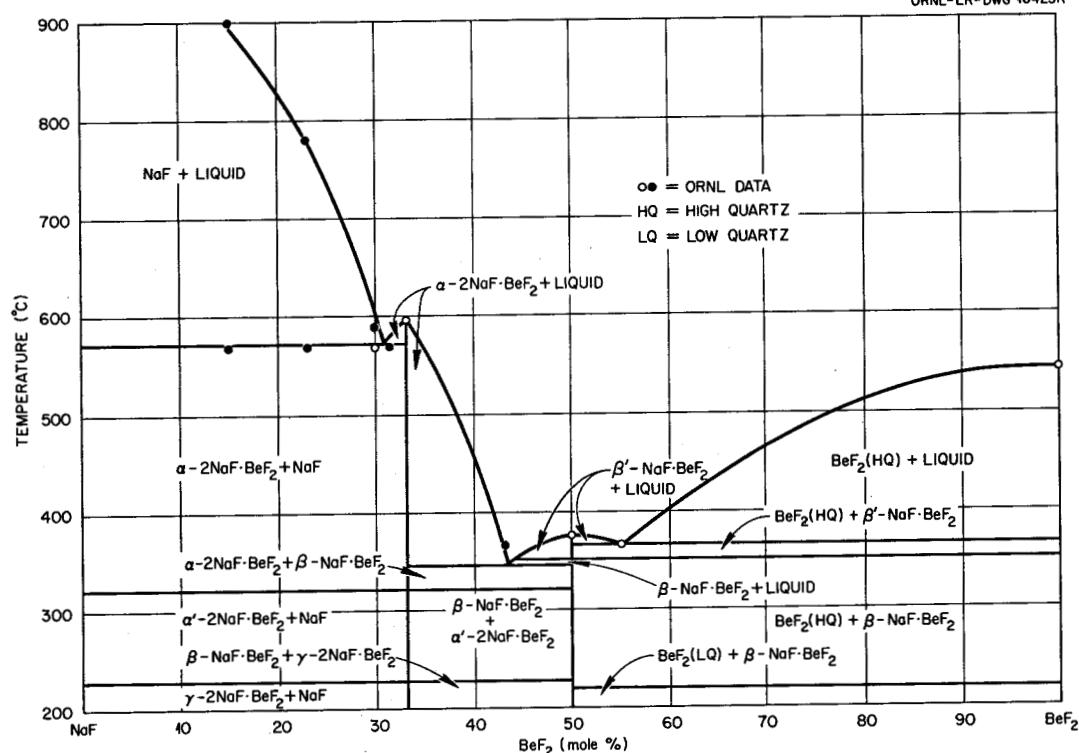
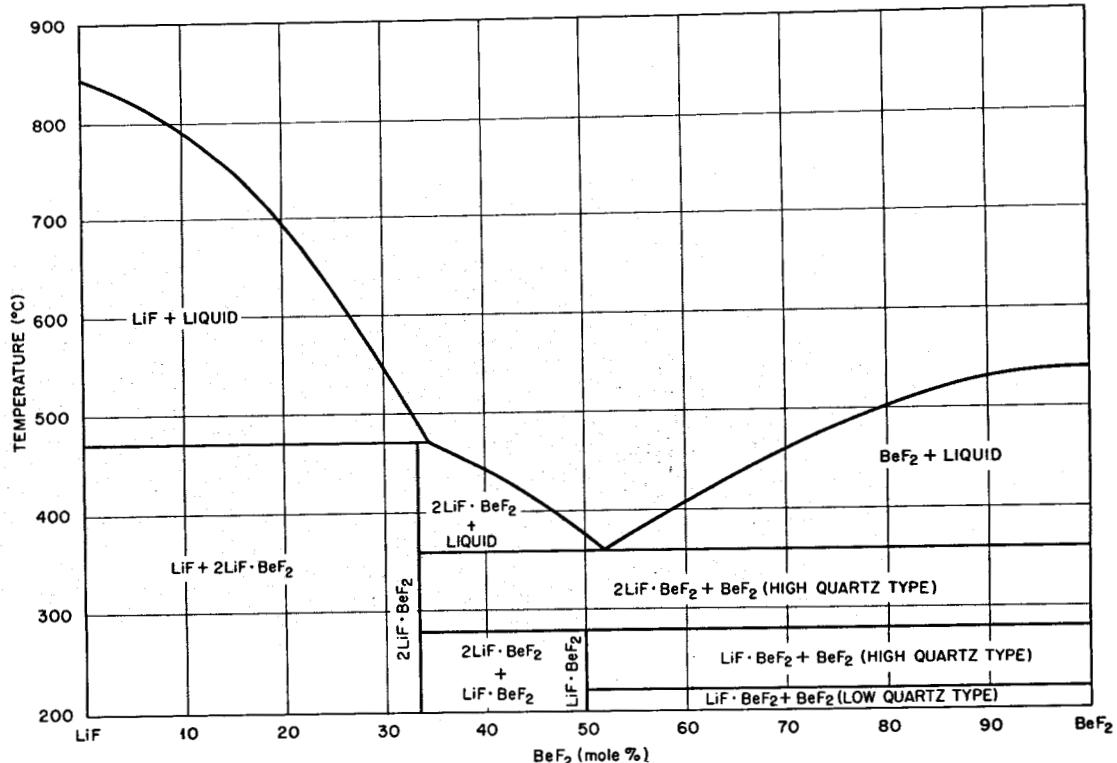
UNCLASSIFIED  
ORNL-LR-DWG-22105Fig. 2. The System NaF-ZrF<sub>4</sub>.

solid-solution series without a maximum or a minimum also exists between the isomorphous congruent compounds  $7\text{NaF}\cdot6\text{UF}_4$  and  $7\text{NaF}\cdot6\text{ZrF}_4$ ; the liquidus decreases with increasing  $\text{ZrF}_4$  content. The liquidus surface over the area below 8 mole %  $\text{UF}_4$  and between 60 and 40 mole % NaF is relatively flat. All fuel compositions within this region have acceptable melting points. Minor advantages in physical and thermal properties accrue from choosing mixtures with minimum  $\text{ZrF}_4$  content in this composition range.

The lowest-melting binary systems of the usable diluent fluorides are those containing  $\text{BeF}_2$  with NaF (Fig. 4) or LiF. (The ternary system LiF-NaF- $\text{BeF}_2$  has been examined in some detail, but it seems to have no important advantage over either binary.) Since beryllium offers the best cross section of the diluents (and  $^7\text{Li}$  ranks very high), fuels based on the LiF- $\text{BeF}_2$  diluent system have been chosen for MSRE.

The binary system LiF- $\text{BeF}_2$  has melting points below 500°C over the concentration range from 33 to 80 mole %  $\text{BeF}_2$ . The presently accepted LiF- $\text{BeF}_2$  system diagram, presented in Fig. 5, is characterized by a single eutectic<sup>4</sup> between  $\text{BeF}_2$  and  $2\text{LiF}\cdot\text{BeF}_2$  that freezes at 356°C and

UNCLASSIFIED  
ORNL-LR-DWG 19886RFig. 3. The System NaF-ZrF<sub>4</sub>-UF<sub>4</sub>.

UNCLASSIFIED  
ORNL-LR-DWG 16425RFig. 4. The System NaF-BeF<sub>2</sub>.UNCLASSIFIED  
ORNL-LR-DWG 16426RFig. 5. The System LiF-BeF<sub>2</sub>.

contains 52 mole %  $\text{BeF}_2$ . The compound  $2\text{LiF}\cdot\text{BeF}_2$  melts incongruently to  $\text{LiF}$  and liquid at  $460^\circ\text{C}$ ;  $\text{LiF}\cdot\text{BeF}_2$  is formed by the reaction of solid  $\text{BeF}_2$  and solid  $2\text{LiF}\cdot\text{BeF}_2$  below  $274^\circ\text{C}$ .

### $\text{LiF-BeF}_2$ Systems with Active Fluorides

The phase diagram of the  $\text{BeF}_2\text{-UF}_4$  system (Fig. 6) shows a single eutectic containing very little  $\text{UF}_4$ . That of the  $\text{LiF-UF}_4$  system (Fig. 7) shows three compounds, none of which melts congruently and one of which shows a low temperature limit of stability. The eutectic mixture of  $4\text{LiF}\cdot\text{UF}_4$  and  $7\text{LiF}\cdot6\text{UF}_4$  occurs at 27 mole %  $\text{UF}_4$  and melts at  $490^\circ\text{C}$ . The ternary system<sup>5</sup>  $\text{LiF-BeF}_2\text{-UF}_4$ , of primary importance in reactor fuels, is shown as Fig. 8. The system shows two eutectics. These are at 1 mole %  $\text{UF}_4$  and 52 mole %  $\text{BeF}_2$  and at 8 mole %  $\text{UF}_4$  and 26 mole %  $\text{BeF}_2$ ; they melt at  $350$  and  $435^\circ\text{C}$  respectively. Moreover, the system shows a very wide range of compositions melting below  $525^\circ\text{C}$ .

The system  $\text{BeF}_2\text{-ThF}_4$  is very similar to the analogous  $\text{UF}_4$  system. The  $\text{LiF-ThF}_4$  system (Fig. 9) contains four compounds. The compound  $3\text{LiF}\cdot\text{ThF}_4$  melts congruently at  $580^\circ\text{C}$  and forms eutectics at  $570^\circ\text{C}$  and 22 mole %  $\text{ThF}_4$  and  $560^\circ\text{C}$  and 29 mole %  $\text{ThF}_4$  with  $\text{LiF}$  and with  $7\text{LiF}\cdot6\text{ThF}_4$  respectively. The compounds  $7\text{LiF}\cdot6\text{ThF}_4$ ,  $\text{LiF}\cdot2\text{ThF}_4$ , and  $\text{LiF}\cdot4\text{ThF}_4$  melt incongruently at  $595$  and  $890^\circ\text{C}$ . The ternary system  $\text{LiF-BeF}_2\text{-ThF}_4$  (see Fig. 10) shows only a single eutectic<sup>6</sup> with the composition 47.0 mole %  $\text{LiF}$  and 1.5 mole %  $\text{ThF}_4$  melting at  $356^\circ\text{C}$ . In spite of small differences due to the phase fields of  $\text{LiF}\cdot2\text{ThF}_4$ ,  $3\text{LiF}\cdot\text{ThF}_4$ , and  $4\text{LiF}\cdot\text{UF}_4$ , the systems represented by Figs. 8 and 10 are very similar.

Moreover,  $\text{ThF}_4$  and  $\text{UF}_4$  form a continuous series of solid solutions with neither maximum nor minimum, and the  $\text{LiF-ThF}_4\text{-UF}_4$  system (see Fig. 11) shows no ternary compounds and a single eutectic which contains 1.5 mole %  $\text{ThF}_4$  with 26.5 mole %  $\text{UF}_4$  and freezes at  $488^\circ\text{C}$ . Most of the area

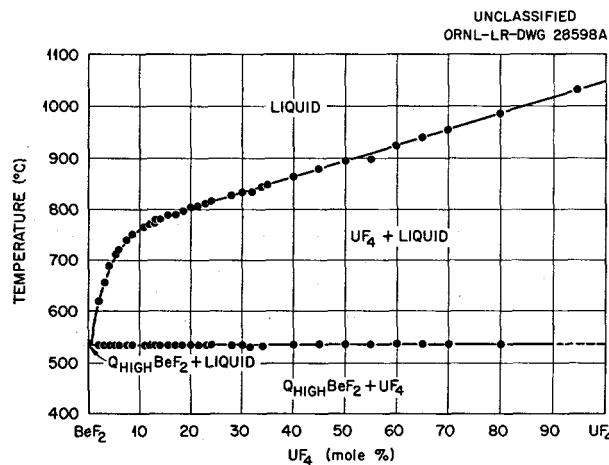


Fig. 6. The System  $\text{BeF}_2\text{-UF}_4$ .

UNCLASSIFIED  
ORNL-LR-DWG 17457

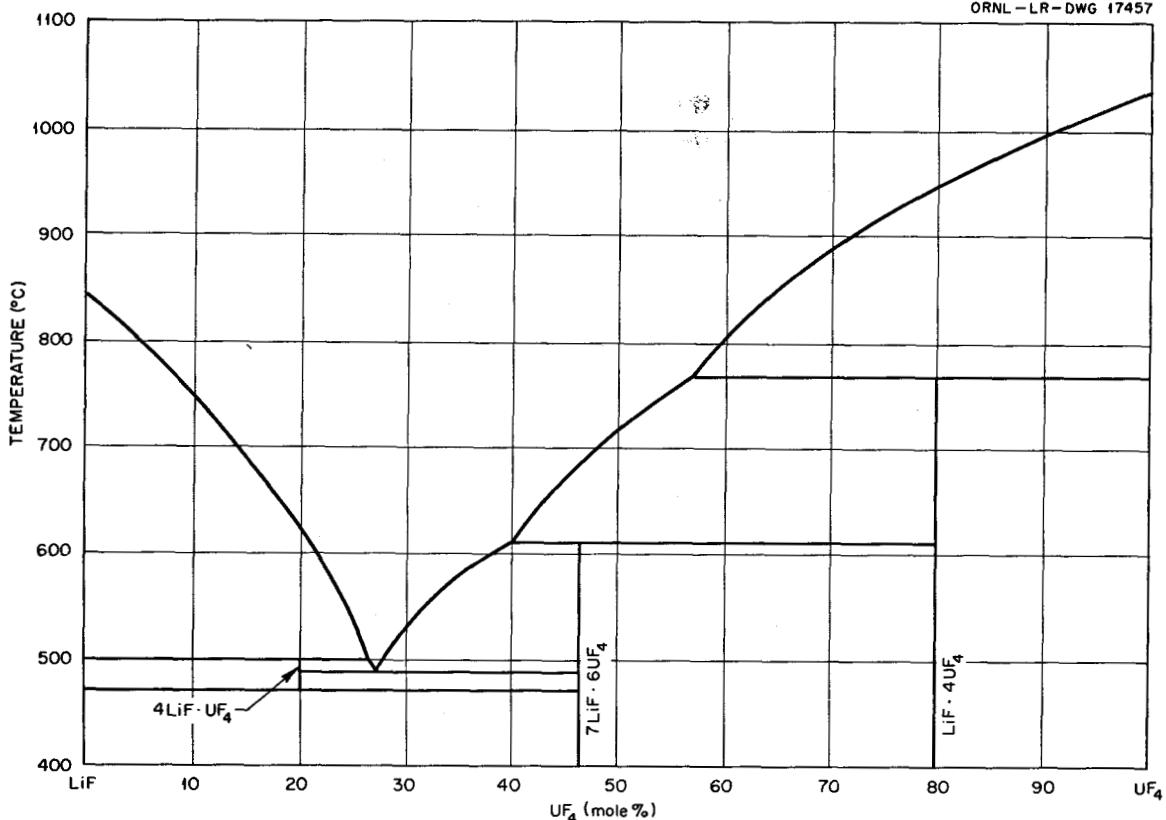


Fig. 7. The System LiF-UF<sub>4</sub>.

on the diagram is occupied by primary phase fields of the solid solutions UF<sub>4</sub>-ThF<sub>4</sub>, LiF·4UF<sub>4</sub>-LiF·4ThF<sub>4</sub>, and 7LiF·UF<sub>4</sub>-7LiF·ThF<sub>4</sub>. Liquidus temperatures decrease, generally, to the LiF-UF<sub>4</sub> edge of the diagram.

It is clear from examination of the diagrams shown that fuel systems melting below 500°C are available over a wide range of compositions in the LiF-BeF<sub>2</sub>-UF<sub>4</sub> system. Since up to 28 mole % of ThF<sub>4</sub> can be melted at temperatures below 1100°F (see Fig. 10), blanket systems with very large ThF<sub>4</sub> concentrations can be obtained. Moreover, the very great similarity in behavior of ThF<sub>4</sub> and UF<sub>4</sub> permits fractional replacement of ThF<sub>4</sub> by UF<sub>4</sub> with little effect on freezing temperature over the composition range of interest as fuel. Fuels for single-region thermal converters are, accordingly, available in the LiF-BeF<sub>2</sub>-ThF<sub>4</sub>-UF<sub>4</sub> quaternary system.<sup>7</sup>

Oxide-Fluoride Equilibria. When a molten mixture containing only LiF, BeF<sub>2</sub>, and UF<sub>4</sub> is treated with appreciable quantities of a reactive oxide (i.e., H<sub>2</sub>O, CO<sub>3</sub><sup>2-</sup>, FeO), precipitation of UO<sub>2</sub> results. The UO<sub>2</sub> so produced is stoichiometric, and if it is maintained in contact with the melt for sufficient time, it forms transparent ruby crystals of UO<sub>2</sub>.<sup>10</sup>

UNCLASSIFIED  
MOUND LAB. NO.  
56-11-29 (REV)

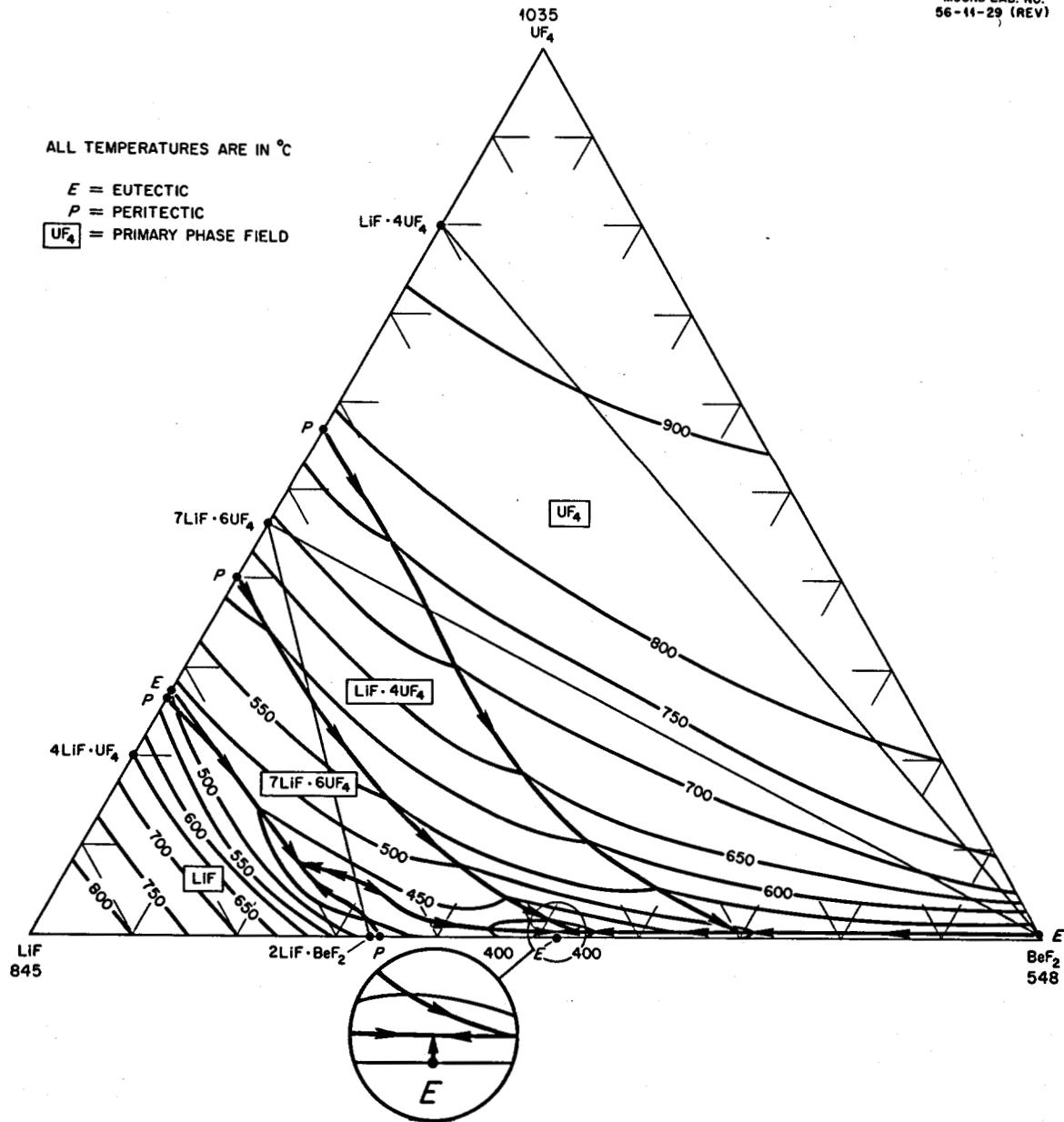
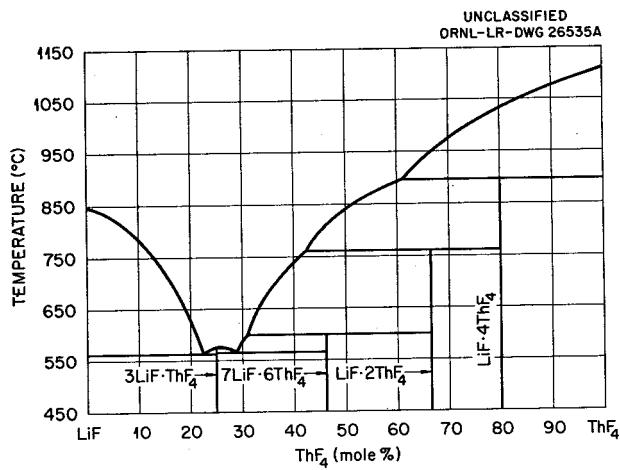
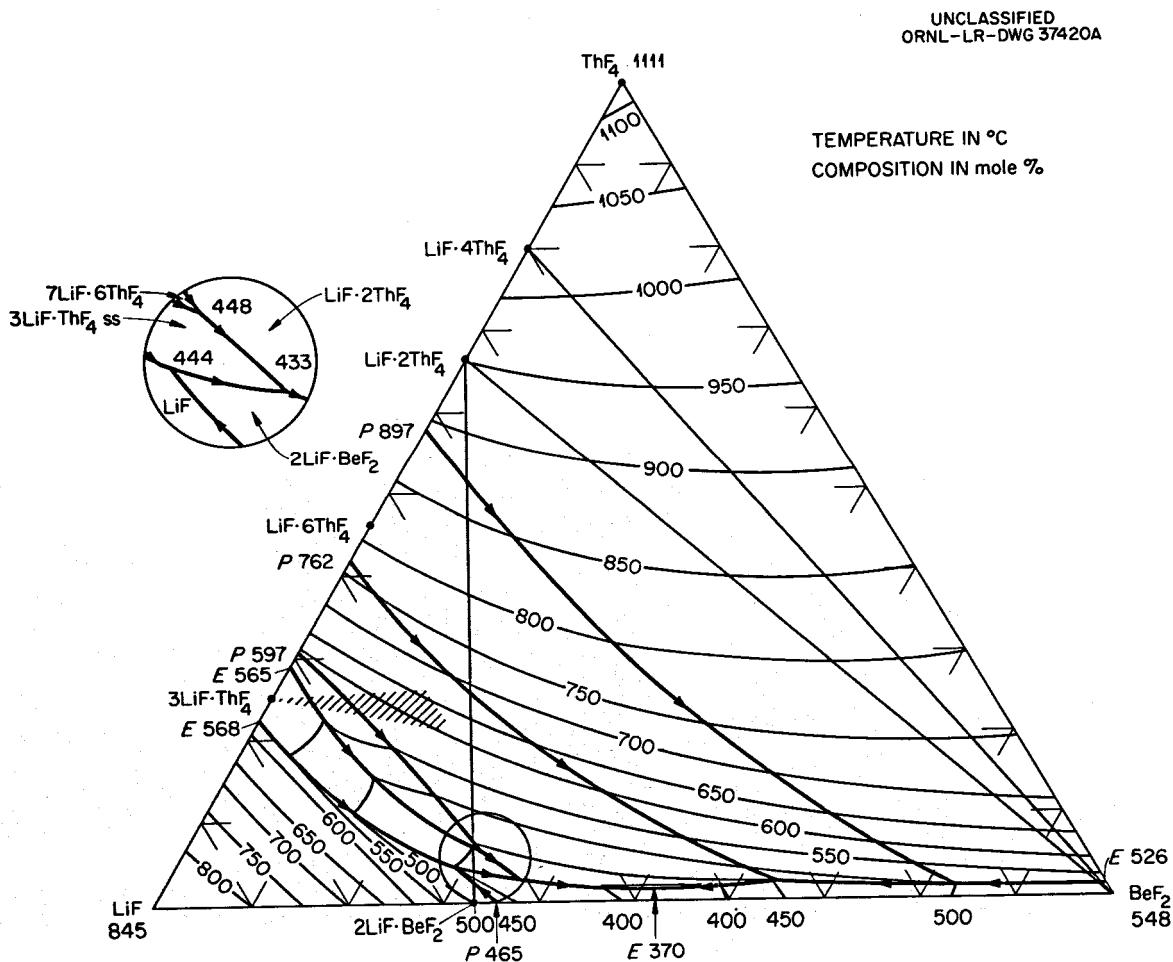
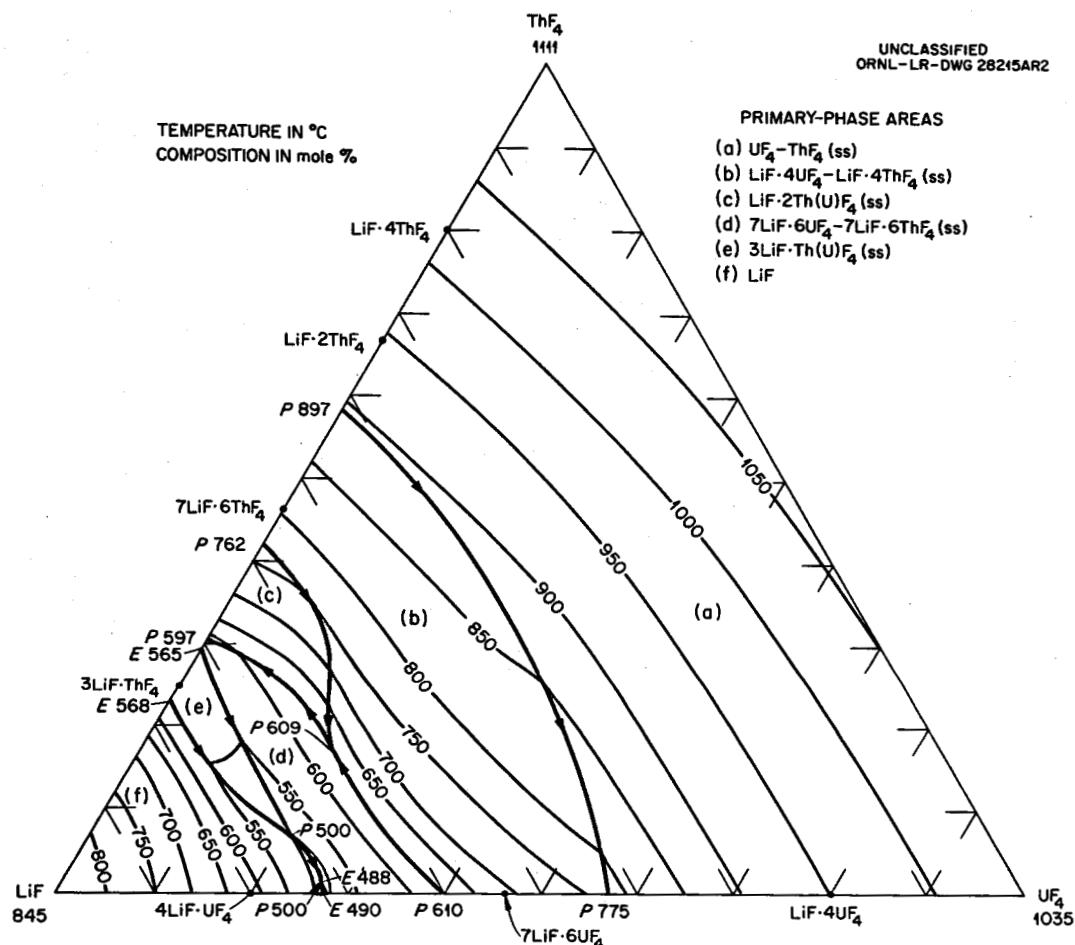
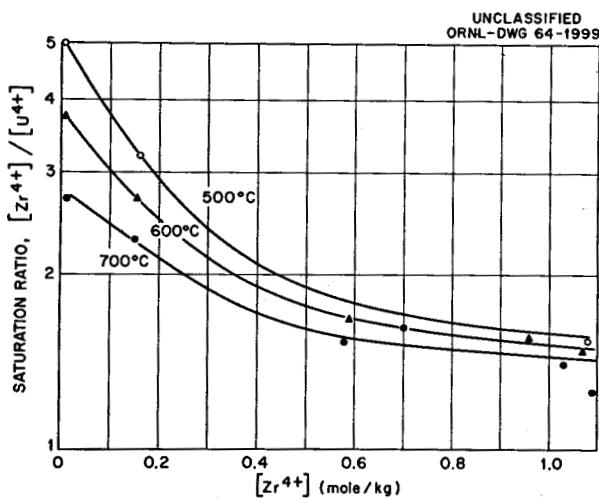


Fig. 8. The System  $\text{LiF}-\text{BeF}_2-\text{UF}_4$ .

Fig. 9. The System LiF-ThF<sub>4</sub>.Fig. 10. The System LiF-BeF<sub>2</sub>-ThF<sub>4</sub>.

Fig. 11. The System LiF-ThF<sub>4</sub>-UF<sub>4</sub>.Fig. 12. Ratio of [Zr<sup>4+</sup>]/[U<sup>4+</sup>] at UO<sub>2</sub> and ZrO<sub>2</sub> Saturation of 2LiF-BaF<sub>2</sub> as a Function of [Zr<sup>4+</sup>].

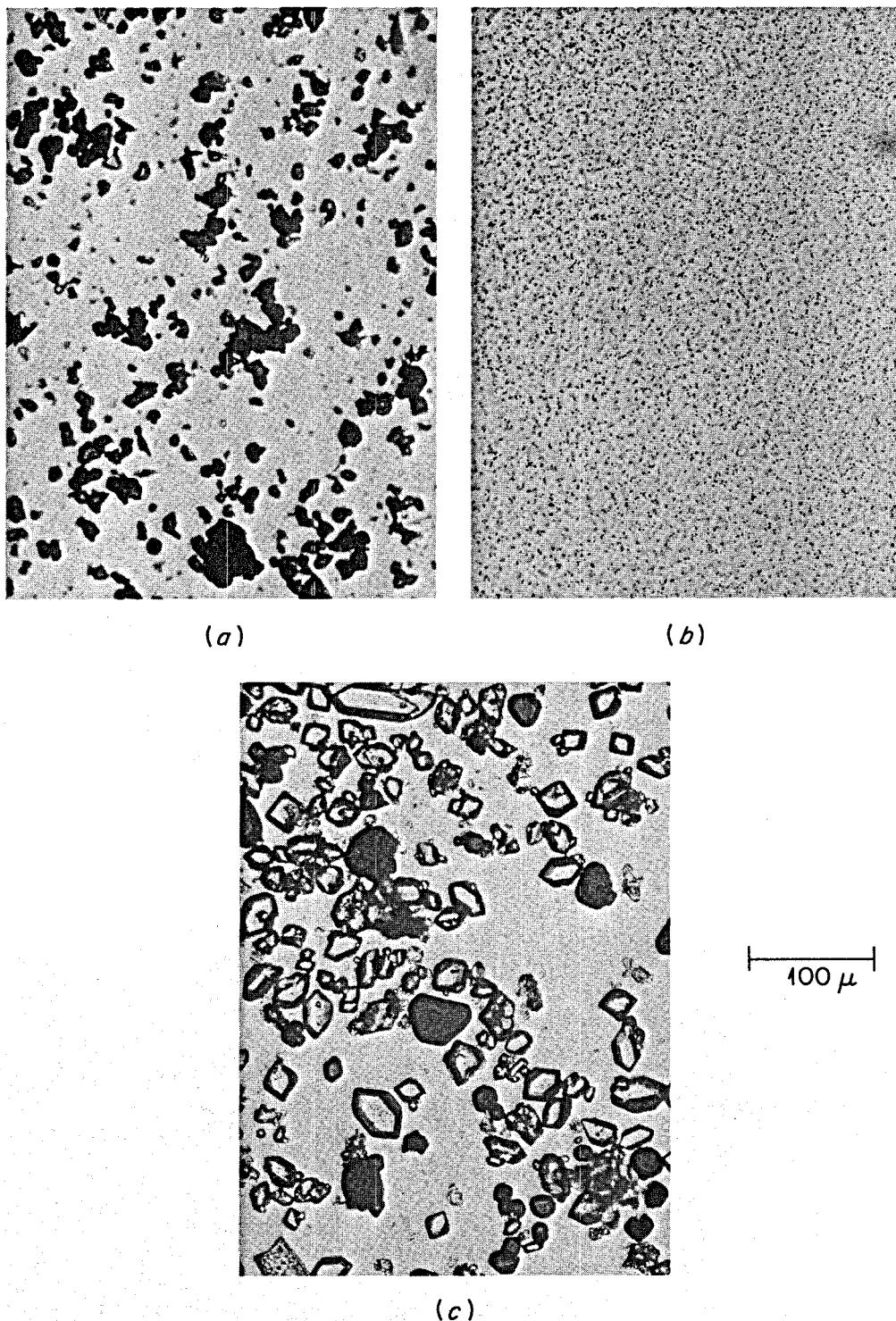
UNCLASSIFIED  
PHOTO 62267

Fig. 13. Photomicrographs of (a)  $\text{UO}_{2.12}$  Starting Material, (b)  $\text{ZrO}_2$  Starting Material, and (c) Mixture of Well-Crystallized  $\text{UO}_2$  and  $\text{ZrO}_2$  Resulting from Equilibration with  $2\text{LiF}\cdot\text{BeF}_2\cdot\text{UF}_4\cdot\text{ZrF}_4$  at 500–700°C.

Precipitation of  $\text{UO}_2$  has been suggested as a separations process of possible value.<sup>8</sup> However, such precipitation constitutes a possible danger for the MSRE since slow precipitation of  $\text{UO}_2$  followed by a sudden entrance of the material into the core would permit uncontrolled increases in reactivity. While precautions will be taken to assure cleanliness of the system, the fuel mixture, and the cover gas, it must be anticipated that some inadvertent contamination of the system will occur. Accordingly, an additional safeguard against precipitation of  $\text{UO}_2$  was developed.

If  $\text{ZrF}_4$  is added in reasonable concentration to the fuel mixture, then contamination of the melt by oxide ion (from  $\text{H}_2\text{O}$  or  $\text{BeO}$ ) results in precipitation of  $\text{ZrO}_2$  (Fig. 12). Continued addition of oxide ion leads to continued precipitation of  $\text{ZrO}_2$  until the  $\text{Zr}^{4+}/\text{U}^{4+}$  ratio falls to a value slightly below 2; additional oxide leads to precipitation of both  $\text{ZrO}_2$  and  $\text{UO}_2$  as separate species (Fig. 13).<sup>9</sup> Recent studies suggest that the relationship between these  $M^{4+}$  concentrations and  $O^{2-}$  concentration follows the mass action behavior expected for the reaction



The  $\text{ZrO}_2$  so precipitated from solution shows the x-ray pattern and the optical properties expected for pure  $\text{ZrO}_2$ . Solid solutions of  $\text{UO}_2$  in  $\text{ZrO}_2$  do not form even when both solids are equilibrated at 700°C for weeks with a fluoride melt under conditions such that gross crystal growth of both species occurs. Since this behavior appears to contradict published phase diagrams of the  $\text{ZrO}_2-\text{UO}_2$  system and since it may be important to the MSRE, it has been demonstrated repeatedly. As a further step it has recently been established that solid solutions of  $\text{UO}_2$  and  $\text{ZrO}_2$  prepared by heating the mixed oxides to high temperatures are decomposed into  $\text{ZrO}_2$  and  $\text{UO}_2$  by equilibration in a molten  $\text{Li}_2\text{BeF}_4$  mixture.

Use of  $\text{ZrF}_4$  in the MSRE fuel at concentrations such as five times that of  $\text{UF}_4$  should effectively prevent precipitation of  $\text{UO}_2$  and should completely avoid criticality hazards from this source. The  $\text{Zr}^{4+}/\text{U}^{4+}$  ratio has, accordingly, been set arbitrarily at a value of 5 or more.

Addition of sufficient oxide ion to  $\text{LiF}-\text{BeF}_2$  mixtures results in precipitation of  $\text{BeO}$ , although the solubility of  $\text{BeO}$  in such melts is considerably larger than the solubilities of  $\text{UO}_2$  and  $\text{ZrO}_2$ . No inherent hazard is apparent from the precipitation of small quantities of  $\text{BeO}$ . The precautions of system cleanliness and original melt purity are expected to suffice for the coolant circuit.

#### MSRE Fuel and Coolant Composition

The final fuel composition for the MSRE will, in fact, depend on the amount of uranium required to bring the system to the critical, and then to the operating, condition. At present it is anticipated that the composition will be (in mole %) 65  $\text{LiF}$ , 29.1  $\text{BeF}_2$ , 5  $\text{ZrF}_4$ , and 0.9  $\text{UF}_4$ . The pertinent physical properties for this mixture are shown in Table 3.

Table 3. Composition and Properties of Fuel and Coolant Salts

|   |                  | Fuel        | Coolant     |
|---|------------------|-------------|-------------|
| Composition, mole %   | LiF              | 65          | 66          |
|   | BeF <sub>2</sub> | 29.1        | 34          |
|   | ZrF <sub>4</sub> | 5           |             |
|   | UF <sub>4</sub>  | 0.9         |             |
| Liquidus temperature, °F  |                  | 842         | 851         |
| Physical properties   |                  | (at 1200°F) | (at 1062°F) |
| Density, lb/ft <sup>3</sup>   |                  | 146         | 120.5       |
| Heat capacity, Btu lb <sup>-1</sup> (°F) <sup>-1</sup>                            |                  | 0.455       | 0.526       |
| Viscosity, centipoises  |                  | 7.6         | 8.3         |
| Thermal conductivity, Btu ft <sup>-2</sup> hr <sup>-1</sup> (°F) <sup>-1</sup> ft |                  | 3.2         | 3.5         |
| Vapor pressure  |                  | Negligible  | Negligible  |

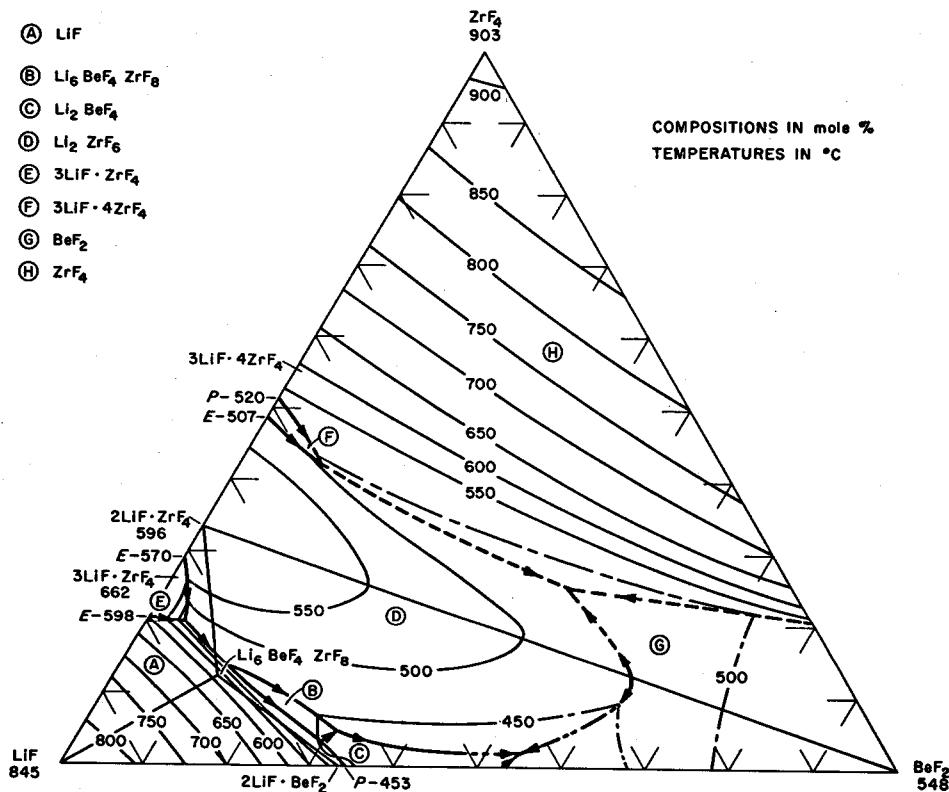
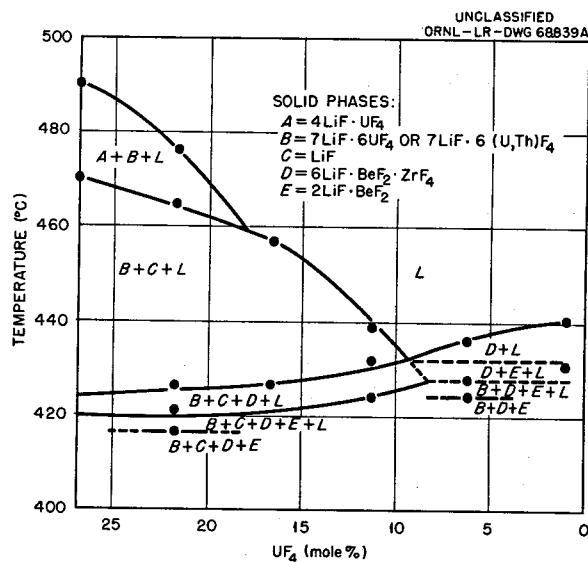
Introduction of ZrF<sub>4</sub> as an important constituent of the MSRE fuel adds, of course, to the complexity of the phase behavior of the system. No complete diagram exists at present for the quaternary system so produced. Figure 14 shows the (essentially completed) diagram for the LiF-BeF<sub>2</sub>-ZrF<sub>4</sub> ternary system.<sup>10</sup> A single ternary compound (6LiF·BeF<sub>2</sub>·ZrF<sub>4</sub>) and two ternary eutectics (at 3 mole % ZrF<sub>4</sub> and 54 mole % BeF<sub>2</sub>, mp 370°C, and at 25 mole % ZrF<sub>4</sub> and 48 mole % BeF<sub>2</sub>, mp 470°C) occur in the system.

Careful study of phase behavior of the complex quaternary system in the region chosen as fuel reveals no phase-instability problems at or near the reactor temperature. Figure 15 shows, as an approximation of behavior to be expected of the MSRE charge, an appropriate section across the more complex quinary system, with ThF<sub>4</sub> as an additional minor component.<sup>11</sup>

The final MSRE fuel will be obtained by deliberate and controlled addition of molten LiF-UF<sub>4</sub> eutectic (27 mole % UF<sub>4</sub>, mp 490°C) to the appropriate uranium-free LiF-BeF<sub>2</sub>-ZrF<sub>4</sub> solution. From Figs. 14 and 15, it is apparent that, if the reactor is maintained at temperatures above 500°C, addition of the LiF-UF<sub>4</sub> material will not produce separation of solid phases at intermediate or at extreme concentrations.

Choice of secondary coolant is, of course, a more simple matter. We decided to use a <sup>7</sup>LiF-BeF<sub>2</sub> mixture as coolant to avoid energetic reactions with the fuel (as with a NaK coolant) or contamination of the fuel if a leak developed between fuel and coolant.

Secondary coolants that have extremely low liquidus temperatures could be chosen (Fig. 5) from mixtures containing 40 to 60 mole % of BeF<sub>2</sub>.

UNCLASSIFIED  
ORNL-DWG 64-1992Fig. 14. The System  $\text{LiF}-\text{BeF}_2-\text{ZrF}_4$ .Fig. 15. The Section  $\text{LiF}-\text{UF}_4$  (73-27 mole %)- $\text{LiF}-\text{BeF}_2-\text{ZrF}_4-\text{ThF}_4-\text{UF}_4$  (70-23-5-1-1 mole %).

Safety considerations, however, gave a mild advantage to a coolant freezing at a temperature slightly above that of the fuel. This fact, plus the advantage in viscosity gained by diminishing the  $\text{BeF}_2$  content, led to choice of the mixture with 66 mole %  $\text{LiF}$  (mp  $851^\circ\text{F}$ ) as the secondary coolant. Values for certain pertinent physical properties of this material are included in Table 3.

Premuclear operation of the reactor will use a uranium-free  $\text{LiF-BeF}_2$  mixture essentially identical with the coolant to test the circulating system and to remove some or all of the oxides and oxygen-bearing species from the MSRE system. This material, commonly referred to as the flush salt, will also be used to flush and clean the reactor circuitry when necessary maintenance is required after nuclear operation.

MSRE operation will require about  $75 \text{ ft}^3$  of fuel mixture,  $75 \text{ ft}^3$  of flush salt, and about  $44 \text{ ft}^3$  of coolant. A total of nearly 25,000 lb of material must be prepared and transferred in pure form into the fuel, coolant, and flush tanks of the MSRE. Details of the preparation, purification, and handling operations on these materials are described in the following section.

### Physical Properties

The physical properties of the MSRE fuel and coolant salts are listed in Table 3, taken from a recent review of molten salts as reactor materials.<sup>12</sup>

The vapor pressures of the coolant and fuel salt were stated to be negligible. This conclusion was established by extrapolation to lower temperatures<sup>13</sup> of measured vapor pressures in the temperature range 1000 to  $1300^\circ\text{C}$ . Figure 16 illustrates the effect of doubling the concentration

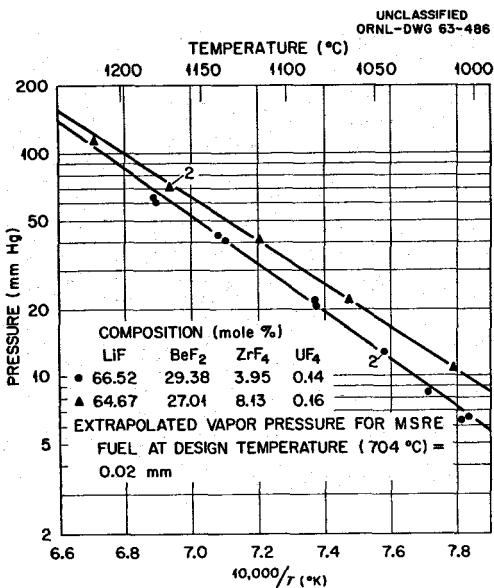


Fig. 16. Vapor Pressure of Two Mixtures in the System  $\text{LiF-BeF}_2-\text{ZrF}_4-\text{UF}_4$ .

of  $ZrF_4$  in a fuel salt mixture, while Fig. 17 shows the effects of changes in the lithium to beryllium ratio. The possible exploitation of vacuum distillation as a means of chemical reprocessing of irradiated MSRE fuel (in which the volatile  $BeF_2$  and  $LiF$  are removed, leaving  $UF_4$  and non-volatile rare-earth fluorides behind) will call for additional study of the vapor pressure and vapor composition of fluoride mixtures.

In addition to the data on viscosities of molten fluorides previously available,<sup>1</sup> an experimental program is currently devoted to the systematic

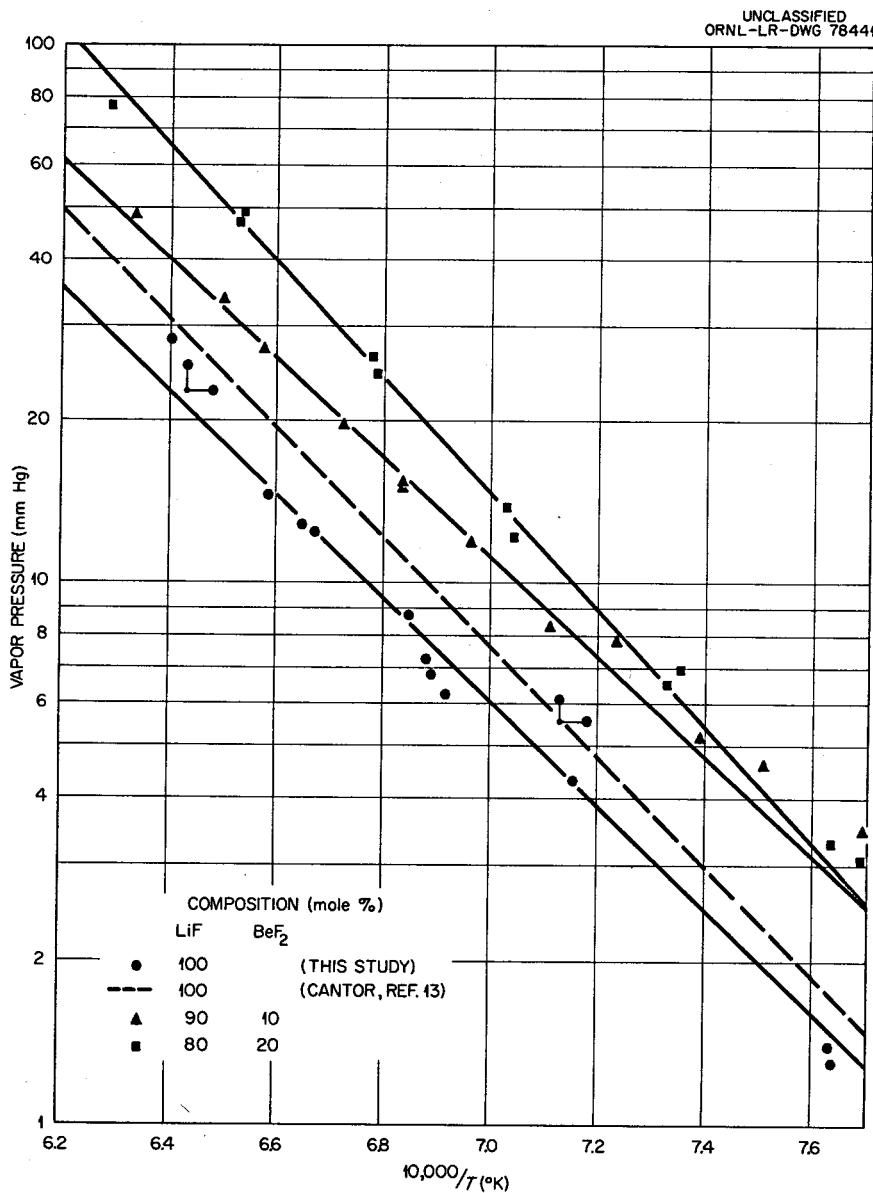


Fig. 17. Vapor Pressures in the LiF-BeF<sub>2</sub> System.

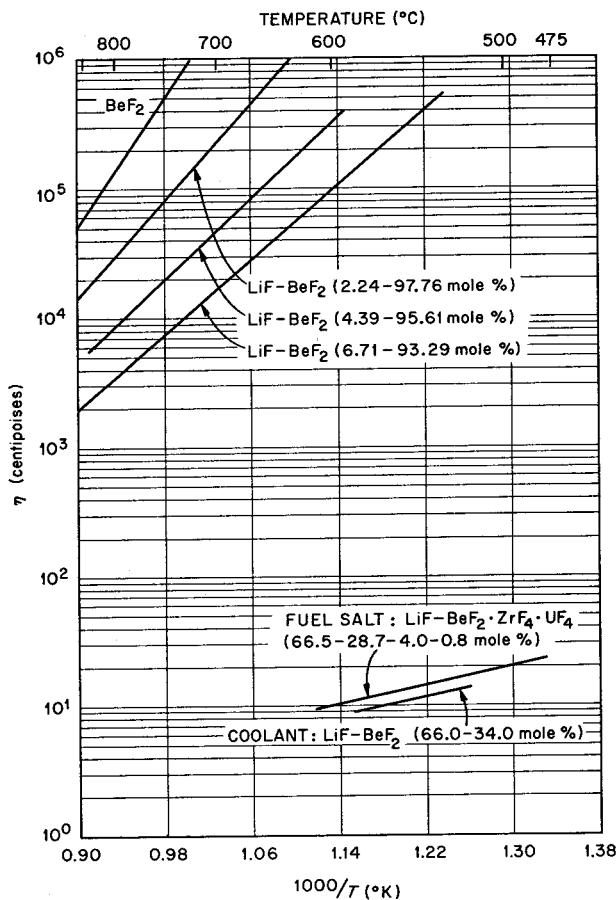
UNCLASSIFIED  
ORNL-DWG 64-2004

Fig. 18. Viscosity-Temperature Relation for LiF-BeF<sub>2</sub> Mixtures and for an MSRE-Type Fuel Mixture.

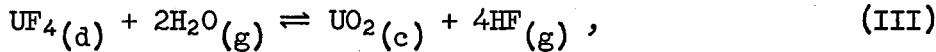
measurement of viscosities of molten fluoride salts over ranges of temperature and composition.<sup>14</sup> Figure 18 illustrates the tremendous influence of LiF in lowering the viscosity of BeF<sub>2</sub> as well as the comfortably low viscosity of the compositions used as fuel and coolant in the MSRE.

#### Stability of UF<sub>4</sub> and UF<sub>3</sub>

Uranium tetrafluoride is the least-stable necessary component of the MSRE fuel. Since some reduction of UF<sub>4</sub> to UF<sub>3</sub> must be anticipated through corrosion reactions (as described below) and since UF<sub>3</sub> is known to disproportionate to UF<sub>4</sub> and metallic uranium under some conditions, the stability of these materials both as solids and in solution has been examined.

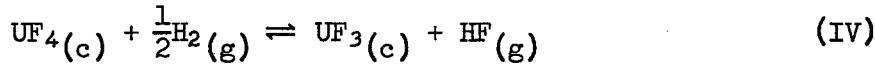
The standard free energy of formation ( $\Delta F_f^0$ ) of  $\text{UF}_4$  appears accurately known. Rand and Kubachewski give the value  $-95.3 \text{ kcal}/\text{F}^0 \text{ atom}$  for  $\Delta F_f^0$  at  $1000^\circ\text{K}$  for the crystalline solid.<sup>15</sup>

Baes has used an  $\text{LiF-BeF}_2$  mixture (67 mole %  $\text{LiF}$ ) in a study of the reaction



where g and c represent gaseous and crystalline solid states, and d indicates that the species is dissolved in the molten solvent.<sup>16</sup> He has shown that the activity coefficient ( $\gamma$ ) for  $\text{UF}_4$  in this solution, based upon the crystalline solid as reference state, has the value 0.55 at  $1000^\circ\text{K}$ . In solutions like the MSRE fuel, therefore, the activity (a) of  $\text{UF}_4$  is approximated by half its mole fraction ( $N$ ).

Long has studied the reduction of  $\text{UF}_4$  to  $\text{UF}_3$  by hydrogen.<sup>17</sup> In his work equilibrium values were defined both with  $\text{UF}_4$  and  $\text{UF}_3$  as crystalline solids and with these materials dissolved in a molten  $\text{LiF-BeF}_2$  (67 mole %  $\text{LiF}$ ) mixture. For the reaction

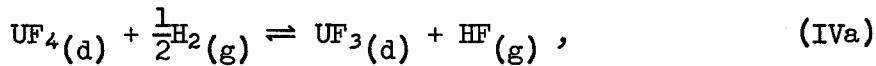


at  $1000^\circ\text{K}$  he obtains

$$K_a = \frac{f_{\text{HF}}}{f_{\text{H}_2}^{1/2}} = \frac{P_{\text{HF}}}{P_{\text{H}_2}^{1/2}} = 7 \times 10^{-4} \text{ atm}^{1/2}. \quad (1)$$

From this value, and from the  $\Delta F_f^0$  values of  $-65.8 \text{ kcal}/\text{mole}$  for HF and  $-381.2 \text{ kcal}/\text{mole}$  for  $\text{UF}_4$ , he obtains  $\Delta F_f^0 = -301.2 \text{ kcal}/\text{mole}$  for  $\text{UF}_3$  (all at  $1000^\circ\text{K}$ ). This latter figure agrees well with that estimated by Brewer<sup>18</sup> in 1945.

When the reduction is accomplished at  $1000^\circ\text{K}$  in the  $\text{LiF-BeF}_2$  solution,\* Long has shown that for



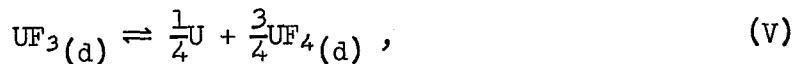
$$K_N = \frac{N_{\text{UF}_3} P_{\text{HF}}}{N_{\text{UF}_4} P_{\text{H}_2}^{1/2}} = 8 \times 10^{-6}. \quad (2)$$

---

\*These experiments were done with about 5 mole %  $\text{UF}_4$  in solution. The values should approximate very well those in MSRE fuel with 1%  $\text{UF}_4$  and 5%  $\text{ZrF}_4$ .

Since the fugacities ( $f$ ) and the pressures ( $P$ ) of the gases are identical and since (after Baes)  $N_{UF_4} \cong a_{UF_4}$ , these values of  $K_a$  and  $K_N$  can be combined to yield the activity coefficient ( $\gamma$ ) of  $UF_3$  with the crystalline solid as reference state; this combination yields  $\gamma_{UF_3} = 50$ .

From these data the extent of the disproportionation reaction may be assessed. For the reaction



the equilibrium quotient ( $K_N$ ) is given by

$$K_N = \frac{N_{UF_4}^{3/4}}{N_{UF_3}} a_U. \quad (3)$$

From the free-energy change the value  $K_a$  for Reaction V with products and reagents in their standard (crystalline solid) states is known to be

$$K_a = \frac{(N\gamma)_{UF_4}^{3/4}}{(N\gamma)_{UF_3}} a_U = 4.7 \times 10^{-4}. \quad (4)$$

From the activity coefficients given above for  $UF_3$  and  $UF_4$ , the value of  $K_N$  [identified in Eq. (3)] may be computed to be  $3.5 \times 10^{-2}$ . From this value the ratio of  $UF_4$  to  $UF_3$  or the extent of reduction of  $UF_4$  which is in equilibrium with any designated activity of  $U^0$  can be estimated.

In the MSR the activity of  $U^0$  might be controlled by formation of a uranium carbide or by alloying of  $U^0$  with the INOR-8. The values at which  $a_U$  would be controlled may be calculated from values of  $\Delta F_f^0$  of the

Table 4. Calculated Values of the Fraction of the Total Uranium in Solution Present in the Trivalent State ( $UF_3$ /Total U) in Equilibrium at 1000°K with Various Phases  
(total uranium in solution = 1 mole %)

| Phase    | $U^0$ Activity           | $UF_3$ /Total U (%) |
|----------|--------------------------|---------------------|
| U metal  | 1.0                      | >99                 |
| UC       | $3 \times 10^{-5}$       | 89                  |
| $UC_2$   | $5 \times 10^{-7}$       | 68                  |
| Ni alloy | $\sim 10^{-8}$           | 49                  |
| Ni alloy | $\sim 2 \times 10^{-10}$ | 20                  |
| Ni alloy | $\sim 1 \times 10^{-15}$ | 1                   |

appropriate carbide and may be estimated ( $a_U = 10^{-8}$  seems pessimistic) for the alloys with Ni<sup>0</sup>. Table 4 shows the calculated ratios of UF<sub>3</sub>/total uranium for several such uranium activities.

These numbers suggest strongly that quite high ratios of UF<sub>3</sub> to total uranium could be tolerated in MSRE before precipitation of uranium or its reaction with other MSRE components became a problem. Conversely, if, by any process, as much as 70% of the uranium were reduced to UF<sub>3</sub>, then one could expect the formation of UC<sub>2</sub> in the presence of graphite.

#### Chemical Compatibility of MSRE Materials

Successful operation of the MSRE requires compatibility of the molten fuel mixture with unclad graphite and INOR-8 during years of rapid circulation of the fuel through an appreciable temperature gradient. Such compatibility must, moreover, be assured while the fission process proceeds with its consequent intense radiation field and the buildup of fission product species. The evaluation of these implied problems has required a large research and development program in which many tests have been conducted over a period of several years. Details and specific findings of the large program of corrosion testing are presented as a separate chapter ("Metallurgical Development") in this report. The chemical properties of the materials and the chemical nature of their several interactions are described briefly in the following section. The effect of irradiation on compatibility of the fuel-graphite-INOR system is described below.

#### Corrosion of INOR-8 by Fluorides

Fluids that are circulated in metal circuits at rapid rates through pronounced temperature gradients frequently attack the metal by very complex processes. Such corrosion, or its prevention, often depends upon the stability and self-healing quality of insoluble corrosion product films; the corrosion resistance of aluminum to hot water (in spite of the thermodynamic instability of aluminum to water) is a familiar example of such behavior.

Molten fluorides such as those proposed for use in MSRE react with (and generally serve as fluxes for) oxides of the common metals. Accordingly, protection of the metal by an oxide or other film seems to be of no value in minimizing corrosion by fluorides. Corrosion behavior seems to be governed by the thermodynamic stability of the systems involved and by rates of migration of the reactive species within the alloy.

The corrosive attack (shown in detail in the chapter "Metallurgical Development"), which is extremely slight, occurs by selective oxidation of the chromium in INOR-8. Selective removal of chromium from the surface of the alloy results in diffusion of chromium atoms from interior layers toward the surface.<sup>19</sup> The process, accordingly, leads to an

excess of vacant sites in the solid solution; these vacancies agglomerate in areas of disregistry, principally at grain boundaries and at the sites of impurity atoms in the lattice, to form voids. These voids tend to agglomerate and to grow in size with increasing time and temperature. The subsurface voids are not interconnected with each other or with the surface. Under MSRE conditions subsurface void formation may be expected to depths of perhaps 0.5 mil/year.

A considerable fraction of the slight corrosive attack occurs shortly after startup of the test assembly. However, the evidence (and especially the older evidence obtained with Inconel, which is more severely attacked than is INOR-8) suggests that attack continues at a slow rate through some sustained-corrosion mechanism.

Nature of the Chemical Reactions. Selective attack upon the chromium in INOR-8 by oxidizing impurities in the molten fluorides is not surprising. Casual inspection of the thermochemical data of Table 2 suggests that both  $\text{FeF}_2$  and  $\text{NiF}_2$  should oxidize Cr to  $\text{CrF}_2$ . Blood<sup>20</sup> has made a careful study of the reaction



where M represents either Cr or Fe, and c, g, and d indicate that the species are crystalline solid (at unit activity), gaseous, or dissolved in a molten  $\text{LiF-BeF}_2$  mixture. In these experiments the solvent contained 62 mole % of LiF. Results of his studies show (see Table 5) that at 1000°K the experimentally determined equilibrium constants ( $K_N$ ) have the values  $8 \times 10^{-1}$  and  $1.3 \times 10^{-4}$  for  $\text{FeF}_2$  and  $\text{CrF}_2$  respectively. The equation for  $K_N$  is

$$K_N = \frac{P_{\text{HF}}^2}{N_{\text{MF}_2} \times P_{\text{H}_2}}, \quad (5)$$

where P and N indicate partial pressure and mole fraction of the designated species. The reaction of  $\text{FeF}_2$  dissolved in molten  $\text{LiF-BeF}_2$  with pure chromium should proceed (producing pure Fe and dissolved  $\text{CrF}_2$ ) until the ratio  $N_{\text{CrF}_2}/N_{\text{FeF}_2} \approx 6000$ .

Attack of dissolved  $\text{FeF}_2$  upon chromium in INOR-8 will, of course, be somewhat different. INOR-8 is a solid solution alloy with 0.083 atom fraction of chromium and 0.055 atom fraction of iron. Activities of the two metals should be approximated by these atom fractions. The reaction of chromium in the alloy with dissolved  $\text{FeF}_2$  to produce iron in the alloy should be slightly more complete than indicated above. Another likely reaction,

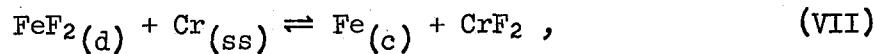


Table 5. Experimentally Determined Equilibrium Constants  
for the Reaction  $MF_2(d) + H_2(g) \rightleftharpoons M(c) + 2HF(g)$  in  
LiF-BeF<sub>2</sub> Mixture Containing 62 mole % LiF

| Temperature<br>(°C) | $K_N^{(a)}$          |                      |                      |
|---------------------|----------------------|----------------------|----------------------|
|                     | For CrF <sub>2</sub> | For FeF <sub>2</sub> | For NiF <sub>2</sub> |
| 800                 | $4.4 \times 10^{-4}$ | 1.9                  |                      |
| 727                 | $1.3 \times 10^{-4}$ | 0.80                 |                      |
| 700                 | $7.5 \times 10^{-5}$ | 0.53                 | $7 \times 10^5$      |
| 600                 | $1.2 \times 10^{-5}$ | 0.13                 | $1.5 \times 10^4$    |

$$a \quad K_N = \frac{P_{HF}^2}{N_{MF_2} \times P_{H_2}}.$$

where Cr<sub>(ss)</sub> is in solid solution in INOR-8 and Fe<sub>(c)</sub> is crystalline iron at unit activity, should proceed until the ratio  $N_{CrF_2}/N_{FeF_2} \cong 500$ . Depletion of chromium in the surface layers of INOR-8 (to be replenished slowly by diffusion from the interior) would, of course, lower this ratio.

Selective attack upon the chromium can occur by any of several reactions. These include:

1. Reactions with Dissolved Impurities in Melt - The fused fluorides are purified (see the chapter "Preparation of MSRE Fuel, Coolant, and Flush Salt" for details) by successive treatments with HF-H<sub>2</sub> mixtures and with H<sub>2</sub>. Incomplete removal of HF or of any easily reducible fluoride will subsequently lead to corrosion of the INOR-8. Reactions such as

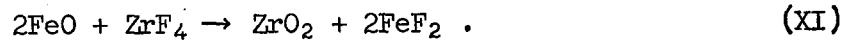
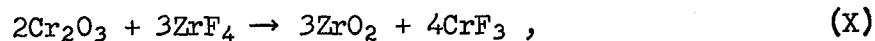


and



are examples. Available free-energy data and direct experimentation confirm that these reactions are even more complete than Reaction (VII).

2. Reactions Due to Oxides on the Metal - Oxide films on the INOR-8 are attacked by the molten fluoride by reactions such as



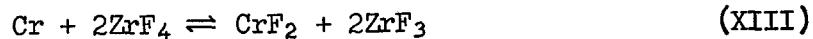
The resulting  $\text{ZrO}_2$  appears to be of little consequence in corrosion, but the  $\text{CrF}_3$  and  $\text{FeF}_2$  are strong oxidants to chromium in INOR-8.

Reactions of the type shown under 1 and 2 above can, if the fuel and the container are not carefully prepared, lead to serious initial corrosion. Such reactions can be minimized (or even avoided) by careful purification and manufacturing procedures. It is likely that these two classes of reactions will produce  $\text{CrF}_2$  in the fuel equivalent to about 250 parts of chromium per million parts of fuel. The  $\text{CrF}_2$  from these sources should, therefore, be at concentration  $N_{\text{CrF}_2} = 2.5 \times 10^{-4}$ .

3. Reactions with Necessary Constituents of Melt - Attempts to disclose the existence of  $\text{Zr}^{3+}$  and  $\text{Be}^+$  species in molten fluoride solution lead to the conclusion that reactions such as



do not occur;  $\text{Zr}^{3+}$  species do not exceed concentrations of 10 ppm if they are present at all. Accordingly, reactions such as

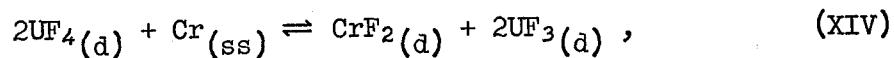


apparently need not be considered.

Uranium trifluoride is, however, a well-known compound that is relatively stable in molten fluorides of the type to be used in MSRE. The extent of reaction is relatively small; the values in Table 2 indicate a free-energy change of +12 kcal for oxidation of Cr by  $\text{UF}_4$ . In spite of this, the reaction is an important contributor to the corrosion process; an evaluation of its contribution is examined in detail in the following.

Extent of Chemical Reactions. The data obtained from studies of hydrogen reduction equilibria by Long and by Blood (described above) can be used to yield reasonable (and consistent) estimates of the activity coefficients of the several species in melts similar to the MSRE fuel. These activity coefficients, based on the crystalline solid as reference state, are shown in Table 6.

From these values and the values (Table 2) of  $\Delta F_f^0$  for the several compounds, we may assess the extent of the reaction



where the  $\text{UF}_4$ ,  $\text{CrF}_2$ , and  $\text{UF}_3$  are in solution in MSRE fuel and the Cr is at the relatively low activity it has in unaltered INOR-8. For this reaction,

$$K_a = 2.4 \times 10^{-3} = \frac{a_{\text{UF}_3}^2 \cdot a_{\text{CrF}_2}}{a_{\text{UF}_4}^2 \cdot a_{\text{Cr}}} = \frac{(N\gamma)_{\text{UF}_3}^2 (N\gamma)_{\text{CrF}_2}}{(N\gamma)_{\text{UF}_4}^2 a_{\text{Cr}}}. \quad (6)$$

If, initially, the salt were completely pure and the metal contained no oxide (so that all  $\text{CrF}_2$  was generated by this reaction), then

$$N_{\text{UF}_3} = 2N_{\text{CrF}_2}. \quad (7)$$

For reaction of a fuel with 1 mole %  $\text{UF}_4$  ( $N_{\text{UF}_4} = a_{\text{UF}_4} = 0.01$ ) with INOR-8 ( $a_{\text{Cr}} = 0.083$ ), the equilibrium indicated in Eq. (6) is satisfied at

$$N_{\text{CrF}_2} = 1.1 \times 10^{-4}$$

and

$$N_{\text{UF}_3} = 2.2 \times 10^{-4}.$$

Accordingly, less than 3% of the  $\text{UF}_4$  would be reduced to  $\text{UF}_3$ , and the chromium fluoride concentration of the melt would be 130 ppm (as Cr). In a more realistic case if  $\text{CrF}_2$  equivalent to some 250 ppm of chromium arose from other sources, then the total  $\text{CrF}_2$  concentration at equilibrium would rise to slightly more than 300 ppm (as Cr), and  $N_{\text{UF}_3}$  would be about  $1 \times 10^{-4}$ .

Table 6: Activity Coefficients<sup>a</sup> Estimated for Various Fluorides in Molten LiF-BeF<sub>2</sub> Solutions at 1000°K

| Species        | $\Delta F_f^0$<br>(kcal/F atom) | Equilibrium Studied  | Approximate<br>Concentration<br>(mole fraction) | $\gamma$ |
|----------------|---------------------------------|--|---|----------|
| $\text{UF}_4$  | -95.3                           | $\text{UF}_4 + 2\text{H}_2\text{O} \rightleftharpoons \text{UO}_2 + 4\text{HF}$  | 0.02  | 0.55     |
| $\text{UF}_3$  | -101.4                          | $\text{UF}_4 + \frac{1}{2}\text{H}_2 \rightleftharpoons \text{UF}_3 + \text{HF}$ | 0.0001  | 50       |
| $\text{FeF}_2$ | -66.5                           | $\text{FeF}_2 + \text{H}_2 \rightleftharpoons \text{Fe} + 2\text{HF}$            | 0.005   | 1.6      |
| $\text{CrF}_2$ | -74                             | $\text{CrF}_2 + \text{H}_2 \rightleftharpoons \text{Cr} + 2\text{HF}$            | 0.001   | 0.5      |

<sup>a</sup>Based on the crystalline solid as reference state.

It is easy to show that if, as a consequence of  $\text{FeF}_2$  impurity, the INOR-8 surface were severely depleted of chromium and if iron at unit activity were available within the system, the reaction would yield at equilibrium  $N_{\text{UF}_3} = 3 \times 10^{-5}$  (corresponding to reduction of only 0.3% of the available  $\text{UF}_4$ ) and  $N_{\text{FeF}_2} = 1.5 \times 10^{-5}$  (corresponding to  $\text{FeF}_2$  at about 15 ppm as Fe). It is highly unlikely that any tests have been run under such circumstances.

This reaction will certainly not produce sufficient  $\text{UF}_3$  to cause trouble from disproportionation of this material. Moreover, the total quantity of chromium removed from the metal should prove trivial in any uniform temperature system.

However, in a nonuniform temperature system such as MSRE the small, but real, temperature dependence of reactions such as (XIV) can result in removal of chromium from the metal in the hotter regions and its deposition in the colder regions of the circuit. However, since the temperature dependence of the reaction is so slight, the deposition can result only in a slight increase in chromium activity (concentration) in the INOR-8 in the cooler regions.

If nickel, iron, and molybdenum are assumed (as is approximately true) to be completely inert diluents for chromium, and if the circulation rate of 1200 gpm for MSRE can be considered infinitely rapid, the process can be simply described. Under such conditions uniform concentrations of  $\text{UF}_3$  and  $\text{CrF}_2$  are maintained in the fluid; these concentrations satisfy (at some intermediate temperature) the equilibrium constant for the reaction shown. Under these steady-state conditions, there exists a temperature ( $T$ ), intermediate between the maximum and minimum temperatures of the loop, at which the initial composition of the structural metal is at equilibrium with the fused salt. Since the equilibrium constant for the chemical reaction increases with increasing temperature, the chromium concentration in the alloy surface is diminished at temperatures higher than  $T$  and is augmented at temperatures lower than  $T$ . In some melts ( $\text{NaF-LiF-KF-UF}_4$ , e.g.) the equilibrium constant of reaction changes sufficiently under extreme temperature conditions to cause formation of nearly pure chromium crystals in the cold zone. In other melts ( $\text{LiF-BeF}_2-\text{UF}_4$ , e.g.) the temperature dependence of the corrosion equilibrium is small, and the equilibrium is satisfied at all useful temperatures without the formation of crystalline chromium. In the  $\text{LiF-BeF}_2-\text{UF}_4$  system the rate of chromium removal from the salt stream at cold-leg regions is dependent on the rate at which chromium can diffuse into the cold-leg wall. If the chromium concentration gradient tends to be small, or if the bulk of the cold-leg surface is held at a relatively low temperature, the corrosion rate in such systems is almost negligible.

As the alloy surface in the hot region at the circuit becomes depleted in chromium, chromium from the interior diffuses down the concentration gradient toward the surface. Since diffusion occurs by a vacancy process and in this particular situation is essentially monodirectional, it is possible, as previously mentioned, to build up an excess number of

vacancies in the metal. These precipitate in areas of disregistry, principally at grain boundaries and impurities, to form voids. These voids tend to agglomerate and grow in size with increasing time and temperature. The subsurface voids are not interconnected with each other or with the surface.

The mechanisms described above seem to explain such observations as the complete independence of corrosion rate and flow rate for a given system, and the increase in corrosion with increase in temperature drop as well as with increase in mean temperature within a system.

The results of many, long-term tests of corrosion of INOR-8 and Inconel by MSRE fuel mixtures and other salt combinations (see the chapter "Metallurgical Development") seem to substantiate very well the expectations from these thermodynamic considerations.

#### Compatibility of Graphite with Fluorides

Graphite does not react chemically with molten fluoride mixtures of the type to be used in the MSRE. Available thermodynamic data suggest that the most likely reaction:



should come to equilibrium at a concentration of  $\text{CF}_4$  which is below the detection limit (about 1 ppm) of this compound by mass spectrometry. Moreover, graphite has been used as a container material for many  $\text{NaF-ZrF}_4-\text{UF}_4$ ,  $\text{LiF-BeF}_2-\text{UF}_4$ , and other salt mixtures, with no evidence of chemical instability.

The MSRE will contain about  $70 \text{ ft}^3$  (nearly 8000 lb) of graphite. Even though chemical stability is assured, several possible problems remain. These include (1) hazardous increase in uranium content of core through permeation of the graphite by fuel, (2) reaction of fuel material with oxygenated gaseous species desorbed from the graphite, and (3) carburization of the INOR-8 structure by carbon dissolved, suspended, or otherwise carried in the circulating salt. These possibilities have been studied experimentally and found to be inconsequential or to have practicable solutions.

Graphite is not wetted by MSRE fuel mixtures (or by other similar mixtures) at elevated temperatures. The extent to which graphite is permeated by the fuel is, accordingly, defined by well-known relationships among applied pressure, surface tension of the nonwetting liquid, and the pore-size spectrum of the graphite specimen. Typical tests<sup>21</sup> with MSRE graphite have exposed evacuated specimens to MSRE fuel mixtures at  $1300^\circ\text{F}$ ; applied pressures were set at 150 lb, a value three times the reactor design pressure. The observed permeation did not change with time after a few hours. In these tests 0.3% of the graphite bulk volume was permeated by the salt; such permeation is well within that considered tolerable during MSRE operation. Specimens permeated to this extent have

been given 100 cycles between 390 and 1300°F without detectable change in properties or appearance.

Graphites contain appreciable quantities of gases that are not removed by pumping at room temperature but that are desorbed on heating in vacuum to high temperatures. These gases typically consist of H<sub>2</sub>O, CO<sub>2</sub>, CO, N<sub>2</sub>, H<sub>2</sub>, and small quantities of hydrocarbons.<sup>22</sup> The MSRE graphite was specified to contain less than 30 STP cm<sup>3</sup> of CO (or equivalent O) per 100 cm<sup>3</sup> of graphite after pumping at 30°C to a pressure of 10<sup>-3</sup> mm Hg<sup>0</sup>; subsequent tests<sup>21</sup> have shown the graphite to contain about 6 cm<sup>3</sup> of these gases per 100 cm<sup>3</sup>. The fuel mixture could, if necessary, withstand much larger quantities of active oxide without difficulty from precipitation of ZrO<sub>2</sub>. In addition, it has been shown that a helium purge, maintained while the graphite is slowly heated to 400°C, effectively removes the small quantity of physically absorbed and chemisorbed water from the MSRE specimens.<sup>23</sup> Carbon monoxide and CO<sub>2</sub> react slowly if at all with the molten fluoride mixtures, and most of the water should be readily removable during preliminary heatup of the reactor. It is unlikely that desorption of gases from the moderator will be of consequence in MSRE operation.

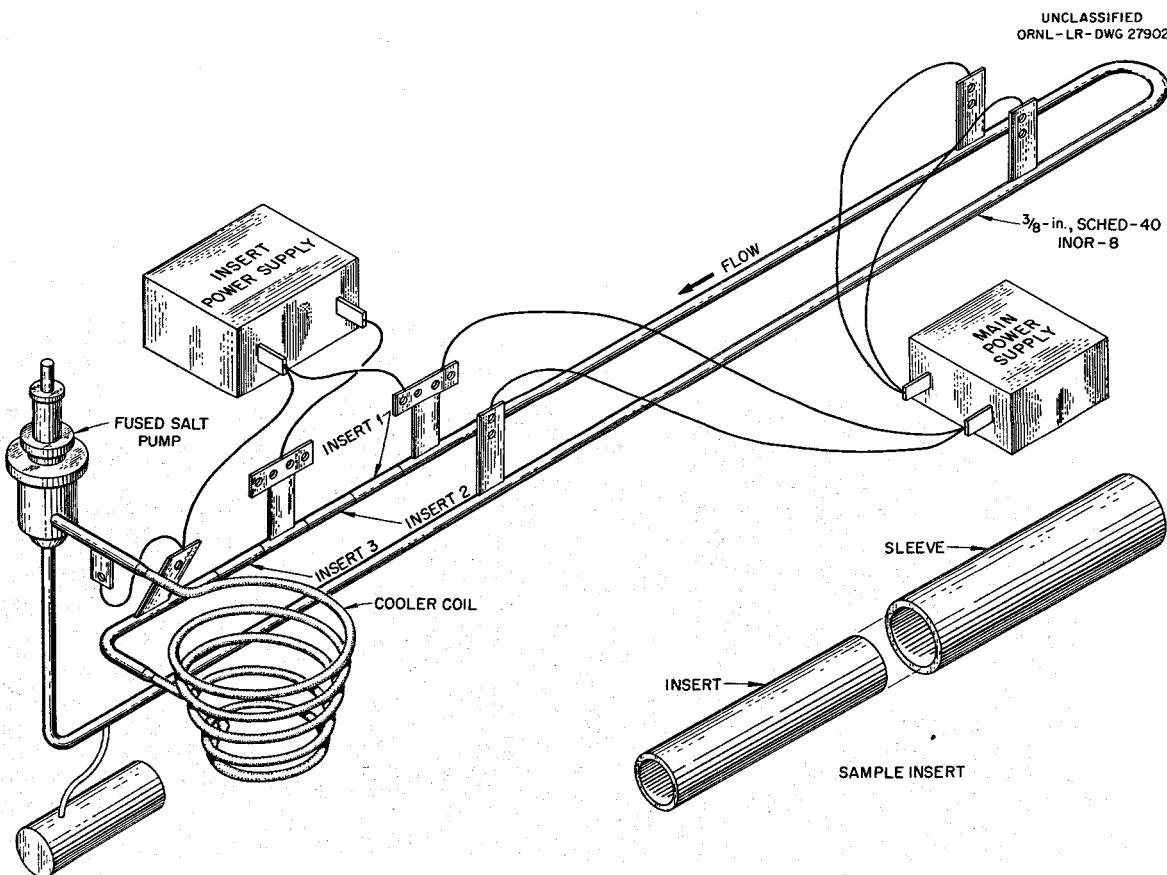


Fig. 19. Diagram of Forced-Circulation Loop for Weight-Loss Studies of INOR-8 Exposed to Circulating Fused Salts.

Carburization of INOR-8 by graphite in contact with molten fluorides has been studied in static capsule tests<sup>24</sup> and in a long-lived forced-circulation loop.<sup>25</sup>

The static capsules were run at 1300°F with INOR-8 specimens, graphite, and an LiF-BeF<sub>2</sub>-UF<sub>4</sub> fuel mixture contained in capsules of INOR-8. Exposures were for multiples of 2000 hr up to 14,000 hr. All tests indicated no carburization and no appreciable alteration of the tensile properties of the metal. The longest test (14,000 hr) produced a slight roughening (less than 0.5 mil) of the INOR-8 specimens.

The forced-circulation loop<sup>25</sup> of INOR-8 was operated at 1300°F for 1 year with an LiF-BeF<sub>2</sub>-UF<sub>4</sub> (62-37-1 mole %) mixture as the circulating medium. An INOR-8 box, located at the heater outlet of a standard loop (see Fig. 19), contained 32 rods (11 × 1/2 in.) and 18 rods (11 × 3/16 in.) of a special experimental graphite from National Carbon Company; this graphite was generally similar to the proposed MSRE moderator material. Each of the larger rods was fitted with four spacer rings of INOR-8 wire to obtain the desired flow characteristics and to provide samples for metallurgical tests for carburization. The graphite specimens after test are shown in Fig. 20. Weight changes, dimensional changes, and chemical analyses of machinings from the graphite<sup>26</sup> revealed no detectable erosion of the specimens, and permeation of the graphite by only traces of fuel. Carburization of the INOR-8 appeared to be absent.

No difficulties with out-of-radiation compatibility of the fluoride-graphite-metal MSRE system have so far been found.

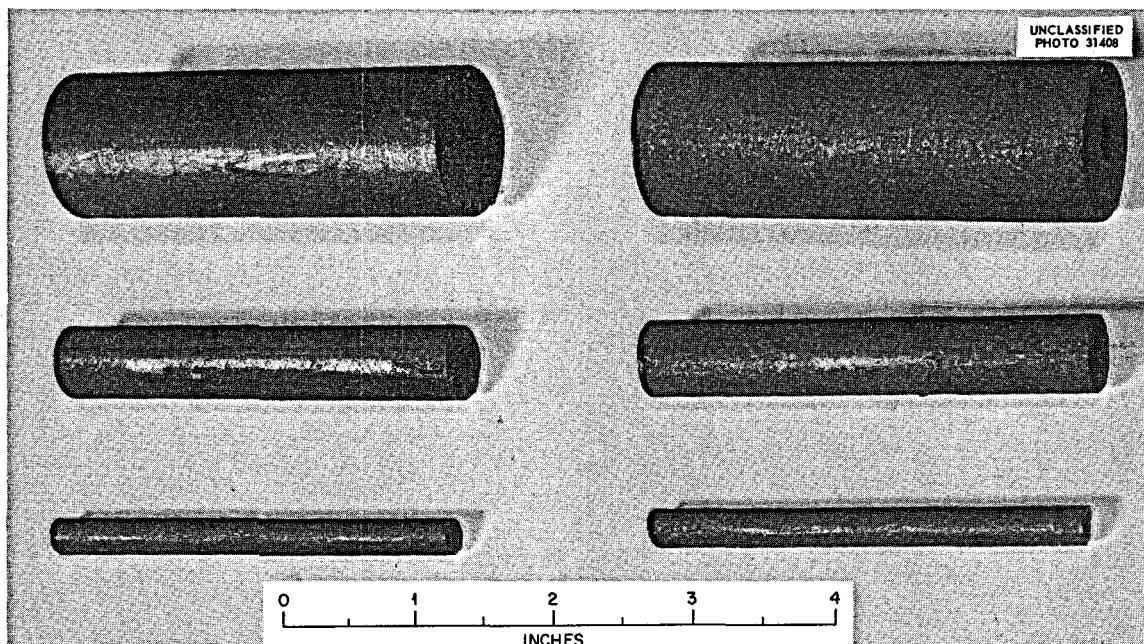


Fig. 20. Graphite Specimens After Exposure to Molten Fluoride.

### Behavior of Fission Products

When fission occurs, the fragments originate in energy states and ionization levels very far from those normally encountered. When fission occurs in a well-mixed liquid medium, these fragments must, as they quickly lose energy through collisions in the liquid, come to a steady state (made very complicated by the radioactive decay of many species) as common chemical entities. The valence states which they assume in the liquid are, presumably, defined by the requirements that cation-anion equivalence be maintained in the liquid and that redox equilibria be established both among the components of the melt and between the melt and the surface layers of the container metal.

When fission occurs in aqueous solution, the requirement of cation-anion equivalence can, if necessary, be satisfied by  $H^+$  or  $OH^-$  ions supplied by the solvent. No such mechanism is available to the MSRE fuel. In these media, since  $F_2$  and valence states of uranium higher than 4 are unstable toward reduction by the container, the fission product cations must neutralize the fission product anions plus the 4 fluoride ions associated with the fissioned atom. If the fission product cations are inadequate, or if they become adequate only by assuming oxidation states incompatible with INOR-8, then the container metal must supply the deficiency.

Thermochemical data, from which the stability of fission product fluorides in complex dilute solutions can be predicted, are lacking in many cases. No precise definition of the valence states of all fission products can be given, and the complex situation in the MSRE fuel cannot be defined in real detail. Such information as seems definite is briefly described in the following. The data obtained in many in-pile tests (see below) suggest strongly that the fuel mixture survives the fission process without requiring substantial contributions from the container metal.

### Rare Gases

The fission products krypton and xenon are volatilized from the high-temperature melts as elements. The solubilities of these gases in molten fluoride mixtures obey Henry's law, increase with increasing temperature, decrease with increasing atomic weight of the gas, and vary somewhat with composition of the solvent.<sup>27</sup> Henry's law constants and heats of solution for the rare gases in  $NaF-ZrF_4$  and  $LiF-BeF_2$  mixtures are shown in Table 7. The positive heat of solution ensures that blanketing or sparging of the fuel with helium or argon in a low-temperature region of the reactor cannot lead to difficulty due to decreased solubility and bubble formation in higher-temperature regions of the system.

The very low solubilities of these gases suggest that they should be readily removed from reactor systems. Only a small fraction of the calculated xenon poisoning was observed during operation of the Aircraft Reactor Experiment, where the only mechanism for xenon removal was the helium purge of the pump bowl. Removal of xenon from the MSRE will be

Table 7. Solubilities at 600°C and Heats of Solution for Noble Gases in Molten Fluorides

| Gas | NaF-ZrF <sub>4</sub><br>(53-47 mole %) |                                 | LiF-BeF <sub>2</sub><br>(64-36 mole %) |                                 |
|-----|--|---------------------------------|--|---------------------------------|
|     | K* × 10 <sup>8</sup>                   | Heat of Solution<br>(kcal/mole) | K* × 10 <sup>8</sup>                   | Heat of Solution<br>(kcal/mole) |
| He  | 21.6 ± 1                               | 6.2                             | 11.55 ± 0.4                            | 5.2                             |
| Ne  | 11.3 ± 0.3                             | 7.8                             | 4.63 ± 0.2                             | 5.9                             |
| A   | 5.1 ± 0.15                             | 8.2                             | 0.98 ± 0.02                            | 8.6                             |
| Xe  | 1.94 ± 0.2                             | 11.1                            | 0.233 ± 0.01                           | 12.1                            |

\* K = moles of gas/(cm<sup>3</sup> of solvent) (atm).

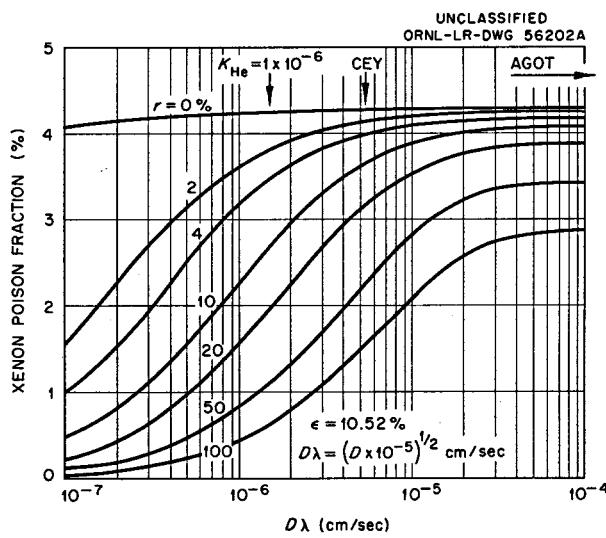


Fig. 21. Possible Xenon Poisoning in Molten-Salt Reactors.

complicated by holdup of this gas in the pores of the graphite and by the relatively small fraction (5 to 10%) of the fuel flow which is bypassed through the pump bowl. Figure 21 shows a family of curves which relate poison fraction to be expected as a function of recycle rate (percentage of fuel flow equilibrated with a stripping gas) and of permeability of the moderator graphite. It is clear from this figure that very marked improvement in tightness of graphite will be required to solve the problem at low recycle rates, but that a simple gas-stripping system operating on the entire fuel flow should solve the problem for a reactor with any reasonable moderator graphite.

#### Elements of Groups I-A, II-A, III-B, and IV-B

Rubidium, cesium, strontium, barium, zirconium, yttrium, and the lanthanides form very stable fluorides. These fission products should, accordingly, exist in the molten fuel in their ordinary valence states. Many studies show that large amounts of  $ZrF_4$ , the alkali fluorides, and the alkaline earth fluorides can be dissolved in the MSRE fuel mixture at operating temperatures. Since the trifluorides are less soluble, the solubility behavior of the fluorides of yttrium and the rare earths, and of plutonium have been examined in some detail.<sup>28,29</sup> The saturating phase from solutions in  $LiF-BeF_2$  and related mixtures is the simple trifluoride; when more than one rare earth is present, the saturating phase is a (nearly ideal) solid solution of the trifluorides. The solubilities of these materials depend strongly on composition of the melt and may be near the minimum in compositions close to that of the MSRE fuel. Even in this region, however, the solubility (near 0.5 mole % at MSRE operating temperatures) is such that many years would be required for the reactor to saturate its fuel with any of these fission products.

The statements regarding rubidium and cesium above do not apply to those fractions of these elements which originate in the graphite as daughters of the rare gases which have permeated the moderator. These alkali metals form compounds with graphite at high temperature; the quantities involved, however, are so small that no damage to the graphite seems possible.

#### Other Fission Products

The fission of the uranium atom of  $UF_4$  would yield more cation equivalents than anion equivalents if the noble-gas isotopes of half-life greater than 10 min were lost from the fuel and if each of the other fission products formed a fluoride of its lowest recognized valence state; if this were the case, the system would retain cation-anion equivalence by depositing the most noble fission products as metal and by reduction, if necessary, of some  $UF_4$  to  $UF_3$ . The sparse thermochemical data suggest that the fluorides of germanium, arsenic, niobium, molybdenum, ruthenium, rhodium, palladium, silver, cadmium, tin, and antimony should be reduced by chromium at its activity in INOR-8. In dilute solution in the MSRE fuel, not all these reductions would be complete, but some of these elements (and perhaps part of all of them) must be expected to exist as

metals. Only about 3.2 cation equivalents result from fission in  $\text{UF}_4$  if all these fission products exist entirely as metals; the fission process would in that event result in oxidation of INOR-8. Considerable qualitative information from in-pile capsules and in-pile loops suggests that the true situation is comfortably between these extremes and in a region where the cation-anion equivalence is satisfied at a redox potential near to that of INOR-8.

#### References

1. W. R. Grimes *et al.*, "Chemical Aspects of Molten-Fluoride-Salt Reactor Fuels," in Fluid Fuel Reactors, ed. by J. A. Lane, H. G. MacPherson, and Frank Maslan, Addison-Wesley, Reading, Mass., 1958; and W. R. Grimes and D. R. Cuneo, "Molten Salts as Reactor Fuels," in Reactor Handbook, 2d ed., vol. I, Materials, ed. by C. R. Tipton, Jr., Interscience, New York, 1960.
2. W. R. Grimes and D. R. Cuneo, "Molten Salts as Reactor Fuels," p. 457 in Reactor Handbook, 2d ed., vol. I, Materials, ed. by C. R. Tipton, Jr., Interscience, New York, 1960.
3. R. E. Thoma (ed.), Phase Diagrams of Nuclear Reactor Materials, ORNL-2548 (Nov. 2, 1959), p. 116.
4. *Ibid.*, p. 33.
5. L. V. Jones *et al.*, J. Am. Ceram. Soc. 45(2), 79-83 (1962).
6. R. E. Thoma *et al.*, J. Phys. Chem. 64, 865 (1960).
7. C. F. Weaver *et al.*, Phase Equilibria in Molten Salt Breeder Reactor Fuels. I. The System  $\text{LiF}-\text{BeF}_2-\text{UF}_4-\text{ThF}_4$ , ORNL-2896 (Dec. 27, 1960).
8. J. H. Shaffer *et al.*, Nucl. Sci. Eng. 18, 177-81 (1964).
9. Reactor Chem. Div. Ann. Progr. Rept. Jan. 31, 1963, ORNL-3417, p. 38; C. F. Baess, Jr., J. H. Shaffer, and H. F. McDuffie, Trans. Am. Nucl. Soc. 6(2), 393 (1963); Reactor Chem. Div. Ann. Progr. Rept. Jan. 31, 1964, ORNL-3591, p. 45.
10. Reactor Chem. Div. Ann. Progr. Rept. Jan. 31, 1964, ORNL-3591, p. 4.
11. Reactor Chem. Div. Ann. Progr. Rept. Jan. 31, 1963, ORNL-3417, p. 5.
12. W. R. Grimes, Nucl. News 7(5), 3-8 (1964).
13. MSRP Semiann. Progr. Rept. Jan. 31, 1963, ORNL-3419, pp. 116-19.
14. Reactor Chem. Div. Ann. Progr. Rept. Jan. 31, 1964, ORNL-3591, pp. 52-53.

15. M. H. Rand and O. Kubaschewski, The Thermochemical Properties of Uranium Compounds, Interscience, New York, 1963.
16. Reactor Chem. Div. Ann. Progr. Rept. Jan. 31, 1964, ORNL-3591, pp. 46-50.
17. MSRP Semiann. Progr. Rept. Jan. 31, 1964, ORNL-3626, pp. 119-20.
18. L. Brewer et al., The Thermodynamic Properties and Equilibria at High Temperatures of Uranium Halides, Oxides, Nitrides, and Carbides, MDDC-1543 (1945).
19. W. R. Grimes et al., "Radiotracer Techniques in the Study of Corrosion by Molten Fluorides," pp. 559-74 in Proceedings of Conference on the Uses of Radioisotopes in the Physical Sciences and Industry, Copenhagen, Sept. 16-18, 1960, vol. 3, IAEA, Vienna, 1962.
20. C. M. Blood, Solubility and Stability of Structural Metal Difluorides in Molten Fluoride Mixtures, ORNL-CF-61-5-4 (Sept. 21, 1961); and C. M. Blood et al., "Activities of Some Transition Metal Fluorides in Molten Fluoride Mixtures," in Proceedings of the International Conference on Coordination Chemistry, 7th, Stockholm and Uppsala, June 25-29, 1962, Butterworths, London, 1963.
21. W. H. Cook, "Evaluation of MSRE Graphite," Metals and Ceramics Div. Ann. Progr. Rept. July 1, 1963, ORNL-3420, pp. 165-67.
22. L. G. Overholser and J. P. Blakely, "The Degassing Behavior of Commercial Graphites," in Proceedings of the Fifth Conference on Carbon, Pergamon, 1962.
23. MSRP Semiann. Progr. Rept. Jan. 31, 1963, ORNL-3419, pp. 122-27.
24. MSRP Semiann. Progr. Rept. Aug. 31, 1961, ORNL-3215, p. 93.
25. J. L. Crowley, MSRP Semiann. Progr. Rept. Jan. 31, 1958, ORNL-2474, p. 31.
26. Reactor Chemistry Div. Ann. Progr. Rept. Jan. 31, 1960, ORNL-2931, pp. 69-70.
27. W. R. Grimes, N. V. Smith, and G. M. Watson, J. Phys. Chem. 62, 862 (1958); M. Blander et al., J. Phys. Chem. 63, 1164 (1959); G. M. Watson et al., J. Chem. Eng. Data 7(2), 285 (1962).
28. W. T. Ward et al., Solubility Relations Among Rare-Earth Fluorides, ORNL-2749 (Oct. 13, 1959).
29. A. J. Singh, G. D. Brunton, and R. E. Thoma, Zone Melting of Inorganic Fluorides, ORNL-3658 (to be published).

EFFECTS OF RADIATION ON THE COMPATIBILITY OF MSRE MATERIALS

F. F. Blankenship

Summary

Postirradiation examination of the several capsules from three in-pile tests of MSRE fuel-graphite-metal compatibility continues to furnish evidence of evolution of  $F_2$  and  $CF_4$ , graphite damage, and other potentially unfavorable phenomena. All cases of unusual behavior, however, seem to be consequences of  $F_2$  generation at low temperatures under conditions which will not normally obtain in MSRE.

Radiolytic formation of  $F_2$  at temperatures below  $100^\circ C$  was observed over a 5-month interval in two capsules that were fitted for sampling of the evolved gases. Fluorine release proceeded at a maximum rate near room temperature ( $G = 0.01$  to  $0.02$  molecule of  $F_2$  per 100 ev absorbed) and decreased to zero rate at  $-70^\circ C$  and  $+80^\circ C$ . At the low temperature, slow diffusion in the crystals presumably limited the evolution rate, while at high temperatures the back reaction of radiolytic products appeared to be controlling. Deliberate addition of  $F_2$  produced results which confirmed this picture and which demonstrated that  $F_2$  reacts more rapidly with salt which has previously lost most of its  $F_2$  radiolysis. These observations conclusively eliminated the specter of fluorine generation at reactor operating temperatures. In reactor components such as freeze valves or freeze flanges and in tanks for storage of irradiated salt, however, the temperature must be kept high enough ( $200^\circ C$  seems sufficient) to prevent salt radiolysis.

Chemical analyses of graphite cores from the large capsules of one assembly revealed the presence of appreciable (0.1 to 0.5 wt %) quantities of uranium, as well as molybdenum, lithium, and container metals. Autoradiography, before and after neutron activation, and x radiography of transverse sections of the cores showed that the uranium was present in a 2-mil-thick layer on the surface of the specimens. Neutron activation analyses gave slightly lower results for uranium than those obtained by chemical analyses. The deposition of uranium is believed to have been a consequence of fuel radiolysis during reactor shutdowns in the course of the in-pile exposure. To test this conjecture, the design of the last in-pile experiment (47-6) provided for heaters on each capsule to prevent radiolysis during shutdown. The performance of this experiment supported, in every way tested, the conclusion that the MSRE components are compatible for use as designed, and the gross visual appearance of the components on disassembly of the experiment has given further support to this conclusion. The components (INOR-8, graphite, salt, and molybdenum specimens) have been separated and packaged for return to ORNL and detailed hot-cell examination.

Introduction

Many familiar examples of systems displaying stability at high temperatures depend on the formation of protective films; but the MSRE fuel-metal-graphite compatibility relationships are not among these. As indicated in the preceding chapter, the components of the fluoride melts used as a fuel are chosen with a view toward complete thermodynamic stability with respect to nickel alloys and graphite, and the resulting combination is substantially corrosion free, isothermally at least, without the intermediation of interfacial films. Pertinent details of corrosion-related behavior of the fuel that have been described previously present no phenomena which obviously render them inherently susceptible to adverse effects from fissioning. The possibility that off-equilibrium species might cause undesirable effects has been examined experimentally and found to be vanishingly small or beyond the limit of detection. However, the history of these experiments provides some interesting sidelights, particularly in connection with the difference in behavior of crystalline and molten fuel.

There exists, as a legacy from the ANP Program, an impressive and reassuring collection of irradiation experiments involving fissioning molten fluorides in contact with nickel-based alloys - more than 100 exposures to reactor irradiation in various fluoride mixtures in Inconel capsules and three in-pile forced-circulation loop experiments. The conclusion, as stated on May 1, 1958, was as follows:<sup>1</sup>

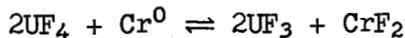
"Within the obvious limitations of the experience up to the present time, there is no effect of radiation on the fuel and no acceleration of corrosion by the radiation field."

But, less was known about the compatibility of graphite with fissioning fuel. Owing to the chemical inertness of graphite with respect to the fuel, there was little reason to suspect gross corrosive effects, but the interfacial behavior was a matter of concern.

The fuel, because of its high surface tension, does not soak into the pores of graphite. It was of great importance to ensure that such a favorable interfacial behavior persisted in spite of irradiation effects, since about 10% of the volume in the core is comprised of the voids in graphite.

Another point of interest for long-term operation is the nature of the deposition of the noble metals produced as fission products. When a uranium cation fissions, the resulting fission fragments correspond, on the average, to cations having a combined valence of about +3.4 in place of the +4 of the uranium cation. The exact replacement valence deficiency depends on the rate of removal of short-lived xenon and krypton that decay to cation-forming elements and also, more importantly, on the fact that the valences adopted by the fission products will be those for equilibrium with the chromium metal at the chemical activity chromium possesses in the INOR-8 container. The net effect is a gradual chemical oxidation at a rate which would increase the Cr<sup>2+</sup> concentration in the

MSRE by about 50 ppm/year. Concurrently, there is a deposition of fission products such as molybdenum and ruthenium as elemental metals. In practice, the change in oxidation level of the fuel (i.e., in the  $\text{UF}_4$  to  $\text{UF}_3$  ratio) is readily adjusted by scheduled reprocessing treatments, and any mismatch with the corrosion equilibrium



is spontaneously corrected by a shift in concentrations toward values corresponding to equilibrium.

An underlying premise of the foregoing considerations was that the chromium in the INOR-8 container remains available as a reducing agent, and that this is the main factor influencing the deposition of noble metals. Should the INOR-8 become plated with noble metals, then occasional reprocessing may be necessary to prevent the slow oxidizing effect of fissioning from tending to release iodine and tellurium from the fissioning fuel.

#### Preliminary Experiments

Beginning in 1960, a sequence of in-pile experiments was directed toward resolving uncertainties regarding the compatibility, under irradiation, of MSRE components.

The first two of these, Experiments 47-1 and 47-2, were essentially duplicates and suffered from an experimental shortcoming such that the results were quite limited and need only brief mention. The experimental difficulty derived from an attempt to maintain pressure on the irradiated system by using a bellows completely filled with salt as the capsule wall submerged in a pressurized bath of liquid sodium. Freeze-thaw cycles during operation of the pile led to rupture of the bellows and to the loss of seven out of eight capsules. The tendency to rupture was probably aggravated by fluorine gas that might have been present in accord with phenomena to be described below.

The single surviving capsule gave generally reassuring results in that the surface of a graphite core appeared unaffected by exposure to fissioning fuel. Numerous observations with a microscope of metallographically mounted sections of the graphite indicated that no significant penetration of the graphite by salt had occurred and that the graphite appeared unchanged.

Autoradiographs and radiochemical analyses showed minor intrusions of fission products into the graphite by two mechanisms. There were a few fissures or faults in the graphite that were repositories for fission product radioactivity resembling that in the fuel. Otherwise the activity in the interior of the graphite was quite low. The other mode of pickup of activity may have been augmented by diffusion of gases; this was in the form of an annulus of activity at the circumference of the graphite core. The inner fringe of this annulus, as studied by drilling

with a hypodermic needle and gamma spectroscopy of the drillings, showed only one major gamma activity, that of cesium. Approximately two-thirds was  $^{134}\text{Cs}$  and one-third was  $^{137}\text{Cs}$ ; the decrease in concentration with increasing penetration suggested that the cesium was deposited by xenon that diffused into the graphite, but there were discrepancies that prevented establishment of this mechanism with certainty.

### Experiment 47-3

While it appeared from the preliminary trials that nothing drastic happened to graphite when irradiated in the presence of fuel, there were still several questions on which further information was desired. For example, the matter of the penetration of the moderator by fuel was sufficiently important to require further confirmation.

A 1 to 2% permeation of the graphite by fuel could be tolerated in reactor operation. But, should penetration attain or exceed the 4% accessible voids in the graphite, as might occur if the wetting characteristics changed during operation, serious difficulties with reactor control could be anticipated. Initially, this problem was thought to be the most serious one the MSRE faced; several design features such as an increased ratio of core volume occupied by fuel to that occupied by moderator, diluting the  $^{235}\text{U}$  content of the salt, and increasing the capacity of the control elements were invoked to reduce the seriousness of a change in wetting behavior to manageable proportions. But there was still a question regarding the extent of fission fragment damage that could occur in the matrix of permeated graphite.

As far as was known at the time, radiation-induced wetting might have been caused by two possible paths: (1) changes in the surface tension of the molten salt by fission products and (2) alteration of the surface energy of the graphite by either radiation damage or chemical interaction such as the formation of carbides or interlamellar compounds, although most of such mechanisms appeared unlikely. Since graphites of varying degrees of graphitization had been shown to exhibit no wetting by the fuel, there was little reason to suspect that damaged graphite would show an enhanced tendency to wet.

In evaluating the integrity of the moderator, one factor which was considered was the stripping of the surface of carbon atoms by the energy deposited in the surface layer by fission fragments. If it were assumed that each fission fragment striking the surface sputters 20 carbon atoms, and that the mean fragment range normal to the surface was  $10 \mu$ , then for  $10^9$  fragments/sec incident on  $1 \text{ cm}^2$  of surface,  $2 \times 10^{10}$  carbon atoms would be sputtered per  $\text{cm}^2$  per second. This amounts to about one atom layer per day, a relatively negligible amount of graphite.

Another potential problem centered on the possibility that a portion of voids near the surface of the graphite might become occupied by salt and that fission heat produced in these regions might develop more rapidly than it could be removed by thermal transport. This could lead to fragmentation of the surface layer adjacent to the void, but probably the salt would merely expand into interconnecting voids.

The fission fragment range in graphite is about  $20 \mu$ , and graphite within this distance of the fuel could be severely damaged. Little is known about the nature of fission fragment damage in graphite; but, if it is an accentuation of the effect of fast neutrons, it could conceivably cause contraction to such a degree that microscopic checking would occur. Progressive and cumulative fission fragment damage could then proceed, with a resulting spalling off of surface material.

Still another problem was the possibility of chemical attack by reactive fission products. The two most likely agents, because of both chemical behavior and fission yield, were the halogens bromine and iodine. It is well known that halogens form intercalation compounds with graphite. Extensive compound formation leads to a separation of the graphite layers and eventual breakup of the material. In the fuel the halogens would exist in the atomic state only during an exceedingly brief transitory period, and their concentration would probably be too low to give a detectable amount of reaction.

During steady irradiation, iodine reaches a maximum yield of 0.13 atom/fission at  $10^4$  sec, from which it declines to a small value at longer times. At the end of 10 days' operation, the surviving yield is only about 0.03 atom of iodine per fission, and this would be in the form of iodide under reactor operating conditions. The bromine accumulation is lower than this value by an order of magnitude. Therefore, chemical attack is not expected to be a serious factor for moderator integrity.

The extent of carburization of the reactor vessel or the metal components is another detail that requires consideration. Mild carburization is of little concern, but enough carburization to cause a hard case is another matter. Sacrificial pieces of INOR were used to prevent the graphite pieces from contacting structural members to avoid damage from carburization in the MSRE.

#### Description of Experiment

Relatively extreme exposure conditions were used to accentuate the effects of fissioning in Experiment 47-3. A power density of  $200 \text{ w/cm}^3$  was developed by adjusting the concentration of  $^{235}\text{UF}_4$  to 1.5 mole % instead of the 0.3 mole % to be used in the MSRE. Consequently, the four 3-week cycles in the MTR, accumulating 1594 hr at power, gave a burnup of 8.5% in comparison with the 6%/year anticipated for the MSRE at 10 Mw. The contact angle of the fuel meniscus was chosen as a convenient and reliable index of possible changes in wetting.

To make the contact angle manifest, a vertical blade of graphite was arranged to dip into a pool of fuel (11.4 g or 5 ml) in a graphite boat, as shown in Fig. 1. A step along a portion of the length of the bottom or submerged edge of the blade extended to within  $1/16$  in. of the floor of the pool of salt; molten fuel, with a surface tension of about 200 dynes/cm, does not normally penetrate a  $1/16$ -in. crevice without pressurization, and thus another device for detecting wetting behavior was incorporated in the capsule design.

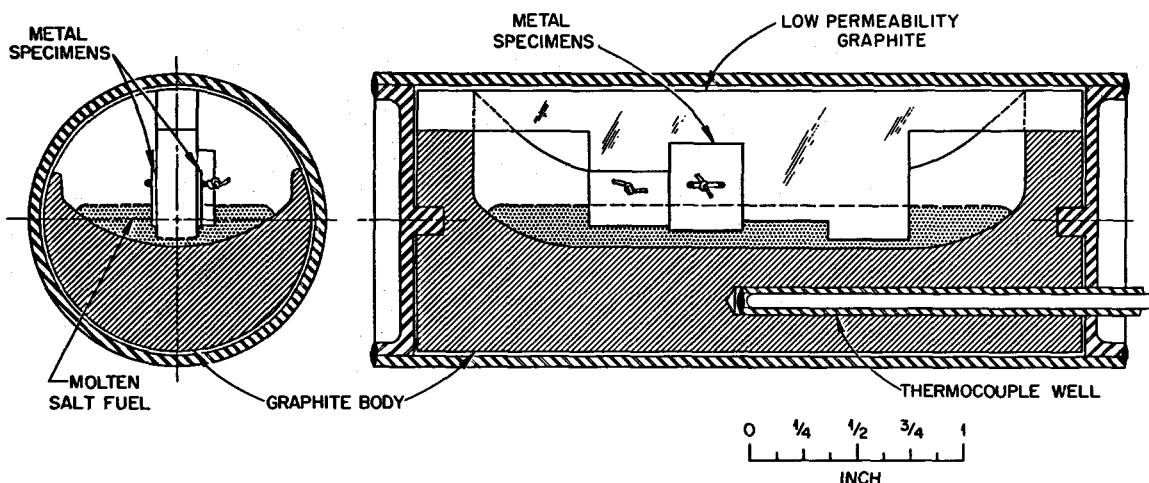
UNCLASSIFIED  
ORNL-LR-DWG 56754

Fig. 1. MSRE Graphite-Fuel Capsule Test, ORNL-MTR-47-3.

There was room in the irradiated assembly for four capsules holding boats 3 in. long by 1-1/4 in. wide. To provide a contrast in behavior and to answer questions regarding the effects of penetrated fuel, two of the boats were prepermeated with fuel. This was accomplished by transferring fuel into a previously evacuated container holding AGOT graphite boats and using an overpressure of 60 psig of helium above the submerged boats. AGOT graphite is sufficiently permeable that this allowed 9 g of fuel to penetrate the boat (66 g). The fuel was LiF-BeF<sub>2</sub>-ZrF<sub>4</sub>-ThF<sub>4</sub>-UF<sub>4</sub> (69.5-23-5-1-1.5 mole %) purified by treatment at 800°C with HF and H<sub>2</sub>. The other two boats, as well as all the blades (3/16 in. wide), were R-0025 graphite, a relatively impermeable grade.

To gain further information from the irradiation, coupons of INOR-8, pyrolytic graphite, and molybdenum were attached to the blade in a manner such that the liquid level of the fuel extended half way up the coupons. This was to provide a contrast between vapor and liquid contact.

The capsules were arranged in the sodium bath so that capsules 3 and 8 were at the top and bottom of a diamond array, and capsules 15 and 16 were at the midplane. The upper capsule ran hotter than the lower one because of thermal convection in the sodium. Capsules with preimpregnated fuel in the graphite boats (3 and 8) ran hotter than the capsules with R-0025 graphite boats (15 and 16). The resulting temperatures, as given in Table 1, were relatively high in comparison with MSRE operating temperatures.

Table 1. Time-Averaged Operating Temperatures and Identification of Irradiated Capsules

| Capsule No. | Graphite <sup>a</sup> | Pretreatment                    | Average Operating Temperature (°C) |                                     |                                    |                          |
|-------------|-----------------------|---------------------------------|------------------------------------|-------------------------------------|------------------------------------|--------------------------|
|             |                       |                                 | Fuel, Maximum (estimated)          | Blade Fuel <sup>b</sup> (estimated) | Boat Fuel <sup>b</sup> (estimated) | Thermocouple in Graphite |
| 15, 16      | R-0025                | 2000°C in vacuum                | 835                                | 790                                 | 730                                | 710                      |
| 8           | AGOT                  | Preimpregnated with 9 g of fuel | 850                                | 810                                 | 750                                | 730                      |
| 3           | AGOT                  | Preimpregnated with 9 g of fuel | 945                                | 900                                 | 850                                | 825                      |

<sup>a</sup>R-0025 graphite is relatively impervious compared to AGOT.<sup>b</sup>Interface temperatures; no allowance for films at the fuel interface was made.

### Results of Experiment

After irradiation was completed, on July 27, 1961, the in-pile assembly was dismantled. The individual capsules were punctured by a hermetically sealed drilling rig so that the released cover gas could be collected by a Toepler pump for analyses.

Although the main results of the experiment were that no change in wetting behavior had occurred, the most surprising results were found in the gas analyses shown in Table 2. As could be later surmised, in light of subsequent experiments, the CF<sub>4</sub> that was found came from F<sub>2</sub> evolved from radiation damage to the fuel at room temperature (during intermediate shutdown periods of the MTR). The much lower yield of CF<sub>4</sub> from capsules 3 and 8 as contrasted with 15 and 16 is believed to be a consequence of higher F<sub>2</sub> yield in capsules 15 and 16. This is consistent with the fact that the expected amount of xenon is found in capsules 3 and 8 but is

Table 2. Off-Gas Compositions

(averaged values from mass spectrometric results obtained at ORNL and BMI)

| Capsule No.          | Standard cm <sup>3</sup> Sampled <sup>a</sup> | Components (vol %) |       |                 |       |      |                 |                 |
|----------------------|---|--------------------|-------|-----------------|-------|------|-----------------|-----------------|
|                      |   | Air <sup>b</sup>   | He    | CF <sub>4</sub> | Xe    | Kr   | CO <sub>2</sub> | Ar <sup>c</sup> |
| 15                   | 10  | 5.84               | 80.6  | 9.85            | 0.012 | 1.40 | 0.04            | 2.29            |
| 16                   | 19  | 22.75              | 61.45 | 8.73            | 0.003 | 1.14 | 4.73            | 1.62            |
| 8                    | 7   | 5.36               | 76.9  | 2.32            | 11.82 | 1.96 | 0.11            | 4.20            |
| 3                    | 17  | 4.57               | 79.6  | 0.67            | 11.43 | 1.78 | 0.10            | 0.96            |
| Control <sup>d</sup> | 10  | 7.38               | 87.0  | <0.0003         |       |      | 0.17            | 5.54            |

<sup>a</sup>Apparent volume of gas transferred from gas-release chamber.<sup>b</sup>Mainly inleakage to the evacuated release chamber while drilling the capsules.<sup>c</sup>Argon was supplied as a blanket gas for the welding arc used in a helium-atmosphere glove box to seal the capsules.<sup>d</sup>The control was heated through cycles roughly corresponding to the thermocouple reading vs time for capsules 15 and 16.

missing from capsules 15 and 16. A lack of xenon is now associated with the presence of sufficient  $F_2$  to form the relatively nonvolatile xenon fluorides, although, indeed, the existence of such compounds was not discovered until after the low xenon yields had remained a perplexing problem for months. Needless to say, the formation of  $CF_4$  had also been quite perplexing until it was realized that  $F_2$  which had evolved at room temperature had been responsible. The difference in the  $F_2$  yields in the two types of capsules has not been explained but is thought to be related to the freezing history of the crystals. Slower freezing, according to one hypothesis, produces crystals that are both larger and less strained and, consequently, less vulnerable to radiation damage. This could conceivably account for the low  $F_2$  yields in capsules 3 and 8, which contained prepermeated graphite and could have cooled more slowly than capsules 15 and 16.

There was sufficient potential cause for alarm in the results of the gas analyses that the gas behavior tended to eclipse the initial purpose of the tests and the important favorable results in regard to the persistence of nonwetting behavior. The meniscus of the irradiated fuel was the same as that of the control specimens and showed definitely nonwetting behavior toward graphite; the metal coupons were wetted. Fuel was not found in the 1/16-in. clearance between the blade and boat but did fill the region under the blade, where the clearance was 1/8 in. The nonwetting behavior was confirmed by metallography of the graphite, which showed no evidence of penetration by salt.

Dimensions of the graphite parts did not change within the precision that measurements in the hot cell were made; changes greater than 0.1% should have been detectable. Weight changes were not very meaningful since they represented the combined effect of broken or lost graphite, of distilled salt condensed in the pores, and of some sticking salt that was difficult to remove. The information from weight changes was at least indicative of no pronounced permeation of the graphite by fuel.

The electrical resistance of the graphite approximately doubled as a result of the irradiation; such increases have been attributed to trapping conductance electrons in defects induced by radiation.

In looking for evidence of damage to the surface of the graphite, particular attention was paid to hardness tests. Rockwell hardness measurements on the R-0025 graphite increased from about 94 to 108 as a result of the exposure. The hardness of the AGOT graphite boats increased from about 56 to about 80 as a result of preimpregnation with salt, and the readings after radiation were not significantly higher. Most importantly, no differences were found between regions under the salt pool and chambers in the same boat; this was indicative that no measurable sloughing of the surface was occurring in response to fission fragment damage.

Autoradiography and gamma-ray spectrometry were used to study the distribution of activity in the capsule; no consistent patterns of unusual interest were found. In general, it was noted that the principal activity was  $Zr-^{95}Nb$  and that  $^{103-106}Ru$  tended to plate out at fuel interfaces.

Visually and photographically, the INOR-8 coupons initially appeared undamaged, although weight changes and metallography showed that the extreme conditions encountered by coupons had indeed caused appreciable amounts of corrosion. The extent to which the effects of  $F_2$  are shown in the results is difficult to assess but is probably large. The INOR-8 specimens lost about 1.5 mils in thickness and were carburized to a further depth of 1 to 2 mils. Molybdenum specimens from capsules 3 and 8 (low fluorine yield) appeared visibly much less corroded than those from capsules 15 and 16, in which the submerged molybdenum edges were corroded to resemble a knife blade. The molybdenum sample from capsule 15 lost 39 mg, or 15%, of its weight, and the thickness of molybdenum from capsule 16, originally 20 mils, varied from 7.5 to 13 mils.

Three of the pyrolytic-carbon samples showed no abnormalities in the metallographs or in dimensions, with the exception of a thin, unidentified black film on the specimen from capsule 16. The sample from capsule 15, however, showed a thickness decrease of 7 to 12 mils, and one spot of the metallographic cross section showed a leafing open of several layers of pyrolytic carbon at the surface. The rest (more than 95%) of the section appeared normal metallographically, with the usual incidence of cracks parallel to the carbon layers. The observed damage in this carbon may be related to the high-yield  $CF_4$  in the cover gas from this capsule; however, the possibility of mechanical damage during dismantling may not be excluded.

In general, the coupons underwent worse corrosion than was encountered in other capsule parts of this or subsequent experiments that presumably involved comparable amounts of  $F_2$ ; the extreme temperatures were the most obvious difference and must therefore have been primarily responsible for the accentuated corrosion.

#### Experiment 47-4

At the time the  $CF_4$  was encountered during the postirradiation examination of Experiment 47-3, the origin of the  $CF_4$  was not known except that it was coming from graphite and fuel. The  $F_2$  that undoubtedly accompanied the  $CF_4$  escaped detection in the gas train used for the collection and analysis of gas; the  $F_2$  reacted before it could be detected. Since fuel and graphite were not thermodynamically expected to react, the origin of the  $CF_4$  was very perplexing. It was assumed that  $CF_4$  formed at the fuel-graphite interface could somehow make its way into the voids in the graphite and there be preserved from reacting with the fuel in the manner that would have been expected for thermodynamic equilibrium. The configuration in the capsules of Experiment 47-3, which was a pool of fuel in a graphite boat, would have favored isolation of the  $CF_4$ . Accordingly, a new experiment was designed, in which central graphite cores were submerged in vertical cylinders of fuel. This configuration was pictured as perhaps accumulating  $CF_4$  in the voids in graphite; but because of the submersion of the graphite, the  $CF_4$  could not make its way to the capsule vapor space without a good opportunity to react with the fuel.

### Description of Experiment

The 47-4 assembly contained six capsules constructed of 1/16-in.-walled INOR-8 tubing. Each of four large capsules, Fig. 2, was 1 in. in diameter, 2.25 in. tall, and contained a CGB graphite core (1/2 in. in diameter by 1 in. long) submerged approximately 0.3 in. in about 25 g of fuel. The fuel generated from 67 to 117 w/cm<sup>3</sup>, depending upon capsule location. The temperature at the graphite-fuel interface was 730°C.

Two smaller capsules of the type shown in Fig. 3 were designed to study the effect of power density and temperature; they contained fuel to operate at 43 and 260 w/cm<sup>3</sup> at 720 and 900°C respectively; and, because they had graphite liners that extended into the gas space, they were thought to provide a favorable configuration for the accumulation of CF<sub>4</sub>. The experiment was irradiated in the MTR from March 12 to June 4, 1962, again in a molten-sodium heat transfer medium.

The large capsules were filled by a transfer of molten fuel of the nominal composition LiF-BeF<sub>2</sub>-ZrF<sub>4</sub>-ThF<sub>4</sub>-UF<sub>4</sub> (70-23.3-5-1-0.7 mole %). The small capsules were loaded with molded ingots of about 10 g of fuel, and in one of them a UF<sub>4</sub> concentration of 1.4 mole % was used.

Exposure data for assembly 47-4 are summarized in Table 3.

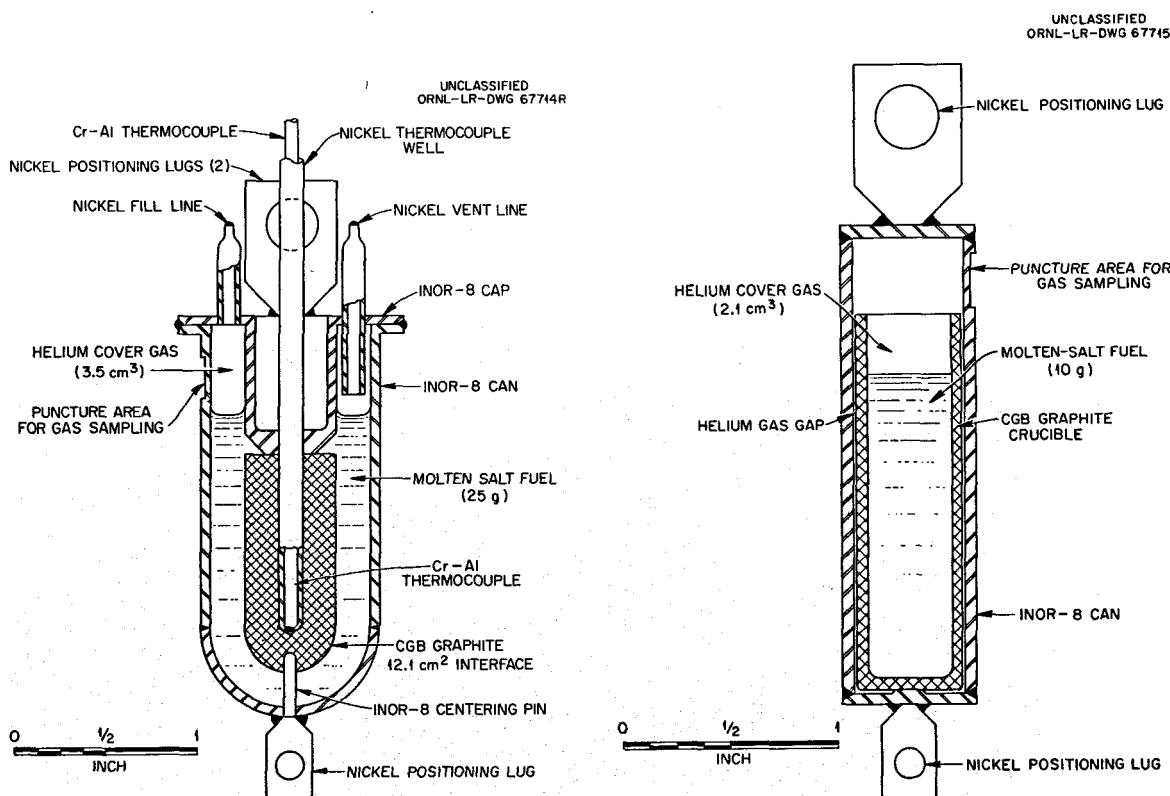


Fig. 2. Experiment MTR-47-4,  
Large Capsule.

Fig. 3. Experiment MTR-47-4,  
Small Capsule.

Table 3. Exposure Data for Capsules in Assembly 47-4

| Capsule<br>No.         | Uranium<br>Content<br>(mole %) | Thermal-Neutron<br>Flux <sup>a</sup> Based on<br>$^{60}\text{Co}$ Activation<br>(neutrons $\text{cm}^{-2} \text{ sec}^{-1}$ ) | Fast-Neutron<br>(>3-Mev) Flux<br>Based on $^{58}\text{Co}$<br>Activation<br>(neutrons $\text{cm}^{-2} \text{ sec}^{-1}$ ) | Temperature (°C)                           |  | Power<br>Density<br>(w/ $\text{cm}^3$ ) | Calculated<br>Burnup<br>(% $^{235}\text{U}$ ) |
|------------------------|--------------------------------|---|---|--|--|---|---|
|                        |                                |   |   | Graphite-to-Salt<br>Interface <sup>c</sup> | INOR-8-to-Salt<br>Interface <sup>b</sup> |   |   |
| $\times 10^{13}$       |                                |   |   | $\times 10^{12}$                           |  |   |   |
| Large                  |                                |   |   |  |  |   |   |
| 12                     | 0.7                            | 2.10  | 2.1   | 680  | 610                                      | 67                                      | 5.5   |
| 24                     | 0.7                            | 2.70  | 3.2   | 760  | 605                                      | 83                                      | 7.0   |
| 36                     | 0.7                            | 2.71  | 3.3   | 710  | 595                                      | 85                                      | 7.0   |
| 45                     | 0.7                            | 3.85  | 3.8   | 710  | 600                                      | 117                                     | 9.7   |
| Central Region<br>(°C) |                                |   |   |  |  |   |   |
| Small                  |                                |   |   |  |  |   |   |
| 4                      | 1.47                           | 4.79  | 5.2   | 895  | 260                                      | 11.4                                    |   |
| 6                      | 0.7                            | 1.31  | 1.3   | 715  | 43                                       | 1.3                                     |   |

<sup>a</sup>Average external neutron flux.<sup>b</sup>Estimated temperatures.<sup>c</sup>Thermocouple readings prior to termination of final irradiation cycle.

Results of Experiment

After 1553 hr of exposure between March 12 and June 4, 1962, the experiment was returned for disassembly in ORNL hot cells. The capsules again were punctured to obtain gas for analysis. The gas was delivered into a calibrated collection system that had been evacuated and checked for leaks. A Toeppler pump was intended for use in transferring gases collected at low pressures. The analyses were made by mass spectrometry.

Capsule 6, one of the crucible types, which had received the minimum exposure in the assembly, was the first to be punctured; its cover gas was found to contain 4.2 vol %, or  $0.07 \text{ cm}^3$ , of  $\text{CF}_4$ , which did not seem surprising in view of the fact that  $\text{CF}_4$  had been found in the 47-3 series.

The next capsule to be punctured was No. 24, and considerable amazement prevailed when the cover gas was found to be predominantly  $\text{F}_2$  gas. The  $\text{F}_2$  was first noticed when the mercury in the Toeppler pump was blackened by the transferred gas.

It was necessary to rebuild the gas-collection system of nickel and to pretreat the nickel with fluorine in order to provide the capability of measuring fluorine. When this was done, the gas from the remainder of the capsules was analyzed; the results are shown in Table 4. In the extreme case (capsule 45), about 3.5% of the total fluoride in the capsule was converted to  $\text{F}_2$  or  $\text{CF}_4$  in the gas phase; the resulting pressures were 50 atm of  $\text{F}_2$  and a tenth that much  $\text{CF}_4$ . Fortunately, these figures were high enough that it appeared very implausible that the  $\text{F}_2$  could have been present at operating temperatures. All the evidence combined to support the suggestion that the fluorine was evolved from low-temperature radiation damage to the frozen fuel rather than high-temperature radiolysis of molten fissioning fuel. The  $\text{CF}_4$  could then be explained as being derived from the subsequent interaction of the fluorine with graphite (perhaps in the brief period of temperature rise after the MTR shutdown was concluded). Two other factors were associated with the presence of  $\text{F}_2$ . In the first place, whenever  $\text{F}_2$  was found, xenon was absent. This was recognized to be a consequence of the then newly discovered compounds of xenon and fluorine. In the second place, a prominent radioactivity due to  $^{129}\text{Te}$  accompanied the  $\text{F}_2$  and hampered studies of the gas. This afforded a contrast between the mildly reducing conditions anticipated at operating temperatures where no  $^{129}\text{Te}$  activity was expected and conditions such that  $\text{F}_2$  was being produced, in which case  $^{129}\text{Te}$  activity was volatilized from the salt as  $\text{TeF}_4$  or  $\text{TeF}_6$ .

At these temperatures, fluorine at any appreciable pressure should have reacted violently with the graphite and noticeably with the INOR-8. A longitudinal section through capsule 24 (Fig. 4) did not reveal any visual evidence of corrosion of metal or damage to graphite. A metallographic examination of a section of the wall of this capsule (Fig. 5) showed no evidence of damage.

Assuming that half of the decay energy released during the 95-day cooling period was absorbed in the fuel, a G value of 0.035 (molecules

Table 4. Data on  $F_2$  and  $CF_4$  Produced Following an Exposure of Experimental Assembly ORNL-MTR-47-4 to an Integrated Flux of  $10^{20}$  neutrons/cm<sup>2</sup>

| Capsule Identification            | Fission Power Density <sup>a</sup><br>(w/cm <sup>3</sup> ) | Krypton Found<br>(% of theoretical) | Xenon Found<br>(% of theoretical) | Milliequivalents of F in Gas per Millimole of U Burned | Decay Period (days) | Total F in Gas (meq) | Total F Converted to $CF_4$ (%) |
|-----------------------------------|--|-------------------------------------|-----------------------------------|--|---------------------|----------------------|---------------------------------|
| <b>Small capsules<sup>b</sup></b> |  |                                     |                                   |  |                     |                      |                                 |
| 6                                 | 43   | 145                                 | 140                               | 0.2  | 63                  | 0.012                | 100                             |
| 4                                 | 260  | 85                                  | 0                                 | 23.4   | 137                 | 8.6                  | 8.5                             |
| <b>Large capsules<sup>b</sup></b> |  |                                     |                                   |  |                     |                      |                                 |
| 24                                | 83   | 140                                 | 0                                 | 28.0   | 71                  | 8.2 <sup>c</sup>     | 31.4                            |
| 36                                | 85   | 125 <sup>d</sup>                    | 0                                 | 59.6   | 95                  | 17.2                 | 18.2                            |
| 45                                | 117  | 65                                  | 0                                 | 61.5   | 134                 | 25.3                 | 15.5                            |
| 12                                | 67   | 130                                 | 0                                 | 72.9   | 141                 | 16.7 <sup>c</sup>    | 57.2                            |

<sup>a</sup>Calculated from cobalt activity in stainless steel dosimeter wire.

<sup>b</sup>Capsules listed in order of sampling.

<sup>c</sup>Flourine analyses were corrected to include fluorine reaction products formed during sampling.

<sup>d</sup>An average based on Kr-to-He and Kr-to- $CF_4$  ratios in three confirmatory samples; direct analyses from the first samples were higher by a factor of 2.

UNCLASSIFIED  
R-11213

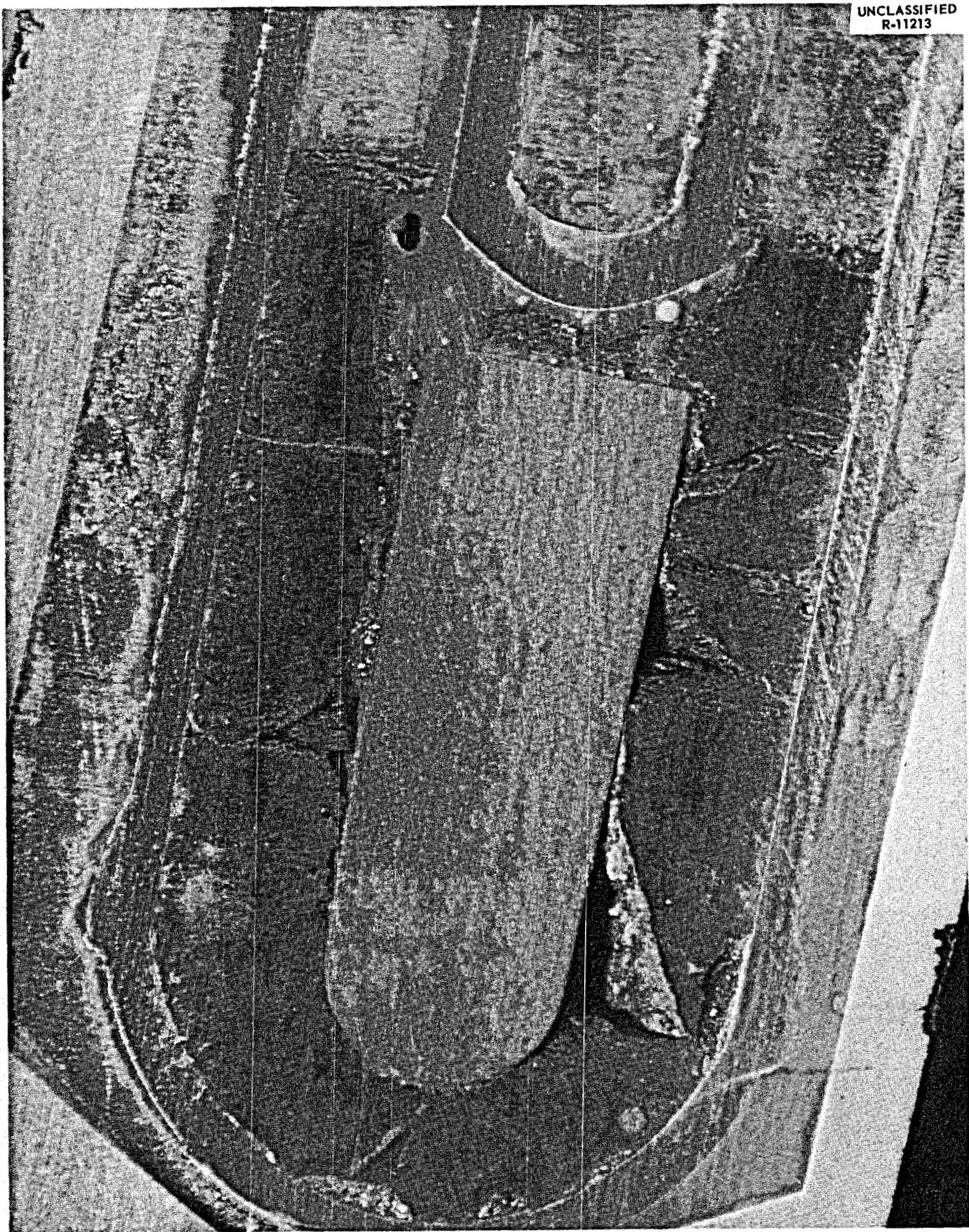


Fig. 4. Cross Section of Capsule 24 Embedded in Resin.

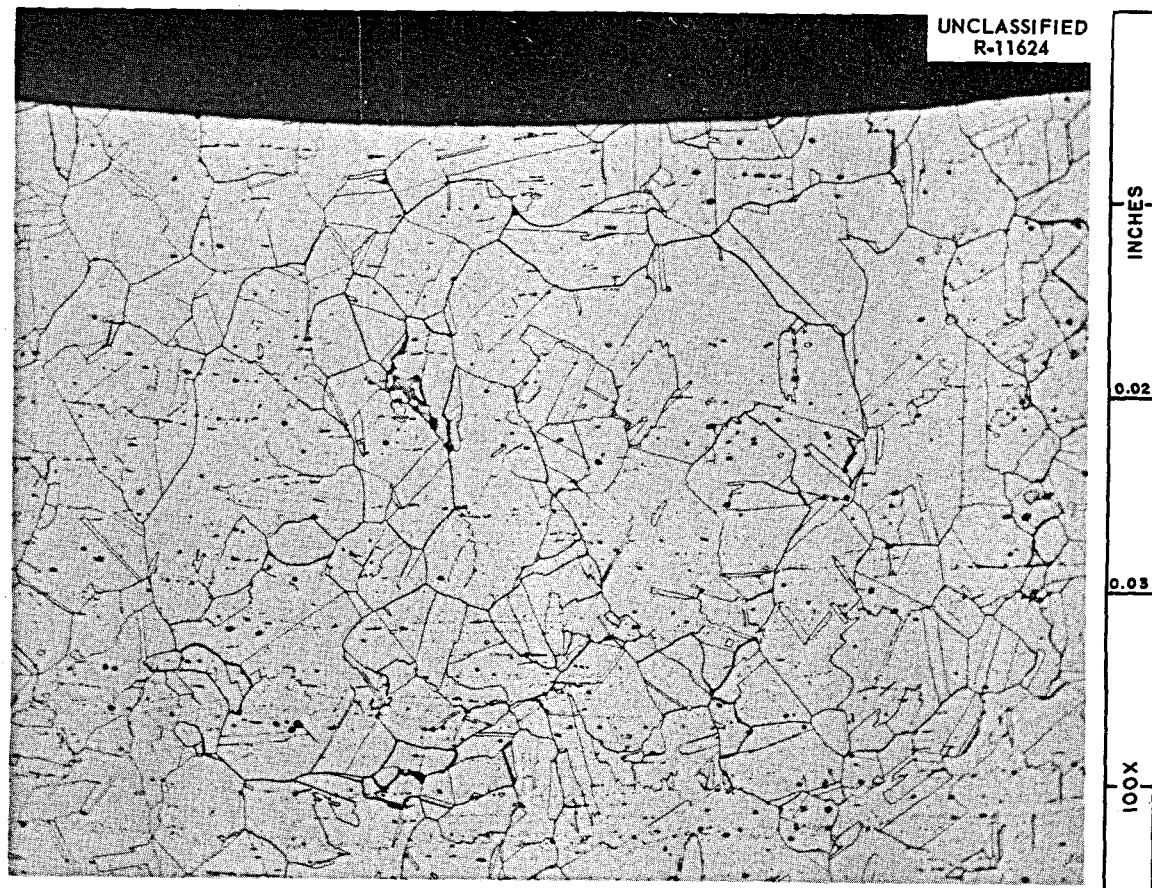


Fig. 5. Longitudinal Section at Bottom of Wall of Capsule 24, MTR-47-4.

of  $F_2$  per 100 ev of energy absorbed) would have been required to produce the fluorine found in capsule 36. However, a wide and puzzling variation in the amount of  $F_2$  production from different capsules was apparent.

Subsequently, all the capsules were opened for examination. Although the fuel was darkened by radiation damage to the point that it appeared black, the fuel showed no unusual tendency to crumble or shatter. One bit of curious behavior, not found in the out-of-pile controls, was the occurrence of bubbles in the fuel. The bubbles were attached to the metal at the bottom hemispherical section of the capsules and appeared to be associated with nonwetting of the metal by fuel. The bubbles are thought to have been formed in response to the difference in helium solubility along the temperature gradient in the capsule.

Metallographs of the metal and of the graphite were prepared. There was no evidence of attack on the INOR-8 and, with one exception, the same was true of the graphite. Capsule 4 contained graphite in the form of a liner. The portion of the liner that projected above the liquid level appeared to have been attacked by fluorine.

Small samples of salt from the irradiated capsules have been examined carefully with the optical microscope to determine the nature of the crystalline material. These materials are, in general, and as is frequently the case for rapidly cooled specimens, too fine grained to be positively identified. However, a sample from near the graphite at the center of capsule 24 has been shown to contain the normally expected phases, though some are discolored and blackened; these phases included  $7\text{LiF}\cdot 6\text{ThF}_4$ , which was shown to contain  $\text{UF}_4$  (green in color) in solid solution. It seems certain, therefore, that the uranium was not markedly reduced at the time the fuel was frozen.

An attempt was made, with capsule 35, to remove the salt by melting under an inert atmosphere to provide representative samples for chemical analysis and, especially, for a determination of the reducing power of the fluorine-deficient salt. This melting operation was not successful since only about one-half of the salt was readily removed in this way. That portion which melted and flowed from the capsule was green in color and obviously contained some tetravalent uranium. Since the salt was highly reduced - 2% of the fluorine, approximately equivalent to that as  $\text{UF}_4$ , had been lost - melting of the material would be expected to result in deposition of some metal; this metal may have resulted in a high-melting heel of uncertain composition.

A variety of chemical analyses were performed on materials from these capsules. No evidence of unusual corrosion behavior was observed in any of the analyses.

Salt specimens have been examined by gamma-ray spectrometry to evaluate gross behavior of fission product elements. In general, the ruthenium activity appears to be concentrated near the bottom of the capsules; this may indicate its existence largely in the metallic state so that a gravity separation could occur. Cerium as well as zirconium-niobium activity appears, as expected, to be fairly evenly distributed in the fuel. Some cesium, with some zirconium-niobium activity, is found on metal surfaces exposed to the gas phase.

After the graphite cores were removed from capsules 45 and 12 and examined, they were stored in screw-cap plastic bottles for 5 months. The necessary manipulation involved many hours of exposure to hot-cell air. On removal from storage, the graphite was heated to  $1000^\circ\text{C}$  under vacuum, and the evolved gases were collected for analysis by mass spectrometry. Xenon was recovered in an amount of 7.5% of the originally anticipated yield on the basis of the burnup.

The xenon fluorides should not have remained as such in the graphite during the long exposure to air because of both their sublimation pressure and their reactivity to form the nonvolatile  $\text{XeO}_3$ . The  $\text{XeO}_3$  molecule has a dipole moment and should adsorb on graphite much more readily than the symmetrical  $\text{XeF}_4$ ; however, the dipole moment of  $\text{XeO}_3$  is probably not large because of the compensating effect of the unshared electrons on the xenon atom at the apex of a triangular pyramid with three oxygens at the base at  $\text{Xe-O}$  distances of 1.76 Å and O-Xe-O angles of  $103^\circ$ . Oxygen that might

have resulted from decomposition of  $\text{XeO}_3$  during heating was apparently converted to CO.

Large pieces of sample (0.8 g or more), for which the ratio of mass-to-surface area originally exposed to the salt was similar to that for the entire core of the MSRE, were analyzed chemically to produce the data shown in Table 5. These data show that of all constituents of the fuel, uranium, lithium, and molybdenum were selectively concentrated in the graphite; analyses from capsule 36, whose fuel was removed by melting, were not notably different from the others. The mechanism by which deposition in the graphite occurred is not known; but subsequent examinations, including metallography, agreed with the chemical analyses that it was not by penetration as fuel. Tests by chemical leaching and by metallographic examination showed that there was no deposition of uranium in or on the metal (INOR-8) capsule walls.

Circular cross sections of the graphite cores were activated in the ORNL Graphite Reactor at a flux of  $5 \times 10^{11}$  neutrons  $\text{cm}^{-2} \text{ sec}^{-1}$  for 8 hr. Contact autoradiography before and after the activation showed that the uranium was in the outer rim, and gamma spectrometry provided a measure of the amount present. The results by activation analyses are compared with those by chemical analyses in Table 6. The chemical analyses suggest a correlation of deposited uranium with power level (or perhaps with the consequent rate of  $\text{F}_2$  generation after irradiation). Analysis by neutron activation, which should probably be preferred because of the simplicity and directness of the technique, does not support such a correlation. Both analyses, however, show the deposition to be substantial; if the graphite contains 1 mg of uranium per gram, it has taken up about 0.5% of all uranium in the capsule.

Contact autoradiography showed a high concentration of radioactivity from fission products (presumably mostly from daughters of gaseous products) to a depth of about 0.2 mm in the periphery of the graphite cross sections. Neutron activation did not appreciably affect this radioactivity; this indicated that the uranium was in the same region as the fission products.

A closer resolution of the uranium distribution was obtained from x radiography by a technique (recently developed in the ORNL Metals and Ceramics Division) in which the interference from fission product activity is negligible. The main deposit of uranium penetrated the graphite to a depth of less than 0.05 mm; however, there were also fringed proliferations that extended perhaps three times as deep. Facilities for attempted identification by x-ray diffraction are nearing completion, but nothing is yet known of the chemical form of the uranium in the graphite.

It seems clear that uranium is deposited in the outer layers of the graphite but not on or in the metal wall and that uranium, lithium, molybdenum, and other metallic constituents of INOR-8 are deposited in the graphite in preference to beryllium, zirconium, and thorium. Mechanisms, such as oxidation to  $\text{UF}_6$  or reduction to  $\text{UF}_3$  and to uranium and formation of  $\text{UC}_2$ , for which the situations resulting from  $\text{F}_2$  release might provide

Table 5. Chemical Analyses on Samples from ORNL-MTR-47-4 Graphite-Fuel Compatibility Test

|                         | Composition (wt %) |        |        |         |                 |        |        |                 |        |        |
|-------------------------|--------------------|--------|--------|---------|-----------------|--------|--------|-----------------|--------|--------|
|                         | U                  | Li     | Zr     | Be      | Th              | Ni     | Cr     | Fe              | Mn     | Mo     |
| Original fuel           | 3.89               | 11.6   | 10.1   | 4.8     | 5.8             | 0.0025 | 0.0024 | 0.0096          |        |        |
| Irradiated fuel         |                    |        |        |         |                 |        |        |                 |        |        |
| Capsule 12              | 3.36<br>4.08       |        |        |         |                 | <0.018 | <0.004 | <0.004          | <0.001 | <0.013 |
| Capsule 45              | 3.96<br>3.81       |        |        |         |                 | 0.016  | <0.007 | <0.007          | <0.007 | <0.025 |
| Graphite                |                    |        |        |         |                 |        |        |                 |        |        |
| Capsule 12              | 0.136              | 0.04   | <0.017 | 0.0008  | ND <sup>a</sup> | 0.013  | 0.014  | ND <sup>a</sup> | 0.019  | 0.062  |
| Capsule 24              | 0.214              | 0.052  | 0.0054 | 0.003   |                 | 0.015  | <0.012 | <0.015          | <0.005 | 0.089  |
| Capsule 36              | 0.13               | 0.06   | 0.004  | 0.0003  |                 | <0.03  | 0.01   | <0.006          |        | 0.04   |
| Capsule 45              | 0.523              | 0.062  | <0.016 | 0.002   | ND <sup>a</sup> | 0.01   | 0.04   | ND <sup>a</sup> | 0.01   | 0.062  |
| Capsule 3A <sup>b</sup> | 0.00088            | <0.001 |        | 0.00003 |                 | 0.012  | 0.004  | 0.067           | <0.014 | <0.035 |

<sup>a</sup>ND, not detected.<sup>b</sup>Unirradiated control capsule.

Table 6. Uranium in ORNL-MTR-47-4 Graphite

| Capsule No. | Power Density <sup>a</sup><br>(w/cm <sup>3</sup> ) | Sample Location <sup>b</sup> | Chemical Analysis<br>(mg of U per g) | Activation Analysis<br>(mg of U per g) |
|-------------|--|------------------------------|--------------------------------------|--|
| 12          | 67   | D                            | 1.3                                  |  |
| 24          | 83   | B                            |                                      | 0.6                                    |
|             |  | C                            |                                      | 1.5                                    |
|             |  | D                            | 2.1                                  |  |
| 45          | 117  | B                            |                                      | 1.5                                    |
|             |  | C                            |                                      | 1.4                                    |
|             |  | D                            | 5.2                                  |  |
| 36          | 85   | A                            |                                      | 0.7                                    |
|             |  | B                            |                                      | 1.2                                    |
|             |  | D                            | 1.3                                  |  |

<sup>a</sup>Nominal power density in fuel surrounding graphite.

<sup>b</sup>Relative locations along core, top to bottom, are designated A-D.

appropriate conditions can be imagined. None of these mechanisms, however, predicts in detail the observed behavior, and they all appear even less applicable at high (reactor-operating) temperatures where no off-equilibrium behavior has been demonstrated. Additional experiments were necessary to decide whether these deposition phenomena can be a problem in the MSRE or are an artifact of our present experimental procedures.

#### Conclusions from MTR-47-4

Of the six capsules in assembly 47-4, five were found to contain large quantities of F<sub>2</sub> and CF<sub>4</sub> while the sixth, which had received a considerably smaller radiation dose, showed a small quantity of CF<sub>4</sub> but no F<sub>2</sub>. This latter capsule alone yielded the expected quantity of xenon while all others retained this element nearly quantitatively. The quantity of F<sup>-</sup> released from the fuel melt generally increased with increase in uranium fissioned (or any of the consequences of this), but no quantitative correlation was found. Neither the quantity of CF<sub>4</sub> nor the ratio CF<sub>4</sub>:F<sub>2</sub> showed an obvious correlation with fission rate, burnup, or time of cooling before examination.

The appearance of the opened capsules and all completed examination of components from these seem to preclude the possibility that the F<sub>2</sub> was present for any appreciable period during the high-temperature operation of this assembly. Accordingly, the generation of F<sub>2</sub> from the salt at low temperatures during the long cooling period must have occurred.

Considerable energy is, of course, available from fission product decay to produce radiolytic reactions in the frozen salt, and the quantity of energy increases with burnup of uranium in the fuel salt. Capsules as small as those can absorb only a small fraction of the gamma energy released by fission product decay. On the other hand, a substantial fraction (perhaps as much as one-half) of the beta energy would be absorbed. A yield (G value) of less than 0.04 fluorine atom per 100 ev absorbed would suffice to produce the fluorine observed in any capsule. Production of  $F_2$  with such a low G value seems a reasonable hypothesis, though no observations of fluorine production from salts on bombardment by beta irradiation had been published.

#### Experiment 47-5

Assembly ORNL-MTR-47-5 was designed, after the observations of  $CF_4$  in the gas space in capsules from 47-3 referred to above, to include six capsules of INOR-8; four of these capsules contained graphite specimens such that a large variation in salt-graphite interface area and in the ratio of graphite area to metal area in contact with salt was provided. The other two capsules, whose behavior is described below, were generally similar to the large capsules of assembly 47-4. However, these capsules

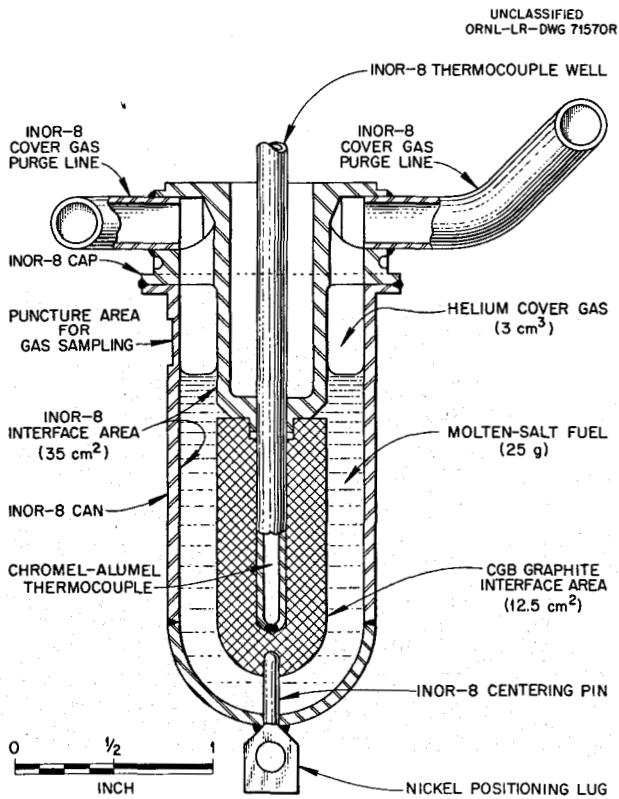


Fig. 6. Assembly MTR-47-5 Purged Capsule.

included additional vapor space above the molten salt, and each was provided with inlet and outlet gas lines extending to manifold systems beyond the reactor. It was possible, accordingly, to sample the cover gas above the melt during reactor operation as well as during and after reactor shutdown.

The two purged capsules, referred to as 3 and 4 in the following and illustrated in Fig. 6, were 0.050-in.-thick INOR-8 vertical cylinders, 1 in. in diameter by 2.25 in. long, with hemispherical end caps. Each capsule contained a core of CGB graphite, 1/2 in. in diameter by 1 in. long, submerged to a depth of approximately 0.3 in. in about 25 g of salt. The top cap contained two 1/4-in.-diam purge lines, a 1/8-in.-diam thermocouple well, and a projection to keep the graphite submerged. The two capsules differed only in the composition (primarily in the uranium concentration) of the fuel salt. Table 7 shows the nominal composition of the salt mixtures in each capsule.

Table 7. Fuel Composition

Specific gravity at 1200°F: 2.13

Liquidus, °F: 842

Thermal conductivity at 1200°F,  $\text{Btu hr}^{-1} \text{ft}^{-2} (\text{°F})^{-1}$ : 3.21

Specific heat at 1200°F,  $\text{Btu lb}^{-1} (\text{°F})^{-1}$ : 0.455

| Component        | Composition (mole %) |           |
|------------------|----------------------|-----------|
|                  | Capsule 3            | Capsule 4 |
| LiF              | 67.19                | 67.36     |
| BeF <sub>2</sub> | 27.96                | 27.73     |
| ZrF <sub>4</sub> | 4.51                 | 4.26      |
| UF <sub>4</sub>  | 0.34                 | 0.66      |

Preparation of the salt and handling and filling operations were very similar to those described for assembly 47-4 above, with the exception that the filling was accomplished with frozen ingots of salt under a helium atmosphere.

The six capsules were, as was the case in previous experiments, suspended in a tank filled with sodium, which served to transfer the thermal energy from the capsules to the tank wall. Heat was removed from the sodium tank through a variable annulus filled with helium to cooling water flowing in an external jacket. As in past experiments, no auxiliary heating was provided. The capsule wall attained temperatures of about 600°C during high-level power operation.

The twin manifolds which comprise the pressure monitoring and gas collection systems were moderately complex. A schematic diagram of one

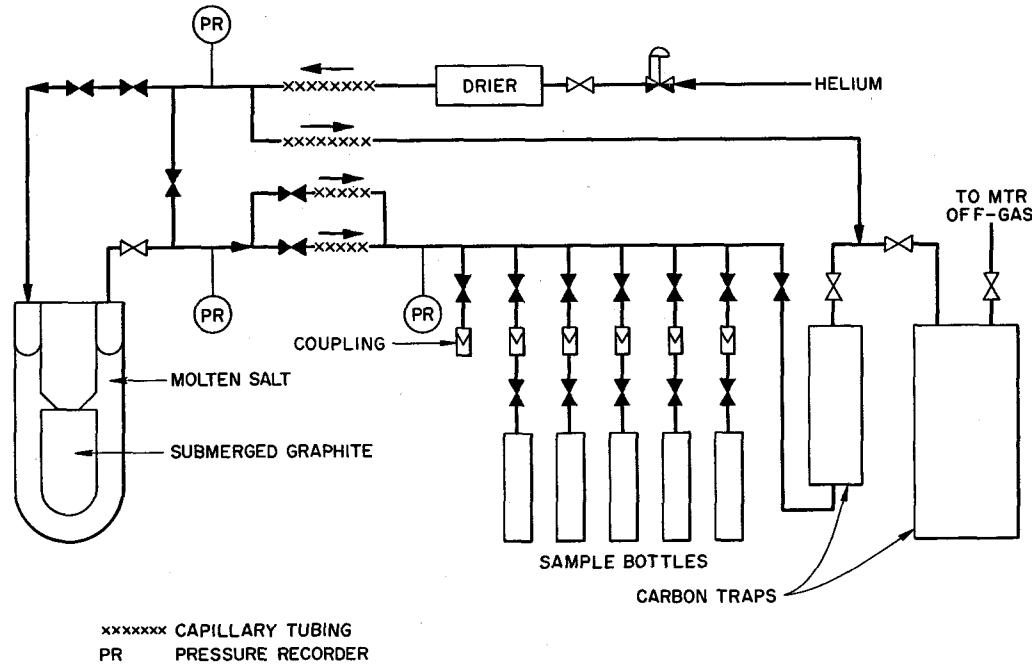
UNCLASSIFIED  
ORNL-LR-DWG 77838

Fig. 7. ORNL-MTR-47-5 Gas-Collection System.

of the assemblies is shown as Fig. 7. The equipment was carefully calibrated to ensure that the samples drawn as desired into 200-cm<sup>3</sup> metal sampling bulbs included a large and known fraction of the gas contained in the capsule.

#### Behavior Under Irradiation

Assembly MTR-47-5 was carried through five MTR cycles during the 4-1/2 months ending January 23, 1963. Operating conditions for this assembly were varied as desired throughout the test to include conditions anticipated in different regions of the MSRE. Temperature and power level in capsules 3 and 4 were varied independently over a considerable interval but were, insofar as possible, held constant during periods represented by accumulation of the gas samples. Fuel temperatures during reactor operation varied from about 190 to 1500°F, with power levels ranging from 3 to 80 w/cm<sup>3</sup> within the fuel.

Gas samples were taken by isolating the capsule for a known and predetermined interval (6 to 96 hr) and then purging the accumulated gases into the sample bulb. Pressure was carefully monitored (to the nearest 0.1 psi) while the capsule was isolated. Fifty-nine gas samples were taken from the two capsules during the first four MTR cycles under five distinct sets of conditions within the capsules. These sets of conditions (and numbers of samples) are:

1. reactor at full power (40 Mw) with fuel molten (34),
2. reactor at intermediate power (5 to 20 Mw) with fuel frozen (8),
3. reactor shut down with the fuel at about 90°F (9),
4. periods spanning fuel melting at reactor startup (4),
5. periods spanning freezing of fuel following reactor shutdown (4).

Partly because the amounts of  $\text{CF}_4$  produced were generally too low to measure accurately, there was much scatter in the results on any of the bases on which correlations were attempted. The most enlightening information was obtained from plots such as Figs. 8 and 9, wherein the

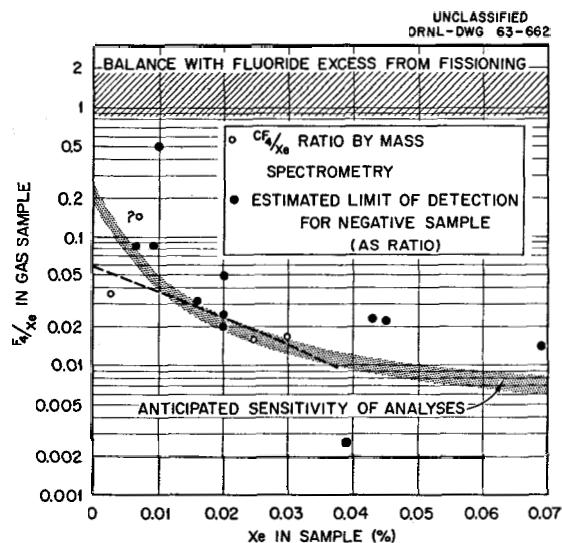


Fig. 8. Production of  $\text{CF}_4$  from Fuel and Graphite at MSRE Power Densities (Although Slightly Lower Temperatures).

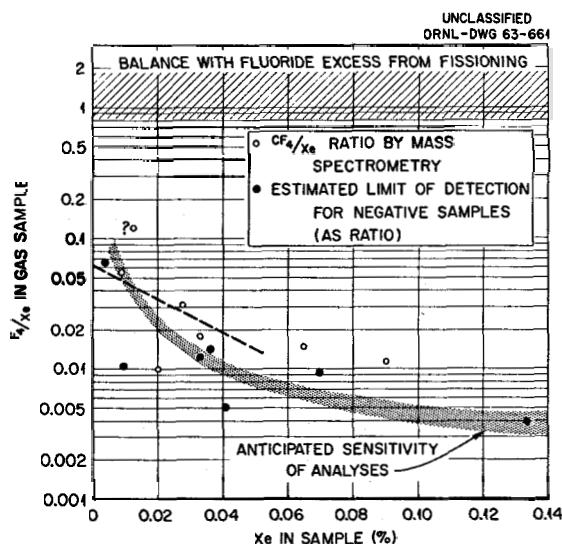


Fig. 9. Production of  $\text{CF}_4$  from Fuel and Graphite at MSRE Temperatures (Although Slightly Higher Power Densities).

amount of xenon (long lived) in a sample served as an internal dosimeter and measured the exposure in terms of the relative amounts of fission energy that were released while the samples accumulated. The amounts of  $\text{CF}_4$  in a sample were presented as ratios of  $\text{CF}_4$  to xenon in the same sample for the following reasons: (1) the primary generation of  $\text{CF}_4$  is probably strongly influenced by the energy, as is of course certainly true of xenon; (2) comparison of mass spectrometric peaks on the same sample eliminates many possible discrepancies that might stem from unrecognized differences in sampling; and (3) also a convenient reference factor is available for assessing the chemical effects on fuels of any given loss of fluoride as  $\text{CF}_4$ . The excess of fluoride ions arising from fissioning  $\text{UF}_4$ , because the fission product cation valences for equilibrium with the container do not accommodate the available anions from the fissioned  $\text{UF}_4$ , gives a small increase in oxidizing power of the fuel with increased burnup. Ordinarily, this oxidation should in principle be manifested as a relatively insignificant increase in corrosion product concentration. However, if the moles of  $\text{CF}_4$  evolved from a fuel were approximately equal to the gram-atoms of stable xenon produced during the same interval, the oxidation-reduction level would tend to remain favorably balanced. The exact ratio for balance varies with conditions of operation but for purposes of estimation can be considered as unity or a little higher. Thus, the cross-hatched bands at the top of Figs. 8 and 9 denote the upper limit of the  $\text{CF}_4/\text{Xe}$  ratios below which the removal of  $\text{CF}_4$  is a corrosion problem of negligible proportions for the MSRE. Higher rates of fluoride removal could conceivably require occasional re-treatment of the fuel with HF, but such a chemical tolerance limit (due to the approach to sufficient reduction to deposit uranium) would be encountered only after an appreciable reduction of  $\text{UF}_4$  to  $\text{UF}_3$ .

Estimated limits of sensitivity for each of the samples that gave negative results have been plotted as filled circles in Figs. 8 and 9 for use as upper limits. The shaded area shows the locus of points corresponding to about 5 ppm  $\text{CF}_4$ , and the open circles correspond to samples for which definite  $\text{CF}_4$  contents were found. Taking into account both positive and negative samples, if  $\text{CF}_4$  were present in amounts proportional to xenon production, the quantity was too small to be measured with certainty. On the other hand, there was a possibility that  $\text{CF}_4$  underwent decomposition and/or reaction with the wall because of the radiation field in the capsule; thus the amount present in samples collected over long periods could represent a steady state between formation and disappearance. The straight dashed lines in Figs. 8 and 9 represent trial extrapolations to zero time, effectively at least, and thus show a possible relative primary rate of generation of  $\text{CF}_4$  compared to xenon in the vapor space in the capsule. In principle, a curve for  $\text{CF}_4$  concentration should pass through all open circles and beneath all filled ones; but, because of the scatter of the data, the curves remained indeterminate. However, the trial values obtained from the dashed extrapolations were considered representative of the rate of production of  $\text{CF}_4$  that could have prevailed. Thus the conclusion would be reached that  $\text{CF}_4$  was produced in the vapor space at about 6% of the rate of xenon and that a steady-state concentration at, or just under, 5 ppm  $\text{CF}_4$  was approached. A simple basis, though not a rigorous or necessarily correct one, for scaling such results from capsules to a

reactor could be the assumption that for given power density in the fuel the  $\text{CF}_4$  production was proportional to the area of the interface between graphite and fuel. Then, since xenon production varies with the fuel volume in the core and the MSRE core contains  $7 \times 10^5 \text{ cm}^3$  of fuel in contact with about  $10^6 \text{ cm}^2$  of graphite, compared to the capsules with  $10 \text{ cm}^3$  of fuel in contact with  $12 \text{ cm}^2$  of graphite, the scaling factor would be

$$\frac{10^6 \text{ cm}^2}{12 \text{ cm}^2} \times \frac{10 \text{ cm}^3}{7 \times 10^5 \text{ cm}^3},$$

or roughly unity. Thus, to the extent that the assumptions involved in the foregoing consideration are justified, the loss of  $\text{CF}_4$  from the MSRE is not expected to cause difficulty.

It was during the reactor shutdowns, which periodically interrupted the collection of gas at operating conditions, that the true nature of the evolution of  $\text{F}_2$  came to light. At shutdowns the capsules were promptly cooled to about  $40^\circ\text{C}$ , and, after variable induction periods, an accumulation of gas in the capsules was noted by pressure measurements. The accumulating gas was found to be  $\text{F}_2$  and to be released from the frozen fuel at  $G_{\text{F}_2}$  values (molecules of  $\text{F}_2$  per 100 ev of absorbed energy) from about 0.005 to 0.031, although on occasion the induction period persisted throughout the shutdown. No correlation between capsule power density just before shutdown and either  $G_{\text{F}_2}$  values or duration of induction periods was observed. There were seven shutdowns of sufficient duration for the effects to be noted.

Short periods of low-power operation (4 hr) were arranged during MTR startups in order to observe the behavior of the solid fuel at varied levels of fissioning which covered the range from 2 to  $10 \text{ w/cm}^3$  and temperatures from  $85$  to  $325^\circ\text{C}$ . Except for some suspicious indications at the lower temperatures, no accumulation of gas was detectable; this indicated, as was later confirmed, that the susceptibility of the solid fuel to radiolytic decomposition diminishes greatly or disappears at relatively low annealing temperatures (e.g.,  $200^\circ\text{C}$ ). An accelerated rate of recombination with increasing temperatures was found in subsequent postirradiation studies, and this is undoubtedly related to the pronounced and favorable temperature effect. At any rate, the operating ranges in which frozen salt in freeze valves and freeze flanges can be maintained without evolving  $\text{F}_2$  appear to be ample for practical purposes.

#### Evolution of $\text{F}_2$ During Postirradiation Decay

On January 23, 1963, after 2000 hr of irradiation at an average thermal flux of  $2 \times 10^{13} \text{ neutrons cm}^{-2} \text{ sec}^{-1}$ , the assembly was withdrawn from the reactor; 11 days later the gas evolution from the two capsules was being monitored in an ORNL hot cell. The  $\text{F}_2$  evolved into an evacuated gas space in which the rate of accumulation was followed by pressure measurements precise to 0.01 psia or  $0.1 \text{ std cm}^3$  of  $\text{F}_2$ . The gas was occasionally collected and analyzed; this restored the vacuum and provided a measure of the leak rate, which was generally quite small. The loss of  $\text{F}_2$  for

the first 95 days of the cooling period is shown in Fig. 10, where the loss is expressed in terms of the percent of the fluoride ions removed from the fuel.

The effect of temperature was found to be quite pronounced, as shown in Fig. 11, which is a differential form of the data in Fig. 10. The calculated yield curve in Fig. 11, which approximates the initial ambient-temperature fluorine-generation curve for the higher-power capsule, represents a  $G_{F_2}$  value of 0.02. A revision of this value may be necessary

when better estimates of capsule power densities are available from uranium isotopic analyses of the irradiated fuels. The jagged rate curve is a consequence of equilibration periods at various temperatures. Either cold (-70°C) or warm (80°C) temperatures sufficed to suppress the evolution. Intermediate behavior found between these extremes implied that a maximum, which shifted somewhat with time, occurred near 35°C or higher. Bursts of  $F_2$  occurred immediately after a temperature rise, and several days were sometimes required for a steady state after a drop in temperature.

Beginning on day 113, the effect of various partial pressures of added  $F_2$  gas was explored. Above 50°C there was a pronounced pressure effect in the expected direction, that is, decreasing loss at increasing pressure, but since the actual rates seemed to depend markedly on the history of the fuel (probably on the state of chemical reduction in the surface layers), it was not possible to determine a quantitative expression for the effect of pressure. Qualitatively the reaction order with respect to  $F_2$  pressure appears to have been initially near unity and to have decreased to 0.5 or lower. Below 50°C, evolution continued even at 1 atm of  $F_2$ . The results are depicted in integral form for the higher-powered capsule in Fig. 12. Consumption of  $F_2$  was clearly evident at increasing rates as the temperature was increased. As the fuel consumed more fluorine, higher temperatures were required to give further consumption at measurable rates.

These data suggest that the  $F_2$  rate of evolution is controlled at low temperatures by rates of diffusion of radiolytic species within the solid, and at higher temperatures by a back reaction whose rate is strongly temperature dependent.

#### Analyses of Gas from Sealed Capsules

For the first 5 months following the in-pile irradiation, the assembly could not be dismantled without disturbing the investigation of  $F_2$  evolution described above. As soon as the rate of  $F_2$  evolution in the swept capsules diminished to the point that it was difficult to measure changes, the four other sealed capsules in the assembly were punctured and their cover gases were analyzed.

Two of the sealed capsules had been designed to provide extremes in the ratio of graphite to metal areas to which the fuel was exposed. Capsule 1 (Fig. 13) had a graphite liner and a graphite core with a total salt-graphite interface area of 27 cm<sup>2</sup>; the liquid extended above the liner and flooded 7 cm<sup>2</sup> of INOR-8 wall. Capsule 2 (see Fig. 14) had only a small

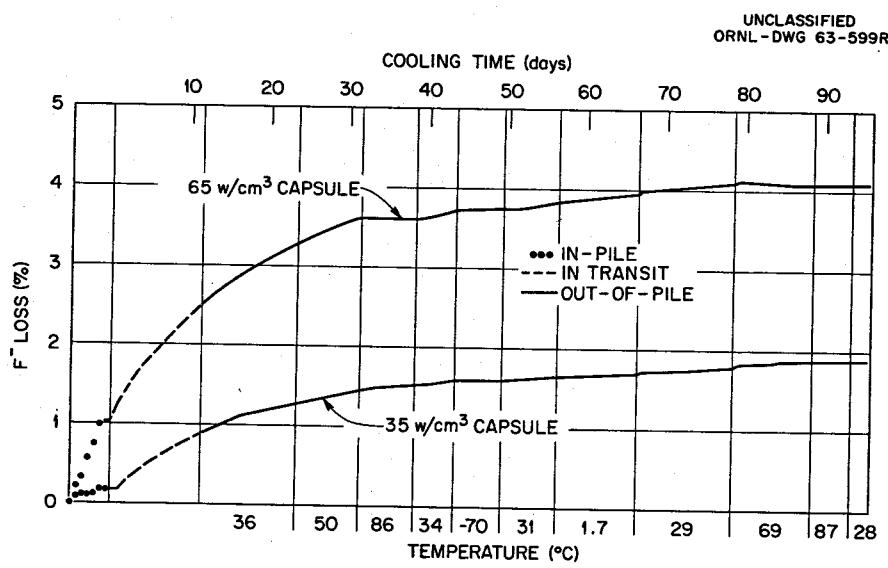


Fig. 10. Loss of Radiolytic Fluorine from MTR-47-5 Capsules.

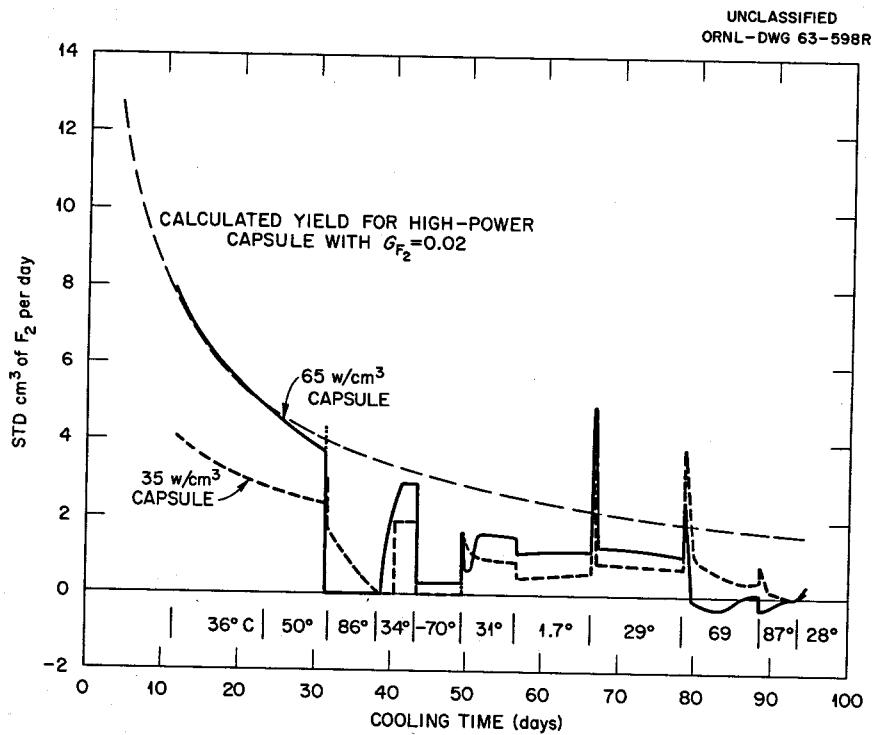


Fig. 11. Postirradiation Fluorine Release in MTR-47-5 Capsules.

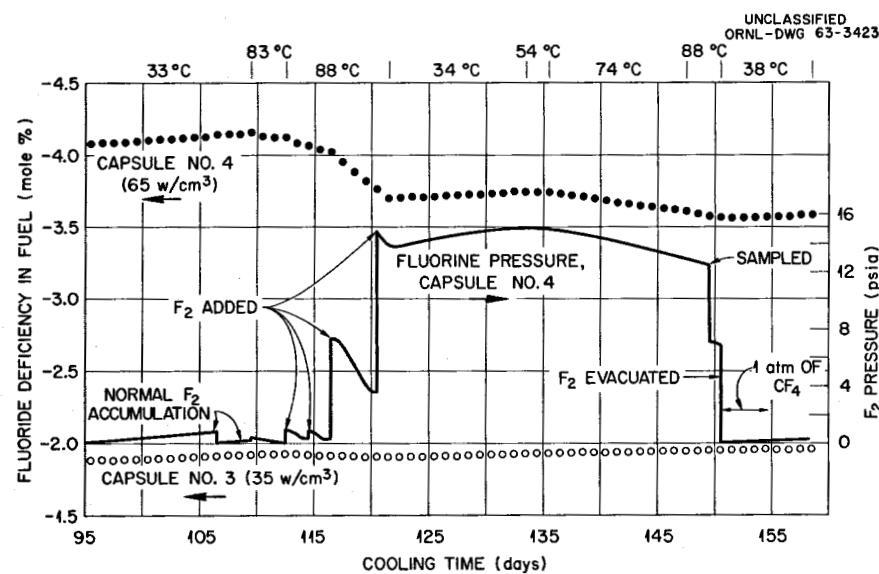


Fig. 12. Effect of Pressure and Temperature on Recomposition of Radiatively Reduced Fuel.

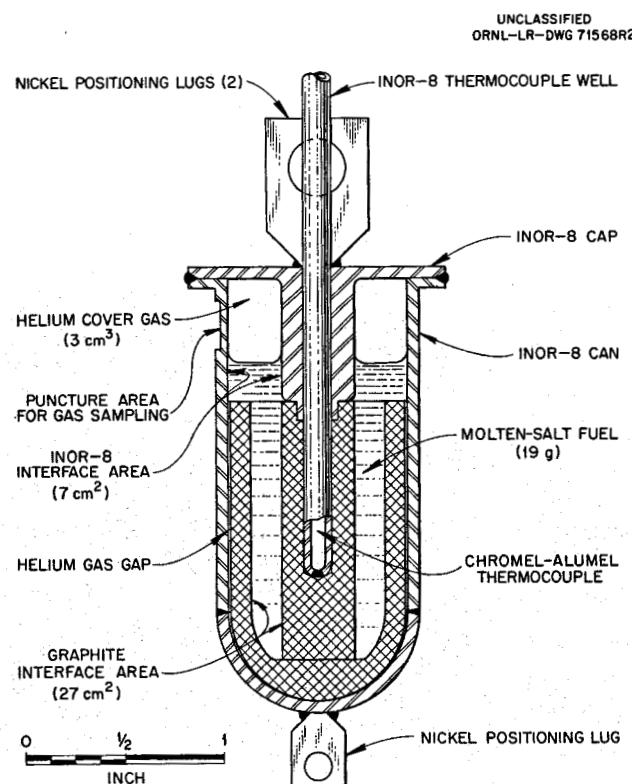


Fig. 13. Capsule Design with Large Area of Graphite-Fuel Interface.

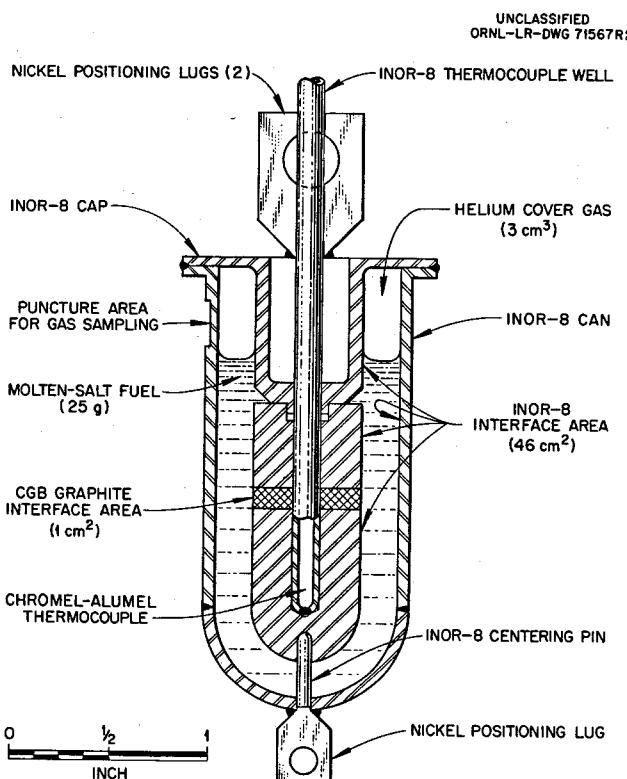


Fig. 14. Capsule Design with Small Area of Graphite-Fuel Interface.

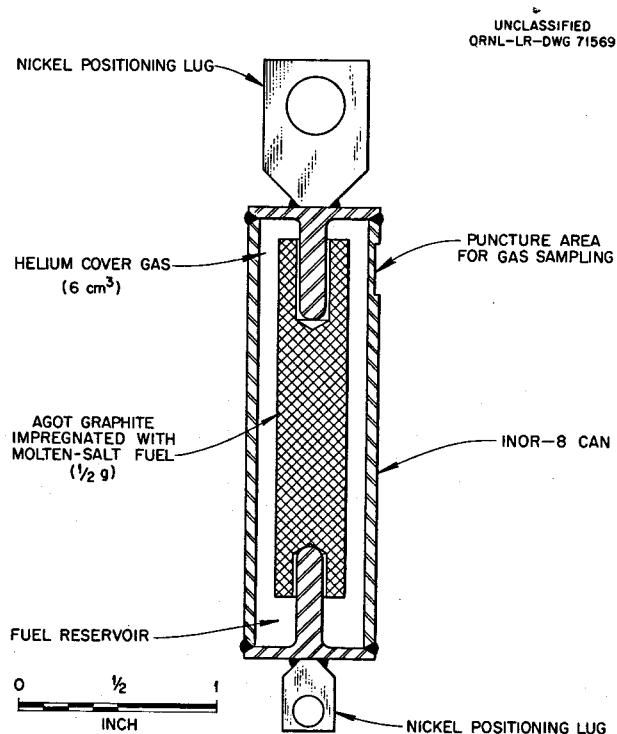


Fig. 15. Capsule Design for Graphite Impregnated with Fuel.

disk of graphite ( $1 \text{ cm}^2$  of graphite-fuel interface) and provided  $46 \text{ cm}^2$  of metal-fuel interface. The other two capsules (Fig. 15) were of smaller diameter; they each contained a mounted graphite (AGOT) bar (3 g) that had been prepermeated with fuel. No other fuel was added; therefore, these capsules, initially at least, exposed no metallic surface to the salt.

Analyses of the gas drawn from these four capsules are shown in Table 8 along with some details of the in-pile exposures. It is clear that the three capsule geometries yielded very different quantities of  $\text{F}_2$  and  $\text{CF}_4$ ; capsule 2 yielded about  $39 \text{ cm}^3$  of  $\text{F}_2$  and  $70 \text{ cm}^3$  of  $\text{CF}_4$ , capsule 1 yielded about  $2.5 \text{ cm}^3$  of  $\text{F}_2$  and  $0.6 \text{ cm}^3$  of  $\text{CF}_4$ , and the small capsules yielded none of either gas. The notion that the salt-metal interface area affects radiolytic generation of  $\text{F}_2$  from solid salt now appears absurd. The possibility that graphite surfaces somehow catalyze back reactions or otherwise slow the generation process now seems almost equally unlikely. It appears more plausible to ascribe the pronounced difference in behavior to large differences in cooling rates of the fuel and to consequent differences in crystallite size and degree of stress introduced into the crystallites. The small capsules, with the gas envelope around the fuel, cooled most slowly and, perhaps, produced least readily damaged fuel. Capsule 2 clearly should have cooled most rapidly.

The particle size of the fuel dispersed through the graphite bars in the rear and front capsules must have been very small. The fact that no detectable amount of  $\text{F}_2$  was generated in these capsules suggests that small particle size alone is not a sufficient factor to induce  $\text{F}_2$  generation.

No evidence of decomposed  $\text{CF}_4$  residues or products, nor even deposits of a suspicious nature in this regard, was found on visual inspection and attempted sampling of the interior of gas lines from Experiment 47-5.

Metallographic results from this experiment have not yet been reported, but no evidence of attack on the INOR-8 is expected to be found. The loss of fluorine from the swept capsules during the in-pile portion of the test might be expected to contribute toward additional uranium deposition in the graphite in these capsules.

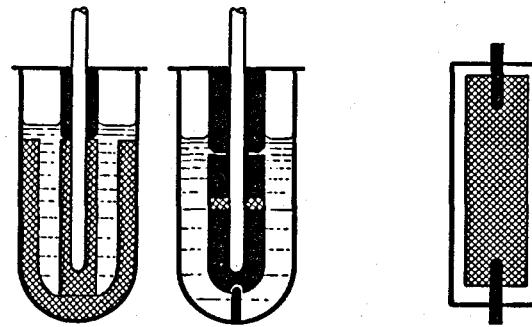
#### Experiment 47-6

##### Description of Experiment

This experiment was designed after low-temperature fluorine generation had been established and after its significance with respect to  $\text{CF}_4$  production, metal corrosion, and uranium deposition in graphite had been considered. Based on these considerations, some questions to which the experiment was addressed, in order of importance in complicating the structural array of the assembly and accessories, are as follows:

Table 8. ORNL-MTR-47-5 Gas Analyses and Exposure Conditions

| Capsule Designation   | Capsule Type          |                       |                       |                       |
|---|-----------------------|-----------------------|-----------------------|-----------------------|
|   | 1                     | 2                     | Rear                  | Front                 |
| Weight of graphite, g   | 14.362                | 0.536                 | 3.6655                | 3.6353                |
| Weight of fuel, g   | 18.928                | 25.240                | 0.6465                | 0.5037                |
| U in fuel, mole %   | 0.659                 | 0.659                 | 0.339                 | 0.659                 |
| Weight of 93.26% $^{235}\text{U}$ , g                                 | 0.770                 | 1.027                 | 0.01345               | 0.0205                |
| Neutron flux, <sup>a</sup> neutrons $\text{cm}^{-2} \text{ sec}^{-1}$ | $1.94 \times 10^{13}$ | $2.24 \times 10^{13}$ | $1.91 \times 10^{13}$ | $3.87 \times 10^{13}$ |
| Fission power density, <sup>b</sup> w/ $\text{cm}^3$                  | 65.0                  | 75.0                  | 32.5 <sup>c</sup>     | 130.0 <sup>c</sup>    |
| Burnup, <sup>d</sup> %  | 7.7                   | 8.8                   | 7.6                   | 14.7                  |
| Volume of cover gas, ml (STP)   | 5.67                  | 115                   | 2.63                  | 2.76                  |
| $\text{F}_2$ , <sup>e</sup> %   | 43                    | 34                    | 0                     | 0                     |
| $\text{CF}_4$ , %   | 10                    | 61                    | 0                     | 0                     |
| He + Ar, %  | 41                    | 2.0                   | 99.6                  | 98.2                  |
| $\text{Kr}$ , <sup>f</sup> %  | 2.7 (73%)             | 0.11 (40%)            | 0.055 (40%)           | 0.20 (51%)            |
| $\text{Xe}$ , <sup>f</sup> %  | <0.01<br>(<0.05%)     | 0.024 (1.7%)          | 0.32 (46%)            | 1.57 (81%)            |
| Air + $\text{CO}_2$ , %   | 3.5                   | 2.7                   | 0                     | 0                     |

<sup>a</sup>Calculated from  $^{60}\text{Co}$  analysis of capsule metal.<sup>b</sup>Calculated from the tabulated neutron fluxes and the known fuel densities at 1300°F.<sup>c</sup>Calculated for fuel itself; overall power densities in the impregnated graphite are 15% of these.<sup>d</sup>Calculated from the tabulated neutron fluxes.<sup>e</sup>Corrected to include  $\text{SiF}_4$ ,  $\text{OF}_2$ ,  $\text{COF}_2$ , etc.<sup>f</sup>Numbers in parentheses are percentages observed of yields calculated from burnups.

1. Can a more sensitive measurement of the production of  $\text{CF}_4$  be obtained?
2. Can the conjectured absence of deposition of uranium in graphite under operating conditions be more clearly confirmed?
3. Does the concentration of  $\text{U}^{4+}$  cations in the fuel, through catalytic-type mechanisms involving the variable valence of the uranium, have a perceptible effect on the recombination of nonequilibrium oxidizing and reducing species that are produced by radiation?
4. Was a previously noted augmented corrosion of molybdenum metal (Experiment 47-3) due to attack at operating conditions or was it a consequence of gaseous  $\text{F}_2$  released by radiation damage from decaying fission products in the frozen fuel?
5. Can the radiolysis of added  $\text{CF}_4$  be detected?

Foremost was the provision for heating the four irradiated test capsules to avoid freezing during reactor shutdowns. This was to avoid release of  $\text{F}_2$  and much of the ensuing obfuscation encountered in recent postirradiation examinations. But this also entailed a problem in opening and dissecting the capsules without allowing  $\text{F}_2$  to intrude again after removal from the MTR. The remedy involved a prompt dissection in MTR hot cells before removal to ORNL hot cells.

Figure 16 shows one of the four test capsules in cross section. All four INOR-8 capsules are vertical right cylinders (~2 in. in height) containing a 1/4-in. annulus of fuel (25 g) that surrounds and covers a central core of graphite (1/2 in. diam), leaving a gas space of about 3  $\text{cm}^3$  above the liquid level. Central thermocouple wells penetrated the graphite. Two capsules were swept by helium, at measured flow rates variable to 5000  $\text{cm}^3/\text{hr}$ , which passed to a sampling assembly that included a molecular sieve column for concentration of  $\text{CF}_4$ . The other two capsules were sealed.

The question of  $\text{CF}_4$  evolution was approached by having the two gas-swept capsules identical in all respects except graphite area (and depth of submersion). An INOR-8 core section replaced the upper half of one of the graphite cores and reduced the graphite area from approximately 14  $\text{cm}^2$  to approximately 7  $\text{cm}^2$ . Both swept capsules contained 0.9 mole %  $\text{UF}_4$  which included a sufficient enrichment of  $^{235}\text{U}$  to give 14 w/ $\text{cm}^3$  at minimum insertion; these values were chosen in conformance with MSRE operating conditions and provided 52 w/ $\text{cm}^3$  as a maximum.

The gas flow system was designed to sweep any  $\text{CF}_4$  from the gas space faster than it could be radiolytically decomposed. Additionally, there were facilities, including thermal conductivity meters, for measuring the rate of radiolysis of  $\text{CF}_4$  as prepared mixtures of  $\text{CF}_4$  and helium were passed through the capsule. Also, sensitive analyses at low concentrations of  $\text{CF}_4$  were available from a "helium breakdown" sensor being developed by the Analytical Chemistry Division. Previous results implied a steady-state concentration of  $\text{CF}_4$  so low that the rate of loss of added  $\text{CF}_4$  might be very much easier to measure than the rate of appearance of evolved  $\text{CF}_4$  in the capsule gas space.

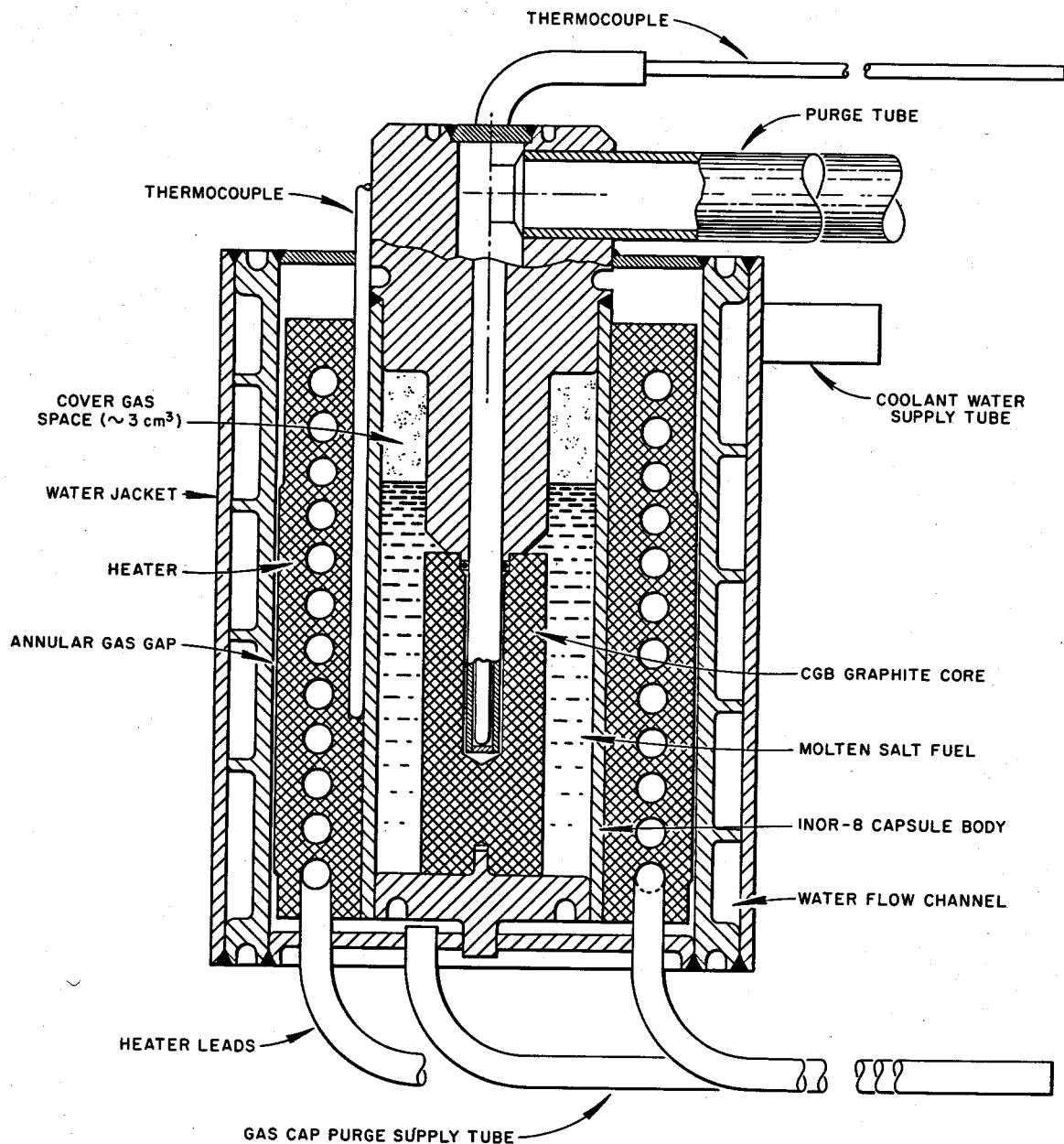
UNCLASSIFIED  
ORNL-DWG 64-4010

Fig. 16. Typical Capsule Assembly Equipped for Purging, for Experiment ORNL-MTR-47-6.

The question of uranium in or on the graphite was approached by designing flat areas on the graphite cores; this should greatly facilitate examination by x-ray diffraction. Further, the two sealed capsules are addressed primarily to comparing minimum with large concentrations of UF<sub>4</sub> in the fuel; one has 4 mole % UF<sub>4</sub>, with the maximum enrichment consistent with safe temperature, while the other contains highly enriched uranium, but in the minimum amount sufficient to duplicate the power density in the swept capsules.

On the one hand there is the possibility, if deposition does indeed occur, that the higher the uranium concentration and the higher the power density, the more uranium might be deposited on the graphite. On the other hand, there is a theory that uranium cations might serve as a recombination catalyst for off-equilibrium radiolytic "free radicals," and that the steady-state concentration of these might be higher with lower concentrations of UF<sub>4</sub>, and hence conceivably induce greater deposition in low-concentration fuels. With the available neutron flux for the experiment, the lowest concentration of fully enriched UF<sub>4</sub> consistent with power densities of interest is about 0.5 mole %. This precludes testing at this time with quite low concentrations that presumably would be of greatest interest in checking for catalytic effects and that would represent a relatively unexplored concentration range, but neither have the higher concentration ranges been explored. Thus, as far as uranium content is concerned, the experiment carries one low, two medium (swept), and one high concentration capsule.

Both sealed capsules contain coupons of molybdenum which are expected, on the basis of corrosion encountered in 47-3, possibly to be more sensitive than INOR-8 as indicators of corrosive influences. Also, the comparison of uranium behavior in the presence of pure molybdenum, as contrasted with the presence of only 17 at. % of molybdenum in INOR-8 in the swept capsules, may prove to be of interest.

The question of the corrosion of molybdenum seemed to be one that could probably be answered without interfering with the other main purposes of the experiment. Admittedly, there was risk of confusion from superposition of variables, but the advantages were deemed to outweigh the risks. In the absence of radiation, molybdenum and INOR-8 form a bimetallic couple, and electrochemical transfer of metal is expected; in practice the rate is alleged to be so slow that no clear evidence of transfer has been obtained. In the absence of radiation, molybdenum is carburized when in contact with graphite; in this experiment the molybdenum is in submerged radial sheets or slivers that touch INOR-8 on one edge and do not touch graphite. Molybdenum and carbon both give rise to volatile fluorides under oxidizing conditions; this could conceivably be the basis for a response (different than nickel, e.g.) to the off-equilibrium species produced by radiation in the fuel. In the absence of irradiation, molybdenum behaves as rather more noble than nickel toward fluoride melts.

Results of Experiment

The experiment was exposed to radiation in the MTR from June 8 to August 10, 1964. During the first two 3-week cycles of the MTR, 26 gas samples were swept from INOR-8 capsules containing MSRE fuel and graphite. A variety of sweep rates, temperatures, and power densities were explored, but no  $\text{CF}_4$  has been found in the samples that have been analyzed thus far, nor has there been any detectable radioactivity other than that of xenon and krypton. This indicates that neither  $\text{F}_2$  nor  $\text{CF}_4$  was produced at rates that would be of significance to the MSRE.

For the first 24 hr following the final MTR shutdown, the assembly was maintained at a temperature above the salt liquidus temperature in order to prevent fluorine generation during the period of most rapid radioactive decay of the fission products in the salt. Then the salt was allowed to freeze at a relatively slow rate ( $10^\circ\text{C}/\text{hr}$ ) through the temperature range 450 to  $400^\circ\text{C}$ , in which the primary, secondary, and tertiary phases are found to appear. Through this slow freezing it was hoped that the fuel would be deposited in a relatively good state of crystallization, permitting petrographic confirmation of the expected phases and further minimizing fluorine evolution. Having cooled the salt to a solid, the assembly was removed from the reactor as quickly as possible and disassembled in the hot cells at the MTR. The capsules were opened and the components separated to prevent any postirradiation effects which might obscure the in-pile behavior of the system.

Visual examination of the components during disassembly did not reveal any unexpected or disturbing information. The salt was either green, gray-green, or black, as frequently seen in the past. There were small droplets of salt components on the metal above the liquid phase. The salt broke cleanly away from the graphite with no evidence that the graphite had been wetted, though the metal was apparently wetted by the salt. The molybdenum coupons appeared not to have been attacked. In the swept capsules the INOR-8 surfaces above the liquid appeared to be covered with a dirty gray film or series of mottled spots similar to the observations in other experiments; this is currently attributed to the effects of traces of water or other reactive components in the helium sweep gas. In the unswept capsule (No. 2) the salt was green, the graphite looked very clean, and all metal below the salt was shiny. The thermocouple well was also shiny. The contact angle of the salt on metal was about  $90^\circ$ , and there were a few beads of salt above the liquid line.

All the components from the experiments have been packed for shipment to ORNL and detailed examination in our hot laboratory facilities. More satisfactory statements confirming the excellent results suggested by the gross visual observations will have to await this examination.

It should be recalled that provisions have been made in the MSRE for the direct exposure of graphite and metal test specimens in the very center of the reactor. An access port has been provided through which these can be removed for observation and replaced by additional specimens as required to confirm and extend the results of the small-scale irradiation test program which has been discussed.

Out-of-Pile Experiments

Salient features of the fluorine generation and recombination processes have been verified with simulated MSRE fuels, and with some of the component fluorides, on exposure to pure gamma, beta, and x radiation.

An INOR-8 capsule containing MSRE salt and graphite was exposed to gamma radiation from a  $^{60}\text{Co}$  source for  $\sim 7400$  hr at temperatures ranging from 38 to  $150^\circ\text{C}$ . The salt received a calculated  $0.45 \times 10^{20}$  ev  $\text{hr}^{-1} \text{g}^{-1}$ . After an induction period of about 600 hr, fluorine gas was generated at rates ( $G$  values) varying between 0.03 to 0.07 molecule of fluorine per 100 ev absorbed at temperatures up to  $110^\circ\text{C}$ . At  $150^\circ\text{C}$  any fluorine gas which had been generated was recombined. At  $130^\circ\text{C}$  recombination rates roughly equaled generation rates. No evidence of any appreciable reaction of the  $\text{F}_2$  gas with the graphite to generate  $\text{CF}_4$  was obtained.<sup>2</sup>

Experiments to investigate fluorine evolution from studies of behavior of solid MSRE fuel mixtures under fast electron bombardment have yielded values of  $G_{\text{F}_2}$  as a function of dose up to a total dose of about  $1.6 \times 10^{18}$  Mev per g of salt. At doses below about  $8 \times 10^{17}$  Mev/g, maximums in the fluorine production rates were observed or indicated in each experiment. In one of the experiments exposed to a greater dose, a second increase in fluorine evolution rate was observed after a total dose of about 9 to  $10 \times 10^{17}$  Mev/g. It is observed that reduction of the dose rate by a factor of about 2 causes an increase in the initial rates of fluorine evolution per unit dose ( $G_{\text{F}_2}$ ). The maximum  $G_{\text{F}_2}$  observed was 0.02. Similar experiments with solid LiF showed that fluorine was not evolved as a result of bombardment with fast electrons but was taken up in small amounts.<sup>3</sup>

Soft x-ray irradiation of a solid mixture similar to the MSRE fuel gave evidence of radiolytic decomposition with yields of volatile fluorine compounds equivalent to  $G_{\text{F}_2}$  (moles of  $\text{F}_2$  per 100 ev absorbed) values ranging from 0.0006 to 0.04. In some cases elemental fluorine was identified, but, generally, the products were carbon tetrafluoride and carbonyl fluoride. Prefluorination of the salt removed carbon-containing impurities and encouraged liberation of elemental fluorine. Fine particles liberated volatile fluorine-containing products at about ten times the rate from coarse particles. The compound  $6\text{LiF} \cdot \text{BeF}_2 \cdot \text{ZrF}_4$ , one of the complex compounds which crystallize from the MSRE fuel, decomposed with an equivalent  $G_{\text{F}_2}$  of about 0.02. Prefluorinated thorium fluoride liberated elemental fluorine at rates of about 0.005 molecule per 100 ev. Neither lithium nor zirconium fluorides gave any evidence of radiolysis.<sup>4</sup>

References

1. MSRP Status Report, May 1, 1958, ORNL-2634.
2. MSRP Semiann. Progr. Rept. Jan. 31, 1964, ORNL-3626, pp. 101-5.
3. MSRP Semiann. Progr. Rept. Jan. 31, 1964, ORNL-3626, pp. 105-10.
4. MSRP Semiann. Progr. Rept. Jan. 31, 1964, ORNL-3626, pp. 110-11.

PREPARATION OF MSRE FUEL, COOLANT, AND FLUSH SALTS

J. H. Shaffer

The initial operation of the Molten-Salt Reactor Experiment (MSRE) will utilize about 26,560 lb of fused fluorides as fuel, coolant, and flush salt mixtures. The reactor fuel mixture will have the composition LiF-BeF<sub>2</sub>-ZrF<sub>4</sub>-UF<sub>4</sub> (65.0-29.1-5.0-0.9 mole % respectively). Fissionable <sup>235</sup>U will comprise about one-third of the uranium inventory; the balance, as nonfissionable uranium, has been included for chemical purposes. An initial loading of about 11,260 lb of fuel salt mixture will be required for a desired fill volume of approximately 73 ft<sup>3</sup> in the reactor assembly. The coolant and flush salt mixtures will be chemically identical and will have the composition LiF-BeF<sub>2</sub> (66-34 mole %). Approximately 15,300 lb of this mixture is needed for a coolant salt volume of 42 ft<sup>3</sup> and a flush salt volume equivalent to that of the fuel mixture.

Techniques for preparing fused fluoride mixtures at ORNL were developed to support the Aircraft Nuclear Propulsion Program and were successfully demonstrated during the preparation of fluoride mixtures for the Aircraft Reactor Experiment.<sup>1</sup> The production facility has since become an integral part of the Molten-Salt Reactor Program to provide fused fluoride mixtures for its chemical and engineering test programs and for other related projects of the Laboratory and the USAEC. Since March 1964, the facility has been operated at capacity for the production of MSRE fluoride mixtures. Sufficient quantities of LiF-BeF<sub>2</sub> (66-34 mole %) for the coolant salt mixture and about 50% of that required as the flush salt have been prepared to date. Production of the fuel salt mixture will follow the loading of coolant and flush salt into the reactor facility.

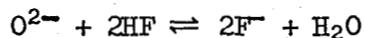
Process Chemistry

Although starting materials of very high purity are used in production of fused fluoride mixtures, further purification is needed before they are acceptable for use in the MSRE. The removal of a limited number of impurity species during production operations is achieved by treatment of the fluoride melts with anhydrous HF, hydrogen, and, in some instances, by the use of beryllium metal as a strong reducing agent. Impurities which can be volatilized are removed in the process gas effluent stream; those which can be rendered as insoluble particles are removed by filtration.

Oxide Removal

On heating the starting materials above the liquidus temperature of the salt mixture, oxides are formed by pyrohydrolysis of the fluoride salts with their absorbed water. Although oxide impurities, in themselves, are probably not detrimental, their presence in the fluoride mixtures of the MSRE could result in the deposition of solid oxide particles or scale. The resulting heterogeneous system could alter heat transfer properties of the reactor components and might also create localized heat sources in the reactor core by the deposition of uranium dioxide.

Oxides are removed during the initial gas sparging of the fluoride melt at 600°C with an anhydrous mixture of HF in hydrogen. They react directly with hydrogen fluoride by the reaction



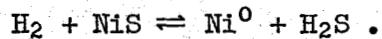
and are conveniently removed from the process as water vapor. Although precise analytical methods for determining the oxide content of fluoride melts have not been suitably developed, recent measurements of equilibrium quotients for this reaction show that the efficiency of oxide removal by this process should be high.<sup>2</sup> In the production process, treatment with HF is continued to a practical reaction completion which should provide a suitable "oxide capacity" of these fluoride mixtures for inadvertent contamination during reactor operations.

#### Sulfur Removal

Sulfur impurities need also to be removed because of their corrosive attack on nickel-base alloys at elevated temperatures. In the starting materials these impurities are found primarily as sulfates and require multiple treatment to effect their removal from the fluoride mixtures. During a preliminary treatment, sulfates are reduced to sulfides by the addition of beryllium metal turnings to the molten raw material mixture.<sup>3</sup> Hydrogen sulfide is produced simultaneously with oxide removal by the reaction



and is removed from the system in the gas effluent. However, the rate at which H<sub>2</sub>S can be removed is low and is proportional to the hydrogen flow rate.<sup>4</sup> This condition may result from an intermediate reaction of H<sub>2</sub>S with the nickel salt container; sulfur removal would be controlled by the reaction

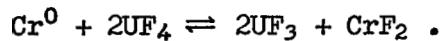


Hydrogen flow rates of about 10 liters/min are used in the production process; the maximum sulfur-removal rate has been approximately 0.7 g/hr.

Because of these difficulties in removing sulfur impurities from molten fluoride mixtures, efforts are made to obtain sulfur-free starting materials. Of the fluoride salts that have been purchased for the production of fluoride mixtures for the MSRE, only beryllium fluoride has been found to contain sulfur impurities; however, through cooperative efforts with the vendors, these impurities have been virtually eliminated. Approximately two-thirds of the BeF<sub>2</sub> required by the MSRE is sulfur-free; the balance contains concentrations of 10 to 1000 ppm.

### Removal of Structural-Metal Impurities

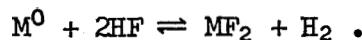
The INOR-8 alloy (Hastelloy N) used as the structural metal container in the MSRE contains 6 to 8% chromium as a constituent. It is expected<sup>5</sup> that the chromium activity in the surface layer of metal in contact with MSRE fuel will be depleted until the following equilibrium is established:



If the molten fluoride mixtures introduced into the MSRE contain nonequilibrium concentrations of structural-metal fluorides more easily reduced than  $\text{UF}_4$  (e.g.,  $\text{NiF}_2$  or  $\text{FeF}_2$ ), the INOR-8 container would corrode.

Structural-metal fluorides are present as impurities in the fluoride raw materials and may also be introduced by corrosion of the process equipment during production operations. Thus, the control of structural-metal fluoride concentrations in the purified fluoride mixtures is an important process consideration.

Hydrogen fluoride will readily attack structural metals and alloys that are suitable as salt containers at the operating temperatures of the production process by reactions of the type



This reaction is arrested in the gas phase of the treatment vessel by the formation of a rather impervious layer of the structural-metal fluoride on the metal surfaces. However, metal surfaces which are in contact with the fluoride mixture are continually renewed by the dissolution of the structural metal fluorides into the melt. Experimental studies of the thermodynamics of corrosion processes in molten fluorides<sup>6</sup> have shown that the corrosion of nickel could be controlled by admixing HF with hydrogen in concentrations which would also be effective for oxide and sulfur removal. Concentrations of HF in hydrogen which would be needed to control the corrosion of iron and chromium are too low to be of practical value by current production techniques. Accordingly, nickel metal is used as the primary salt containment material in the process equipment. A gas mixture containing approximately 1/10 mole fraction of HF in  $\text{H}_2$  has been used effectively in the fluoride purification process. As suggested by studies of high-temperature thermocouple research,<sup>7</sup> the presence of hydrogen should also reduce the corrosiveness of the HF- $\text{H}_2\text{O}$  effluent gas mixture which accompanies the conversion of oxides to fluorides.

Gas sparging of the melt at 700°C with hydrogen alone is used as a final phase of the purification process to reduce  $\text{FeF}_2$  and remaining  $\text{NiF}_2$  concentrations to low values. The reduction of  $\text{CrF}_2$  by hydrogen is too slow to be effective at process temperatures. However, chromium concentrations of 25 to 50 ppm that are present in the starting materials are not prohibitive for reactor applications and remain essentially unchanged by the production process. When structural-metal fluoride concentrations are exceedingly high, beryllium metal, a strong reducing agent, is added to the melt. This treatment is followed by a mild hydrofluorination to

convert the unreacted excess of beryllium metal to its fluoride salt. Insoluble metallic impurities are separated from the purified fluoride mixture by decantation and by filtration through sintered nickel during transfer of the molten mixture to its storage container.

#### Production Operations

Fused fluoride mixtures are prepared in two batch processing units from fluoride salts that are normally purchased from commercial sources. Although the units are operated independently of each other, both are charged with molten raw materials from a single meltdown furnace assembly. Figure 1 shows the floor plan of the main operating level of the production facility and indicates the flow of materials through the processing units. All operations are coordinated so that the batch processing units will operate on a semicontinuous schedule.

#### Starting Materials

Fluoride salts that are used as starting materials for the production of fused fluoride mixtures for the MSRE were purchased, when possible, from commercial sources on a competitive bid arrangement. Since further purification of these materials during the production process is limited, only those of highest purity, within the competitive market, were accepted; chemical specifications are shown in Table 1. Although all materials obtained for use in preparing MSRE fluoride mixtures were generally within these specified limits, iron concentrations of 250 and 500 ppm were allowed in  $\text{BeF}_2$  and  $\text{LiF}$  respectively. Some carbonaceous impurities were also allowed since they are readily removed as carbon by gas sparging and are inherent in some manufacturing processes. Approximately 12,000 lb of beryllium fluoride was purchased for preparing the first reactor loading of fluoride mixtures. Zirconium tetrafluoride that is relatively free of hafnium (<100 ppm) and otherwise of high purity was also found to be readily available from commercial sources. Approximately 2300 lb of this material was purchased for use in the MSRE fuel mixture.

For neutron-absorption cross-section considerations, all lithium fluoride used in salt mixtures for the MSRE must be essentially free of  ${}^6\text{Li}$ . Sufficient  ${}^7\text{LiF}$  (22,000 lb) was obtained from the USAEC for one complete reactor loading and the planned replacement of the flush and fuel salt mixtures. The isotopic assay of this material is at least 99.9%  ${}^7\text{Li}$ ; however, those batches having the highest  ${}^6\text{Li}$  content have been used in preparing the coolant salt mixture.

Although the  ${}^{235}\text{U}$  enrichment in the MSRE fuel mixture during power operation will be approximately 30%, all  ${}^{235}\text{U}$  will be obtained for processing as highly enriched (92% in  ${}^{235}\text{U}$ ) uranium tetrafluoride. About 90 kg of  ${}^{235}\text{U}$  will be required for reactor tests currently scheduled. The balance of uranium inventory in the reactor fuel system will be made up of  $\text{UF}_4$  that is depleted of  ${}^{235}\text{U}$ . These materials are readily available from USAEC.

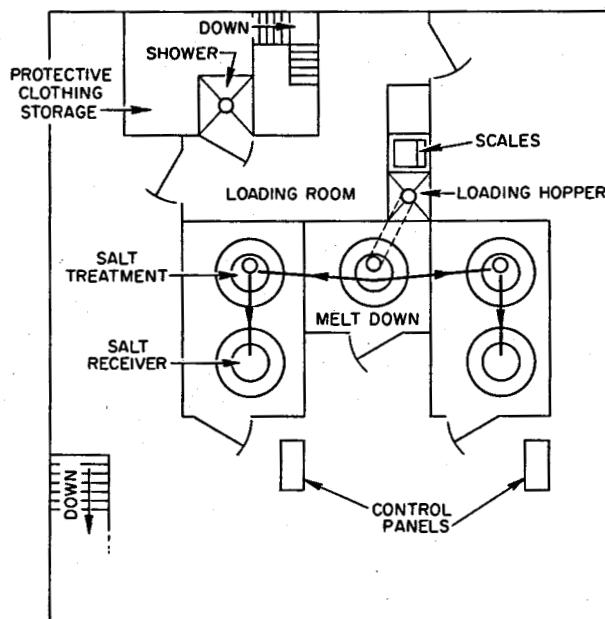
UNCLASSIFIED  
ORNL-DWG 64-6998

Fig. 1. Fluoride Production Facility - Layout of Operating Level.

Table 1. Fluoride Production for MSRE - General Chemical Specifications for Starting Materials

| Impurity            | Allowable Concentration<br>(wt %)<br>(1 ppm = 0.0001 wt %) |
|---------------------|--|
| Water               | 0.1  |
| Cu                  | 0.005  |
| Fe                  | 0.01   |
| Ni                  | 0.0025   |
| S                   | 0.025  |
| Cr                  | 0.0025   |
| Al                  | 0.015  |
| Si                  | 0.01   |
| B                   | 0.0005   |
| Na                  | 0.05   |
| Ca                  | 0.01   |
| Mg                  | 0.01   |
| K                   | 0.01   |
| Li (natural)        | 0.005  |
| Zr (natural)        | 0.025  |
| Cd                  | 0.001  |
| Rare earths (total) | 0.001  |

### <sup>7</sup>LiF Densification

With the exception of <sup>7</sup>LiF, all raw materials obtained for preparing the MSRE fluoride mixtures can be charged directly to the meltdown furnace. The lithium fluoride, as received, was found to have a very low bulk density. Subsequent examination showed that it also contained substantial amounts of water. Since the direct use of this material would result in loss of production capacity and excessive oxide contamination, pretreatment of the <sup>7</sup>LiF to improve these properties was desired.

Densification of LiF by heating to 650°C had appeared promising in laboratory experiments.<sup>8</sup> Intermediate-scale tests were made preparatory to production-scale operations to develop a processing procedure and to examine the feasibility of pretreating the 22,000 lb of material that was on hand. These tests showed that periodic agitation of the LiF while heating to 650°C was necessary to produce a free-flowing granular product. Anhydrous HF was mixed with the helium sweep gas while the charge was being heated to about 400°C to convert LiOH, either initially present or formed by pyrohydrolysis, to LiF; otherwise, heating to 650°C would permit the LiOH to be fused with the LiF to give an intractable mass.

The production-scale equipment is a horizontal Monel reaction vessel (17 in. in diameter by 8 ft long) equipped with a full-length agitator and a heating jacket. The apparatus had been used during the ANP Program in the conversion of solid ZrCl<sub>4</sub> to ZrF<sub>4</sub> by treatment with anhydrous HF at elevated temperatures. This equipment is shown in Fig. 2. Up to 300 lb of <sup>7</sup>LiF has been processed in a single batch; approximately 11,500 lb has been processed to date. The average bulk density of the <sup>7</sup>LiF has been increased from about 0.6 g/cm<sup>3</sup> to 1.1 g/cm<sup>3</sup> by this operation.

### Raw-Materials Charge and Meltdown

Because of the toxicity of fluoride salts (beryllium fluoride in particular), the raw materials are handled by operating personnel in a loading room isolated from other areas of the production plant by shower facilities and air locks. Personnel working within the loading room wear fully protective, plastic, fresh-air suits to avoid exposure to these hazardous chemicals. Raw materials are assembled in this area, weighed into appropriate batch sizes in a well-ventilated hood enclosure, and transferred to the meltdown furnace by a vibratory conveyer. A part of this operation is illustrated in Fig. 3.

The meltdown furnace assembly shown in Fig. 4 adjoins the raw-materials loading room and is operated to provide a molten raw-material charge to each of the two adjacent batch processing units. After meltdown the molten fluoride mixture is sparged with hydrogen and helium at relatively high flow rates to remove insoluble carbon by entrainment. Beryllium metal turnings are also added to the molten charge to reduce sulfate impurities to sulfides and to reduce structural-metal impurities to their insoluble metallic states. During subsequent transfer of material to a batch processing unit, some of these insoluble impurities are separated by decantation.

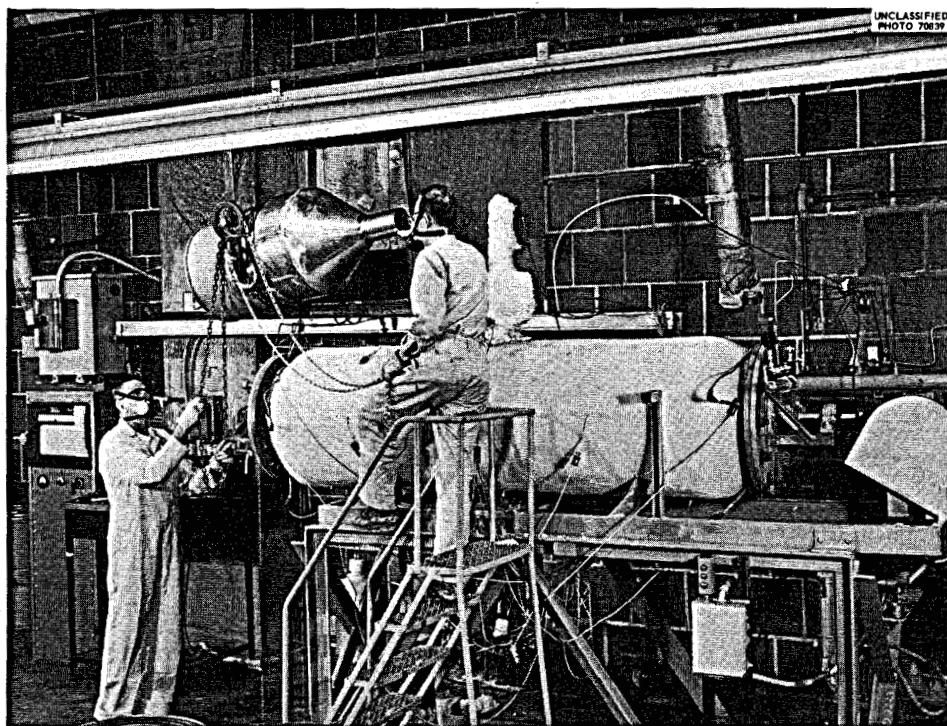


Fig. 2. Fluoride Production Facility - Horizontal Densification Kiln.



Fig. 3. Fluoride Production Facility - Raw Materials Handling Area.

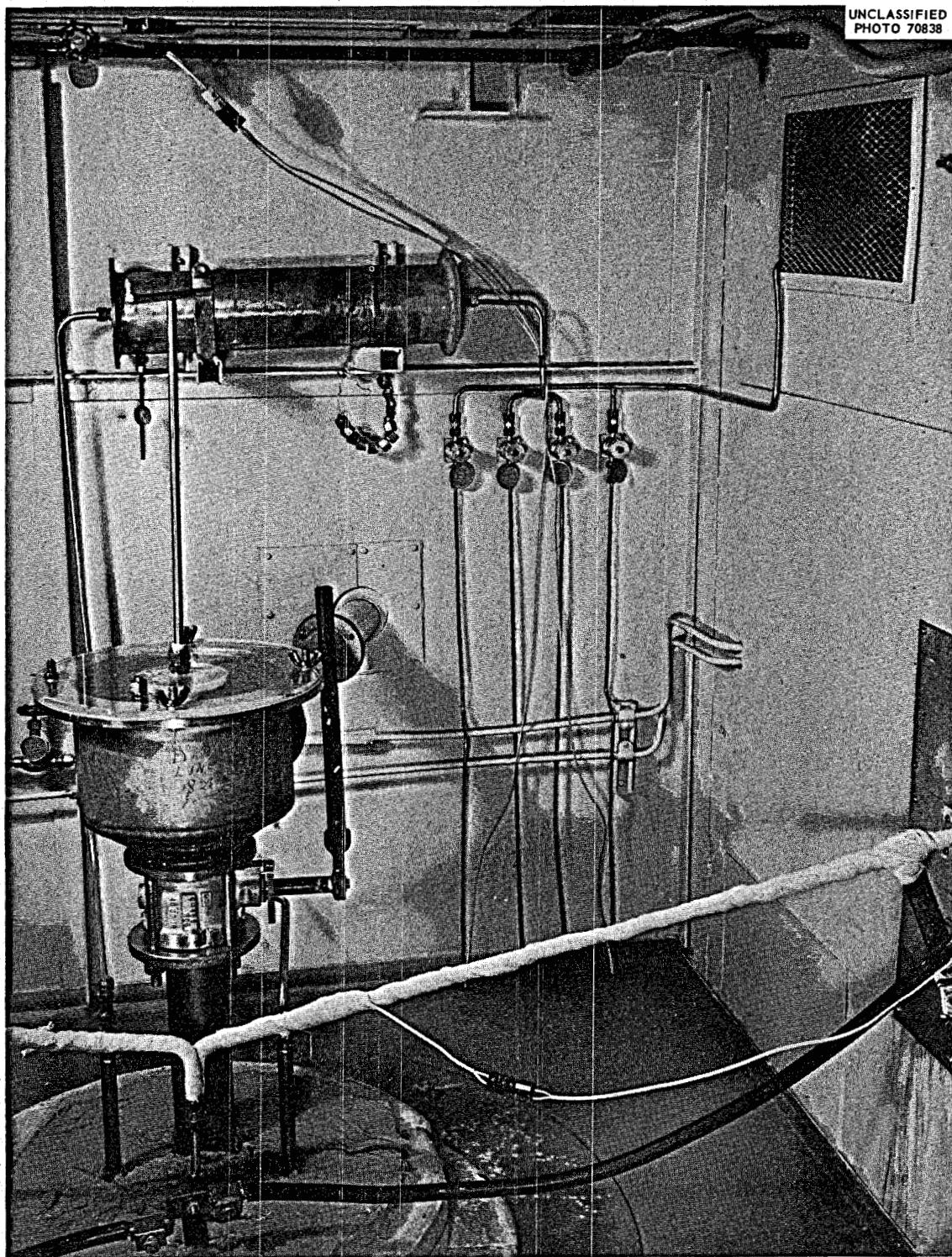


Fig. 4. Fluoride Production Facility - Premelting Furnace Assembly.

### Melt Purification

Each of the two processing units has a capacity of 2 ft<sup>3</sup> of salt per batch. Thus, the production of all fluoride mixtures for the MSRE will require a minimum of 94 batch preparations. A 10% production excess is planned to allow for usual contingencies. Although the production rate varies with the quality of the starting materials, the average batch cycle encountered thus far, including maintenance shutdown periods, is 164 hr.

Salt treatment vessels used in the process units as well as in the meltdown furnace are constructed of 12-in. iron pipe size 304L stainless steel pipe and are approximately 6 ft long. An inner liner fabricated from 1/8-in. grade A nickel sheet provides primary salt containment. Except for conventional loading ports and gas-line connections, the vessel is of welded construction. Salt storage containers are of the same approximate diameter but are only 3 ft in length. These vessels are made of nickel and are used only to store and dispense purified salt mixtures. The treatment vessels and salt storage vessels are heated by commercial resistance furnaces of 50 and 25 kw respectively. Figure 5 shows the arrangement of equipment in one of the two identical batch processing units.

A simplified schematic flow diagram of the unit process is shown in Fig. 6. The salt treatment vessel connects directly to the receiver vessel (salt storage container) through a small-diameter tube which functions as the process gas entry line during purification of the fluoride mixture and as the salt transfer line at the completion of the process. These vessels are also connected through the gas manifold system to provide centralized control over process conditions during salt purification and regulation of the differential gas pressure on the system during transfer of the molten charge to its storage container.

The gas effluent from the process is passed through a bed of sodium fluoride pellets to reduce HF concentrations to low values before discharge to the atmosphere. Since large quantities of hydrogen are used, exhaust gases are bubbled through an inert-liquid trap to isolate the process equipment from the atmosphere.

At the completion of the production cycle, the purified fluoride mixture is transferred to the salt storage container and allowed to cool. Interim storage under a static helium cover gas is provided within the production facility. The containers will be shipped to the reactor site, as they are needed, for remelting and transfer into the fluoride drain tanks of the MSRE.

### Process Control

To ensure delivery of acceptable fluoride mixtures to the MSRE, material balances and process conditions must be controlled during each phase of the production operation. In addition to accounts that show the source, quality, and amounts of raw materials used in each production batch, various measures are exercised during the processing cycle to provide quality control of the finished product. Primary process control is

UNCLASSIFIED  
PHOTO 70834

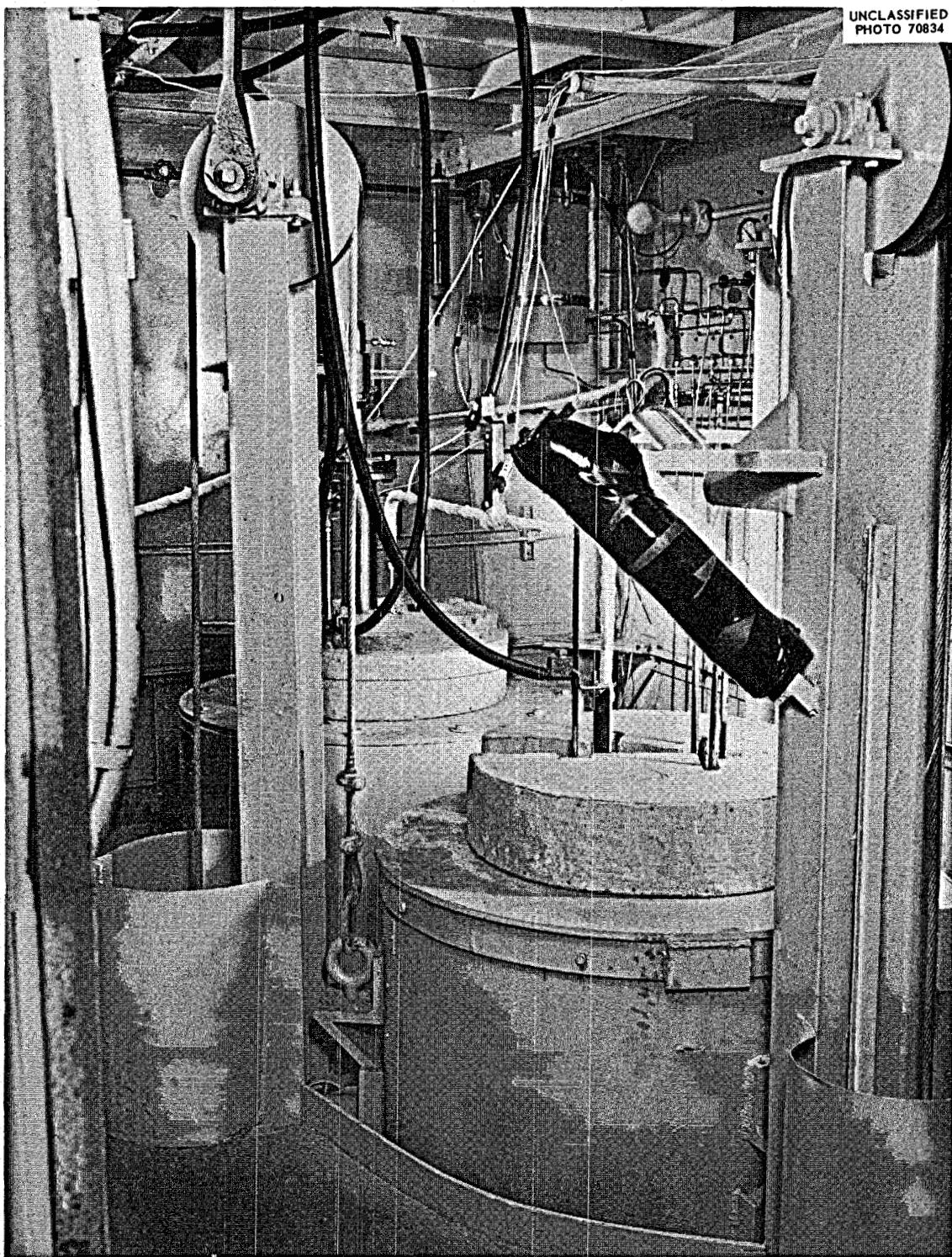


Fig. 5. Fluoride Production Facility - Batch Processing Unit.

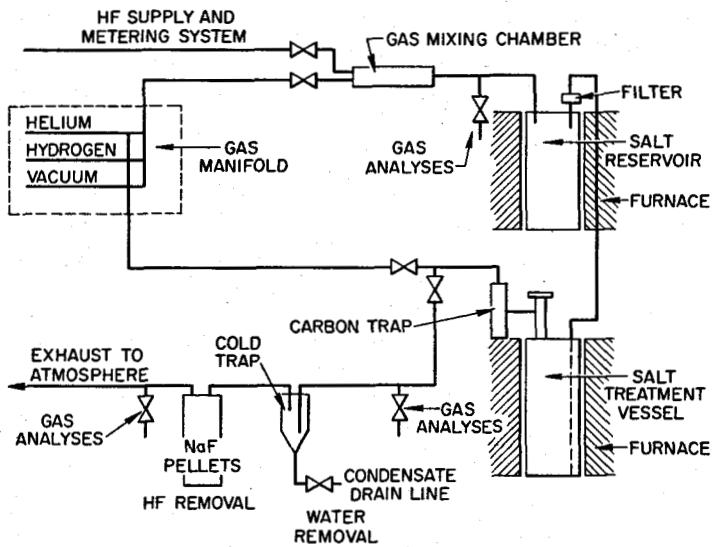
UNCLASSIFIED  
ORNL-DWG 64-6993

Fig. 6. Fluoride Production Facility - Simplified Schematic Process Diagram.

achieved by frequent analyses of the process gas streams. These analyses are used as guides for alteration or termination of process conditions and are, therefore, directly related to production efficiency and quality control. Secondary control of product quality is derived from chemical analyses of salt samples that are withdrawn from melts during processing operations. These results are used to determine the acceptability of the finished batches.

#### Process Gas analyses

The HF-H<sub>2</sub> concentration ratio in the gas influent to the salt treatment vessel is regulated according to results obtained by direct titration of a side stream with a standard KOH solution. A similar titration of the gas effluent stream is used to determine HF utilization. Typical results obtained during preparation of the MSRE coolant salt mixture are illustrated in Fig. 7 and show the high degree of HF utilization that is characteristic during initial treatment of the molten raw materials.

Hydrogen sulfide is collected in an ammoniacal cadmium chloride solution from the gas effluent stream and is titrated with a standard iodine solution. Material balances on sulfur evolved as H<sub>2</sub>S from the treatment vessel as compared with the quantity of sulfur believed to be present in the raw-materials charge are often in disagreement and probably result from the precipitation of sulfur compounds in the meltdown furnace. However, experience obtained thus far shows that the rate of H<sub>2</sub>S evolution is indicative of the concentration of sulfur remaining in the melt. This condition appears valid only when all sulfates have been reduced to sulfides. Removal of sulfur from the melt, therefore, is not considered complete until a subsequent addition of beryllium metal fails to result in

an increase in the  $H_2S$  evolution rate. Results shown in Fig. 8 illustrate the sensitivity of this control measure.

Water vapor which results from the reaction of HF with oxide ion in the melt is condensed, with some HF, from the gas effluent stream in a

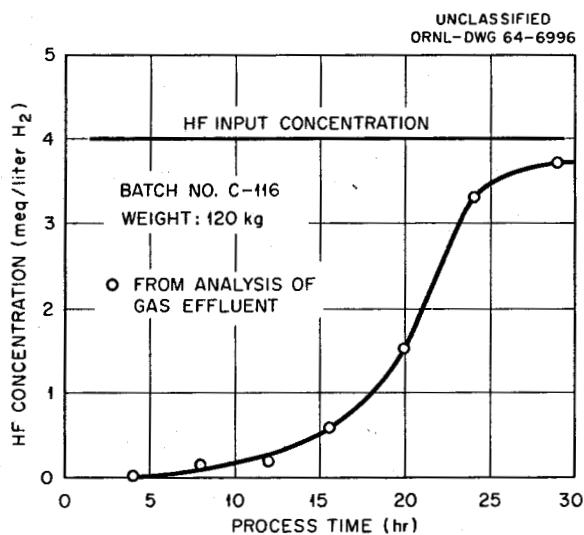


Fig. 7. Fluoride Production for MSRE - Utilization of HF During Purification of  $^7\text{LiF-BeF}_2$  (66-34 mole %) at  $600^\circ\text{C}$ .

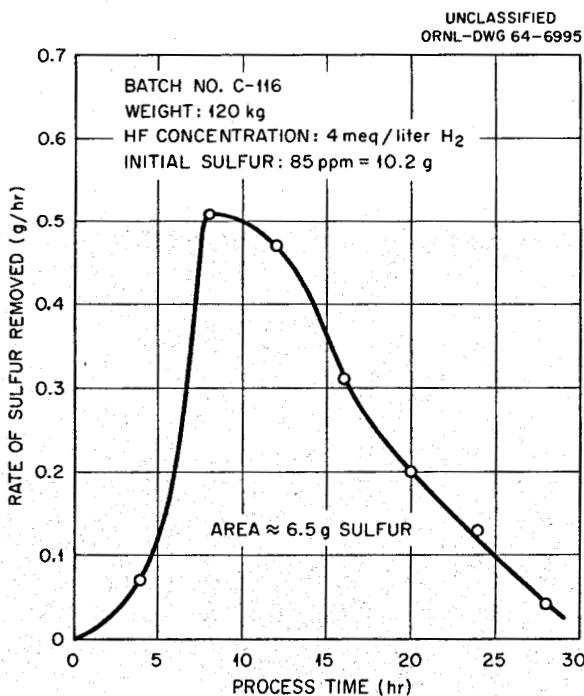


Fig. 8. Fluoride Production for MSRE - Removal of Sulfur Impurities from  $^7\text{LiF-BeF}_2$  (66-34 mole %) During HF- $H_2$  Treatment at  $600^\circ\text{C}$ .

cold trap. The condensation chamber is maintained at about  $-12^{\circ}\text{C}$  by refrigerating a surrounding ethylene glycol-water bath. Development tests have shown that essentially all water vapor can be condensed from an HF-H<sub>2</sub> stream at this temperature. The contents of the cold trap are drained periodically and analyzed for water content. The reproducibility of results obtained by this process control method on a number of salt preparations is shown in Fig. 9. Oxide removal is considered complete when the water-removal rate becomes negligible.

During the final hydrogen sparging treatment, the reduction of structural metals results in the evolution of HF. The rate of HF evolution is indicative of the reduction rate and is also a function of the structural-metal ion concentration of the melt. Therefore, the HF content of the gas effluent is monitored periodically by direct titration with a standard KOH solution. Values obtained by this procedure are used to determine process completion.

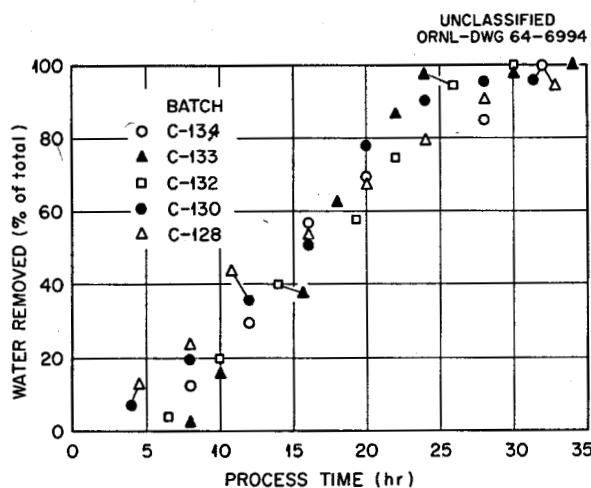


Fig. 9. Fluoride Production for MSRE - Removal of Oxides from  ${}^7\text{LiF-BeF}_2$  (66-34 mole %) During HF-H<sub>2</sub> Treatment at  $600^{\circ}\text{C}$ .

#### Salt Analyses

Chemical analyses are obtained on salt samples that are withdrawn from the melts into copper filter tubes during processing operations. These tubes are previously fired in an atmosphere of flowing hydrogen and installed in a sampler device. This assembly is fitted onto a valved port of the treatment vessel and permits sampling under existing process conditions without extraneous contamination to the sample. Salt is crushed from these sample tubes in a glove box and stored in glass sample bottles.

The concentrations of impurities found by chemical analyses of final salt samples taken for production thus far are shown in Table 2. Values for "oxides removed" were determined from quantities of water collected

Table 2. Fluoride Production for MSRE - Results of Chemical Analyses of Batch Preparations of  $^7\text{LiF}$ - $\text{BeF}_2$  (66-34 mole %)<sup>a</sup>

| Batch Nos. | Average Concentrations of Impurities (ppm) |    |     |                 | Oxides Removed |
|------------|--|----|-----|-----------------|----------------|
|            | Cr   | Ni | Fe  | S               |                |
| 101-105    | 13   | 31 | 183 | <5              | 1391           |
| 106-110    | 11   | 26 | 161 | <5              | 1110           |
| 111-115    | 10   | 19 | 180 | <5              | 1828           |
| 116-120    | 15   | 20 | 164 | <5              | 1473           |
| 121-125    | 50   | 21 | 115 | <5              | 1465           |
| 126-130    | 14   | 22 | 127 | <7 <sup>b</sup> | 2301           |

<sup>a</sup>Batch size, 120 kg of salt mixture.

<sup>b</sup>Batch 126 at 37 ppm of sulfur, all others at <5 ppm.

in the effluent gas cold trap. The values for chromium concentrations are low but significant because they reflect the integrity of the treatment vessel. Should the nickel liner in this vessel fail, a rapid increase in chromium concentrations would occur by corrosion of the stainless steel outer vessel.

#### Reactor Loading

The fluoride production method is generally independent of fluoride mixture composition provided that the liquidus temperature of the mixture is within the capability of the process equipment. The production of multicomponent mixtures, however, is sometimes facilitated by the preparation and subsequent combination of simpler binary or ternary mixtures. As applied to the production of the fuel salt mixture for the MSRE, this technique is advantageous to both production and reactor operations.

To provide for conservation of fissionable material, for nuclear safety, and for planned reactor operations, the MSRE fuel salt will be prepared as a fuel concentrate mixture and as a barren fuel solvent mixture. The fuel concentrate mixture will consist of the binary eutectic mixture  $^7\text{LiF}$ - $\text{UF}_4$  (73-27 mole %); the barren fuel solvent mixture will consist of the balance of fluoride salts required to achieve the overall fuel composition  $\text{LiF}$ - $\text{BeF}_2$ - $\text{ZrF}_4$ - $\text{UF}_4$  (65.0-29.1-5.0-0.9 mole % respectively).

The fuel concentrate mixture will be further segregated as the enriched fuel concentrate mixture, which will contain all  $^{235}\text{U}$  as highly enriched  $^{235}\text{UF}_4$ , and as the depleted fuel concentrate mixture, which will

contain the balance of nonfissionable uranium required for the fuel salt mixture. This depleted material will be prepared in two batches by conventional processing techniques.

The enriched fuel concentrate mixture will be produced in six small batch preparations. Each batch will contain approximately 60 lb of salt mixture, of which 33 lb will be  $^{235}\text{U}$ . Although the processing technique will be essentially the same as that used for conventional fluoride production, the operation will be carefully regulated according to established criticality-control procedures.

Before critical experiments are conducted in the reactor, uranium analyses and inventory procedures will be checked out on a mixture of the depleted fuel concentrate and the barren fuel solvent. Approach to the critical and then to the operating conditions of the MSRE will be achieved by incremental additions of enriched fuel concentrate mixture to the reactor fuel.

#### Production Economics

During the course of fused fluoride production at ORNL, modifications and revisions have been made on the facility to meet specific safety requirements and to incorporate procedural changes which have resulted from process development programs. When the use of beryllium fluoride in fused fluoride mixtures became attractive to the Molten-Salt Reactor Program, extensive modifications in the physical plant were made to cope with health hazards which accompany the handling of beryllium compounds. The required preparation of large quantities of identical fluoride mixtures for the MSRE also made possible the effective use of a single meltdown furnace assembly. Other production features developed for the process have required only minor revision of the facility. The replacement value of the production facility is probably in the range of \$300,000 to \$500,000.

Present operation of the production facility for the preparation of MSRE materials is conducted on a seven-day, three-shift schedule. Each shift requires a technical operator and an assistant for routine maintenance. Other supporting crafts are employed for nonroutine maintenance as required. Operation, maintenance, and equipment costs are budgeted at an average of \$20,000/month.

Data on the fluoride starting materials that have been acquired for the production of MSRE materials are shown in Table 3. The cost of the raw materials for the coolant and flush salt mixture,  $^7\text{LiF-BeF}_2$  (66-34 mole %), is \$11.29/lb, and that of the fuel salt, excluding  $^{235}\text{U}$ , is \$10.13/lb. As calculated from operating and raw-materials costs, the coolant and flush salt mixture has an estimated value of \$19.71/lb. A similar cost for the fuel salt mixture, excluding  $^{235}\text{U}$ , is estimated at \$17.33/lb. Thus, the initial charge of coolant, flush, and fuel salt mixtures for the MSRE will have an estimated value of \$496,400, exclusive of plant amortization and uranium costs.

Table 3. Costs of Raw Materials Used in MSRE Fluoride Production

| Material       | Quantity                           | Unit Cost (\$)     | Total Cost (\$) |
|----------------|------------------------------------|--------------------|-----------------|
| $^7\text{LiF}$ | 22,000 lb                          | 16.50 <sup>a</sup> | 363,000         |
| $\text{BeF}_2$ | 12,000 lb                          | 5.70               | 68,400          |
| $\text{ZrF}_4$ | 2,300 lb                           | 8.00               | 18,400          |
| $\text{UF}_4$  | 90 kg<br>( $^{235}\text{U}$ basis) | 12,000.00          | 1,080,000       |
|                |                                    | Total              | 1,529,800       |

<sup>a</sup>Includes \$1.82/lb for preparation as fluoride salt.

#### References

1. G. J. Nessle and W. R. Grimes, Chem. Eng. Progr., Symp. Ser. 56(28), 51 (1960).
2. MSRP Semiann. Progr. Rept. Jan. 31, 1964, ORNL-3626, p. 137.
3. MSRP Semiann. Progr. Rept. July 31, 1963, ORNL-3529, p. 117.
4. C. F. Baes, Jr., and H. H. Stone, private communication to H. F. McDuffie, July 27, 1964.
5. Fluid Fuel Reactors, ed. by J. A. Lane, H. G. MacPherson, and F. Maslan, p. 599, Addison-Wesley, Reading, Mass., 1958.
6. C. M. Blood, Solubility and Stability of Structural Metal Difluorides in Molten Fluoride Mixtures, ORNL-CF-61-5-4 (Sept. 21, 1961).
7. G. W. Keilholtz et al., Reactor Chem. Div. Ann. Progr. Rept. Jan. 31, 1961, ORNL-3127, p. 133.
8. B. J. Sturm, A Method for Densifying Lithium Fluoride Powder, MSR-62-94 (Nov. 20, 1962) (internal use only).

FUTURE CHEMICAL DEVELOPMENT

H. F. McDuffie

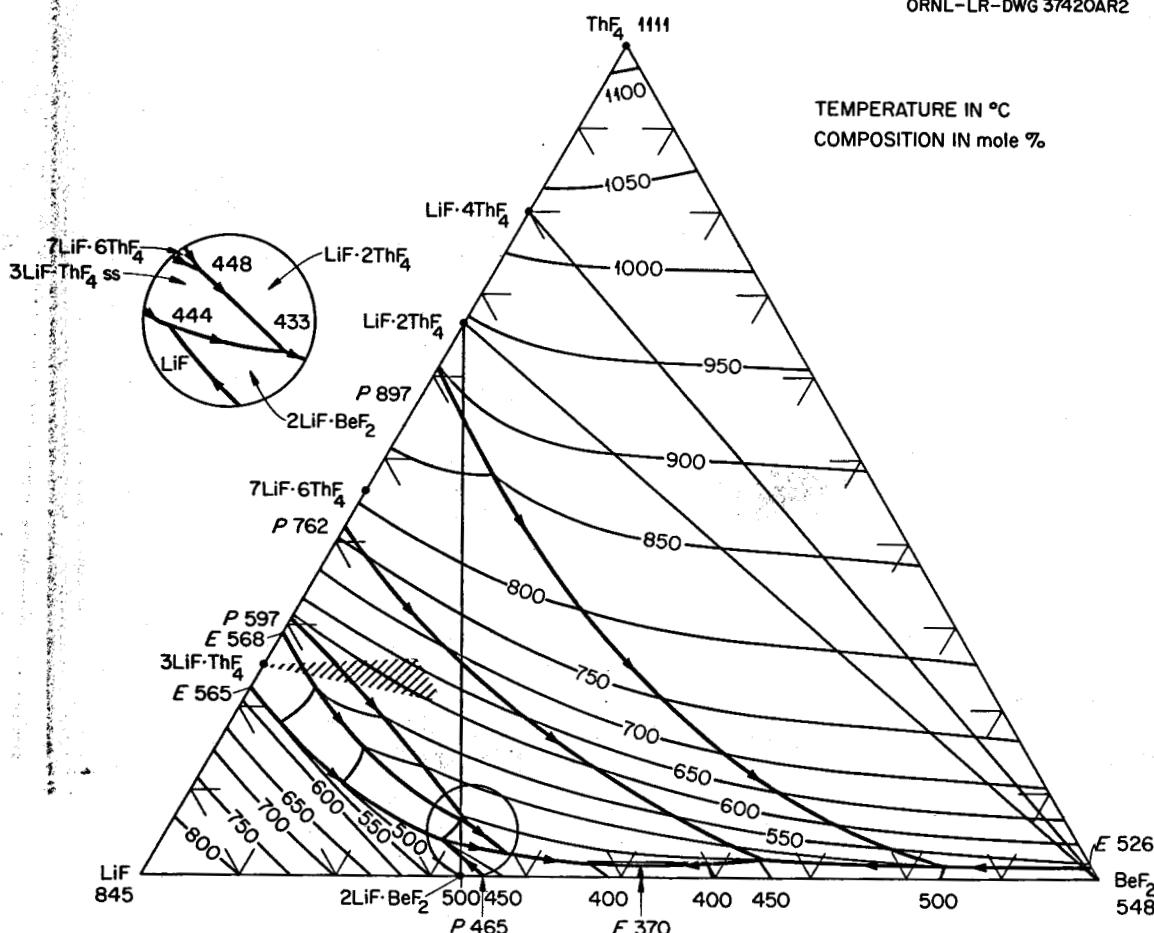
The MSRE illustrates a reactor concept - the fluid fuel concept - which has been espoused and under development in two different embodiments by ORNL since 1949. The major advantage of this concept, and the one which supports continuing chemical research and development, is that changes in the fuel or blanket compositions can be made without the requirement of metallurgical or ceramic refabrication. Fertile material can be added, bred fissionable material and fission products can be removed, and samples can be taken for analysis, all without interrupting the operation of the reactor. The accompanying major disadvantage is that the radioactive fission products are dispersed throughout the system, complicating the containment and maintenance problems.

As a consequence of the research and development work done for the ARE and the MSRE, and also the fundamental research studies of molten salts supported by the AEC Division of Research throughout the last 15 years, there are a number of chemical developments which permit a tentative look ahead to the extension of the molten-salt concept to economical operation and to a broader range of reactors. Reactors closely related in type to the MSRE will be discussed first, with other types of thermal and fast reactors discussed later.

One- and Two-Region Molten Fluoride ReactorsFuels and Blankets

The importance of using thorium and the existence of possibly suitable vehicles have been discussed in previous sections, but a restatement will be made for emphasis. Figure 1 shows the system LiF-BeF<sub>2</sub>-ThF<sub>4</sub> as studied by Thoma et al.;<sup>1</sup> a maximum of 24 mole % ThF<sub>4</sub> can be accommodated in solution at 550°C. This is equivalent to 78 wt % ThF<sub>4</sub>, or 2400 g of thorium per liter. The system LiF-BeF<sub>2</sub>-UF<sub>4</sub> (ref. 2) is quite similar to the thorium system, with even a slight lowering of the liquidus temperatures upon the fractional substitution of the uranium for thorium in the quaternary system LiF-BeF<sub>2</sub>-UF<sub>4</sub>-ThF<sub>4</sub> (ref. 3). Thus both thorium blankets for two-region breeder reactors and thorium-uranium fuels for single-region converters are potentially available.

Barton and co-workers have also measured the solubility of PuF<sub>3</sub> in alkali fluoride-beryllium fluoride mixtures<sup>4</sup> and found values of 0.2 to 1.0 mole % in the temperature range 500 to 600°C. Figure 2 illustrates the effect of temperature and shows, also, that there is a substantial effect of solvent composition on plutonium solubility. Thus, molten fluoride reactors should be operable with plutonium as the fissionable fuel component instead of uranium.

UNCLASSIFIED  
ORNL-LR-DWG 37420AR2Fig. 1. The System LiF-BeF<sub>2</sub>-ThF<sub>4</sub>.

Consideration has also been given to reactors in which a fast reactor core can be surrounded by a static molten-salt blanket. (All moderator materials would have to be absent from the core; and lithium and beryllium could not be used in the blanket, but fluorine could be present.) The system NaF-KF-ThF<sub>4</sub> (ref. 5) provides molten mixtures which appear suitable for such a blanket; the lowest melting eutectic in the system, as shown in Fig. 3, contains 26 mole % ThF<sub>4</sub> and melts at about 562°C. This mixture contains 65 to 70 wt % ThF<sub>4</sub> and about 2400 g of thorium per liter.

#### Materials Compatibility

The compatibility of molten fluorides with INOR-8 (or Hastelloy N) and graphite is apparently excellent, as indicated by the chapters on chemistry, radiation effects, graphite, and metallurgy, as well as by the long history of development work with molten fluorides in both the MSR and the ANP programs. Nevertheless, many questions of long-term

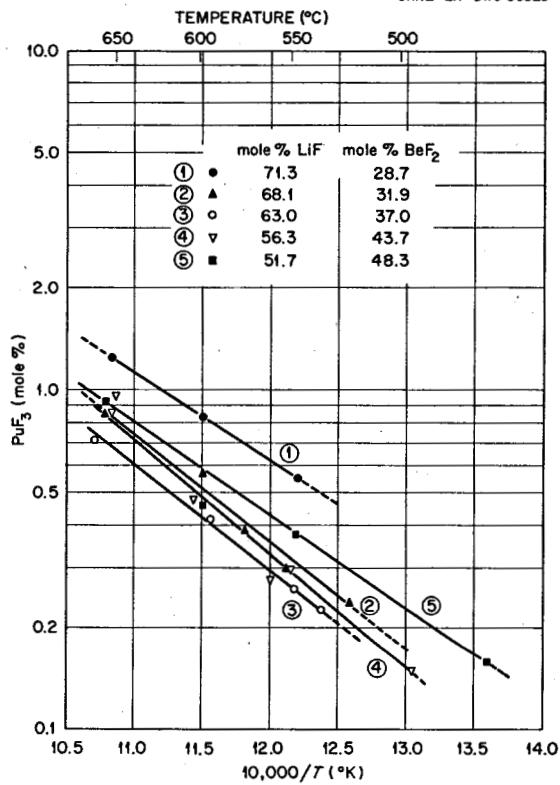
UNCLASSIFIED  
ORNL-LR-DWG 36820

Fig. 2. Solubility of PuF<sub>3</sub> as a Function of Temperature for LiF-BaF<sub>2</sub> Solvents.

compatibility remain to be determined. The chemical effects of the accumulation of fission products will certainly require study, and the irradiation tests should be extended to cover progressively more severe conditions which ultimately exceed by a substantial margin the projected reactor operating conditions.

#### Chemical Reprocessing

The main advantage of the fluid fuel concept, the ready availability of the fuel for whatever physical or chemical treatment is desired, furnishes the main source of future chemical development — laying a basis for selective chemical reprocessing. The addition of components to a molten-salt mixture is a relatively simple operation, but the removal of either dissolved or suspended materials is considerably more difficult.

A number of fuel-reprocessing schemes have been proposed, and some have been developed. Dawson and Sowden,<sup>6</sup> in their excellent recent book, discuss these under the following headings:

1. Fluorination — to remove volatile uranium hexafluoride (described in a previous section),

UNCLASSIFIED  
ORNL-DWG 64-4014

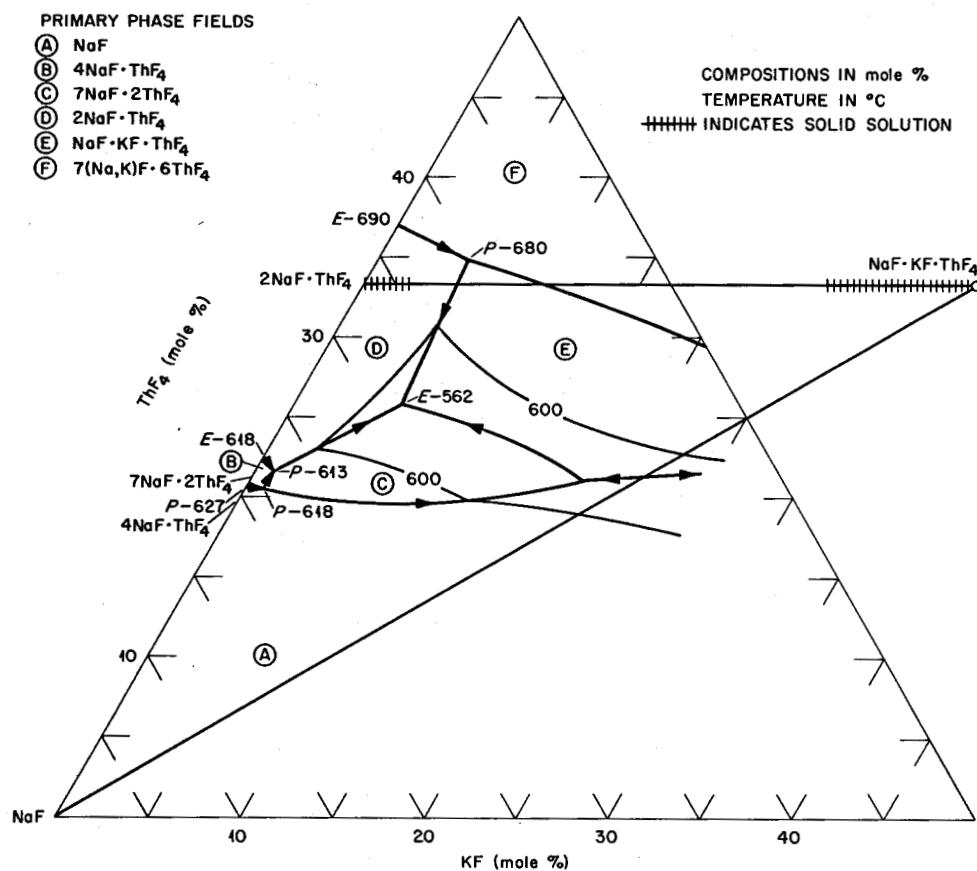


Fig. 3. The System  $\text{NaF-KF-ThF}_4$ .

2. Fluoride precipitation - including the exchange of rare earths with cerium trifluoride,
3. Electrolysis - which would remove elements whose decomposition potential is lower than that of the main melt constituents (leaving lanthanides in solution),
4. Oxide precipitation - including the use of beryllium oxide and water vapor to precipitate uranium dioxide.

Fission Product Rare Gases. Of the fission products produced in a molten fluoride fuel, the noble gases should most readily escape as a consequence of their low solubility.<sup>7</sup> Figure 4 illustrates the low solubility of helium, neon, argon, and xenon in molten  $\text{LiF-BeF}_2$  over a temperature range of interest to reactor operation. Future chemical development in this field will be limited to confirmatory measurements of solubility in new fuel or blanket compositions. The factors governing the diffusion of gases through graphite and other porous media have been thoroughly studied<sup>8</sup> in connection with the development of gas-cooled reactors. For application to the unclad graphite in molten-salt reactors, it may be important in the future to determine the diffusive behavior of

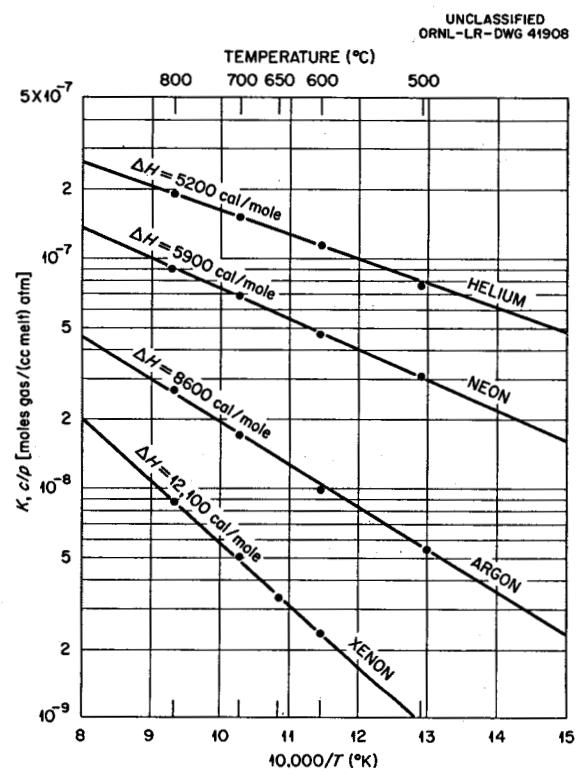


Fig. 4. Temperature Dependences of Solubilities of Noble Gases in LiF-BeF<sub>2</sub> (64-36 mole %).

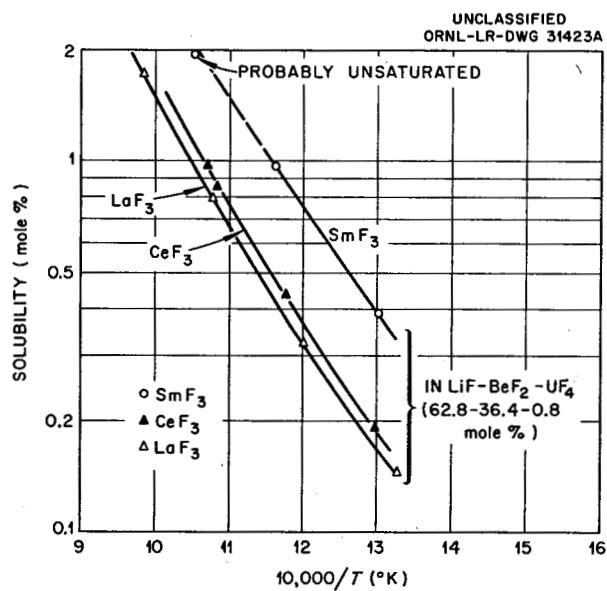


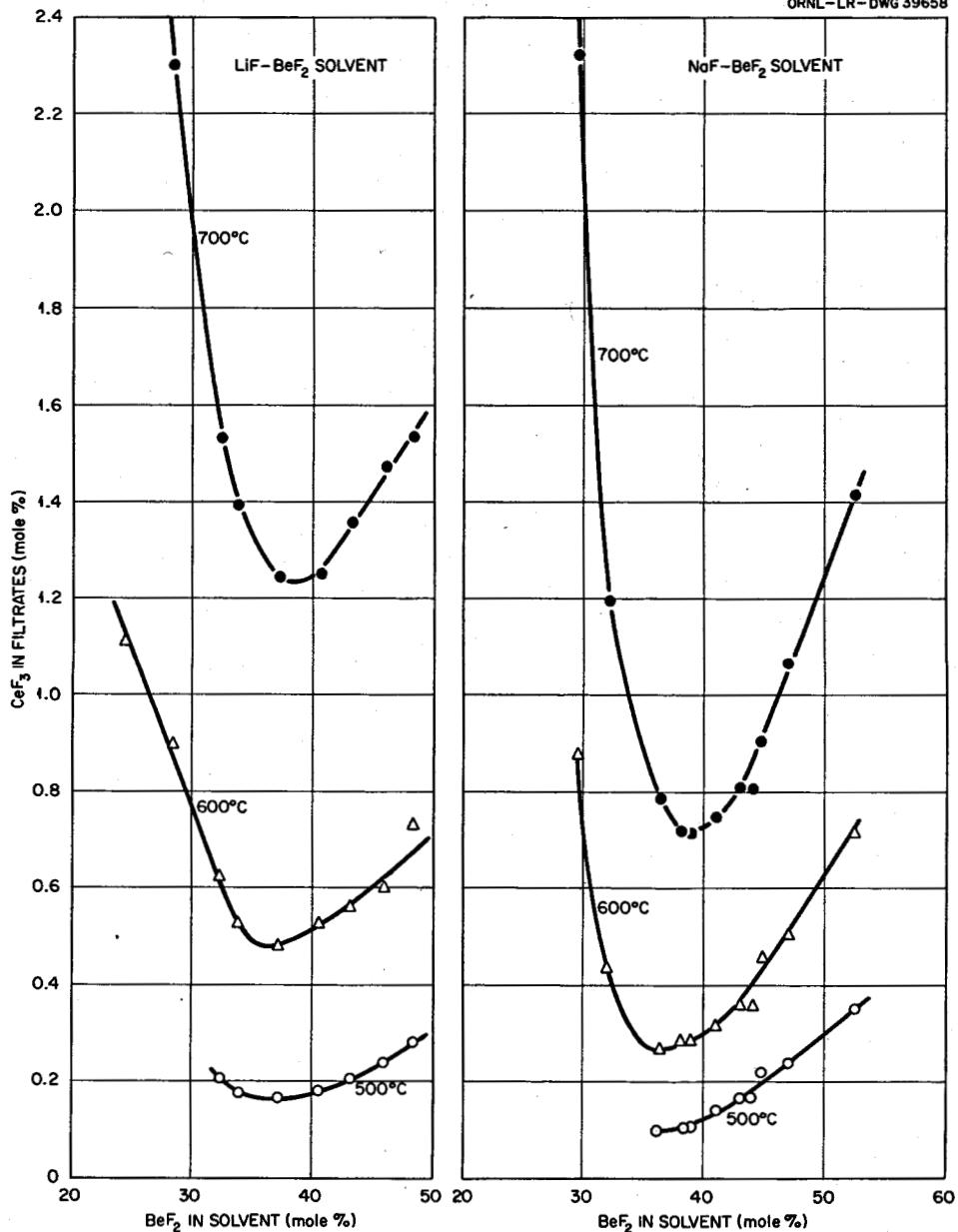
Fig. 5. Solubility of CeF<sub>3</sub> and LaF<sub>3</sub> in LiF-BeF<sub>2</sub>-UF<sub>4</sub> (62.8-36.4-0.8 mole %).

the fission product gases in the very impermeable graphites which are suitable for use with molten fluorides.

Rare Earths. The long-lived rare-earth fission products form very stable trifluorides and contribute a large proportion of the total fission product poisoning. Their removal is very necessary for economic operation. Figure 5 illustrates the solubility of  $\text{CeF}_3$ ,  $\text{LaF}_3$ , and  $\text{SmF}_3$  in a  $\text{LiF-BeF}_2$  mixture of the same ratio as the MSRE solvent.<sup>9</sup>

The work of Ward *et al.*<sup>10</sup> showed that exchange reactions between solid cerium trifluoride and dissolved rare-earth fluorides of higher cross section would occur, with the molten fluoride becoming saturated with cerium fluoride and the solid phase being a solid solution of a small amount of rare-earth fluoride in cerium fluoride. The solubility of cerium fluoride has been shown to be extremely dependent on the composition of binary fluoride solvent mixtures such as  $\text{LiF-BeF}_2$  and  $\text{NaF-BeF}_2$ , as illustrated by Fig. 6; strong dependence on temperature is also shown by these studies. Although it is not attractive to consider use of a fuel saturated with even ~0.1 mole % of cerium, it seems quite likely that more study of the solubility and composition relationships involving the rare-earth fluorides may be profitable.

A technique, which from recent results appears simple and feasible, involves the vacuum distillation of an irradiated fluoride fuel to recover  $^7\text{LiF}$ ,  $\text{BeF}_2$ , and  $\text{ZrF}_4$ , leaving the uranium and rare-earth fission products behind. Vapor phase transport of salt components is, of course, well known. Kirsilis, Savolainen, and Blankenship<sup>11</sup> noted distillation as a consequence of the temperature gradients present in capsules under irradiation. Their evidence suggested that the distillate had a composition near that of  $2\text{LiF}\cdot\text{BeF}_2$ . Kreyger,<sup>12</sup> in studies of the behavior of sessile drops of molten  $2\text{LiF}\cdot\text{BeF}_2$ , noted that the surface became rich in  $\text{LiF}$  and that distillate drops were 95%  $\text{BeF}_2$ . Thoma, Singh, and Ross studied the purification of  $\text{LiF}$  by vacuum distillation;<sup>13</sup> they reported that the impurities and the  $\text{LiF}$  distilled in the order of the vapor pressures of the components, with  $\text{NaF}$  and  $\text{MnF}_2$  coming over ahead of the bulk of the  $\text{LiF}$  and with  $\text{CaF}_2$  and  $\text{MgF}_2$  being left behind. In very recent studies, Kelly has examined the vacuum distillation of MSRE fuel, to which he had added europium to represent the rare-earth fission product poisons. A charge of 57.2 g of fuel was distilled from a stainless steel pot at temperatures in the range of 1000 to 1050°C. Samples of approximately 5 g each were taken serially and analyzed for the fuel components Li, Be, Zr, F, U, and (by counting techniques) Eu. Figure 7 shows the smooth change in Li to Be ratio of the distillate, the inclusion of the zirconium along with the beryllium, and the very low concentration of europium. Actually, the relatively larger concentration of europium observed in the initial stages of the experiment is attributed entirely to the result of dusting, as the initial charge was powdered and the vacuum was applied before the charge was first melted. If these results are confirmed by tests with other rare earths, a "brute-force" technique for recovering the lithium and beryllium fluorides seems assured, with the residue containing the rare earths plus the uranium being a much more desirable charge for the fluoride volatility process than the entire fuel volume would have been.

UNCLASSIFIED  
ORNL-LR-DWG 39658Fig. 6. Solubility of  $\text{CeF}_3$  in  $\text{LiF-BeF}_2$  and  $\text{NaF-BeF}_2$ .

Zone melting is also being explored as a potential basis for purification of irradiated fuel. Singh, Brunton, and Thoma<sup>14</sup> have reported that 12 passes of a 3-cm zone at 1 cm/hr removed an initial concentration of 1000 ppm each of  $\text{CeF}_3$ ,  $\text{GdF}_3$ , and  $\text{LuF}_3$  from a 30-cm ingot of  $\text{LiF}$ . The choice of the three rare earths was such as to provide representatives of the three classes of phase behavior observed in  $\text{MF-MF}_3$  systems — no intermediate compound, an incongruously melting intermediate compound, and a congruently melting intermediate compound.

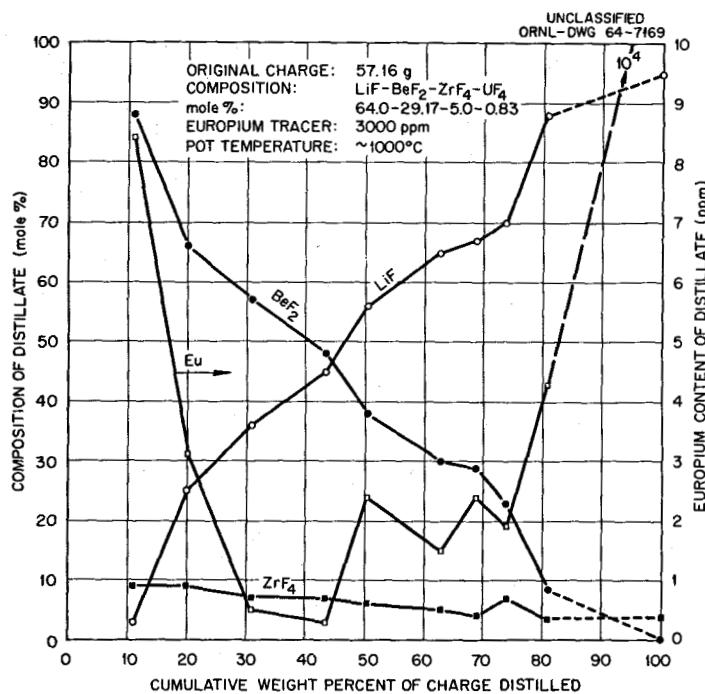


Fig. 7. Distillation of MSRE Fuel.

The extraction of rare-earth fission products from liquid-metal reactor fuels into molten salts was explored at Brookhaven National Laboratory in connection with the LMFR.<sup>15</sup> Favorable distribution coefficients were found for rare-earth removal when the composition and redox potential of the salt were properly controlled. The converse extraction, from molten fluorides into liquid metals, would be necessary if rare-earth fission products were to be removed from the fuel of the MSRE or similar reactors. Baes<sup>16</sup> has recently considered the application of this process to molten fluoride reactors in the light of available thermodynamic knowledge. The higher stability of the rare-earth trifluorides as compared with beryllium fluoride would require that an extremely stable intermetallic compound of the rare earth and a reduced metal be formed in order for the extraction to be successful. Recent information on the activity coefficients of cerium in molten zinc and lead<sup>17</sup> suggests that these metals would not be suitable; further consideration of tin and bismuth may be worthwhile. A current paper<sup>18</sup> indicates that, at 600°C, in the system Mg-40% Th/KCl-LiCl-25% MgCl<sub>2</sub>/Zn-7% Mg, the three solutes yttrium, cerium, and neodymium were each extracted from the Mg-40% Th through the salt and into the Zn-7% Mg alloy - to the extent of over 95% in 2 hr. Modifications of the composition of the molten-salt portion of a metal-salt extraction system are known to have profound effects upon the distribution of solutes; Moore<sup>19</sup> has shown that changes in the AlCl<sub>3</sub>:KCl mole ratio can change the distribution coefficient for uranium between the molten chlorides and molten aluminum at 725°C by a factor of 50 or more. In future chemical development, considerable emphasis in fundamental

studies will be placed on the determination of the activities of various solutes in molten fluorides, as a function of solvent composition, redox potential, and temperature. The techniques of electrochemistry, liquid-liquid extraction into molten metals, and control of gas-phase composition will be used in these studies.

Removal of Uranium and Protactinium. Shaffer et al.<sup>20</sup> have reported the recovery of protactinium and uranium from molten fluoride systems by precipitation as oxides. Initially, trace quantities (1 to 2 ppb of  $^{233}\text{Pa}$ ) were removed from the molten solvent mixture  $\text{LiF-BeF}_2\text{-ThF}_4$  (67-18-15 mole %) by the addition of powdered  $\text{BeO}$  or  $\text{CaO}$ , as shown by Fig. 8. In subsequent tests more realistic concentrations (with respect to reactor applications) of protactinium in the fluoride solvent were obtained by dissolving  $^{231}\text{Pa}$  to the extent of 50 to 75 ppm in the fluoride melt. The removal of this larger concentration of protactinium from solution by the addition of powdered  $\text{BeO}$  or  $\text{ThO}_2$  is shown in Fig. 9. When both protactinium and uranium were present initially in solution, the addition of  $\text{BeO}$  appeared to precipitate both, with the protactinium removed first and preferentially, as shown in Fig. 10. Even  $\text{UO}_2$  was able to remove the  $^{231}\text{Pa}$  from solution, as shown in Fig. 11. After each removal of protactinium from solution, the precipitated protactinium was returned to solution easily when the contents of the pot (melt and precipitate) were treated with gaseous HF. These results suggest a number of ways in which selective precipitation could be used in connection with reactors which depend on the conversion of thorium to  $^{233}\text{U}$ .

Studies of the crystallization path of MSRE fuel revealed that uranium was not present in the first two phases to appear ( $2\text{LiF}\cdot\text{BeF}_2$  at  $434^\circ\text{C}$  and

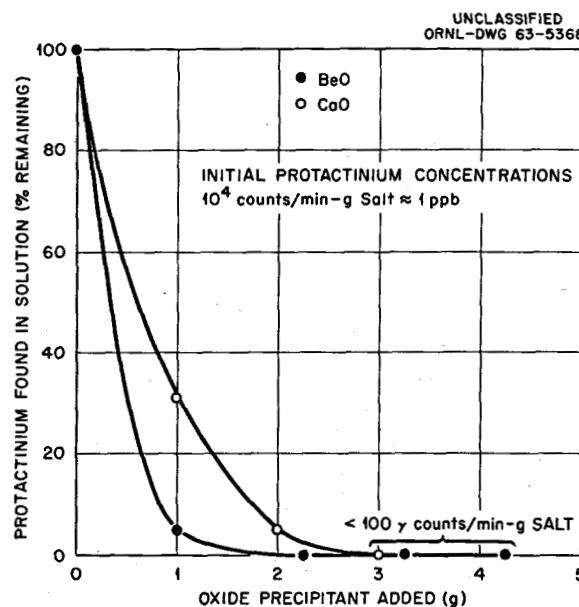


Fig. 8. Removal of Protactinium ( $^{233}\text{Pa}$ ) from Solution in  $\text{LiF-BeF}_2\text{-ThF}_4$  (67-18-15 mole %) by Reaction with  $\text{BeO}$  and  $\text{CaO}$  at  $650^\circ\text{C}$ .

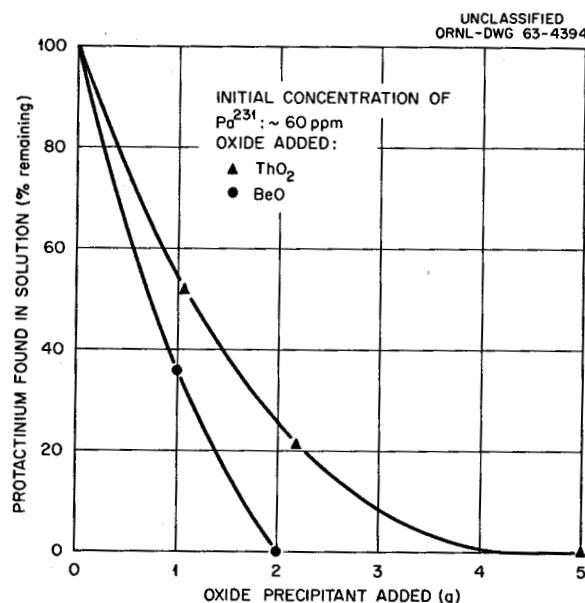


Fig. 9. Removal of Protactinium ( $^{231}\text{Pa}$  Labeled with  $^{233}\text{Pa}$ ) from Solution in  $\text{LiF-BeF}_2\text{-ThF}_4$  (67-18-15 mole %) by Reactions with  $\text{BeO}$  and  $\text{ThO}_2$  at  $650^\circ\text{C}$ .

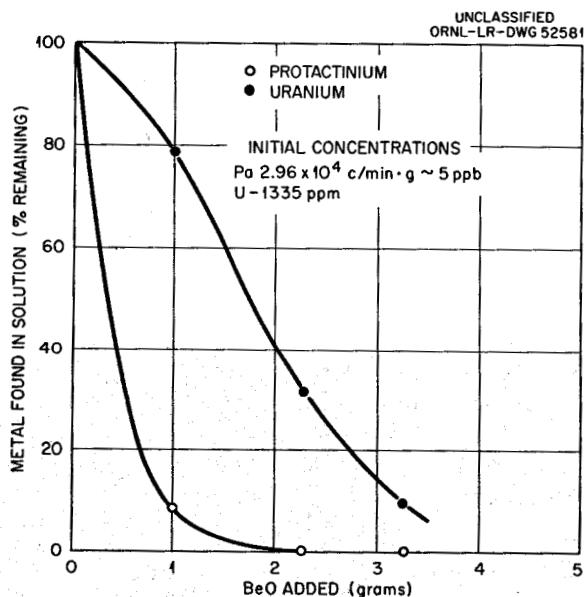


Fig. 10. Reaction of  $\text{BeO}$  with Protactinium and Uranium Dissolved in  $\text{LiF-BeF}_2\text{-ThF}_4$  (67-18-15 mole %) at  $650^\circ\text{C}$ .

$2\text{LiF}\cdot\text{ZrF}_4$  at  $431^\circ\text{C}$ ). Zone-melting experiments with a vertical tube and upward passes failed to cause any unusual concentration of uranium, but, as illustrated by Fig. 12, 20 downward passes gave a very substantial concentration of uranium. An effect of gravity has been reported in zone melting but only for insoluble trash in the material; this new effect involving soluble uranium should prove very interesting and rewarding to

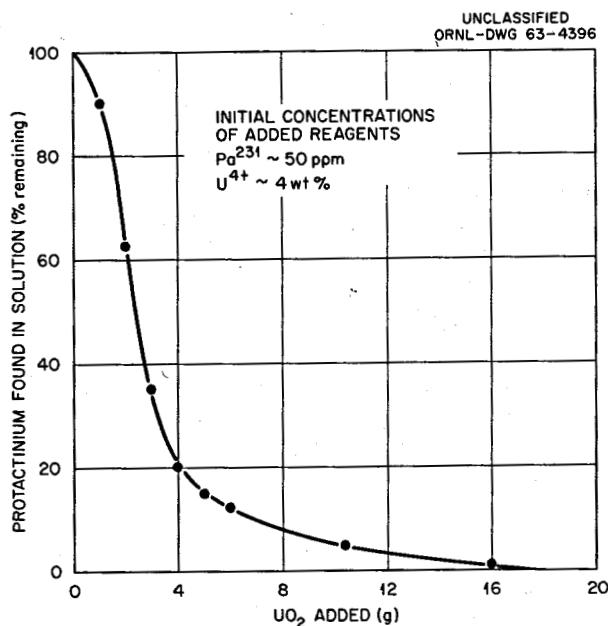


Fig. 11. Removal of Protactinium ( $^{231}\text{Pa}$  Labeled with  $^{233}\text{Pa}$ ) from Solution in LiF-BeF<sub>2</sub>-ThF<sub>4</sub> (67-18-15 mole %) by Reaction with UO<sub>2</sub> at 650°C.

exploit. There is a report from previous work that stratification sometimes resulted from thermal cycling melts containing uranium or thorium.<sup>21</sup>

#### Other Types of Molten-Salt Reactor Systems

##### Direct Heat Exchange

Direct heat exchange between molten salts (fluorides or chlorides) and liquid lead has been given consideration as an innovation which would permit the use of a nearly static core and blanket system, with the liquid lead circulated through the molten salt and an external heat exchanger. Such a system would greatly lower the fuel inventory and might offer better heat transfer characteristics. Blankenship, Kreyger, and Kirslis<sup>22</sup> found that molten lead gave good phase separation after being dispersed in molten chlorides or fluorides, even in the presence of solid oxides. In an NaCl-KCl melt at about 500°C, sparging a suspension of lead in the melt with an oxygen-containing gas caused the development of a red color (from dissolved lead oxide); subsequent sparging with hydrogen reduced the lead salt to finely divided lead, which coalesced into liquid lead within 5 min. Many chemical studies remain to be made in the development of direct heat exchange.

##### Alternative Coolants

The possibility of using a mixture of LiF, NaF, and KF as the coolant for a molten-salt reactor has been discussed in the chapter on chemistry.

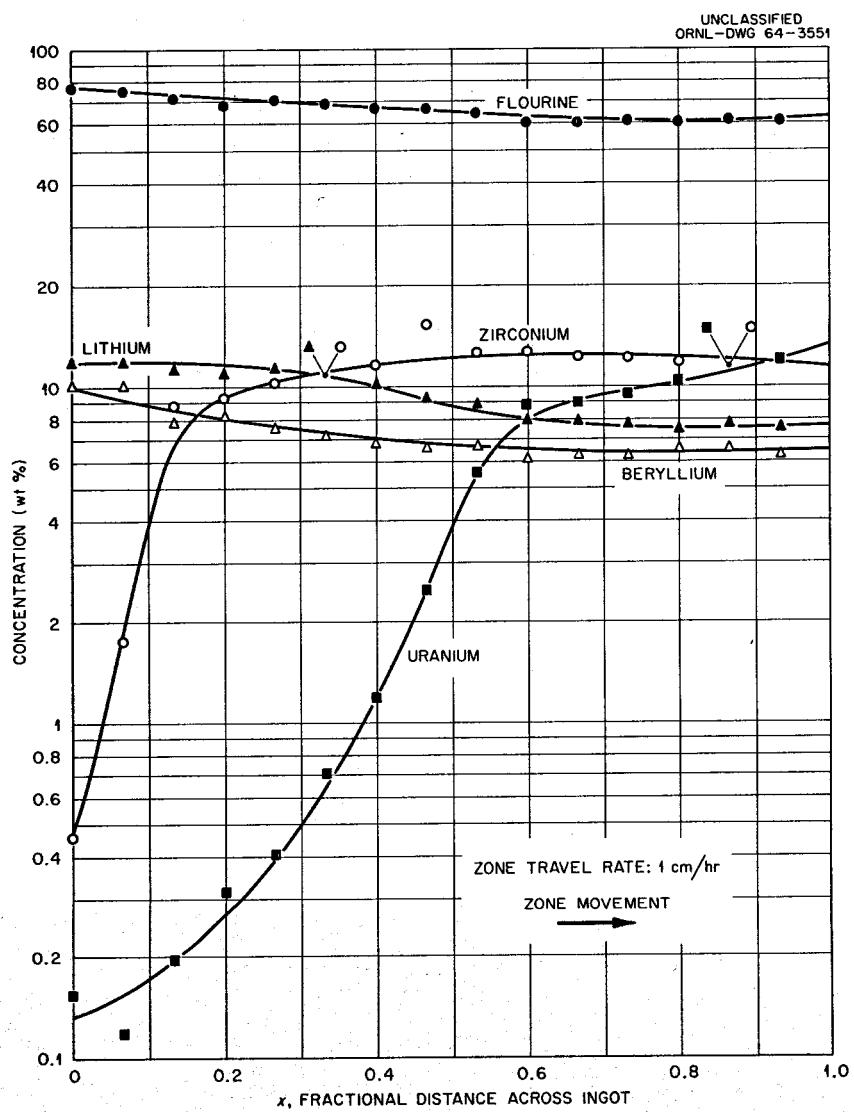


Fig. 12. Element Concentration (wt %) in  $\text{LiF-BeF}_2\text{-ZrF}_4\text{-UF}_4$  Mixture, vs Fractional Distance ( $x$ ) Across Ingot, After 20 Downward Zone Passes.

This would require that the entire coolant system be resistant to the action of molten fluorides. It has been recently suggested that molten carbonates be used as the coolant fluid.<sup>23</sup> Owing largely to the work of Janz and his associates at RPI,<sup>24</sup> a number of properties of molten carbonates have been established. Figure 13 presents a phase diagram of the ternary system  $\text{Li}_2\text{CO}_3$ - $\text{Na}_2\text{CO}_3$ - $\text{K}_2\text{CO}_3$ . The eutectic of the composition Li-Na-K (43.5-31.5-25.0 mole %), melts just below 400°C and should require less than 1 atm of  $\text{CO}_2$  cover gas for stability in the temperature range of interest. The mixture has been used for a number of years as a heat-treating medium and is known to be noncorrosive to steel at 1400°F over many months of exposure. No obvious corrosion has been observed after about 4000 hr exposure at 1200°F to INOR-8. In recent tests at ORNL, Bettis found that molten carbonate is apparently quite stable toward molten lead at temperatures of 900 to 1000°F. Development of molten carbonate fluids will require study of radiation stability, corrosion, thermal conductivity and viscosity, and compatibility with fuel salts (the consequence of a leak).

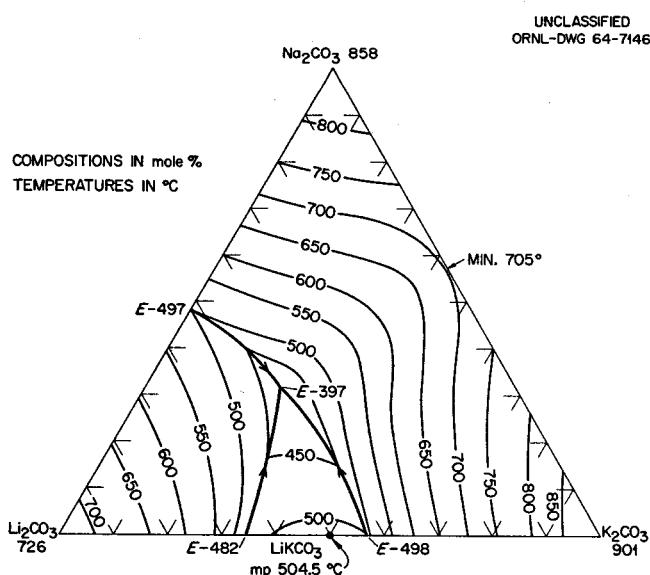


Fig. 13. Ternary System  $\text{Li}_2\text{CO}_3$ - $\text{Na}_2\text{CO}_3$ - $\text{K}_2\text{CO}_3$ .

#### Molten Salts as Fast Reactor Fuels

The availability of large amounts of plutonium and the potential advantages in the use of fast neutrons for breeding have prompted consideration of molten chloride fuels. Separated isotopic  $^{37}\text{Cl}$  would be used (at 98% enrichment) but would have to be conserved. Some information is available on the binary systems of alkali metal chlorides with  $\text{UCl}_3$ , the valence state of uranium which, for compatibility reasons, would be used in a chloride system. Additional study of the system  $\text{KCl}-\text{UCl}_3$  is in progress at ORNL. From the available information on

binary mixtures,<sup>25</sup> Thoma has predicted the behavior of relatively simple ternary systems.<sup>26</sup> Figure 14 presents a predicted diagram for the system NaCl-KCl-PuCl<sub>3</sub>. Very substantial solubility of plutonium is predicted at temperatures between 500 and 600°C. Figure 15 presents a similar diagram for the system NaCl-KCl-UCl<sub>3</sub>, and, again, very substantial solubilities of uranium are predicted for the temperature range 500 to 600°C. The similarities in the uranium and plutonium systems suggest that it may be feasible to achieve the desired plutonium to uranium ratios of 5:1, a heavy metal concentration of 30 to 55 mole %, and a liquidus temperature below 550°C. Testing of these predictions will be included in future chemical development.

The thermodynamic stability of metals and their chlorides in the presence of UCl<sub>3</sub> and PuCl<sub>3</sub> has been the subject of calculations by

UNCLASSIFIED  
ORNL-DWG 64-1994

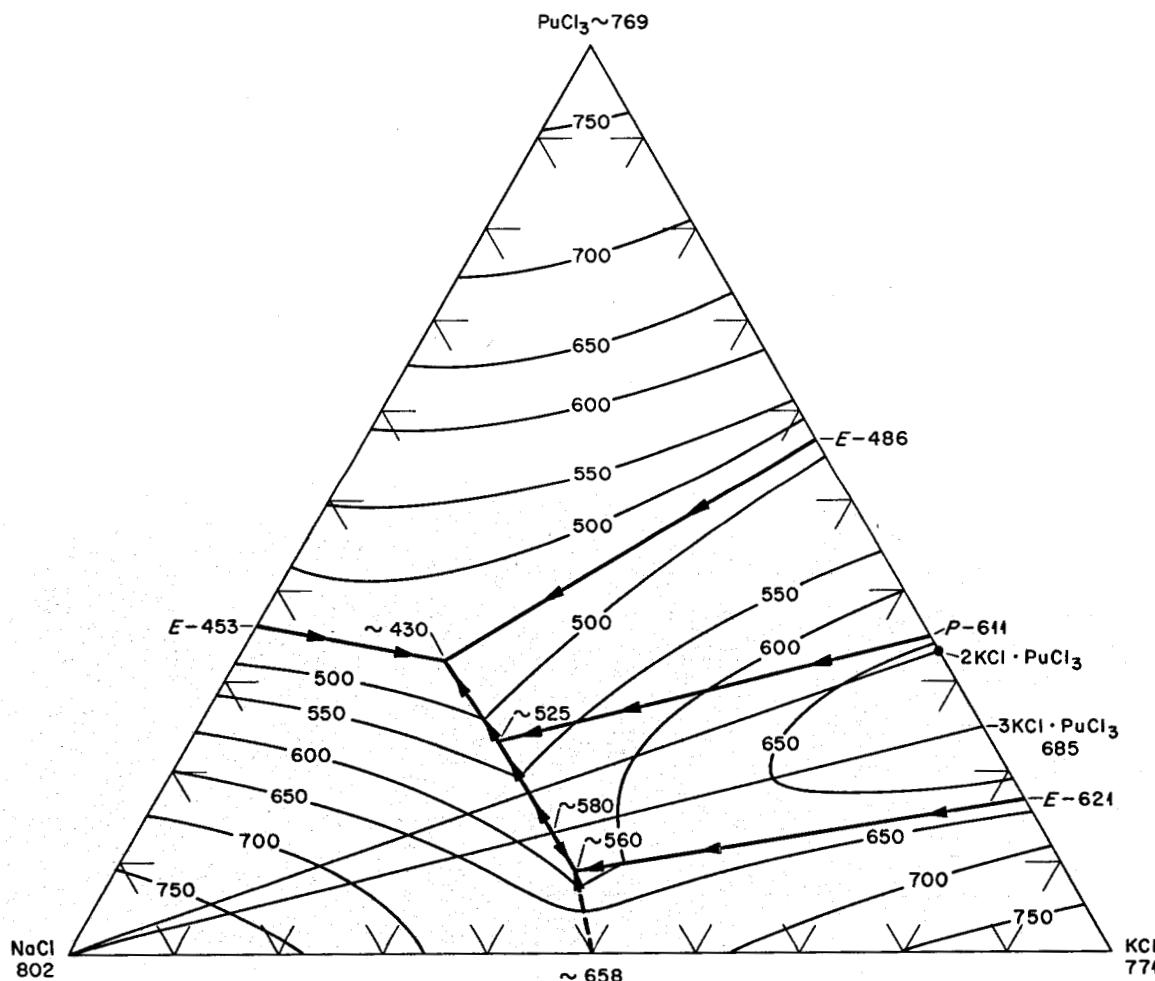


Fig. 14. Predicted Phase Behavior for the System NaCl-KCl-PuCl<sub>3</sub>.

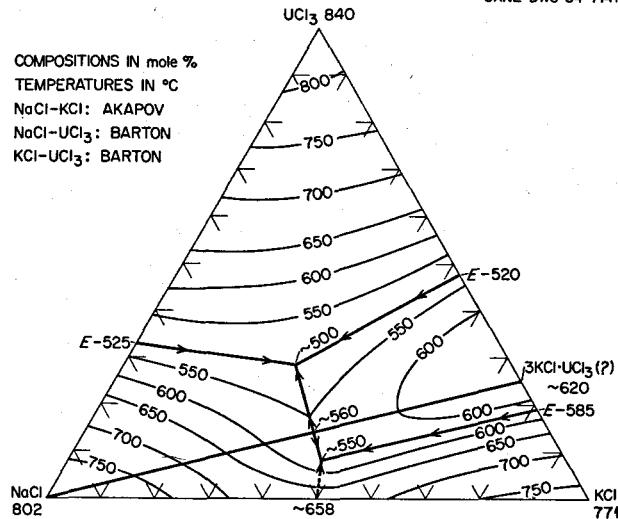
UNCLASSIFIED  
ORNL-DWG 64-7147

Fig. 15. System  $\text{NaCl}-\text{KCl}-\text{UCl}_3$ , Phase Diagram Predicted on Basis of Limiting Binary Systems.

Newton<sup>27</sup> and by Long.<sup>28</sup> From the point of view of corrosion by the salt, chromium is considered to be somewhat worse than iron, nickel is better, and tungsten and molybdenum are much better; iron is considered to be probably good enough. The combination of an iron-molten chloride-molten lead system, based on available thermodynamic information, appears to be acceptable chemically with respect to corrosion of the iron by lead, to contamination of the melt by  $\text{FeCl}_2$ , and to uptake of uranium by the molten lead. Future chemical development will require laboratory and intermediate-scale loop testing of these tentative conclusions.

#### References

1. R. E. Thoma *et al.*, *J. Phys. Chem.* **64**, 865 (1960).
2. L. V. Jones *et al.*, Phase Equilibria in the  $\text{LiF}-\text{BeF}_2-\text{UF}_4$  Ternary Fused Salt System, MLM-1080 (1959); *J. Am. Ceram. Soc.* **45**, 79 (1962).
3. C. F. Weaver *et al.*, Phase Equilibria in Molten Salt Breeder Reactor Fuels. 1. The System  $\text{LiF}-\text{BeF}_2-\text{UF}_4-\text{ThF}_4$ , ORNL-2896 (Dec. 27, 1960).
4. C. J. Barton, *J. Phys. Chem.* **64**, 306 (1960).
5. MSRP Semiann. Progr. Rept. Jan. 31, 1964, ORNL-3626, p. 125.
6. J. K. Dawson and R. G. Sowden, Chemical Aspects of Nuclear Reactors, vol. 3, *Miscellaneous Topics*, p. 103, Butterworths, London, 1963.

7. W. R. Grimes, N. V. Smith, and G. M. Watson, J. Phys. Chem. 62, 862 (1958); M. Blander et al., Ibid., 63, 1164 (1959); G. M. Watson et al., J. Chem. Eng. Data 7, 285 (1962).
8. R. B. Evans III, G. M. Watson, and E. A. Mason, J. Chem. Phys. 35(6), 2076 (1961); Ibid., 36(7), 1894 (1962); Ibid., 38(8), 1808 (1963); R. B. Evans III, Jack Truitt, and G. M. Watson, J. Chem. Eng. Data 6(4), 522 (1961); R. B. Evans III, G. M. Watson, and J. Truitt, J. Appl. Phys. 33(9), 2682 (1962); Ibid., 34(7), 2020 (1963).
9. W. T. Ward et al., Solubility Relations Among Rare-Earth Fluorides in Selected Molten Fluoride Solvents, ORNL-2749 (Oct. 13, 1959).
10. W. T. Ward et al., J. Chem. Eng. Data 5(2), 137-42 (1960).
11. Reactor Chem. Div. Ann. Progr. Rept., Jan. 31, 1962, ORNL-3262, p. 21.
12. P. J. Kreyger, Euratom, private communication, intralaboratory memorandum to F. F. Blankenship, June 25, 1963.
13. A. J. Singh, R. G. Ross, and R. E. Thoma, "Vacuum Distillation of LiF," Journal of Applied Physics (submitted for publication).
14. A. J. Singh, G. D. Brunton, and R. E. Thoma, Zone Melting of Inorganic Fluorides, ORNL-3658 (to be published).
15. Fluid Fuel Reactors, ed. by J. A. Lane, H. G. MacPherson, and Frank Maslan, Chap. 22, p. 791, Addison-Wesley, Reading, Mass., 1958.
16. C. F. Baes, private communication, intralaboratory memorandum to W. R. Grimes, June 4, 1964.
17. F. A. Cafasso, Harold M. Feder, and Irving Johnson, J. Phys. Chem. 68(7), 1944-48 (1964).
18. P. Chiotti and J. S. Klepfer, Transport of Solutes Between Liquid Alloys in Mutual Contact with a Fused Salt - Application to Fuel Reprocessing, 148th American Chemical Society Meeting, Chicago, Ill., Aug. 31-Sept. 3, 1964, Abstract 39 (to be presented).
19. R. H. Moore, Cation Effects on the Distribution of Uranium in the System: Aluminum-Aluminum Chloride-Alkali Chloride, HW-67574 (Nov. 28, 1960).
20. J. H. Shaffer et al., Nucl. Sci. Eng. 18(2), 177-81 (1964).
21. H. G. MacPherson, MSRP Quart. Progr. Rept. Jan. 31, 1959, ORNL-2684, p. 111; G. J. Nessle and J. Truitt, Reactor Chem. Div. Ann. Progr. Rept. Jan. 31, 1960, ORNL-2931, p. 17.

22. MSRP Semiann. Progr. Rept. Jan. 31, 1962, ORNL-3626, p. 126.
23. H. F. Bauman and E. S. Bettis, Selection of the Heat Exchange System for Advanced Molten Salt Reactors (to be published).
24. George J. Janz and Max R. Lorenz, J. Chem. Eng. Data 6(3), 321-23 (1961).
25. J. A. Leary, Temperature-Composition Diagrams of Pseudo-Binary Systems Containing Plutonium(III) Halides, LA-2661 (Apr. 9, 1962).
26. R. E. Thoma, Predicted Phase Behavior in Ternary Systems of Uranium and Plutonium Chlorides, MSR-63-52 (June 6, 1963) (internal use only).
27. R. F. Newton, Thermodynamic Stability of Metals and Their Chlorides in the Presence of UCl<sub>3</sub> and PuCl<sub>3</sub>, MSR-63-53 (Oct. 31, 1963) (internal use only).
28. G. Long, private communication, intralaboratory memorandum to W. R. Grimes, May 26, 1964.

---

#### ANALYTICAL CHEMISTRY FOR THE MOLTEN-SALT REACTOR

---

J. C. White

The program being carried out by the Analytical Chemistry Division for the MSRE can be classified into two categories: (1) development and evaluation of the methods required for the analysis of the MSRE fuel and related problems and (2) investigation of the feasibility of various techniques for in-line monitoring of the fuel.

Development and evaluation of methods have occupied the major portion of the program. This phase should be essentially completed by the end of this period. In-line analysis is in the initial phases of investigation. Among the analytical techniques being considered for in-line monitoring are: electrochemical analyses of the molten state, electron spin resonance, and x-ray measurements. It is not contemplated to use these in-line measurements on the MSRE but to evaluate them for possible future use on molten-salt reactors.

Methods DevelopmentSample Preparation

Since the MSRE fuel samples will be extremely radioactive, considerable effort has been given to sampling, transfer, and handling of the fuel sample. The maximum expected activity of the sample taken for analysis (at 10 Mw power level) will be of the order of 15 curies. The fuel salt is also quite hygroscopic and consequently subject to hydrolysis. Thus chemical as well as activity considerations are of paramount importance. The actual operation of sample preparation will be performed in the High Radiation Level Analytical Laboratory hot cells using tools and apparatus controlled by remote master slave manipulators. This equipment has been especially designed for the MSRE.

The sample will be obtained by dipping a copper ladle into the molten fuel. The ladle is removed from the fuel, which is allowed to solidify, and then placed into a lead-shielded container for transport to the analytical examination cell. The transport container decoupling device is shown in Fig. 1. The copper ladle, filled with approximately 10 g of salt (Fig. 2), is then placed into the pulverizer-mixer and agitated for 45 sec on the mixer mill to crush and mix the salt. The top of the ladle is removed prior to the operation by cutting with a specially built tubing cutter. The powdered salt is then removed from the pulverizer-mixer and transferred to a polyethylene bottle by means of the equipment shown in Fig. 3. Portions of the salt can now be taken for the appropriate analysis. The elapsed time from receipt of sample to transfer of prepared salt sample is about 2 hr.

Dissolution of Sample

The salt will be dissolved in a mixture of boric, nitric, and sulfuric acids. It is then diluted with water to ensure an acidity of 0.5 M  $H_2SO_4$ . The approximate concentrations of the major constituents of the fuel in the diluted solution (1 g of salt per 100 ml of 0.5 M  $H_2SO_4$ ) are: 1.2 Li, 0.7 Be, 0.1 U, and 1.0 Zr (these are expressed in mg/ml). Appropriate size aliquots are then taken for specific determinations. Approximately 3 hr is required to weigh, dissolve, and dilute the sample.

Separate samples will be taken for reducing power, fluoride, and oxide analyses. In order to avoid possible evolution of fluorine from the salt sample upon prolonged standing due to radiation damage, the remaining salt will be weighed and dissolved in a like manner and set aside for possible future use.

Uranium

The determination of uranium is perhaps the most important analysis to be made. A number of well-evaluated methods that are compatible with hot-cell operation are available. Controlled-potential coulometry<sup>1</sup> will be used as the primary method of analysis because of its inherent high

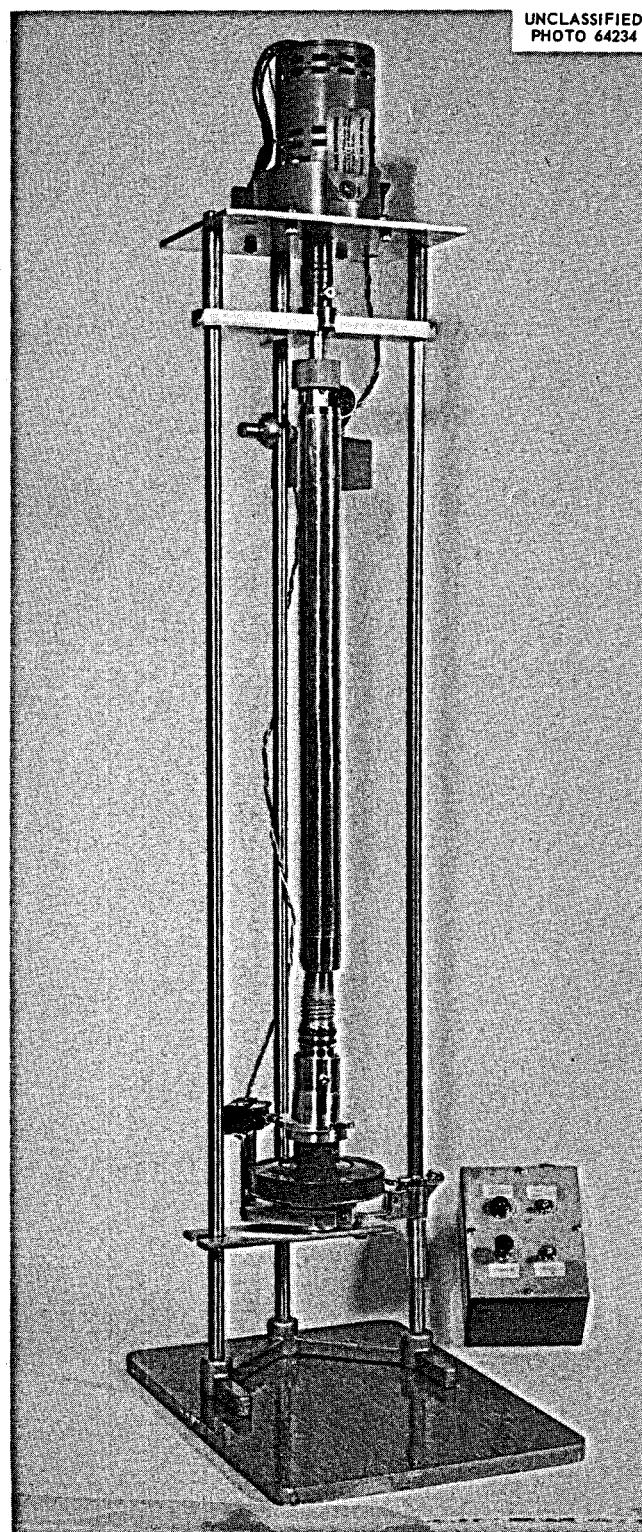


Fig. 1. Transport Container Decoupling Device for MSRE Fuel.

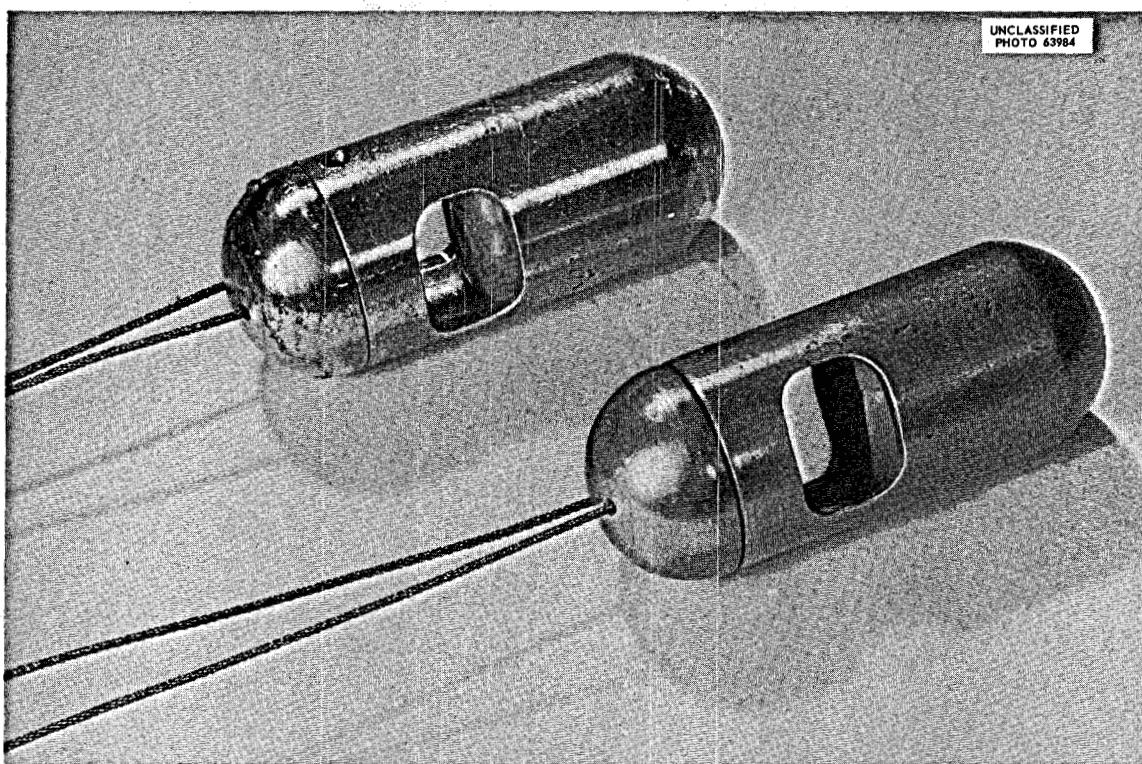


Fig. 2. Container for Sampling MSRE Salt.

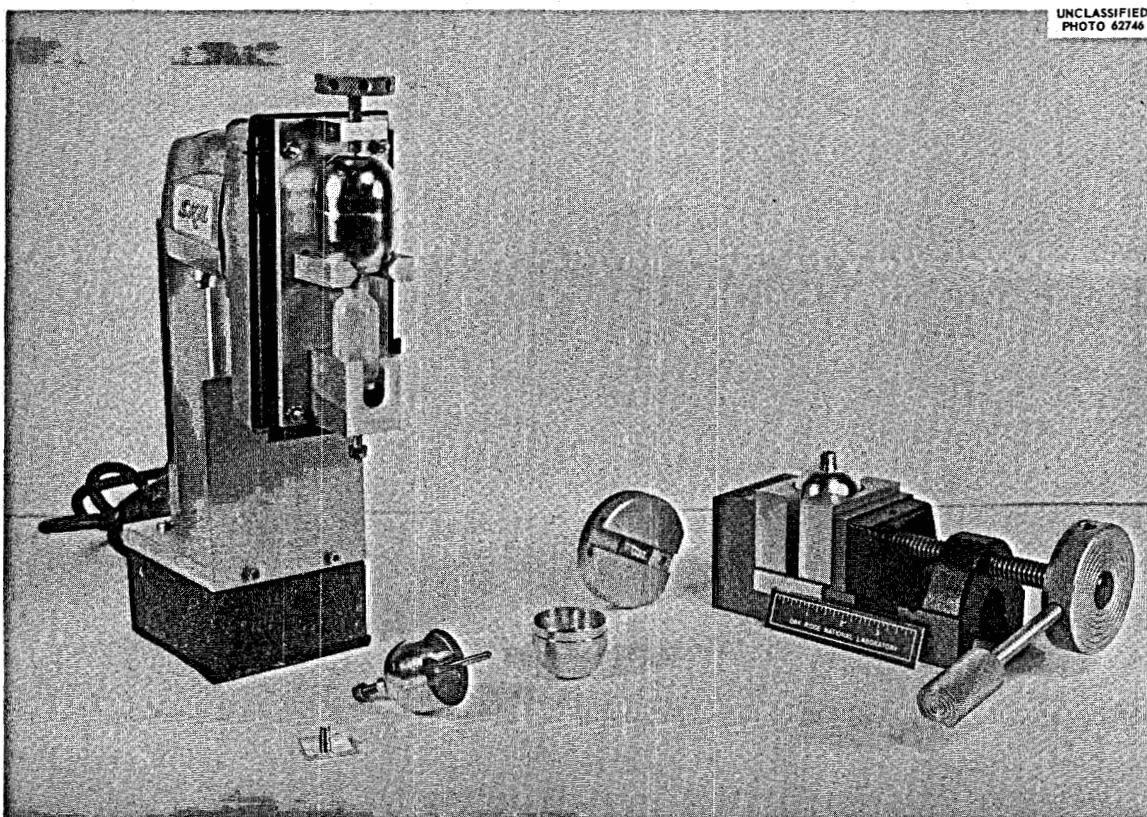


Fig. 3. Apparatus for Removing MSRE Salt from Pulverizer-Mixer to Polyethylene Sample Bottle.

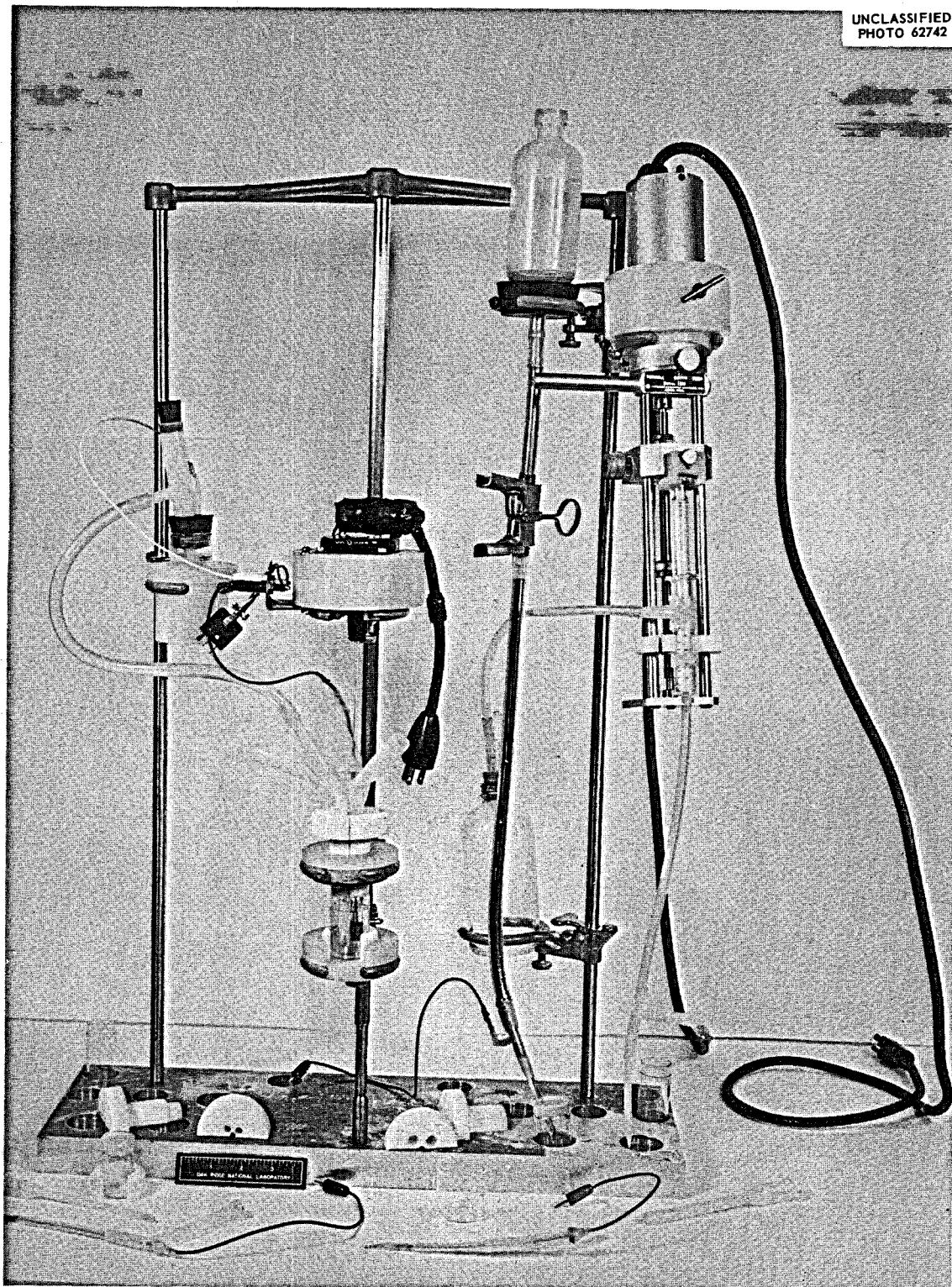
UNCLASSIFIED  
PHOTO 62742

Fig. 4. Cell Assembly for Coulometric and Amperometric Remote Titration of Uranium, Zirconium, and Chromium.

order of precision, easy adaptability to remote operation, and applicability to sulfuric acid solutions. A titration cell (Fig. 4) which includes an S.C.E. reference electrode, a separated electrode of coiled platinum wire contained in 0.5 M H<sub>2</sub>SO<sub>4</sub>, and a Teflon-sleeved platinum wire to connect to the mercury was designed for this method. A test solution representing approximately 500 µg of uranium is added to the cell which contains 3 ml of mercury and 4 ml of 0.5 M H<sub>2</sub>SO<sub>4</sub>. The solution is deaerated for 10 min while stirring. Essentially complete elimination of interference is accomplished by a prereduction at +0.075 v. The U(VI) is then reduced to U(IV) at -0.325 v. The progress of the titration at the 10-µ equivalent range is followed by means of an ORNL model Q-2514 high-sensitivity coulometer and continued until the potential is reduced to approximately 5 µamp. The readout voltage due to the titration is read from an attached potentiometer. From 50 to 500 µg of uranium can be titrated with a precision of the order of less than 1%. The method is essentially free of interferences under normal circumstances of MSRE operation. An extraction procedure is available to separate uranium quantitatively in case a bias in the method is found.

#### Zirconium

An amperometric method<sup>2</sup> for the titration of zirconium with cupferron has been developed for the determination of zirconium. A titration assembly (Fig. 4) was fabricated in order to adapt this method to remote manipulation. Zirconium forms a complex with cupferron in 0.5 M H<sub>2</sub>SO<sub>4</sub>; the concentration of this complex is measured electrically. The progress of the titration is followed by an ORNL polarograph model Q-1160 with the mercury pool at -0.5 v respective to the platinum. The titration is continued until a sharp, vertical inflection in the titration curve is observed. The method can be performed without any prior separations with a precision of about 1.5%.

#### Beryllium

Beryllium will be determined by gamma activation<sup>3</sup> using a <sup>124</sup>Sb source. The neutrons liberated by the  $\gamma, n$  reaction are counted by means of BF<sub>3</sub> tubes. Instrument settings are established at which the net sample counting rate is at a maximum and is independent of high voltage and pulse-height discriminator settings. A test aliquot, usually 5 mg of beryllium in 0.5 M H<sub>2</sub>SO<sub>4</sub>, is exposed to the <sup>124</sup>Sb source, and neutrons are counted until 10,000 counts are collected. A calibration factor, obtained from standard solutions of beryllium, is established to permit final calculations of concentration. Large (2-in.) <sup>10</sup>BF<sub>3</sub> neutron counter tubes are used which increase the neutron detection efficiency of the instrument so that a gamma source activity of only about 300 mc of <sup>124</sup>Sb is necessary. Interference caused by elements which absorb neutrons at this energy level can be eliminated by the cadmium shield technique. The precision of the method is about 2.5%.

Lithium

Lithium will be analyzed, when required, by flame photometry. Since this determination is relatively unimportant, no estimate of its precision has been made as yet.

Fluoride

The pyrolytic determination of fluoride<sup>4</sup> is carried out in an apparatus designed for remote operation (Fig. 5). A nickel reaction tube is first heated to 1000°C, and moist oxygen is passed through it at a rate of about 2 liters/min. A test portion, usually 100 mg of the salt, is placed in a nickel boat and mixed with about 3 g of powdered U<sub>3</sub>O<sub>8</sub> catalyst. The boat is inserted in the heated reaction tube, which is immediately sealed to prevent loss of fluoride. The evolved fluoride is trapped in a known quantity of sodium hydroxide. After about 30 min the absorber solution is removed from the apparatus, and the excess caustic is titrated with standard hydrochloric acid. The fluoride is equivalent to the sodium hydroxide neutralized by the absorbed hydrogen fluoride. The precision is of the order of 1%.

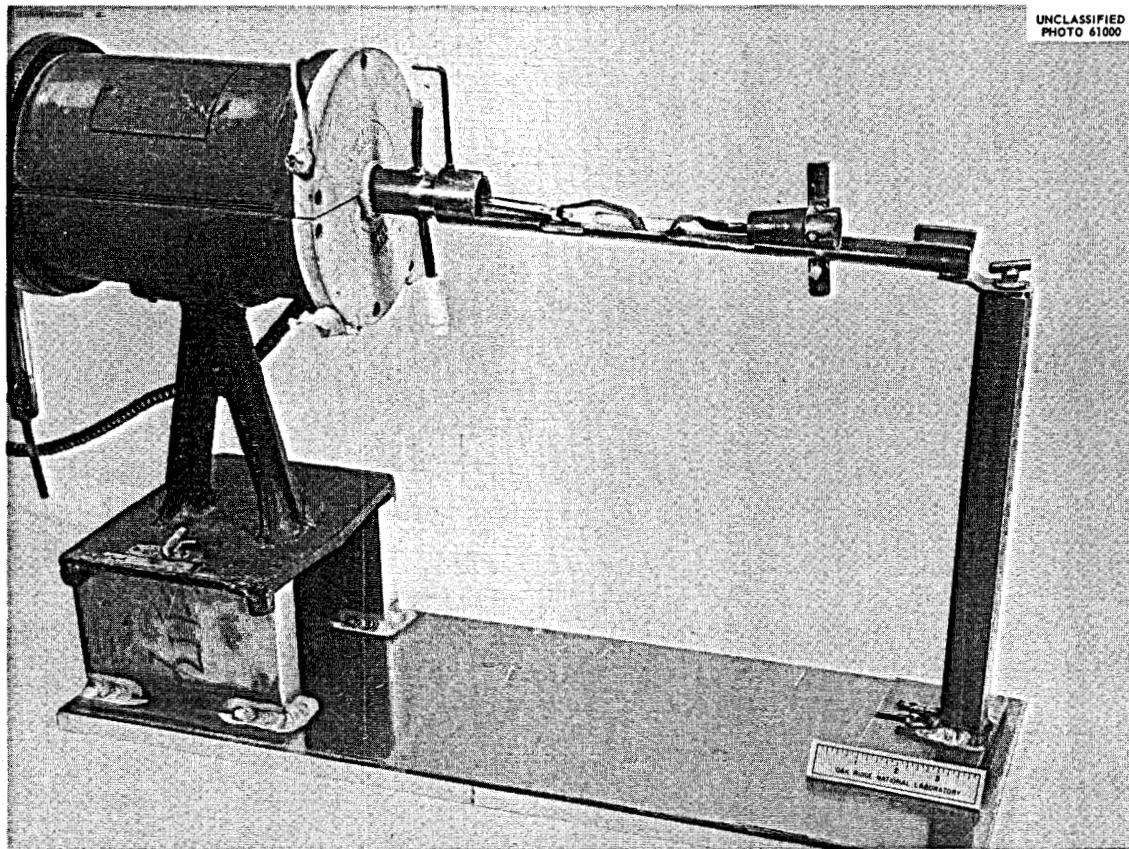


Fig. 5. Apparatus for Pyrolysis of Fluoride for Hot-Cell Operation.

Chromium

Since chromium serves as a means of monitoring the corrosion by the fuel, a reliable and accurate method of analysis is required. This has been achieved<sup>5</sup> by development of an amperometric titration with  $\text{Fe}^{2+}$ . A titration cell assembly which includes a pyrolytic-graphite electrode and an S.C.E. was designed for this method (Fig. 4). Chromium, in 5- to 50- $\mu\text{g}$  quantities, is oxidized to Cr(VI) with argentic oxide in 0.5 M  $\text{H}_2\text{SO}_4$ . The Cr(VI) is subsequently reduced to Cr(III) by titration with  $\text{Fe}^{2+}$ ; this reduction causes a decrease in diffusion current, which is measured amperometrically. The progress of the titration is followed by an ORNL polarograph, model Q-1160, with the pyrolytic-graphite electrode at +1.0 respective to the S.C.E. The titration is continued until a sharp deflection in the curve is observed. The titration of chromium can be performed without any prior separations, and the precision is of the order of 1.5%.

Iron, Nickel, and Molybdenum

These corrosion products will be determined by emission spectroscopy or by spectrophotometric procedures. Standard methods are available for this application.

Fission Products

The fission products will be determined by standard radiochemical procedures.

Oxide

Knowledge of the oxide concentration of the MSRE fuel is highly desirable in the course of operation of the reactor. The determination of small amounts of oxide in the MSRE fuel is, unfortunately, extremely difficult and complicated due to problems imposed in handling highly radioactive materials. The high-pressure high-temperature fluorination method<sup>6</sup> used on nonradioactive salts is not applicable because of hot-cell limitations. As a result, most effort has been devoted to the inert-gas fusion technique,<sup>7</sup> in which the salt is confined in an enclosed graphite cup and heated by induction to about 2400°C. Under these conditions the oxides react with the graphite to form CO, which is then measured gas chromatographically after oxidation to CO<sub>2</sub>. This method is still being studied; pure ZrO<sub>2</sub> has been used as a standard source of oxygen since much, if not all, of the oxide in the MSRE fuel will probably be present in this form.

Reducing Power

The reducing power of the fuel is considered to be an indication of its trivalent uranium concentration. The method used is not specific for U<sup>3+</sup>; any element or compound capable of reacting with the hydrogen ion to liberate hydrogen will be included in the reducing-power value. The

method currently under investigation is that of reacting the salt with tritiated HCl to liberate tritium as well as hydrogen. The two gases are converted to water and collected, and the tritium is counted by scintillation techniques. The method is capable of the great sensitivity which is needed to detect trace quantities of trivalent uranium.

In all these procedures, such factors as ease of installation, manipulation, and replacement of equipment and apparatus have been given foremost consideration. The size of equipment and apparatus is held to a minimum since hot-cell space is drastically limited. Manual operations that must be performed with master slave manipulators are also reduced to a minimum.

#### Reactor Off-Gas Analysis

A gas chromatograph featuring the high-sensitivity helium breakdown detector was specially designed for installation in the sample station of ORNL-MTR-47-6. The objectives of this instrument were (1) to determine sub-ppm concentrations of CF<sub>4</sub> together with ppm concentrations of krypton and xenon emerging from the capsules; (2) to detect traces of permanent gas impurities in the helium purge gas; and (3) to obtain data essential for the design of a chromatograph for the analysis of off-gas from the MSRE reactor.

The essential feature of this chromatograph is the helium discharge detector in which the voltage that is developed across the gas gap between two closely spaced electrodes reflects the gas composition. With pure helium in the detector and currents in the microampere range, a potential of about 500 v is developed across the electrodes. This potential is reduced by as much as several hundred volts by the passage of contaminants eluted from a chromatographic column. The sensitivity of the detector is limited primarily by the noise level so that under optimum conditions certain permanent gas impurities can be detected at concentrations as low as 5 ppb. During periods of stable operation, detection limits are about 3 ppb for krypton, 5 ppb for xenon, and 30 ppb for CF<sub>4</sub>.

The following data were obtained with the instrument from the in-pile test:

1. Permanent gas contaminants were present in the purge gas in much greater than anticipated concentrations. Hydrogen, oxygen, nitrogen, methane, and occasionally CO were observed, frequently in concentrations above the range of the instrument (estimated >200 ppm). The purification system removed at least 99% of the oxygen and about 90% of the nitrogen. Oxygen, when present, was almost quantitatively removed on passage through the capsules.
2. The concentration of fission gases in the capsule purge was subject to rapid fluctuations, sometimes severalfold, apparently either the result of bubbling of the fuel or of flow perturbations introduced by check valves. The concentration of krypton paralleled that of

xenon so that an Xe/Kr ratio of 4.2 was maintained in agreement with mass spectrographic measurements.

3. No CF<sub>4</sub> was detected in the purge gas (<250 ppb) at maximum insertion and low purge rates (400 cm<sup>3</sup>/hr). Moreover, CF<sub>4</sub> was not detected in capsule effluent when the capsules were purged with helium containing 1 ppm of CF<sub>4</sub>.
4. No evidence of adverse effects on the chromatograph or changes in sensitivity of the detector resulting from radioactivity were observed. Standard additions of krypton and xenon through the capsules were recovered within the reproducibility of the fission-gas-generation rate.
5. For a particular current the response for krypton and xenon remained constant within about 10% despite variation in temperature and radioactivity. The response for CF<sub>4</sub> was variable over a factor of 2 and depended on the immediate history of samples analyzed.
6. As had been noted in laboratory tests, reducing gases such as hydrogen and methane frequently introduced violent base-line noise, while CF<sub>4</sub> diminished this noise.

On the basis of this experience it is concluded that this type of instrument offers considerable promise for applications to the MSRE reactor. The detector should be modified to provide improved stability for CF<sub>4</sub> analysis. (Tests of various electrode materials are in progress.) In addition, a multicolumn instrument, which would permit the determination of CO<sub>2</sub> and possible resolution and identification of the unknown contaminants, should be considered. An all-metal sampling valve should be developed to provide long-term service at higher activity levels.

#### In-Line Analysis

The advantages of in-line analysis and control of the fuel chemistry are so obvious and appealing that a portion of the analytical effort has been turned toward this objective. Not the least of such advantages is the immediate knowledge of chemical behavior of the fuel. Unfortunately, the magnitude of the task is as great as its potential. Much basic information is required before adequate assessments of any of the techniques can be made. Electrochemical analysis is, in theory, adaptable to in-line control and is especially attractive with regard to direct analysis of corrosion products and other electroactive species in the molten MSRE fuel. The electrochemical behavior of iron<sup>8</sup> and nickel<sup>9</sup> in fluorides has been reported. Investigations are under way on the characteristics of chromium. Oxide analysis is also possible, and efforts are being made in this direction also. Solid electrodes made from such materials as pyrolytic graphite, "glassy" carbon, and pyrolytic boron nitride are being used in molten-salt solutions and offer much potential also. In this area lie the most promising prospects for in-line analysis.

Feasibility studies of the possible determination of oxidation states of uranium in the MSRE fuel by electron-spin-resonance measurements have

been carried out. Initial results are mildly encouraging. Adequate sensitivity is only achieved at very low temperatures ( $77^{\circ}\text{K}$ ) which poses obvious difficulties when applied to a fuel at high temperature. X-ray fluorescence and absorbance measurement techniques are also under study.

#### References

1. L. G. Farrar, P. F. Thomason, and M. T. Kelley, Anal. Chem. 30, 1511 (1958).
  2. Hisashi Kubota and J. G. Surak, Anal. Chem. 35, 1715 (1963).
  3. G. Goldstein, Anal. Chem. 35, 1620 (1963).
  4. R. F. Apple, Fluoride in MSRE Fuel, Pyrolysis Method, Method No. 9 021203, July 1964, ORNL Master Analytical Manual.
  5. R. F. Apple and H. E. Zittel, Anal. Chem. 36, 983 (1964).
  6. G. Goldberg, A. S. Meyer, Jr., and J. C. White, Anal. Chem. 32, 314 (1960).
  7. E. J. Beck, Determination of Oxygen by the Inert Gas Fusion Method Using Graphite Capsules, Parma Research Center, Report URS-29 (Feb. 1, 1961).
  8. D. L. Manning and Gleb Mamantov, J. Electroanal. Chem. 7, 102-8 (1964).
  9. D. L. Manning, J. Electroanal. Chem. 7, 302-6 (1964).
- 

#### METALLURGICAL DEVELOPMENTS *for MSRE*

A. Taboada

#### Introduction

The development of molten-salt reactors that circulate fluoride mixtures depends on the availability of a material of construction that will contain the mixtures for the life of the reactors and also afford the required structural properties at operating temperatures. In the MSRE, the material must be compatible with a graphite-fluoride system and resistant to oxidation in air or air-nitrogen mixtures as well as resistant to corrosion of fluorides; all while in the presence of a neutron flux. Since the reactor is a dynamic system that operates at about  $1200^{\circ}\text{F}$ , the material should have good elevated-temperature strength

and ductility. It is further required that the material be metallurgically stable in this environment of high temperatures, corrosive fluids, and irradiation. Finally, such a material must be fabricable into large and complex engineering structures, such as pumps and heat exchangers. Thus, it must be easily welded, cast, and worked into such forms as tubes, plates, forgings, etc.

The container material<sup>1</sup> selected for the MSRE is the alloy INOR-8, also known as Hastelloy N and INCO. This alloy was developed at ORNL in the Aircraft Nuclear Propulsion Program and was viewed as the most promising container material for molten fluorides exposed to the severe (1500°F) ANP conditions. The properties of this alloy are considered to be more than adequate for MSRE application. Considerable effort and expense were devoted by the ANP Program to determine general metallurgical and fabrication data for INOR-8. Although several changes in the chemistry of the alloy appeared desirable in order to make it more economical and give it improved properties under MSRE conditions, these changes were precluded by the adequacy of the material, the availability of INOR-8 data, and the cost and time required to obtain metallurgical data for a new alloy. INOR-8 has therefore been selected as the structural material for all parts of the MSRE exposed to molten salts.

The metallurgical developments in support of the MSRE have been limited to establishing the compatibility of INOR-8 in a molten-salt-graphite system at MSRE conditions and to generating the metallurgical information necessary to design, fabricate, and operate the reactor. Included in this work was the preparation of standards for materials procurement and for the fabrication of components. A description of these metallurgical achievements is presented.

#### Description of INOR-8

INOR-8 is a nickel-base alloy (see Table 1) that is solution-strengthened with molybdenum and has sufficient chromium to be oxidation resistant; however, the chemistry has been controlled to preclude aging embrittlement. The aluminum, titanium, and carbon contents are limited to minimize severe fabrication and corrosion problems, and the boron content is limited to prevent weld cracking. Iron is included to allow flexibility in starting materials during melting. The extreme examples of permissible combinations of elements allowed by the chemistry specification were studied, and in no case did any undesirable brittle phases develop. Carbides of the form  $M_23C_6$  and  $M_6C$  exist in the alloy and are stable to at least 1800°F.

Physical properties of INOR-8 are shown in Table 2. Specific heat, electrical resistivity, thermal expansion, and thermal conductivity data all show inflections in temperature curves, indicating that an order-disorder reaction may be occurring in this alloy at approximately 1200°F.

Table 1. Chemical Composition Requirements for the  
Ni-Mo-Cr Alloy - INOR-8

| Element             | Percent <sup>a</sup> |
|---------------------|----------------------|
| Nickel              | Remainder            |
| Molybdenum          | 15.00-18.000         |
| Chromium            | 6.00-8.00            |
| Iron                | 5.00                 |
| Carbon              | 0.04-0.08            |
| Manganese           | 1.00                 |
| Silicon             | 1.00                 |
| Tungsten            | 0.50                 |
| Aluminum + titanium | 0.50                 |
| Copper              | 0.35                 |
| Cobalt              | 0.20                 |
| Phosphorus          | 0.015                |
| Sulfur              | 0.020                |
| Boron               | 0.010                |
| Others, total       | 0.50                 |

<sup>a</sup>Single values are maximum percentages unless otherwise specified.

Table 2. Physical Properties of INOR-8

| Temperature              | Density,<br>$\rho$                         |                                  | Electrical Resistivity,<br>$\rho$           |                 | Thermal Conductivity,<br>$k$ |   |
|--------------------------|--|----------------------------------|---|-----------------|------------------------------|---|
|                          | (g/cm <sup>3</sup> )                       | (lb/in. <sup>3</sup> )           | Temperature<br>(°F)                         | ( $\mu$ ohm-cm) | Temperature<br>(°F)          | [Btu ft <sup>-2</sup> hr <sup>-1</sup> (°F) <sup>-1</sup> ft] |
| RT                       | 8.93                                       | 0.320                            | RT  | 120.5           | 300                          | 6.94  |
|                          |  |                                  | 1300  | 126.0           | 575                          | 8.21  |
|                          |  |                                  | 1500  | 124.1           | 825                          | 9.25  |
|                          |  |                                  |   |                 | 985                          | 10.40   |
|                          |  |                                  |   |                 | 1165                         | 11.56   |
|                          |  |                                  |   |                 | 1475                         | 13.87   |
| Specific Heat            |  | Coefficient of Thermal Expansion |   |                 |                              |   |
| Temperature<br>(°F)      | [Btu lb (°F) <sup>-1</sup> ]               | Temperature<br>(°F)              | [in. in. <sup>-1</sup> (°F) <sup>-1</sup> ] |                 |                              |   |
| 140                      | 0.098                                      | 212-752                          | $7.0 \times 10^{-6}$                        |                 |                              |   |
| 572                      | 0.109                                      | 752-1112                         | $8.4 \times 10^{-6}$                        |                 |                              |   |
| 1000                     | 0.115                                      | 1112-1832                        | $9.9 \times 10^{-6}$                        |                 |                              |   |
| 1292                     | 0.138                                      | 212-1832                         | $8.6 \times 10^{-6}$                        |                 |                              |   |
| Modulus of Elasticity, E |  |                                  |   |                 |                              |   |
| Temperature<br>(°F)      | E (lb/in. <sup>2</sup> × 10 <sup>6</sup> ) | Temperature<br>(°F)              | E (lb/in. <sup>2</sup> × 10 <sup>6</sup> )  |                 |                              |   |
| 55                       | 31.5                                       | 1475                             | 23.7  |                 |                              |   |
| 425                      | 29.0                                       | 1575                             | 22.7  |                 |                              |   |
| 775                      | 28.0                                       | 1650                             | 21.9  |                 |                              |   |
| 925                      | 27.0                                       | 1750                             | 20.7  |                 |                              |   |
| 1075                     | 26.3                                       | 1825                             | 19.1  |                 |                              |   |
| 1175                     | 26.0                                       | 1925                             | 17.7  |                 |                              |   |
| 1300                     | 24.8                                       |                                  |   |                 |                              |   |

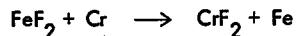
Corrosion Resistance of INOR-8 to Molten Salts

Corrosion of metals in salt mixtures occurs by oxidation of the metal components to their fluoride salts, which are readily dissolved by the molten fluorides. This precludes any possibility of protection by passivation of the metal surface by corrosion products, and the extent of corrosion is then controlled by the thermodynamic driving force of the oxidation reaction. Oxidation reactions stem from three sources, which are indicated in Fig. 1. These reactions involve (1) impurities in the salt, (2) impurities on the metal, and (3) components of the salt ( $UF_4$ ).

In the case of INOR-8 and similar multicomponent systems, corrosion is manifested by the selective oxidation and removal of the least-noble constituent. In INOR-8 this element is chromium. When it becomes depleted, subsurface voids form in the depletion zone.

UNCLASSIFIED  
ORNL-DWG 64-96781. Impurities in the Melt:

Example:

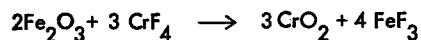


Other Impurities:

$\text{NiF}_2$ ,  $\text{CrF}_3$ ,  $\text{CrF}_4$ ,  $\text{FeF}_3$ , HF, and  $\text{UF}_5$

2. Oxide Films on Metal Surfaces:

Example:



Importance:

$\text{FeF}_3$  now reacts with Cr by 1

3. Constituents in the fuel:

Example:

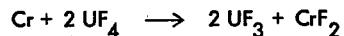


Fig. 1. Types of Reactions Associated with Chromium Removal.

An extensive corrosion program was conducted to determine the extent to which nickel alloys would be attacked by molten salts in polythermal systems. The program was conducted in three sequential phases. In the first phase, the corrosion properties of 13 fluoride salt mixtures were compared in INOR-8 thermal-convection loops operated for 1000 hr. Specific salt mixtures, whose compositions are listed in Table 3, were selected to provide an evaluation of (1) the corrosion properties of beryllium-bearing fuels, as compared with earlier property data amassed for zirconium-base fuels; (2) the corrosion properties of beryllium-fluoride mixtures containing large quantities of thorium; and (3) the corrosion properties of non-fuel-bearing fluoride coolant salts.

The second phase of testing, which again used thermal-convection loops, subjected systems that demonstrated their compatibility in phase I tests to more extensive investigations for longer time periods and at two temperature levels. The third phase of out-of-pile testing was conducted in forced-circulation loops<sup>2</sup> at flow rates and temperature conditions simulating those of an operating reactor system. The temperature conditions employed in each test phase are shown in Table 4.

Table 3. Compositions of Molten-Salt Mixtures To Be Tested for Corrosiveness in Inconel and INOR-8 Thermal-Convection Loops

| Salt Designation       | Composition (mole %) |     |      |                  |                  |                 |                  |
|------------------------|----------------------|-----|------|------------------|------------------|-----------------|------------------|
|                        | NaF                  | LiF | KF   | ZrF <sub>4</sub> | BeF <sub>2</sub> | UF <sub>4</sub> | ThF <sub>4</sub> |
| Fuel and Blanket Salts |                      |     |      |                  |                  |                 |                  |
| 122                    | 57                   |     | 42   |                  |                  | 1               |                  |
| 129                    | 55.3                 |     | 40.7 |                  |                  | 4               |                  |
| 123                    | 53                   |     |      | 46               |                  | 1               |                  |
| 124                    | 58                   |     |      | 35               |                  |                 | 7                |
| 125                    | 53                   |     |      | 46               | 0.5              | 0.5             |                  |
| 126                    |                      | 53  |      | 46               |                  | 1               |                  |
| 127                    |                      | 58  |      | 35               |                  |                 | 7                |
| 128                    |                      | 71  |      |                  |                  |                 | 29               |
| 130                    |                      | 62  |      | 37               | 1                |                 |                  |
| 131                    |                      | 60  |      | 36               | 4                |                 |                  |
| 133                    |                      | 71  |      | 16               |                  | 13              |                  |
| 134                    |                      | 62  |      | 36.5             | 0.5              | 1               |                  |
| 135                    | 53                   |     |      | 45.5             | 0.5              | 1               |                  |
| 136                    |                      | 70  |      | 10               | 20               |                 |                  |
| BULT-14 + 0.5U         |                      | 67  |      | 18.5             | 0.5              | 14              |                  |
| Coolant Salts          |                      |     |      |                  |                  |                 |                  |
| 12                     | 11.5                 |     | 42   |                  |                  |                 |                  |
| 84                     | 27                   |     |      |                  | 38               |                 |                  |

Table 4. Operating Temperatures To Be Used in Various Phases of Corrosion Testing

| Operating Temperatures (°F) |           |  |
|-----------------------------|-----------|--|
|                             | Maximum   | Difference Between Hot and Cold Sections |
| Phase 1                     |           |  |
| Fuel mixtures               | 1250      | 170                                      |
| Coolant salts               | 1125      | 125                                      |
| Phase 2                     |           |  |
| Fuel mixtures               | 1250-1350 | 170                                      |
| Coolant salts               | 1050-1250 | 170                                      |
| Phase 3                     |           |  |
| Fuel mixtures               | 1300      | 200                                      |
| Coolant salts               | 1200      | 200                                      |

Initial screening studies of INOR-8-fluoride salt systems produced no measurable attack during the 1000-hr test interval. Results of these tests are summarized in Table 5. Accordingly, the majority of salt systems developed for phase I testing were included in the phase II corrosion program. Results of phase II tests, which were conducted for 8760 hr, are summarized in Table 6. The maximum attack in phase II tests was limited to surface roughening and pitting to a depth of 1/2 mil. Figure 2 is representative of the attack found in these loops. Attack in most cases was accompanied by the formation of a thin surface layer which is discussed below in conjunction with phase III tests. Examination of cold regions of these loops revealed no deposits or other evidence of mass transfer.

Chemical analyses of salt samples removed from hot- and cold-leg sections of phase I and II tests showed increases in chromium concentration of 50-100 ppm. Nickel and iron concentrations tended to either hold steady or drop slightly during loop operation.

In the third phase of the program, 15 of the forced-convection loops were made of INOR-8 and 9 of Inconel. Table 7 gives a summary of the duration of these tests. Tubular inserts in the heated sections of some of the loops provided information about the weight losses occurring during the tests; salt samples taken from the pump bowls provided a semicontinuous indication of corrosion product concentration in the circulating system.

A summary of the operating conditions and the results of metallographic examination of the INOR-8 loops are presented in Table 8. Metallographic examination of inserts removed after 5000 hr of loop operation showed no evidence of surface attack. When tests exceeded 5000 hr, however, a thin, continuous surface layer was evident along exposed surfaces, as shown in Fig. 3. In the most severe case of attack found in a 20,000-hr test, this layer reached a maximum depth of 2 mils and was found to contain subsurface voids (see Fig. 4). No transition or diffusion zone was apparent between the layer and the base metal, and analysis of the layer showed it to be composed predominantly of nickel with smaller amounts of iron, chromium, and molybdenum. The layer had a composition<sup>3</sup> similar to the intermetallic phase Ni<sub>4</sub>Mo.

Increasing the maximum temperature of the forced-convection loop from 1300°F to 1400°F did not vary the results. However, in loops with 1500°F maximum temperature, surface attack was manifested by the appearance of subsurface voids to a depth of 4 mils, as shown in Fig. 5, and the surface layer was not observed.

The weight losses of corrosion inserts contained in the hot legs of loops at 1300, 1400, and 1500°F are shown in Table 9. At MSRE temperatures, weight losses were 2 to 5 mg/cm<sup>2</sup> and showed little change after 5000 hr of loop operation. No measurable changes were found in the wall thicknesses; however, if uniform attack is assumed, weight losses indicate wall reductions of 2 to 12  $\mu$ .

Table 5. Operating Conditions and Results of Phase I INOR-8  
Thermal-Convection Loop Tests  
(operating time: 1000 hr)

| Loop No. | Salt No. | Temperature of Hot Section (°F) | Depth of Attack (mils) | Chromium Concentration of Salt Mixture (ppm) |            |
|----------|----------|---------------------------------|------------------------|--|------------|
|          |          |                                 |                        | Before Test                                  | After Test |
| 1203     | 125      | 1250                            | 0                      | 72   | 235        |
| 1204     | 131      | 1250                            | 0                      | 30   | 79         |
| 1221     | 128      | 1250                            | 0                      | 37   | 70         |
| 1164     | 124      | 1250                            | 0                      | 200  | 300        |
| 1165     | 12       | 1250                            | 0                      |  |            |
| 1179     | 130      | 1250                            | 0                      | 120  | 10(?)      |
| 1197     | 126      | 1250                            | 0                      | 15   | 150        |
| 1205     | 129      | 1250                            | 0                      | 20   | 163        |
| 1227     | 134      | 1250                            | 0                      | 265  | 315        |
| 1228     | 133      | 1250                            | 0                      | 96   | 78         |
| 1229     | 135      | 1250                            | 0                      | 190  | 193        |
| 1241     | 136      | 1250                            | 0                      | 90   | 49         |
| 1242     | 136      | 1350                            | ~1/2                   | 80   | 209        |
| 1195     | 84       | 1125                            | 0                      | 30   | 30         |
| 1194     | 12       | 1125                            | 0                      | 68   | 284        |

Table 6. Results of Metallographic Examination of Phase II INOR-8 Thermal-Convection Loops

| Loop No. | Test Period (hr) | Maximum Fluid-Metal Interface Temperature (°F) | Salt No. | Metallographic Examination  |   |
|----------|------------------|--|----------|---|---|
|          |                  |  |          | Hot-Leg Appearance  | Cold-Leg Appearance                                   |
| 1162     | 6360             | 1250   | 123      | Moderate surface roughening and pitting to 3/4 mil                            | No attack   |
| 1224     | 8760             | 1350   | 123      | Moderate surface roughening and pitting to 1 mil                              | No attack   |
| 1226     | 8760             | 1250   | 131      | Moderate surface roughening, film 1/2 to 1 mil thick                          | Light surface roughening, with 1/2-mil corrosion film |
| 1231     | 8760             | 1250   | 134      | Light surface roughening and pitting to < 1/2 mil                             | No attack   |
| 1238     | 8760             | 1350   | 134      | Light surface roughening  | No attack, very shallow corrosion film present        |
| 1244     | 8760             | 1250   | 135      | Light surface roughening, moderate voids and pits to < 1 mil                  | No attack   |
| 1246     | 8760             | 1350   | 135      | Light surface roughening  | No attack   |
| 1233     | 8760             | 1250   | 133      | No attack; very shallow corrosion film  | No attack   |
| 1240     | 8760             | 1350   | 133      | Light surface roughening  | No attack   |
| 1216     | 8760             | 1350   | 127      | Moderate surface roughening and pitting to < 1/2 mil, light voids to < 2 mils | No attack   |
| 1219     | 8760             | 1350   | 122      | Light surface roughening  | No attack   |
| 1200     | 8760             | 1250   | 130      | Light surface roughening, pits less than 1 mil                                | Light surface roughening                              |
| 1196     | 8760             | 1350   | 130      | Light surface roughening  | No attack   |
| 1185     | 8760             | 1250   | 126      | Light surface roughening  | No attack   |
| 1206     | 8760             | 1350   | 126      | Light surface pitting   | No attack   |
| 1212     | 8760             | 1250   | 125      | Moderate pits < 1 mil in depth  | No attack   |
| 1215     | 8760             | 1350   | 125      | Moderate surface roughening   | Light surface roughening                              |
| 1209     | 8760             | 1350   | 128      | Heavy surface roughening  | No attack   |
| 1190     | 8760             | 1250   | 127      | Light surface roughening, pits less than 1 mil                                | No attack   |
| 1208     | 8760             | 1250   | 12       | Moderate surface roughening and pits up to 1 mil deep                         | No attack   |

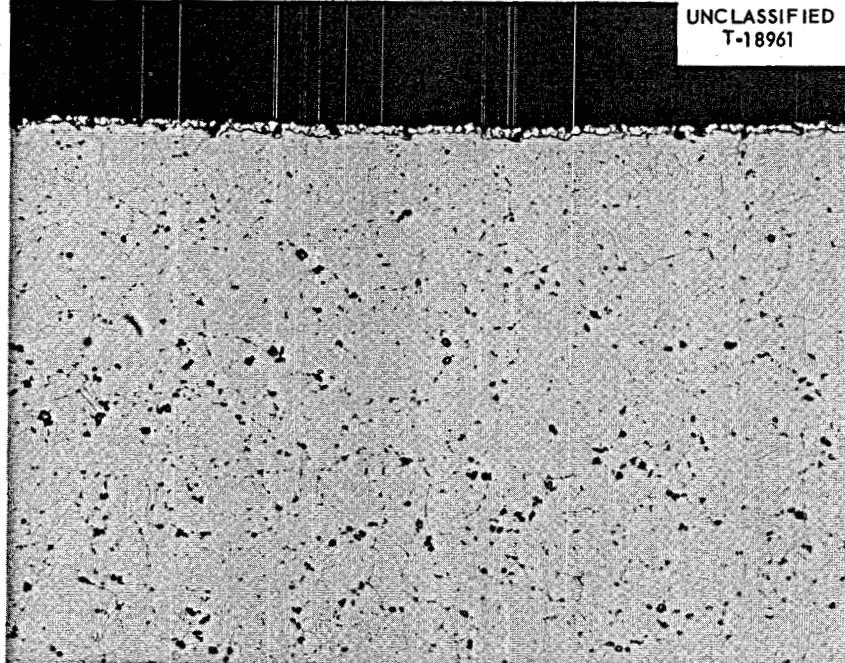
UNCLASSIFIED  
T-18961

Fig. 2. Typical Appearance of Metallographic Specimen at Hot Leg of INOR-8 Thermal-Convection Loop in Phase II Tests.

Table 7. Summary of Forced-Convection Loop Operation

| Length of Test<br>(hr)  | INOR-8             |                         | Inconel            |                         |
|-------------------------|--------------------|-------------------------|--------------------|-------------------------|
|                         | Number of<br>Tests | Total Hours<br>Operated | Number of<br>Tests | Total Hours<br>Operated |
| 3,000- 5,000            |                    |                         | 2                  | 6,440                   |
| 6,000-10,000            | 6                  | 52,680                  | 5                  | 44,760                  |
| 11,000-15,000           | 4                  | 54,370                  | 2                  | 28,190                  |
| 16,000-20,000           | 5                  | 99,950                  |                    |                         |
| Total hours accumulated |                    | 207,000                 |                    | 79,390                  |

Table 8. INOR-8 Operating Conditions of Forced-Convection Loops and Results of Metallographic Examinations of Loop Materials

| Loop No. | Duration of Test (hr) | Salt Mixture   | Maximum Fluid-Metal Interface Temperature (°F) | ΔT (°F) | Reynolds No. | Flow Rate (gpm) | Results of Metallographic Examination                      |
|----------|-----------------------|----------------|--|---------|--------------|-----------------|--|
| 9354-1   | 14,563                | 126            | 1300   | 200     | 2000         | 2.5             | Heavy surface roughening and pitting to 1-1/2 mils         |
| 9354-3   | 19,942                | 84             | 1200   | 100     | 3000         | 2.0             | No attack, slight trace of metallic deposit in cooler coil |
| 9354-4   | 15,140                | 130            | 1300   | 200     | 3000         | 2.5             | No attack  |
| 9354-5   | 14,503                | 130            | 1300   | 200     | 3000         | 2.5             | No attack  |
| MSRP-6   | 20,000                | 134            | 1300   | 200     | 2300         | 1.5             | Pitted surface layer to 2 mils                             |
| MSRP-7   | 20,000                | 133            | 1300   | 200     | 3100         | 1.8             | Pitted surface layer to 1 mil                              |
| MSRP-8   | 9,633                 | 124            | 1300   | 200     | 4000         | 2.0             | No attack  |
| MSRP-9   | 9,687                 | 134            | 1300   | 200     | 2300         | 1.8             | No attack  |
| MSRP-10  | 20,000                | 135            | 1300   | 200     | 3400         | 2.0             | Pitted surface layer to 1/2 mil                            |
| MSRP-11  | 20,000                | 123            | 1300   | 200     | 3200         | 2.0             | Pitted surface layer to 1 mil                              |
| MSRP-12  | 14,498                | 134            | 1300   | 200     | 2300         | 1.8             | No attack  |
| MSRP-13  | 8,085                 | 136            | 1300   | 200     | 3900         | 2.0             | Heavy surface roughening and pitting                       |
| MSRP-14  | 9,800                 | BULT-14 + 0.5U | 1300   | 200     |              |                 | Pitted surface layer to 1/2 mil                            |
| MSRP-15  | 10,200                | BULT-14 + 0.5U | 1400   | 200     |              |                 | Pitted surface layer to 2/3 mil                            |
| MSRP-16  | 6,500                 | BULT-14 + 0.5U | 1500   | 200     |              |                 | Moderate subsurface void formation to 4 mils               |

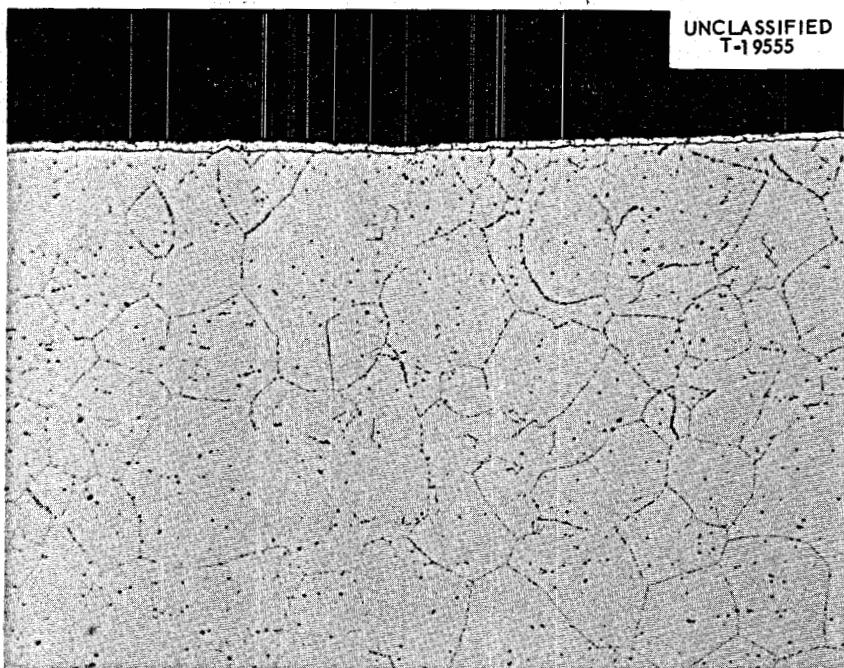


Fig. 3. Typical Appearance of Metallographic Specimen at Point of Maximum Wall Temperature of INOR Forced-Convection Loop.

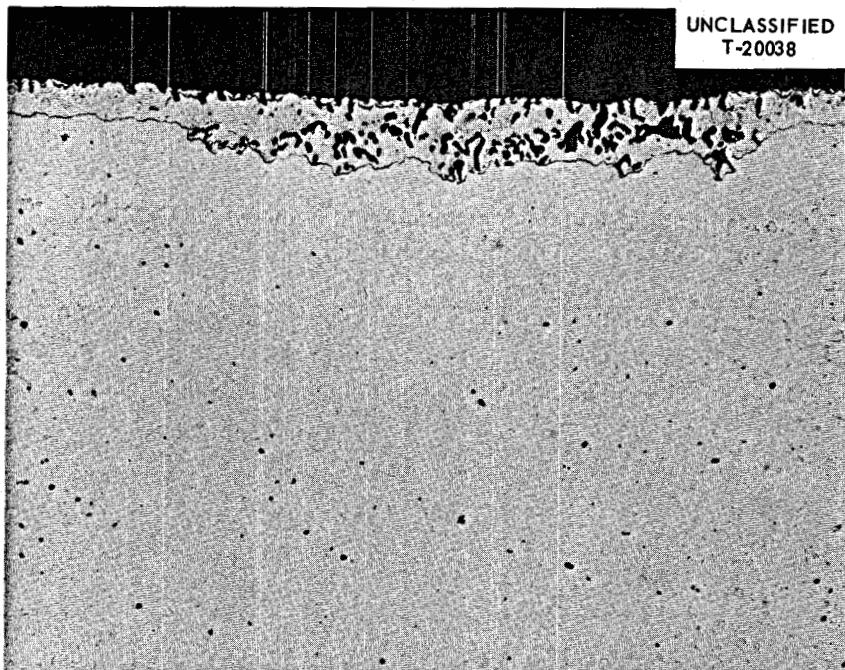


Fig. 4. Metallographic Specimen, Showing Maximum Corrosion Observed in Forced-Convection Loop Operating at 1300°F for 20,000 hr.

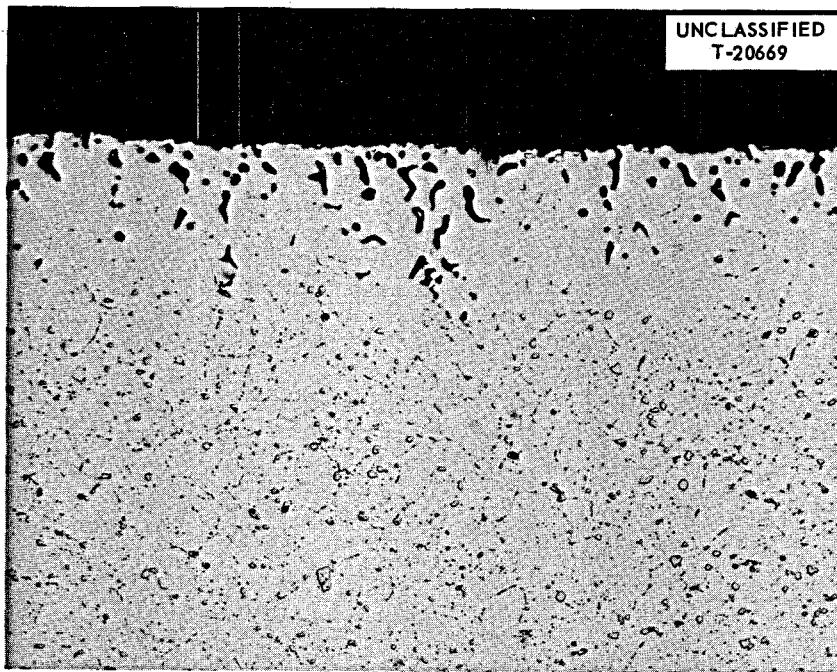


Fig. 5. Typical Appearance of Corrosion at Point of Maximum Temperature of Forced-Convection Loop Operating at 1500°F.

Table 9. Corrosion Rates of Inserts Located in the Hot Legs of INOR-8 Forced-Convection Loops as a Function of Operating Temperature

Loop temperature gradient: 200°F  
Flow rate: approximately 2.0 gpm  
Reynolds No.: ~3000

| Loop No. | Salt Mixture         | Insert Temperature <sup>a</sup> (°F) | Time (hr) | Weight Loss per Unit Area (mg/cm <sup>2</sup> ) | Equivalent Loss in Wall Thickness (μ) |
|----------|----------------------|--------------------------------------|-----------|---|---------------------------------------|
| 9354-4   | 130 <sup>b</sup>     | 1300                                 | 5,000     | 1.8   | 2.0                                   |
|          |                      |                                      | 10,000    | 2.1   | 2.3                                   |
|          |                      |                                      | 15,140    | 1.8   | 2.0                                   |
| MSRP-14  | BULT-14 <sup>c</sup> | 1300                                 | 2,200     | 0.7   | 0.8                                   |
|          |                      |                                      | 8,460     | 3.8   | 4.3                                   |
|          |                      |                                      | 10,570    | 5.1   | 5.8                                   |
| MSRP-15  | BULT-14 <sup>c</sup> | 1400                                 | 8,770     | 11.2  | 12.7                                  |
|          |                      |                                      | 10,880    | 10.0 <sup>d</sup>                               | 11.2                                  |
| MSRP-16  | BULT-14 <sup>c</sup> | 1500                                 | 5,250     | 9.6   | 10.9                                  |
|          |                      |                                      | 7,240     | 9.0 <sup>d</sup>                                | 9.1                                   |

<sup>a</sup>Same as maximum wall temperature.

<sup>b</sup>LiF-BeF<sub>2</sub>-UF<sub>4</sub> (62-37-1 mole %).

<sup>c</sup>LiF-BeF<sub>2</sub>-ThF<sub>4</sub>-UF<sub>4</sub> (67-18.5-14-0.5 mole %).

<sup>d</sup>Average of two inserts.

Chemical analysis of salt samples that were periodically withdrawn from the loop showed a slight increase in chromium concentration, while concentrations of other metals remained unchanged. During a typical run, the chromium concentration reached an asymptotic limit after about 5000 hr of operation, as shown in Fig. 6. This limit was between 300 and 500 ppm at 1300°F and between 600 and 800 ppm at 1400 and 1500°F.

The corrosion data for INOR-8, exposed in the pump loops, indicate that corrosion reactions with fluoride salts at MSRE temperatures are essentially complete within the first 5000 hr of operation, do not generally exceed 1 mil even after 20,000 hr, and are probably associated only with impurity reactions. No significant increase in corrosion occurs due to temperature increase until about 1500°F. At this temperature, noticeable depletion of chromium occurs, as indicated by subsurface voids, and the corrosion mechanism associated with components of the salt is probably effective. The safety factor of the corrosion resistance of INOR-8 appears to be ample, even for the temperature excursions or hot spots that could occur during the MSRE reactor operation.

#### Compatibility of Graphite and INOR-8 in Molten Salt

Since the MSRE uses a graphite moderator in direct contact with molten-salt fuel, the compatibility of graphite and INOR-8 in a fluoride fuel was investigated.

The tendency for INOR-8 to be carburized was investigated in static pots containing LiF-BeF<sub>2</sub>-UF<sub>4</sub> (67-32-1 mole %) and graphite at 1300°F for times ranging from 2000 to 12,000 hr.

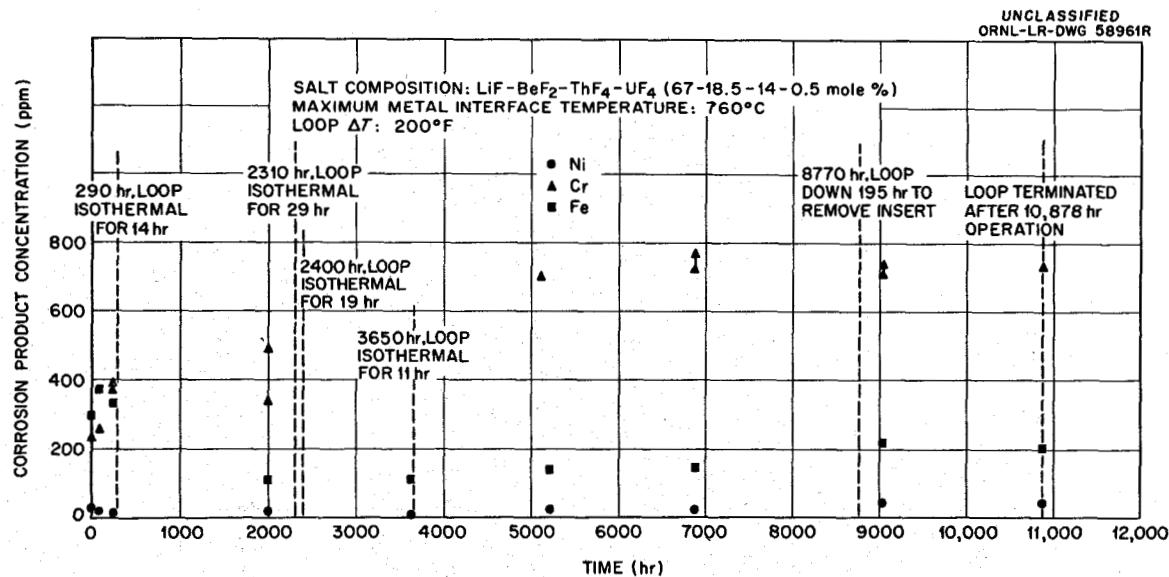


Fig. 6. Concentration of Corrosion Products in Fluoride Salt Circulated in an INOR-8 Forced-Convection Loop.

No carburization was metallographically detected on specimens from any of the above tests. Tensile properties were determined on specimens included in each test, and these properties are listed in Table 10. A comparison of the tensile strengths and elongation values of the tested specimens with those of the control specimens indicates that no significant change occurred.

These data indicate that unstressed INOR-8 is not detectably carburized in the fuel-graphite system at the conditions described above.

For the purpose of evaluating the compatibility of graphite and INOR-8 in a circulating fluoride fuel, an INOR-8 forced-convection loop of the design shown in Fig. 7 was operated<sup>4</sup> for 8850 hr. The loop operated at a maximum temperature of 1300°F and circulated a fluoride mixture of LiF-BeF<sub>2</sub>-UF<sub>4</sub>.

Upon completion of the test, components from the loop were checked metallographically and chemically, and specimens were checked for dimensional changes and weight changes. The tests indicated that

Table 10. Tensile-Test Results on INOR-8 Specimens Exposed to Fuel-Graphite Systems Compared with Control Specimens Exposed to Argon for Various Times

| Time of Test           | Control Specimens <sup>a</sup>                |                            | Test Specimens <sup>b</sup>                   |                            |
|------------------------|---|----------------------------|---|----------------------------|
|                        | Tensile Strength<br>(psi × 10 <sup>-3</sup> ) | Elongation<br>(% in 2 in.) | Tensile Strength<br>(psi × 10 <sup>-3</sup> ) | Elongation<br>(% in 2 in.) |
| Room-Temperature Tests |   |                            |   |                            |
| 2,000                  | 123.2   | 42.5                       | 124.8   | 41.0                       |
| 4,000                  | 123.0   | 42.0                       | 124.5   | 43.0                       |
| 6,000                  | 124.7   | 39.0                       | 124.2   | 36.0                       |
| 8,000                  | 127.7   | 43.5                       | 128.2   | 36.5                       |
| 10,000                 | 130.8   | 43.0                       | 130.3   | 41.0                       |
| 12,000                 | 130.6   | 36.5                       | 126.7   | 36.3                       |
| 1250°F Tests           |   |                            |   |                            |
| 2,000                  | 74.6  | 18.0                       | 75.6  | 18.5                       |
| 4,000                  | 75.9, 76.0                                    | 19.0, 20.0                 | 76.2, 74.3                                    | 18.5, 18.5                 |
| 6,000                  | 72.8  | 16.5                       | 74.5  | 16.0                       |
| 8,000                  | 76.7  | 17.5                       | 76.6  | 19.0                       |
| 10,000                 | 78.9  | 15.0                       | 80.8  | 17.5                       |
| 12,000                 | 72.8  | 15.5                       | 75.8  | 17.0                       |

<sup>a</sup>Control specimens were exposed to argon at 1300°F for the times indicated.

<sup>b</sup>Test specimens were exposed to LiF-BeF<sub>2</sub>-UF<sub>4</sub> (62-37-1 mole %) and graphite at 1300°F for the times indicated.

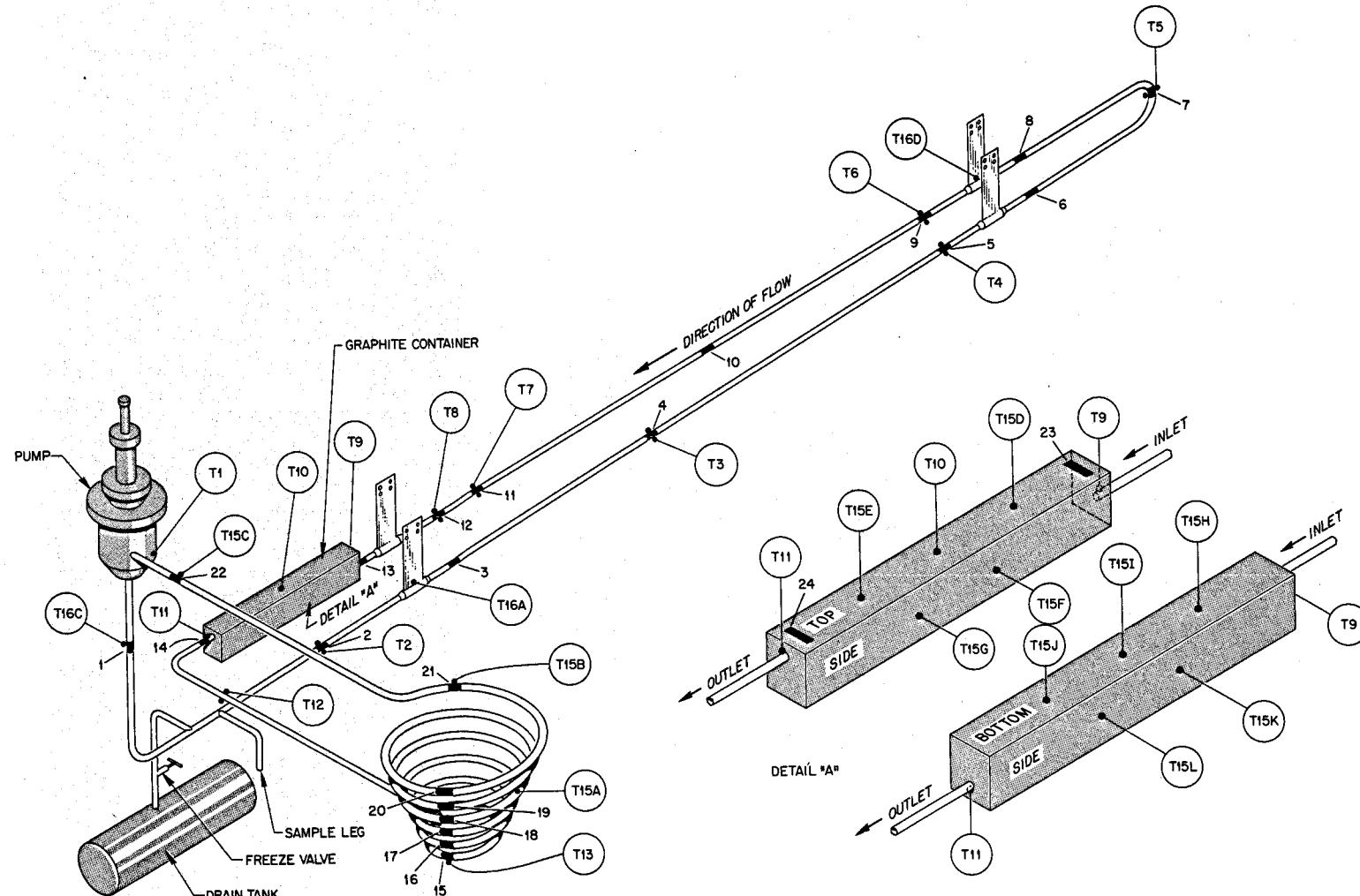


Fig. 7. Molten-Salt Corrosion Loop 9354-5 Containing Graphite Specimens, Showing Thermocouple and Specimen Locations.

1. There was no corrosion or erosion of the graphite by the flowing salt.
2. There was very little permeation of the graphite by the salt, and the permeation that occurred was uniform throughout the graphite rods.
3. The various INOR-8 loop components exposed to the salt were not carburized.
4. The INOR-8 components exposed to the salt and graphite were negligibly attacked.
5. With the possible exception of oxygen contamination, the salt appeared to have undergone no chemical changes as a result of exposure to the graphite test specimens.

#### Oxidation Resistance of INOR-8

The oxidation resistance of nickel-molybdenum alloys depends on the service temperature, the temperature cycle, the molybdenum content, and the chromium content. The oxidation rate of the binary nickel-molybdenum alloy passes through a maximum for the alloy containing 15% Mo, and the scale formed by the oxidation is  $\text{NiMoO}_4$  and  $\text{NiO}$ . Upon thermal cycling from above 1400°F to below 660°F, the  $\text{NiMoO}_4$  undergoes a phase transformation which causes the protective scale on the oxidized metal to spall. Subsequent temperature cycles then result in an accelerated oxidation rate. Similarly, the oxidation rate of nickel-molybdenum alloys containing chromium passes through a maximum for alloys containing between 2 and 6% Cr. Alloys containing more than 6% Cr are insensitive to thermal cycling and to the molybdenum content because the oxide scale is predominantly stable  $\text{Cr}_2\text{O}_3$ . An abrupt decrease (by a factor of about 40) in the oxidation rate at 1800°F is observed; then the chromium content is increased from 5.9% to 6.2%.

The oxidation resistance of INOR-8 is excellent, and continuous operation at temperatures up to 1800°F is feasible. Intermittent use at temperatures as high as 1900°F could be tolerated. For temperatures up to 1200°F, the oxidation rate is not measurable; it is essentially zero after 1000 hr of exposure in static air, as well as in nitrogen containing small quantities of air (the MSRE cell environment). It is estimated that oxidation of 0.001 to 0.002 in. would occur in 100,000 hr of operation at 1200°F. The effect of temperature on the oxidation rate of the alloy is shown in Fig. 8.

#### Mechanical Properties of INOR-8

Mechanical properties tests were performed on eight commercial-size heats of INOR-8. Tests were conducted at ORNL,<sup>5</sup> the Haynes Stellite Company,<sup>6</sup> the Battelle Memorial Institute,<sup>7</sup> and the University of Alabama.<sup>8</sup> Results indicated that the strength of INOR-8 compares favorably with austenitic stainless steels.

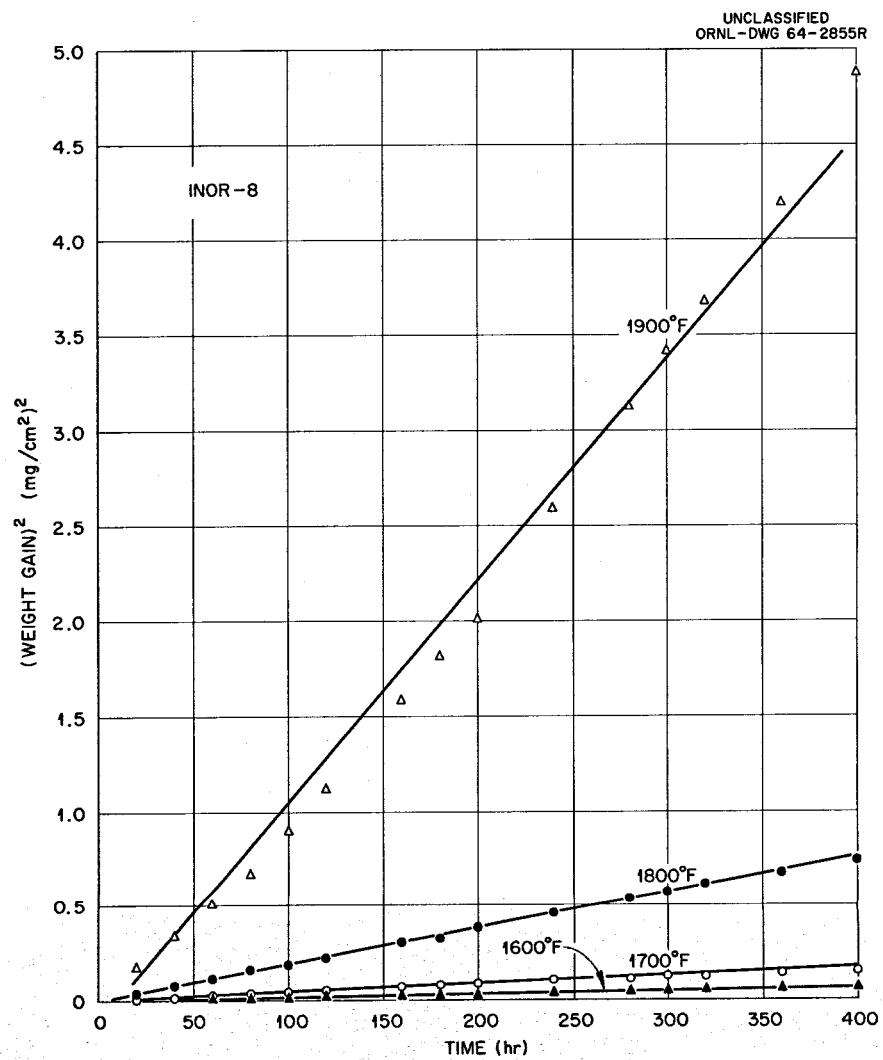


Fig. 8. Effect of Temperature on Oxidation of INOR-8.

Five of the heats were experimental ones and were used to establish design data for the alloy. These data were reviewed by the ASME Boiler and Pressure Vessel Code Committee, and INOR-8 was approved for code construction in Code Case L3L5, subject to the allowable stresses cited in Table 11. The original design values used for the MSRE were approximately 30% below these values to allow an added safety factor for possible unknown irradiation effects.

The remaining three heats, randomly selected from material used to fabricate MSRE components, were tested to evaluate the effects of large-scale production and improved quality requirements. In general, the mechanical properties of these three heats were significantly better than those of the earlier experimental heats, from which design data were established.

#### Tensile Properties

Tensile tests were performed in air using sheet- and rod-type specimens. Figure 9 is a summary of the ultimate tensile strengths at temperatures from ambient to about 1800°F. The minimum specified tensile strength for purchase specifications is included. The 0.2% offset yield strength over the same temperature range is shown in Fig. 10. The values for elongation and for reduction in area are illustrated in Figs. 11 and 12 respectively. Metallographic data indicated that heats with very low carbon and, consequently, large grain size tend to exhibit lower tensile and yield strengths. Heats with similar grain size showed comparable values at all temperatures.

Tensile tests of notched specimens were performed using a notch radius of 0.005 in. The notched-to-unnotched strength ratios varied from 1.07 to 1.38 at test temperatures from ambient to 1500°F.

#### Creep Properties

Creep tests were performed on sheet and rod specimens in both air and molten salts. Most of the testing was confined to the 1100 to 1300°F range, but a few tests were conducted at temperatures up to 1700°F. Summary curves representing stress vs minimum creep rate for the MSRE heats of INOR-8 are shown in Fig. 13. These data for heat 5055 are plotted to show the time to various strains at 1300°F in Fig. 14. The rupture life of INOR-8, plotted as a function of stress, is shown in Fig. 15.

#### Fatigue Properties

Rotating-beam fatigue tests were conducted on INOR-8 at 1100 and 1300°F by Battelle Memorial Institute.<sup>7</sup> Grain size and frequency were the major variables studied. The results are shown in Figs. 16 and 17.

Table 11. Maximum Allowable Stresses for INOR-8 Reported by ASME Boiler and Pressure Vessel Code

| Temperature<br>(°F) | Maximum Allowable Stress<br>(psi) |         |
|---------------------|-----------------------------------|---------|
|                     | Material Other<br>Than Bolting    | Bolting |
| 100                 | 25,000                            | 10,000  |
| 200                 | 24,000                            | 9,300   |
| 300                 | 23,000                            | 8,600   |
| 400                 | 21,000                            | 8,000   |
| 500                 | 20,000                            | 7,700   |
| 600                 | 20,000                            | 7,500   |
| 700                 | 19,000                            | 7,200   |
| 800                 | 18,000                            | 7,000   |
| 900                 | 18,000                            | 6,800   |
| 1000                | 17,000                            | 6,600   |
| 1100                | 13,000                            | 6,000   |
| 1200                | 6,000                             | 3,500   |
| 1300                | 3,500                             | 1,600   |

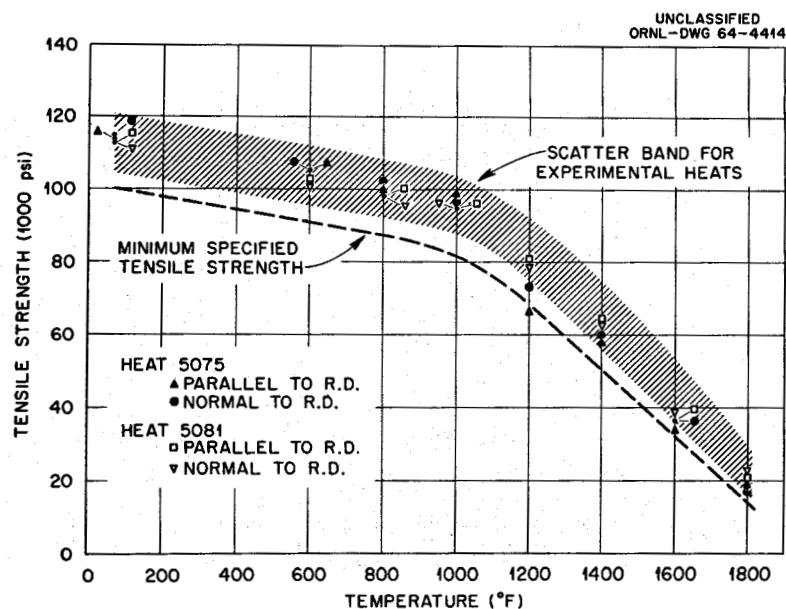


Fig. 9. Ultimate Tensile Strength for INOR-8 to 1800°F.

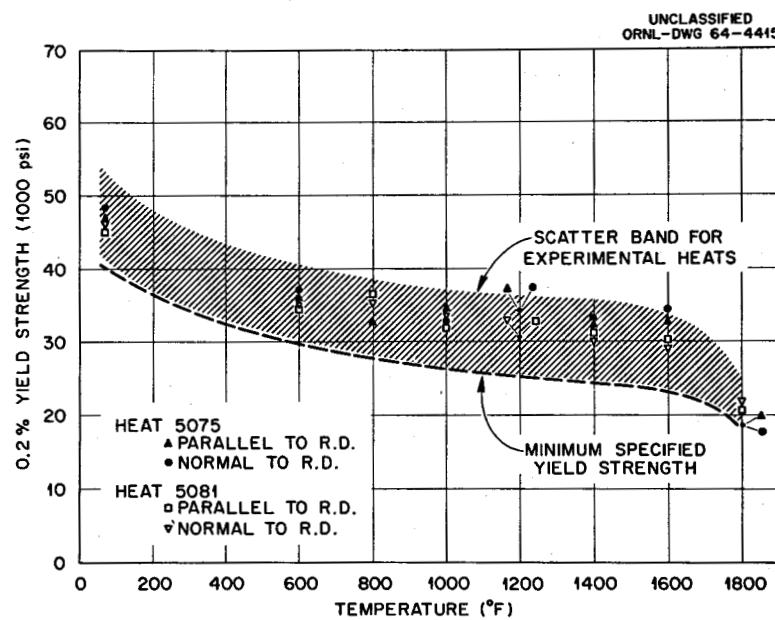


Fig. 10. Yield Strength for INOR-8 to 1800°F.

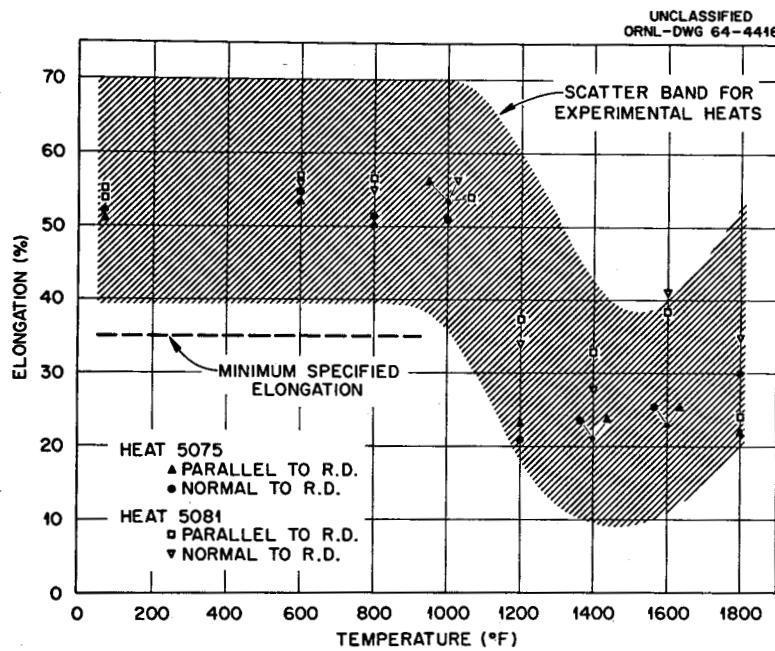


Fig. 11. Percent Elongation for INOR-8 to 1800°F.

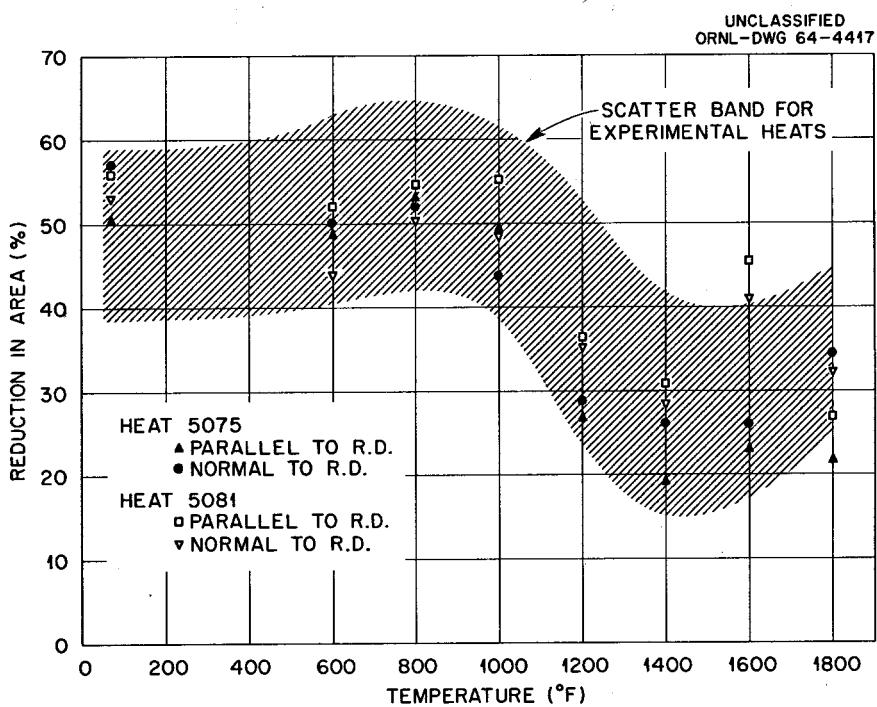


Fig. 12. Reduction in Area for INOR-8 to 1800°F.

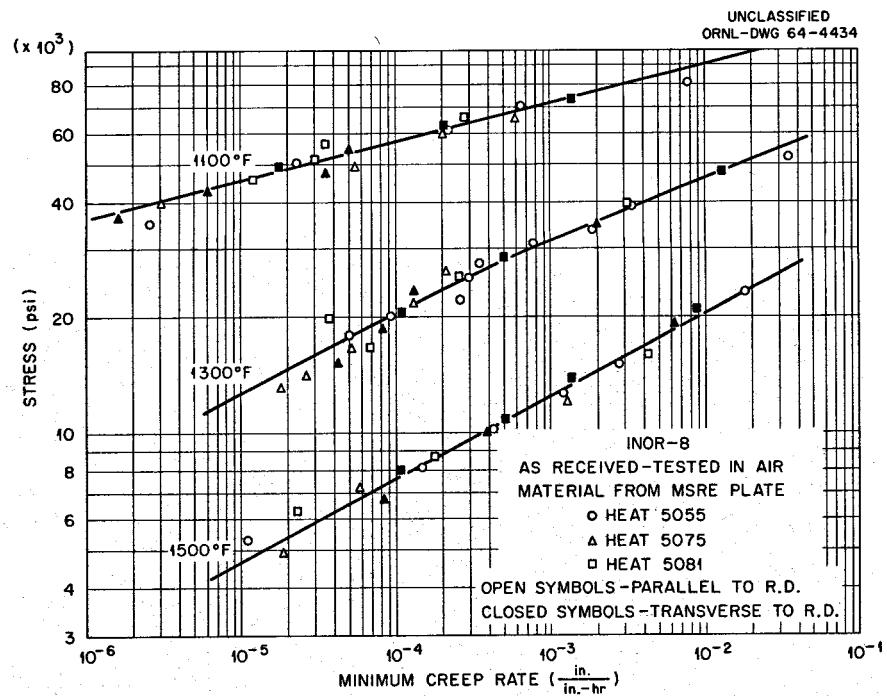


Fig. 13. Minimum Creep Rate for INOR-8 at 1100, 1300, and 1500°F.

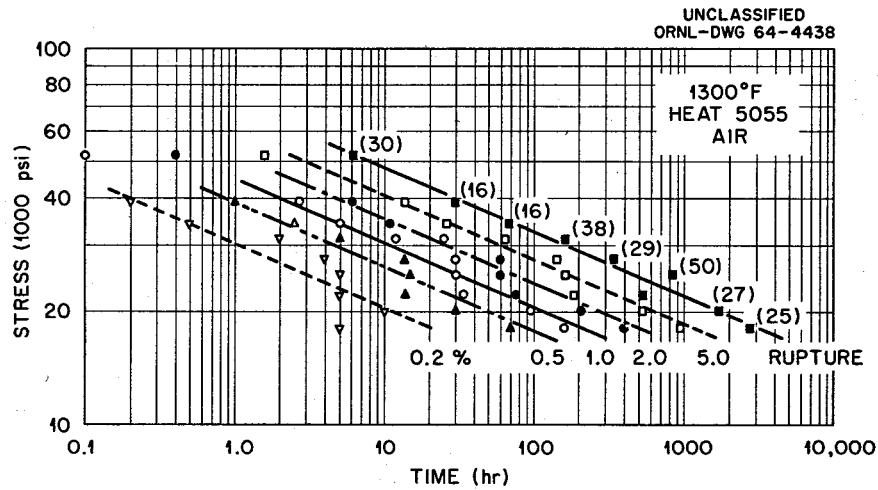


Fig. 14. Stress vs Time to Produce Various Strains for INOR-8.

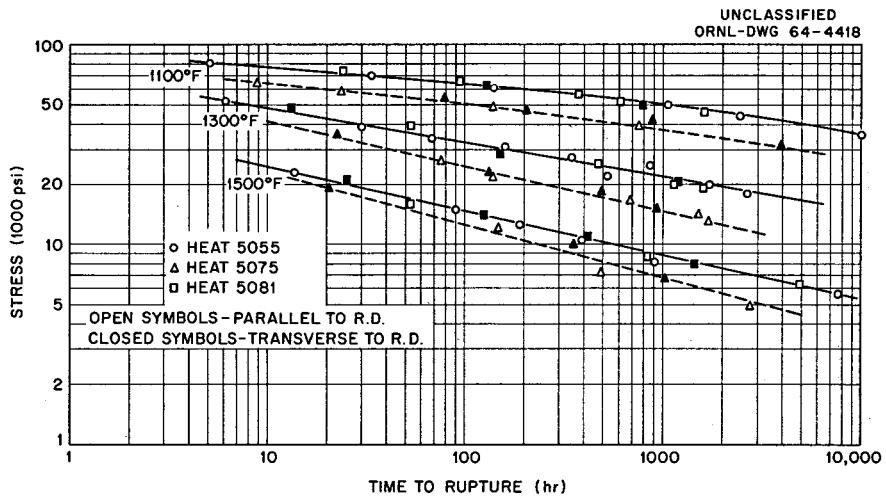


Fig. 15. Creep Rupture Curves for INOR-8 at 1100, 1300, and 1500°F.

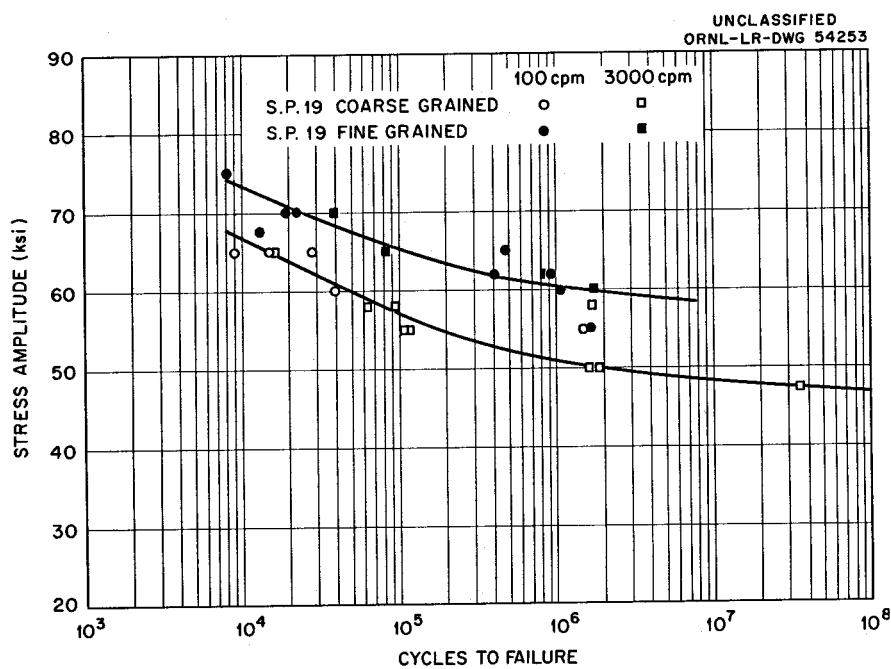


Fig. 16. Fatigue Properties of INOR-8 at 1100°F; Rotating Beams.

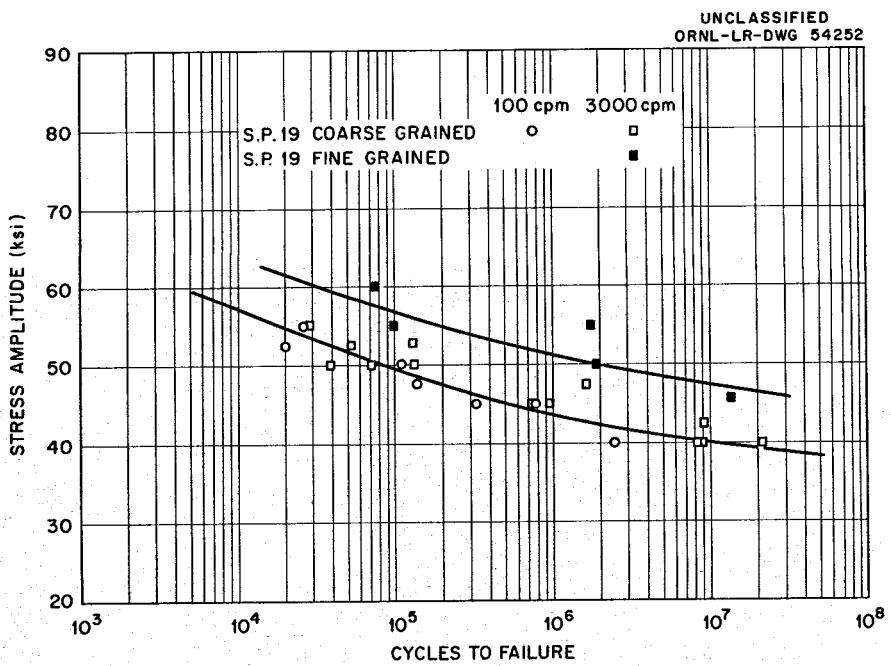


Fig. 17. Fatigue Properties of INOR-8 at 1300°F; Rotating Beams.

The thermal-fatigue behavior of INOR-8 was investigated at the University of Alabama. Figure 18 presents a graph of the plastic strain range vs cycles to failure, and results are seen to obey a Coffin-type relation. The tests involved several maximum temperatures, as noted, as well as rapid cycling and hold-time cycling. Furthermore, the data were obtained from two specimen geometries. These data show good agreement with isothermal strain-fatigue data on this alloy.

An analysis of these same tests, based on a plastic strain energy criterion, indicates that the total plastic work for failure of INOR-8 by fatigue is constant in this temperature range. The data have been plotted in Fig. 19 as plastic strain energy vs cycles to failure. It is seen that the data for 1300 and 1600°F fit curves having the same slope ( $\sim -1$ ) but different intercepts. The intercept values (at  $N_p = 1/2$ ) are in fair agreement with plastic strain energy values derived from tensile tests at the appropriate temperatures.

#### Mechanical Properties of INOR-8 Irradiated at Elevated Temperatures

Subsize tensile specimens of INOR-8 have been irradiated in the B-8 lattice position of the ORR. The specimens (heat 5081) were given a solid-solution heat treatment at 1175°F prior to irradiation. They were irradiated at 1300°F for approximately 2000 hr to a dose of 5 to  $12 \times 10^{20}$  nvt (fast and thermal).

The tensile properties of irradiated and unirradiated alloys with similar thermal histories are compared in Table 12 as functions of deformation temperatures for given strain rates. No significant differences in yield stresses were observed, although the yield stress behaviors were slightly different at 600 to 750°F. However, irradiation markedly reduced the ultimate and true tensile stresses for deformation temperatures of 1112°F and above. The ductility was also affected by irradiation, and again the effect was confined to deformation at elevated temperatures. The true fracture strain was approximately equal to the true uniform elongation for the irradiated specimens. Therefore, the fracture strain, uniform strain, and total elongation were all reduced by irradiation.

The influence of strain rate at elevated temperatures was investigated, and these data are given in Table 13. The effect of irradiation increases with decreasing strain rate. Figure 20 indicates that the effect of irradiation on the uniform elongation and true fracture strain may reach a maximum at a temperature that is strain-rate sensitive.

The effect of postirradiation annealing on the elevated-temperature properties has been investigated. Numerous investigations have shown that postirradiation heat treatments at 1750 to 2000°F anneal the damage that causes irradiated stainless steel to be brittle when deformed at ambient temperature to 212°F. Irradiated INOR-8 samples were heated for 0.75 hr at 2150°F prior to deforming at 1300 and 1650°F. The properties of the irradiated alloy given the postirradiation heat treatment are compared to those of the irradiated alloy not heat treated in Table 14. The

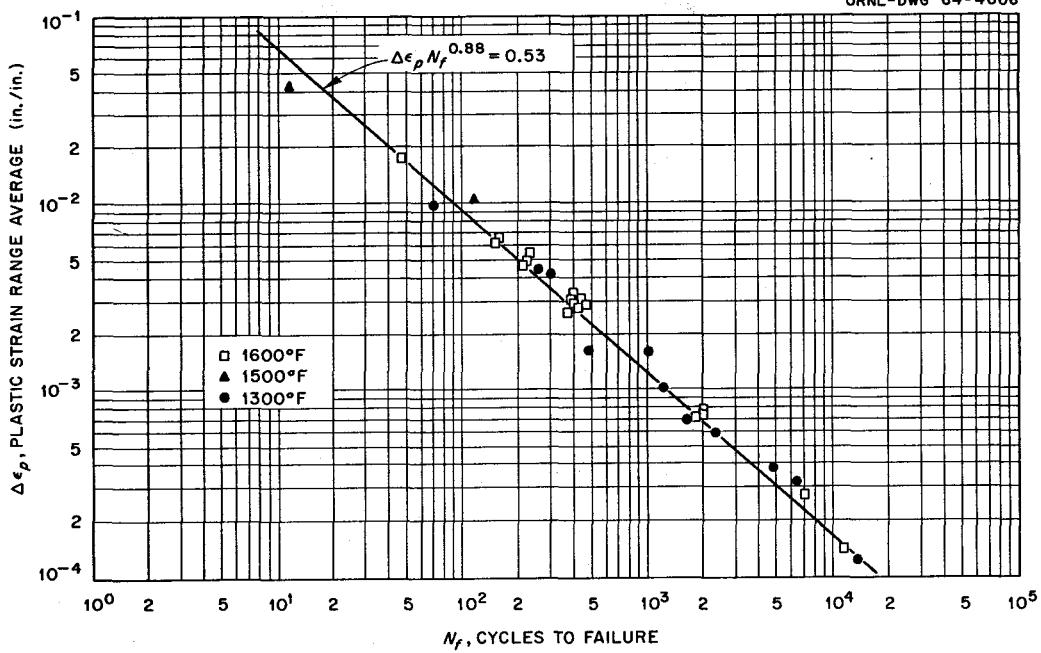
UNCLASSIFIED  
ORNL-DWG 64-4006

Fig. 18. Effects of Strain Range on the Thermal-Fatigue Life of INOR-8.

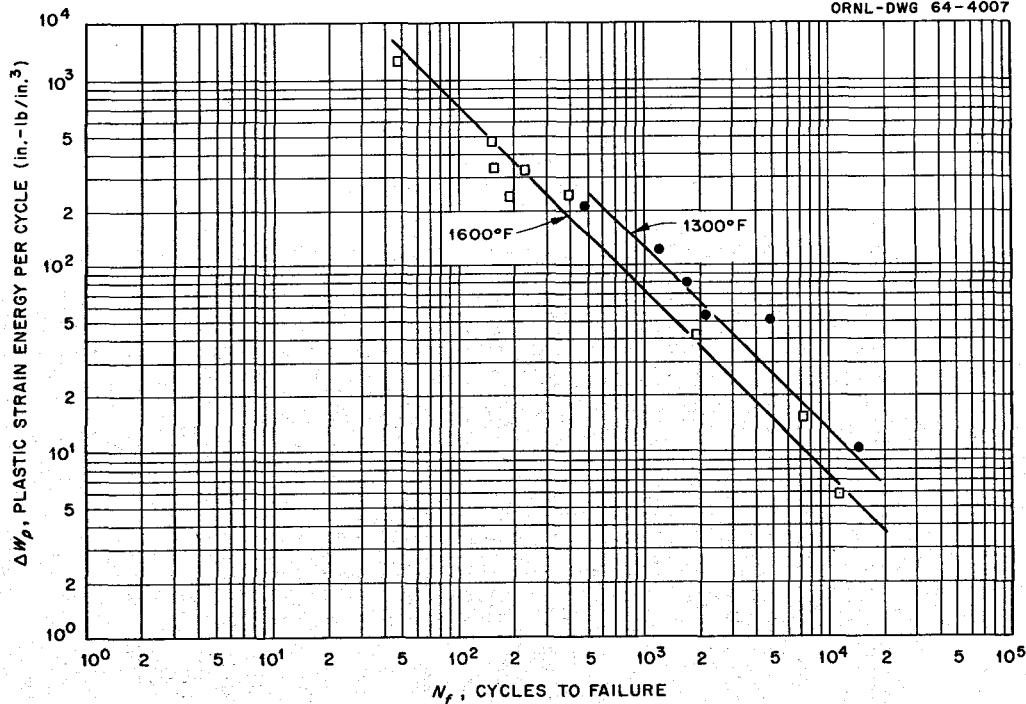
UNCLASSIFIED  
ORNL-DWG 64-4007

Fig. 19. Relation of Plastic Strain Energy Absorbed per Cycle to the Fatigue Life of INOR-8.

Table 12. Tensile Strength and Ductility of Irradiated and Unirradiated INOR-8 (Heat 5081)

| Deformation<br>Temperature<br>(°C) | Stress (ksi)   |          |                       |          | Ductility (%)       |          |                      |          |
|------------------------------------|----------------|----------|-----------------------|----------|---------------------|----------|----------------------|----------|
|                                    | Yield Strength |          | True Tensile Strength |          | True Uniform Strain |          | True Fracture Strain |          |
|                                    | Irrad.         | Unirrad. | Irrad.                | Unirrad. | Irrad.              | Unirrad. | Irrad.               | Unirrad. |
| RT                                 | 46.3           | 45.5     | 168.6                 | 166.5    | 42.3                | 40.6     | 42.5                 | 39.0     |
| 100                                | 43.9           | 43.9     | 159.5                 | 161.0    | 40.1                | 40.3     | 44.6                 | 37.2     |
| 200                                | 38.4           | 40.7     | 150.6                 | 157.5    | 40.3                | 41.9     | 42.5                 | 50.7     |
| 300                                | 36.0           | 40.7     | 154.3                 | 147.0    | 42.2                | 37.9     | 44.6                 | 41.4     |
| 400                                | 35.0           | 40.7     | 146.9                 | 153.0    | 40.2                | 39.3     | 42.5                 | 46.9     |
| 500                                | 35.8           | 35.8     | 129.5                 | 144.0    | 35.3                | 42.4     |                      |          |
| 600                                | 32.5           | 36.2     | 82.4                  | 109.0    | 11.8                | 26.7     | 21.9                 | 31.6     |
| 700                                | 31.0           | 34.1     | 53.4                  | 102.8    | 8.0                 | 30.8     | 11.6                 | 42.1     |
| 800                                | 28.5           | 30.9     | 38.4                  | 59.9     | 3.7                 | 12.2     | 6.9                  | 86.6     |

Table 13. Strain-Rate Sensitivity of Irradiated and Unirradiated INOR-8 (Heat 5081)

| Deformation<br>Temperature<br>(°C) | Strain<br>Rate<br>(per min) | Stress (ksi)   |          |                          |          | Ductility (%)          |          |                         |          |
|------------------------------------|-----------------------------|----------------|----------|--------------------------|----------|------------------------|----------|-------------------------|----------|
|                                    |                             | Yield Strength |          | True Tensile<br>Strength |          | True Uniform<br>Strain |          | True Fracture<br>Strain |          |
|                                    |                             | Irrad.         | Unirrad. | Irrad.                   | Unirrad. | Irrad.                 | Unirrad. | Irrad.                  | Unirrad. |
| 500                                | 0.2                         | 32.7           | 34.9     | 136.1                    | 145.6    | 41.2                   | 42.3     | 46.6                    | 53.4     |
| 500                                | 0.02                        | 35.8           | 35.8     | 129.5                    | 144.0    | 35.3                   | 42.4     |                         | 51.4     |
| 500                                | 0.002                       | 34.4           | 37.4     | 122.5                    | 131.5    | 32.3                   | 33.3     | 36.5                    | 34.2     |
| 600                                | 0.2                         | 32.9           | 34.1     | 112.7                    | 134.4    | 31.2                   | 38.9     | 36.5                    | 48.7     |
| 600                                | 0.02                        | 32.5           | 36.2     | 82.4                     | 109.0    | 17.7                   | 26.7     | 21.9                    | 31.6     |
| 600                                | 0.002                       | 34.2           | 34.6     | 63.1                     | 106.0    | 10.3                   | 29.9     | 13.2                    | 29.7     |
| 700                                | 0.2                         | 30.5           | 30.9     | 66.8                     | 106.5    | 13.5                   | 32.2     | 19.2                    | 39.2     |
| 700                                | 0.02                        | 31.0           | 34.1     | 53.4                     | 102.8    | 8.0                    | 30.8     | 11.6                    | 42.1     |
| 700                                | 0.002                       | 32.1           | 33.7     | 47.0                     | 80.5     | 5.6                    | 20.0     | 7.8                     | 29.0     |
| 800                                | 0.2                         | 29.3           | 29.3     | 45.7                     | 79.8     | 6.7                    |          | 11.6                    |          |
| 800                                | 0.02                        | 28.5           | 30.9     | 38.4                     | 59.9     | 3.7                    | 12.2     | 6.9                     | 86.6     |
| 800                                | 0.002                       | 29.3           | 32.5     | 32.2                     | 42.9     | 1.8                    | 6.5      | 4.9                     | 93.7     |

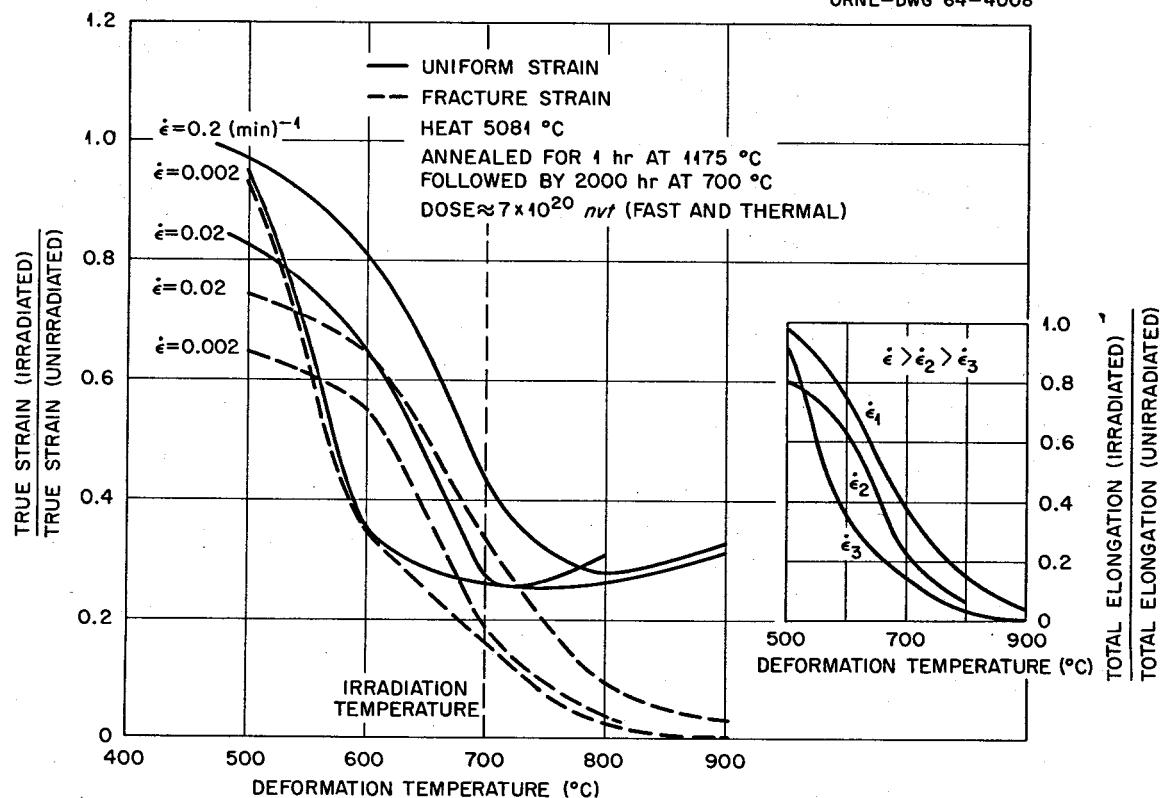
UNCLASSIFIED  
ORNL-DWG 64-4008

Fig. 20. Effect of Irradiation on the Ductility of INOR-8 at Elevated Temperatures.

Table 14. Influence of Postirradiation Heat Treatment of 1 hr at 2150°F on the Tensile Properties of INOR-8 at a Strain Rate of  $0.002 \text{ min}^{-1}$

| Deformation Temperature (°F) | Postirradiation Heat Treatment | Yield Stress (ksi) | Tensile Strength (ksi) |      | Elongation Measured in 1 in. (%) |       |
|------------------------------|--------------------------------|--------------------|------------------------|------|----------------------------------|-------|
|                              |                                |                    | Ultimate               | True | Uniform                          | Total |
| 1300                         | As irradiated                  | 32.1               | 44.3                   | 47.0 | 5.8                              | 6.1   |
| 1300                         | 1 hr at 2150°F                 | 30.5               | 41.5                   | 44.2 | 6.3                              | 6.4   |
| 1650                         | As irradiated                  | 23.2               | 23.2                   | 23.3 | 0.4                              | ≈0.4  |
| 1650                         | 1 hr at 2150°F                 | 23.5               | 23.5                   | 23.6 | 0.6                              | 0.7   |

stability of the irradiation-induced defect associated with the elevated temperature problem is remarkable.

A comparison of the effects of irradiation at the lower and upper limit of neutron exposure given the INOR-8 are shown below:

| Neutron Dose<br>(nvt) |                      | Yield<br>Stress<br>(ksi) | Ultimate<br>Strength<br>(ksi) | True<br>Tensile<br>Strength<br>(ksi) | Elongation<br>(%) |       |
|-----------------------|----------------------|--------------------------|-------------------------------|--------------------------------------|-------------------|-------|
| Fast                  | Thermal              |                          |                               |                                      | Uniform           | Total |
| $5 \times 10^{20}$    | $6 \times 10^{20}$   | 33.3                     | 44.0                          | 46.0                                 | 4.5               | 4.7   |
| $12 \times 10^{21}$   | $1.2 \times 10^{21}$ | 32.1                     | 44.3                          | 47.0                                 | 5.8               | 6.1   |

The differences observed in these data obtained at 1300°F and at a strain rate of  $0.002 \text{ min}^{-1}$  are believed to be insignificant.

In summary, the ductility of INOR-8 in the absence of irradiation is considered to be low at deformation temperatures of 1472 and 1650°F. The low, uniform elongations decrease with decreasing strain rate. The decrease in uniform strain is accompanied by a large increase in fracture strain and a reduction in true fracture stress. The alloy appears to work-soften at elevated temperature at a specific temperature that is strain rate sensitive.

The effect of irradiation at high temperatures on the mechanical properties of INOR-8 is similar to the effect observed on austenitic stainless steels and other nickel-base alloys. This effect is caused by thermal neutrons that apparently produce helium when boron atoms in the grain boundaries are irradiated. The deterioration in the ductile properties of the irradiated metal occurs only at temperatures above 1112°F. The magnitude of the effect increases with decreasing strain rate. The effect is primarily one of lowering the ductility. However, the ultimate stress and the true tensile stress are markedly reduced for those deformation temperatures at which the alloy's work-hardening coefficient is high.

Studies are now in progress to determine the effects of irradiation on the creep strength of INOR-8 which is the primary criterion for MSRE designs.

#### Fabrication of INOR-8

##### Melting and Casting

The melting and casting of INOR-8 can be carried out by using conventional practices for nickel and its alloys. Air and vacuum induction,

electric arc, and consumable arc melting methods have been successfully employed. The usual precautions must be taken to avoid gassy melts together with sulfur contamination. Manganese, silicon, aluminum, and titanium are added to deoxidize the metal. Care must be exercised in the use of boron as a deoxidizer because of its adverse effects on weldability.

The alloy has been cast in molds of water-cooled copper, graphite, rammed magnesia, and cast iron. Both the fuel and coolant pump impellers and volutes were made from INOR-8 sand castings. More than 15 sets of these castings were made by the Cerami-Sand Process of General Alloys Company. Chemistry requirements for the castings did not deviate from the chemistry specification for wrought material. Radiographic quality levels of the castings were class 1 (ASME Boiler and Pressure Vessel Code) in areas of high stress and class 2 in other areas; however, considerable weld repair was required to obtain this quality.

Mechanical properties tests were performed on specimens made from sand-cast blanks as well as on investment cast material. Results indicated that the tensile strength of sound cast metal is about 60% of that for wrought metal and the 0.2% offset yield strength for cast material is about 80% of that for wrought material. Most castings had elongations of greater than 20% at all temperatures. Short-term stress rupture tests for cast material at 1100 to 1700°F indicated that it was stronger than wrought material, and the conventional MSRE design strengths are therefore considered suitable for cast metal.

#### Forming

INOR-8 has been produced on a commercial basis in a variety of shapes, such as plate, sheet, rod wire, and welded and seamless tubing, by conventional methods of hot and cold forming. More than 27 heats of INOR-8 were made for the MSRE, amounting to almost 200,000 lb of material.

Hot forging of INOR-8 ingots has been successfully carried out both on press- and hammer-type forges between 1832 and 2250°F. Hot rolling is readily accomplished between 2100 and 2200°F using reductions of about 10% per pass. The optimum extrusion temperature range is 2150 to 2200°F for extrusion ratios of 4:1 to 12:1. Extrusion rate is one of the most critical variables in tube blank extrusion; it should be kept to about 1 in. of billet length per second in order to avoid hot cracking.

The ductility of INOR-8 at room temperature allows cold-working operations such as rolling, swaging, tube reducing, and drawing to be performed successfully. The alloy work-hardens rapidly, as shown in Fig. 21, and therefore requires frequent annealing in order to prevent the formation of splits and cracks. Between anneals a reduction in area of about 50% is possible.

The forming of INOR-8 heads for the MSRE was attempted using hot spinning techniques as well as hot- and cold-forming methods. Spinning

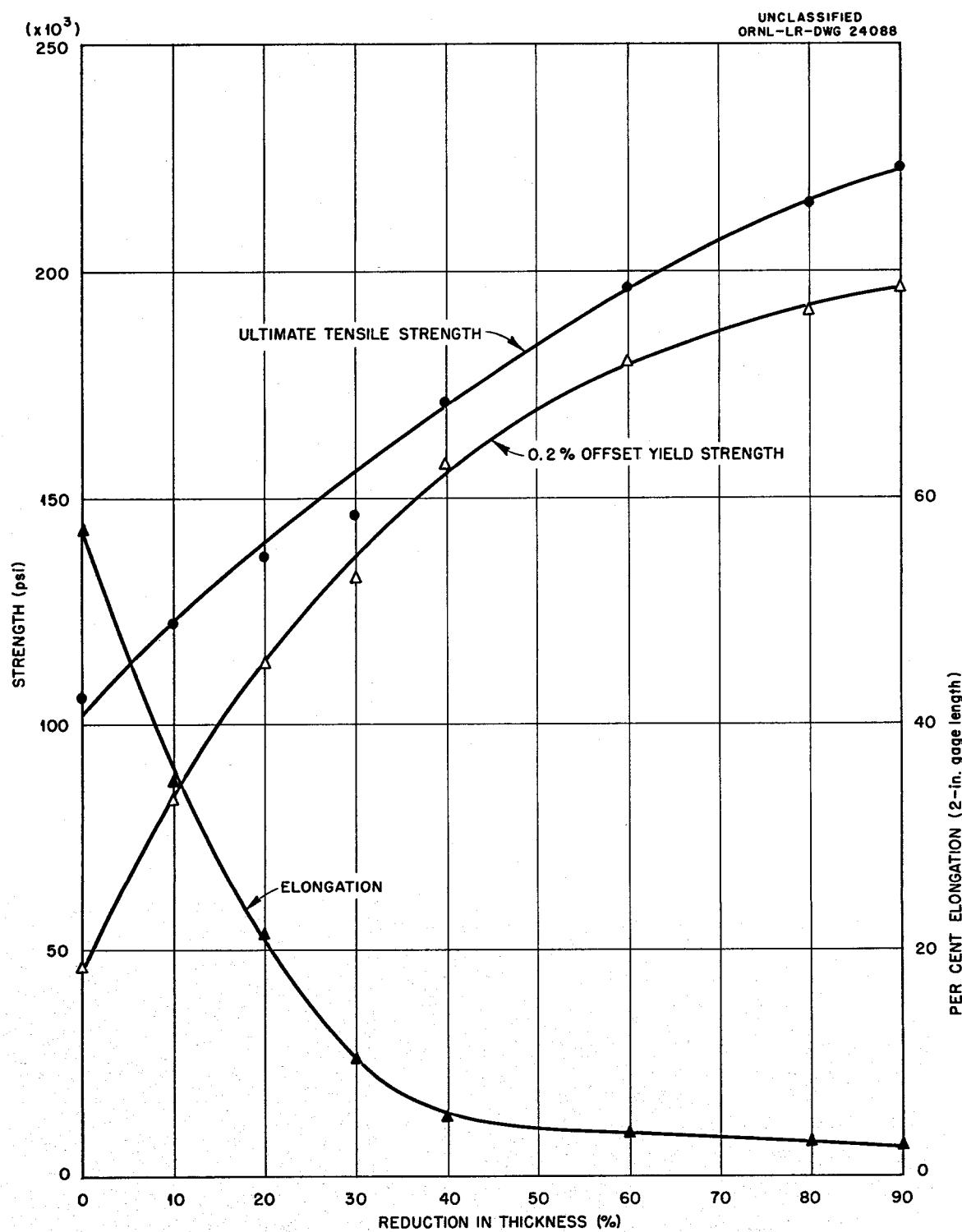


Fig. 21. Work-Hardening Curves for INOR-8.

was attempted at 2100 to 2150°F with the INOR-8 plate sandwiched between steel plates. Cracking occurred in the flanges and radii of all the shells. This was due to the material's cooling too rapidly into the region of low ductility. As a result spinning was discontinued as a method for producing INOR-8 heads.

Heads 3 to 4 ft in diameter were successfully made by the hot-forming method using starting temperatures of 2000 to 2100°F. This material cooled to temperatures as low as 1550°F during working but did not crack. Cold forming was the most successful method used to fabricate INOR-8 heads. Heads as small as 9 in. in diameter by 1/2 in. thick and as large as 60 in. in diameter by 1-1/8 in. thick (reactor vessel) were made in this manner without the use of intermediate anneals.

#### Machining

INOR-8 was found to machine in a manner similar to other nickel-base alloys, such as the Hastelloy type. Standard cemented carbide tools, cutting speeds of about 35 to 50 fpm and feeds of 0.015 in. or less, gave best machining results. Depths of finishing cuts were kept greater than 0.005 in. in order to machine below the work-hardened surface that occurs in this alloy. Rough machining using a cutting depth of 0.250 to 0.375 in. was accomplished at speeds up to 150 fpm.

#### Heat Treatment

INOR-8 can be fully annealed by treating it at 2150 ± 25°F for approximately 1 hr per inch of thickness, or a minimum time of 10 to 15 min. For bright annealing an atmosphere of dry hydrogen is satisfactory.

The approximate recrystallization temperatures for INOR-8 have been determined to be 1350 and 1500°F for 80 and 10% cold-worked materials respectively; this was with annealing times of 1 hr.

The chemical specification for INOR-8 is such that the alloy is not able to be age hardened by the precipitation of  $Ni_x Mo_y$  intermetallic compounds at 1100 to 1500°F. Carbides initially present in the alloy will precipitate eutectically and will spheroidize as a result of the fabrication and annealing treatment. High-temperature annealing of the wrought material, for example, between 2100 and 2250°F, results in partial solution of the carbides which then precipitate as fine particles when the temperature of material is lowered to, for example, 1500°F. A slight aging response has been attributed to the reprecipitation of the carbides.

Heat-treatment requirements for INOR-8 parts in the MSRE call for the material to be annealed after any forming or working and to be stress-relieved after final fabrication. The temperature used for annealing is 2150 ± 25°F, and the temperature used for stress-relieving is 1600 ± 25°F.

The cooling rate at temperatures above 600°F for any complex component is 400°/hr per inch of thickness. Where possible, stress-relieving was done after welding and heavy machining in order to give dimensional stability at operating temperatures and to improve ductility in the 1400 to 1800°F range.

#### Cleaning and Descaling of INOR-8

Special precautions were taken to keep INOR-8 components clean and free of harmful materials. After machining, forming, etc., and prior to any welding or heat treatment, the alloy was degreased using a solvent such as perchloroethylene and then inspected for cleanliness. At no time were sulfur-containing compounds allowed in contact with the alloy. Also, aluminum, lead, and mercury were not allowed to contact the alloy in order to preclude their presence at elevated temperatures where undesirable reactions occur between these materials and INOR-8.

Oxide removal from INOR-8 was generally done by the vapor blast method because of the safety and convenience of this technique; however, other methods were also successfully used, such as processing with sodium hydride and also pickling in a 30% HNO<sub>3</sub>-5% HF bath at 140°F.

#### Welding

INOR-8 is readily weldable by the inert-gas-shielded tungsten-arc process using weldrod with no changes in chemistry from the wrought material. Welding procedures and specifications for welding the alloy to Inconel and to austenitic stainless steels, as well as to itself, are listed in Table 15. These procedures are similar to the welding procedures for other nickel-base alloys, such as Inconel.

The mechanical properties of INOR-8 weld metal are very similar to those of INOR-8 wrought metal. That no aging occurs is shown in Fig. 22, which compares INOR-8 with age-hardenable Hastelloy B and Hastelloy W.

Early tests of some experimental heats of INOR-8 indicated a susceptibility to weld-metal cracking of the type shown in Fig. 23 when these materials were subjected to welding under restraint. Consequent studies showed that weld-metal cracking tendencies can be induced in heats with an abnormally high boron content and that the cracking tendencies can be eliminated by the addition of 2% Nb or by improving deoxidation and purification procedures during melting. A change to the chemistry specification (see Table 16) and a weldability testing of all heats of material purchased for the MSRE has resulted in weldments of the quality shown in Fig. 24. A comparison of the mechanical properties of the experimental heat that had cracking tendencies (INOR-8 SP-23) with the properties of an INOR-8 having a revised chemistry is shown in Table 17.

Table 15. Welding Specifications for INOR-8 Material

| Specification No. | Date Issued | Title  |
|-------------------|-------------|--|
| MET-WR-2          | 8/23/63     | Welding of High-Nickel Alloy Components for Nuclear Service  |
| MET-WR-3          | 6/23/61     | Welding and Brazing Requirements of Nickel-Molybdenum-Chromium Alloy Test for Plate                                |
| QTS-23            | 1/1/58      | Qualification Test Specification Inert-Gas Shielded Tungsten Arc Welding of INOR-8 Alloy Tubing                    |
| PS-24             |             | ORNL Procedure Specification D.C. Inert-Gas Shielded Tungsten Arc Welding of INOR-8 Alloy                          |
| PS-25             | 1/5/60      | ORNL Procedure Specification D.C. Inert-Gas Shielded Tungsten Arc Welding of INOR-8 Alloy Pipe, Plate and Fittings |
| PS-26             | 3/15/60     | ORNL Procedure Specification D.C. Inert-Gas Shielded Tungsten Arc Welding of INOR-8 Alloy Pipe, Plate and Fittings |
| MET-WS-1          | 12/20/61    | Joint Design for Welding of INOR-8   |
| MET-WS-2          | 11/21/61    | Machining Details for Matching Single-Welded Joints  |
| MET-WS-3          | 2/16/62     | Interpretation of Weld Symbols of Company Drawings   |
| MET-WR-200        | 11/6/63     | Procedure for Inspection of Welding of High Nickel Alloys  |

Table 16. Chemical Composition Requirements for the Ni-Mo-Cr Alloy - INOR-8

| Element             | Percent <sup>a</sup>   |                       |
|---------------------|------------------------|-----------------------|
|                     | Original Specification | Revised Specification |
| Nickel              | Remainder              | Remainder             |
| Molybdenum          | 15.00-18.00            | 15.00-18.00           |
| Chromium            | 6.00- 8.00             | 6.00- 8.00            |
| Iron                | 5.00                   | 5.00                  |
| Carbon              | 0.04- 0.08             | 0.04- 0.08            |
| Manganese           | 0.80                   | 1.00                  |
| Silicon             | 0.50                   | 1.00                  |
| Tungsten            | 0.50                   | 0.50                  |
| Aluminum + titanium | 0.50                   | 0.50                  |
| Copper              | 0.35                   | 0.35                  |
| Cobalt              | 0.20                   | 0.20                  |
| Phosphorus          | 0.010                  | 0.015                 |
| Sulfur              | 0.015                  | 0.020                 |
| Boron               | 0.010                  | 0.010                 |
| Vanadium            |                        | 0.50                  |
| Others              | 0.50                   |                       |

<sup>a</sup>Single values are maximum percentages unless otherwise specified.

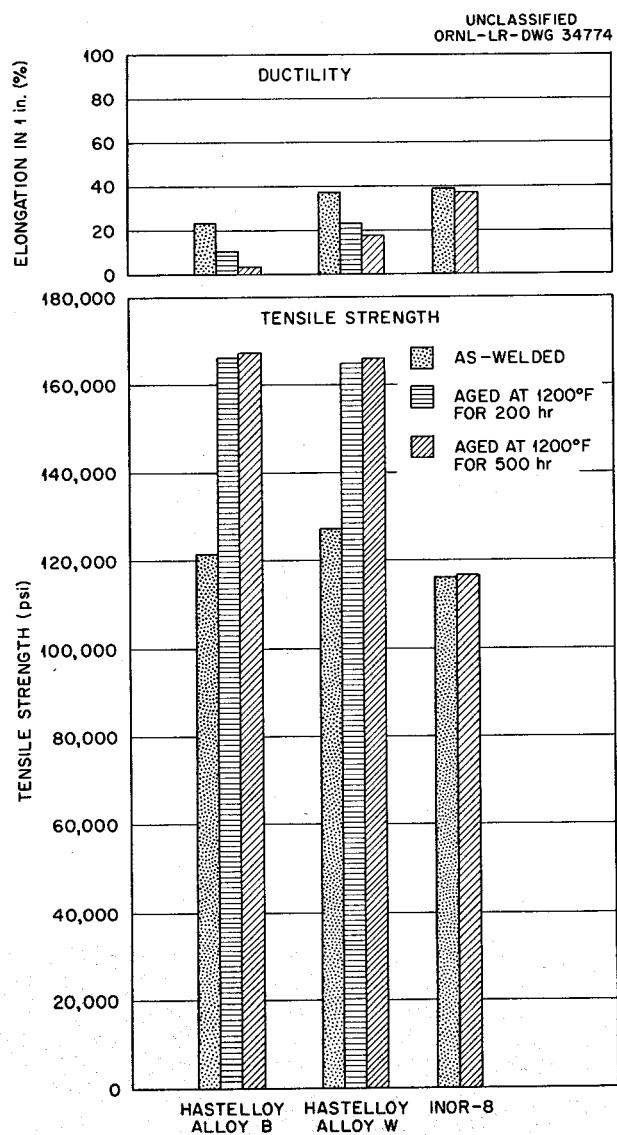


Fig. 22. Room-Temperature Mechanical Properties of Hastelloy B, Hastelloy W, and INOR-8 Weld Metal in the As-Welded Condition and After Aging at 1200°F.

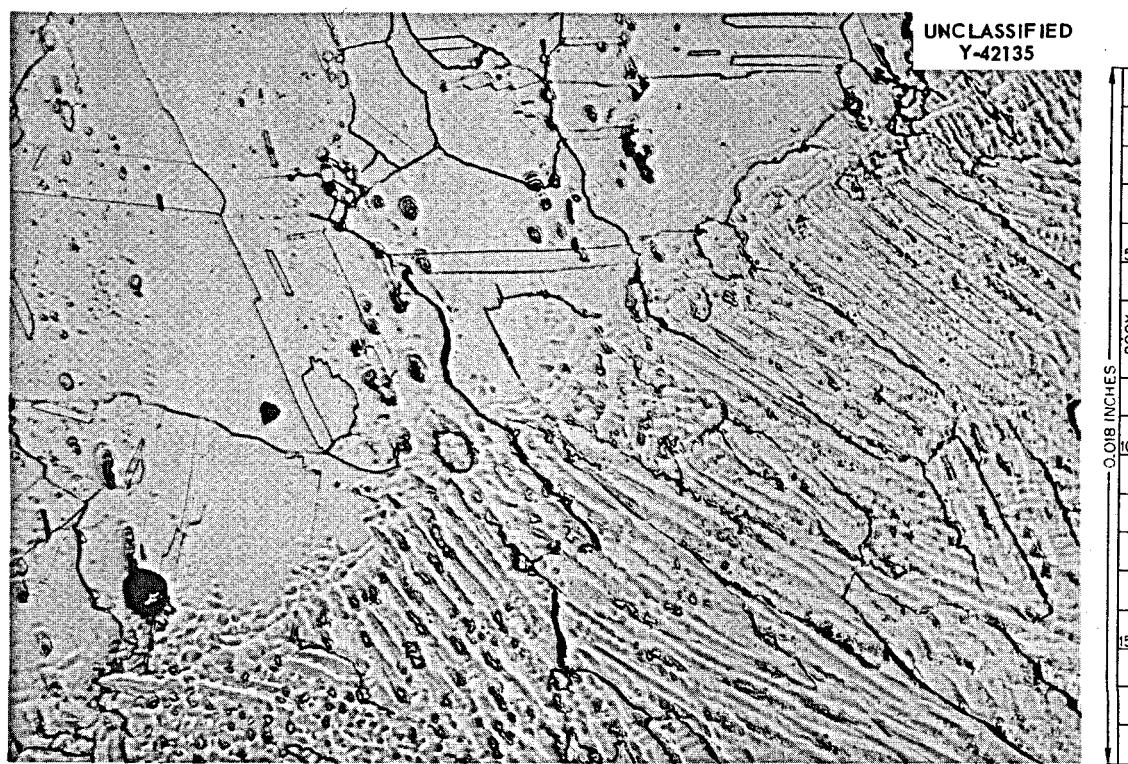


Fig. 23. Weld Metal Cracking in Heat SP-23 of INOR-8.

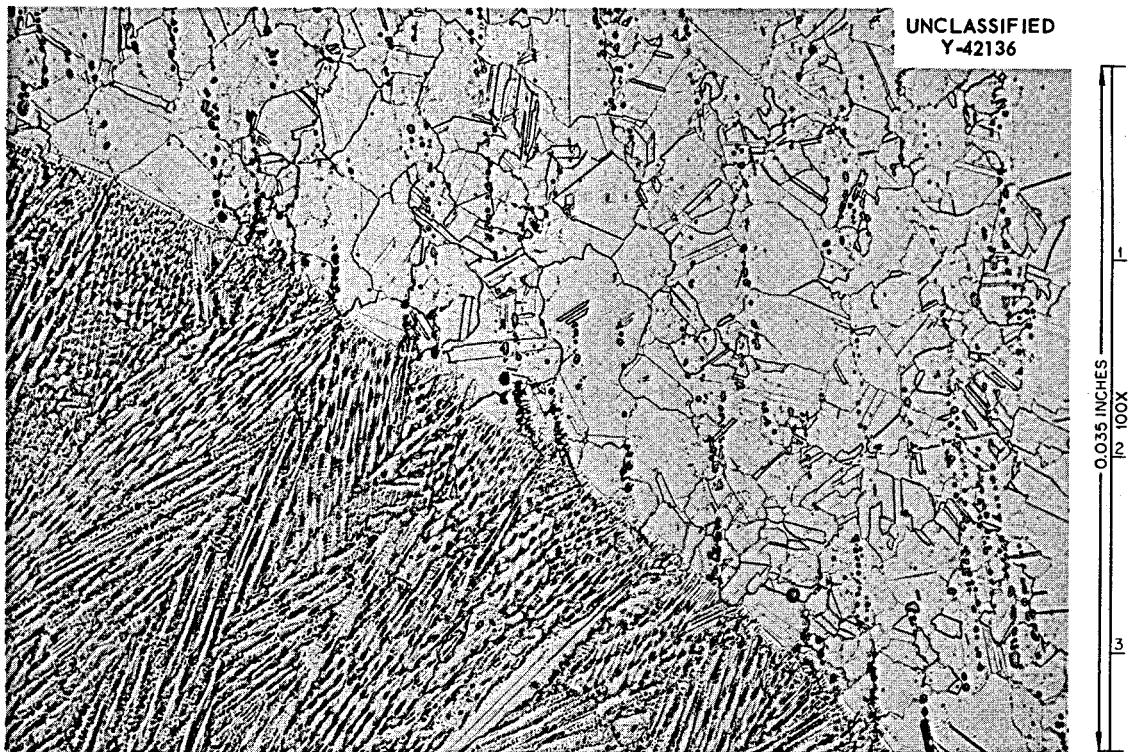


Fig. 24. Weld Metal Structure of Heat 5055 of INOR-8, Showing No Cracking.

Table 17. Comparison of the Mechanical Properties of Transverse Specimens from High Restraint INOR-8 Welds Before and After Material Composition Revision

| Material Designation | Room Temperature Tensile |                  |                | 1300°F Tensile |                  |                | Stress Rupture <sup>a</sup> |                  |
|----------------------|--------------------------|------------------|----------------|----------------|------------------|----------------|-----------------------------|------------------|
|                      | Elongation (%)           | Tensile Strength | Yield Strength | Elongation (%) | Tensile Strength | Yield Strength | Rupture Time (hr)           | Total Strain (%) |
| Original composition | 28                       | 105,600          | 67,800         | 8              | 59,600           | 43,100         | 7.5                         | 1.7              |
| Revised composition  | 40                       | 114,200          | 70,000         | 16             | 67,200           | 47,200         | 96.5                        | 5.8              |

<sup>a</sup> Stress of 27,500 psi at 1300°F.

Component Fabrication DevelopmentHeat Exchanger Tube-to-Tube-Sheet Attachment

The INOR-8 tube bundle of the primary heat exchanger of the MSRE, shown in Fig. 25, contains 163 1/2-in.-diam  $\times$  0.42-in.-wall U-tubes welded to a 1-1/2-in.-thick tube sheet 18 in. in diameter. Procedures were successfully developed for welding and back brazing the 326 closely spaced tube-to-tube sheet joints in the unit, and the actual tube bundle was fabricated without incident. **The welded and back-brazed design** shown in Fig. 26 provides a double seal between the fuel and coolant salts and was used because of the necessity for high joint integrity.

Grooves were trepanned in the weld side of the tube sheet so that low-restraint edge-type welds could be made. **This technique greatly** reduces the cracking problems associated with welding thin-walled tubes to thick tube sheets. Welding and assembly procedures were developed that provided welds of high quality with a minimum of roll-over. Welding conditions are given in Table 18.

The 82 Au-18 Ni (wt %) brazing alloy used in this application is corrosion resistant, ductile, and produces joints exhibiting satisfactory mechanical strength. A unique joint design, incorporating a trepan groove and feeder holes in the tube sheet, was used for the braze side. The purpose was to prevent the brazing alloy from melting and flowing along the thin-walled tubes before the heavy tube sheet reached the brazing temperature.

After the determination of optimum welding and brazing conditions on several subsize and full-size mockup samples, the actual unit was constructed. Nondestructive inspection of the welds revealed no defects. The general flow of the brazing alloy was good, and ultrasonic examination of brazed joints showed only minor, scattered porosity. The completed unit passed both the helium leak test and the 800-psi hydrostatic test.

Development and Manufacture of MSRE Control Rod Elements

A total of 160 MSRE control rod elements were manufactured by Westinghouse Atomic Fuel Department. **The elements are gadolinium oxide-aluminum oxide bushings clad with Inconel**, as shown in Fig. 27. **They are** about 1-1/2 in. long with an ID slightly larger than 3/4 in. and a wall thickness of about 3/8 in. **Each element contains three bushings which** are made by pressing and sintering prereacted powder, starting as 70% gadolinium oxide and 20% aluminum oxide. **The use of prereacted powder was** developed at ORNL in order to minimize shrinkage and eliminate the possibility of hydrolysis, with subsequent deterioration of the solid pellets.

The prereacted materials have densities as high as 6.0 g/cm<sup>3</sup>. This compares with a theoretical maximum of 5.89 g/cm<sup>3</sup> for a fully dense mixture. X-ray diffraction analysis identified the reacted material to be primarily a perovskite-type phase GdAlO<sub>3</sub> with an excess of  $\alpha$ -Al<sub>2</sub>O<sub>3</sub>.

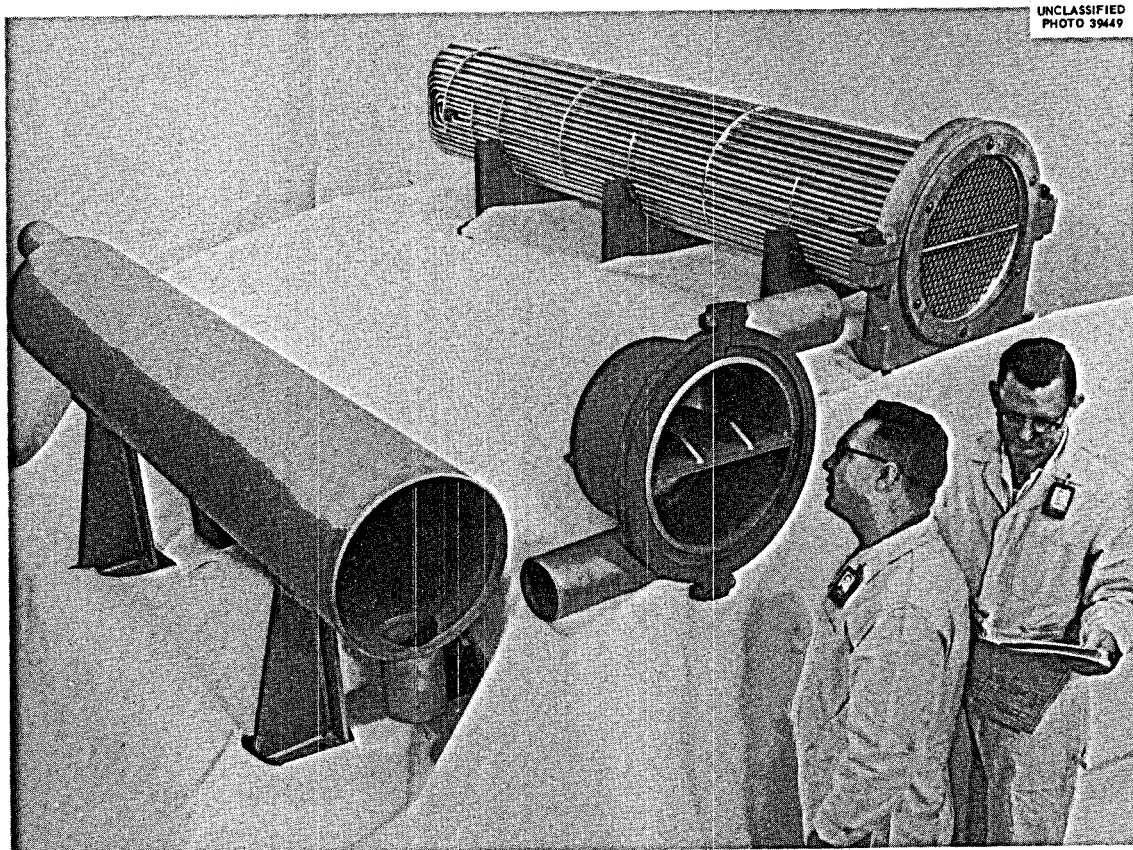


Fig. 25. MSRE Primary Heat Exchanger Components.

Table 18. Welding Conditions for MSRE Tube-to-Tube-Sheet Joints

|                               |  |
|-------------------------------|--|
| Electrode material            | Tungsten + 2% thoria   |
| Electrode diameter            | 3/32 in.   |
| Electrode taper               | 30° including angle  |
| Electrode-to-work distance    | 0.035 in. (determined by feeler gage)  |
| Electrode position            | 0.005 in. outside joint interface for full 360° rotation ( $\pm 0.002$ in. concentric) |
| Inert gas                     | Argon (99.995% purity)   |
| Gas flow rate                 | 12-13 cfh  |
| Welding amperage              | 39-40  |
| Electrode travel speed        | 7.3 in./min  |
| Weld overlap (full amperage)  | 30-60°   |
| Weld overlap (amperage taper) | 120-150°   |
| Welding position              | Flat   |

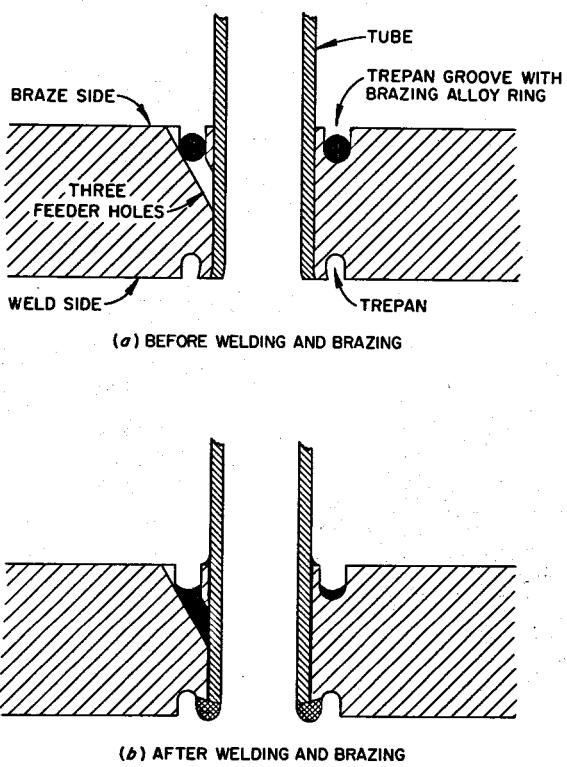
UNCLASSIFIED  
ORNL-LR-DWG 65682R3

Fig. 26. Schematic Drawing of Welded and Back-Brazed Joint Design.

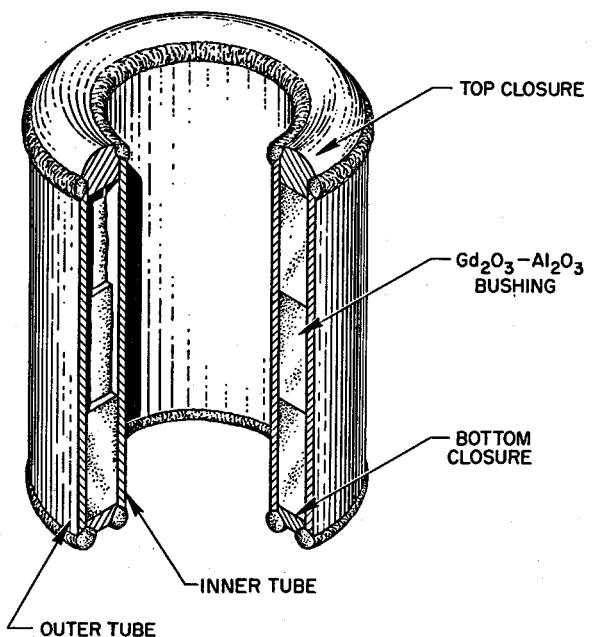
UNCLASSIFIED  
ORNL-DWG 64-1105R

Fig. 27. MSRE Control Rod Element.

The manufacturing process for the bushing included the mixing of the  $\text{Al}_2\text{O}_3$  and  $\text{Gd}_2\text{O}_3$  powder and prereacting at 1700°F. The reaction products were crushed, ball milled, sized, pressed into a bushing, and sintered at 1450°F. Each bushing was then given a thermal shock test by heating to 1400°F and quenching in water. After grinding, the bushings were visually inspected for any chips or cracks.

The top closure was welded to the outer and inner walls by the automatic tungsten-arc, inert-gas shield process (TIG). The bushings were heated to 1500°F to drive off absorbed gases. This heat treatment was found necessary because some of the first elements bulged owing to gas-pressure buildup during heating after canning. The bushings were then loaded into the can, the bottom closure was pressed on in a helium atmosphere, and the final two bottom closure welds were made.

After a preliminary dimensional inspection, a helium leak check, and a fluorescent penetrant inspection, the elements were heated to 1700°F in air in order to preoxidize the Inconel and thus prevent self-welding.

Prototype control rod elements were subjected to repeated thermal and mechanical shocks in the control-rod rig test from room temperature to 1400°F.

These were examined radiographically and dimensionally after 24 (1 cycle), 350, and 600 hr of operation that included approximately 11,000 cycles and 1700 simulated scrams. Holes were made in one can to expose the  $\text{Gd}_2\text{O}_3$ - $\text{Al}_2\text{O}_3$  to air for the final 250 hr of testing.

No measurable dimensional changes in the metal cans were noted throughout the test. Axial cracks were radiographically observed after the first cycle, and severe cracking in both the axial and transverse direction was observed at later stages. However, no crumbling or ratchetting was evident, and no condition was observed that might affect the nuclear or mechanical performance of the control-rod elements.

#### MSRE Material Surveillance Program

Surveillance specimens of INOR-8 and type CGB graphite will be placed in a central position of the reactor core to survey the effects of reactor operations on these materials. The specimens will be made from the stock used to fabricate the reactor primary system and moderator. Identical control specimens will be exposed to a duplicate thermal history while submerged in fuel salt in an INOR-8 container to differentiate between the effects of temperature and the effects of irradiation. Specimens will be removed from the reactor and examined after six months of operation and then again after periods of operation that should result in meaningful data based on the results of the first set of specimens. New specimens will replace the material removed.

The analysis of INOR-8 specimens will include metallographic examination for structural changes and corrosion effects, mechanical properties, and a general check for material integrity and dimensional changes. The analysis of the graphite specimens will include metallographic and radiographic examination for salt permeation and possible wetting effects, mechanical properties tests, dimensional checks for shrinkage effects, chemical analysis for deposits on the graphite, electrical resistivity measurements, and a general inspection for material integrity.

#### Summary

The materials problems attendant to containing molten salts as the fuel-bearing fluid for a power reactor have been studied extensively for a number of years. The mechanisms by which alloys are attacked by these salts have been defined, and an alloy inherently resistant to such corrosion has been developed. Thermal- and forced-convection loop tests, operating for periods of from one to two years, have demonstrated the validity of the corrosion model and the corrosion resistance of the alloy.

Problems of melting, casting, forming, and joining have been investigated, and it is noted that INOR-8 offers no unusual difficulties in any of these categories. The physical and mechanical properties of the alloy have been measured, and sufficient data are available to establish design criteria. Irradiation effects are being studied and large reactor components have been made from this alloy. It is therefore concluded that INOR-8 successfully meets the requirements of a construction material for the MSRE. For additional assurance, surveillance specimens will be placed in the core of the MSRE and examined periodically.

#### References

1. W. D. Manly et al., Progr. Nucl. Energy, Ser. IV 2, 164-79 (1960).
2. J. L. Crowley, W. B. McDonald, and D. L. Clark, Trans. Am. Nucl. Soc. 2(1), 174 (June 1959).
3. Met. Div. Ann. Progr. Rept. July 1, 1960, ORNL-2988.
4. R. C. Schulze et al., INOR-8 Graphite-Fused Salt Compatibility Test, ORNL-3124 (June 1, 1961).
5. R. W. Swindeman, The Mechanical Properties of INOR-8, ORNL-2780 (January 1961).
6. Development Data on Hastelloy Alloy N, Haynes Stellite Company Brochure, May 1959.
7. R. G. Carlsen, Fatigue Studies of INOR-8, BMI-1354 (January 1959).
8. A. E. Carden, "Thermal Fatigue of a Nickel Base Alloy," to be published in the Journal of Basic Engineering.



MSRE GRAPHITE for MSRE

W. H. Cook

Summary

The graphite purchased for the MSRE, grade CGB, is a new nuclear graphite that is basically an extruded petroleum coke bonded with coal tar pitch heated to 2800°C. Low permeation is obtained through a series of impregnations and heat treatments. The final heat treatment was at 2800°C or higher. Experimental equipment and processes were used on a commercial scale for the first time. The graphite was produced as 2-1/2-in.-square X 72-in.-long bars which were machined to the required shapes. The average bulk density is 1.86 g/cm<sup>3</sup>. Its matrix is not permeated by molten salts under conditions more severe than those expected in the MSRE. It exceeded all the requirements specified for the MSRE except that it had longitudinal cracks. Tests indicated that the cracks should not have any significant adverse effect on the operation of the MSRE. The shrinkage of the graphite at 350 to 475°C under exposures between  $0.60 \times 10^{20}$  to  $1.40 \times 10^{20}$  nvt ( $E > 2.9$  Mev) indicated that this should not create any important adverse effects on the operation of the MSRE.

Major Requirements and Procurement

The major requirements for unclad graphite for the MSRE and for large central-station power plants are low permeation by salt, low permeability to gas, and a fully graphitized structure that would be least affected by irradiation. When we began looking for graphite for molten-salt reactors, only small pieces of superior-grade graphite produced in the laboratory appeared to have the desirable qualities. Therefore, the specifications for the MSRE were written around the properties of these laboratory-prepared superior grades of graphite, the requirements of large-scale power reactors, and reasonable limits of current graphite technology. The latter required that the gas permeability requirement not be specified since it certainly would be better than the best commercial grades of extruded and fully graphitized material. The technology also dictated that a 2-in.-square extruded bar was about the maximum practical size.

Fixed-fee bids were solicited. Only one vendor, the Carbon Products Division of Union Carbide Corporation, bid to supply the graphite for the MSRE.

Experimental equipment and processes were used on a commercial scale for the first time to produce the MSRE graphite designated as grade CGB. It was produced as 2-1/4-in.-square  $\times$  72-in.-long bars which were machined by the vendor to the shapes required for the MSRE.

The graphite is basically an extruded petroleum coke bonded with coal tar pitch heated to 2800°C. Low permeation is obtained through a series of impregnations and heat treatments. All components of the material are fired to 2800°C or higher. Since all components graphitize readily, this means that the product should be essentially a well-graphitized material. It is highly anisotropic.

The properties of grade CGB graphite are summarized in Table 1. These data are combinations of those obtained by the Carbon Products Division as part of their fulfillment of the purchase contract plus those obtained by ORNL as part of their studies. The discussion that follows is limited to some of the major properties of the graphite as related to the requirements of the MSRE and large-scale power plants.

#### Chemical Composition and Oxygen Content

Chemical analyses made by the Carbon Products Division on samples taken from 5% of the graphite supplied for the MSRE indicated that it meets the chemical composition requirements. These are compared in Table 2 with the specified values and those of a spot-check analysis made by ORNL.

The boron level is moderate and was set to keep the nuclear cross section of the graphite reasonably low. The sulfur was limited to avoid the sulfur embrittlement of the INOR-8.

A composite sample from three bars was analyzed spectrochemically. Calcium and magnesium were the only additional elements present, and these were less than 10 and 100 ppm respectively.

Grades of graphite tested prior to the grade CGB graphite had relatively high oxygen contamination, which tended to detrimentally contaminate the molten fluoride salts.<sup>1</sup> Because of this, the compositions of salts were adjusted to protect against uranium precipitation as an oxide. However, the quantity of chemisorbed oxygen in grade CGB graphite is relatively low, and it does not appear to present a problem to the MSRE.

The measurement of the chemisorbed oxygen was determined by placing specimens in a closed gas system, evacuating to  $\leq 10^{-3}$  torr at room temperature, and measuring the STP volume of carbon monoxide evolved from the graphite at 1800°C. The oxygen content was determined to be 4 and 9 cm<sup>3</sup> of CO per 100 cm<sup>3</sup> of graphite, respectively, at ORNL<sup>2,3</sup> and the Carbon Products Division. These are well under the maximum of 30 cm<sup>3</sup> of CO per 100 cm<sup>3</sup> of graphite permitted by the specification.

Table 1. Properties of MSRE Core Graphite, Grade CGB

|   |                         |
|---|-------------------------|
| <b>Physical properties</b>  |                         |
| Bulk density, <sup>a</sup> g/cm <sup>3</sup>  |                         |
| Range   | 1.82-1.89               |
| Average   | 1.86                    |
| Porosity, <sup>b</sup> %  |                         |
| Accessible  | 4.0                     |
| Inaccessible  | 13.7                    |
| Total   | 17.7                    |
| Thermal conductivity, <sup>a</sup> Btu ft <sup>-1</sup> hr <sup>-1</sup> (°F) <sup>-1</sup> |                         |
| With grain  |                         |
| At 90°F   | 112                     |
| At 1200°F   |                         |
| Normal to grain   |                         |
| At 90°F   | 63                      |
| At 1200°F   | 34                      |
| Temperature coefficient of expansion, <sup>c</sup> (°F) <sup>-1</sup>                       |                         |
| With grain  |                         |
| At 68°F   | 0.27 × 10 <sup>-6</sup> |
| Normal to grain   |                         |
| At 68°F   | 1.6 × 10 <sup>-6</sup>  |
| Specific heat, <sup>d</sup> Btu lb <sup>-1</sup> (°F) <sup>-1</sup>                         |                         |
| At 0°F  | 0.14                    |
| At 200°F  | 0.22                    |
| At 600°F  | 0.33                    |
| At 1000°F   | 0.39                    |
| At 1200°F   | 0.42                    |
| Matrix coefficient of permeability <sup>e</sup> to helium<br>at 70°F, cm <sup>2</sup> /sec  | 3 × 10 <sup>-4</sup>    |
| Salt absorption at 150 psig, <sup>a</sup> vol %   | 0.20                    |
| Mechanical strength <sup>b</sup> at 68°F  |                         |
| Tensile strength, psi   |                         |
| With grain  |                         |
| Range   | 1500-6200               |
| Average   | 1900                    |
| Normal to grain   |                         |
| Range   | 1100-4500               |
| Average   | 1400                    |
| Flexural strength, psi  |                         |
| With grain  |                         |
| Range   | 3000-5000               |
| Average   | 4300                    |

Table 1 (continued)

|   |                   |
|---|-------------------|
| Mechanical strength <sup>b</sup> at 68°F                          |                   |
| Flexural strength, psi  |                   |
| Normal to grain   |                   |
| Range   | 2200-3650         |
| Average   | 3400              |
| Modulus of elasticity, psi  |                   |
| With grain  | $3.2 \times 10^6$ |
| Normal to grain   | $1.0 \times 10^6$ |
| Compressive strength, <sup>d</sup> psi                            | 8600              |
| Chemical purity <sup>f</sup>                                      |                   |
| Ash, wt %   | 0.0041            |
| Boron, wt %   | 0.00009           |
| Vanadium, wt %  | 0.0005            |
| Sulfur, wt %  | 0.0013            |
| Oxygen, cm <sup>3</sup> of CO per 100 cm <sup>3</sup> of graphite | 9.0               |
| Irradiation data <sup>a</sup>                                     |                   |
| (Exposure: $1.0 \times 10^{20}$ nvt, E > 2.9 Mev)                 |                   |
| Shrinkage, % (350-475°C)  |                   |
| A <sub>0</sub>  | 0.10              |
| C <sub>0</sub>  | 0.07              |

<sup>a</sup>Measurements made by ORNL.<sup>b</sup>Based on measurements made by the Carbon Products Division and ORNL.<sup>c</sup>Measurements made by the Carbon Products Division.<sup>d</sup>Representative data from the Carbon Products Division.<sup>e</sup>Based on measurements made by the Carbon Products Division on pilot-production MSRE graphite.<sup>f</sup>Data from the Carbon Products Division.

Table 2. Chemical Composition of Grade CGB Graphite

| Specified Maximum<br>(wt %) | Analysis<br>(wt %) |                  |
|-----------------------------|--------------------|------------------|
|                             | ORNL <sup>a</sup>  | CPD <sup>b</sup> |
| Ash                         | 0.07               | 0.0005           |
| Boron                       | 0.0001             | 0.00008          |
| Vanadium                    | 0.01               | 0.0009           |
| Sulfur                      | 0.001              | <0.0005          |

<sup>a</sup>Analyses made by ORNL on a composite sample from three randomly selected bars.

<sup>b</sup>Each value is an average of values obtained on composite samples from 4 bars of each of the 13 lots.

#### Bulk Density

A minimum bulk density of 1.87 g/cm<sup>3</sup> was specified for the MSRE graphite because the laboratory materials that were examined and found to have low salt permeation had about this density. The bulk density of grade CGB graphite ranges from 1.82 to 1.89 g/cm<sup>3</sup> and averages 1.86 g/cm<sup>3</sup>. Calculations indicate that an average bulk density of 1.84 g/cm<sup>3</sup> is acceptable for the MSRE if the graphite meets the salt permeation requirements.<sup>4</sup> The grade CGB graphite meets these conditions.

#### Porosity

The graphite has a total void volume or porosity of ~18.0%, about 77% of which is inaccessible or closed. Therefore, the accessible void space should be ~4.0% of the bulk volume of the graphite. The pore entrance diameters to the accessible voids range approximately between the two extremes shown in Fig. 1 for grades CGB and CGB-X (an experimental grade). This means that the major portion of the accessible voids have entrances less than 0.4  $\mu$  in diameter. The molten fluoride salts do not wet the graphite, and it has been calculated that a differential pressure of >300 psia would be required to force salt into these voids. This is supported in the impregnation tests, which are discussed later.

#### Microstructure

The attainment of the high density and low accessible voids with small pore entrance diameters is reflected in the microstructure of the graphite,<sup>5</sup> as shown in Fig. 2. Note that almost all the original voids

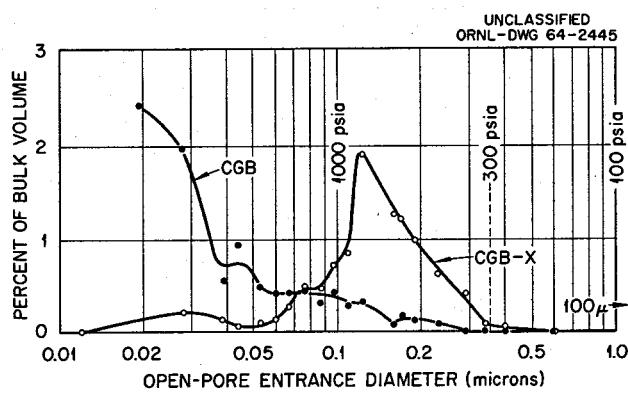


Fig. 1. Pore Sizes of Accessible Voids in Graphite.

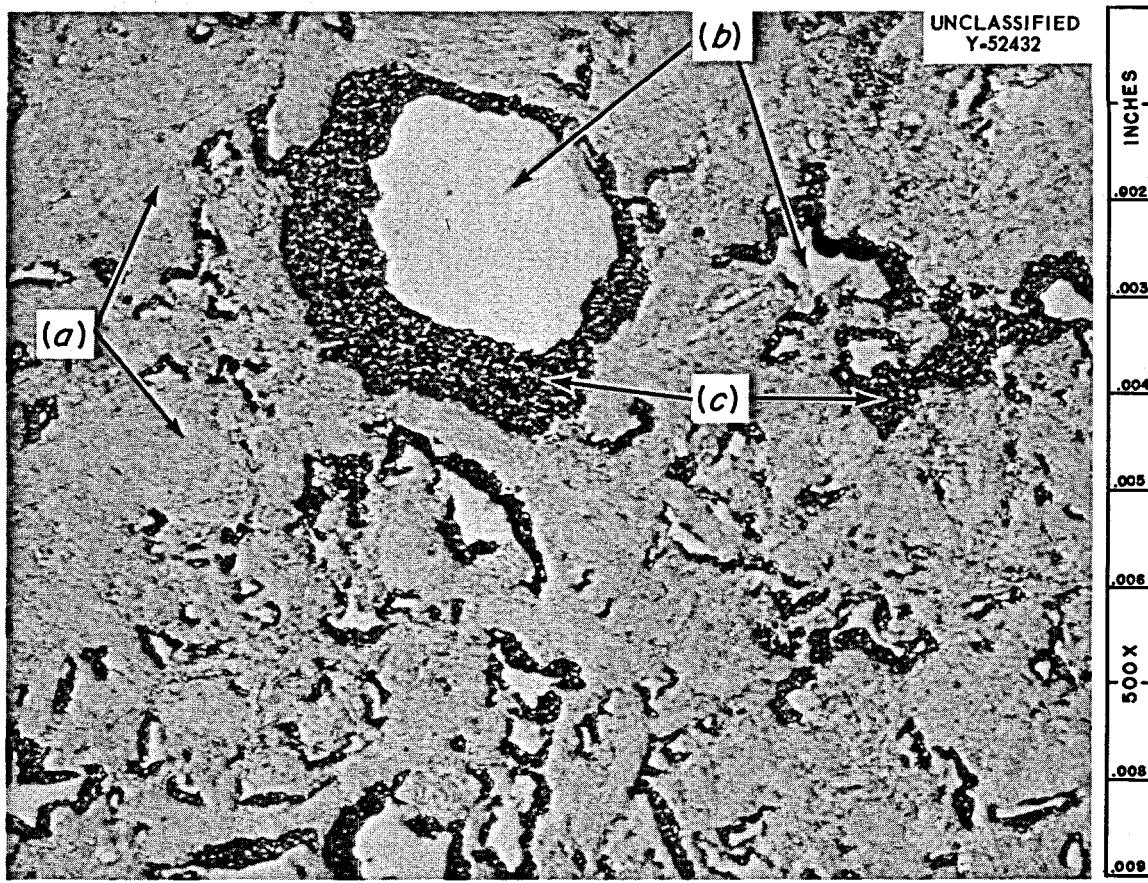


Fig. 2. Some Microstructural Details of MSRE Graphite, Grade CGB.  
 (a) The major constituent, graphitized coke particles (graphite particles); and (b and c) types of structures developed through impregnations and heat treatments. As-polished. 500X.

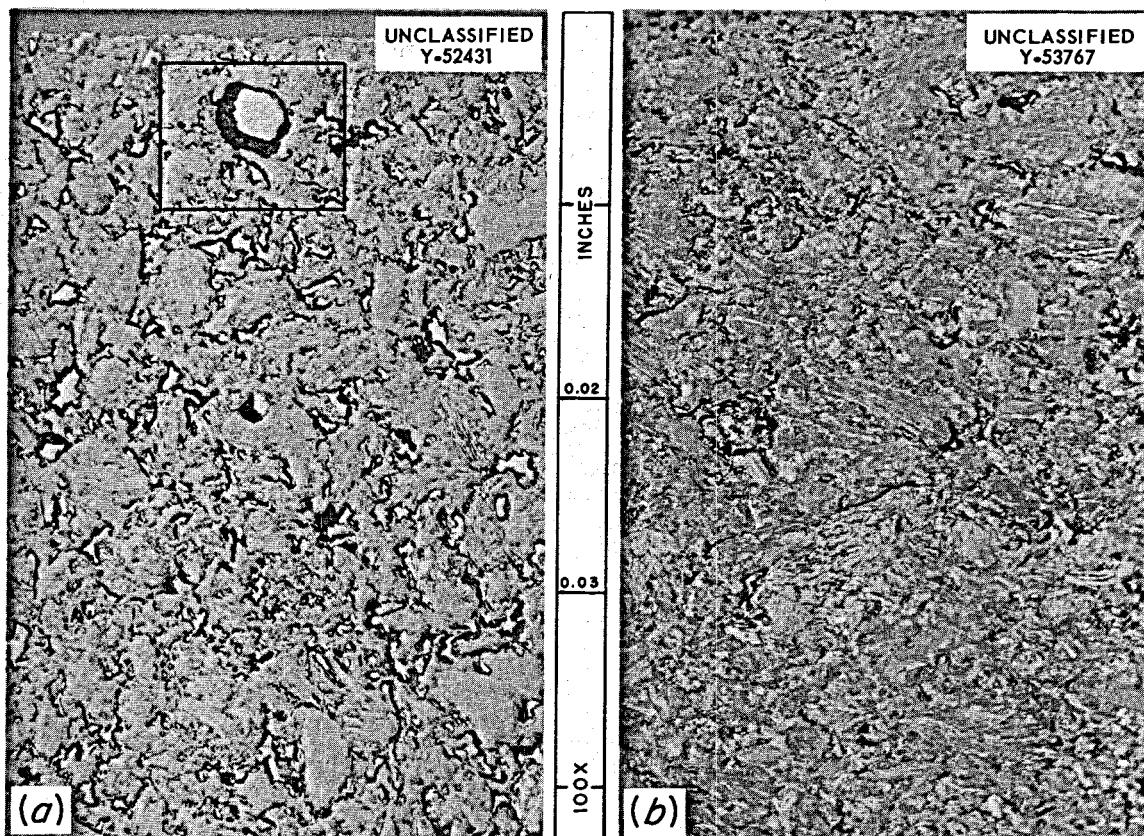


Fig. 3. Variations of the General Microstructure of the MSRE Graphite, Grade CGB. As-polished. 100X.

in the base stock have been impregnated, and these impregnants fill or almost fill each void although they have been subjected to 2800°C heat treatments. There is some structure variation in the graphite which is illustrated in Fig. 3. In general, all the black areas are voids filled with graphitized impregnants.

#### Cracks

The high density and small pore structure are desirable characteristics for unclad graphite in molten-salt reactors. However, this particular structure was apparently so dense, or tight, that hydrocarbons produced through the pyrolysis of the impregnants could not escape rapidly enough through the natural pores of the graphite during the fabrication processes. Consequently, the matrix of the graphite was cracked as these gases forced their way out. The appearance and results of these cracks on the more severely cracked bars are shown in Fig. 4.

The majority of the cracks were 0.001 in. (25  $\mu$ ) to 0.002 in. (50  $\mu$ ) thick, 1/8 to 1/4 in. wide, and less than 3 in. long as determined by visual, microscopic, and radiographic techniques.

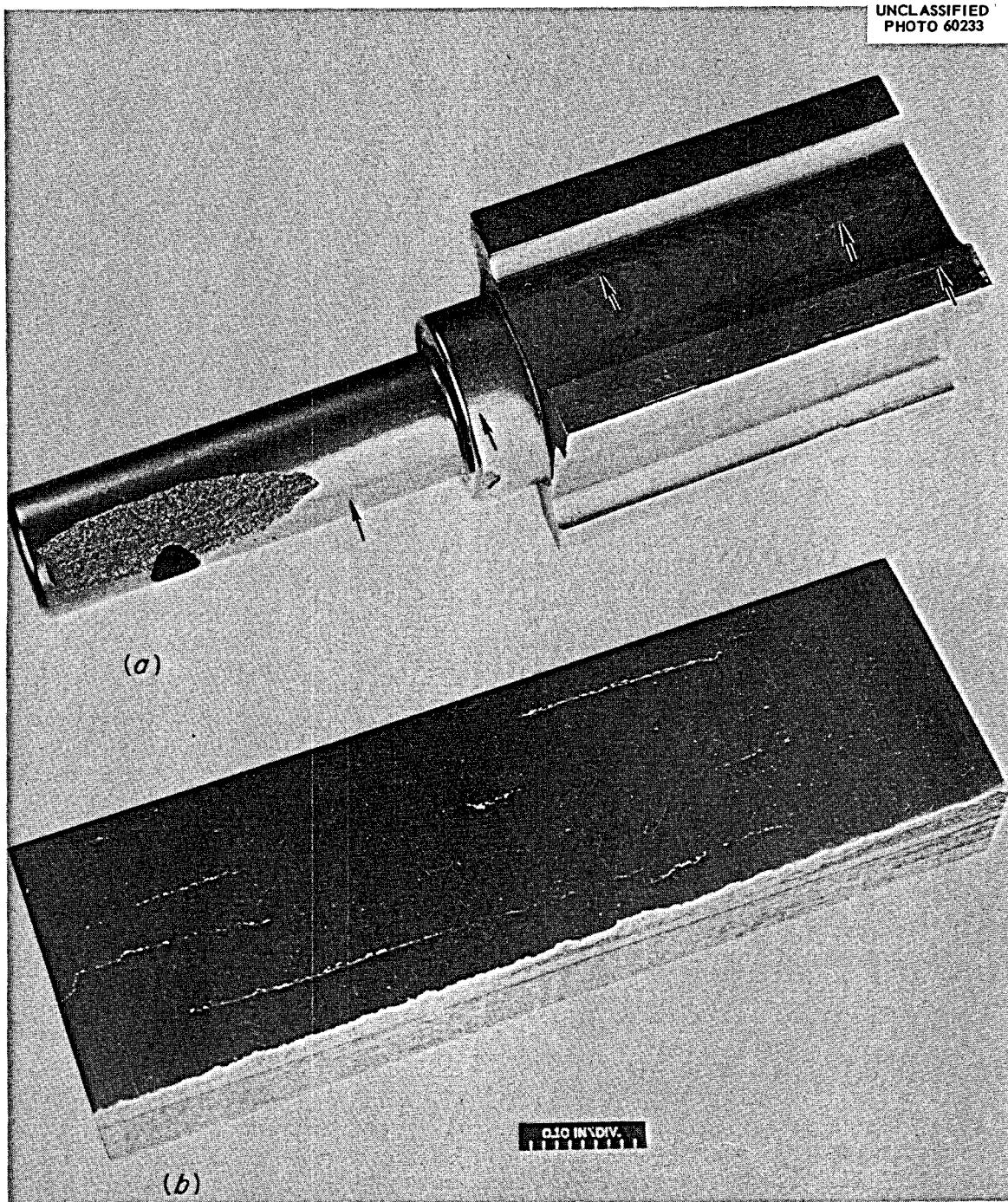
UNCLASSIFIED  
PHOTO 60233

Fig. 4. Appearance of Spalls and Cracks in Samples of Severely Cracked Grade CGB Graphite in (a) Spindle End of a Machined Bar and (b) Midplane of an As-Received Bar. Cracks are indicated by arrows or are clearly visible as ragged white lines.

Most of the graphite had been manufactured when the cracking, which occurred in the final processing step, was discovered. Additional process development, production, and machining of replacement material would have delayed the reactor at least 1 year.

With the exception of the cracks, the material met the specification. Studies were made on defects in representative bars. The graphite would not be good enough for the core of a high-performance breeder, but our analyses showed that sizable flaws should not adversely affect the operation of the MSRE.<sup>4</sup> The specifications were revised to define the flaws that could be accepted. In addition to the integrity tests in the original specification and additional modified macroscopic examinations, the vendor agreed to make a 100% radiographic examination of all the bars. Each bar used in the MSRE passed limits set for the results of two radiographs made perpendicular to, and along the full length of, two adjoining lateral surfaces of each bar.<sup>6</sup>

#### Thermal Cycling of Salt-Impregnated Graphite

Mechanical tests indicated that the cracks resisted propagation.<sup>7,8</sup> However, since it is probable that some of the cracks in graphite will be filled with salt, tests were made to determine if repeated melting and freezing of the salt would propagate the cracks.

#### One Hundred Cycles

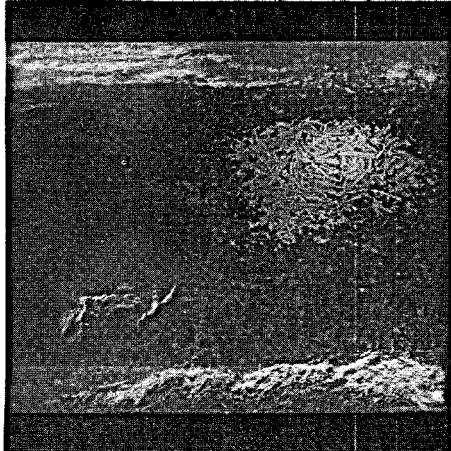
Laboratory thermal cycling tests were made on specimens of grade CGB graphite with salt-impregnated cracks to determine whether damage would occur under conditions simulating the draining, cooling, and reheating of the MSRE core.

The specimens were 2-in.-long transverse sections cut from a machined CGB graphite bar in a zone having a relatively high concentration of cracks.

Specimens were impregnated with salt at 700°C (1300°F) during 100-hr exposures at 50 or 150 psig. The lower pressure was selected because it is approximately the maximum pressure expected in the reactor. The higher pressure was selected to ensure that the cracks would be deeply penetrated by the salt. The average bulk volume of the specimens permeated by the salt was 0.08% at 50 psig and 0.14% at 150 psig. The salt impregnation appeared to be limited to the fissures, as shown in Fig. 5. The specimens were subjected to 100 thermal cycles in which the temperature was increased from 200°C to 700°C in the first 9 min of each cycle; this is more than 100 times faster than the maximum electrical heating rate of the core. After this treatment there were no detectable changes in the appearance of the graphite or in the lengths of the cracks (Fig. 5).

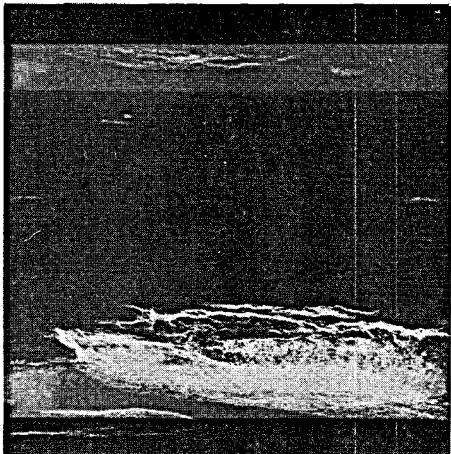
UNCLASSIFIED  
PHOTO 60329

Y-48960



(a)

Y-48961



(b)

Y-48955



(d)

Y-48962



(c)

Fig. 5. GCB Graphite Specimens Impregnated with Molten Salt at 50 psig. (a,b,c) As-radiographed and (d) after 100 thermal cycles.

### High-Temperature Cycle

For more severe, high-temperature tests of this kind, two additional specimens were impregnated in the standard way; that is, they were evacuated, and then were exposed for 100 hr to molten salt at 150 psig at 700°C (1300°F). Radiography, as for the previously reported work, indicated that the salt was primarily confined to the cracks in the graphite specimens. It was equivalent to 0.09% of the bulk volume of one specimen and 0.11% of the other.

Each impregnated specimen was subjected to a single high-temperature cycle from 200 to 1000°C. The rate of temperature rise for each is summarized in Table 3.

There were no detectable changes in the graphite specimens or their cracks as a result of these thermal cycles. These exceeded the maximum temperature, 730°C (1350°F), expected in the MSRE.

The maximum electrical heating rate<sup>9</sup> of the core is expected to be 30°C/hr (54°F/hr). On this basis the slowest of the high-temperature thermal cycles was >250 times faster in reaching 700°C (1300°F) than the maximum preheating rate.

The results of the preceding tests indicate that the thermal cycling of the MSRE probably would not cause the salt to expand and break up the graphite.

Table 3. Rates of Temperature Rise for the Thermal Cycles of Two Salt-Impregnated Segments from a Machined MSRE Graphite Bar

| Temperature<br>[°C (°F)] | Time to Indicated Cycle Temperature <sup>a</sup><br>(min) |                |
|--------------------------|---|----------------|
|                          | Specimen 198-4  | Specimen 198-5 |
| ~200 (~390) <sup>b</sup> | 0   | 0              |
| 700 (1300)               | 3.7   | 3.4            |
| 1000 (1830)              | 36.0  | 23.0           |

<sup>a</sup>The differences in heating rates are due to different quantities of argon cover gas used in each test.

<sup>b</sup>Starting temperature of cycle.

Impregnation TestsMercury

It was established that mercury impregnation into graphite at room temperature could be correlated with molten-salt permeation into graphite.<sup>10</sup> Therefore, a mercury-impregnation test of graphite specimens at room temperature was specified to provide a convenient quality control for the manufacturer. It was specified that  $0.125 \times 1.500 \times 1.500$  in. evacuated specimens should not gain more than 3.5 wt % when submerged for 20 hr in mercury at 470 psig. The vendor was required to apply this test to a sample taken 1 in. from the end of every bar. The average weight gain was 1.8%. Most of this was due to mercury pickup in cracks in the specimens. The maximum permitted by the specification was 3.5%.

Salt

The molten salts are used at ORNL to screen various grades of graphite. An average of less than 0.2% of the bulk volumes of specimens (0.500 in. in diameter  $\times$  1.500 in. long) from grade CGB graphite were filled when evacuated and then exposed for 100 hr to LiF-BeF<sub>2</sub>-ThF<sub>4</sub>-UF<sub>4</sub> (67-18.5-14-0.5 mole %) salt at 700°C (1300°F) under 150 psig pressure, the standard screening test. The design limit for the MSRE is 0.5% of the bulk volume of the graphite. The maximum pressure expected in the MSRE is 50 psig, which is one-third that of the standard screening pressure. The bulk volume of the small specimens impregnated with salt ranged from 0.01 to 0.46%. It should be emphasized that a full-scale bar would have even less salt pickup. The small screening specimens tend to magnify the degree of salt impregnation.

The MSRE designers did not want the molten salt to penetrate into the matrix of the graphite. This was essentially accomplished. The pattern of the impregnating salt is illustrated in Fig. 6, which shows reproductions of radiographs of thin sections cut from an unimpregnated specimen and three salt-impregnated specimens. As was the case for the large thermal cycling specimens, the salt is limited to small penetrations at the surface and along cracks where the cracks intersect the exterior surfaces. Note that the salt is confined to the limits of the crack and does not permeate the matrix.

Mechanical Properties

The tensile and flexural strength measurements on grade CGB graphite averaged 1860 and 4340 psi, respectively, despite the presence of cracks in the graphite. There were no values less than the minimums of 1500 and 3000 psi specified for the tensile and flexural strengths respectively. These strength values were specified primarily to assure a good quality of graphite. The stresses expected in the reactor are relatively modest in comparison. The stresses are all less than 100 psi in the absence of irradiation.<sup>11</sup> Under fast-neutron irradiation at MSRE temperatures, the

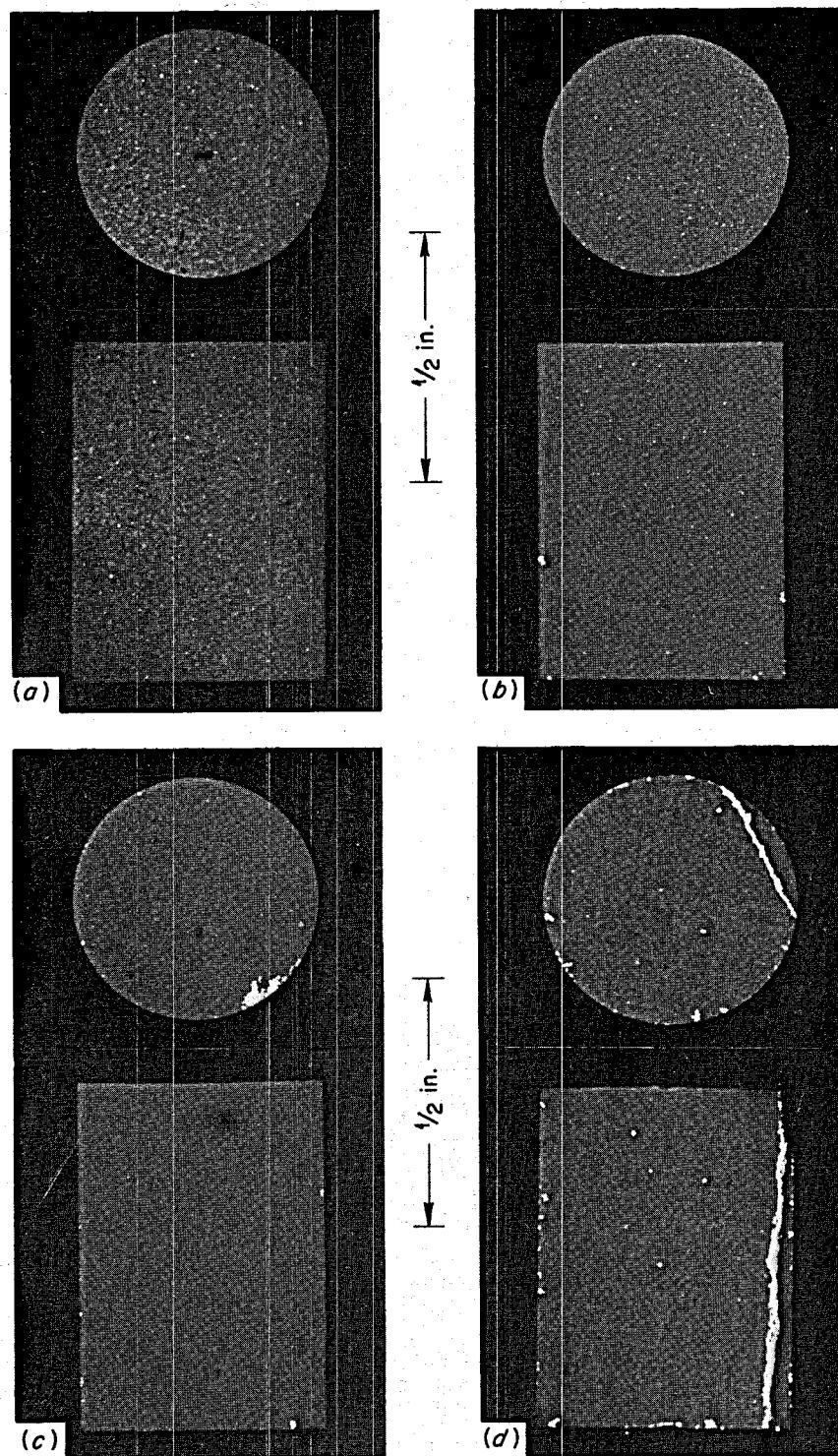
UNCLASSIFIED  
PHOTO 66313

Fig. 6. Typical Salt Distribution in Grade CGB Graphite Cylinders as Shown by Radiographs of Their Thin Sections. (a) Control (no salt present) and (b,c,d) salt-impregnated specimens; white phase is salt.

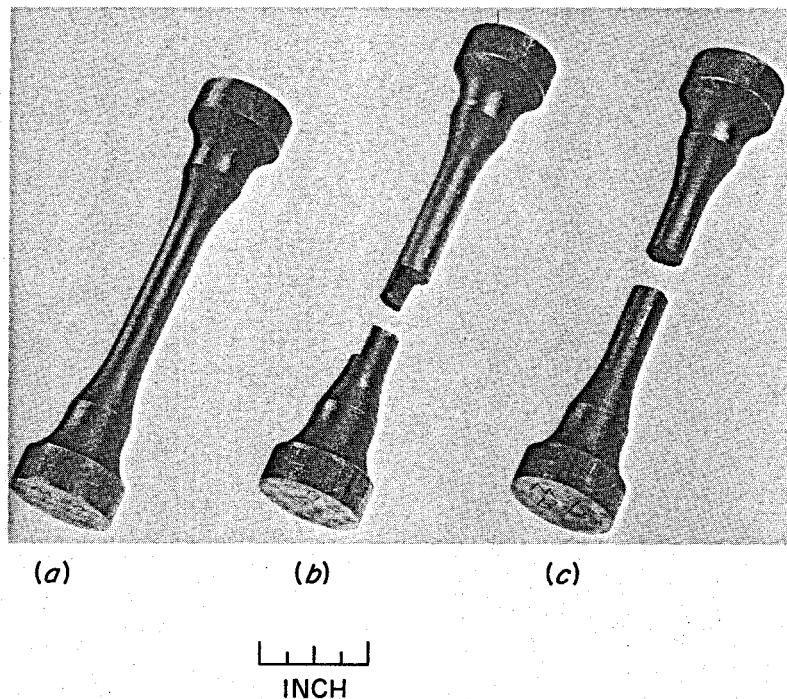
UNCLASSIFIED  
Y-48954

Fig. 7. Tensile Specimens of Grade CGB Graphite. (a) As-machined.  
(b) Typical stair-step fracture. (c) Normal fracture.

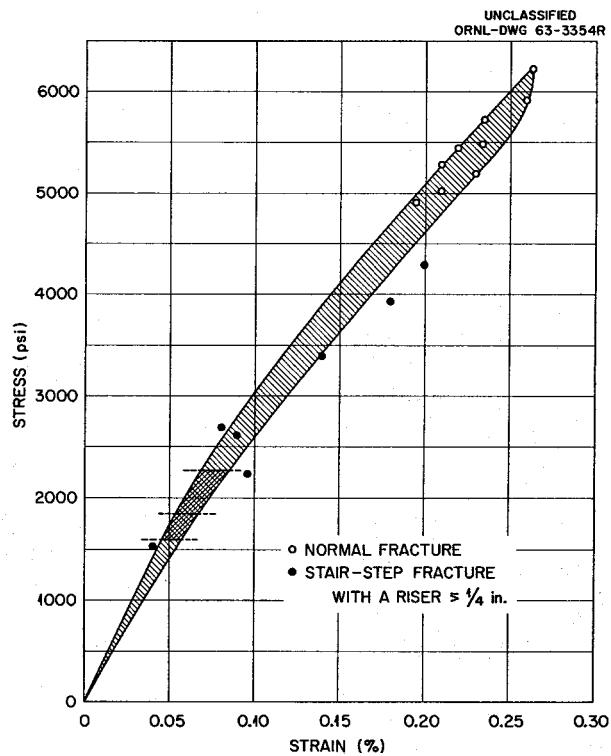


Fig. 8. Tensile Properties of Grade CGB Graphite Parallel with Grain (Axis of Extrusion) Bar 45, 2 x 2 in.

flux gradient across the bars will create a difference in shrinkage and will cause most of them to bow away from the center of the core. The stress in tension on a completely restrained beam will increase at a rate of 950 psi per full-power year.<sup>12</sup>

To say that the mechanical properties of the graphite meet the expected requirements of the MSRE does not adequately describe the graphite for use in the MSRE or future molten-salt reactors. The tensile strength of the material was examined in zones with and without cracks with a specimen as shown in Fig. 7a. A typical fracture in the presence of a crack is shown in Fig. 7b, and a normal fracture in the absence of cracks is shown in Fig. 7c. The ultimate tensile strength values obtained by the Mechanical Properties Laboratory of the Metals and Ceramics Division are shown in Fig. 8 with the overall range of tensile strength values just discussed for the batch of MSRE graphite superimposed with double cross-hatching. This corresponds to the specimens that demonstrated definite effects of cracks, the black points, that had a minimum strength of 1510 psi and an average strength of 2940 psi. Specimens that were not appreciably affected by cracks, the open circles, yielded an average strength of 5440 psi and a modulus of elasticity of  $3.2 \times 10^6$  psi. This is an unusually strong graphite.

#### Stability Under Irradiation

The effects of irradiation on grade CGB graphite have been studied by Kennedy<sup>13</sup> with grade EGCR-AGOT (grade AGOT), a needle coke graphite, at 350 to 475°C under exposures between  $0.60 \times 10^{20}$  to  $1.40 \times 10^{20}$  nvt ( $E > 2.9$  Mev). He reports that contraction of the grade CGB graphite is initiated at lower dosage in the direction perpendicular to the grain than in the parallel direction, but the increase rates for both are almost identical. These contractions are shown graphically in Figs. 9 and 10. In the same studies the effect on the average modulus of elasticity was reported as changing from  $3.25 \times 10^6$  psi to  $8.42 \times 10^6$  psi in the parallel direction and from  $1.06 \times 10^6$  psi to  $3.78 \times 10^6$  psi in the perpendicular direction. Calculations using greater contraction values than

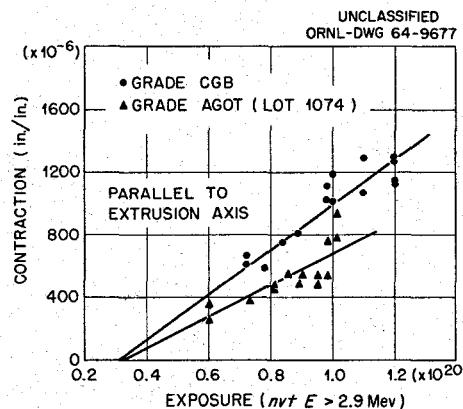


Fig. 9. Effect of Irradiation on Graphite Dimensional Changes Parallel to the Extrusion Axis.

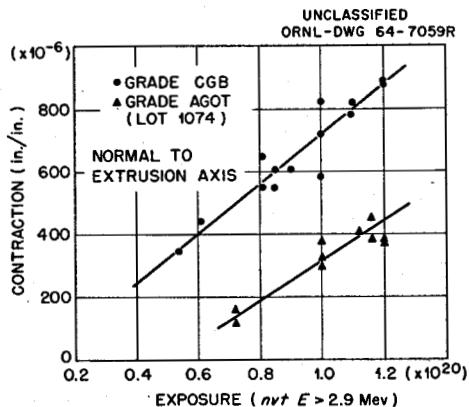


Fig. 10. Effect of Irradiation on Graphite Dimensional Changes Normal to the Extrusion Axis.

these indicate that these should not adversely affect the operation of the MSRE.<sup>14,15</sup> The actual contraction rates should be even smaller at the operating temperature of the MSRE, because at these higher temperatures nuclear grades of graphite are approaching a minimum contraction rate.<sup>16</sup> This, plus the creep of the grade CGB graphite,<sup>17</sup> provide additional safety factors for conditions that appear satisfactory without them.

#### Lattice and Ring Bars

The preceding information has been for the MSRE core bars that are vertical in the reactor. These core bars are supported on a lattice of horizontal bars and held together at the top by a graphite retainer ring (sections of graphite pieces joined with INOR-8 pins). The graphite fabricated for the lattice bars and ring sections was fabricated with a higher permeability to help eliminate cracks and to secure more structural integrity for these pieces. Radiographic examination of this material was the only technique that showed any flaws.<sup>18</sup> There were a few isolated, small cracks. These closely approach being structurally flaw-free bars. Limited sampling indicates that the properties of this material are similar to the core material except that it takes up an average of 4.67 wt % in the mercury test, about 2.6 times that of the core bars. However, this is equivalent to a molten-salt takeup in the graphite of only 0.6% of the bulk volume of the graphite. This is tolerable for the MSRE because the lattice bars and retainer ring are a small fraction of the total graphite and are in low-neutron-flux zones that are not subject to the more severe operating conditions of the MSRE.

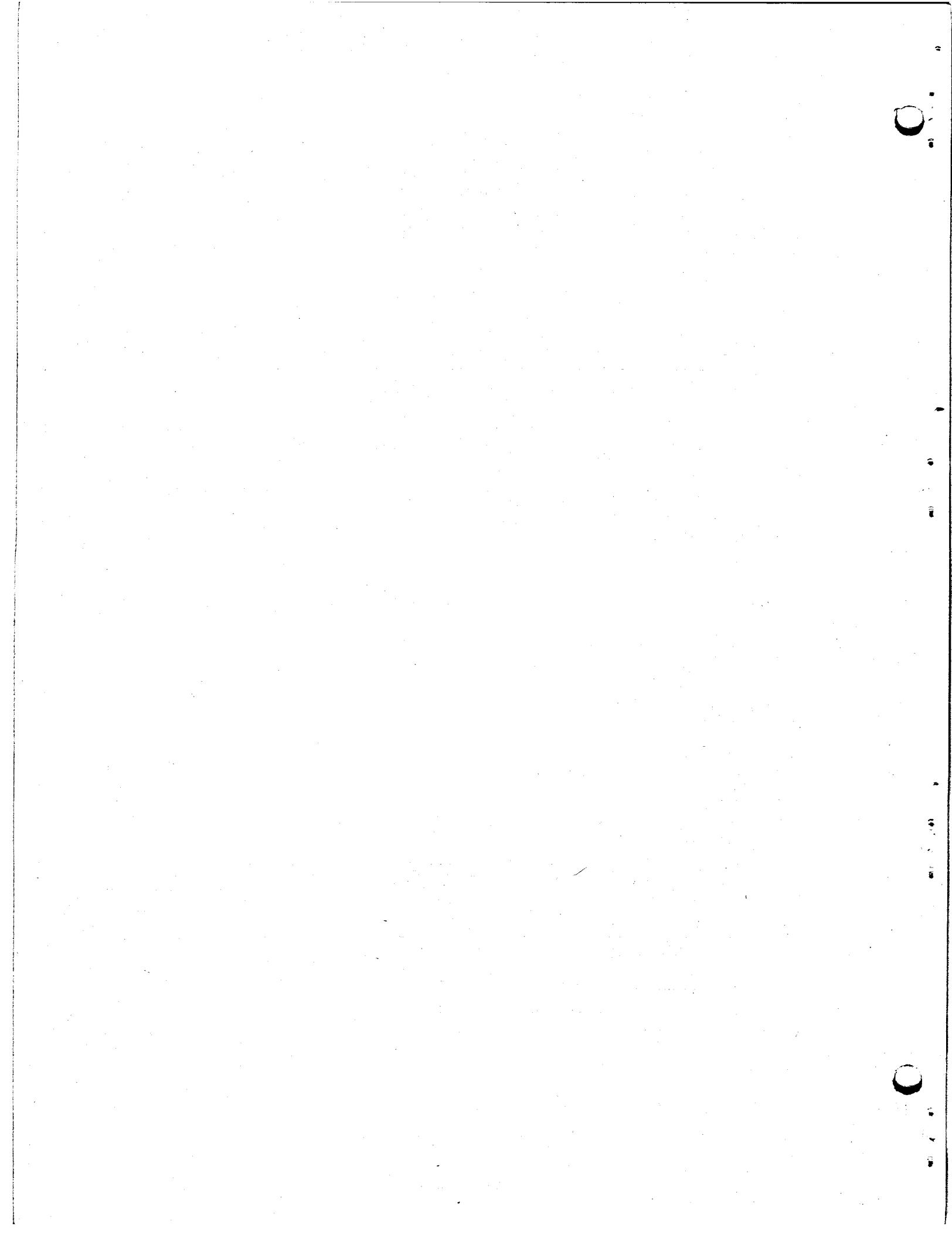
Developmental studies on MSRE-type graphite are being continued by the Carbon Products Division. They report that in recent work they have produced core-quality graphite without flaws without resorting to this minor sacrifice to permeation.

Conclusions

At this time all the graphite for the MSRE appears to meet all the requirements. The grade CGB graphite appears to be a substantial step forward in the development of a high-density, low-permeability nuclear graphite, but further improvement is needed to obtain a material for structural units in molten-salt power reactors.

References

1. MSRP Quart. Progr. Rept. Oct. 31, 1958, ORNL-2626, pp. 61-64.
2. MSRP Semiann. Progr. Rept. July 31, 1963, ORNL-3529, p. 75.
3. Unpublished work.
4. R. B. Briggs, W. H. Cook, and A. Taboada, internal memorandum, Feb. 14, 1963.
5. MSRP Semiann. Progr. Rept. Jan. 31, 1964, ORNL-3626, pp. 67-69.
6. R. B. Briggs, W. H. Cook, and A. Taboada, internal memorandum, Feb. 14, 1963.
7. Ibid.
8. C. R. Kennedy, GCRP Semiann. Progr. Rept. Mar. 31, 1963, ORNL-3445, p. 221.
9. MSRP Semiann. Progr. Rept. Jan. 31, 1963, ORNL-3419, p. 123.
10. MSRP Semiann. Progr. Rept. Feb. 28, 1962, ORNL-3282, p. 92.
11. R. B. Briggs, W. H. Cook, and A. Taboada, internal memorandum, Feb. 14, 1963.
12. Ibid.
13. C. R. Kennedy, Metals and Ceramics Div. Ann. Progr. Rept. June 30, 1964, ORNL-3670 (to be published).
14. R. B. Briggs, W. H. Cook, and A. Taboada, internal memorandum, Feb. 14, 1963.
15. P. N. Haubenreich et al., MSRE Design and Operations Report. Part III, ORNL-TM-730 (Feb. 3, 1964), pp. 183-84.
16. J. M. Davidson and J. W. Helm, "Effect of Temperature on Radiation-Induced Contraction of Reactor Graphite," p. 286 in Proceedings of the Fifth Conference on Carbon, vol. I, Macmillan, New York, 1962.
17. GCRP Semiann. Progr. Rept. Mar. 31, 1964, ORNL-3619, pp. 151-54.
18. MSRP Semiann. Progr. Rept. Jan. 31, 1964, ORNL-3626, p. 70.



ORNL-3708  
UC-80 - Reactor Technology  
TID-4500 (35th ed.)

Internal Distribution

- |         |                   |      |                   |
|---------|-------------------|------|-------------------|
| 1.      | G. M. Adamson     | 200. | E. N. Fray        |
| 2.      | L. G. Alexander   | 201. | J. W. Freels      |
| 3.      | R. F. Apple       | 202. | H. A. Friedman    |
| 4.      | T. Arnwine        | 203. | J. H. Frye, Jr.   |
| 5.      | C. F. Baes        | 204. | C. H. Gabbard     |
| 6.      | S. J. Ball        | 205. | W. R. Gall        |
| 7.      | S. E. Beall       | 206. | R. B. Gallaher    |
| 8.      | E. S. Bettis      | 207. | J. J. Geist       |
| 9.      | D. S. Billington  | 208. | C. A. Gifford     |
| 10.     | F. F. Blankenship | 209. | T. G. Godfrey     |
| 11.     | E. P. Blizard     | 210. | W. W. Goolsby     |
| 12.     | R. Blumberg       | 211. | W. R. Grimes      |
| 13.     | A. L. Boch        | 212. | J. L. Griffith    |
| 14.     | E. G. Bohlmann    | 213. | A. G. Grindell    |
| 15.     | C. J. Borkowski   | 214. | E. H. Guinn       |
| 16.     | G. E. Boyd        | 215. | R. H. Guymon      |
| 17.     | E. J. Breeding    | 216. | P. H. Harley      |
| 18-168. | R. B. Briggs      | 217. | C. S. Harrill     |
| 169.    | W. M. Brown       | 218. | P. N. Haubenreich |
| 170.    | F. R. Bruce       | 219. | F. K. Heacker     |
| 171.    | G. H. Burger      | 220. | G. M. Hebert      |
| 172.    | J. C. Cable       | 221. | P. G. Herndon     |
| 173.    | S. Cantor         | 222. | M. R. Hill        |
| 174.    | D. W. Cardwell    | 223. | T. G. Hill        |
| 175.    | R. E. Carnes      | 224. | E. C. Hise        |
| 176.    | T. M. Cate        | 225. | B. F. Hitch       |
| 177.    | C. E. Center      | 226. | H. W. Hoffman     |
| 178.    | J. A. Conlin      | 227. | A. Hollaender     |
| 179.    | W. H. Cook        | 228. | V. D. Holt        |
| 180.    | L. T. Corbin      | 229. | P. P. Holz        |
| 181.    | G. A. Cristy      | 230. | A. S. Householder |
| 182.    | J. L. Crowley     | 231. | A. Houtzeel       |
| 183.    | F. L. Culler      | 232. | T. L. Hudson      |
| 184.    | D. G. Davis       | 233. | C. C. Hurt        |
| 185.    | J. H. DeVan       | 234. | R. S. Jackson     |
| 186.    | D. T. Dice        | 235. | W. Jennings       |
| 187.    | T. E. Diggs       | 236. | B. J. Jones       |
| 188.    | S. J. Ditto       | 237. | C. Jones          |
| 189.    | R. G. Donnelly    | 238. | W. C. Jordan      |
| 190.    | D. A. Douglas     | 239. | W. H. Jordan      |
| 191.    | W. H. Duckworth   | 240. | P. R. Kasten      |
| 192.    | N. E. Dunwoody    | 241. | R. J. Kedl        |
| 193.    | J. D. Emch        | 242. | M. T. Kelley      |
| 194.    | J. R. Engel       | 243. | M. J. Kelly       |
| 195.    | E. P. Epler       | 244. | C. R. Kennedy     |
| 196.    | W. K. Ergen       | 245. | T. W. Kerlin      |
| 197.    | H. E. Felts       | 246. | S. S. Kirslis     |
| 198.    | W. K. R. Finnell  | 247. | A. I. Krakoviak   |
| 199.    | A. P. Fraas       | 248. | J. W. Krewson     |

- |      |                  |      |                  |
|------|------------------|------|------------------|
| 249. | C. E. Lamb       | 298. | R. J. Ross       |
| 250. | J. A. Lane       | 299. | W. E. Sallee     |
| 251. | C. E. Larson     | 300. | H. W. Savage     |
| 252. | E. J. Lawrence   | 301. | A. W. Savolainen |
| 253. | T. A. Lincoln    | 302. | D. Scott         |
| 254. | S. C. Lind       | 303. | H. E. Seagren    |
| 255. | R. B. Lindauer   | 304. | D. R. Sears      |
| 256. | R. S. Livingston | 305. | J. H. Shaffer    |
| 257. | M. I. Lundin     | 306. | E. D. Shipley    |
| 258. | H. G. MacPherson | 307. | J. R. Shugart    |
| 259. | W. L. Maddox     | 308. | M. J. Skinner    |
| 260. | E. R. Mann       | 309. | G. M. Slaughter  |
| 261. | E. J. Manthos    | 310. | A. N. Smith      |
| 262. | W. R. Martin     | 311. | P. G. Smith      |
| 263. | H. C. McCurdy    | 312. | R. Smith, Jr.    |
| 264. | W. B. McDonald   | 313. | A. H. Snell      |
| 265. | H. F. McDuffie   | 314. | I. Spiewak       |
| 266. | D. L. McElroy    | 315. | R. Steffy        |
| 267. | C. K. McGlothlan | 316. | C. E. Stevenson  |
| 268. | E. C. Miller     | 317. | H. H. Stone      |
| 269. | W. R. Mixon      | 318. | C. D. Susano     |
| 270. | B. H. Montgomery | 319. | J. A. Swartout   |
| 271. | J. P. Moore      | 320. | A. Taboada       |
| 272. | R. L. Moore      | 321. | J. R. Tallackson |
| 273. | K. Z. Morgan     | 322. | E. H. Taylor     |
| 274. | J. C. Moyers     | 323. | J. W. Teague     |
| 275. | M. L. Nelson     | 324. | W. P. Teichert   |
| 276. | T. E. Northup    | 325. | R. E. Thoma      |
| 277. | W. R. Osborn     | 326. | W. D. Todd       |
| 278. | R. B. Parker     | 327. | G. M. Tolson     |
| 279. | L. F. Parsly     | 328. | D. B. Trauger    |
| 280. | P. Patriarca     | 329. | R. W. Tucker     |
| 281. | H. R. Payne      | 330. | W. C. Ulrich     |
| 282. | L. E. Penton     | 331. | F. J. Underwood  |
| 283. | A. M. Perry      | 332. | J. L. Underwood  |
| 284. | D. Phillips      | 333. | J. A. Watts      |
| 285. | W. B. Pike       | 334. | J. T. Venard     |
| 286. | H. B. Piper      | 335. | D. C. Watkin     |
| 287. | B. E. Prince     | 336. | G. M. Watson     |
| 288. | L. P. Pugh       | 337. | B. H. Webster    |
| 289. | W. E. Ramsey     | 338. | A. M. Weinberg   |
| 290. | J. L. Redford    | 339. | R. Weis          |
| 291. | M. Richardson    | 340. | S. R. West       |
| 292. | C. E. Roberts    | 341. | J. H. Westsik    |
| 293. | R. C. Robertson  | 342. | J. C. White      |
| 294. | T. K. Roche      | 343. | L. V. Wilson     |
| 295. | H. C. Roller     | 344. | C. H. Wodtke     |
| 296. | K. A. Romberger  | 345. | J. E. Wolfe      |
| 297. | M. W. Rosenthal  | 346. | B. J. Young      |

|  |  |
|--|--|
| 347. Biology Library   | 353-355. Central Research Library      |
| 348-349. Reactor Division Library                                      | 356-385. Laboratory Records            |
| 350-352. ORNL-Y-12 Technical<br>Library, Document<br>Reference Section | Department                             |
|  | 386. Laboratory Records,<br>ORNL R. C. |

External Distribution

387-388. D. F. Cope, AEC, ORO  
389. R. W. Garrison, AEC, Washington  
390. R. W. McNamee, Manager, Research Administration, UCC, New York  
391. R. L. Philippone, AEC, ORO  
392. W. L. Smalley, AEC, ORO  
393. M. J. Whitman, AEC, Washington  
394. Division of Research and Development, AEC, ORO  
395-1012. Given distribution as shown in TID-4500 (35th ed.) under  
Reactor Technology Category (75 copies - CFSTI)